JAAVSO

Volume 40
Number 2
2012

The Journal of the American Association of Variable Star Observers

ε Aurigae Special Edition

Historic first: 1.6-μ wavelength image of ε Aur, 2009 Nov. 2, as initially processed by John Monnier, based on four telescope beam combination data acquired by MIRC at the CHARA Array and showing the shadow of the disk crossing the face of ε Aur. *see page 618*

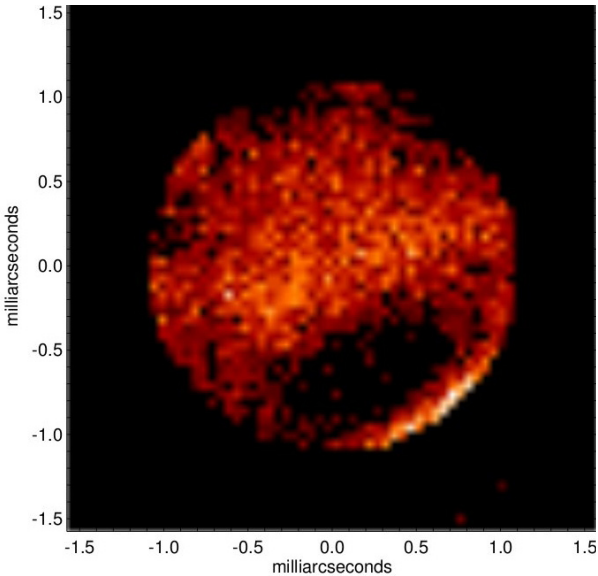

Image courtesy of John Monnier, Univ. Michigan

Also in this issue...

THE AMERICAN ASSOCIATION OF VARIABLE STAR OBSERVERS
FOUNDED 1911

49 Bay State Road
Cambridge, MA 02138
U. S. A.

ISSN 0271-9053

JAAVSO

The Journal of
The American Association
of Variable Star Observers

Volume 40
Number 2
2012

ε Aurigae Special Edition

ISSN 0271-9053

49 Bay State Road
Cambridge, MA 02138
U. S. A.

The *Journal of the American Association of Variable Star Observers* is a refereed scientific journal published by the American Association of Variable Star Observers, 49 Bay State Road, Cambridge, Massachusetts 02138, USA. The *Journal* is made available to all AAVSO members and subscribers.

In order to speed the dissemination of scientific results, selected papers that have been refereed and accepted for publication in the *Journal* will be posted on the internet at the *eJAAVSO* website as soon as they have been typeset and edited. These electronic representations of the *JAAVSO* articles are automatically indexed and included in the NASA Astrophysics Data System (ADS). *eJAAVSO* papers may be referenced as *J. Amer. Assoc. Var. Star Obs., in press,* until they appear in the concatonated electronic issue of *JAAVSO*. The *Journal* cannot supply reprints of papers.

Page Charges

Unsolicited papers by non-Members will be assessed a charge of $15 per published page.

Instructions for Submissions

The *Journal* welcomes papers from all persons concerned with the study of variable stars and topics specifically related to variability. All manuscripts should be written in a style designed to provide clear expositions of the topic. Contributors are strongly encouraged to submit digitized text in MS WORD, LATEX+POSTSCRIPT, or plain-text format. Manuscripts may be mailed electronically to journal@aavso.org or submitted by postal mail to *JAAVSO*, 49 Bay State Road, Cambridge, MA 02138, USA.

Manuscripts must be submitted according to the following guidelines, or they will be returned to the author for correction:

Manuscripts must be:
1) original, unpublished material;
2) written in English;
3) accompanied by an abstract of no more than 100 words.
4) not more than 2,500–3,000 words in length (10–12 pages double-spaced).

Figures for publication must:
1) be camera-ready or in a high-contrast, high-resolution, standard digitized image format;
2) have all coordinates labeled with division marks on all four sides;
3) be accompanied by a caption that clearly explains all symbols and significance, so that the reader can understand the figure without reference to the text.

Maximum published figure space is 4.5" by 7". When submitting original figures, be sure to allow for reduction in size by making all symbols and letters sufficiently large.

Photographs and halftone images will be considered for publication if they directly illustrate the text.

Tables should be:
1) provided separate from the main body of the text;
2) numbered sequentially and referred to by Arabic number in the text, e.g., Table 1.

References:
1) References should relate directly to the text.
2) References should be keyed into the text with the author's last name and the year of publication, e.g., (Smith 1974; Jones 1974) or Smith (1974) and Jones (1974).
3) In the case of three or more joint authors, the text reference should be written as follows: (Smith *et al.* 1976).
4) All references must be listed at the end of the text in alphabetical order by the author's last name and the year of publication, according to the following format:
   Brown, J., and Green, E. B. 1974, *Astrophys. J.*, **200**, 765.
   Thomas, K. 1982, *Phys. Report*, **33**, 96.
5) Abbreviations used in references should be based on recent issues of the Journal or the listing provided at the beginning of *Astronomy and Astrophysics Abstracts* (Springer-Verlag).

Miscellaneous:
1) Equations should be written on a separate line and given a sequential Arabic number in parentheses near the right-hand margin. Equations should be referred to in the text as, e.g., equation (1).
2) Magnitude will be assumed to be visual unless otherwise specified.
3) Manuscripts may be submitted to referees for review without obligation of publication.

Journal of the American Association of Variable Star Observers
Volume 40, Number 2, 2012

ε Aurigae Special Edition

Table of Contents continued on following pages

***JAAVSO* Volume 40, Number 2—other papers received**

Table of Contents continued on next page

Highlighting ε Aurigae and Citizen Sky

John R. Percy
Department of Astronomy and Astrophysics, University of Toronto, Toronto. ON M5S 3H4, Canada; john.percy@utoronto.ca

Welcome to this special issue of the *Journal of the American Association of Variable Star Observers*, featuring papers on ε Aurigae and the Citizen Sky project (www.citizensky.org). As Price *et al.* explain in the opening paper, Citizen Sky grew out of International Year of Astronomy 2009, brilliantly piggybacking on the international campaign to observe the 2009–2011 eclipse of a bright but mysterious star. It incorporated the "citizen astronomy" philosophy on which the AAVSO is founded—skilled volunteers participating in and advancing astronomical research. It was a complex multidisciplinary project which required careful organization, facilitated by a generous grant from the National Science Foundation. The papers in this issue represent the culmination of the astronomical research aspects of the project but, as Price *et al.* explain, there were many other positive outcomes of the project which, we hope, will continue to bear fruit in the future. In particular, it provides an excellent model for how to organize and manage a complex project, and evaluate the results—something which is rarely done.

I've been actively involved in astronomical research for exactly half a century, so I have experienced three eclipses of ε Aurigae (if I include the 1955–1957 one which I read about as a graduate student). I was educated in an astronomy department (at the University of Toronto) which had special expertise in variable and binary stars—of which ε Aurigae is a prominent example. I have a specific interest in the intrinsic variability of the supergiant component of the system so, unlike many observers, I don't have to wait for the eclipses every twenty-seven years. What fascinates me about the papers in this issue, and in Citizen Sky in general, is how they illustrate so many diverse and intriguing facets of variable star astronomy.

First and foremost: ε Aurigae is a genuine astronomical mystery. It consists of a pulsating blue supergiant and a secondary component, in a 9,896-day (27.09-year) orbit. The secondary component is surrounded by a donut-shaped disk of gas and dust, which eclipses the primary component for almost exactly two years each orbit. It is still not clear whether the primary is a normal massive supergiant, in which case the secondary is most likely a pair of stars in close orbit (the "high-mass model"), or whether the primary is a low-mass supergiant, and the secondary is a single star (the "low-mass model"). We hope that the papers in this special issue will help to resolve this mystery. For an excellent overview of ε Aurigae prior to the 2009–2011 eclipse, see Templeton (2008).

This is frontier astronomy. Disks of gas and dust are widely studied, because they are ubiquitous in the universe. They are found around forming stars, in

cataclysmic binary systems, and around supermassive black holes at the nuclei of galaxies. Binary and multiple star evolution is poorly understood, even though binary and multiple stars are the norm, not the exception. It is a topic which is relevant to some of the most exciting topics in astrophysics today. The origin of Type Ia supernovae, which are the most important "measuring sticks" in modern cosmology, is one example.

ε Aurigae has an apparent V magnitude of about 3.0—not much fainter than the stars in the Big Dipper—so it is visible even in cities such as mine. Beginning skywatchers tend to think that all stars are the same so, at star parties, I like to tell them about the particular characteristics of individual bright stars, especially bizarre stars such as ε Aurigae. Beginning skywatchers can then become beginning observers; ε Aurigae is easy to measure with the unaided eye (though binoculars help). Indeed, this was the whole point of Citizen Sky; it brings astronomy and astronomical research to anyone, of any age, anywhere.

As others have pointed out, each eclipse of ε Aurigae brings a new generation of astronomers, and a new generation of technology. The 1982–1984 eclipse coincided with the blossoming of amateur photoelectric photometry (PEP). The 2009–2011 eclipse was observed with CCD and DSLR cameras, as well as PEP and visual techniques.

It was also observed with spectroscopy, a technique which is increasingly available to amateurs, and with polarimetry—a frontier technique for suitably-equipped advanced amateurs. Very few professional observatories are carrying out long-term spectroscopic and polarimetric observations, so this is an area in which amateurs could take up the slack in the future. This eclipse was also observed with an optical interferometer—Georgia State University's CHARA array—so, for the first time, we can "see" this mysterious system.

Finally, this eclipse campaign benefitted from modern information and communication technology, including email, the Internet, and social media. These made the transfer, display, and storage of information efficient and effective. They also helped to connect the international network of amateur and professional observers as never before.

You will notice that the authors of the papers in this issue come from many countries. The observations which amateurs and professionals have contributed during this eclipse campaign come from even more countries, so every contributor is part of an international community of variable star observers.

Furthermore, the archival data on ε Aurigae stretch back for over 160 years. The data in the AAVSO International Database cover the last seven eclipses (1847–1849, 1874–1876, 1901–1903, 1928–1930, 1955–1957, 1982–1984, and 2009–2011), including observations by the eminent Friedrich Argelander of the first of these. The variability of the star was first suspected by Johann Fritch in 1821, during the 1820–1822 eclipse. The 1847–1849 eclipse was observed systematically by Argelander and others. Hans Ludendorff (1904) suggested that the star was an eclipsing variable. By 1937, it had engaged the minds of

some of the foremost astronomers of the time: Gerard Kuiper, Otto Struve, and Bengt Strömgren (1937) stated that "the photometric and the spectroscopic data on ε Aur seem to lead to contradictions unparalleled in the study of other eclipsing systems". By the 1955–1957 eclipse, the situation was even more critical, as stellar astrophysics had matured greatly. Various models were proposed, including the possibility (since ruled out) that the system contained a black hole. Today's observers are thus connected, across time, with yesterday's observers and interpreters. The AAVSO centennial, the centennial history (Williams and Saladyga 2011), and the historical papers in the centennial issue of *JAAVSO* (volume 40, number 1) were timely vehicles for helping to make these historical connections.

Citizen Sky, and this special issue, would not have been possible without the support of many organizations and people: the National Science Foundation for grant support (DRL-0840188); the AAVSO and its staff who provided in-kind support; the Citizen Sky team: Aaron Price, Rebecca Turner, Robert E. Stencel, Brian Kloppenborg, and Arne A. Henden; partner organizations and individuals who contributed to parts of the project such as the workshops and tutorials; the authors of the papers in this issue; and all the observers and other volunteers who contributed to the diverse scientific and educational aspects of the project. Special thanks, as always, to the staff of this *Journal*: Associate Editor Elizabeth Waagen, Assistant Editor Matthew Templeton, and Production Editor Michael Saladyga. We hope that you enjoy this issue!

References

Kuiper, G., Struve, O., and Strömgren, B. 1937, *Astrophys. J.*, **86**, 570.

Ludendorff, H. 1904, *Astron. Nachr.*, **164**, 81.

Templeton, M. 2008, http://www.aavso.org/vsots epsaur

Williams, T. R., and Saladyga, M. 2011, *Advancing Variable Star Astronomy: The Centennial History of the American Association of Variable Star Observers*, Cambridge Univ. Press, Cambridge.

ε Aurigae Papers

The Origins and Future of the Citizen Sky Project

Aaron Price
Rebecca Turner
AAVSO Headquarters, 49 Bay State Road, Cambridge, MA 02138; address email correspondence to R. Turner, aavso@aavso.org

Robert E. Stencel
Brian K. Kloppenborg
University of Denver, Department of Physics and Astronomy, 2112 E. Wesley Avenue, Denver, CO 80208; rstencel@du.edu; bkloppen@du.edu

Arne A. Henden
AAVSO Headquarters, 49 Bay State Road, Cambridge, MA 02138; arne@aavso.org

Received June 12, 2012

Citizen Sky arose as a product of the 2009 International Year of Astronomy (IYA) project. Aaron Price was appointed to the U.S. IYA Program Committee when it was first constituted in 2006. After about a year of planning, the committee established a Working Group for Research Experiences for Students, Teachers, and Citizen Scientists with Aaron as the chair. The goal was to use the IYA initiative to promote citizen science projects to the general public. The group met for the first time at the Astronomical Society of the Pacific meeting in Chicago—2007. At the meeting they decided to focus their efforts around one project instead of promoting a slate of projects. Many specific ideas were discussed during a morning meeting, but nothing caught the excitement of the entire group.

In the afternoon, Aaron had a hallway discussion with Rick Fienberg, then editor-in-chief of *Sky & Telescope* magazine. Rick mentioned the upcoming ε Aurigae eclipse as a possible topic. He had previously co-presented a paper on the topic with Robert Stencel ("Dr. Bob") at the 2006 meeting of the International Astronomical Union. It seemed like an ideal project. And as the working group researched it more, it became more and more enticing. ε Aur is bright enough to be seen from the city, its eclipse has an amplitude that can be detected with the naked eye, it happens very rarely, it is difficult for professionals to monitor (due to limited large telescope time) and, above all, it was still an enigma—even after over a century of research and speculation.

U.S. IYA funding was a constant issue. The Program Committee only had enough funds to support a small staff and a few projects. The Working Group knew that any project they came up with would be targeted at a narrow audience and so would not receive the same level of support from the Program Committee that a more generalized topic—such as the Galileoscope—received. So the Working Group came up with two plans. One was aimed at what they would

do with zero funding—what each member of the group could contribute gratis and/or can do as part of their regular job. For the AAVSO, this meant issuing an *Alert Notice* on the topic, making charts, and running a regular campaign, but not much more. They also came up with a program to implement if they could raise substantial levels of support. After these two plans were in place, they looked for funding.

The National Science Foundation (NSF) seemed like a natural fit. They fund citizen science, have a nice history with the AAVSO, and the working group had some experience writing proposals for them. However, strong NSF proposals are not easy to assemble. It took almost six months to write the Citizen Sky proposal. Aaron wrote a draft, circulated it amongst the Working Group, and then they held conference calls to discuss revisions. The process went very smoothly, but took a lot of time.

AAVSO Director Arne Henden was chosen as the project's principal investigator (PI) because Aaron did not yet have a Ph.D. (he was in graduate school at the time). All of the co-PIs contributed to the proposal. In addition to Aaron, they were Lucy Fortson, Jordan Raddick, and Bob Stencel. Ryan Wyatt also contributed to the proposal and was a member of the advisory board along with Chris DuPree, Suzanne Jacoby, Hee-Sun Lee, and David Anderson. The proposal itself was originally called STARS—Science Through the Astronomical Research of Stars. It was after funding that it was changed to Citizen Sky, a name first proposed by Rebecca Turner.

Robert Stencel served as scientific advisor from the very beginning. The original idea to involve web cams and DSLR cameras began with him. He provided much needed scientific advice and also a welcome sense of humor when things got tight and deadlines loomed. He also recruited a graduate student of his, Brian Kloppenborg, into the project.

By the time we submitted the proposal to the NSF's Informal Science Education (ISE) program, which funds their citizen science projects, the budget had increased to about $796,000 for a three-year project. It was an interdisciplinary project with funding for modeling software, workshops, a high-end planetarium show, journal publication, Science Olympiad materials, and much more. The scientific goal of the project was to collect data to help researchers uncover what is causing the ε Aur eclipse. The educational goal was to involve the public in all aspects of a scientific project. Instead of focusing solely on data collection, the project aimed to train participants to analyze data, pose their own research questions, and write up results for a peer-reviewed journal. This had not been done before in a large scale citizen science project, and the AAVSO was in a unique position to do so thanks to our history of having an engaged membership. The goal with Citizen Sky was to put it all together in one package and make it accessible to novice amateur astronomers with the belief that participants will get a better understanding of the scientific method if they are more engaged with it at every step of the way.

The proposal was submitted in June 2008. In November 2008 we received the word that it had been favorably reviewed by the NSF. Over the next few months we answered questions and responded to suggestions from the NSF to strengthen the project. In mid-April 2009 we finally received official notification that the project would be fully funded. However, we were new to the NSF so there were substantial administrative tasks to complete before funding could begin. This additional delay caused a problem because, as we all know, the sky waits for no one. The eclipse was predicted to begin in the latter half of the year and we needed pre-eclipse observations. In the original proposal we planned to have almost a year to build the project, materials, and so on, before the eclipse began. Now we had to do a year's work in a few months.

Rebecca Turner was assigned the position of Project Manager, meaning she was responsible for overall implementation of the project. Dr. Bob was the scientific advisor. Brian Kloppenborg was hired as a staff member to assist Rebecca. The first author was funded to conduct an evaluation of the project, which eventually morphed into his dissertation at Tufts University. The Morrison Planetarium at the California Academy of Sciences, acting under Ryan Wyatt, was contracted to produce an eight-minute planetarium film for the project. The Adler Planetarium and Astronomy Museum, acting under Mark SubbaRao, was hired to develop an interactive eclipsing binary modeling software. Jordan Raddick at Johns Hopkins was hired to consult on web site development, which was mostly done by Kate Davis, the AAVSO webmaster at the time.

The first year of the project was dedicated to building infrastructure and data collection. The web site was officially launched in June 2009. It consisted of simplified versions of WebObs, the light curve generator, and the Quick Look file, tutorials on observing and reading light curves, online forums, and a blog maintained by the staff and Dr. Bob. The first Citizen Sky workshop was held in September 2009 at the Adler Planetarium in Chicago. The focus of the workshop was on data collection (visual, photoelectric, and spectra) and on the science behind the system.

The second year of the project was dedicated to building teams and training in data analysis. The non-observing aspect of Citizen Sky was designed around the concept of teams of participants working together. It was inspired by the success of the chart and comparison star database teams that were active in the AAVSO in the previous decade. A second workshop was held in August 2010 at the California Academy of Sciences in San Francisco. The focus of that workshop was on data analysis and writing scientific papers.

The third year of the project was dedicated to observing the end of the eclipse and writing papers for the *Journal of the AAVSO* (*JAAVSO)*. This was a less publicly active period as the teams worked on their papers, most of which are published in this edition of *JAAVSO,* about ε Aur, Citizen Sky, and related topics.

So what is happening next with Citizen Sky? One of the lessons we learned in this project is that teams can indeed do great work. Evidence of that is in

this *JAAVSO* issue. However, some teams did not achieve their goals. There are many reasons for this, but in our view there was one overall lesson to learn: project staff cannot appoint leaders of teams; they have to grow organically from among the participants. The most successful teams were mostly the ones that had self-nominated leaders. The teams which had staff-invited leaders were less successful, with a few notable exceptions.

At the end of the third year of the Citizen Sky Project the AAVSO received a supplemental NSF grant to fund a third workshop. This workshop will focus on generating a manual for DSLR Photometry. Applications will be accepted in late 2012 and early 2013. It will take place March 22–24, 2013, at AAVSO Headquarters in Cambridge, Massachusetts. The program will comprise a mix of 1) talks by experienced DSLR photometrists and 2) breakout sessions during which small groups of participants (each with a designated leader) will develop preassigned sections of the manual. These groups will be determined well in advance and will be based on participant interest, experience, and skills. No prior DSLR experience is required, but there will be some pre-workshop reading and preparation required. The workshop will produce an easy to use, introductory manual that will help the AAVSO support observers who are interested in giving DSLR photometry a try.

With the conclusion of the ε Aur eclipse and news of the DSLR workshop, the AAVSO has given Citizen Sky a new mission: to be the new home of the AAVSO's bright variable star activities. Initially, the Citizen Sky area of the AAVSO website will host the AAVSO Binocular Observing Program and the DSLR Photometry Program. Additional bright object programs/projects will be added to the Citizen Sky pages as they develop. Important Citizen Sky materials will be moved from its existing website to the Citizen Sky section of the AAVSO website. The original Citizen Sky website will be frozen in 2013 but will stay online as an archive.

As for staff, they have also built on what they have learned as part of this project. Dr. Brian Kloppenborg, who received his Ph.D. at Univ. of Denver in spring 2012, is now a visiting scientist at the Max Planck Institute for Radio Astronomy in Bonn, Germany, working on interferometry. He continues to involve amateur astronomers in his research. Dr. Aaron Price is now Manager of Research and Evaluation at the Museum of Science and Industry in Chicago, where he is applying the social science research skills he learned through his dissertation on Citizen Sky's impact on the scientific beliefs of its participants. Rebecca Turner has been promoted to Operations Director at the AAVSO, where she is applying many of the project and personnel management skills she learned as Project Manager of the Citizen Sky project. Dr. Arne Henden continues as Director of the AAVSO, and Dr. Robert Stencel continues as a professor at the University of Denver, and is now planning observations for the next eclipse of ε Aur in 2036!

ε Aurigae—an Overview of the 2009–2011 Eclipse Campaign Results

Robert E. Stencel
University of Denver, Department of Physics and Astronomy, 2112 E. Wesley Avenue, Denver, CO 80208; rstencel@du.edu

Received March 19, 2012; revised May 30, 2012; accepted June 19, 2012

Abstract Evidence is provided from the array of observations amassed during the 2009–2011 eclipse, that defines the enigmatic binary ε Aurigae as comprised of an unstable F0-1 Iab star in orbit around a comparable mass upper main sequence star (or stars) enshrouded in a disk resulting from F star mass loss. In this picture, the F star may be undergoing rapid evolutionary changes, and the recent 67-day primary quasi-period may make it suitable for asteroseismic studies. The hidden star(s) may have gained mass from the F star, and the disk itself provides opportunities for study of accretion, dust evolution, and dynamics.

1. Introduction

During the 20th century, the bright star ε Aurigae confounded astronomers because the visible member of this single-lined spectroscopic binary star appeared to be a massive, F-type supergiant star, with an equally-massive but invisible companion (Guinan and deWarf 2002). Unimpeachable evidence for the eclipsing object, a disk in transit, was obtained with interferometric imaging during the 2009–2010 eclipse (Kloppenborg *et al.* 2010), building on the infrared detection of same by Backman *et al.* (1984). Hoard *et al.* (2010), and previous authors, argued that the F star is in a volatile, reduced mass, post-Asymptotic Giant Branch (AGB) evoutionary phase, with the companion being a disk-enshrouded B-type main sequence star—possibly now the more massive object in the system. Resolution of the masses and evolutionary state of stars in this system is a primary motivator for the recent eclipse campaign, results of which are summarized in this paper. This article is part of a group of articles collected in the *Journal of the AAVSO*, intended to document results of an international effort to collect high quality observations of the ε Aur system during its 2009–2011 eclipse. Those reports provide details for each facet, but here we summarize some of the important findings, in relation to findings recognized as a result of the studies of previous eclipses.

2. Results

As discussed by Jeff Hopkins (2012), photometric V-band timings of the latest eclipse are as follows:

First contact:	RJD 55070	2009 August 16
"Second" contact:	RJD 55250	2010 February 22
Mid-eclipse:	RJD 55400	2010 July 22
"Third" contact:	RJD 55620	2011 February 27
Fourth contact:	RJD 55800	2011 August 26

where RJD = JD – 2,400,000 and the uncertainty in timings is at least one to two weeks. The notion of contact times historically refers to tangent crossings between objects that appear circular in projection, but with a ellipsoidal disk shape involved, the normal meanings of second and third contacts are changed. Also, these timings are complicated by persistent ~0.1 magnitude light variations on a quasi-period of 67 days (Kim 2008). Spectroscopic evidence suggests that disk material encroached on the line of sight months prior to photometric first contact (for example, in K I 7699A—see Leadbeater *et al.*, this issue), or even years prior (Hα, see Chadima *et al.* 2011). Spectroscopic fourth contact was recently announced by observer Thierry Garrell, who reported excess blue-shifted Hα and Na D-line absorption disappeared circa RJD 55950 (2012 January 25).

The eclipsing object is a large, 550K flattened structure, based on recent infrared photometry and imaging. Although speculated to be a "swarm of meteors" by Hans Ludendorff early in the 20th century, the first photometric evidence for the eclipsing object was provided by Mitchell (1964) with nine-color photometry, who claimed a 500K excess, with a projected linear size of 50AU! Later, Backman *et al.* (1984) observed ε Aur entering eclipse and confirmed the result, reporting a 500K blackbody, with an apparent size of 8×10^{-16} ster-radians. At the reference distance of 650 pc, this translates to an area of 14 AU squared, or equivalent to a rectangular shape 1 AU tall and 14 AU long.

The eclipsing object is disk shaped as seen in the near-IR. Thanks to remarkable progress in interferometric imaging over the past decade, it was possible in autumn 2009, during ingress, to detect the shadow of the disk crossing the face of the F star (Figure 1), using the MIRC beam combiner at the Center for High Angular Resolution Astronomy (CHARA) Array of telescopes atop Mt. Wilson, California (Kloppenborg *et al.* 2010). More about this below.

The neutral potassium line at 7699Å reappeared and showed velocity shifts that associate it with the disk and its rotation. Originally reported by Lambert and Sawyer (1986), extensive monitoring by Robin Leadbeater (reported in this issue) showed a repeat of the phenomenon, demonstrating disk rotation and showing stepwise changes in the added equivalent width of the line, suggestive of disk substructure (Leadbeater and Stencel 2010). Subsequent study of spectra reveals a number of lines with this behavior (see Leadbeater *et al.* 2012; Schanne *et al.* 2012; Griffin and Stencel 2012).

The only molecule detected in ε Aur, so far, is transient carbon monoxide. This was originally reported by Hinkle and Simon (1987), and shown by Stencel *et al.* (2011) to reappear again after mid-eclipse, using both moderate resolution IRTF+SpeX and high dispersion Gemini North Near-IR Spectrometer (GNIRS) spectra. The data do not clearly confirm the low isotopic $^{12}C/^{13}C$ ratio ~10 (compared to the solar value, 89). The overlap of a P_{fund} series line of hydrogen atop the ^{13}CO bandhead demands post-eclipse observations where the CO contribution is removed, allowing disentanglement of the relative contribution. See Figures 2a and 2b. A less extreme $^{12}C/^{13}C$ ratio reduces the evidence for the F star being a lower mass, post-AGB star.

For the first time, transient He I 10830Å absorption was detected, and it strengthened around mid-eclipse (Stencel *et al.* 2011), using NASA's IRTF+SpeX instrument; see Figure 3. This line arises from a 19.8 eV level and suggests a high temperature central region in the disk. This is consistent with accretion onto a B0-B5 central star (Pequette *et al.* 2011).

Infrared monitoring confirmed the prediction by Takeuti (1986) that the side of the disk facing the F star is heated to 1100K (Hoard *et al.* 2012), in contrast to the 550K side facing away from the F star. Among the implications of this are that the binary separation might be evaluated, independent of the uncertain distance, and this degree of heating is related to the material properties of the dust in the disk.

A series of three in-eclipse observations of the the far-ultraviolet spectrum of ε Aur were obtained with the Cosmic Origins Spectrograph (COS) on Hubble Space Telescope (Howell *et al.* 2011), and it was found that the continuum output is somewhat eclipsed. The far-UV emission lines show evidence for a P Cygni-like outflow (Figure 4). Both facts point to surface activity of the F star, although contributions from the disk central regions cannot be ruled out.

Attempts to observe solid state spectral features (ices, PAHs, or 10-micron silicates) failed to detect any. Instruments involved included SpeX and BASS at NASA's IRTF, plus MIRAC at Mount Hopkins (see Stencel *et al.* 2011). The broadband infrared excess, combined with lack of spectral features, argues that the dust is comprised of large particles (greater than ~1 micron size). Kopal (1954) concluded similarly when studying the similarity of eclipse depth at many optical wavelengths—the eclipse is "gray" due to large particle sizes, much greater than the wavelengths involved. As noted above, eclipse depth departure from grayness is seen at wavelengths longer than several microns and in the ultraviolet, and these may provide useful constraints on particle size and type.

Photometric monitoring shows persistence of ~0.1 magnitude variations with a quasi-period of ~67 days (Kim 2008), both in and out of eclipse (Figure 5, and see Hopkins (2012)). These have been associated with F star oscillations and perhaps wind events (see Griffin and Stencel 2012).

3. System parameters

Among the generally agreed system parameters are the eclipse period, 9890±2 days, and the mass function in this single line spectroscopic binary, f(M) = 2.51±0.12 (Stefanik *et al.* 2010). System inclination seems securely established at very close to 90 degrees, based on interferometric images showing the disk eclipsing the primary star (Kloppenborg 2010). Given these parameters, possible solutions for the mass ratio (q) include the "high mass" case, q~1.1 (sum of masses, M+m~25 $M_{\odot}$, and semi-major axis, a~25AU) and the "low mass" case, q~0.5 (M+m~9 $M_{\odot}$, a~18AU), where M is the F star mass, and m refers to the mass of the secondary object – assumed to be a star inside the disk, and where a is the semi-major axis of the orbit. Astrometric solutions for both extremes have been published (Strand 1959; van de Kamp 1978). Work is underway to include interferometric results as a new constraint on combined astrometric and photometric solutions (Kloppenborg 2012), which favors the higher mass solution.

What constraints do we have on the *mass (M) of the primary star*? Classically, the spectral type of the primary star has been classified as an F0 Ia star (7500K). Yellow supergiant stars have cataloged masses of 12 $M_{\odot}$ and absolute magnitude, M_V=–6.6 (see, for example, Straizys and Kuriliene 1981). The historic q=1 solution for this single lined spectroscopic binary immediately called into question how a high mass companion could remain invisible outside of the eclipses it causes (Struve and Elvey 1930). Using the apparent magnitude, V=3.05 and the reddening, A_V=0.3, the implied distance is 740 pc (about 20% larger than that used by Kloppenborg (2010) based on the first Hipparcos parallax). From this, the implied luminosity is 3.7×10^4 $L_{\odot}$, and the implied radius is 115 $R_{\odot}$—larger than most Cepheids! At 740 pc, the angular diameter would be 1.5 milli-arcsec (hereafter, mas), at least 0.5 mas smaller than recent interferometric determinations (2.27 mas, K-band, Stencel *et al.* 2008). This requires the star to either have unusual limb darkening, or perhaps not be as distant as 740 pc. Formally, a 2.1 mas V-band uniform disk diameter indicates a distance of 650 pc.

An interesting constraint on binary separation can be deduced from recent thermal IR data, which shows that the portion of the disk nearest the F star rises to ~1100K (Stencel *et al.* 2011; Hoard *et al.* 2012). This equilibrium temperature for dust particles, with low albedo (0.3 to zero), implies a separation from the 7500K F0 star of 9 to 12 AU. For a disk radius of 4 to 5AU (see Kloppenborg 2010), the implied binary separation is 13 to 17 AU, which is more consistent with the q=0.5 solution. The sum of masses in this case ranges from 3 to 7 $M_{\odot}$. However, a distance of 1kpc distance, for example, requires a wider separation (25AU) to yield the same disk temperature, in a q=1 binary where the sum of masses would be 25 $M_{\odot}$.

In terms of resolving the ambiguity in distance and masses, two developments deserve mention. Dissertation work by Brian Kloppenborg, at the University of Denver at the time of this writing, combined astrometric, spectroscopic, and interferometric constraints on the orbit absolute dimensions. This resulted in a solution that places the system at 737 ± 67 pc, with a separation of 25 AU and masses of M = 13 and m = 11 $M_{\odot}$. The interferometrically constrained disk diameter of 7.31 ± 0.66 AU refers to the optically thickest portions and hence a minimum disk size, relative to the larger sizes implied by spectroscopic constraints.

What other constraints are possible on the mass (m) of the secondary star? Disk rotation curves may be obtained from the optically thin neutral potassium lines at 7699Å (Lambert and Sawyer 1986; Leadbeater *et al.* 2012), seen only during eclipse phases, and arguably arising from extreme outer portions of the disk. Their measured disk rotation speed is ~35 ± –5 km/sec. Rotation curves from optically thicker metallic lines (for example, Ti II 4028Å) indicate the disk rotation speed is 42 ± –2 km/sec (Saito *et al.* 1987). Then, with a disk radius value, we can determine a Keplerian rotation period at these speeds. Interferometric images were fitted by Kloppenborg (2010) with a 3.8 AU elliptical semi-major axis, assuming a 625 pc distance. Said rotation speeds (35, 42 km/sec) have implied circumferential rotation rates of 3.25 and 2.70 years, respectively, implying a central mass of 5.2 to 7.5 $M_{\odot}$. Saito *et al.* (1987), using eclipse timing arguments, deduced that m < 5.3 $M_{\odot}$, whereas Lambert and Sawyer (1986) deduced m = 3 to 6 $M_{\odot}$ from their neutral potassium line velocity as a measure of disk rotation. These results strongly suggest the secondary star mass, m, is close to 4 to 6 $M_{\odot}$, comparable to that of a main sequence, B-type star. However, with a larger distance (737 pc) and using an optically thin disk radius (10 AU), these orbital speeds are consistent with a larger secondary mass (m = 11 $M_{\odot}$).

Another constraint on the mass of the secondary can be inferred from observed disk dust and gas scale heights. As shown by VEGA+CHARA observations (Mourard *et al.* 2012), the eclipse in Hα is total in comparison to the partial eclipse seen in the near-IR with the Michigan InfraRed beam Combiner (MIRC) at CHARA—that is, the hydrogen gas extends at least a full F star diameter above and below the disk plane. For strictly thermal dispersion of material, the scale height (H) to disk radius (R_D) ratio equals the sound speed-to-orbital velocity ratio, which is:

$$[H/R_D] = [(\gamma kT/\mu)/(Gm/R_D)]^{1/2} \quad (1)$$

(see Lissauer *et al.* 1996), where γ is the ratio of specific heats (5/3 for ideal gases), μ is the atomic mass, and m is the central star mass. Tables and Figures in Lissauer *et al.* illustrate that the observed thickness is several times the scale height. The observed ratio of the minimum VEGA-observed thickness of gas

disk (2.1 milli-arcsec, mas) relative to the estimated optically thick disk radius (8.92 mas – Kloppenborg 2012), is 0.24, suggesting a scale height to disk radius ratio of 0.12 to 0.08. For the Hipparcos reference distance of 650 pc, the implied optically thick disk radius is 5.8 AU. Given the range of disk temperatures, 550 to 1100K, the thermal speed of hydrogen atoms ranges from 2.8 to 3.9 km/sec, and we deduce the quantity $(Gm/R)^{1/2}$ to be less than or equal to 35 km/sec, or implying again that the secondary star mass, m, is less than or equal to 10.7 $M_{\odot}$. For the larger distance estimate, 1 kpc, the implied disk radius becomes 8.9 AU and the disk temperatures result in a maximum mass of 16.5 $M_{\odot}$. In the absence of dynamical stirring, these masses are an upper limit, as the disk's hydrogen atmosphere could be thicker. Higher gas temperatures and/or a thicker disk scale height both point to a lower secondary mass. If the optically thin disk radius is larger than implied by the photometric eclipse duration, the resultant mass could be larger.

Are there any additional distance-independent discriminators? One might be the Eddington limit on luminosity, which is classically computed to be:

$$L_{Edd} / L_{\odot} = 3.8 \times 10^4 \, M / M_{\odot}. \quad (2)$$

For the two solutions offered, m = 3 to 4 and m = 15 to 25 $M_{\odot}$, the respective Eddington luminosities are $1.1 - 1.5 \times 10^5 L_{\odot}$ versus $5 - 9.5 \times 10^5 L_{\odot}$. Both ranges exceed the upper estimates for $L / L_{\odot}$. Other distance-independent means of establishing binary star parameters are needed.

3.1. Nature of the disk

Kloppenborg *et al.* (2010) estimated that the disk-fitted semi-major axis is 6.10 mas, meaning the full major axis is 12.2 mas, or ~5.8 times F star diameter (2.1 mas). Given the reported 0.62 mas E-W motion per month during ingress (plus a N-S component 0.34 mas/month, for a net motion of 0.72 mas/month), and a 2.1 mas uniform disk diameter star, it should take ~2.9 months for a given point in the disk to move across the F star disk, assuming uniform motion, and ~18 months to have the entire disk move past, which is close to the observed first to third contact eclipse duration. The ellipse model devised during ingress was poorly constrained, dictated mainly by the expected length of eclipse. Afterwards, we obtained the complete light curve (Figure 5) and the first to fourth contact length in days is of order RJD 5800–5060 = 740 days, or ~24 months, and larger still in spectroscopic terms, suggesting the disk is larger than originally estimated and/or the relative velocities are varying (slowing, post-periastron).

Evidence exists that the disk is structured and asymmetric. There has been outstanding spectroscopic monitoring of Hα by Mauclaire *et al.* (2012) and of K I 7699Å by Leadbeater *et al.* (2012) and blue spectroscopic features by Griffin and Stencel (2012), reported in this issue and elsewhere, indicating an

extended, asymmetric spectroscopic signature of the disk. The Hα equivalent width changes versus time suggest a compact ring may contribute to late phases of ingress (RJD 55150–55250), while the disk main body is seen during totality (with a possible mid-eclipse decline circa RJD 55450, perhaps due to ionization related to the appearance of He I 10830Å (Stencel *et al.* 2011)). A more diffuse following ring associates with egress, but lasting past nominal fourth contact (RJD 55800) with excess Hα absorption still present in early 2012, a good 150 days past fourth contact. Similarly, the neutral potassium monitoring has been interpreted to show stepwise changes in equivalent width related to internal ring structure (Leadbeater and Stencel 2010). These were labeled as rings A through F. Rings D and E might contribute to the late ingress Hα behavior, while rings D-A associate with egress phenomena. As reported elsewhere, however, the relationship between the dust and gas components is only just being revealed by spectro-interferometry obtained with the VEGA instrument at the CHARA Array (Mourard *et al.* 2012).

Additional suggestions of an ionizing photon induced shock in the ingress side of the disk has been made by Saito *et al.* (1987). Similarly, a matter transfer stream impacting the egress side of the disk had been advanced by Struve and colleagues early on, and something to this effect was seen again in blue region spectra reported by Griffin and Stencel (2012). Finally, the out-of-eclipse photometric variations are consistent with surface phenomena-driven mass loss episodes from the F star that contribute to a stellar wind, asymmetrically shaped toward the center of mass and ionized by UV light scattered away from the source internal to the disk (Figure 6).

3.2. Dust scattering

The composition of the disk is of interest because determining dust size would provide evidence for the age of the object and the degree to which planetessimal formation may have occurred in the disk. Kopal (1954) noted the wavelength-independence of eclipse depths and concluded that large grains must be present with multi-micron sizes, much greater than optical wavelengths. However, observations to date have not detected any typical spectroscopic bands due to solids, such as ice (3 microns), PAHs, or 10-micron silicates (Stencel *et al.* 2011). An estimate for disk mass can be made, based on the far IR/sub-mm fluxes reported by Hoard *et al.* (2012):

$$M(\text{dust}) = F\nu\, \lambda^2\, d^2 / (2\, k\, T_{\text{dust}}\, \kappa_\nu) \qquad (3)$$

where $F\nu$(250 microns) = 57 mJy = 3×10^{-22} W/cm^2/micron. Using 650 pc as the distance, a dust temperature of 550K and a mass absorption coefficient, $\kappa_\nu = 3$ cm^2/gm (Jura *et al.* 2001), we deduce a dust mass of 1.2×10^{31} gm or nearly 6 Jupiter masses. This seems too large if the gas to dust ratio is ~100, because the disk mass would be dynamically significant in the system.

Disk volume (Kloppenborg *et al.* 2010) and deduced densities (Hinkle and Simon 1987) argue for a lower dust mass, roughly an Earth-mass. Dust opacity based on sub-mm disk studies suggests that mass absorption coefficients are not well determined. Further work is needed to better characterize the material in the ε Aurigae disk (see Pearson and Stencel 2012).

Another avenue for exploring the disk content involves polarimetry. Broadband polarimetric studies have been reported by Kemp *et al.* (1986) and by Cole (2012). These show an out of eclipse baseline value in photometric V band of 2.0 percent, presumed to be interstellar, but growing and varying during eclipse to 2.4 percent. The substructure of V-band polarization during eclipse does not simply correlate with photometric changes. Kemp *et al.* (1986) correctly deduced the position angle of the eclipsing disk decades prior to the interferometric imaging of it. Recently, line polarization monitoring has become possible, greatly increasing insight into disk and star phenomena, and greatly complicating the analysis (see Geise *et al.* 2012).

One more line of evidence to be explored involves a difference between eclipse behavior among red wavelength lines like Hα and K I 7699Å, and blue wavelength lines like Fe I 3920Å and others. The former show equivalent width variation due to the eclipse, but remain substantially enhanced around mid-eclipse, while the bluer lines have equivalent width excess that nearly vanishes at mid-eclipse and then returns strongly during late eclipse. This is to say that the line depth changes are less in the blue regions compared to the red regions, suggestive of particle sizes dominated by the greater-than-micron scale.

4. Archives

Table 1 lists observations that this author proposed and conducted, many of which will appear in public data archives maintained by the institutions involved. The AAVSO provides a comprehensive photometry archive. There are a number of spectroscopic data sources that might not be fully reflected in this report, but well worth the mention. In addition to the careful digitization by Elizabeth Griffin of Mt. Wilson and DAO photographic spectra (plus new digital observations), additional modern high dispersion digital spectra were obtained regularly during eclipse by Hideyuki Izumiura at Okayama Observatory, by William Ketzeback and collaborators at Apache Point Observatory (see Barentine *et al.* 2012), by Nadine Manset and collaborators at CFHT (see Geise *et al.* 2012), by John Martin at the University of Illinois, Springfield, Observatory, by Nancy Morrison at the University of Toledo Ritter Observatory, by Ulisse Munari and collaborators at Asiago Observatory, by Klaus Strassmeier and collaborators (Astronomical Institute at Potsdam) STELLA telescope at IAC (see Schanne *et al.* 2012), and several others. Ideally, these data archives can be maintained by their originators and made available to interested researchers. This author would be happy to try to help coordinate analysis efforts.

5. Conclusions

Clarification of the nature of the eclipsing object in ε Aur will stand as one of the major achievements of this eclipse cycle. While the eclipse has brought attention to the study of ε Aur and its mysteries, we now have entered the long inter-eclipse period, prior to the start of the next eclipse circa 2036. Current orbital elements (Stefanik *et al.* 2010) predict key times that should be of interest to observers: the F star reaches maximum blue shift circa autumn 2017 (and it reached maximum redshift during autumn 2006). Eclipse of the disk by the F star is anticipated during 2020 and this should be detectable in the infrared, insofar as the observational capability exists then. There is merit in photometric monitoring of out-of-eclipse behavior, although the characteristic behavior (67-day quasi-period plus overtones and evolution) seems established (for example, Kim (2008) and Kloppenborg (2012)). The AAVSO's photometric data archive (www.aavso.org) provides an excellent resource. Nonetheless, with robotic telescopes and dedicated persons, the slow changes in this system can yet be followed during this newest orbital cycle.

6. Acknowledgements

There are many, many people to thank for help in this overall effort, making coverage of the recent eclipse the most complete in human history. Without Jeff Hopkins' and Lou Boyd's dedication to long term photometry, we would have a much sparser dataset. My thanks to Hal McAlister for accepting my proposals to use the CHARA Array for interferometric study of the eclipse, and to John Monnier for access to the MIRC instrument that made the imaging possible. Many facets of the work presented here were facilitated by Brian Kloppenborg and his amazing computer skills. I am grateful to Aaron Price, Rebecca Turner, and Arne Henden at AAVSO for their efforts with the Citizen Sky observer campaign that enriched the data archives with thousands of new measures, all carefully archived. Additional spectroscopic monitoring was contributed by Robin Leadbeater, Thierry Garrel, Christian Buil, Elizabeth Griffin, and many others. Key collaborators on HST COS and Spitzer/IRAC data acquisition included Steve Howell and Donald Hoard, with excellent advice received from COS team members Stephane Beland, Jim Green, Steven Penton, and others. Collaborators obtaining and reducing Gemini North GNIRS data were Tom Geballe and Rachel Mason. Helpful comments on this paper from an anonymous referee are appreciated. My participation was supported in part by the bequest of William Herschel Womble in support of Astronomy at the University of Denver, for which I am extremely grateful (as the project would not have been possible otherwise), along with an NSF-RAPID grant, AST 10-16678, to the University of Denver, organized by the prescient program director Donald Terndrup, who deserves public thanks for recognizing the singular opportunity afforded by ε Aur.

References

Backman, D. E., Becklin, E. E., Cruikshank, D. P., Joyce, R. R., Simon, T., and Tokunaga, A. 1984, *Astrophys. J.,* **284**, 799.

Barentine, J., *et al.* 2012, *Bull. Amer. Astron. Soc.*, **44**, 433.312.

Chadima, P., *et al.* 2011, *Astron. Astrophys.*, **530A**, 146.

Cole, G. 2012, *J. Amer. Assoc. Var. Star Obs.,* **40**, 787.

Geise, K., Stencel, R., Manset, N., Harrington, D., and Kuhn, J. 2012, *J. Amer. Assoc. Var. Star Obs.,* submitted.

Griffin, R. E. M. G., and Stencel, R. 2012, *J. Amer. Assoc. Var. Star Obs.,* **40**, 714, and *Publ. Astron. Soc. Pacifc*, submitted.

Guinan, E., and Dewarf, L. 2002, in *Exotic Stars as Challenges to Evolution*, eds. C. A. Tout and W. Van Hamme, ASP Conf. Ser., 279, Astron. Soc. Pacific, San Francisco, 121.

Hinkle, K., and Simon, T. 1987, *Astrophys. J.,* **315**, 296.

Hoard, D., Howell, S., and Stencel, R. 2010, *Astrophys. J.,* **714**, 549.

Hoard, D., Ladjal, D., Stencel, R., and Howell, S. 2012, *Astrophys. J., Lett. Ed.*, **748**, L28.

Hopkins, J., 2012, *J. Amer. Assoc. Var. Star Obs.,***40**, 633.

Howell, S., Hoard, D., and Stencel, R. 2011, *Bull. Amer. Astron. Soc.*, **43**, 257.07.

Jura, M., Webb, R. A., and Kahane, C. 2001, *Astrophys. J., Lett. Ed.*, **550**, L71.

Kemp, J. C., Henson, G. D., Kraus, D., Beardsley, I., Carroll, L., Ake, T., Simon, T., and Collins, G. 1986, *Astrophys. J., Lett. Ed.*, **300**, L11.

Kim, H. 2008, *J. Astron. Space Sci.*, **25**, 1.

Kloppenborg, B. 2012, Ph.D. thesis, University of Denver.

Kloppenborg, B., *et al.* 2010, *Nature*, **464**, 870.

Kopal, Z. 1954, *Observatory*, **74**, 14.

Lambert, D., and Sawyer, S. 1986, *Publ. Astron. Soc. Pacific*, **98**, 389.

Leadbeater, R., and Stencel, R. 2010, http://arxiv.org/abs/1003.3617.

Leadbeater, R., *et al.* 2012, *J. Amer. Assoc. Var. Star Obs.,* submitted.

Lissauer, J., Wolk, S., Griffith, C., and Backman, D. 1996, *Astrophys. J.*, **465**, 371.

Mauclaire, B., Buil, C., Garrel, T., Leadbeater, R., and Lopez, A. 2012, *J. Amer. Assoc. Var. Star Obs.,* **40**, 718.

Mitchell, R. 1964, *Astrophys. J.*, **140**, 1607.

Mourard, D., *et al.* 2012, *Astron. Astrophys.*, **544A,** 91.

Pearson, R., and Stencel, R. 2012, *J. Amer. Assoc. Var. Star Obs.,* **40**, 802.

Pequette, N., Stencel, R., and Whitney, B. 2011, *Bull. Amer. Astron. Soc.*, **43**, 225.05.

Saito, M., Kawabata, S., Saijo, K., and Sato, H. 1987, *Publ. Astron. Soc. Japan*, **39**, 135.

Schanne, L., Strassmeier, K., Weber, M., Leadbeater, R., and Stencel, R. 2012, *J. Amer. Assoc. Var. Star Obs.,* submitted.

Stefanik, R., Torres, G., Lovegrove, J., Pera, V., Latham, D., Zajac, J., and Mazeh, T. 2010, *Astron. J.*, **139**, 1254.

Stencel, R. E., Creech-Eakman, M., Hart, A., Hopkins, J. L., Kloppenborg, B. K., and Mais, D. E. 2008, *Astrophys. J., Lett. Ed.*, **689**, L137.
Stencel, R., *et al.* 2011, *Astron. J.*, **142**, 174.
Straizys, V., and Kuriliene, G. 1981, *Astrophys. Space Sci.*, **80**, 353.
Strand, K. 1959, *Astron. J.*, **64**, 346.
Struve, O., and Elvey, C. 1930, *Astrophys. J.*, **71**, 136.
Takeuti, M. 1986, *Astrophys. Space Sci.*, **121**, 127.
van de Kamp, P. 1978, *Astron. J.*, **83**, 975.

Table 1. Selected new observations of ε Aur during eclipse, 2009–2011.

*RJD**	*Calendar Date*	*Telescope*	*Mode*
55084	2009 Sep 10	IRTF/SpeX	1–5-micron med-res spectra
55139	2009 Nov 2–4	CHARA+MIRC	1.6-micron interferometric imaging
55140	2009 Nov 3	IRTF/SpeX	1–5-micron med-res spectra
55169	2009 Dec 2–4	CHARA+MIRC	1.6-micron interferometric imaging
55197	2010 Jan 1	MMTO/MIRAC	10-micron photometry/spectra
55245	2010 Feb 18	CHARA+MIRC	1.6-micron interferometric imaging
55250	2010 Feb 23	IRTF/SpeX	1–5-micron med-res spectra
55428	2010 Aug 19–21	CHARA+MIRC	1.6-micron interferometric imaging
55432	2010 Aug 24	IRTF/SpeX	1–5-micron med-res spectra
55441	2010 Sep 1	HST/COS	far-UV spectra
55462	2010 Sep 22–23	CHARA+MIRC	1.6-micron interferometric imaging
55467	2010 Sep 27	IRTF/SpeX	1–5-micron med-res spectra
55494	2010 Oct 24	MMTO/CLIO	JHKLM photometry
55495	2010 Oct 25–26	CHARA+MIRC	1.6-micron interferometric imaging
55499	2010 Oct 29	IRTF/SpeX	1–5-micron med-res spectra
55500	2010 Oct 29	Spitzer/IRAC	3.6 and 4.6-micron photometry
55513	2010 Nov 12	IRTF/SpeX	1–5-micron med-res spectra
55523	2010 Nov 22	Spitzer/IRAC	3.6 and 4.6-micron photometry
55537	2010 Dec 6	IRTF/SpeX	1–5-micron med-res spectra
55540	2010 Dec 9–10	CHARA+MIRC	1.6-micron interferometric imaging
55540	2010 Dec 9	HST/COS	2nd far-UV spectrum
55553	2010 Dec 22	MMTO/MIRAC	10-micron photometry/spectra
55559	2010 Dec 28/9	GNIRS SV	2.3-micron high-res CO spectra
55565	2011 Jan 04	GeminiN+GNIRS	2.3-micron high-res spectra
55567	2011 Jan 06	IRTF/SpeX	1–5-micron med-res spectra
55582	2011 Jan 19	CHARA+MIRC4T	1.6-micron interferometric imaging
55567	2011 Mar 3/4	IRTF+SpeX	attempt, 1–5-micron med-res spectra
55637	2011 Mar 17	HST+COS	1150–1800Å spectra (3rd epoch)
55637	2011 Mar 17/18	CHARA+CLIMB	3T interferometry
55649	2011 Mar 29	IRTF+SpeX	JTR, 1–5-micron med-res spectra

Table continued on next page

Table 1. Selected new observations of ε Aur during eclipse, 2009–2011, cont.

RJD[1]	*Calendar Date*	*Telescope*[2]	*Mode*
55650	2011 Mar 30	GeminiN+GNIRS	2.3-micron high-res spectra
55651	2011 Apr 1–5	CHARA+CLIMB	3T interferometry
55663	2011 Apr 12	IRAC	3.5 and 4.5-micron photometry
55663	2011 Apr 12	GeminiN+GNIRS	2.3-micron high-res spectra
55663	2011 Apr 12	Spitzer/IRAC	3.6 and 4.6-micron photometry
55678	2011 Apr 25	IRTF+MIRSI	10-micron photometry
55680	2011 Apr 29	Spitzer/IRAC	3.6 and 4.6-micron photometry
55814	2011 Sep 10	HSO–PACS	70, 110, 160-micron photometry
55824	2011 Sep 18	CHARA+MIRC6T	1.6-micron interferometric imaging
55826	2011 Sep 21	HSO–SPIRE	250, 350, 500-micron photometry
55830	2011 Sep 24	CHARA+MIRC6T	1.6-micron interferometric imaging
55830	2011 Sep 24	IRTF+SpeX	1–5-micron med-res spectra
55846	2011 Oct 10	CHARA+MIRC6T	1.6-micron interferometric imaging
55869	2011 Nov 03	CHARA+MIRC6T	1.6-micron interferometric imaging
55871	2011 Nov 05	MMT+MIRAC4	clouded out
55884	2011 Nov 17	Spitzer/IRAC	3.6 and 4.6-micron photometry
55894	2011 Nov 27	IRTF+SpeX	1–5-micron med-res spectra
55899	2011 Dec 02	Spitzer/IRAC	3.6 and 4.6-micron photometry
55913	2011 Dec 16	CHARA+MIRC	clouded out
55915	2011 Dec 18	IRTF+SpeX	1–5-micron med-res spectra

[*]*RJD = JD– 2400000.*

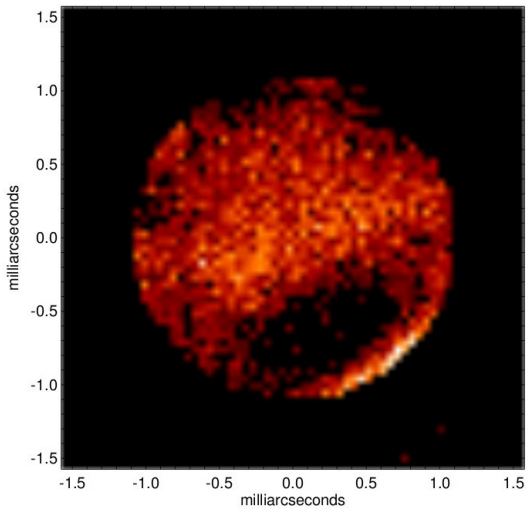

Figure 1. Historic first: the 1.6-micron wavelength image of ε Aur 2009 November 2 as initially processed by John Monnier, based on four telescope beam combination data acquired by MIRC at the CHARA Array, and showing the shadow of the disk crossing the face of ε Aur. The scales are in milli-arcsecond units. *Image courtesy of John Monnier, Univ. Michigan.*

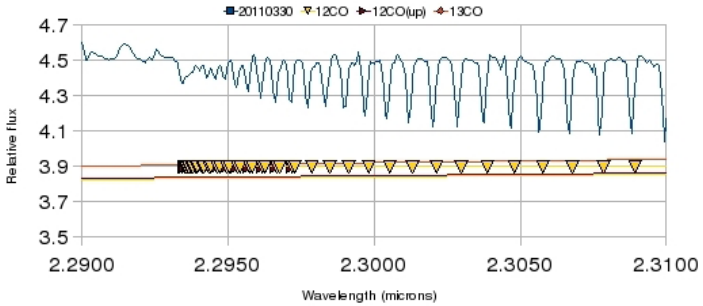

Figure 2a. A portion of the Gemini North GNIRS spectrum of ε Aur spanning the ^{12}CO (2-0) bandhead at 4360 cm-1 region (2.293 microns) showing spectral lines of ^{12}CO(2-0 up) and ^{12}CO(2-0 down), illustrating the GNIRS resolution capable of separating these contributions. The lines show a –25 km/sec systematic blueshift, characteristic of the disk at this epoch.

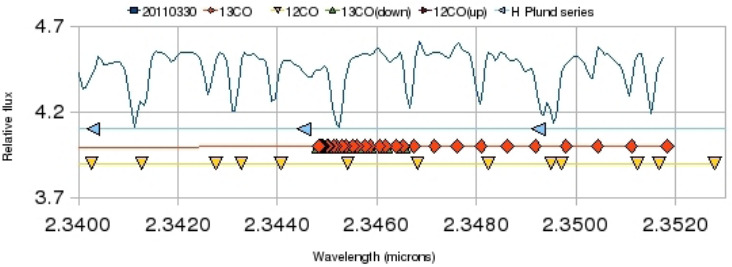

Figure 2b. A portion of the Gemini North GNIRS spectrum of ε Aur spanning the ^{13}CO (2-0) bandhead at 4265 cm-1 region (2.344 microns) showing spectral line positions of ^{13}CO(2-0), ^{12}CO(2-0), ^{12}CO (3-1) lines and hydrogen P_{fund} lines. Redshifted P_{fund} line absorption may account for some, or all, of the previously reported ^{13}CO bandhead near 2.345 microns.

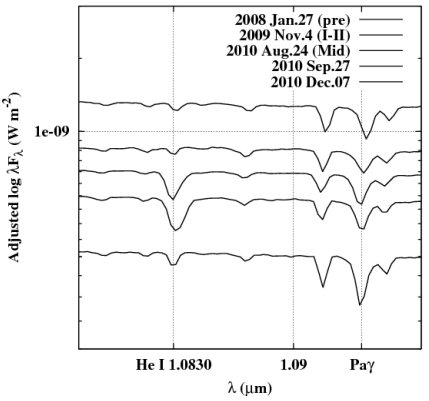

Figure 3. Time series of IRTF+SpeX data showing mid-eclipse appearance of He 10830Å.

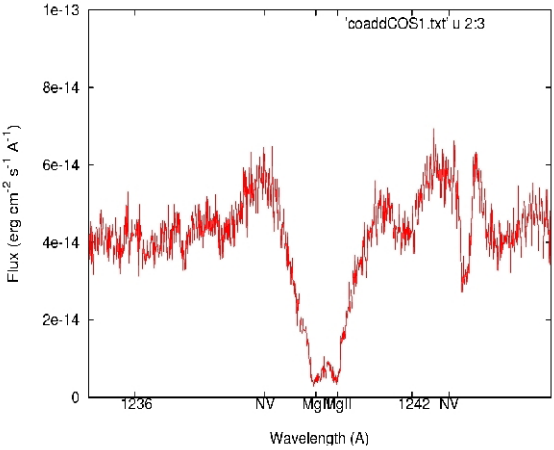

Figure 4a. HST/COS spectra of ε Aur. The strong UV Mg II doublet at 1240Å (1239.925, 1240.395) but lack of N V (1238.821, 1242.804). The line near 1243.3 could be N I.

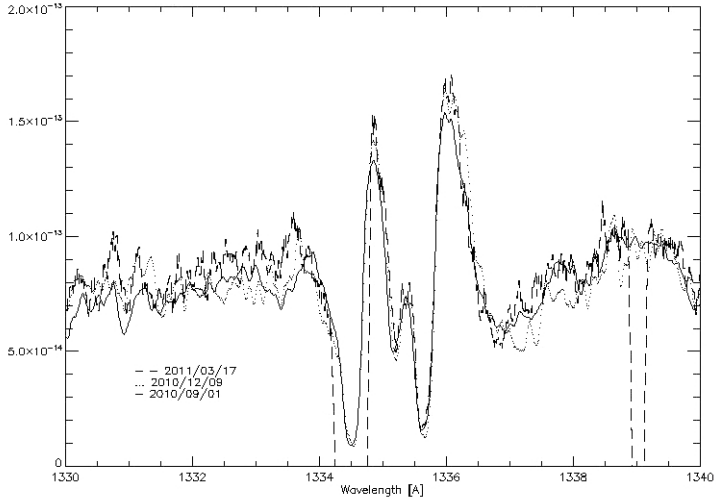

Figure 4b. C II profiles showing clear P Cygni outflow, unaffected by eclipse phase.

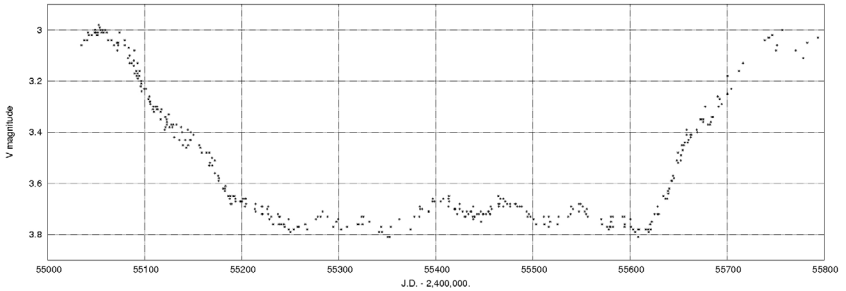

Figure 5. V magnitude record of the 2009–2011 eclipse of ε Aur as recorded by a variety of observers. See Stencel *et al.* (2011) for details.

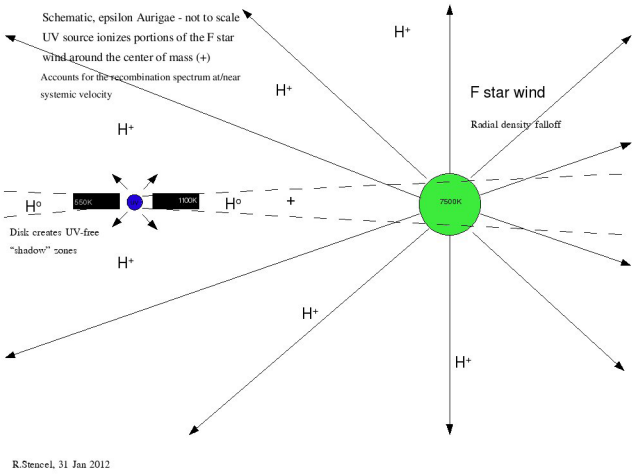

Figure 6. Schematic model of ε Aur that incorporates F star wind focusing and ionization effects due to scattering of UV photons originating inside the dark disk. This model accounts for many of the newly observed spectroscopic and radial velocity details reported here and in related papers, and provides predictions for advanced high-resolution imaging in the future.

The International ε Aurigae Campaign 2009 Photometry Report

Jeffrey L. Hopkins
Hopkins Phoenix Observatory, 7812 West Clayton Drive, Phoenix, AZ 85033; phxjeff@hposoft.com

Received February 23, 2012; revised April 25, 2012, and June 29, 2012; accepted July 3, 2012

Abstract An International Campaign and Web site were started in May of 2006 for the 2009–2011 eclipse of the mysterious star system ε Aurigae. Photometric and spectroscopic observations of the eclipse were coordinated and reported. The eclipse started in the summer of 2009 and lasted until the spring of 2011. During the campaign twenty-four newsletters were published on the web site and made available free as .pdf files to read and download. Twenty-six observers from fourteen different countries submitted photometric data in the UBVRI bands. Over 3,600 high-quality photometric observations were submitted with nearly 2,000 observations in just the V band. This paper discusses the Campaign and report the results.

1. Introduction

Prior to the eclipse, data from previous eclipses and from between eclipses were consolidated in the form of a book (see Hopkins and Stencel 2008). A paper was given at the Society for Astronomical Sciences 2010 Symposium that discussed the ingress of the latest eclipse (Hopkins *et al.* 2010). Most of the photometric data for the 2009–2011 eclipse were obtained in the V band. The largest photometric changes were in the in the shorter wavelengths, however. The U band, which was only observed with the PMT-based systems, provided the largest changes.

Some people thought that during the late spring and early summer the star system went behind the Sun and was not observable. This is not true. The declination of the star system is high above the plane of the solar system and it never goes behind the Sun.The problem is that at lower latitudes it gets very close to the horizon during the dark hours and thus the light passes through very high air mass. Extinction becomes a very significant problem. Those observers at higher latitudes could observe the system at lower air masses, but as one goes farther north the number of dark hours decreases to the point of the midnight Sun. Some of the higher-latitude observers did heroic work during these poor observing times. Even then the data are somewhat confusing and noisy. The mid-eclipse brightening period was at one of these poor times. Some data indicate the brightening and some indicate no brightening. Also, midway

during egress was a poor time and something interesting happened then too. There seems to be a knee in the egress photometric plots. Perhaps more and better data during these times can be obtained during the next eclipse in 2036.

A Campaign was formed during the 1982–1984 eclipse and thirteen newsletters published. The current Campaign's web site has some of these newsletters available on line. For the 2009–2011 eclipse there were twenty-four newsletters published by the Hopkins Phoenix Observatory. All of these are available as .pdfs on the Campaign web site along with a great deal of other pertinent data on ε Aur. In addition to the 2009 Campaign's web site at http://www.hposoft.com/Campaign09.html, a Campaign Yahoo forum was started and can be accessed at: http://tech.groups.yahoo.com/EpsilonAurigae/

2. Observations summary

As of December 26, 2011, we had nearly 3,700 total observations reported during the eclipse, with the visual band having by far the most at nearly 2,000 observations. Twenty-six observers from around the world contributed observational data. Table 1 is a summary of the observers contributions.

3. Data quality

ε Aur is bright enough to be visually seen easily even in most light polluted areas. One can even notice the dimming of the eclipse visually. While the use of visual observations for plotting changes in the brightness of stars works well with some stars, the eclipse of ε Aur was not a good project for visual work. To be of value magnitudes estimates must be of a resolution of 0.05 magnitude or better. This is an order of magnitude less than what even experienced visual observers can produce under the best of conditions. For this reason the International Campaign did not use any visual magnitude estimates.

Photometric data submitted to the campaign had average standard deviations for three or more data points of magnitude 0.01. Many observations approached a standard deviation of magnitude 0.001. The standard deviation is used as an indication of the quality of the data by representing a data spread of three or more data points. The photometric plots do not have error bars because the standard deviations, which would be used for the error bars, are too small in relation to the plot scale. Most submitted data have been transformed and corrected for nightly extinction. The Hopkins Phoenix Observatory (HPO) used a high-precision UBV 1P21-based photon counting system. All HPO data were dead time corrected, transformation coefficients determined for each band, and nightly extinction coefficients determined for each band. Data reduction was done using the Hardie equations. Magnitudes were determined for both λ Aur and ε Aur and then differential calculations done and normalized to the standard values for λ Aur's magnitudes. Nightly sessions consisted of three comparison

star measurements in each band, three adjacent sky measurements in each band, followed by the same routine for the program star. There were three sets of these measurements made with the program star bracketed by the comparison star. The data were all transformed and extinction corrected. Three magnitudes were determined for each band, a standard deviation calculated, and the magnitude average for each band reported to four places.

There has been some concern about the U and B magnitudes from the Hopkins Phoenix Observatory. First, there are no standard U and B magnitudes for ε Aur. The star system varies significantly and randomly out-of-eclipse. The variation is greatest in the U and B bands. If one were to suggest out-of-eclipse magnitudes then the average of several seasons of out-of-eclipse magnitudes could be specified, but a warning would be needed indicating that these are averages. From data taken out-of-eclipse between March 1986 and February 2008, the following are maximum, minimum, and average magnitudes for the UBV bands:

Vavg = 3.04	Vmin = 3.16	Vmax = 2.94
Bavg = 3.61	Bmin = 3.53	Bmax = 3.69
Uavg = 3.73	Umin = 3.60	Umax = 3.92

One of the great things about a campaign like this is that one gets a chance to compare their photometric data taken at approximately the same time against others. Photometric light curves for the campaign were updated and published on the web around once a month. Observers could identify their data and see how well they compared to others. Noisy data are obvious. If the observer was interested, he or she could investigate the differences and improvements in technique and data reduction.

4. Comparison star

There are a vast number of observations of ε Aur covering many decades that use λ Aur as a comparison star. Because during this time λ Aur has been found to be very stable over several decades, no check star is needed. The UBV magnitudes are those used in the previous two eclipses. The longer wavelength magnitudes were obtained from the AAVSO.

The data used for the comparison star are:

Comparison star: λ Aur
Other identification: SAO40233, HR1729, HD34411
Position: R.A. (2000) $05^h\ 19^m\ 08.4^s$, Dec. (2000) +40° 05' 57"
Magnitudes: U = 5.46, B = 5.34, V = 4.71, Ij = 3.88, Ic = 4.00, Rj = 4.19, Rc = 4.30, J = 3.62, H = 3.33

5. Equipment

There were four types of instrumentation used to acquire data for the 2009 Campaign: Digital Single Lens Reflex (DSLR) cameras, CCD cameras, Pin Diode photometers (SSP-3 and SSP-4), and photon counting photometers (PMT-based). The photon counting provided highest quality UBV data followed by the SSP-3 for BV data. Obtaining CCD data was more difficult as the brightness caused problems. CCD provided BVRI data. The last and newest equipment for photometry were the DSLR cameras. The DSLR provided V-band data by using the green channel of the RGB images. With the exception of a couple DSLR observers the data submitted were very noisy. However, DSLR cameras offer an excellent introduction to photometry. Once an observer is confident with doing photometry with a DSLR, an entry level monochrome CCD camera with BVRI photometric filters would be a great way to start doing professional photometry.

6. Results

6.1. Hopkins Phoenix Observatory data

The Hopkins Phoenix Observatory data were taken with a high-precision UBV photon counting system. All data were transformed, dead time corrected, and nightly extinction determined and corrected. Details of the photometric work at the Hopkins Phoenix Observatory is reported in Hopkins *et al.* (2007).

When out-of-eclipse the star system has presented tantalizing data (Figure 1). The light is not constant, but varies at a pseudo-periodic rate in all the photometric bands. The period is not stable, and varies unpredictably between 50 and 70 days. In addition to the period variations the amplitudes vary unpredictably. Period analysis was done using PERANSO period analysis software (Vanmunster 2007), but no period could be determined. Details of this work are reported in Hopkins and Stencel (2007) and Hopkins *et al.* (2008).

While not photometry, in an attempt to shed light on the out-of-eclipse variations high-resolution out-of-eclipse spectroscopy of the star system's Hα region was done at Hopkins Phoenix. The main Hα absorption line is bracketed by emission lines (horns) that go up and down, sometimes together and sometimes completely independently (see Figure 2). They sometimes reach a large peak and at other times disappear completely. This is known as the "Hydrogen Alpha Horn Dance." No connection was found between the out-of eclipse Hα spectroscopic variations and the out-of-eclipse photometric variations. The emission horns did seem to decrease and even go away for a while during the eclipse, however. Details of the spectroscopic observations at Hopkins Phoenix Observatory are reported in Hopkins and Stencel (2009a, 2009b) and Hopkins (2012).

6.2. Campaign data

High data producers for the ε Aur campaign were as follows:

DSLR: Des Loughney, Edinburgh, Scotland—238 V-band observations.
CCD: Gerard Samolyk, Greenfield, Wisconsin—721 BVRcIc observations.
SSP: Paul J. Beckmann, Jim Beckmann Observatory, Mendota Heights, Minnesota—89 BVRjIj observations;
Photon counting: Jeff Hopkins, Hopkins Phoenix Observatory, Phoenix, Arizona—565 UBV observations.

Observation techniques varied among observers. Details of each observer are presented on the 2009 Campaign's web site at http://www.hposoft.com/Campaign09.html.

6.3. Campaign light curves

See Figures 3 through 7. UBVRIJH photometric data from 1982 to 2012 are archived and available in multiple formats at http://www.hposoft.com/Eaur09/Data/UBVRIJHData.html.

7. Analysis

There has been some concern expressed by armchair photometrists about the contact times. The following may help understand the complexity of this system and the methodology used to determine the contact points.

The ε Aur star system is very different from most eclipsing binary systems. For the analysis of the contact points the classical method was used. In addition to the non-classical eclipsing body, complicating the analysis are the pseudo-periodic out-of-eclipse (OOE) variations (see Figure 8).

Figure 9 shows the procedure for determining the current eclipse contact points. The average ingress and egress slopes were used to find the intersection with the average totality and out-of-eclipse magnitudes.

An archive of UBVRIJH photometric data is available to the public at http://www.hposoft.com/EAur09/Photometry.html and http://www.hposoft.com/EAur09/Data/UBVRIJHData.html.

A summary of the data is given in Table 2.

8. Predictions for the 2036–2038 eclipse

While I am unlikely to be around for the next eclipse in 2036 it is still interesting to offer photometric predictions about it. Only the V-band contact points are included. There is still controversy about the second and third contact points. These dates were calculated by adding 9,898 days to the first contact, mid-eclipse, and fourth contact of the 2009–2011 contact times.

The V-band predictions are:

first contact: JD 2464964 ± 12 days, September 27, 2036;
mid-eclipse: JD 2465283 ± 9.5 days, August 12, 2037;
fourth contact: JD 2465601± 7 days, June 26, 2038.

9. Conclusion

Each eclipse of ε Aur sees a new breed of equipment and observers. While more was learned from this latest eclipse, the star system is not giving up its secrets easily. It seems to be taunting us. During some of the most interesting times, the system was extremely difficult to observe. The eclipse may be over for another twenty-seven years, but the star system still presents some interesting challenges. Monitoring and understanding the out-of-eclipse variations will be a major objective. This is followed by the strange Hα horn dance. A continued following of the star system with both photometric and spectroscopic observations is suggested. This may provide some additional insights into these mysteries. One of the nice things about observing out-of-eclipse is the times of high air mass can usually be avoided. Observing can be done during favorable times, such as in the early fall, during winter, and in early spring. As indicated earlier, the most active regions for photometry are the shorter wavelengths. U band is a especially important band in which to make observations. The system also offers excellent spectroscopic learning for the hydrogen Balmer lines as well as the sodium D lines.

10. Acknowledgements

I would like to thank all the observers who contributed data to the Campaign. In particular I want to thank Dr. Robert Stencel ("Dr. Bob") and Brian Kloppenborg for their help, encouragement, and the honor of working with them both with the Campaign and especially with the observing sessions at CHARA on Mount Wilson in California, and the MMT on Mount Hopkins in southern Arizona. Those are treasured experiences and memories.

References

Hopkins, J. L. 2012, *Small Telescope Astronomical Spectroscopy*, Hopkins Phoenix Observatory, Phoenix, AZ.

Hopkins, J. L., Schanne, L., and Stencel R. E. 2008, in *The Society for Astronomical Sciences 27th Annual Symposium on Telescope Science*, Society for Astronomical Sciences, Rancho Cucamonga, CA, 67.

Hopkins, J. L., and Stencel, R. E. 2007, in *The Society for Astronomical Sciences 26th Annual Symposium on Telescope Science*, Society for Astronomical Sciences, Rancho Cucamonga, CA, 37.

Hopkins, J., and Stencel, R. E. 2008, *Epsilon Aurigae: A Mysterious Star System*, Hopkins Phoenix Observatory, Phoenix, AZ.

Hopkins, J. L., and Stencel, R. E. 2009a, ε Aurigae Hydrogen-α Emission Line Variations: The Horn Dance, *J. Amer. Assoc. Variable Star Obs.*, **37**, 213.

Hopkins, J. L., and Stencel R. E. 2009b, in The *Society for Astronomical Sciences 28th Annual Symposium on Telescope Science*, Society for Astronomical Sciences, Rancho Cucamonga, CA, 157.

Hopkins, J. L., *et al.* 2010, in *The Society for Astronomical Sciences 29th Annual Symposium on Telescope Science*, Society for Astronomical Sciences, Rancho Cucamonga, CA, 13.

Vanmunster, T. 2007, PERANSO period analysis software, http://www.peranso.com.

Table 1. 2009 ε Aur campaign photometric observer count.

Observer[1]	*V*	*B*	*U*	*Rc*	*Rj*	*Ic*	*Ij*	*Total*	*Equipment*[2]
CH	143	—	—	—	—	—	—	143	DSLR
CO	3	—	—	—	—	—	—	3	CCD
CQJ	100	100	—	—	—	95	—	295	CCD
DES	242	—	—	—	—	—	—	238	DSLR
EAO	68	—	—	—	—	—	—	68	CCD
EGO	81	—	—	—	—	—	—	81	DSLR
EUO	1	39	9	—	40	—	—	89	PMT
FJM	65	—	—	—	—	—	—	65	SSP-3
GHO	165	—	—	—	—	160	—	325	CCD
GO	22	—	—	20	—	—	—	42	CCD
GS	179	178	—	183	—	181	—	721	CCD
GVO	13	8	—	—	13	—	13	47	SSP-3
HPO	147	209	209	—	—	—	—	565	PMT
JBO	16	41	—	—	16	—	16	89	SSP-3
JESO	34	—	—	—	—	—	—	34	CCD
KO	111	—	—	—	—	—	—	111	CCD
LO	87	—	—	—	—	—	—	87	SSP-3
MSO	3	3	—	—	—	—	—	6	CCD
NKO	38	—	—	—	—	—	—	38	DSLR
NPO	—	—	—	—	18	—	18	36	SSP-3
RES	56	—	—	—	—	—	—	56	DSLR
RLO	29	—	—	—	—	—	—	29	DSLR
SGGO	67	17	—	59	—	—	—	143	CCD
TP	86	—	—	—	—	—	—	86	DSLR
VO	193	—	—	—	—	—	—	193	DSLR
WWC	50	42	—	—	—	—	—	92	DSLR
Total	1999	637	218	262	87	436	47	3686	

Table continued on next page

Table 1. 2009 ε Aur campaign photometric observer count, cont.

[1] Observers (AAVSO observer initials are given in parentheses):
CH (HEN), Colin Henshaw, Tabuk, Saudi Arabia
CO (OSC), Steve Orlando, Custer Observatory, East Northport, NY
CQJ (CQJ), John Centala, Eastern Iowa
DES (LDS), Des Loughney, Edinburgh, Scotland, UK
EAO (SIAK), Iakovos Marios Strikis, Elizabeth Observatory of Athens, Haldrf (Athens), Greece
EGO, Charles Hofferber, East Greenwood Observatory, East Grand Forks, MN
EUO, Serdar Evren, Ege University Observatory, Izmir, Turkey
FJM (MFR), Frank J. Melillo, Holtsville, NY
GHO (MXL), Richard Miles, Golden Hill Observatory, Dorset, England
GO (CLZ), Laurent Corp, Garden Observatory, Rodez, France
GS (SAH), Gerard Samolyk, Greenfield, WI
GVO (MBE), Brian E. McCandless, Grand View Observatory, Elkton, MD
HPO (HPO), Jeff Hopkins, Hopkins Phoenix Observatory, Phoenix, AZ
JBO (BPJ), Paul J. Beckmann, Jim Beckmann Observatory, Mendota Heights, MN
JESO, Dr. Mukund Kurtadikar, Jalna Education Society Observatory, Maharashtra, India
KO (LHG), Hans-Goran Lindberg, Kaerrbo Observatory, Skultuna, Sweden
LO (GSN), Snaevarr Gudmundsson, Lindarberg Observatory, Hafnarfjordur, Iceland
MSO, Arvind Paranjpye, MVS IUCAA Observatory, Ganeshkhind Pune, India
NKO, Nils Karlsen, Nils Karlsen Observatory, Umea, Sweden
NPO, Gary Frey, North Pines Observatory, Mayer, AZ
RES (SVR), Dr. Robert E. Stencel, University of Denver, Denver, CO
RLO (HHU), Hubert Hautecler, Roosbeek Lake Observatory, Boutersem Brabant, Belgium
SGGO (CTIO), Tiziano Colombo, S. Giovanni Gatano al Observatory, Pisa, Italy
TP, Tom Pearson, Virginia Beach, VA
VO (KTHA), Thomas Karlsson, Varberg Observatory, Varberg, Sweden
WWC (CDK), Donald Collins, Warren Wilson College, Ashville, NC

[2] Equipment key: CCD, CCD Camera and telescope; DSLR, Digital Single Lens Reflex Camera, unguided; SSP-3, PIN Diode photometer with telescope; PMT, Photomultiplier Tube, photon counting with telescope.

Table 2. 2009 ε Aur campaign data summary.

Parameter	*Observed RJD = JD–2400000*	*Error*	*Predicted[1] RJD = JD–2400000*
U band			
OOE Mag.	3.725 Mag.		3.73 Mag. (1982–1984)
	Δ0.230 Mag.		
1st Contact	RJD = 55,062	± 21 days	RJD = 55,065
2nd Contact	RJD = 55,193	± 21 days	RJD = 55,237
Ingress	131 days	± 26.5 days	120 days (1982–1984)
Mid-Eclipse	RJD = 55,377	± 14 days	
Totality			
Average Mag.	4.525 Mag.		4.57 Mag. (1982–1984)
Average Depth	0.800 Mag.		
Duration	438 days	± 10 days	455 days (1982–1984)
3rd Contact	RJD = 55,631	± 09 days	

Table continued on following pages

Table 2. 2009 ε Aur campaign data summary, cont.

Parameter	*Observed RJD = JD–2400000*	*Error*	*Predicted*[1] *RJD = JD–2400000*
4th Contact	RJD = 55,693	± 09 days	
Egress	62 days	± 37.5 days	55 days (1982–1984)
Eclipse			
Duration	631 days	± 14 days	630 days (1982–1984)
Average Depth	0.800 Mag.	0.84 Mag.	
Period	9,882 days	± 21 days	9,885 days
B band			
OOE Mag.	3.605 Mag. Δ0.150 Mag.		3.61 Mag. (1982–1984)
1st Contact	RJD = 55,089	± 12 days	RJD = 55,054
2nd Contact	RJD = 55,202	± 12 days	RJD = 55,214
Ingress	113 days	± 12 days	135 days (1982–1984)
Mid-Eclipse	RJD = 55,391	± 19.5 days	
Totality			
Average Mag.	4.325		4.32 Mag. (1982–1984)
Average Depth	0.720 Mag.		
Duration	432 days	± 09.5 days	437 days (1982–1984)
3rd Contact	RJD = 55,634	± 07 days	
4th Contact	RJD = 55,693	± 07 days	
Egress	59 days	± 07 days	71 days (1982–1984)
Eclipse			
Duration	604 days	± 19.5 days	643 days (1982–1984)
Average Depth	0.720 Mag.	0.71 Mag.	
Period	9,919 days	± 12 days	9,884 days
V band[2]			
OOE Mag.	3.035 Mag. Δ0.130 Mag.		3.03 Mag. (1982–1984)
1st Contact	RJD = 55,066	± 12 days	RJD = 55,056
2nd Contact	RJD = 55,199	± 12 days	RJD = 55,213
Ingress	133 days	± 12 days	142 days (1982–1984)
Mid-Eclipse	RJD = 55,384.5	± 09.5 days	
Totality			
Average Mag.	3.710 Mag.		3.73 Mag. (1982–1984)
Average Depth	0.675 Mag.		0.70 Mag. (1982–1984)
Duration	430 days	± 09.5 days	447 days (1982–1984)
3rd Contact	RJD = 55,629	± 07 days	
4th Contact	RJD = 55,703	± 07 days	
Egress	74 days	± 07 days	65 days (1982–1984)
Eclipse			
Duration	637 days	± 09.5 days	654 days (1982–1984)

Table continued on following pages

Table 2. 2009 ε Aur campaign data summary, cont.

Parameter	*Observed RJD = JD–2400000*	*Error*	*Predicted[1] RJD = JD–2400000*
Average Depth	0.675 Mag.	0.70 Mag.	
Period	9,898 days	± 12 days	9,908 days
Rc band			
OOE Mag.	2.745 Mag.		
	Δ0.630 Mag.		
1st Contact	RJD = 55,073	± 67 days	
2nd Contact	RJD = 55,217	± 67 days	
Ingress	144 days	± 67 days	
Mid-Eclipse	RJD = 55,333	± 45.5 days	
Totality			
Average Mag.	3.415 Mag.		
Average Depth	0.670 Mag.		
Duration	406 days	± 17.5 days	
3rd Contact	RJD = 55,623	± 34 days	
4th Contact	RJD = 55,695	± 34 days	
Egress	72 days	± 34 days	
Eclipse			
Duration	622 days	± 45.5 days	
Average Depth	0.670 Mag.		
Period	—		
Ic band			
OOE Mag.	2.255 Mag.		
	Δ0.410 Mag.		
1st Contact	RJD = 55,054	± 42 days	
2nd Contact	RJD = 55,202	± 42 days	
Ingress	148 days	± 42 days	
Mid-Eclipse	RJD = 55,414	± 32.5 days	
Totality			
Average Mag.	2.985 Mag.		
Average Depth	0.720 Mag.		
Duration	424 days	± 32.5 days	
3rd Contact	RJD = 55,626	± 23 days	
4th Contact	RJD = 55,707	± 23 days	
Egress	81 days	± 23 days	
Eclipse			
Duration	625.3 days	± 37.5 days	
Average Depth	0.730 Mag.		
Period	—		

Table continued on next page

Table 2. 2009 ε Aur campaign data summary, cont.

Parameter	*Observed RJD = JD–2400000*	*Error*	*Predicted[1] RJD = JD–2400000*
J band			
OOE Mag.	1.840 Mag.		
	Δ0.160 Mag.		
1st Contact	RJD = 55,060	± 30 days	
2nd Contact	RJD = 55,210	± 30 days	
Ingress	150 days	± 30 days	
Mid-Eclipse	RJD = 55,391	± 18 days	
Totality			
Average Mag.	2.480 Mag.		
Average Depth	0.640 Mag.		
Duration	404 days	± 18 days	
3rd Contact	RJD = 55,614	± 14 days	
4th Contact	RJD = 55,722	± 14 days	
Egress	108 days	± 14 days	
Eclipse			
Duration	662 days	± 18 days	
Average Depth	0.640 Mag.		
Period	—		
H band			
OOE Mag.	1.605 Mag.		
	Δ0.645 Mag.		
1st Contact	RJD = 55,057	± 15 days	
2nd Contact	RJD = 55,202	± 15 days	
Ingress	145 days	± 15 days	
Mid-Eclipse	RJD = 55,395	± 15.5 days	
Totality			
Average Mag.	2.050 Mag.		
Average Depth	0.645 Mag.		
Duration	388 days	± 15.5 days	
3rd Contact	RJD = 55,590	± 14 days	
4th Contact	RJD = 55,733	± 14 days	
Egress	143 days	± 14 days	
Eclipse			
Duration	676 days	± 09.5 days	
Average Depth	0.645 Mag.		
Period	—		

[1] The predicted times were calculated by adding the previous eclipse times to the previous determined periods. [2] There were no predictions for the longer wavelengths in the V band.

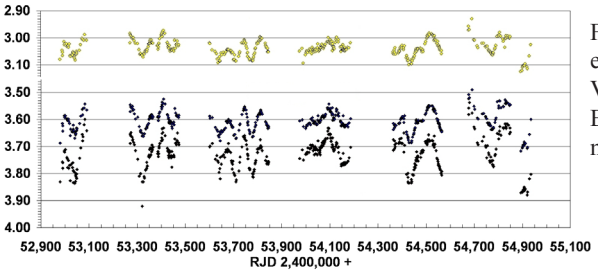

Figure 1. ε Aur out-of-eclipse light curves: top, V magnitude; middle, B magnitude; bottom, U magnitude.

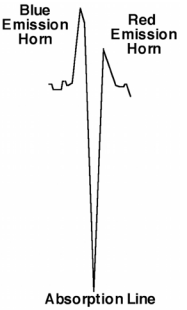

Figure 2. ε Aur Hα spectrum.

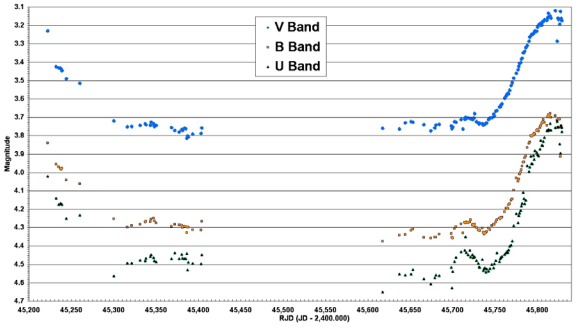

Figure 3. ε Aur light curve, September 1982–May 1984: top, V band; middle, B band; bottom, U band. Hopkins Phoenix Observatory data.

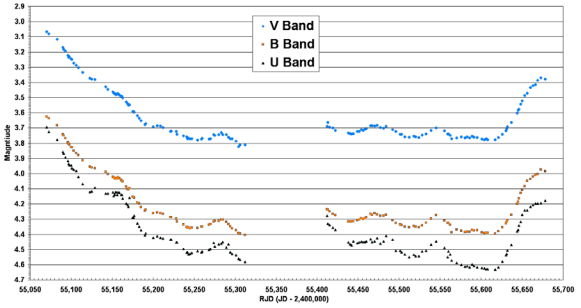

Figure 4. ε Aur light curve, August 2009–April 2009: top, V band; middle, B band; bottom, U band. Hopkins Phoenix Observatory data.

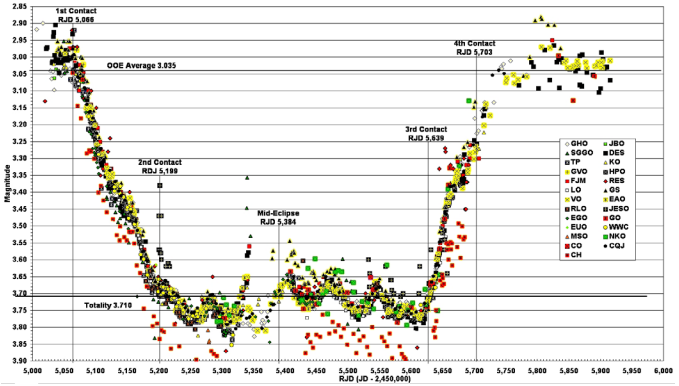

Figure 5. ε Aur campaign V data. See Table 1 for key to observer identification.

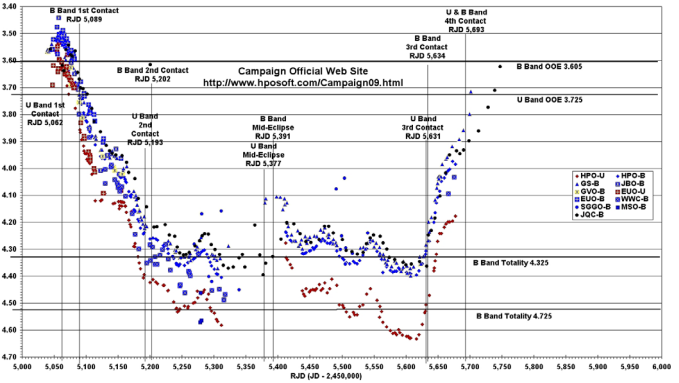

Figure 6. ε Aur campaign U and B data. See Table 1 for key to observer identification.

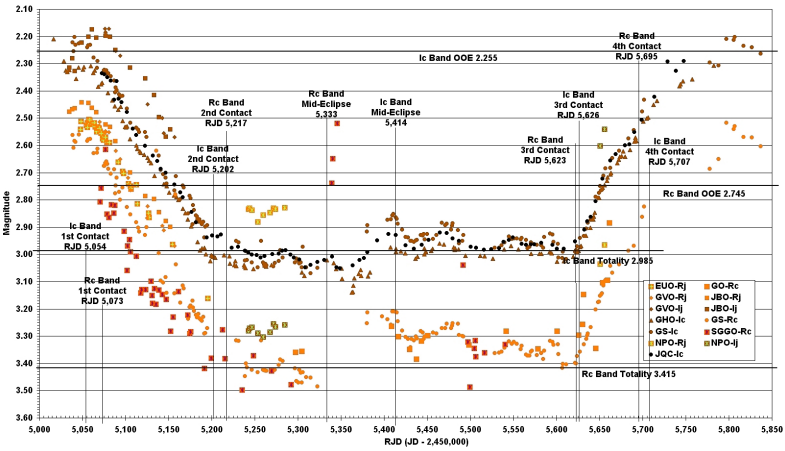

Figure 7. ε Aur campaign R and I data. See Table 1 for key to observer identification.

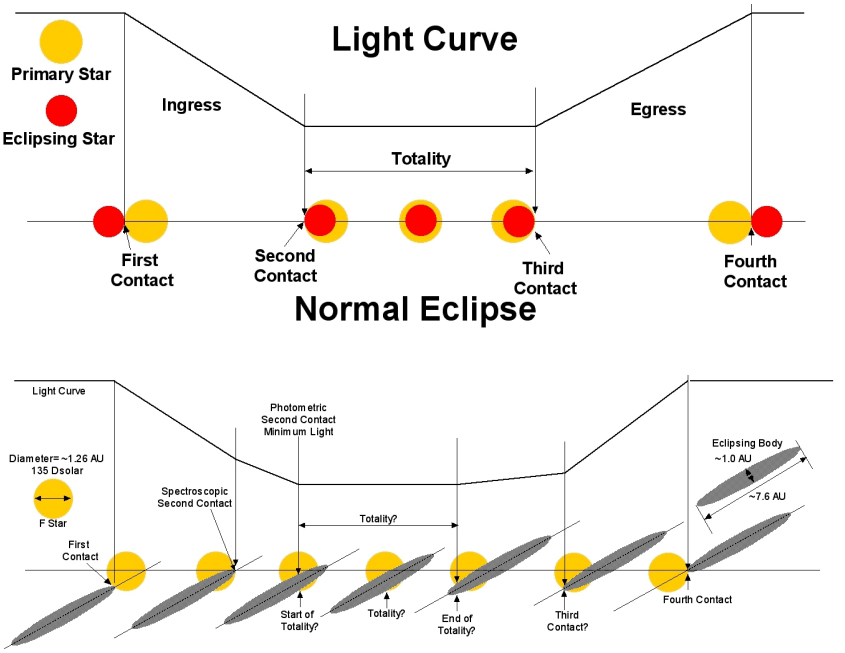

Figure 8. Classical contact points (top) and ε Aur new contact points (bottom).

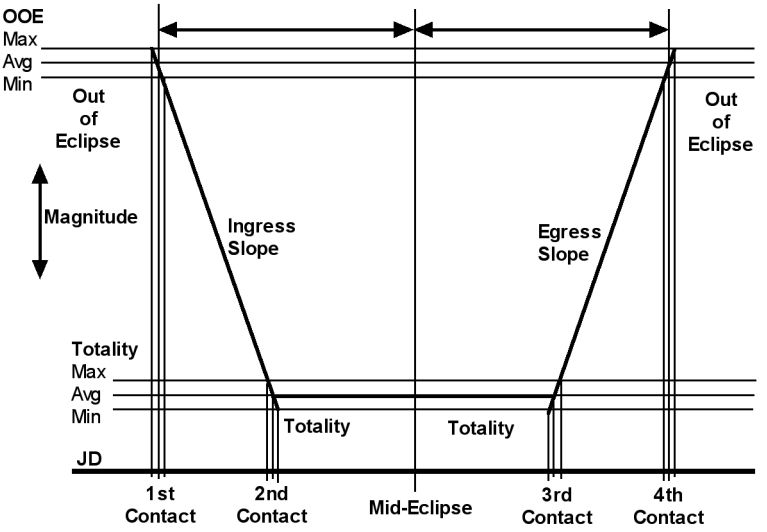

Figure 9. Contact point determination methodology.

An Analysis of the Long-term Photometric Behavior of ε Aurigae

Brian K. Kloppenborg
Department of Physics and Astronomy, University of Denver, 2112 East Wesley Avenue, Denver, CO 80208; bkloppen@du.edu

Jeffrey L. Hopkins
Hopkins Phoenix Observatory, 7812 West Clayton Drive, Phoenix, AZ 85033; phxjeff@hposoft.com

Robert E. Stencel
University of Denver, Department of Physics and Astronomy, 2112 E. Wesley Avenue, Denver, CO 80208; rstencel@du.edu

Received June 1, 2012; revised October 4, 2012; accepted October 4, 2012

Abstract

The lure of a 50% reduction in light has brought a multitude of observers and researchers to ε Aur every twenty-seven years, but few have paid attention to the system outside of eclipse. As early as the late 1800s, it was clear that the system undergoes some form of quasi-periodic variation outside of totality, but few considered this effect in their research until the mid-1950s. In this work we focus exclusively on the out-of-eclipse (OOE) variations seen in this system. We have digitized twenty-seven sources of historic photometry from eighty-one different observers. Two of these sources provide twenty-seven years of inter-eclipse *UBV* photometry which we have analyzed using modern period finding techniques. We have discovered the F-star variations are multi-periodic with at least two periods that evolve in time at $\Delta P \approx -1.5$ day/year. These periods are detected when they manifest as near-sinusoidal variations at 3,200-day intervals. We discuss our work in an evolutionary context by comparing the behavior found in ε Aur with bona-fide supergiant and post-AGB stars of similar spectral type. Based upon our qualitative comparison, we find the photometric behavior of the F-star in the ε Aur system is more indicative of supergiant behavior. Therefore the star is more likely to be a "traditional supergiant" than a post-AGB object. We encourage continued photometric monitoring of this system to test our predictions.

1. Introduction

ε Aurigae is a 27.1-year single line eclipsing spectroscopic binary that has long been wrapped in an enigma. Ever since a dimming of the system was

discovered by Fritsch (1824), and its periodicity established (Ludendorff 1903), astronomers have speculated about the cause of this variation. Based upon radial velocity measurements, ε Aur was classified as a spectroscopic binary (Vogel 1903), which hinted that the dimming might be an eclipse. Later application of Henry Norris Russel's binary star theory (Russell 1912a, 1912b) came to a striking revelation: the companion to the F-type supergiant was nearly equal in mass, yet spectroscopically invisible (Shapley1915).

Over the next decade several theories were advanced to explain this startling conclusion (for example, Ludendorff 1912; Kuiper *et al.* 1937; Schoenberg and Jung 1938; Kopal 1954); however, it was Huang (1965) who proposed that the eclipse was caused by a disk of opaque material that enshrouded the secondary component. Although Huang's analytic model replicated the eclipse light curve, the disk theory remained unproven until Backman (1985) detected an infrared excess that corresponded to a 500 K blackbody source. Recently, the disk theory was vindicated by interferometric observations of the eclipse. These images show the F-star is partially obscured by a disk of opaque material (Kloppenborg *et al.* 2010, 2011) which is responsible for the dimming observed photometrically.

Although most research on this system concentrated on the eclipse itself, a few works have looked at the system outside of eclipse. Since the early 1900s, it has been known that the F-star exhibits 0.1-magnitude variations in *V*-band outside of eclipse. Indeed, the earliest discussion of these out-of-eclipse (OOE) variations were by Shapley (1915, p. 20). He comments on variations in visual photometry with an amplitude of ΔVis = 0.3 magnitude. Because observational errors were not fully characterized, Shapley treated these results with caution. Later, Güssow (1928) spotted a ΔVis = 0.15-magnitude variation outside of eclipse that was corroborated by two photoelectric photometers (Shapley 1928), thereby confirming the presence of the OOE variations. Shapley (1928) concluded that these variations arose from a ~355-day quasi-periodic variation; however, the exact period was poorly constrained by these data.

After the 1983–1985 eclipse, Kemp *et al.* (1986) proposed that a ~100-day period may exist in polarimetry data. Later, Henson (1989) showed there was little to no wavelength dependence in the variations, implying that the source of polarization is Thompson scattering from free electrons. In his dissertation, Henson found intervals where there were variations in Stokes Q, but little to nothing in Stokes U. This was interpreted to be caused by the F-star having two major axes for polarization, inclined at an angle of 45 degrees with respect to each other. Like many of the other studies, a visual inspection of Henson's data showed that some long trends may indeed exist, but nothing was strictly periodic. From the post-eclipse polarimetry, Henson concluded that the photometric and polarimetric variations might be caused by non-radial pulsation in low-order $\ell = 1,2$ $m = \pm 1$ modes. This notion is supported by the recent automated classification of ε Aur as an α Cyg variable (Dubath *et al.* 2011a).

After the 1985 eclipse, many authors sought to determine periods of the OOE variation. Using data from the first five years after the eclipse, Nha *et al.* (1993) found occasional stable variational patterns would set in (in particular around JD 2447085–2447163) with $\Delta U = 0.27$, $\Delta B = 0.17$, and $\Delta V = 0.08$, and a characteristic period of 95.5 days. Later, Hopkins and Stencel (2008) analyzed their inter-eclipse V-band photometric data using the PERANSO software package (Husar 2006). They found two dominant peaks in the Fourier power spectra with 65- and 90-day periods.

Perhaps the most comprehensive period analysis effort was made by Kim (2008). They used the CLEANest Fourier transform algorithm (Foster 1995) and the Weighted Wavelet Z-transform (WWZ; Foster 1996) on nearly 160 years of photometry of ε Aur. Using these two algorithms they identified several periods which led them to conclude ε Aur may be a double or multi-periodic pulsator.

Here we extend the work of our predecessors by analyzing twenty-seven-years worth of inter-eclipse *UBV* photometry. In the following sections we discuss our sources of data, our analysis methods, and the results. We then conclude with a discussion of our results in a stellar evolution context.

2. Data sources

2.1. Historic photometry

ε Aur has a rich history of photometric observations. We conducted a comprehensive literature review and found twenty-seven sources of photometry from eighty-one different observers. We digitized all of these data and intend to submit them to the AAVSO International Database or VizieR (when copyright allows) after the publication of this article. A full discussion of the data sources, assumed uncertainties, and digitization methods is in Kloppenborg (2012); however, we have summarized the important aspects of these data in Table 1.

2.2. Phoenix-10

The Phoenix-10 Automated Photoelectric telescope, designed by Louis Boyd, obtained a total of 1,570 *U*-, 1,581 *B*-, and 1,595 *V*-band observations of ε Aur between 1983 and 2005. The system consisted of a 1P21 photomultiplier mounted on a 10-inch *f*/4 Newtonian telescope. A detailed description of this setup can be found in Boyd *et al.* (1984b). The telescope was originally located in downtown Phoenix, Arizona, until it was moved to Mount Hopkins during the summer of 1986. The system was then moved to Washington Camp in Patagonia, Arizona, in 1996 where it operated until 2005.

The earliest data on ε Aur were obtained in 1983 November and covered most of the 1983–1984 eclipse (Boyd *et al.* 1984a). These data cover intervals JD 2445646–2455699 (Breger 1982, file 131), JD 2445701–2445785 (Breger 1985, file 136), and JD 2445792–2445972 (Breger 1988, file 137) (1983 November 3–1984 September 29). Although the photometer collected data

between 1984 September and 1987 September, the original data were lost due to a hardware failure (Boyd 2010). As far as we have been able to determine, these data were not published in subsequent issues of the *IAU Archives of Unpublished Observations of Variable Stars*. In addition to these data, our publication includes unpublished data from the APT-10 which starts on JD 2447066 (1987 September 27) and ends on 2453457 (2005 March 27).

The standard observing sequence for ε Aur was KSCVCVCVCSK (K=Check, S=Sky, C=Comparison, V=Variable) iterating through the *UBV* filters (see Boyd *et al.* 1984b, Table 1) with 10-second integrations. Information on the target, check, and comparison stars are summarized in Table 2. These differential measurements were corrected for extinction and transformed into the standard *UBV* system. The automated reduction pipeline discarded any observations with an internal standard error of ± 20 milli-magnitudes or greater. Typical external errors are ± 0.011, ± 0.014, ± 0.023 magnitude in *V*, *B*, and *U* filters, respectively, with mean internal errors of ± 0.005, ± 0.005, and ± 0.009 (Strassmeier and Hall 1988). The stability of the system has been satisfactory on decade-long timescales (Hall and Henry 1992; Hall *et al.* 1986).

2.3. Hopkins *UBV*

Co-author Jeffrey Hopkins collected 811 *U*, 815 *B*, and 993 *V* differential magnitudes at the Hopkins Phoenix Observatory (HPO) in Phoenix, Arizona. The data consist of two large blocks: the first began on 1982 September 09 and ended on 1988 December 23, and the second series started on 2003 December 04 and ended on 2011 April 25. At this time the photometric program at HPO ended.

The HPO setup consisted of a 1P21 photomultiplier mounted to an 8-inch Celestron C-8 telescope with standard Johnson *UBV* filters. Observations of ε Aur were conducted in CSVSCSVSCSVSCS format, each composed of three 10-second integrations in one of the three filters. Nightly extinction coefficients were determined and applied. Color correction was determined on a monthly basis. After the 1980 observing season, λ Aurigae was used as the sole comparison star. The assumed magnitudes for λ Aurigae were $V = 4.71$, $(B–V) = 0.63$, and $(U–B) = 0.12$. A subset of these data have been discussed in Chadima *et al.* (2011).

2.4. AAVSO Bright Star Monitor

Starting on 2009 October 16, ε Aur was placed on the American Association of Variable Star Observers' Bright Star Monitor (BSM) observing program. The BSM consisted of a Takahashi FS-60CB with a field flattener; 60-mm *f*/6.2 telescope and a SBIG ST-8XME camera with Johnson/Cousins BVR_cI_c and clear filters. Data were reduced by Arne Henden at AAVSO headquarters to the standard photometric system. All color and extinction corrections were applied before data were submitted to the AAVSO International Database. Ongoing observations from this instrument can be found in the AAVSO database under the observer code "HQA."

2.5. Solar mass ejection imager

For the sake of completeness, we also mention our work on data from the Solar Mass Ejection Imager (SMEI; Simnett *et al.* 2003). Although SMEI's primary mission is to map the large-scale variations in heliospheric electron densities by observing Thompson-scattered sunlight, it also collected precision photometry on ~20,000 stars with $V < 8$. Through each 102-minute orbit, most regions in the sky were covered by a dozen or more frames through one of SMEI's three baffled, unfiltered CCD cameras.

The instrument was designed for 0.1% photometry and, when proper photometric extraction is performed, this precision was realized on stars brighter than fifth magnitude. On average the uncertainty on fainter stars was proportionally worse by the ratio of the star's brightness to fourth magnitude, meaning faint eighth magnitude stars still have better-than-ground photometry precision. The instrument was operational from launch until September 2011 when it was deactivated due to budget constraints. Our work with these data will be discussed in a future publication.

3. Analysis

The sources of photometry listed above were very inhomogeneous; consisting of multiple filters, reduction methods, observatories, instruments, and even reference star magnitudes. We created a script that finds overlaps between two data sets of the same filter, bins the data, and then calculates the coefficients required to scale/offset the data to the same quasi-system using a weighted least-squares technique using the following equation:

$$Ai = a + bB_j + ct_j \quad (1)$$

Here A_i is the i^{th} entry in the reference photometry set, B_j is the j^{th} entry in the comparison photometry data set occurring at time t_j, a is a zero-point offset, b accounts for non-Pogson magnitudes (present in only our earliest visual photometric data), and c corrects for a time-dependent drift of the comparison photometry set. In all of the filtered photometry, only a was required. In the visual data, a and b were required. As our work here is concerned with the variations, rather than absolutely calibrated photometry, we selected Hopkins U, BSM B, and BSM V as references. Offsets (a) between various photometric sources are summarized in Table 3.

After the offsets were determined we passed the data through the Windows implementation of WWZ, WINWWZ. Here we have used data from the range JD 2446000–2455000 in 10-day steps with $f_{low} = 0.004$, $f_{high} = 0.05$, and $\Delta f = 0.0001$. Our WWZ decay constant was 0.0125.

4. Results

In Figure 1 we plot the twenty-seven-years worth of inter-eclipse *UBV* photometry from the APT-10 and HPO observatories. The V data have been plotted unaltered, but *U* have been offset by –1.3 magnitude and *B* by –0.8 magnitude. Internal photometric uncertainties (~ 10 milli-magnitudes) are about the thickness of the lines. Each observing season consists of approximately 200 days of data with bi-nightly sampling followed by 165-day gaps where the star was not visible at night. All of the data were corrected for extinction and transformed to the standard *UBV* photometric system. A visual inspection of the data reveals no single consistent period is present.

Historically, there have been several reported instances of short-term (that is, few-day long) events which we suspect are flares. Albo and Sorgsepp (1974) reported a $\Delta U = 0.2$, $\Delta B = 0.1$, and $\Delta V = 0.06$ brightening that lasted five days around JD 2439968 (1968 April 21). Similarly, Nha and Lee (1983) noted a rapid (few hour) 0.4 magnitude rise in the blue filter and 0.2 magnitude in the yellow filter on JD 2445356 (1983 January 21). We have noticed a two-night flare in our data set starting on JD 2446736 (1986 November 01). This event resulted in a $\Delta U = 0.2$, $\Delta B = 0.1$, and $\Delta V = 0.7$ photometric increase, strangely opposite of historic records. Continued *UBV* photometry appears to be a efficient way of detecting these events.

In Figure 2 we plot the current eclipse light curve in *UBVRIJH* filters from the above sources and the AAVSO database. We note that the eclipse appears to be slightly wavelength-dependent, particularly from mid-eclipse to third contact. This can be seen from the downward slope of the *U*-band data and flat trend in *H*-band. We suggest this is due to additional small particles coming into the line of sight from a sublimation zone on the F-star facing side of the disk.

In Figures 3 through 5 we plot the WWZ results for the *U*, *B*, and *V* filters, respectively. The color in these figures is the WWZ output with higher value indicating stronger presence of that particular period. Because the APT-10 was not operational during the interval JD 2449500–JD 245000, we blocked out the WWZ result in this region.

From inspection of these figures, it is clear that no single period can accurately describe the variations seen in ε Aur. In Table 4 we list peaks whose WWZ coefficient was greater than 100. In the *U*-band data the two most dominant periods are centered at (8977, 102.7) and (12259, 87.9) (henceforth the "upper track''). These peaks were spaced apart by 3,282 days with $\Delta P = -14.8$ days. When the WWZ output was high, the radial velocity (see Stefanik *et al.* 2010 for data) and photometric changes were in phase. The combination of these two effects lead us to believe these events should be regarded as significant.

Operating on the assumption that these peaks provided a glimpse of period evolution in the F-star, we intentionally sought variations following a parallel evolutionary path. Three peaks located at (7166, 90), (10492, 82.7), and

(13744, 68.9) (hereafter the "lower track") followed a similar evolution. Like the "upper track," these peaks were separated by nearly 3,300 days.

Peaks at these locations also appeared in the *B*- and *V*-band data, although with much lower significance. The WWZ value in WINWWZ was determined by a χ^2-like metric that does not consider the uncertainties in the data. Therefore the additional scatter seen in adjacent *B* or *V* photometry, although within uncertainties, results in a lower WWZ value. The higher amplitudes and greater night-to-night consistency causes the *U* data to have larger WWZ values, on average, than the *B* and *V* data.

In the *B*-band WWZ, we see a few peaks in the 80- to 100-day range appearing from time to time, although they are clearly not stable. Likewise, in the *V*-band WWZ there is a single dominant peak of (6100, 90), but otherwise little hint of a stable variational pattern. We do not suggest the WWZ <100 results should be given much consideration; however, in the range JD 24450000–24455000 there were several commensurate periods that appeared to evolve downward at a rate of several days/year.

In Table 5 we used the above observations as a guide and predicted dates when stable pulsational patterns should develop and their periods. We note that the 118-day period around JD 2445695 (near third contact of the 1984 eclipse) did not manifest; however, near the end of the 2009–2011 eclipse a sawtooth-like pattern with a 61- to 76-day period developed (see Figure 2). This is tantalizingly close to the ~73-day period we predicted would develop at this time.

To test our extrapolation, we attempted a WWZ analysis on the visual data. The only set that spanned an entire inter-eclipse interval was collected by Plassman (Güssow1936). Data within the interval 2422000–2428000 (see Figure 6) clearly show the presence of the OOE variations with characteristic periods of 330–370 days. This value was nearly 100 days longer than what we predict for this time interval, implying our extrapolation should not be regarded as highly predictive until further period characterization is conducted.

5. Discussion and conclusion

We have created the first long-term *UBV* photometric record of ε Aur using the data from the APT-10 and HPO observatories. These data show stable variational patterns developed on 3,200-day timescales. In the *U*-band WWZ output, we have identified two parallel tracks of stable variations that evolve at a rate of $\Delta P = -1.6$ day/year and $\Delta P = -1.2$ day/year for the "upper" and "lower" track, respectively. Extrapolating these results, we have identified dates at which we anticipate stable variational patterns will manifest and predicted the periods that they should have. Our extrapolation to JD 2455541 predicts a 73-day period should have developed; it is tantalizingly close to the 61- to 76-day period that was observed during the second-half of the 2009–

2011 eclipse. Our interpretation below is based on this "two-track" notion and likely underestimates the true complexity in this system. In Table 4 we provide all peaks with a WWZ > 100 for the *UBV* photometry in hopes that they will be useful to future researchers.

At the time of this writing, a consistent asteroseismic interpretation for evolved supergiant-class stars does not exist due to the uncertainties underlying the theoretical calculations of mixing theory and radiation pressure (Aerts *et al.* 2010, ch. 2). Therefore, we cannot provide a rigorous, quantitative interpretation of the periods which we have observed. Instead, we interpret the observed periods qualitatively by comparing them with observed supergiant and post-AGB behavior. Regrettably, few comparative studies of F-type supergiant/post-AGB stars exist, especially multi-decade surveys. Therefore our interpretations are inherently biased. We have attempted to discuss these biases throughly and indicate where our study could benefit from future research.

It had been known for some time that stars near the F0Ia spectral and luminosity class show low-level variations with 0.015–0.025 magnitude amplitudes in the V-band (Maeder 1980). An investigation by van Leeuwen *et al.* (1998) of twenty-four super- and hyper-giant stars from the LMC, SMC, and the Milky Way using HIPPARCOS photometry showed that all of these B to late-G stars exhibited photometric changes that were not strictly periodic. Indeed, many of these "periods" would be better described as "quasi-" or "pseudo-periods." Across this region of the HR diagram, stars tended to show variations on 10- to 100-day timescales.

Indeed, in this respect ε Aur could easily be regarded as a recently-evolved supergiant. Several stars in the van Leeuwen *et al.* (1998) sample were a close match for ε Aur: At a slightly higher temperature, HD 269541 (HIP 25448, A8:Ia+, in the LMC) has ΔV_T = 0.1-magnitude variations with several short periods in the 8- to 40-day interval, and two longer periods at 146 and 182 days. The slightly cooler HD 269697 (HIP 25892, F5Ia, in the LMC) had two equally significant periods at 48 and 84 days with photometric variations between 0.01 and 0.05 magnitude in ΔV_T. HD 74180 (HIP 42570, F2Ia, in the Milky Way) was the closest match to ε Aur in the van Leeuwen *et al.* (1998) sample. This star showed quasi-periods at 53, 80, and 160 days with variations of 0.06 magnitude. It is also worth mentioning that an automated photometric classification scheme considered ε Aur to be an α Cyg variable (Dubath *et al.* 2011), a class of luminous supergiants undergoing non-radial pulsation.

Post-AGB stars make up a very heterogeneous class of objects, therefore it is difficult to discuss their properties, let alone discuss any reasons for membership (or lack thereof) for one particular star. We have searched the "Torun catalogue of Galactic post-AGB and related objects" (Szczerba *et al.* 2007) for systems of similar spectral type and identical luminosities to ε Aur. The best-match is AR Pup (F0Iab, HIP 39376) which features multi-periodic (RVb) pulsation with ΔV = 0.5 and timescales of 76.4 ± 4- and 1,250 ± 300-

day periods (Kiss *et al.* 2007). Although the timescales match, the variational pattern (that is, highly predictable, stable) does not match what is seen in ε Aur. Likewise the pattern seen in the cooler V340 Ser (HD 158616, F8) has similar timescales (87.7d and 131d, Arkhipova *et al.* 2011), but is obviously multi-periodic and easily predicted. To complete our view of variations seen around the F0Ia class, long-term photometric studies of the post-AGB stars IRAS 10197-5750 (A2Iab:e, 2MASS J10213385-5805476), IRAS 16206-5956 (A3Iab:e, 2MASS J16250261-6003323), IRAS 06530-0213 (F0Iab, 2MASS J06553181-0217283), HD 101584 (F0Iabpe, HIP 56992), and HD 187885 (F2/F3Iab, IRAS 19500-1709) would be beneficial.

Aggregate statistics of post-AGB stars imply systems of similar spectral types to ε Aur have significantly shorter periods than their supergiant counterparts. For example, Hrivnak *et al.* (2010) studied a series of C-rich post-AGB stars and found a strong correlation between the effective temperature and period. The relationship predicts that higher-temperature post-AGBs will have shorter periods following a linear trend: $\Delta P / \Delta T_{eff} = -0.047$ day K^{1}. Their Figure 18 suggested ε Aur should exhibit variations with a ~40-day timescale, a factor of 1.7 less than what we have observed. Their work on O-rich stars appears to be forthcoming (see Shaw *et al.* 2011). In a sample of five post-AGB stars Arkhipova *et al.* (2011) found a similar trend. Their Figure 8 predicts periods of ~65 days, a factor of 1.25 to 1.5 shorter than what we have observed. A majority of their program stars also were multiperiodic, with ratios of P_1/P_2 ~1.03 to 1.09, whereas ε Aur shows a higher ratio of 1.24 to 1.27.

Until this point we have compared the variational patterns in ε Aur against single stars. As noted above, the stable variation patterns develop at 3,200-day intervals, which is nearly 1/3 of the 27.1-year (9,890-day) orbital period. It would appear the companion is influencing the pulsational properties of the F-star. As the orbit is eccentric (e ~0.227 or e ~0.249–0.256, Stefanik *et al.* 2010, Chadima *et al.* 2010, respectively) one might anticipate tidal flows to be induced in the F-star's tenuously-bound atmosphere (log g ~1, Sadakane *et al.* 2010) during periastron passage; however, dissipation timescales would certainly be less than the nine-year interval seen between stable variational patterns (see Moreno *et al.* 2011, and references therein for a discussion of the theoretical framework). Instead we speculate that gravitational forcing due to orbital motion is exciting natural resonant frequencies in the F-star (this theory is shown to be possible in main sequence objects—see Goldreich and Nicholson 1989; Rocca 1989; Witte and Savonije 1999a, 1999b; Zahn 1975, 1977). This conjecture predicts that the excitations should repeat at the same orbital phases and is therefore testable by continued photometric monitoring. The next dates when such events might happen are JD ~2457000 (2014 December) and JD ~2457000 (2019 December). The development of a consistent asteroseismic theory for supergiants may provide an earlier test of our hypothesis.

Given this information and the photometric behavior discussed above,

we consider it unlikely that the F-star is a post-AGB object and conclude, on a qualitative basis, that the F-star is more likely a traditional supergiant. Implications for the evolutionary state and physical properties of the disk will be discussed in forthcoming publications.

6. Acknowledgements

Participants from the University of Denver are grateful for the bequest of William Hershel Womble in support of astronomy at the University of Denver. They acknowledge support from National Science Foundation through ISE grant DRL-0840188 (Citizen Sky) to the American Association of Variable Star Observers and AST grant 10-16678 to the University of Denver. We acknowledge with thanks the variable star observations from the AAVSO International Database contributed by observers worldwide and used in this research. This research has made use of NASA's Astrophysics Data System Bibliographic Services and the SIMBAD database, operated at CDS, Strasbourg, France.

References

Aerts, C., Christensen-Dalsgaard, J., and Kurtz, D. W. 2010, *Asteroseismology*, Springer, New York.

Albo, H. 1977, *Tartu Astrofüüs. Obs. Publ.*, **45**, 284.

Albo, H., and Sorgsepp, L. 1974, *Tartu Astrofüüs. Obs. Publ.*, **42**, 166.

Arkhipova, V. P., Ikonnikova, N. P., and Komissarova, G. V. 2011, *Astron. Lett.*, **37**, 635.

Backman, D. E. 1985, in *The 1982–1984 Eclipse of Epsilon Aurigae*, NASA, Washington, DC, 23.

Backman, D. E., Becklin, E. E., Cruikshank, D. P., Joyce, R. R., Simon, T., and Tokunaga, A. 1984, *Astrophys J.*, **284**, 799.

Bhatt, H. C., Ashok, N. M., and Chandrasekhar, T. 1984, *Inf. Bull. Var. Stars*, No. 2509, 1.

Boyd, L. J. 2010, personal communication.

Boyd, L. J., Genet, R. M., and Hall, D. S. 1984a, *Inf. Bull Var. Stars*, No. 2562, 1.

Boyd, L. J., Genet, R. M., and Hall, D. S. 1984b, *Int. Amateur-Professional Photoelectric Photom. Commun.*, **15**, 20.

Breger, M. 1982, *Inf. Bull. Var. Stars*, No. 2246, 1.

Breger, M. 1985, *Publ. Astron. Soc. Pacific*, **97**, 85.

Breger, M. 1988, *Publ. Astron. Soc. Pacific*, **100**, 751.

Chadima, P., *et al.* 2010, *Inf. Bull. Var. Stars*, No. 5937, 1.

Chadima, P., *et al.* 2011, *Astron. Astrophys.*, **530A**, 146.

Chochol, D., and Žižovský, J. 1987, *Contrib. Astron. Obs. Skalnaté Pleso*, **16**, 207.

Danjon, A. 1936, *J. Obs.*, **19**, 209.

Dubath, P., *et al.* 2011, *Mon. Not. Roy. Astron. Soc.*, **414**, 2602.

Emberson, R. M., Loevinger, R., and Sterne, T. E. 1938, *Bull. Harvard Coll. Obs.*, No. 908, 11.
Flin, P., Winiarski, M., and Zola, S. 1985, *Inf. Bull. Var. Stars*, No. 2678, 1.
Foster, G. 1995, *Astron. J.*, **109**, 1889.
Foster, G. 1996, *Astron. J.*, **112**, 1709.
Fredrick, L. W. 1960, *Astron. J.*, **65**, 97.
Fritsch, J. M. 1824, *Astron. Jahr.*, 252.
Goldreich, P., and Nicholson, P. D. 1989, *Astrophys. J.*, **342**, 1079.
Güssow, M. 1928, *Astron. Nachr.*, **232**, 207.
Güssow, M. 1936, *Veröff. Univ. Berlin-Babelsberg*, **11**, 1.
Hall, D. S., and Henry, G. W. 1992, in *Automated Telescopes for Photometry and Imaging*, eds. S. J. Adelman, R. J. Dukes, Jr., and C. J. Adelman, ASP Conf. Ser. 28, Astron. Soc. Pacific, San Francisco, 13.
Hall, D. S., Kirkpatrick, J. D., and Seufert, E. R. 1986, *Int. Amateur-Professional Photoelectric Photom. Commun.*, **25**, 32.
Henson, G. D. 1989, Ph.D. Thesis, Oregon Univ.
Hopkins, J., and Stencel, R. E. 2008, *Epsilon Aurigae: A Mysterious Star System*, Hopkins Phoenix Observatory, Phoenix, AZ.
Hrivnak, B. J., Lu, W., Maupin, R. E., and Spitzbart, B. D. 2010, *Astrophys. J.*, **709**, 1042.
Huang, S.-S. 1965, *Astrophys, J.*, **141**, 976.
Huffer, C. M. 1932, *Astrophys. J.*, **76**, 1.
Husar, D. 2006, *BAV Rundbrief*, **55**, 32.
Ivanov, N., and Scharbe, S. B. 1934, *Astron. Nachr.*, **251**, 285.
Japan Amateur Photoelectric Observers Association (JAPOA). 1983, *Inf. Bull. Var. Stars*, No. 2371, 1.
Kemp, J. C., Henson, G. D., Kraus, D. J., Beardsley, I. S., Carroll, L. C., Ake, T. B., Simon, T., and Collins, G. W. 1986, *Astrophys. J., Lett. Ed.*, **300**, 11.
Kim, H. 2008, *J. Astron. Space Sci.*, **25**, 1.
Kiss, L. L., Derekas, A., Szabó, G. M., Bedding, T. R., and Szabados, L. 2007, *Mon. Not. Roy. Astron. Soc.*, **375**, 1338.
Kloppenborg, B. K. 2012, Ph.D. Thesis, Univ. Denver.
Kloppenborg, B. K., *et al.* 2010, *Nature*, **464**, 870.
Kloppenborg, B. K., *et al.* 2011, *Bull. Amer. Astron. Soc.*, **43**, 257.03.
Kopal, Z. 1954, *Observatory*, **74**, 14.
Kopylov, I. M., and Kumaigorodskaya, R. N. 1963, *Proc. Crimean Astrophys. Obs.*, **29**, 251.
Kuiper, G. P., Struve, O., and Strömgren, B. 1937, *Astrophys. J.*, **86**, 570.
Larsson-Leander, G. 1959, *Ark. Astron.*, **2**, 283.
Larsson-Leander, G. 1962, *Ark. Astron.*, **3**, 17.
Low, F. J., and Mitchell, R. I. 1965, *Astrophys. J.*, **141**, 327.
Ludendorff, H. 1903, *Astron. Nachr.*, **164**, 81.
Ludendorff, H. 1912, *Astron. Nachr.*, **192**, 389.

Maeder, A. 1980, *Astron. Astrophys.*, **90**, 311.
Mitchell, R. I. 1964, *Astrophys. J.*, **140**, 1607.
Moreno, E., Koenigsberger, G., and Harrington, D. M. 2011, *Astron. Astrophys.*, **528A**, 48.
Nha, I. S., and Lee, S. J. 1983, I*nf. Bull. Var. Stars*, No. 2405, 1.
Nha, I. S., Lee, Y. S., Jeong, J. H., and Kim, H. I. 1993, in *New Frontiers in Binary Star Research*, eds. K. C. Leung, and I. S. Nha, ASP Conf. Ser. 38, Astron. Soc. Pacific, San Francisco, 291.
Parthasarathy, M., and Frueh, M. L. 1986, *Astrophys. Space Sci.*, **123**, 31.
Rocca, A. 1989, *Astron. Astrophys.*, **213**, 114.
Russell, H. N. 1912a, *Astrophys. J.*, **35**, 315.
Russell, H. N. 1912b, *Astrophys. J.*, **36**, 54.
Sadakane, D., Kambe, E., Sato, B., Honda, S., and Hashimoto, O. 2010, *Publ. Astron. Soc. Japan*, **62**, 1381.
Schoenberg, E., and Jung, B. 1938, *Astron. Nachr.*, **265**, 221.
Shapley, H. 1915, *Contrib. Princeton Univ. Obs.*, **3**, 1.
Shapley, H. 1928, *Bull. Harvard Coll. Obs.*, No. 858, 5.
Shaw, K., Hrivnak, B. J., and Lu, W. 2011, *Bull. Amer. Astron. Soc.*, **43**, 342.10.
Simnett, G. M., *et al.* 2003, *Amer. Geophys. Union*, **2**, 319.
Stefanik, R. P., Torres, G., Lovegrove, J., Pera, V. E., Latham, D. W., Zajac, J., and Mazeh, T. 2010, *Astron. J.*, **139**, 1254.
Strassmeier, K. G., and Hall, D. S. 1988, *Astrophys. J., Suppl. Ser.*, **67**, 439.
Strassmeier, K. G., Serkowitsch, E., and Granzer, T. 1999, *Astron. Astrophys., Suppl. Ser.*, **140**, 29.
Stub, H. 1972, *Astron. Astrophys.*, **20**, 161.
Szczerba, R., Siodmiak, N., Stasinska, G., and Borkowski, J. 2007, *Astron. Astrophys.*, **469**, 799.
Taranova, O. G., and Shenavrin, V. I. 2001, *Astron. Lett.*, **27**, 338.
Thiessen, G. 1957, *Z. Astrophys.*, **43**, 233.
van Leeuwen, F., van Genderen, A. M., and Zegelaar, I. 1998, *Astron. Astrophys., Suppl. Ser.*, **128**, 117.
Vogel, H. C. 1903, *Astrophys. J.*, **17**, 243.
Wendell, O. C. 1913, *Ann. Harvard Coll. Obs.*, **69**, 99.
Widorn, T. 1959, *Mitt. Univ. Sternw. Wien*, **10**, 3.
Witte, M. G., and Savonije, G.J. 1999a, *Astron. Astrophys.*, **341**, 842.
Witte, M. G., and Savonije, G.J. 1999b, *Astron. Astrophys.*, **350**, 129.
Zahn, J.-P. 1975, *Astron. Astrophys.*, **41**, 329.
Zahn, J.-P. 1977, *Astron. Astrophys.*, **57**, 383.

Table 1. All sources of photometry (historic and new).

Source	*Observer*[a]	*JD Start*	*JD End*	*Obs.*	*Type*[b]	*Notes*
Ludendorff (1903)	Argelander	2393950	2404492	56	St	
Ludendorff (1903)	Heis	2394511	2400252	78	St	
Ludendorff (1903)	Oudemaüns	2398490	2399058	16	St	
Ludendorff (1903)	Argelander	2403950	2404492	56	St	
Ludendorff (1903)	Schoenfeld	2404049	2405988	29	St	
Ludendorff (1903)	Schwab	2406614	2416245	65	St	
Ludendorff (1903)	Plassman	2408093	2414961	85	St	
Ludendorff (1903)	Sawyer	2409147	2413645	50	St	
Ludendorff (1903)	Porro	2411360	2411391	3	St	
Ludendorff (1903)	Luitzet	2414288	2416217	55	St	
Ludendorff (1903)	von Prittwitz	2414584	2416080	18	Pm	
Ludendorff (1903)	Plassman	2415259	2416223	29	St	
Ludendorff (1903)	Kopff	2415709	2415825	6	St	
Ludendorff (1903)	Goetz	2416107	2416196	6	St	
Ludendorff (1912)		2395304	2406567	109	St	
Wendell (1913)		2416574	2419706	41	St	
Shapley (1928)		2416574	2419691	26	Pe	
Huffer (1932)		2425267	2426467	98	Pe	
Ivanov and Scharbe (1934)		2417821	2426104	84	St	
Danjon (1936)		2425130	2429238	97	St	
Güssow (1936)	Nijland (1)	2413488	2414280	22	St	
Güssow (1936)	Plassman	2416380	2427785	430	St	

Table continued on following pages

Table 1. All sources of photometry (historic and new), cont.

Source	*Observer*[a]	*JD Start*	*JD End*	*Obs.*	*Type*[b]	*Notes*
Güssow (1936)	Enebo	2416425	2417326	31	St	
Güssow (1936)	Wendell	2416574	2419691	25	Pe	
Güssow (1936)	Schiller	2416848	2416973	12	St	
Güssow (1936)	Lohnert	2417326	2417498	5	St	
Güssow (1936)	Scharbe (1)	2417824	2418653	12	St	
Güssow (1936)	Horning	2418192	2420589	51	St	
Güssow (1936)	Mundler	2418323	2418657	13	St	
Güssow (1936)	Lau	2419275	2429779	16	St	
Güssow (1936)	Menze	2420031	2420958	39	St	
Güssow (1936)	Guthnick	2420147	2420175	10	Pe	
Güssow (1936)	Johasson	2422687	2423374	12	St	
Güssow (1936)	Guthnick and Pavel	2422940	2423361	27	Pe	
Güssow (1936)	Gadomski	2423016	2427060	31	St	
Güssow (1936)	Graff	2424251	2425957	13	Pm	
Güssow (1936)	Kordylewski	2424647	2425953	29	St	
Güssow (1936)	Güssow	2424808	2427762	145	Pm	
Güssow (1936)	Kukarkin	2425100	2426242	34	St	
Güssow (1936)	Beyer	2425126	2426196	44	St	
Güssow (1936)	Danjon	2425139	2426636	34	Pm	
Güssow (1936)	Jacchia	2425177	2426210	41	St	
Güssow (1936)	Pagaczewski	2425185	2426034	13	St	
Güssow (1936)	Scharbe (2)	2425237	2426104	15	St	

Table continued on following pages

Table 1. All sources of photometry (historic and new), cont.

Source	*Observer*[a]	*JD Start*	*JD End*	*Obs.*	*Type*[b]	*Notes*
Güssow (1936)	Stebbins and Huffer	2425267	2426467	98	Pe	
Güssow (1936)	Tschernov	2425296	2426090	25	St	
Güssow (1936)	Mrazek	2425322	2425857	4	Pm	
Güssow (1936)	Nijland (2)	2425322	2426436	40	St	
Güssow (1936)	Dziewulski	2425364	2426096	22	St	
Güssow (1936)	Menze2	2425529	2426065	23	St	
Güssow (1936)	Kopal	2425925	2426465	18	St	
Emberson et al. (1938)		2428903	2428920	7	Broadband-IR	Not used
Thiessen (1957)		2435374	2435942	10	yellow,blue,violet	
Larsson-Leander (1959)		2435428	2436334	121	PV	
Widorn (1959)		2435128	2436295	122	yellow,blue	Not used
Fredrick (1960)		2434761	2435903	143	Pe, 4 color	Not transformed
Larsson-Leander (1962)		2436457	2437023	52	PV	
Kopylov and Kumaigorodskaya (1963)		2435111	2436695	251	PV	
Mitchell (1964)					UBVRIJHKLN	Not used
Low and Mitchell (1965)					UBVRIJHKLN	Not used
Stub (1972)		2438755	2439925	220	Pe, 10 color	
Albo and Sorgsepp (1974)		2439947	2439988	144	UBV	
Albo (1977)		2440460	2440548	42	UBV	
Breger (1982, 1985, 1988)		2445646	2445972	453	UBV	Boyd, IAU
JAPOA (1983)		2445239	2445409	123	UBV	

Table continued on next page

Table 1. All sources of photometry (historic and new), cont.

Source	*Observer*[a]	*JD Start*	*JD End*	*Obs.*	*Type*[b]	*Notes*
Backman et al. (1984)		2444269	2445382	107	JHKL'MNQ	
Bhatt et al. (1984)		2445044	2445798	84	BVRIJHK	
Hopkins UBV (1)		2445222	2447520	1140	UBV	
Flin et al. (1985)		2445065	2445937	330	UBV	
Parthasarathy and Frueh (1986)		2445208	2445426	983	UBV,uvby	
Boyd UBV		2447066	2453457	4746	UBV	Unpublished
Chochol and Žižovský (1987)		2445043	2445664	207	UBV	
Strassmeier et al. (1999)		2450396	2450427	216	by	
Taranova and Shenavrin (2001)		2445032	2451652	243	UBVRJHKLM	Download from CDS
Hopkins UBV (2)		2452979	2455678	1836	UBV	
AAVSO BSM		2455122	present	960	BVRI	

[a] *Identified only if from a compilation source.* [b] *The photometric system used or one of the following: St = Step magnitudes (mechanically assisted visual data), Pm = Photometric, Pe = photoelectric, and PV = photovisual. See original reference for further details.*

Table 2. Star information for Boyd photometric data.

Object	*R. A.* *h m s*	*Dec.* ° ′ ″	*Epoch*	*Role**	*Other Names*
HD 34411	05 19 08	40 05 57	2000	K	HR 1729, SAO 40233
HD 32655	05 06 50	43 10 29	2001	C	HR 1644, SAO 40029
HD 31964	05 01 58	43 49 24	2002	V	HR 1605, SAO 39955
Sky	05 04 24	43 29 57	2003	S	

**Role: K = Check, S = Sky, C = Comparison, V = Variable*

Table 3. Offsets between observers. "ref" indicates this was the reference photometry set for the associated column.

Source	*U*	*B*	*V*
1983 Boyd	6.944964	6.704575	5.955698
1984 Hopkins	–0.022894	–0.056568	–0.075453
1987 Boyd	–0.124972	–0.007964	–0.043503
2011 Hopkins	ref	–0.045311	–0.044434
2011 AAVSO BSM	N/A	ref	ref

Table 4. Peak periods observed in the UBV WWZ transforms roughly grouped by date. Dates have been rounded to the nearest 10. Periods and WWZ output are rounded to integer values. MJD = JD – 2440000.

U			*B*			*V*		
MJD	*Period*	*WWZ*	*MJD*	*Period*	*WWZ*	*MJD*	*Period*	*WWZ*
6180	83	210	6210	90	224	6170	91	478
7170	90	171	7200	76	86	7180	68	44
7840	75	327	7850	78	220	7350	66	43
—	—	—	—	—	—	7620	52	41
—	—	—	—	—	—	7820	83	171
8320	82	112	8400	75	180	8400	85	123
8590	163	65	—	—	—	—	—	—
8980	102	400	—	—	—	—	—	—
9160	99	270	9060	98	171	9160	98	80
—	—	—	9360	85	46	9380	94	66
—	—	—	—	—	—	10150	61	158
10490	83	254	10510	85	114	—	—	—
10930	217	140	10920	212	158	10920	208	139
11220	122	112	11250	123	93	11390	123	92
11400	123	110	11410	123	108	—	—	—

Table continued on next page

Table 4. Peak periods observed in the UBV WWZ transforms roughly grouped by date. Dates have been rounded to the nearest 10. Periods and WWZ output are rounded to integer values. MJD = JD – 2440000, cont.

U			*B*			*V*		
MJD	*Period*	*WWZ*	*MJD*	*Period*	*WWZ*	*MJD*	*Period*	*WWZ*
11690	175	87	11670	172	86	11680	172	70
12260	88	350	12220	89	128	12240	90	81
12550	119	270	12560	121	172	12540	120	147
12960	76	98	12930	75	126	12880	77	108
13250	159	123	13320	149	99	13270	150	62
13740	69	180	13770	69	150	13750	69	71
—	—	—	14260	208	69	14290	204	63
14300	139	117	14540	156	81	14540	156	71

Table 5. Predicted dates of stable pulsation features and their periods based upon extrapolation of trends discussed in section 4.

Upper Track			*Lower Track*		
JD	*Period*	*Observed?*	*JD*	*Period*	*Observed?*
2396465	340		2397831	249	
2399747	325		2401120	239	
2403029	310		2404409	228	
2406311	295		2407698	218	
2409593	280		2410987	207	
2412875	266		2414276	196	
2416157	251		2417565	186	
2419439	236		2420854	175	
2422721	221		2424143	165	
2426003	206		2427432	154	
2429285	192		2430721	144	
2432567	177		2434010	133	
2435849	162		2437299	123	
2439131	147		2440588	112	
2442413	132		2443877	102	
2445695	118		2447166	90.0	Y
2448977	102.7	Y	2450492	82.7	Y
2452259	87.9	Y	2453744	68.9	Y
2455541	73		2457026	66	
2458823	58		2460308	52	
2462105	43		2463590	37	
2465387	29		2466872	22	
2468669	14		2470154	7	

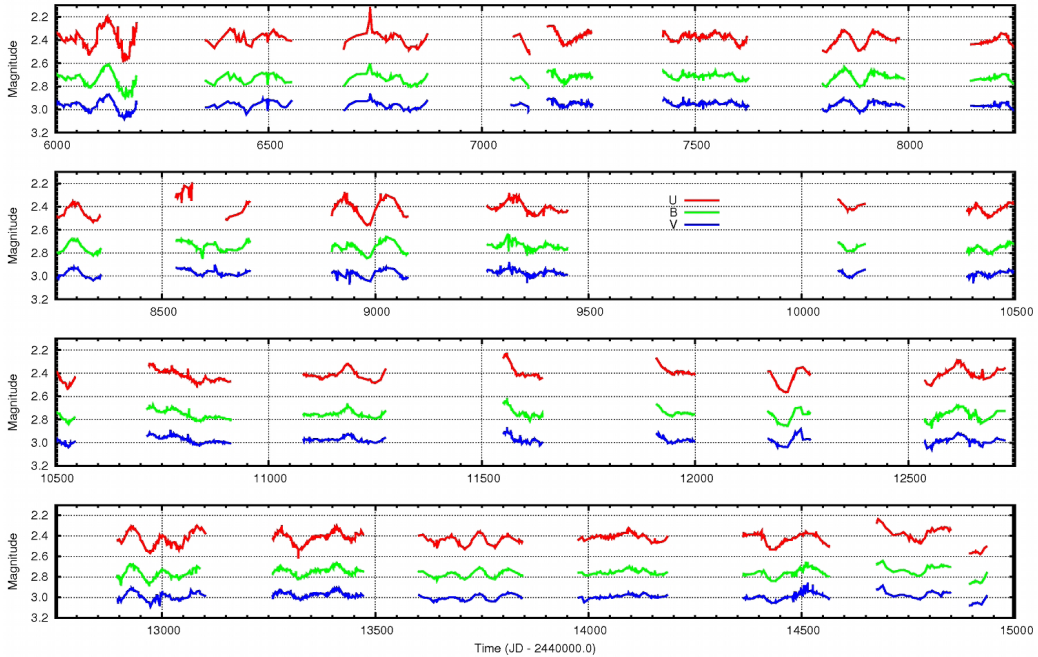

Figure 1. Inter-eclipse *UBV* photometry of ε Aur, JD 2446000–2455000 (1984 October 26–2009 June 17) from the Boyd and Hopkins data sets. For display purposes, we have offset the *U* data by –1.3 magnitude (that is, $U_{plot} = U_{data} + (-1.3)$). Likewise, the *B* data were offset by –0.8 magnitude. The V data are unaltered. Internal uncertainties (~10 mmag) are about the thickness of the lines. The observing windows consist of about 200 days of data followed by 165-day gaps. During the interval 2449500–2450000 the APT-10 photometer was not operational. The out-of-eclipse variations have amplitudes of ~0.1 magnitude in *U* and ~0.05 in *V* with characteristic timescales of 60–100 days. The sudden brightening seen around JD 2446736–2446737 might have been a flare.

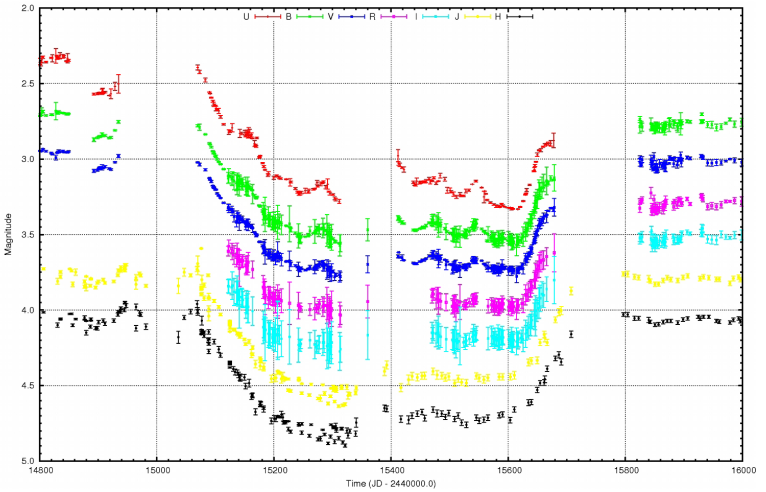

Figure 2. 2009–2011 eclipse of ε Aur in *UBVRIJH* filters, JD 2454800–2456000 (2008 November 29–2012 March 13), as measured by Hopkins (*UBV*), the AAVSO BSM (*BVRI*), and AAVSO observers Brian McCandless and Thomas Rutherford (*JH* data). The *V*-band data are plotted as observed, all other filters have been offset by an arbitrary amount for display purposes. The eclipse may be represented by a linear decrease in brightness of ~0.7 magnitude, followed by a flat minimum and then a sharp rise back to out-of-eclipse brightness. The out-of-eclipse variations are superimposed on this profile and result in 60- to 100-day cycles with characteristic amplitudes of ~0.1 magnitude in *U*, decreasing in amplitude towards longer wavelengths. Notice during the second half of the eclipse the *U*-band light curve slopes downward, whereas the *H*-band has an upward slope. This attests to the fact that the eclipse had wavelength-dependent extinction.

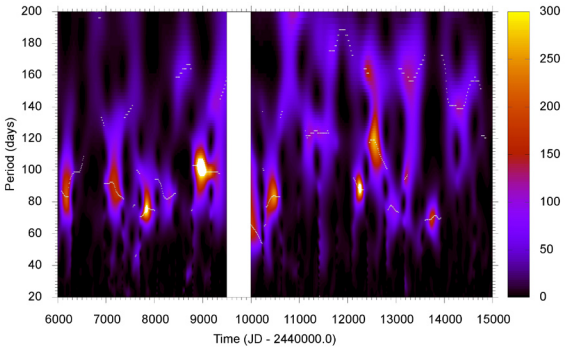

Figure 3. *U*-band WWZ period analysis of ε Aur (c = 1.25E–2). The color indicates power associated with a given period at a particular time, whereas the white dot traces the dominant period at a particular time. The region JD 2449500–2450000 has been blocked out due to a lack of data. We caution the reader that periods within < 200 days of this region may not be trustworthy. See section 4 for a discussion of the periods present and our interpretations.

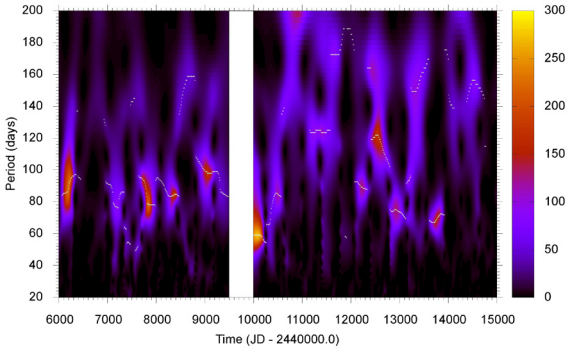

Figure 4. *B*-band WWZ period analysis of ε Aur (c = 1.25E–2). See description in Figure 3.

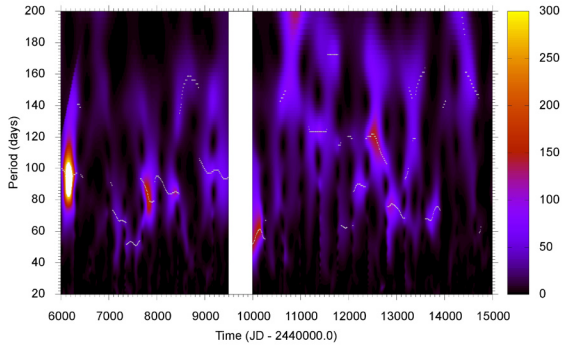

Figure 5. *V*-band WWZ period analysis of ε Aur (c = 1.25E–2). See description in Figure 3.

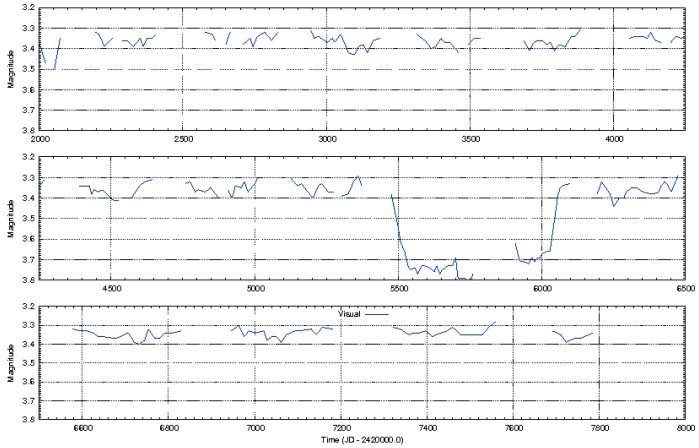

Figure 6. Visual photometry of ε Aur by Plassman (in Güssow 1936) showing the interval JD 2422000–2428000 (1919 February 10–1935 July 16) including the 1927 eclipse. Uncertainties, not plotted, are ±1 in the least significant digit (± 0.01 magnitude). The OOE variations are clearly present. Typical peak-to-peak times are difficult to judge, except right before the 1927 eclipse, where 330- to 370-day periods appear to be present.

V-band Light Curve Analysis of ε Aurigae During the 2009–2011 Eclipse

Thomas Karlsson
Almers väg 19, 432 51 Varberg, Sweden; tkn@seaside.se

Received August 19, 2011; revised October 28, 2011, November 9, 2011; accepted November 14, 2011

Abstract Timings for the eclipse contact points and mid-eclipse, length of ingress and egress, average magnitude during eclipse, and timings for out-of-eclipse variations have been determined in the V band for the long period eclipsing binary ε Aurigae during the 2009–2011 eclipse. This has been done with data from the International Epsilon Aurigae Campaign 2009 and AAVSO. Comparison with data from previous eclipses has also been made.

1. Introduction

The extremely long-period eclipsing binary ε Aurigae (period = ~27.1 years) is still not fully understood. It has been studied by many groups in different wavelengths photometrically, spectroscopically, and interferometrically. The ~2-year eclipse that occurred 2009–2011 presented an opportunity to constrain some parameters for the system. As the system is bright (V = 2.9–3.8) and the duration of the eclipse is long, it is a suitable target for amateur astronomers who can commit a long period of time for this type of project. An international campaign with participants of both advanced amateur and professional astronomers was established (see the campaign website at http://www.hposoft.com/Campaign09.html for further details.) Photometric data from this campaign together with two contributors from the AAVSO, who have covered the whole eclipse, are the basis for this analysis. The campaign produced data in the U, B, V, Rc, Ic, J, and H bands but this analysis only covers the most studied V band.

2. Method

The observers in the campaign used a diversity of equipment and reduction methods (Table 1), from photometers mounted on telescopes, to CCD-cameras with telescopes, or camera-lenses and standard digital single-lens reflex cameras on a tripod. The campaign has published recommended reduction methods and comparison stars to use. But the diversity in equipment and individuality in photometric software and methods used have introduced some differences among the observers. To make the observations comparable to each other the following methods were used.

Prior to the analysis all observations were divided into groups of four-day

periods. In each group the mean of magnitude and JD were calculated. Each observer's individual observations were then subtracted from the corresponding means, and the standard deviation of each observer's differences was calculated. Observers with too much spread in their data (SD > 0.04) were then excluded altogether, and some outlying (> 0.08 from the mean) individual points from the remaining observers were also removed. New four-day means and differences were then calculated for the remaining observers. From these new differences an offset for each observer was calculated, showing the difference for each observer's dataset and the mean for all data. This offset was then subtracted from each observer's data and new one- and four-day means were calculated. These corrected means were then used in the further analysis. The individual observations with the offset applied are seen in Figure 1, the 4-day means are in Figure 2 and the 1-day means in Figure 3.

The offset is based on the assumption that each observer used a similar reduction technique during the eclipse, but the choice of reduction techniques and comparison stars differs among the observers, so that each dataset is to a higher degree consistent with itself than with the other datasets. The idea is that by using this method of reconciling the data more fine details in the light curve should be seen.

3. Results

3.1. Eclipse timings and magnitude

The four contact points for a total eclipse between two spherical bodies are defined as beginning of eclipse, beginning of totality, end of totality, and end of eclipse. In the case of ε Aurigae the main star is partially eclipsed by what is supposed to be a dusty disc seen almost edge on (Huang 1965; Kloppenborg *et al.* 2011), giving rise to an elongated and elliptical eclipsing body from our view. Contact 2 and 3 have therefore for this system an ambiguous definition and not the same physical meaning as for a classical eclipsing binary. For this system they could be interpreted as the points where the leading edge of the elongated disc has crossed the whole face of the main star and where the trailing edge of the disc begins to leave the face of the main star.

The contact points (Table 2) were estimated using a linear trend line applied to the ingress/egress from Figure 2 and were decided by where the line crossed the out-of-eclipse mean magnitude of 3.035 (Hopkins 2011) and the mean during the eclipse of 3.728. Some further work may be done to produce a more precise model of the curve and the means before and after the contact points to obtain more accurate times for the contacts. At contact 2 the curve is especially smooth, which makes the contact point hard to define. Contact 3 could have occurred about a week later than the trend line suggests because of the very steep beginning of the egress. Figures 4 and 5 show the graphs used to establish the contact points.

The totality phase after mid-eclipse is 0.027 magnitude brighter than before mid-eclipse. The brightest part of the totality is during mid-eclipse, and the dimmest just before mid-eclipse. On average, the dimmest part is in the beginning and end of totality and the brightest in between:

- Mean magnitude during totality:
  3.728 (mean over JD 2455208–2455616)

- Mean magnitude during 1st part of totality:
  3.742 (mean over JD 2455208–2455400)

- Mean magnitude during 2nd part of totality:
  3.715 (mean over JD 2455400–2455616)

- Eclipse depth: 0.693 magnitude

- Length of ingress: 142 ± 10 days
  mean drop of brightness: 0.0049 ± 0.0003 magnitude/day

- Length of egress: 121 ± 14 days
  mean increase of brightness 0.0057 ± 0.0007 magnitude/day

- Mid-eclipse, mean of contact 1 and 4:
  JD 2455401 ± 6 (2010 July 23)

- Midpoint of totality, mean of contact 2 and 3:
  JD 2455411.5 ± 6 (2010 August 03)

- Eclipse duration, contact 4–contact 1: 674 ± 12 days

- Totality duration, contact 3–contact 2: 411 ± 12 days

3.2. Out-of-eclipse (OOE) variations

Besides the eclipse, the system shows a smaller variation of 0.1 to 0.2 magnitude with an irregular period of ~2 months (see, for example, Hopkins and Stencel 2006 for a recent study before start of the 2009 eclipse). The out-of-eclipse variations during totality were calculated by applying a fourth-order polynomial fit to the data points 24 and 27 days around each maxima and minima using the 1-day averages from Figure 3. The mean times and magnitudes from the two sets are shown in Table 3. The error for the specified dates is estimated to be on average within ± 2 days and the magnitude within ± 0.01.

Amplitude is calculated as the difference between the maximum and the mean of the two adjacent minima. The first minimum could be affected by the ingress. The observations made 3–4 weeks before and after solar conjunction

that occurred on JD 2455355 (2010 June 07) are contradictory probably because of the difficult observing conditions and differences in extinction calculation among the observers. This gives uncertainty to the data from minimum 2 and maximum 2. During minimum 5 there is a flat part of about 15 days between JD 2455510 and 2455525. The last maximum before start of egress is especially short and low.

The slope of the OOE-variations is between 0.0012 and 0.0029 mag/day with a mean of 0.0022 mag/day, a little less than half of the slope during ingress/egress.

3.3. Ingress and egress characteristics

During ingress there are hints of two OOE variations with maxima about JD 2455080 (2009 September 05) and JD 2455160 (2009 November 24), which can be seen in Figure 4 in the parts of the ingress curve that lie above the linear trend. Another OOE variation just at the end of ingress with a maximum about JD 2455215 (2010 January 18) is also probable and can be seen as a part with low slope at the end of ingress.

The egress started with a high rate of change in magnitude, during JD 2455620 to 2455655 (2011 February 27–2011 April 03). The change was 0.0089 magnitude/day, the highest that was seen during the whole eclipse. Further analysis must be done to tell if a rising OOE variation interacted to generate this high pace. As the last OOE variation just before egress was strangely short and low it is hard to decide by just looking at the light curve if a new OOE variation occurred during this period. During JD 2455655 to 2455670 (2011 April 03–2011 April 18) the slope was lower, at 0.0051 magnitude/day, and then there was a strange standstill or slight decrease of brightness for about 15 days until JD 2455685 (2011 May 03). After that the egress went on at a steady rate of 0.0055 magnitude/day, which is about the same as the mean during the whole egress. The fluctuations that can be seen at the very end of egress are probably caused by the difficult observation conditions during that time near solar conjunction. The big change of slope around JD 2455655 and the later standstill seem too big to be caused by any OOE variation.

3.4 Comparison with previous eclipses

In Figure 6 there is a combined light curve with the 4-day average data from Figure 2 together with two prominent datasets from the previous two eclipses, observations by Gunnar Larsson-Leander 1956–1957 (Larsson-Leander 1959) and Stig Ingvarsson 1982–1984 (Schmidke 1985). The elements from the *General Catalogue of Variable Stars* (GCVS4; Kholopov *et al.* 1984), epoch JD 2435629 and period 9,892 days, were used to phase the data. Table 4 shows data from previous eclipses together with the data from this paper.

Period analyses were made with the light curve and period analysis software PERANSO (Vanmunster 2007) and the ANOVA (analysis of variance) method. The periods calculated (Table 5) are 2–5 days longer than the period from GCVS4.

The trend of decreasing duration of eclipse and egress and increasing duration of totality that was seen during the three or four previous eclipses is broken by the last eclipse. In fact, the 2009–2011 eclipse resembles that of 1955–1957 more than that of 1982–1984, with the more similar length of the different phases, the deep minimum just before mid-eclipse, and the knee half way during the egress. In 1984 the knee was not visible until the system had reached magnitude 3.30–3.25 and the observation season was almost over. The lack of observations at the end of the 1984 eclipse is probably the cause of the very short egress stated, calculated from the slope seen at the first phase of egress.

Differences are the deep minimum, down to 3.85, that was seen at the very end of totality in 1956 but not seen in the two following eclipses. The frequent OOE variations during totality seen during 2010 seem to not occur to the same extent either in 1956 or 1983. Maybe it can be partly explained by the more detailed observations done during the last eclipse.

The pronounced mid-eclipse brightening that was evident in 1983 was not seen to any higher degree in 2010. Although the brightest point during the totality of 2010 occurred at mid-eclipse, it was only 0.02–0.04 magnitude brighter than the two subsequent out-of-eclipse variations. It should also be stated that the mid-eclipse of 1984 coincided with the toughest observation conditions at solar conjunction, and no observations were made at the time of mid-eclipse. If a careful correction for extinction is not done during this period, one could easily obtain values too bright for ε as the most used comparison stars, λ Aur, η Aur, and HR1644, all lie south of ε. This appearance was seen among several observers during May–June 2010.

In Figure 6 one can also notice the placement of the humps from the OOE-variations during the totality phase between the three eclipses. For most part they are not in phase between all three eclipses, with the exception of a brighter phase at mid-eclipse. It contradicts the idea from Ferluga (1990), that the OOE-variations are caused by ring-like structures with Cassini-like divisions in the obscuring disc as it passes the main star. If such a ring structure is stable one should expect that the humps would be in phase between the eclipses.

4. Conclusions

The following conclusions can be drawn from this study:

The OOE variations occur with the same amplitude and periodicity during the eclipse as the period before eclipse and make it much harder to see the features of the eclipse itself.

Ingress and egress have different lengths. In this study egress is about 20 days shorter than ingress. Compared to previous eclipses this relation has varied a great deal. The length of egress, especially, has fluctuated a lot.

The egress has a knee half ways where the slope changes abruptly, a change that is too big to be explained by OOE variations. Further analysis has to be

done to see if the geometry of the eclipsing disc can explain the shape of the egress light curve or if some other process is involved.

If the eclipsing body is an homogeneous elliptical disc, then in purely geometrical terms the biggest loss of light by a partial eclipse should occur half ways, and the light curve during totality should be slightly convex. Instead, the average light curve is slightly concave during totality. This means that another mechanism may be involved to explain the shape of the curve, for example, an optically thinner center of the disc or some sort of scattering effect.

There is also a difference in mean magnitude during the first half of totality compared to the second half that could be a real feature if OOE variations are omitted.

Acknowledgements

Thanks to the observers for the countless hours of work spent on collecting the data that this analysis is based on. Thanks also to Jeff Hopkins, who has done a great job with The International Campaign and who collected and provided the data for this analysis. And thanks to Chris Allen, who has helped me get the English language right.

References

Ferluga, S. 1990, *Astron. Astrophys., Suppl. Ser.*, **238**, 270.

Hopkins, J. L. 2011, "Photometric timing analysis of the 2009–2011 eclipse of Epsilon Aurigae" (http://www.hposoft.com/EAur09/Analysis2011.pdf).

Hopkins, J. L., Schanne, L., and Stencel, R. E. 2008, "Gearing Up for Epsilon Aurigae's First Eclipse of the Millennium," in *The Society for Astronomical Sciences 27th Annual Symposium on Telescope Science*, held May 20–22, 2008 at Big Bear Lake, California, Soc. Astron. Sci., Rancho Cucamonga, CA, 67.

Hopkins, J. L., and Stencel, R. E. 2006, "Single Channel UBV and JH Band Photometry of Epsilon Aurigae," in *The Society for Astronomical Sciences 25th Annual Symposium on Telescope Science*, held May 23–25, 2006, at Big Bear, California, Soc. Astron. Sci., Rancho Cucamonga , CA, 13.

Huang, S. -S. 1965, *Astrophys. J.*, **141**, 976.

Kholopov, P. N., *et al.* 1985, *General Catalogue of Variable Stars*, 4th ed., Moscow.

Kloppenborg, B., *et al.* 2011, poster at the Seattle AAS meeting 11 Jan 2011, "Interferometric Images of the Transiting Disk in the epsilon Aurigae System."

Larsson-Leander, G. 1959, *Arkiv Astron.*, **2**, 283.

Schmidke, P. C. 1985, "UBV photometry of the 1982–4 eclipse of Epsilon Aurigae: A discussion of the observed light curves," in NASA Conf. Publ., NASA CP-2384, 67.

Vanmunster, T. 2007, PERANSO period analysis software, http://www.peranso.com.

Table 1. The observers whose data were used and their offsets and standard deviation.

Observer, Country	*Affiliation**	*Observer Code*	*Equipment*	*Number of observations*	*Offset*	*SD*
John Centala, USA	AAVSO	CQJ	CCD	96	–0.0042	0.017
Donald Collins, USA	IEAC	WWC	DSLR	74	0.0068	0.020
Laurent Corp, France	IEAC	GO	CCD	19	–0.0045	0.030
Serdar Evren, Turkey	IEAC	EUO	PEP	80	–0.0229	0.016
Snaevarr Gudmundsson, Iceland	IEAC	LO	PEP	125	0.0072	0.016
Hubert Hautecler, Belgium	IEAC	RLO	DSLR	28	0.0177	0.020
Charles Hofferber, USA	IEAC	EGO	DSLR	81	0.0137	0.021
Jeff Hopkins, USA	IEAC	HPO	PEP	148	0.0137	0.010
Thomas Karlsson, Sweden	IEAC /AAVSO	VO/KTHA	DSLR	166	0.0004	0.014
Hans-Gîran Lindberg, Sweden	IEAC	KO	CCD	111	0.0073	0.020
Des Loughney, Great Britain	IEAC	DES	DSLR	206	0.0035	0.020
Brian E. McCandless, USA	IEAC	GVO	PEP	11	–0.0054	0.006
Frank J. Melillo, USA	IEAC	FJM	PEP	95	–0.0119	0.017
Richard Miles, Great Britain	IEAC	GHO	CCD	151	0.0011	0.025
Tom Pearson, USA	IEAC	TP	DSLR	106	0.0143	0.019
Roger Pieri, France	AAVSO	PROC	DSLR	160	–0.0137	0.016
Gerard Samolyk, USA	IEAC	GS	CCD	149	–0.0236	0.022
Iakovos Marios Strikis, Greece	IEAC	EAO	CCD	76	0.0020	0.017
Piotr Wychudzki, Poland	IEAC	PW1	CCD	22	0.0001	0.023
Piotr Wychudzki, Poland	IEAC	PW2	CCD	38	0.0237	0.025

** IEAC, International Epsilon Aurigae Campaign 2009; AAVSO, American Association of Variable Star Observers; PEP, Photoelectric photometric equipment as SSP–3 or PMT; CCD, Charge Coupled Device camera; DSLR, Digital Single–Lens Reflex camera.*

Table 2. Timing of the eclipse contact points.

Contact	*JD*	*Date*
1	2455064 ± 5	2009 August 20
2	2455206 ± 5	2010 January 09
3	2455617 ± 7	2011 February 24
4	2455738 ± 7	2011 June 25

Table 3. Data for out-of-eclipse variations during the eclipse.

		Minima		
Nr.	*JD*	*Date*	*Length*	*VMag.*
1	2455259	2010 March 03	—	3.77
2	2455311	2010 April 24	52	3.79
3	2455367	2010 June 19	56	3.78
4	2455437	2010 August 28	70	3.72
5	2455520	2010 November 19	83	3.75
6	2455576	2011 January 14	56	3.75
7	2455610	2011 February 17	34	3.77
Avg			58.5	3.761

		Maxima			
Nr.	*JD*	*Date*	*Length*	*VMag.*	*Amplitude*
1	2455283	2010 March 27		3.72	0.060
2	2455336	2010 May 19	62	3.71	0.075
3	2455407	2010 July 29	60	3.65	0.100
4	2455471	2010 October 01	63	3.67	0.065
5	2455547	2010 December 16	79	3.69	0.060
6	2455590	2011 January 28	43	3.74	0.020
7	—	—	—	—	—
Avg			61.4	3.697	0.063

Table 4. Data from previous eclipses together with the data from this paper.

	Mean of 1901–1903 1928-1930 [1]	*1955–1957 Gyldenkerne* [1]	*1982–1984 Schmidtke*	*2009–2011*
Duration (days)	714	670	647	674
Ingress (days)	182	135	137	142
Totality (days)	330	394	446	411
Egress (days)	203	141	64	121
Depth (mag)	0.80	0.75	0.686 [2]	0.693

[1] *From Hopkins, Schanne, and Stencel (2009).* [2] *Mid-eclipse brightening omitted.*

Table 5. Periods calculated with PERANSO ANOVA.

Comparison	*Period (days)*
1955-57, 1982-84, 2009-11	9897
1955-57, 2009-11	9896
1982-84, 2009-11	9894
GCVS4	9892

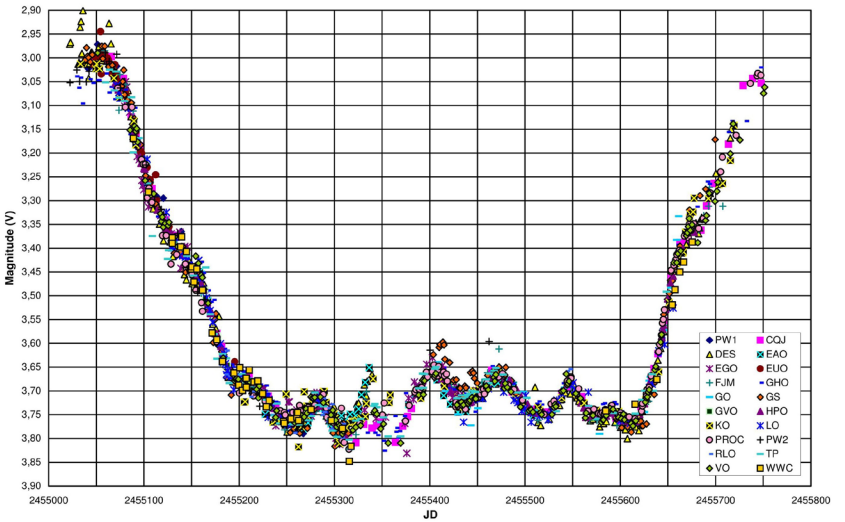

Figure 1. The individual observations, with each dataset corrected with its offset. (The observer PW made observations from two different observatories.)

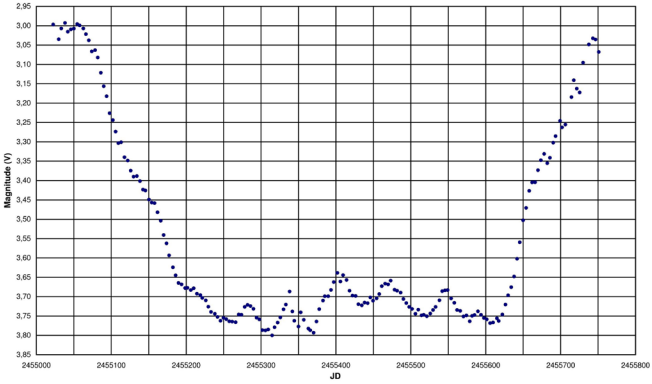

Figure 2. The observations from Figure 1, grouped together as 4-day averages.

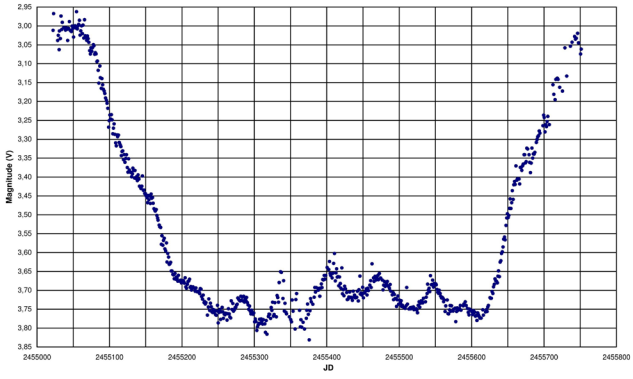

Figure 3. The observations from Figure 1, grouped together as 1 day averages.

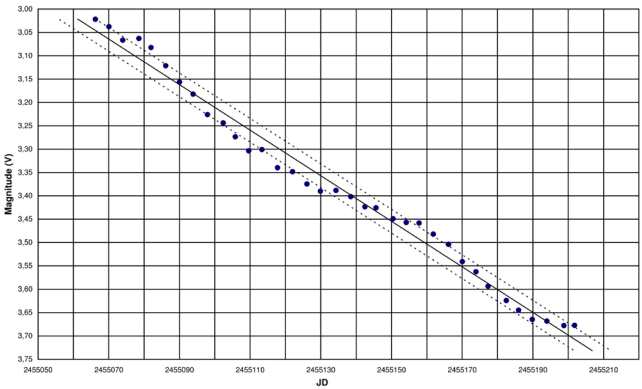

Figure 4. Detail from Figure 2 of the ingress (JD 2455060–22455216) and the linear fit used. The dotted lines show an error of 1 sigma in magnitude.

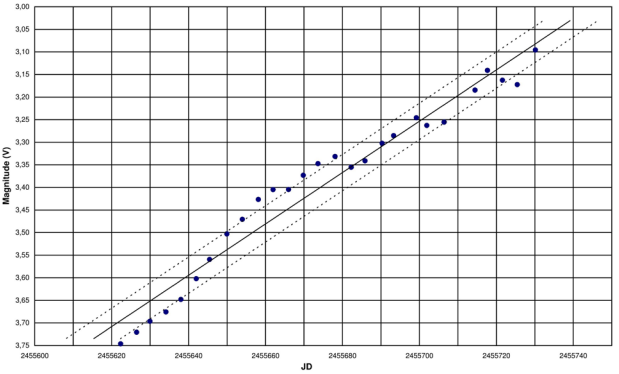

Figure 5. Detail from figure 2 of the egress (JD 2455616–2455740) and the linear fit used. The dotted lines show an error of 1 sigma in magnitude.

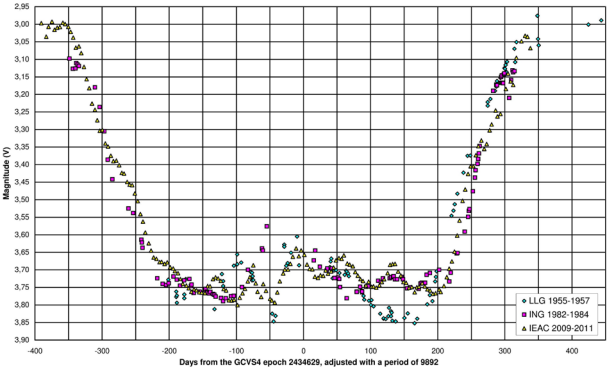

Figure 6. The data from this paper (IEAC) compared with two datasets from the previous two eclipses, Gunnar Larsson-Leander (LLG) from 1955–1957 and Stig Ingvarsson (ING) from 1982–1984.

Report From the ε Aurigae Campaign in Greece

Grigoris Maravelias
Physics Department, University of Crete, GR-71003, Heraklion, Crete, Greece; address email correspondence to G. Maravelias at gmaravel@physics.uoc.gr

Emmanuel (Manos) Kardasis
Department of Electronics Engineering, T.E.I. of Pireaus, GR-12244, Egaleo, Greece

Iakovos-Marios Strikis
Pindarou 15, GR-12461, Chaidari, Greece

Byron Georgalas
Ameipsiou 12, GR-11143, Athens, Greece

Maria Koutoulaki
Physics Department, University of Crete, GR-71003, Heraklion, Crete, Greece

Received May 30, 2012; revised August 27, 2012; accepted September 5, 2012

Abstract We report the results of the Greek campaign to observe the 2009–2011 eclipse of ε Aurigae. We present the activities organized by the Hellenic Amateur Astronomy Association (HAAA) in order to publicize the event and to provide the necessary information and tools to both first-time and experienced observers. Although visual observations were the core method, we proposed and experimented with various techniques. In total, data from 21 observers were acquired combining different techniques: 302 visual, 95 CCD, and 11 DSLR observations, and 5 low-resolution spectra.

We were able to construct the light curve of the eclipse and extract some interesting results, in agreement with previous studies. The system's V-magnitude drops from ~3.0 to ~3.8 in 131 ± 21 days. The ingress date is estimated around the MJD 55087 ± 15d (August 12, 2009) and the system is exiting eclipse after the MJD 55797 ± 15d (August 23, 2011). We estimate the duration of the 2009–2011 eclipse to be 710 ± 21 days. A rather possible trend for mid-eclipse brightening exists only in the CCD/DSLR data, which show oscillations of 0.07 magnitude amplitude.

1. Introduction

The bright (~3 V-magnitude) binary system ε Aurigae (ε Aur, R.A. 05^h 01^m 58.1^s, Dec. +43° 49' 23.9", J2000) has been a long mystery since its discovery in early 1800s. The binary consists of a F0 Iab star and a cool, mysterious

companion which eclipses the supergiant every 27.1 years for almost 2 years. Although the system has been used extensively as a test bed for many theories and observational methods (Carroll *et al.* 1991; Guinan and deWarf 2002, and references therein) the data obtained so far, which extend almost two centuries, have not been adequate to fully explain this system. Even after the last eclipse of 1982–1984, when an international campaign was launched, the mass and luminosity uncertainties remained strong, prohibiting the final solution (Stencel 1985). But all these data provide important constraints allowing two possible scenarios: (i) the high-mass model, where the F0 star is considered a young star of mass ~15 $M_{\odot}$ and radius ~200 $R_{\odot}$ and the eclipsing companion a cool, proto-stellar or proto-planetary disk with total mass of M ~13.7 $M_{\odot}$ and radius ~9.3 AU, (ii) the low-mass model, where the F0 star is an old solar mass post-AGB star and the disk is a remnant of accretion due to mass transfer with a total mass of ~5 $M_{\odot}$ and radius ~7 $R_{\odot}$. But both models have severe problems to fully interpret the observations, and, moreover, new data raise new questions (Hoard *et al.* 2010; Kloppenborg *et al.* 2010).

In 2009–2010 the system would undergo another eclipse, offering a great opportunity to acquire more information. Thus, another international campaign has been launched in order to coordinate, collect, and provide all the necessary material to perform scientific useful observations from both professional and amateur astronomers: the International ε Aur Campaign 2009–2011 (http://www.hposoft.com/Campaign09.html) organized by Jeff Hopkins and Robert Stencel, and the Citizen Sky project (http://www.citizensky.org) organized by the American Association of Variable Star Observers (AAVSO; http://www.aavso.org). The contribution of amateur astronomers is considered valuable since the system is bright enough to be observed by their equipment (even with unaided eye).

This fact motivated us, the Hellenic Amateur Astronomy Association (HAAA; http://www.hellas-astro.gr), to publicize this campaign in Greece. In HAAA our main goal is to promote the amateur astronomy performed using the necessary methodology in order to obtain scientifically valuable observations and contributing to pro-am collaborations. Thus, the contribution to such a project was considered as a unique opportunity to participate in and to promote it to the Greek amateur community.

This work reports the results of this campaign in Greece, including the aims and the activities organized, in section 2, a description of the methods used and the observations collected, in section 3, and a small discussion on the results, in section 4.

2. The campaign in Greece

2.1. Aims

The ε Aur campaign in Greece was directed by the HAAA with the help

of the AAVSO/Citizen Sky staff. The main goals of this campaign were to: (i) inform the Greek community about the rarity and the importance of the ε Aur's eclipse, (ii) provide the necessary material for observations for both experienced and first-time observers, (iii) collect all observations by Greek observers, (iv) forward these to the AAVSO database, (iv) construct the light curve of the eclipse along with any interesting results.

2.2. Activities

In order to better promote the campaign, we have created the dedicated webpage "The observational program of ε Aur" (currently available in Greek at http://www.hellas-astro.gr/article.php?id=765&topic=variables&subtopic=&lang=el) in which we published related material. This included analytical guides on how to perform visual observations, maps, tips, news and updated information on the system, and a frequently updated plot of all observations collected.

This page has already been updated thirteen times and it will continue as new information and results will become available. Updates were mailed to the observers who have already submitted observations and were publicized at the two main fora of amateur astronomers in Greece, Astrovox (under the thread "epsilon Aur", http://www.astrovox.gr/forum/viewtopic.php?t=10578&highlight=\%C7\%ED\%DF\%EF\%F7\%EF\%F5) and AstroForum (under the thread "epsilon Aur", http://astroforum.gr/forum/viewtopic.php?t=3862&highlight=\%C7\%ED\%DF\%EF\%F7\%EF\%F5), with almost 5,000 reads each. At the same time, there was also a thread active in the forum (under the thread "Greek on-going visual observations", http://www.citizensky.org/forum/greek-going-visual-observations) of the Citizen Sky project, which was informing the international campaign about the progress in Greece.

A formal call for observations was made during a talk at the 6th Panhellenic Conference on Amateur Astronomy held in Alexandroupolis, Greece, on September 26, 2009 (Maravelias 2009), with more than 500 participants. The talk was also accompanied by a practical mini-workshop during the night, in which volunteers tried the visual observing technique on the system. In addition, two of the regular meetings of the HAAA were dedicated to ε Aur, regarding the progress of the observations and of the eclipse along with new results obtained. Numerous informal discussions took place at the meetings and via the mailing list.

ε Aur was presented in all talks and workshops related to variable stars that took place after the initialization of the campaign in March 2009. We took advantage of every event to publicize the need for observations and the campaign itself (that is, the Panhellenic Astroparties of 2009 and 2010, at Anavra-Fthiotida and Mt. Parnonas, respectively, and the "Sun and Variable Stars Meeting" at the University of Athens in 2010). Especially in the cases of workshops we offered the opportunity for hands-on experience of visual and digital observations.

Although we did not circulate any press releases about the ε Aur eclipse, there was one article, to the best of our knowledge, published in a national circulation newspaper dedicated to this event ("Vima Science," January 17, 2010). The author referred to both historical and new data about the system and did not fail to refer to the Citizen Sky project and the Greek campaign.

3. Observations

The campaign in Greece was heavily based on visual photometric observations. However, we still experiment with other kind of observations, including DSLR photometry (GM was a member of the DSLR Documentation and Reduction team of the CitizenSky project (http://www.citizensky.org/teams/dslr-documentation-and-reduction, responsible to develop observational methods and tutorials), CCD photometry (IMS was an official member of the International Epsilon Aur Campaign 2009 (http://www.hposoft.com/Campaign09.html)), and low-resolution spectroscopy. The observations will be web-archived and made available through the AAVSO ftp site at ftp://ftp.aavso.org/public/datasets/gmaraj402.txt. We present each method and observations obtained in the following sections.

3.1. Visual

Visual observations are all observations that are obtained using the eye as a photometer, either unaided or through an optical system (that is, binoculars or a telescope). Since ε Aur is a bright object the majority of the observations were made using unaided eye and binoculars.

The method used for visual observations is simply based on the comparison of the target star (ε Aur) with two reference (comparison) stars, usually η Aur with 3.2 V-magnitude (in visual observations all magnitudes are rounded to the first decimal place), ζ Aur with 3.8 V-magnitude (actually it is an eclipsing binary of ~3.75 V-magnitude with a drop of ~0.1 during eclipse, every 2.7 years with eclipse duration ~40 days, but it is considered as non-variable during the major part of the ε Aur eclipse except for the period November–December 2009 when it was in eclipse—during that time it was avoided as a comparison star), or 58 Per with 4.3 V-magnitude. By comparing our target with a fainter and a brighter star, we were able to place it between the two magnitudes. Usually the error of these measurements is not given, and an accuracy of a few tenths of magnitude is assumed with the most experienced observers going down to 0.1, although a subject of controversy (Price *et al.* 2006). In some cases we were able to go down to 0.05 magnitude error, partly due to the small difference between ζ Aur and 58 Per (when ε Aur was in-between) and partly to the growing experience and confidence with the field.

By applying this method we were able to collect 302 observations from twenty-one persons, presented in Table 1.

3.2. CCD

The CCD observations were performed by using an ATik 16 IC monochrome camera, equipped with a Zenit 55 mm *f*/2.8 lens, and a Johnson V photometric filter with the whole setup mounted on an equatorial mount. The reduction procedure followed is the standard one for CCD observations: (i) create the master-dark, the master-bias, and the master-flat images (usually twenty-five images were combined for each master image), (ii) subtract master-dark and master-bias from each science image, (iii) divide each of these by the master-flat, (iv) align and stack images of each set (usually ten sets of thirty science images each), (v) perform photometry using the MaxIm DL software.

The comparison stars used were η Aur and ζ Aur. Since the latter is an eclipsing binary the V-magnitude to use was provided each week by Jeff Hopkins (coordinator of the International ε Aur Campaign 2009). The reduction and the photometry were performed according to the guidelines of the International Campaign.

Using this technique we collected 95 CCD observations, all acquired by a single observer. Details are presented in Table 2.

3.3. DSLR

DSLR photometry refers to the use of a normal Digital Single-Lens Reflex camera (DSLR) or any digital photography camera which: (i) can produce images in a RAW data format, (ii) can focus semi-manually, (iii) is able to manually select a shutter speed/exposure time of several seconds, (iv) has a wide enough field-of-view to get a variable star and a comparison star in the image. In order to obtain the images needed, the camera is usually mounted on a simple tripod with a typical lens of 50–90 mm and exposures of some seconds to capture the bright stars (Kloppenborg *et al.* 2012, in this volume).

The data reduction of DSLR observations follows that of the CCD. In our case though, bias and flat fields were not available, so a slightly different process was followed: (i) the master-dark was created as normal (from dark images), (ii) using three science images we created the master-flat (median combine of the images), (ii) subtract the master-dark from science images, (iii) divide each of these by the master-flat, (iv) align and stack images of each set (usually around eight images), (v) separate stacked images to their RGB Bayer pattern, and keep only the Green channel (closer match to the V filter passband), (vi) perform photometry.

The DSLR Documentation and Reduction team of the Citizen Sky project has developed standard guides (http://www.citizensky.org/content/dslr-documentation-and-reduction) for some widely used software packages within the amateur astronomer community (IRIS, AIP4WIN, MAXIMDL) in order to present easy ways to reduce data and perform photometry. In this work we used IRIS (free software) for image reduction and photometry, along with the spreadsheets provided for this purpose at the Citizen Sky site. We used η Aur

as a comparison star while others (that is, ζ Aur, λ Aur, ο Aur, and 58 Per) were used for color and airmass correction. Two of the DSLR observations were analyzed with the MaxIm DL software, where η Aur and ζ Aur stars were used as comparison stars.

Using this technique we manage to collect eleven observations from three persons. The observers and the systems used are presented in Table 2.

3.4. Spectra

3.4.1. 80-mm refractor

As low resolution spectroscopy is available to amateur astronomers, a sample was obtained with a Sky Watcher 80-mm Apochromatic refractor equipped with an ATiK 16 IC camera (640 × 480 px) and a Baader Blaze Grating Spectroscope (207 lines/mm grating with a dispersion of 1267 Å/mm and wavelength coverage ~ 3800–6800 Å).

The spectra extraction was performed through the RSPEC software. Using the standard libraries, an A7V spectral type star profile was selected for the identification of the Balmer lines as well as for the wavelength calibration. From the calibrated spectrum, the Balmer lines were removed, leaving only a featureless spectrum composed of the continuum emission of the star and the instrumental response of the system. By dividing this result by the instrumental response we obtained the final normalized spectrum.

Using this method we collected four spectra, obtained by a single observer (Table 3). One of these spectra is presented in Figure 1.

3.4.2. 1.3-m reflector

We were also able to use the slit spectrograph mounted on the 1.3-m telescope at Skinakas Observatory (http://skinakas.physics.uoc.gr/en/) to acquire one spectrum of ε Aur during its eclipse, on 30 September, 2010. The telescope is equipped with a slit spectrograph (1302 lines/mm with a dispersion of 70.44 Å/mm and wavelength coverage ~ 5210–7280 Å) and a 2000 × 800 ISA SITe CCD.

The data reduction performed in IRAF included: (i) bias subtraction, (ii) flat-fielding, to correct pixel-to-pixel variations across the chip, and (iii) wavelength calibration. The final correction would be to remove the continuum with the help of a standard star. Since no standard was observed that night and no good one was available we decided to leave the spectrum uncorrected. Although present, the continuum does not prohibit us from identifying basic features in the spectrum.

Only one spectrum was obtained with this setup (Table 3) and is presented in Figure 2.

4. Discussion

4.1. Statistics

The main aim of the campaign in Greece was to collect all the observations made by Greek observers during the 2009–2011 eclipse (Figure 3). A total of twenty-one individuals managed to obtain 302 visual observations. Out of the twenty-one observers, only three were not engaged with the campaign run by the HAAA and their observations were acquired through the AAVSO International Database. However, the majority of the observers (~86%) were participants of this campaign (that is, they submitted their observations directly to HAAA) and provided almost all the observations (93%). It is interesting to point out that thirteen participants (~72%) were first-timers in visual observations of variable stars, but only three of them observed more than a couple of times. Although we were expecting a larger contribution, we hope that the new observers will continue observing other variable stars. In total the vast majority of the data (255 observations, almost 84% of the total sample) came from only four persons, already experienced observers.

Out of the eighteen participants of the campaign, six were not members of the HAAA, which means that actually there was a number of people outside the HAAA interested in the campaign. In addition, seven of the participants were already AAVSO observers (that is, they had an AAVSO observer code).

Although the campaign was heavily biased towards the visual observations (74% of the whole sample), there had been systematic work with digital observations (DSLR/CCD). Only three people observed using digital systems (two DSLR users and one using both). One of our team (IMS) used a CCD camera as part of the International ε Aur Campaign 2009, producing the majority of the digital results (almost 90% of all digital observations).

Spectroscopic observations were also attempted by two observers (ISM and GM), but mainly as tests. Experience and time availability was limited to fully exploit the powerful tool of spectroscopy for ε Aur, but the knowledge gained could be used in future projects.

4.2. Visual observations

In Figure 4 we present all the visual observations obtained (indicated as the "raw data" in the figure). It is obvious that we were completely successful in following the 2009–2011 eclipse of ε Aur. The number of observations is not sufficient to extract solid conclusions but some interesting results can be presented.

In order to perform a basic reduction of the observations we used bins of 15 days. Bins with fewer days are close to the sampling period, as the observations were obtained once per week or ten days. Bins with more days tend to smooth too much the light curve, as it is not realistic for the star to be constant in a time span of 20 to 30 days or more. For each bin the median value and the standard

deviation (σ) were calculated. In the cases where only one observation was obtained, an error of 0.1 magnitude was assumed (corresponding to the best case scenario—experienced observers). Then all the data which were within the $3 \times \sigma$ range were kept (indicated as the "reduced data" in Figure 4). We used these data to obtain the median value and its corresponding error for each bin (represented as the "median" line in the same figure). By visual inspection of the final result some interesting features of the eclipse can be identified.

The V-magnitude of the system before entering eclipse was ~3.0. The small drop of 0.1 magnitude after the MJD 55050 (August 6, 2009) cannot identify the beginning of the eclipse (due to the 0.1-magnitude oscillations of the system (Carroll 1991; Hopkins *et al.* 2008). Only later, within MJD 55077–55097, we have a clearer indication of the ingress, which could be placed around the MJD 55087 (August 12, 2009), with an error equivalent to the bin size (that is, ±15 days). The date is within the predicted range of dates (Hopkins *et al.* 2008).

Only after MJD 55218 (February 2, 2010), ε Aur seems to have reached its faint state (totality) at magnitude ~3.8, losing almost 0.8 magnitude in 131 ± 15 days, in agreement with the values of 137 days for the 1982–1984 eclipse and 135 days for the 1955–1957 eclipse (Carroll *et al.* 1991). There was a small trend of brightening after MJD 55261 (March 5, 2010), which could tempt us to credit it to the mid-eclipse brightening. However, since the errors are large, the brightening is not statistically significant. Moreover, during this period ε Aur was getting lower on the horizon and after passing behind the Sun (June 2010), it was again low on the horizon, when the observations were resumed. This position definitely affected the observations due to the airmass.

After the MJD 55376 (June 28, 2010) we notice a scatter of values around magnitude ~3.7–3.75. There can be no estimation when the system passed from the third contact (start of engress) due to the data scatter. Only after MJD 55797 (August 23, 2011) we can accept that ε Aur was totally out of the eclipse with a V-magnitude ~3.1. Using the previously estimated date of ingress (MJD 55087) we calculate the duration of the 2009–2011 eclipse to be 710 ± 21 days, which is actually within 2–3σ from the previous eclipse durations, 647 days in 1982–1984 and 670 days in 1955–1957 (although there is a trend for decreasing duration (Carroll *et al.* 1991).

4.3. CCD and DSLR observations

We present the digital data (DSLR and CCD observations) in Figure 5. All observations were obtained within MJD 55128–55545 (October 23, 2009–December 14, 2010), when ε Aur was already in eclipse, with the majority of the data obtained during totality. Thus, there are no additional data to allow for the determination of ingress or engress. Nevertheless, we observe modulations of ~0.07 magnitude, in agreement with previous results (Hopkins *et al.* 2008; Carroll *et al.* 1991). The faintest value, within errors, that ε Aur reached was magnitude 3.789 ± 0.003. Moreover, the oscillations displayed in Figure 5,

with maxima near MJD 55285, 55400, and 55470, probably reflects the 67- and 123-day periods identified by Kim (2008).

After MJD 55305 (April 18, 2010) and up to MJD 55335 (May 18, 2010), the system seems to have brightened, with a resulting change in V-magnitude of 0.13 magnitude. It is interesting to observe that this time period coincides with the possible trend observed in the visual data (see Figure 4). Although, the errors are large in visual observations, preventing us from definitely identifying the brightening, the CCD observations are more accurate and they are corrected for the airmass. Thus, this trend in the CCD observations is more realistic and could be attributed to the mid-eclipse brightening.

4.4. Spectra

As there have been only a few tests with spectroscopy, we present the best spectra obtained in Figures 1 (spcA) and 2 (spcB). The observations were obtained during the eclipse of ε Aur and, as such, its spectrum would be a composite of the main star and the disk. Thus, it is out of the scope of this work to present a classification or any spectral results regarding with the nature of the objects, but rather to present a sample of the observations performed and the lines identified.

There is an overlap of the two spectra in the range 5200–6700 Å, where the most prominent features are the NaI Doublet λλ5890,5896 lines (characteristic feature of F- to M-type stars (Montes *et al.* 1999)) and the Hα λ6563 line. Both of these lines are variable during the eclipse, revealing properties for both the disk and the primary star (Barsony *et al.* 1986; Chadima *et al.* 2011). Outside this region in spcA all Balmer lines are evident with some additional features around λλ4040, 4480, and 5050 but we were unable to resolve which lines they are (though the λ4480 line could be the MgII line at λ4481 Å). However, in spcB we were able to identify numerous metallic lines. The most abundant metal is iron with lines such as FeII λλ5235,5274,5316,5363,6148,6238, and 6247 lines and FeI λλ5226,5325,5657, and 5780 lines. Also present are the NiIII λ5534 line and the SiII λλ6347,6371 lines (Chadima *et al.* 2011). In this case, the NaI Doublet is also nicely resolved to its two separate absorption lines (λλ5890,5896, see inset graph in Figure 2).

5. Conclusions

The current work is a report of the results obtained from the Greek campaign dedicated to the observation of the 2009–2011 eclipse of ε Aur. We have been successful in informing the Greek amateur astronomical community about the eclipse and its importance. Furthermore, we publicized the event and the appropriate material for both experienced and first-time observers, by using internet resources (dedicated webpage, threads in well-known fora) and talks/workshops at major astronomical events. We managed to collect 413

observations (302 visual estimates, 95 CCD, and 11 DSLR measurements, 5 low-resolution spectra) from 21 Greek individuals, which have been submitted to the AAVSO International Database.

We were able to construct the light curve of the eclipse and, even under some limitations of the data, to extract some interesting results. By visual examination of the light curve we noticed the system's V-magnitude dropped from ~3.0 to ~3.8, in 131±21 days, in agreement with Carroll *et al.* (1991). We estimated the ingress date around the MJD 55087±15 days (August 12, 2009), within the predicted range of dates, and the exit of the eclipse after the MJD 55797±15 days (August 23, 2011). The duration of the 2009–2011 eclipse was found to be 710±21 days, within the error margins of previous eclipses (Carroll *et al.* 1991). Although we cannot confirm the mid-eclipse brightening by the visual observations, the CCD/DSLR data presented a rather possible indication. Moreover, 0.07-magnitude oscillations were present in the CCD/DSLR data in agreement with previous observations (Hopkins *et al.* 2008; Kim 2008). In addition, we presented our first attempts at spectroscopic observations of ε Aur, which resulted in the identification of the NaI Doublet λλ5890,5896 lines, the SiII λλ6347,6371 lines, and numerous FeI and FeII lines (Barsony *et al.* 1986; Chadima *et al.* 2011).

6. Acknowledgements

The authors are grateful to the observers: Athanasios Douvris, Nikos Flemotomos, Dimitris Gkionis, Panagiotis Kottaridis, Krikis Manolis, Dimitris Manousos, Eleni Maraki, Serafim Ntovolos, Kostas Dimitris Panourakis, Paschos, Giorgos Stefanopoulos, Vasilis Takoudis, Andromachi Tsouloucha, Lefteris Vakalopoulos, George Vithoulkas, Giorgos Voutiras, and Orfeas Voutiras.

The authors would like to thank the AAVSO and its Citizen Sky project, especially Aaron Price and Brian Kloppenborg. GM would like to acknowledge the help of Pablo Reig regarding spectroscopy obtained at Skinakas Observatory and the valuable discussions with Thodoris Bitsakis and Paolo Bonfini. IMS acknowledges the help of Jeff Hopkins and Robin Leadbeater.

Also, we acknowledge the supporting communities of the free/open softwares IRIS, PYTHON/MATPLOTLIB, and IRAF, which have been used for this work. This research has made use of NASA's Astrophysics Data System.

References

Barsony, M., Lutz, B. L., and Mould, J. R. 1986, *Publ. Astron. Soc. Pacific*, **98**, 637.

Carroll, S. M., Guinan, E. F., McCook, G. P., and Donahue, R. A. 1991, *Astrophys. J.*, **367**, 278.

Chadima, P., *et al.* 2011, *Astron. Astrophys.*, **530A**, 146.

Guinan, E. F., and DeWarf, E. 2002, in *Exotic Stars as Challenges to Evolution*, eds. C. A. Tout and W. Van Hamme, ASP Conf. Ser. 279, Astron. Soc. Pacific, San Francisco, 121.

Hoard, D. W., Howell, S. B., and Stencel, R. E. 2010, *Astrophys. J.*, **714**, 549.

Hopkins, J. L., Schanne, L., and Stencel, R. E. 2008, in *The Society for Astronomical Sciences 27th Annual Symposium on Telescope Science, Held May 20-22, 2008 at Big Bear Lake, CA*, Society for Astronomical Sciences, Rancho Cucamonga, CA, 67.

Kim, H. 2008, *J. Astron. Space Sci.*, **25**, 1.

Kloppenborg, B., Pieri, R., Eggenstein, H.-B., Maravelias, G., and Pearson, T. 2012, *J. Amer. Assoc. Var. Star Obs.*, **40**, 815.

Kloppenborg, B., *et al.* 2010, *Nature*, **464**, 870.

Maravelias, G. 2009, In *Proceedings of the 6th Panhellenic Conference on Amateur Astronomy, Alexandroupolis, Greece, 25–27 September 2009*, 143 (in Greek).

Montes, D., Ramsey, L. W., and Welty, A. D. 1999, *Astrophys. J., Suppl. Ser.*, **123**, 283.

Price, A., Foster, G., Skiff, B., and Henden, A. 2006, *Bull. Amer. Astron. Soc.*, **38**, 1126.

Stencel, R. E. 1985, in *1982–1984 Eclipse of Epsilon Aurigae* , ed. R. E. Stencel, NASA Conf. Publ. 2384, NASA, Washington, D.C., v.

Table 1. Visual observations obtained by Greek observers during the 2009–2011 eclipse of ε Aur.

Name	*Number of Observations*	*Participant*[1]	*HAAA Member*[2]	*AAVSO Code*[3]
Douvris, Athanasios	1	yes	no	DXA
Flemotomos, Nikos	1	yes	no	—
Georgalas, Byronas	1	yes	yes	—
Gkionis, Dimitris	5	yes	yes	—
Kardasis, Manos	44	yes	yes	KMO
Kottaridis, Panagiotis	5	yes	yes	KPAA
Krikis, Manolis	1	yes	no	—
Manousos, Dimitris	4	yes	no	MUQ
Maraki, Eleni	1	yes	no	—
Maravelias, Grigoris	64	yes	yes	MGK
Ntovolos, Serafim	1	yes	yes	—
Panourakis, Kostas	1	no	no	PKO
Paschos, Dimitris	1	no	no	PDIA
Stefanopoulos, Giorgos	41	yes	yes	STF
Strikis, Iakovos-Marios	106	yes	yes	SIAK
Takoudis, Vasilis	1	yes	yes	—
Tsouloucha, Andromachi	2	yes	no	—
Vakalopoulos, Lefteris	1	yes	yes	—
Vithoulkas, George	19	no	no	VGK
Voutiras, Giorgos	1	yes	yes	—
Voutiras, Orfeas	1	yes	yes	—
Totals *(persons/observations)*				
21	302	18	12	10

[1] Defined as an observer who submitted his/her observations directly to the HAAA (in "no" cases the data were retrieved from the AAVSO International Database). [2] Member of the Hellenic Amateur Astronomy Association (HAAA). [3] Observer who submits his/her observations to the AAVSO has a unique observer code—this is given when applicable.

Table 2. DSLR and CCD observations obtained by Greek observers during the 2009-2011 eclipse of ε Aur.

Name	*Filter*[*]	*Camera*	*Lens*	*f-ratio*	*Exposure(s)*	*No. Obs.*
Gkionis, Dimitris	Green	Canon 300D	Nikon 200mm	2.8	5	1
Gkionis, Dimitris	Green	Canon 300D	Tamron 300mm	5.6	5	1
Kardasis, Manos	Green	Canon 300D	Canon 17–85mm (@ 85mm)	5.6	10	7
Strikis, Iakovos-Marios	Green	Canon EOS 5D Mrk II	Tamron 24–105mm (@ 105mm)	4.5	5	1
Strikis, Iakovos-Marios	Green	Canon EOS 350D Rebel XTI	Tamron 24–105mm (@ 105mm)	4.5	5	1
Strikis, Iakovos-Marios	V	ATiK 16 IC monochrome	Zenit 55mm	2.8	2–5	95

[*] *Green corresponds to the Green channel of the Bayer pattern (RGB) for DSLR cameras, V corresponds to the Johnson V photometric filter, used for CCD photometry.*

Table 3. Log of spectroscopic observations obtained by Greek observers during the 2009–2011 eclipse of ε Aur.

Name	*Date*	*Telescope*	*Camera*	*Grating (lines/mm}*	*Wavelength (Å)*	*Dispersion (Å/mm)*
Strikis, Iakovos-Marios	2 Jan 2010	ED 80mm	ATiK 16 IC (640×480)	BBG[*] (207)	3800–6800	1267
Strikis, Iakovos-Marios	30 Jan 2010	ED 80mm	ATiK 16 IC (640×480)	BBG (207)	3800–6800	1267
Strikis, Iakovos-Marios	1 Feb 2010	ED 80mm	ATiK 16 IC (640×480)	BBG (207)	3800–6800	1267
Strikis, Iakovos-Marios	27 Aug 2010	ED 80mm	ATiK 16 IC (640×480)	BBG (207)	3800–6800	1267
Maravelias, Grigoris	30 Sep 2010	Skinakas' 1.3m	ISA SITe (2000×800)	1302	5210–7280	70.44

[*] *Baader Blaze grating.*

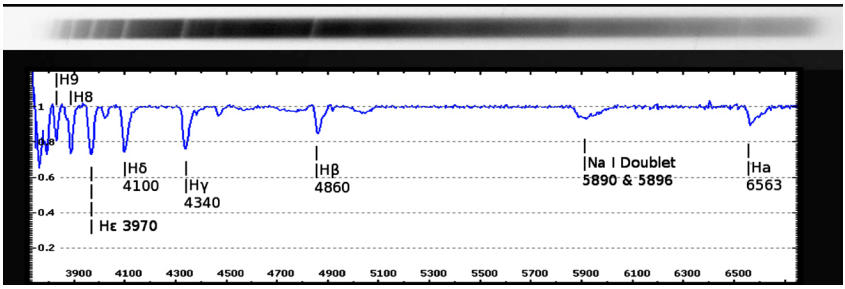

Figure 1. Low-resolution spectrum of ε Aur obtained on August 27, 2010. A Sky Watcher 80-mm Apochromatic refractor was used equipped with an ATiK 16 IC (mono) and a Baader Blaze grating (see section 3.4.1). Characteristic Balmer lines are shown along with the NaI Doublet lines. Spectrum obtained by IMS, reduced by Robin Leadbeater.

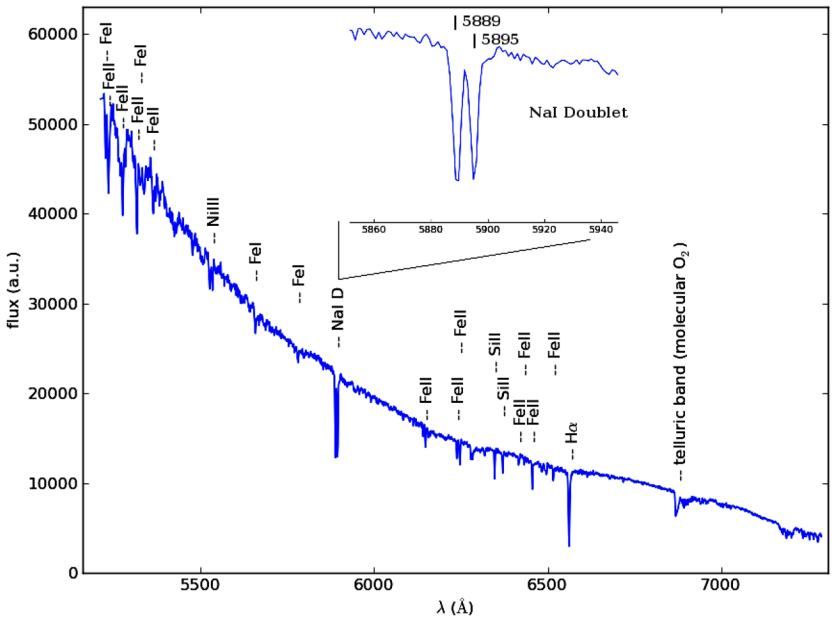

Figure 2. Low-resolution spectrum of ε Aur obtained on September 30, 2010. Skinakas' 1.3-m telescope was used, equipped with an ISA SITe and a slit spectrograph (see section 3.4.2). The Hα and NaI Doublet lines are prominent along with a series of FeI and FeII lines, and SiII lines. Spectrum obtained by GM with the help of Pablo Reig, and reduced by MK.

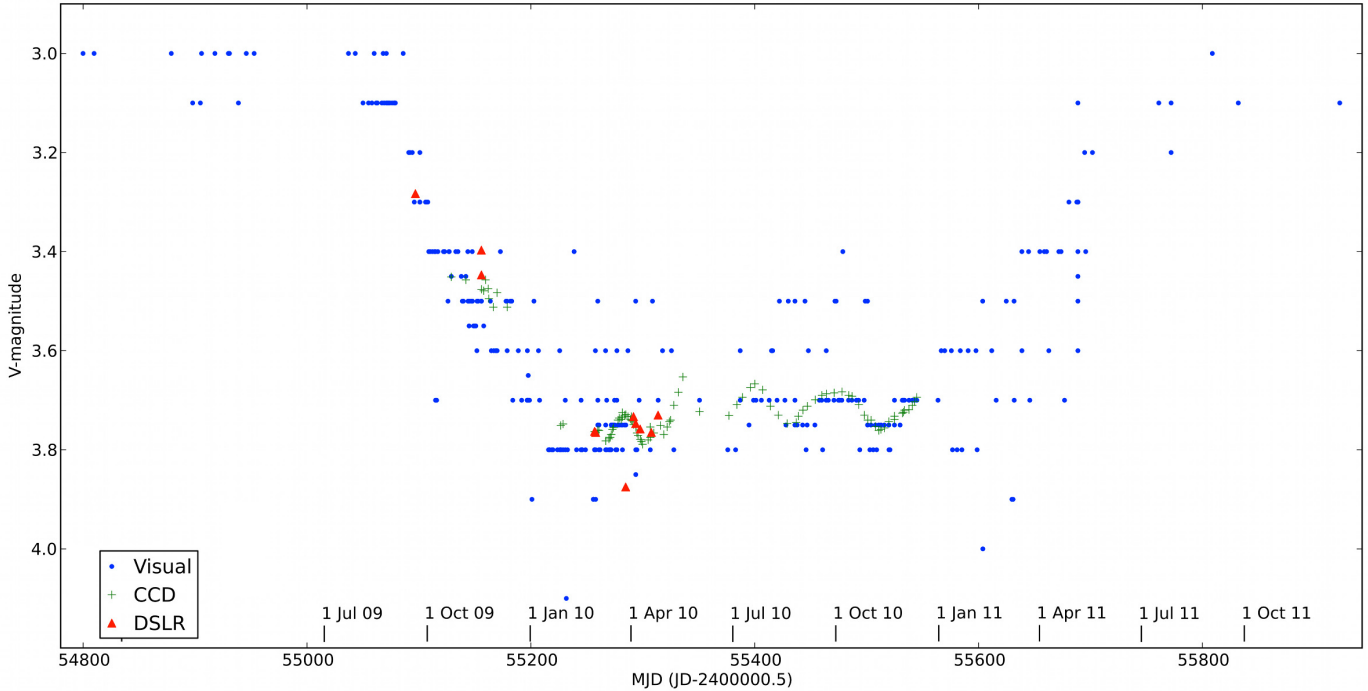

Figure 3. The 2009–2011 eclipse of ε Aur as derived from observations (visual is indicated with a dot, CCD is indicated with a cross, DSLR is indicated with a triangle) obtained by Greek observers, members or not of the Hellenic Amateur Astronomy Association (the list of contributors is presented in Tables 1 and 2).

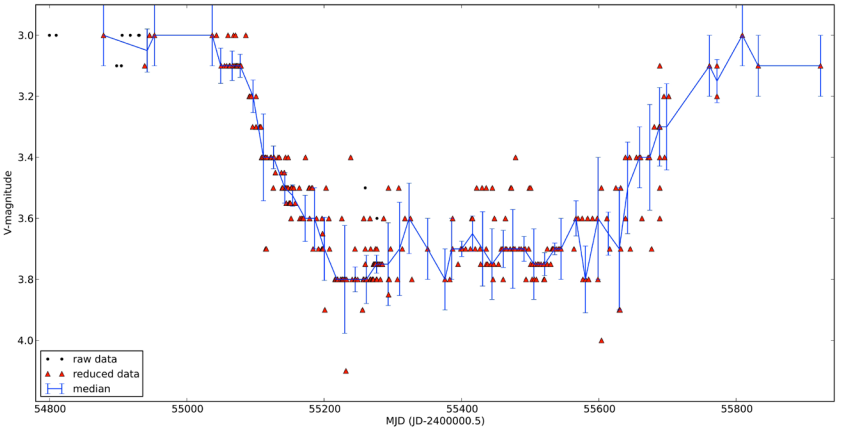

Figure 4. Plot of visual observations along with the median values of the binned data (15 days). From the initial data (indicated as "raw data") values outside the $3 \times \sigma$ were removed and we binned the remaining ones (indicated as "reduced data") providing the median value and its corresponding standard deviation σ (indicated as "median line"). Interesting results are presented in section 4.2.

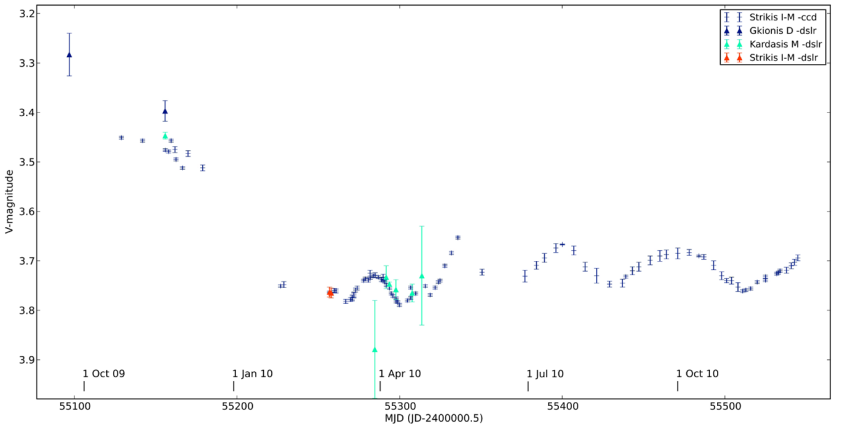

Figure 5. Plot of the digital (DSLR identified as triangles, and CCD identified as crosses) observations during the 2009–2011 eclipse of ε Aur (see section 4.3 for details). The DSLR point just before April 1st, 2010, is a poor result probably due to the presence of thin clouds.

Photoelectric Photometry of ε Aurigae During the 2009–2011 Eclipse Season

Frank J. Melillo
Holtsville Observatory, 14 Glen-Hollow Dr, E-16, Holtsville, NY 11742; FrankJ12@aol.com

Received February 13, 2012; revised March 1, 2012; accepted March 1, 2012

Abstract A total of 100 V-band photometric observations were made at Holtsville Observatory for the 2009–2011 eclipse of ε Aurigae. A light curve has been plotted using data from these observations which covers the phases before, during, and after the eclipse. The light curve shows precise timing during the first, second, third, and fourth contacts, which mark important parts of the eclipse. The magnitudes and duration of the eclipse in the photometric V band are discussed.

1. Introduction

ε Aurigae is different from other binary star systems. It has been a mysterious star to us since 1821 when it was first noticed that it was a variable, but it was not well known until the early1900s. This star is the longest period eclipsing binary ever studied. What's so mysterious about ε Aur is that we do not know much about its eclipsing object. Even though the eclipsing object has been well identified as existing, it is still unclear what it is made of. With its 27.1-year period, it is a slow eclipse lasting a total of 1.75 years. Regardless of what equipment you use to study this binary system, there is no clear clue about the eclipsing object. Using photometry, spectroscopy, polarimetry, and interferometry, we are beginning to get an indication of its nature. During the time of the eclipse, ε Aur dims about 0.8 magnitude and then returns to a normal brightness.

What is known about this binary star system is that the eclipsing body's orbit is in our line of sight. Every 27.1 years, ε Aur undergoes an eclipse which means the unknown secondary object passes in front of a star as seen from the Earth, causing the light to dim (Hopkins *et al.* 2006). The ε Aur system is so strange that it is unique. With such a rare binary star system, it is difficult to study the eclipse every 27.1 years. Something is orbiting ε Aur, but what is it?

ε Aur is known to be a F0-type star and it is a highly luminous supergiant at V magnitude 3.00. The eclipsing object orbiting this F0-type star doesn't exhibit any spectrum of its own but it is most likely to be a hidden B-type star. The disk must be dark but have transparent regions. But during the eclipse, still it is thick enough to obscure some of the light from the F0 star. The visual light can dim about 0.8 magnitude even though the spectrum does not change. Also, the F0

star itself is a variable and it is perhaps a semiregular type. It is a pulsating star outside of the eclipse with a period of 60 to 65 days. The amplitude can change as much as 0.15 magnitude in addition to the eclipse.

ε Aur has been studied substantially every 27.1 years. The 1982–1984 eclipse was observed by many amateur astronomers, by ground-based professional observatories, and from space. No matter what data were collected, still it was a completely mysterious star. There is so much interest in this binary that all observers are trying to squeeze out as much detail as possible about the secondary. What we really see is only the light of the primary star.

The long awaited ε Aur 2009–2011 eclipse is finally over. Prior to 2009, many organizations and observing campaigns were formed (Hopkins *et al.* 2008). This author is participating in one organization, which is run by Jeffrey Hopkins of Phoenix, Arizona. During the 2009–2011 eclipse, many amateur astronomers were equipped with the most advanced technology, especially in spectroscopy, which plays an important role for ε Aur where the secondary can be detected at certain wavelengths. Also, the Center for High Angular Resolution Astronomy (CHARA) operates an interferometer on Mount Wilson in California (Kloppenborg *et al.* 2010). With up to six telescopes combined together in infrared light, they have successfully imaged ε Aur. They were able to detect an elongated object partially obscure the primary disk. The ε Aur eclipse of 1982–1984 was successful but left us many questions for the 2009–2011 season. Hopefully many amateur and professional astronomers can shed new light on the secondary this time. This author carried out photoelectric photometry in V light during the 2009–2011 eclipse, and it is described here.

2. Method

Photoelectric photometry was the only method this author used to monitor the entire eclipse of ε Aur. The observations provided an excellent coverage in V band. It is a Johnson-type filter with a peak spectral response at 5400nm. The readings were taken photometrically using a SSP3 OPTEC photo counting photometer coupled on a Celestron 8-inch *f*/10 telescope. λ Aur was the comparison star at V magnitude 4.71. It is located just four degrees east-southeast of ε Aur and it was an excellent choice to compare its brightness and to minimize the atmospheric coefficient during the 2009–2011 eclipse season.

For each set, four readings were taken at ten seconds' integration time for ε Aur, sky readings, and then the comparison star, λ Aur. This author sometimes monitored three to four sets, depending on the weather condition and time. Once the observing night was over, the readings could be calculated. The photometric readings of ε Aur, the sky, and λ Aur were averaged. Then, the sky was subtracted from both stars' readings. That left the ratio brightness between ε Aur and λ Aur. Once the ratio was calculated, ε Aur's brightness could be determined with the known magnitude of λ Aur. Also, the Standard

Deviation (SD) was calculated to analyze how much error was in the readings. Most of the time, the error amount was from 0.012 magnitude to as much as 0.0427 when all the readings were calculated. The altitude was also calculated to determine the air mass during the time of the observations. During the observing run, the higher the stars, the better chance of getting the accurate readings from the photometer.

Many factors had to be also considered: seeing conditions, the winds, periodic clock drive error, polar alignment, and the stability of the photometer, which can all affect the readings. During most nights, the seeing condition was above average with no winds, and the periodic clock drive error was noticeable at times. Being that a portable observatory was used, the polar axis was aligned as close as possible to the celestial north pole. Therefore, in spite of the small drift, the star still stayed inside the reticle circle during the length of time. For the SSP-3 OPTEC photometer itself, the unit was turned on at least an hour before the start of the first counts. This "warm up" routine stayed on until the photometer dark count was stable enough for accurate readings. In fact, the colder the outside air temperature was, the more time the photometer needed to warm up. The unit was running on a 9-volt battery to avoid the power cord tangle-up during the night's run. In the photoelectric photometry method, the accuracy can be little as 0.01 magnitude. This author's readings were close enough to generate the shape of the light curve (see Figure 1 and Table 1).

3. Observations

ε Aur is located in the constellation Aurigae as a third magnitude object and passes nearly overhead most evenings, as seen from the Holtsville Observatory. All photoelectric photometry results were taken from Holtsville Observatory, located under a moderately light-polluted sky fifty miles east of New York City. ε Aur is easily visible to the naked-eye and it is one of the three stars forming the asterism "The Kids," near α Aur (Capella).

This author was gearing up for the first eclipse of the Millennuim. Prior to the start of the eclipse, the first contact was predicted to occur in August 2009 (Hopkins *et al.* 2009). The observations commenced on December 3, 2008, during the 2008–2009 observing season to develop a baseline for the light curve. The photometric readings were taken nightly, weather permitting, until the star reached a conjunction with the sun in June 2009. Within this period, ε Aur was showing a slight variation averaging V magnitude 3.00 out-of-eclipse (OOE). The variation had nothing to do with the eclipsing object. ε Aur itself is a variable and perhaps a semiregular type with amplitude of 0.10 magnitude. The last readings of the observing season in V band showed no indication of the upcoming eclipse.

After the solar conjunction, the observation resumed for the 2009–2010 observing season. The first reading was on August 14, 2009, in the

morning sky. Even though the exact start of the eclipse was predicted to be on August 6, 2009, everything looked normal. After several weeks, it got very interesting. Since the start of the new observing season, ε Aur had dimmed considerably. This author didn't know whether or not this was due to ε Aur's variation itself or the start of the eclipse. As ε Aur continued to dim, the partial eclipse had actually begun, but it wasn't confirmed until after mid-September when the magnitude dropped below 3.15 V.

The excitement built up as ε Aur's brightness continued to fall. This author took photometric readings in V band on an average of two nights per week. At certain points of the declining phase, ε Aur's brightness reduction slowed down a bit. This was due to the variation of the star itself. It formed a somewhat wavy pattern as it continued to dim.

At this part of the declining stage, the author was getting ready for the second contact. It wasn't until the end of December 2009 when the brightness decline slowed down a lot at 3.70 V. It still showed a slight dimming until late February 2010 when the light curve reached rock-bottom at 3.78 V—but this was not necessarily the second contact. While ε Aur itself varied within 0.10 magnitude the whole time, this might have interfered with the actual time of the second contact, which should be the beginning of the totality. The second contact was predicted on December 19, 2009, and it looked like it was right on schedule, but the OOE variability caused the light curve to dim even further. After the second contact, ε Aur showed a small variation even in totality. The light curve could be easily identified as a semiregular type with a 65-day period.

Here is the interesting part: ε Aur is known to show a surge of brightness as it nears to mid-totality, which may cause perhaps a small gap in the middle of the eclipsing body to allow the F0 star to shine through. This mystery has not been explained yet, but hopefully it can be solved this time. The mid-totality was scheduled to happen by early August 2010. This author tried to take readings as much as possible while ε Aur was approaching solar conjunction, but, unfortunately, the readings were taken at low altitude in the northwest after sunset. The accuracy of the photometric measurement was not as great, but any attempt to take readings was worthwhile. According to the last two nights in May 2010, this author may have caught a surge of brightness to 3.55 V. The photometric results may not been proven yet because the author did not know whether this was caused by atmospheric turbulence from the low altitude, ε Aur's variation itself, or the F0 star shining through the gap. ε Aur was not in a good position to take further readings and it went through the solar conjunction in June 2010.

The 2010–2011 observing season began when ε Aur was just past the mid-eclipse stage. The observations resumed on August 13, 2010, early in the morning sky. There was no surge of brightness at mid-eclipse that was expected just shortly before the solar conjunction. At this time, the expected surge of brightness may or may not have occurred at exactly mid-eclipse. This is yet to be determined.

The brightness of ε Aur varied within 0.10 magnitude throughout the whole second half of the eclipse, with the magnitude averaging at 3.71 V. Even at totality, ε Aur clearly demonstrated a 65-day variation unrelated to the eclipsing body. The star was monitored on an average of once per week, and the author prepared for the third contact, which was predicted for March 19, 2011. During that month, the star's brightness became a little strange. According to the irregular 65-day pattern, ε Aur was expected to get a little brighter. Instead, it went off track a bit. As this time, we don't know if this was related to the eclipsing body or the result of the star's irregular-type behavior. After March 19, 2011, the brightness began to rise quite rapidly, which indicated the third contact had passed. The total eclipse was over and this was the beginning of the partial phase. It had risen at a faster pace than during the declining stage. The fourth contact was scheduled for May 19, 2011. Earlier that month, the brightness leveled off at 3.25 V. Again, this could be ε Aur's variation itself, but at the same time, the photometric readings were getting difficult to obtain due to the lower altitude in the northwest. The fourth contact, which marks the end of the partial phase, was probably not caught. In late May 2011, ε Aur was approaching solar conjunction and therefore no more readings were taken.

More observations of ε Aur began in September 2011, after solar conjunction. Even though the eclipse ended after the fourth contact around late May or June, this author continued to monitor this star just to confirm that the eclipse was over. The star returned to a normal brightness at an average of 3.00 V, just as before the eclipse. After monitoring the entire eclipse of ε Aur, the photometric observations ceased after two years and nine months.

4. Conclusion

Only the V band at a peak spectral response 5400 nm was used to determine the accurate shape of the light curve. The result may be similar to the 1982–1984 eclipse but a closer look might detect some differences, especially in spectroscopy. However, the mid-eclipse brightening is still a mystery and it wasn't well observed due to the time of the solar conjunction. It is still premature to draw any conclusion whether the mid-eclipse brightness took place in this cycle.

The contact points need further analysis in order to draw any conclusion. It is quite difficult to obtain the data of the contact time just by one person. There are gaps between the observations and probably the actual contact time may be missed even by one day. But the author's light curve was constructed (see Figure 1) and we see two different types of variations. While ε Aur is a semiregular type variable star, the 65-day cycle 0.10 magnitude is clearly seen in the light curve. Secondly, the eclipsing object of a 27.1-year period is obvious—seen at 0.70 magnitude amplitude. With 100 data points, one can show that the eclipse took place but not clearly mark the contact points. The

actual time of the contact points may be confused by ε Aur's 65-day cycle, and the 0.10-magnitude variation is enough to bury the actual contact times. Using only the author's data, it would be premature to draw more specific conclusions about the contact times. Data from other observers may fill in the gaps and therefore the contact times may be determined. Also, the results may be compared with eclipses of the past to see whether there is any significant difference. While the photometric data gathered by participants is much more sophisticated than for the past eclipses, the truly new type of data is the spectroscopy. With today's advanced technology, this collective photometric and spectroscopic data set is the best ever obtained. The ε Aur 2009–2011 eclipse is behind us and the results will be studied for many years to come. Still, there will be more questions than answers. Hopefully, we will have more answers by the next eclipse in 2036–2038.

References

Hopkins. J. L., *et al.* 2006, "Long-Period Eclipsing Binary System ε Aur Eclipse Campaign," Presented at the May 2006 Society for Astronomical Sciences Symposium, Big Bear, California.

Hopkins J. L., *et al.* 2008, "Gearing Up for ε Aur's First Eclipse of the Millennium," Proceedings for the 27th Annual Conference of the Society for Astronomical Sciences.

Hopkins, J. L., *et al.* "2009: The eclipse begins—Observing Campaign Status," Presented at the Society for Astronomical Sciences Symposium.

Kloppenborg, B., *et al.* 2010, *Nature*, **464**, 870.

Table 1. Differential photometry of ε Aurigae.

UT Date	*JD*	*V Filter*	
		Magnitude	*Standard Deviation*
2008 Dec 03	2454803.73611	2.97	0.02569
2008 Dec 13	2454813.7222	3.04	0.01987
2008 Dec 26	2454826.6875	2.99	0.02654
2009 Jan 04	2454835.70833	2.98	0.02987
2009 Jan 22	2454853.59722	2.98	0.02226
2009 Jan 30	2454861.70833	2.99	0.02321
2009 Feb 09	2454871.625	3.02	0.00754
2009 Feb 21	2454883.70833	3.07	0.01987
2009 Mar 18	2454908.64583	3.08	0.01402
2009 Apr 06	2454927.58333	3.07	0.01954
2009 Apr 13	2454934.61806	3.0	0.01563
2009 May 21	2454972.5625	2.92	0.04598
2009 Aug 15	2455058 +	2.97	0.01548
2009 Aug 23	2455066.79167	3.01	0.02112
2009 Aug 31	2455074.76389	3.02	0.01548
2009 Sep 06	2455080.76042	3.04	0.01289
2009 Sep 14	2455088.73611	3.1	0.01985
2009 Sep 18	2455092.73611	3.13	0.00874
2009 Sep 20	2455094.75	3.16	0.01482
2009 Sep 26	2455100.72625	3.2	0.01365
2009 Sep 28	2455102.72625	3.21	0.01759
2009 Oct 02	2455106.71139	3.25	0.02236
2009 Oct 06	2455110.69819	3.28	0.02
2009 Oct 12	2455116.71146	3.32	0.01913
2009 Oct 20	2455124.66993	3.33	0.01775
2009 Oct 26	2455130.69507	3.37	0.0188
2009 Oct 30	2455134.6559	3.38	0.01999
2009 Nov 04	2455139.70882	3.4	0.02198
2009 Nov 09	2455144.65146	3.41	0.01559
2009 Nov 18	2455153.71319	3.44	0.02646
2009 Nov 21	2455156.70903	3.44	0.02429
2009 Nov 29	2455164.75347	3.48	0.03114
2009 Dec 04	2455169.71424	3.53	0.01975
2009 Dec 11	2455176.71243	3.57	0.0204
2009 Dec 17	2455182.63146	3.62	0.0173
2009 Dec 22	2455187.72181	3.66	0.0124
2009 Dec 28	2455193.6325	3.67	0.01215
2010 Jan 11	2455207.63194	3.68	0.01614
2010 Jan 15	2455211.52264	3.68	0.02811

table continued on following pages

Table 1. Differential photometry of ε Aurigae, cont.

UT Date	*JD*	*V Filter*	
		Magnitude	*Standard Deviation*
2010 Jan 19	2455215.52937	3.68	0.0363
2010 Jan 23	2455219.75847	3.69	0.02937
2010 Jan 28	2455224.51042	3.7	0.01443
2010 Feb 01	2455228.70486	3.7	0.02712
2010 Feb 08	2455235.62917	3.72	0.01923
2010 Feb 13	2455240.71597	3.73	0.02232
2010 Feb 20	2455247.71347	3.77	0.01564
2010 Mar 03	2455256.63194	3.76	0.02179
2010 Mar 07	2455262.52986	3.76	0.0174
2010 Mar 17	2455272.64306	3.74	0.01712
2010 Mar 25	2455280.64938	3.73	0.02301
2010 Apr 02	2455288.65486	3.74	0.02851
2010 Apr 15	2455301.56736	3.78	0.01706
2010 Apr 20	2455306.62931	3.76	0.02374
2010 Apr 24	2455310.62778	3.76	0.03999
2010 Apr 29	2455315.60361	3.76	0.04549
2010 May 06	2455322.56451	3.78	0.02002
2010 May 16	2455332.5711	3.71	0.03709
2010 May 17	2455333.57111	3.69	0.03997
2010 May 27	2455343.55278	3.56	0.02828
2010 Aug 14	2455422.82389	3.68	0.01155
2010 Aug 21	2455429.81597	3.68	0.02243
2010 Aug 28	2455436.79354	3.7	0.01768
2010 Sep 05	2455444.77292	3.7	0.02137
2010 Sep 15	2455454.73403	3.67	0.02348
2010 Sep 21	2455460.73056	3.65	0.03312
2010 Oct 03	2455472.72431	3.65	0.01199
2010 Oct 09	2455478.71007	3.68	0.03198
2010 Oct 18	2455487.65347	3.67	0.0159
2010 Oct 23	2455492.68597	3.7	0.0128
2010 Nov 01	2455501.64625	3.73	0.02182
2010 Nov 06	2455506.68056	3.73	0.02324
2010 Nov 13	2455513.72514	3.75	0.0194
2010 Nov 20	2455520.72222	3.74	0.01928
2010 Nov 29	2455529.64236	3.72	0.03263
2010 Dec 08	2455538.71181	3.7	0.01633
2010 Dec 18	2455548.71042	3.68	0.01852
2010 Dec 30	2455560.63889	3.71	0.03079
2011 Jan 06	2455567.52431	3.75	0.03577

table continued on next page

Table 1. Differential photometry of ε Aurigae, cont.

UT Date	*JD*	*V Filter*	
		Magnitude	*Standard Deviation*
2011 Jan 14	2455575.52694	3.75	0.01603
2011 Jan 31	2455592.63472	3.74	0.02098
2011 Feb 04	2455596.52847	3.76	0.02623
2011 Feb 11	2455603.53104	3.75	0.01365
2011 Feb 23	2455615.52639	3.76	0.02029
2011 Mar 02	2455622.69104	3.73	0.03067
2011 Mar 09	2455629.69313	3.71	0.03032
2011 Mar 14	2455634.59722	3.67	0.02517
2011 Mar 20	2455640.69722	3.59	0.04129
2011 Mar 25	2455645.69604	3.55	0.02363
2011 Mar 29	2455649.70271	3.5	0.03054
2011 Apr 06	2455657.65646	3.42	0.02266
2011 Apr 22	2455673.65542	3.31	0.03364
2011 May 01	2455682.58889	3.35	0.3777
2011 May 06	2455687.57313	3.32	0.03628
2011 May 11	2455692.57201	3.3	0.01258
2011 May 12	2455693.56646	3.26	0.02463
2011 May 26	2455707.55549	3.3	0.05566

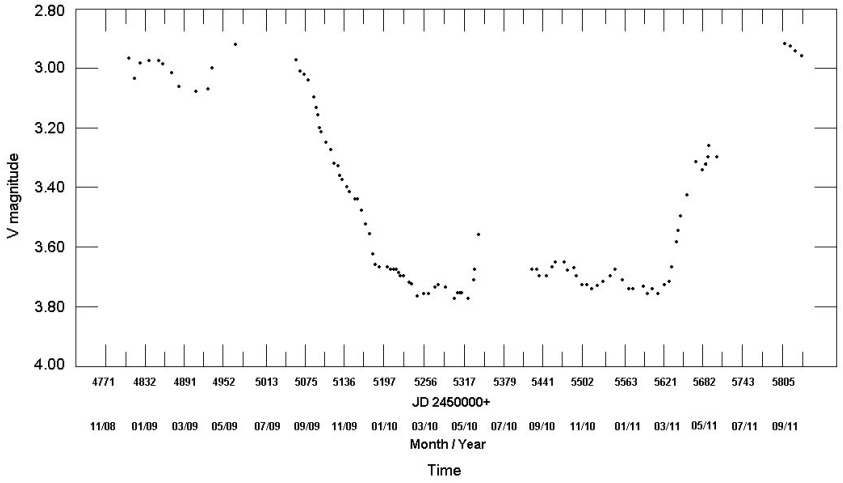

Figure 1. Light curve of ε Aur, 2008–2011. V magnitude is with respect to λ Aur comparison star at V magnitude 4.71.

Small Telescope Infrared Photometry of the ε Aurigae Eclipse

Thomas P. Rutherford
201 Clear Branch Circle, Blountville, TN 37617; sternwachter@netscape.net

Received May 15, 2012; revised June 18, 2012; accepted June 18, 2012

Abstract Near-infrared photometry of ε Aurigae, in the H- and J-bands, was undertaken during the 2009–2011 eclipse using telescopes of moderate size (8-inch and 14-inch diameter). Instruments of this size successfully collected scientific data in the H- and J-bands. Observations were made from the campus of East Tennessee State University (ETSU), Johnson City, Tennessee, the campus of King College, Bristol, Tennessee, and from the author's home. Signal/Noise ratios of approximately 45 were obtained during times of maximum eclipse. Higher S/N ratios could have been obtained by extending the length of time on target. S/N ratios of almost 100 were obtained outside of eclipse. The infrared light curves produced closely parallel the light curve in the visual range (V), being about 0.5 magnitude brighter in H and 0.7 magnitude brighter in J. The eclipse was easily detected and followed throughout its duration. The rate of ingress was shallower than the rate of egress in both the H- and J-bands. The background variations of the primary star were readily detected.

1. Introduction

The variable star ε Aur has been of interest to astronomers for almost two centuries due to its long period (27.1 years) and the long duration (approximately two years) of its eclipses. With such a long eclipse, the occulting object can not be another star, but must be some other type of object. The exact nature of the eclipsing object has been a mystery, although more information becomes available each time an eclipse occurs. This is due to both an increase in the number of observers and also collection of data in additional wavelengths not utilized in previous eclipses. The current model of the occulting object is that of a large, cool disk which contains a central B-type star (Stencel 2011).

Infrared photometry has, until recently, been the province of professional astronomers, using large telescopes, sophisticated infrared detectors, and high-altitude observing sites. UKIRT, SOFIA, IRTF, and Spitzer are a few of the professional instruments that come to mind. It is now possible for the average variable star observer, using a common telescope of modest size, to work in the near-infrared part of the electromagnetic spectrum and to produce high quality, scientifically useful results. The recent eclipse of ε Aur provided an excellent opportunity to demonstrate these capabilities; during previous eclipses, infrared studies were restricted to professional observatories since amateur observers did not have the capabilty.

There are numerous advantages (and some disadvantages) for the observer who works in the near-infrared when compared to visual-band photometry (Templeton 2011a):

1) The sky is very dark in the infrared; there is little infrared light pollution. An infrared observer can work under conditions that would make visual-band photometry difficult.

2) Atmospheric extinction, while present, is low compared to the visual wavelengths. As the eclipse neared its end, some data were collected at the very high airmass of 5; this high airmass did cause an increase in noise, but the S/N ratio was still adequate.

3) Many variable stars are brighter in the infrared than at visual wavelengths (some are much brighter). ε Aur was no exception to this; throughout the eclipse, the J-band readings were about 0.5 magnitude brighter than in V, while the H-band readings ran close to 0.7 magnitude brighter than in V. This can be seen in Figure 1.

4) There are few infrared observers. While for some stars, visual-band observers (V in particular) will find their data lost in the crowd and so contribute little, this is not the case in the infrared. For the duration of this project (November 2008–present) there were only two observers submitting H- and J-band data to the AAVSO.

5) Water is an absorber of infrared radiation. Even though the sky may look clear, there will sometimes be too much water vapor in the air. Some of the noisy data collected early in the eclipse were due to attempts made on poor nights.

2. Equipment

The equipment used during the eclipse consisted of an Optec SSP-4 photoelectric photometer with a manual filter slide holding H- and J-band filters. The H- and J-band filter band-passes are closest to the Mauna Kea Observatory (MKO) and Caltech/Tololo (CIT) systems (Henden 2002). The gallium-arsenide (GaAs) detector in the SSP-4 is one millimeter across (about 100 arc seconds at the focal plane of an 8-inch SCT operating at *f*/10). A version of the photometer is available with a smaller, 0.3-mm detector, but the smaller detector gives less satisfactory results (Hopkins 2006a).

The SSP-4 photometer is the result of a collaborative program between the AAVSO and Optec, Inc. (West 2007). It contains an eyepiece for centering the target and comparison stars, a flip mirror for sending the image to the detector after centering, and a filter slide containing the H- and J-band filters; the filter slide and flip mirror are operated manually.

The software which Optec provided for use with the photometer was utilized for most of the observations, although an alternate software package,

written by Brian Kloppenborg at the University of Denver, was used on occasion (Kloppenborg 2011). This software gave greater control over the photometer, but the Optec software made a better match with the particular spreadsheet that was in use. Both software packages ran without issue on an older laptop computer running Windows XP Pro. This computer was used for both telescope and photometer control. The computer had 1 GB of RAM and a single-core Celeron processor; it had no problems controlling both instruments at the same time.

Three different telescopes were utilized during the eclipse: an 8-inch Meade LX200, a Celestron C14, and a Meade 8-inch LX90. The two Meade SCTs were fork-mounted on equatorial wedges, while the C14 was mounted on a German-equatorial mount (GEM). All of the telescopes proved adequate to the task, although the C14, due to its larger aperture, gave the best results in the shortest period of time.

3. Observations

When preparations began for the upcoming eclipse during the summer of 2008, an 8-inch Meade LX200 located at ETSU's Powell Observatory was utilized. It is reported that a 10-inch telescope is the minimum useful size for infrared photometry of ε Aur due to the faintness of the traditional comparison star, λ Aur (Lucas *et al.* 2006). λ Aur is faint in the infrared (mag_h = 3.33, mag_j = 3.62), making it difficult to use with a smaller telescope. The solution was to use a brighter comparison star—the AAVSO recommendations for telescopes under 0.25 meter (10 inches) are to use Capella as the comparison star and β Tau (el Nath) as the check star (Templeton 2011b).

The two Meade telescopes were controlled with Meade's AUTOSTAR software. Although other control software was tested, the Meade software proved to be very capable and worked well. The C14 was controlled using STARRY NIGHT PRO 5, which also worked well. The goals initially were: 1) collect pre-eclipse data on ε Aur, 2) take measurements of standard stars to be used for calibrating the photometer/telescope combination, and 3) measure other variable stars on the AAVSO's IR photometry list.

The first observations of ε Aur occurred on November 2, 2008. The star was kept under observation (from the ETSU observatory) from that date until it was lost to the sun in late May 2009. ε Aur was re-acquired on the morning of July 24, 2009, and at that point, it became obvious that there would soon be a problem. The author's "day job" is that of a high school chemistry teacher—once school began after the summer break, it would not be possible to make the forty-five-minute drive to ETSU early in the morning, get set up, collect the data, get everything put away, and then get to school in time for the start of classes.

A search for a suitable telescope to use from the author's home was started and a used Meade 8-inch LX90 (UHTC coatings) with an equatorial wedge

was found. It was purchased and set up on a concrete pier at the author's home. The LX90 was not as accurate as the LX200, but its tracking and pointing abilities were more than adequate for use with the 1-mm detector of the photometer. The onset of the eclipse in August 2009 was easily detected.

As the eclipse deepened, it became apparent that a larger telescope would give better results, as the brightness of ε Aur was decreasing. A discussion with AAVSO Director Arne Henden, while he was on a speaking engagement at ETSU, led to the advice that longer time on target was one solution (Henden 2009). This worked, but the time involved increased as well.

At this point, about 1.5 hours of collecting data were required for the two data points (one each in H and J). The infrared sky is not transparent over long periods of time (Henden 2002), especially in the Southeastern United States. A larger telescope would allow shortened observation times. King College, in Bristol, Tennessee, offered the use of their Celestron C14 located at the college's Burke Observatory. The college's physics department allowed use of the telescope when it was not being otherwise utilized.

The C14 made a large difference in the S/N ratio. It was used for the remainder of that observing season, although a move back to the ETSU telescope was required in late May (trees became an issue). During the last year of the eclipse, the C14 began to be utilized more often by King College and so observations moved back to the LX90 and the LX200. Currently, the LX90 is the primary instrument used for post-eclipse monitoring.

4. Data collection

Prior to a night's observations, the photometer was powered up and hooked to the laptop computer. The photometer drew from its own external power supply, but was controlled by software on the laptop through a USB cable. The photometer's temperature control was set to –40° Celsius (below ambient).

When first turned on, the photometer typically produced high dark counts—these decreased as the instrument stabilized (30–60 minutes after power-up). The dark counts would normally drop slowly during the run, but not so far that they became a problem. While the photometer was stabilizing, the telescope was set up, polar-aligned, and placed under control of the laptop (the C14 was permanently mounted, the other two telescopes were not). Prior to starting the data run, the photometer's dark counts were checked and the gain control adjusted to bring them into the range recommended by Hopkins (2006b). The photometer was then set to a gain of 100, with a 10-second exposure.

The comparison star, α Aur (Capella), was measured with both H and J filters. The telescope was then off-set slightly and a reading on the sky was made, once again in both filters; the pattern used was "comp H, comp J, sky J, sky H." The telescope would then be pointed at the variable star (ε Aur) and the same pattern repeated "variable H, variable J, sky J, sky H." Then back to

α Aur where the pattern was repeated once again. The last measurement of the night was of the check star (β Tau) since it had lowest priority (Schmidke and Hopkins 1990). This procedure produced one data point in each filter. A minimum of three such observations were required so that meaningful statistics could be calculated; more than three observations were necessary due to the small size of the telescopes used.

The photometer software, provided by Optec, allowed the photometer to take one exposure, three sequential exposures, or four sequential exposures. When the project first began, three exposures of ten seconds each were taken, followed by three exposures on the sky and then back to the comparison star where three more exposures were made (according to the above description). These three observations were then averaged. This was repeated at least three times (or five or seven, and so on.). Each group of three readings was averaged down to one reading and then the three (or five or seven, and so on) single readings were averaged to give a single number for the star's brightness for that night's observations. This was then repeated using the other filter. The time involved for this was significant, especially in the beginning.

This method worked well, except when the sky was rapidly changing or for observations made at high airmass—the sky would simply change too quickly between one measurment and the next. It was realized that averaging the data twice did not help in terms of S/N and added a great deal of time to the operation. As the eclipse neared its end, "single shot" readings began to be taken—comp, sky, var, sky, comp, sky—one reading each, not grouped into threes. This produced data that were generally better, if the stars were under changing sky conditions, than the "group of three" method mentioned above. Because of the speed at which the readings could be taken, data could be collected at high airmass and still not be too noisy.

Originally this pattern was repeated three times, but it was found that the total counts were low, (except when using the C14), so it was increased to five sets, then to seven, and finally to nine sets. Nine repetitions were not practical, so eventually seven sets were settled upon—this gave the best trade-off between time involved and S/N ratio.

5. Data reduction

A Microsoft EXCEL spread sheet was developed, using a format that allowed the observer to simply cut and past the data from the photometer's native output file directly into the spreadsheet.

The data output of the photometer contained columns of data, representing such things as date, time, filters used, gain settings, length of exposure, and numbers which represent the photons detected during the run. It was in an EXCEL-readable format. Several quantities must be calculated from this information:

1) The telescope's location—this information, along with the sidereal time, was needed to calculate the local hour angle and from that, atmospheric extinction,

2) Time and date of the observation converted into Julian Days—the data run consisted of several readings so the timestamp of the central value of the set was used as the time of observation.

3) Filters used—the EXCEL sheet did not utilize these data, but it allowed sorting of the data prior to pasting them into the spreadsheet.

4) Gain and exposure times—this information was used to reduce the total counts down to "counts per second" so the brightness of the star at the time of the observation could be determined.

The averaged photometer readings mentioned previously represented the number of photons that arrived from the target star during each exposure. Several additional corrections to these raw counts were necessary in order to get the star's true magnitude in each filter. A summary of the procedures are listed below. The full procedures and equations used may be found in Henden and Kaitchuck (1982), Hall (1988), and Schmidke and Hopkins (1990):

1) Convert the raw counts into instrumental magnitudes.

2) Calculate the difference in brightness between the target star (ε Aur) and the comparison star (α Aur). The value used for α Aur was the average of the readings taken just before and just after the reading on ε Aur.

3) Apply an extinction correction to the differential magnitude of the target star. This extinction correction is necessary due to the difference in airmasses between the comp and target stars. In the case of the α Aur-ε Aur pair, the difference was slight while the stars were rising in the east (late summer), but increased as they traveled westward, reaching a maximum in late spring.

4) Apply a correction for the instrumental color response for the system—this final correction adjusts the magnitudes to the standard system.

There are other, additional corrections that could have been performed on the data. However, the impact of those corrections is very slight in the infrared (Henden 1982) and so those corrections were not made.

6. Results

Although this project was primarily instrumental in nature and not analytical, some conclusions about the eclipse can be drawn from the data:

1) ε Aur is fainter in the J band than in the H band, both in and out of eclipse (see Figure 1).

2) The background variations of the primary are evident, both in and out of eclipse (Figure 1).

3) The second half of the eclipse is not as deep as the first half—perhaps the trailing side of the disk is thinner than the leading side or it might not cover the primary to as great an extent.

4) A comparison of the rates of change during ingress and egress in both filters show that the eclipse ended at a greater rate than it began. This can be seen in Figures 2 and 3. The slopes of the ingress stages were 0.0045 mag./JD in H and 0.0048 mag./JD in J, while those of the egress portions were 0.0060 mag./JD in H and 0.0067 mag./JD in J.

These slopes are very shallow due to the long duration of the eclipse. Data points for making slope determinations were chosen from when both the ingress and egress stages were well underway.

5) By taking the slopes of the pre- and post-eclipse stages and overlaying them on the slopes of the ingress and egress stages, it is possible to determine the dates of the eclipse's onset and ending in the H and J bands.

An examination of Figure 2 and Figure 3 shows that the eclipse began around JD 2455046 in H and JD 2455057 in J (3 August 2009 in H and 14 August 2009 in J). There is a large amount of scatter in the pre-eclipse J band data points and this might explain the variation in the starting dates between the two filters. The eclipse appeared to end on JD 2455707 in both the H and J bands (26 May 2011).

7. Conclusions

Near-infrared photometry in the H and J bands can be successfully undertaken using a telescope of modest size, such as an 8-inch Schmidt-Cassegrain. Care should be taken in the choice of comparison, target, and check stars in order to keep signal/noise ratios as high as possible. The ε Aur eclipse did fall within the reach of this type of setup, but at its deepest, the drop in the S/N ratio was very apparent. Target stars for such a setup should be brighter than about magnitude 2 in the chosen filters, if possible. Fainter stars can be monitored, but require long data collection times in order to keep the signal at acceptable levels.

8. Acknowledgements

The author would like to thank the following individuals and institutions for their guidance and assistance in this project: Dr. Gary Henson, ETSU; Dr. Beverly Smith, ETSU; Dr. Ray Bloomer, King College; Dr. Edward Burke, King College (deceased); ETSU Department of Physics and Astronomy; and the American Association of Variable Star Observers.

Special thanks to my wife and family for all the long hours and complaints about the clouds.

References

Hall, D. S., and Genet, R. M. 1988, *Photoelectric Photometry of Variable Stars*, Willmann-Bell, Richmond, VA.

Henden, A. A. 2002, "JHK Standards for Small Telescopes" (http://www.aavso.org/sites/default/files/webpublications/ejaavso/v31n1/11.pdf).

Henden, A. A. 2009, private communication.

Henden, A. A., and Kaitchuck, R. H. 1982, *Astronomical Photometry*, Van Nostrand Reinhold, New York.

Hopkins, J. L. 2006a, "Photoelectric Photometry Whitepaper, SSP-4 Detector" (http://www.hposoft.com/Astro/SSP-4/WhitePapers/Detector.html).

Hopkins, J. L. 2006b, "Photoelectric Photometry Whitepaper, SSP-4 Observation Techniques" (http://www.hposoft.com/Astro/SSP-4/WhitePapers/Techniques.html).

Kloppenborg, B. 2011, "SSP-4 Control Software" (http://finiteline.homeip.net/redmine/projects/ssp-4-control/wiki/Wiki).

Lucas, G. A., Hopkins, J. L., and Stencel, R. E. 2006, in *The Society for Astronomical Sciences 25th Annual Symposium on Telescope Science*, Society for Astronomical Sciences, Rancho Cucamonga, CA, 25.

Schmidke, P. C., and Hopkins, J. L. 1990, *Workbook for Astronomical Photoelectric Photometry*, HPO Desktop Publishing, Phoenix, AZ.

Stencel, R. E. 2011, "A Primary Node in the Epsilon Aurigae Eclipse Campaign" (http://mysite.du.edu/~rstencel/epsaur.htm).

Templeton, M. 2011a, "Infrared Photoelectric Photometry Program" (http://www.aavso.org/infrared-photoelectric-photometry-program).

Templeton, M. 2011b, "SSP-4 Targets and Comparison Stars" (http://www.aavso.org/ssp-4-targets-and-comparison-stars).

West, D. 2007, "Single-Channel Infrared Photometry with a Small Telescope" (http://www.bellatrixobservatory.org/cvaaI/28/).

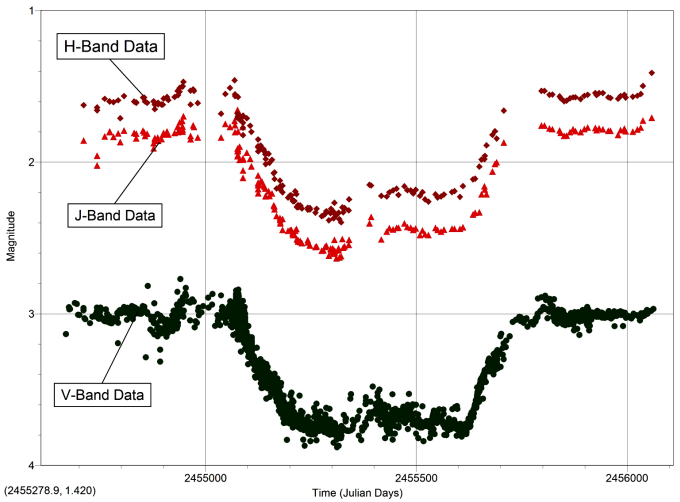

Figure 1. The ε Aur eclipse (2009–2011) in V, H, and J. ε Aur is brighter in both the H and J bands than in the V band in both the in- and out-of-eclipse phases. The background variations of the primary star can also be seen. (Data courtesy AAVSO).

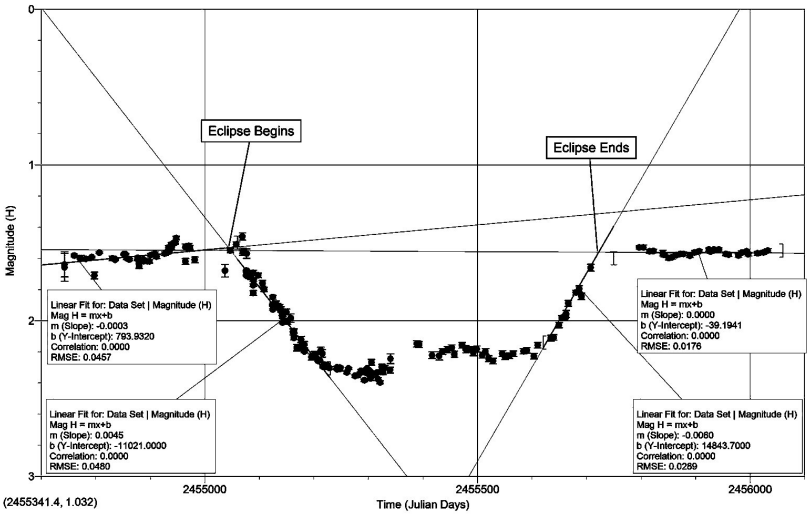

Figure 2. The ε Aur eclipse (H). Once the ingress stage was well underway, the eclipse proceeded at the rate of 0.0045 mag./JD in H. Once egress had begun, ε Aur began to brighten at the rate of 0.0060 mag./Julian Day in H. The dates of eclipse onset and eclipse end can be seen by determining where the pre-and post-eclipse slopes cross the ingress and egress slopes.

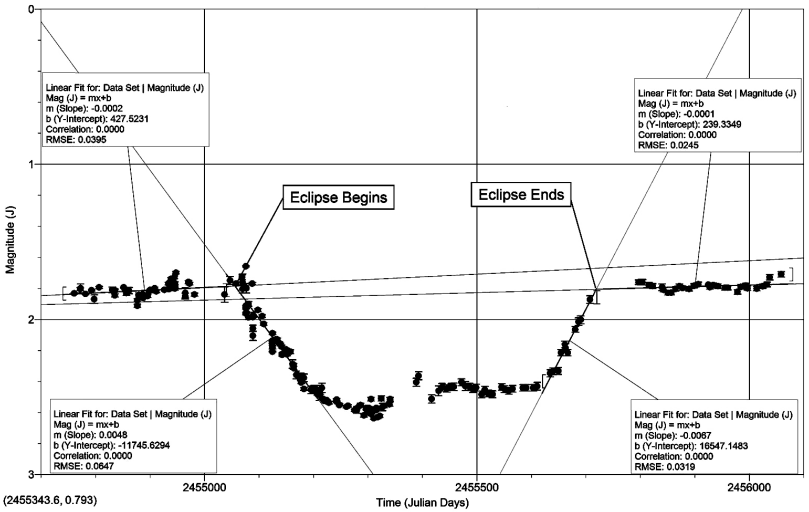

Figure 3. The ε Aur eclipse (J). The ingress phase (J band) of ε Aur proceeded at the rate of 0.0048 mag./JD. As egress occurred, it proceeded at the rate of 0.0067 mag./JD. The dates of eclipse onset and eclipse end can be seen by determining where the pre-and post-eclipse slopes cross the ingress and egress slopes.

UV-Blue (CCD) and Historic (Photographic) Spectra of ε Aurigae—Summary

R. Elizabeth Griffin
Dominion Astrophysical Observatory, 5071 West Saanich Road, Victoria, BC V9E 2E7, Canada; Elizabeth.Griffin@nrc.gc.ca

Robert E. Stencel
Department of Physics and Astronomy, University of Denver, 2112 East Wesley Avenue, Denver, CO 80208; Robert.Stencel@du.edu

Received March 19, 2012; accepted March 27, 2012

Abstract While there are numerous "new spectroscopic studies" of ε Aurigae reported in this special edition of *JAAVSO*, the one summarized here is believed to be unique on two counts: it concentrates on the blue and near-UV spectral regions, and it incorporates historical spectra from the previous eclipses of 1983 and 1956. The more data that can be collated, across all wavelength and time base-lines, the more conclusive the final model of this baffling object is likely to be. A more lengthy paper that includes illustrations of the spectra is being prepared for publication elsewhere. This short contribution summarizes the effort that has so far gone into data acquisition and preparation, and the principal results that are now emerging.

1. Data: recent CCD spectra

We have observed and analysed ~150 new CCD spectra of ε Aurigae at blue and near-UV wavelengths, recorded during the 2010 eclipse with the coudé spectrograph of the Dominion Astrophysical Observatory (DAO) 1.2-m telescope. The wavelength span observable in one exposure is about 145 Å, so we targetted spectral regions of specific interest, and monitored just those as opportunity permitted. The great majority was centred near λ 3950 Å so as to include the Ca II *H* and *K* lines and the nearby strong ground-state Fe I lines; somewhat less frequent monitoring was centred on Hδ and spanned the strong low-excitation Fe I lines between λ 4045–4071 Å, and a comparable number of spectra were centered near the Mg II doublet at λ 4481 Å, where a useful mixture of low- and high-excitation lines occurs. Some observations were also made in the red spectral region, near Hα. All the spectra were reduced in the world co-ordinate system by a semi-automatic pipeline, and were then extracted in steps of 0.01 Å and linearized to an apparent continuum height of 100%. If original S/N ratios were rather low, sequential spectra were co-added.

2. Data: historic photographic spectra

We digitized over 130 historic spectra of ε Aur from Mount Wilson (dating back to the 1930s) and from the DAO (dating from 1971) using the DAO's PDS microphotometer, resurrecting and adopting procedures that have stood the test of time. Spectrophotometric calibrations were determined by means of special exposures to a light source through apertures of known geometrical characteristics. Those spectra were also extracted in regular steps of 0.01 Å and linearized to the local stellar continuum. Many had very acceptable S/N ratios, though none quite as high as can be achieved with a modern CCD detector on a bright star. Nevertheless, these heritage data contribute uniquely to this study, by revealing which of the many line-profile changes have repeated at identical phases of past eclipses, thereby furnishing important constraints for a model of the structure and formation of the occulting disk. They could then be merged with the recent CCD ones so as to provide a more complete dataset, which we examined by ranging each spectral region with phase, within the wavelength spans defined by the CCD spectra.

3. Properties of the disk

We adopted the parameters of the radial-velocity orbit of Stefanik *et al.* (2010) ($P = 9896.0 \pm 1.6$ days, $K = 13.84 \pm 0.23$ kms^{-1}, $T =$ HJD 2434723 ± 80), and aligned the spectra in the velocity rest-frame of the F star. The zero phase of that orbit solution corresponds to periastron, so photometric eclipse began close to phase 0.056 and ended close to phase 0.130. Mid-eclipse (secondary conjunction) was at phase 0.091.

Many authors—e.g., Struve (1956), Wright (1958), Hack (1962), Lambert and Sawyer (1986), and Ferluga and Mangiacapra (1991)—have drawn attention to curious line-profile changes, particularly during early ingress and late egress, often referring to them as "line doubling."

(a) The principal line-profile changes are the extra absorption components that become superimposed on ground-state and low-excitation lines. The new features are red-shifted during ingress and blue-shifted during egress, and are best seen in lines of Fe I on account of the latter's strength and number. The lines themselves do not actually "split," since the two distinct components originate in quite different regions of the system.

(b) Comparisons of the Fe I profiles at different times furnish limits to the phases (and hence on the geometry) when that "doubling" commenced and ceased. It is apparent that the occulting disk has a "tail" which trails much more extensively than does any material at its leading edge. Our spectra also demonstrated the existence of more rarefied material in the extremes of the "tail," not unlike that in a cool-star chromosphere.

(c) Comparisons of spectra of the same phases but different orbital cycles indicate that the structure of the disk is stable, at least on a time-scale of a century

or so: the same "line-doubling" recurs at identical phases and its characteristics repeat quite precisely.

(d) Extra-narrow disk features in both ingress and egress suggest regions of exchange of material (between the disk and the supergiant) that are highly confined in both direction and velocity.

4. Instabilities in the F star

At all orbital phases the spectra of the system reveal more subtle line-profile changes: the absorption lines which presumably originate in the F-star photosphere (since they show no phase-related velocity changes) can weaken, or broaden, or strengthen a little. Dividing all spectra of a given region by one recorded far from eclipse accentuates the changes, and shows broad emission features that grow and fade at all phases on time-scales of days or weeks, with associated narrowing (or deepening) of the *K*-line wings resembling a rise (or fall) in T_{eff}. For the recent eclipse, there was some evidence of correlation between the growth of emission and the Cepheid-like pulsations of ~67 days' period (Kim 2008), but the recorded photometry had not been sufficiently plentiful in the past to investigate such correspondences in earlier years, nor are the available spectra adequate for a thorough investigation: a quarter-phase is only 17 days, and spectra must correspond to null or maximum—a requirement that is unlikely to be fulfilled given the eclectic nature of the archival data for a system of such long period.

5. The spectrum of the disk

The absorption of the disk itself can be isolated by dividing eclipse-phase spectra by one of the system far from eclipse. The procedure cannot be fully precise or absolute because of the small intrinsic variations in the system's spectrum referred to above; the disk spectrum also contributes to the system's one at all phases, though those contributions are small compared to the substantial absorption which the edges of the disk create during eclipse phases. The prime features that we thus isolate are the red-shifted (ingress) and blue-shifted (egress) absorption lines; they vanish during the phases of central eclipse. Their respective velocity displacements are surprisingly constant, and while both are considerably sharp the blue-shifted ones appear broader at phases which are actually beyond the end of photometric eclipse. It is therefore only at the leading and trailing edges of the disk that optically thin material is sufficiently concentrated to give rise to detectable absorption features. However, the presence of variable emission also in the system requires modelling before a quantitative assessment of the properties of that absorbing material can be made.

Qualitatively, the disk features are very similar to the absorption lines which arise in a cool-star chromosphere and which can be isolated during ingress or

egress phases of an "atmospheric" eclipse in a ζ Aur system. The lines in ε Aur are ground-state or low-excitation transitions of easily-ionized elements like Ti I and Fe I, whereas there are no corresponding features in Mg II λ 4481 Å, for example. As with a stellar chromosphere, the total absence of line wings, even for hydrogen lines, indicates a surface gravity, log g, < 1.

A comparison between the ingress and egress features of the disk shows that the disk is not symmetrical: its leading edge is more compressed than its trailing edge. Although the velocity shifts are largely constant, during the extreme end of the egress phases (phase ~0.125 onward) the blue-shift in velocity begins to decrease. Around the same time the sharpness of the features is particularly accentuated. Those observations suggest that we are seeing material which is flowing along a very confined path from the F star to the disk.

6. Transient absorption lines during egress

A few weak, narrow absorption lines appear only between phases 0.111 and 0.123 (or possibly later). They have a constant velocity offset that matches what is shown by the sharp egress features, and their appearances were repeated at identical phases in earlier orbital cycles. Most appear to be low-level lines of Fe I, though not all have yet been identified. The curiously tight restriction in phase suggests an enhanced absorbing mechanism which comes into play *only* during the second stage of egress; there is no counterpart during ingress. Their remarkable sharpness is probably limited by the resolution of the observations and is therefore only an upper limit; a measured half-width suggests an upper limit of ~9 kms.

7. Acknowledgements

We acknowledge the support of the HIA/DAO in granting observing time, when many spectra of the 2010 eclipse were obtained. We are also grateful to the DAO and to Mount Wilson Observatory for the loan of their photographic spectra of the system, and to the American Astronomical Society for a Small Research Grant to digitize them.

References

Ferluga, S., and Mangiacapra, D. 1991, *Astron. Astrophys.*, **243**, 230.
Hack, M. 1962, *Mem. Soc. Astron. Ital.*, **32**, 351.
Kim, H. 2008, *J. Astron. Space Sci.*, **25**, 1.
Lambert, D. L., and Sawyer, S. 1986, *Publ. Astron. Soc. Pacific*, **98**, 389.
Stefanik, R. P., Torres, G., Lovegrove, J., Pera, V. E., Latham, D. W., Zajac, J., and Mazeh, T. 2010, *Astron. J.*, **139**, 1254.
Struve, O. 1956, *Publ. Astron. Soc. Pacific*, **68**, 27.
Wright, K. O. 1958, *Astron. J.*, **63**, 312.

Hα Spectral Monitoring of ε Aurigae 2009–2011 Eclipse

Benjamin Mauclaire
Observatoire du Val de l'Arc, route de Peynier, 13530 Trets, France; bma.ova@gmail.com

Christian Buil
Castanet Tolosan Observatory, 6 place Clémence Isaure, 31320 Castanet Tolosan, France

Thierry Garrel
Observatoire de Juvignac, 19, avenue du Hameau du Golf, 34990 Juvignac, France

Robin Leadbeater
Three Hills Observatory, The Birches, CA7 1JF, England

Alain Lopez
529 rue Buffon, 06110 Le Canet, France

Received February 22, 2012; revised May 30 2012; accepted May 30, 2012

Abstract We present and analyze ε Aurigae data concerning the evolution of the Hα line on the occasion of the 2009 International observation campaign launched to cover the eclipse of this object. We visually inspect the dynamical spectrum constructed from the data and analyze the evolution with time of the EW (Equivalent Width) and of the radial velocity. The spectroscopic data reveal many details which confirm the complexity of the ε Aur system. The object is far from being understood. In particular, according to our measurements, the eclipse duration has been underestimated. A complete analysis of details revealed by our data would require much time and effort. Observers are encouraged to continue monitoring the Hα line out of eclipse in the hope that it will provide further important information.

1. Introduction

ε Aurigae is one of the most intriguing eclipsing star systems which has puzzled astronomers for nearly 200 years. The main eclipsing period is close to 27.1 years and the first spectroscopic surveys were undertaken during the 1929 and 1956 eclipses. A large campaign was also organized for 1982–1984. For a review of literature prior to the 2009–2011 eclipse, see Guinan and De Warf (2008). There are also numerous papers being prepared as a result of the 2009–2011 eclipse. Despite the concentrated efforts, some aspects of ε Aur remain a mystery.

ε Aur is classified as an A8Iab star in an Algol type eclipsing binary system (SIMBAD database 2011). The prevailing model is of an F-type star with a hot clumpy Hydrogen disc and an object of unknown nature which produces an eclipse phenomenon lasting almost 2 years every 27.1 years. There may be a mid-eclipse brightening but solar proximity makes the photometry suspect at those times. Recently, it has been suggested that the eclipsing object is a 550 K dusty disk seen edge on, heated on the side facing the F star to 1100 K. This disk may contain a B5V star (Hopkins *et al.* 2011) that could contribute to emission wings surrounding Ha line. Light curves feature 0.1 magnitude variations both inside and outside eclipse. Variations have also been observed in the Equivalent Width (EW) and Radial velocity of spectral lines outside eclipse. These variations might be F star oscillations and wind.

During the 1982–1984 eclipse, this star was studied by amateur observers using multiband photometric methods. The ε Aur system was not clearly described despite all the acquired data.

Twenty-seven years later, an international campaign was organized to manage both spectroscopic and photometric observations by amateur observers with the aim of producing data with improved time resolution compared with that achieved during previous eclipses. In this article, we present amateur spectroscopic Hα line monitoring from February 12, 2008, to November 12, 2011.

2. Observations

In 2008, Jeff Hopkins (http://www.hposoft.com/Campaign09.html) organized the international observation compaign of the 2009 ε Aur eclipse. We acquired more than 250 high resolution spectra of the Hα line covering the three years around eclipse. These show significant variability throughout this period. The effect of the eclipse is clearly seen in this line from the end of April 2010 to end of April 2011. The spectra used for this study were recorded by five observers in Europe.

Most observations were made using LHIRES3 spectrographs (LHIRES3 and eShell are products from Shelyak Instrument, Grenoble, France: http://www.shelyak.com). C. Buil used an eShell spectrograph that covers wavelengths from 4500 Å to 7000 Å. Telescope diameters were between 0.2 m and 0.3 m. Spectral resolution is above 10,000 and most of the time around 15,000. Mean exposure time was 2,000 s. All setups are reported in Table 1.

3. Reduction and analysis method

The raw observations are available from Robin Leadbeater's ε Aur survey web page (http://www.threehillsobservatory.co.uk/). The spectra were reduced using standard procedures to produce calibrated and normalized line profiles. Most of the reduction was done using SpcAudace (http://bmauclaire.free.

fr/spcaudace/) pipelines. The reduction steps were: preprocessing, geometric corrections, and registration. Then line profiles were extracted with sky background subtraction. Wavelength calibration was done using calibration lamp spectra before and after each acquisition series to minimise the effects of calibration drifts. The instrumental response was then removed. An offset was computed using telluric lines to achieve a final wavelength calibration RMS uncertainty of 0.03 Å. Finally a heliocentric velocity correction was applied depending on the observation date. All wavelengths λ are given in Å (Ångström).

Equivalent Width (EW) measurements were computed between λ6550 and λ6577 using linear integration and an extracted continuum obtained from a fit to the local star continuum (about EW's computation: http://bmauclaire.free.fr/astronomie/spectro/experiences/ew/ewconvention/). The Chalabaev algorithm (Chalabaev 1983) was used to estimate the uncertainty, which is mostly dependent on the signal-to-noise ratio, and appears to overestimate the uncertainty compared with the actual scatter observed around the long term trend.

Radial velocity is computed in two steps because the Hα line is asymmetric:

- The Gaussian flank of the line was reproduced on the opposite side of the symmetry axis (theoretical wavelength of the line) and shifted to fit the line's opposite flank;
- A Gaussian fit of these two flanks gave a measure of the line center.

A dynamical spectrum was computed using 177 spectra corrected to heliocentric velocity and cropped to λ6550–λ6575. A linear interpolation was used to produce an image with a 1-day sampling interval. Such interpolation doesn't introduce bias for our analysis as the purpose of Figure 6 is to show global behavior of the eclipse spread over several hundred days. Dates are logged in MJD (that is, JD–2400000). All computations were performed in SpcAudace. The monitoring covers a period of 720 days. Most of the information generated by our monitoring of the Hα line is contained in this dynamical spectrum.

Analyzing this complex image turns out to be cumbersome, however. This is the reason why we have simplified the analysis by concentrating on the evolution with time of the EW that can be compared to V magnitude, and of the radial velocity that can be used to study eclipsing phenomena. Of course we have to keep in mind that EW loses its physical meaning when applied to complex line profiles lines, as it is the case for ε Aur, are likely to result from a combination of several sources. But before analyzing these quantities, let us first examine the spectral line profiles at dates that show important transitions.

4. Behavior of the wings

Outside eclipse, the Hα line profile comprises a central absorption core flanked by emission features on the red and blue wings (see Figure 1). These features are highly variable as described by Golovin (2007).

In the region of the Hα line are absorption lines identified as telluric lines at λ6543.91, λ6547.71, λ6548.32, λ6552.63, λ6557.17, λ6568.81, λ6572.09, λ6574.85, and λ6586.68.

As we can see in Figures 2 and 6, from MJD 55250 onwards there was additional absorption in the core which broadened rapidly, engulfing first the red emission and by MJD 55340 also the blue emission component. Note this is in contrast to the KI λ7699 line absorption which started decreasing in intensity during this phase (Leadbeater *et al.* 2011).

During ingress and into totality (see spectra at MJD 55390.44 and MJD 55496.42) through the mid-eclipse point, the absorption core deepened and broadened slightly on the red side. The additional absorption moved to the blue and, at MJD 55520, the red emission feature reappeared.

At the beginning of the decreasing phase (see spectrum at MJD 55627.46), the Hα line became narrower, with an emission component at the red side. Then, from MJD 55853.42, the blue edge emission component returned as just before eclipse. After the main eclipse phase (see spectrum at MJD 55878.39), the blue and red wings were both present but small, starting to resemble the pre-eclipse profile (Figure 1).

At the end of the survey period there still appears to be an excess absorption on the blue side of the central absorption region compared with typical pre-eclipse spectra, possibly due to the continued presence of the eclipsing disc. However, the inherent variability of this at all phases makes the statement uncertain.

Today's understanding (Stencel 2011) is that the F star is semi-stable and capable of producing variability in lines in and out of eclipse. The disk is only modifying the optical spectrum during its passage.

5. EW evolution with time

EW measurements were computed between λ6550 and λ6577. Although the signal-to-noise ratio varies between observations and includes telluric lines which impact on EW, the effect most of the time is rather small. The data quality allows a reliable estimation of the EW. As mentioned earlier, the single quantity EW is a gross simplification of the complex nature of the line.

However, this quantity is the integral of the distribution of luminosity versus wavelength. It can thus be compared to similar integrals such as the V magnitude. As shown in Figures 3 and 4, equivalent width (EW) and V magnitude (V mag.) are anti-correlated. Given that EW > 0 for absorption lines, the eclipsing object occults the F star Hydrogen disk as first minimum in EW

and in V mag. evolution are both close to MJD 55250, and as second minimum and V magnitude evolution are also both close to MJD 55630. These dates define totality inner limits (see Table 2).

While second and third contacts (and mid-eclipse) times are well-defined by our EW as a function of Date trend (Figure 3), the definition of first and fourth contact times are less obvious here and do not correspond to photometric contacts: these dates (second and third contacts) are likely to be linked with the densest ends of the eclipsing object.

During the eclipse phase and outside it too, there are many small variations in EW and V mag. This suggests that the occulting object and F star Hydrogen disk may be clumpy. The F star may have also an intrinsic pulsating activity (Kemp *et al.* 1986; Stencel 2011) that produces such variations.

Hα EW has irregular variations like small steps during its increasing and decreasing phases. Similar behavior has been observed on the KI λ7699 asborption line. It has been interpreted as an indication of structures (possibly ring-like) within the disc (Leadbeater and Stencel 2010). Continued observation during egress may help to clarify this.

6. Radial velocity evolution with time

Figures 2 and 6 show how shapes are shifted in radial velocity. During the beginning phase of the eclipse (see spectra at MJD 55390.44 and MJD 55496.42), the absorption line became red shifted (+14.79 ± 1.37 km/s). During the end phase of the eclipse (see spectrum at MJD 55627.46), the Hα line first returned to the position seen at MJD 55390.44 and then the absorption line still remained blue shifted (–31.59 ± 1.54km/s at MJD 55853.42). See Table 3 for measurements at key dates.

An emission component (Figure 5) appeared in the core of the Hα line close to the rest wavelength from MJD 55150 onward as the absorption increased in this region. This became more clearly defined as the surrounding flux level dropped further and moved across the region from red to blue. The shape of the emission component is revealed as the absorption region broadened and swept across it through mid eclipse. It is clear that the constant emission component is only revealed as the surrounding flux level drops.

During our survey, the emission component measured by gaussian fitting remained centered on 6562.71 ± 0.03 Å, which, in terms of radial velocity, amounts to –4.97 ± 1.54km/s. This does not account for the ε Aur systemic radial velocity estimated at –2.26 ± 0.15km/s (Stefanik *et al.* 2010), leading to a correction of +0.049 Å (that is, +2.26 km/s). Note that Figure 6 is not well enough resolved to see such a small shift. Computations were done on the line profiles.

7. In quest of new models

The light variations of ε Aur in and out of eclipse have been the object of many studies.

During 1983 eclipse Kemp *et al.* (1986) analyzed polarization data. They suggested that the F star is a non-radial pulsator and that its surrounding disk is tilted with respect to the orbit.

In 1991, Ferluga and Mangiacapra (1991) suggested that to explain the shape of the light curve, the disk is not a continuous aggregate of dust, but instead a series of rings with a Cassini-like division. This model was more or less validated by observations.

During this eclipse, a wide variety of observations have been undertaken: infrared, ultraviolet, interferometry, photometry, and high resolution spectral monitoring. Thus, a considerable amount of information is now available (see Stencel 2010; Hopkins *et al.* 2011 for an overview). It now remains to develop a model that fits all the data at hand. Undoubtedly, the high resolution spectral monitoring data will be very important for constraining theses models.

8. Conclusions

Our Hα monitoring of ε Aur shows that, contrary to what was forecast, the effects of the eclipse extended beyond December 2011. Post-eclipse observations are needed. R. Stencel welcomes any outside eclipse spectroscopic contributions to the campaign over the coming months and years, especially those covering the Na D lines.

We have observed similarities and discrepancies between the EW and V magnitude evolution with time. The discrepancies remain to be explained, but that is beyond the scope of this article. We also were able to define key dates in the eclipsing phenomenon. However, much remains to be analyzed. Obviously the Hα monitoring brings a lot of information which should place many constraints on the models conceived by scientists about ε Aur.

Amateur spectroscopists are now able to monitor bright targets with a spectral resolution of about 15,000. Suitably equipped amateurs constitute a team with long term monitoring capacity which is widely distributed over the planet.

In any case, we hope that this information will help scientists to solve the mysteries hidden behind this fascinating object.

9. Acknowledgements

This campaign would not have been possible without Jeff Hopkins' motivation and constant efforts to encourage amateur observations. The authors acknowledge Robert Stencel for his help and encouragements

thoughout this campaign. They also kindly thank the referee for constructive comments and very helpful work.

All of the data presented in this paper were obtained from amateur observers. The authors also acknowledge Eric Barbotin, Stéphane Charbonnel, Valérie Desnoux, Stanley Gorodenski, Keith Graham, Torsten Hansen, James Edlin, Brian E. McCandless, Éric Sarrazin, Lothar Schanne, José Ribeiro, François Teyssier, Olivier Thizy, and John Strachan for all the work they carried out at other wavelengths and spectral resolutions on this mysterious star.

References

Chalabaev, A., and Maillard, J. P. 1983, *Astron. Astrophys.*, **127**, 279.

Ferluga, S., and Mangiacapra, D. 1991, *Astron. Astrophys.*, **243**, 230.

Golovin, A., Kuznyetsova, Y., and Andreev, M. 2007, *Odessa Astron. Publ.*, **20**, 55.

Guinan, E. F., and Dewarf, L. E. 2002, in *Exotic Stars as Challenges to Evolution*, eds. C. A. Tout and W. Van Hamme, ASP Conf. Ser. 279, Astron. Soc. Pacific, San Francisco, 121.

Hopkins, J., Stencel, R., and Leadbeater, R. 2011, *Epsilon Aurigae Eclipse International Campaign Newsletter*, No. 24 (Fall/Winter).

Kemp, J., Henson, G., Kraus, D., Beardsley, I., Carroll, L., Ake, T., Simon, T., and Collins, G. 1986, *Astrophys. J., Lett. Ed.*, **300**, L11.

Leadbeater, R., Buil, C., Garrel, T., Gorodenski, S., Hopkins, J., Mauclaire, B., Ribeiro, J., Schanne, L., Thizy, O., and Stencel, R. 2011, *Bull. Amer. Astron. Soc.*, **43**, 257.04.

Leadbeater, R., and Stencel, R. 2010, arXiv:1003.3617v2 (18 March).

Simbad database. 2011, ε Aur web page (http://simbad.u-strasbg.fr/simbad/sim-id?Ident=eps aur).

Stefanik, R. P., Torres, G., Lovegrove, J., Pera, V. E., Latham, D. W., Zajac, J., and Mazeh, T. 2010, *Astron. J.*, **139**, 1254.

Stencel, R. 2010, "Epsilon Aurigae in Total Eclipse 2010, Mid-eclipse report," Univ. Denver Obs. (http://arxiv.org/pdf/1005.3738.pdf).

Stencel, R. 2011, private communication (December 7).

Table 1. Equipment information for observation of ε Aur.

Observer name	*Telescope*	*Spectro-graph**	*Resolution*	*Mean SNR*	*Spectral range (Å)*	*Number of spectra*
C. Buil	SCT 0.28 m	1	10,000	164	4500–7000	96
T. Garrel	SCT 0.21 m	2	15,000	108	6500–6630	87
B. Mauclaire	SCT 0.30 m	2	15,000	224	6520–6690	34
R. Leadbeater	SCT 0.20 m	2	15,000	98	6500–6700	25
A. Lopez	SCT 0.28 m	2	15,000	164	6500–6700	5

**Spectrograph: 1) eShell; 2) Lhires3 2400 1/mm.*

Table 2. Contact dates during ε Aur eclipse.

Main contact	*MJD (day)*
first	55070 ± 3
second	55250 ± 2
third	55630 ± 2
fourth	55800 ± 3

Table 3. Radial velocity measurements of ε Aur at key dates.

MJD (day)	*Radial velocity (km/s)*
55199.24	+19.46 ± 1.54
55390.44	+14.79 ± 1.37
55436.49	−38.10 ± 1.54
55521.46	−60.36 ± 1.54
55819.46	−31.59 ± 1.54

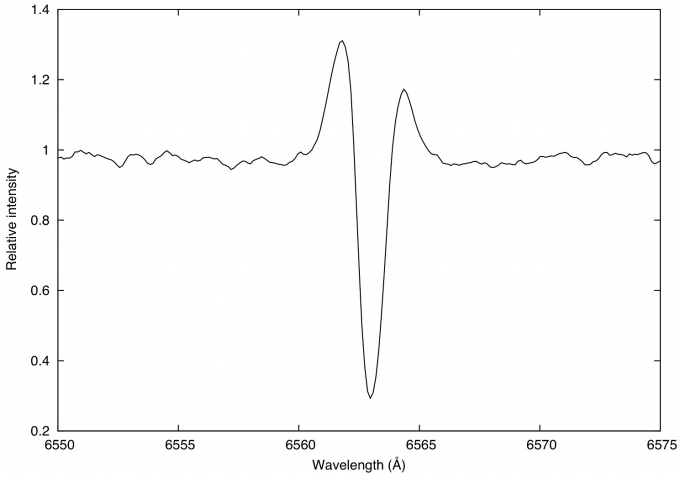

Figure 1. ε Aur spectrum showing Hα wings out of eclipse phase. Observations of 12.881/12/2008, SCT 0.3 m, Lhires3 2400 g/mm, 0.115 Å/pixel, B. Mauclaire, 4 × 600 s.

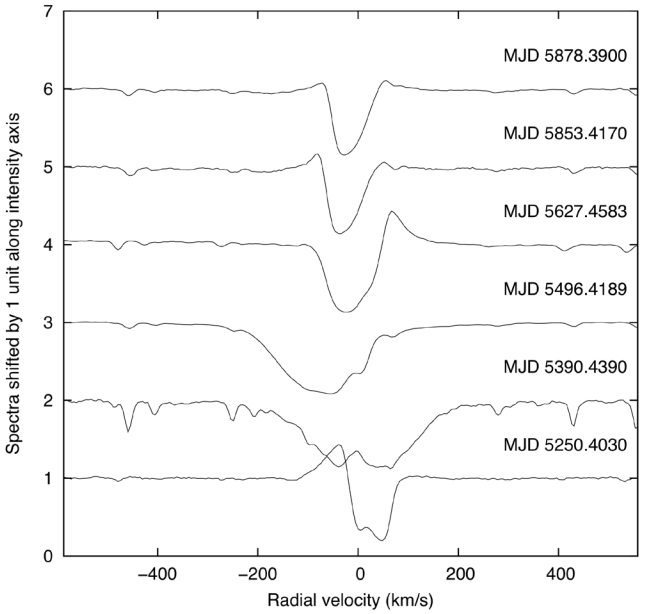

Figure 2. Time evolution of ε Aur from 2455250.403 to 2455878.39. Hα wings are shown at key dates.

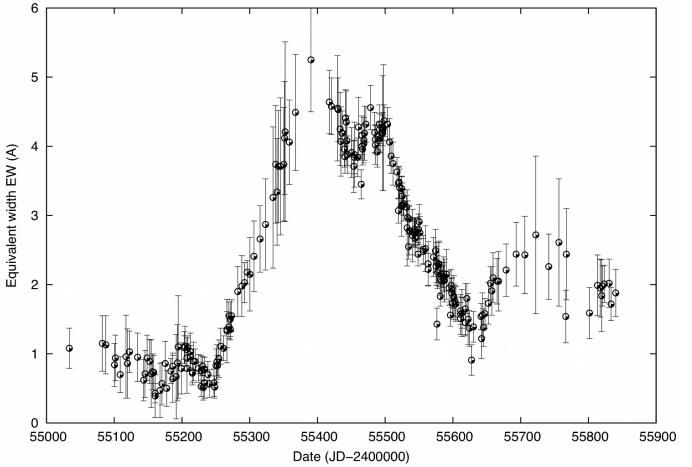

Figure 3. Plot showing evolution with time of Equivalent Width computed between λ6550 and λ6577. Note the two minima at MJD 55250 ± 2 and 55630 ± 2 corresponding to second and third contacts dates.

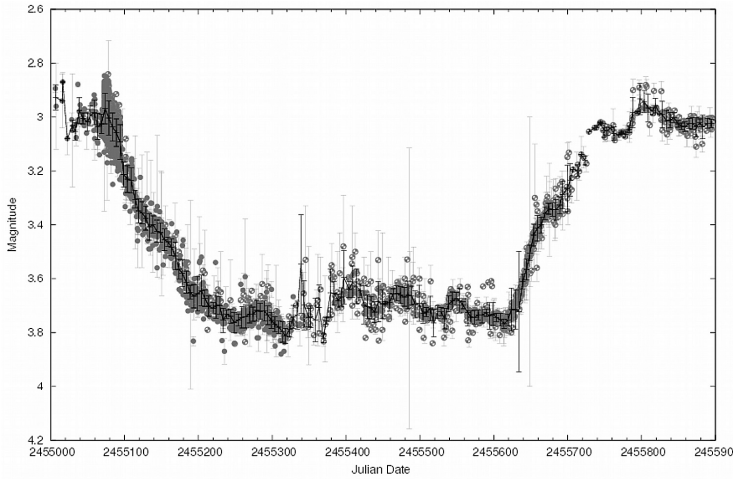

Figure 4. Light curve of ε Aur using data from the AAVSO International Database showing V magnitude evolution within time. Light curve courtesy of AAVSO.

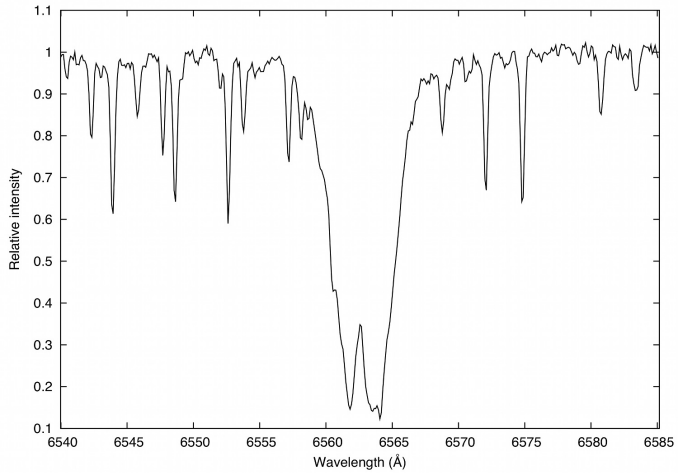

Figure 5. Spectrum of ε Aur showing emission component at bottom of Hα absorption line. Observations of 12.939/7/2010, R. Leadbeater, TN 0.25 m, Lhires3 2400 g/mm, 0.107 Å/pixel.

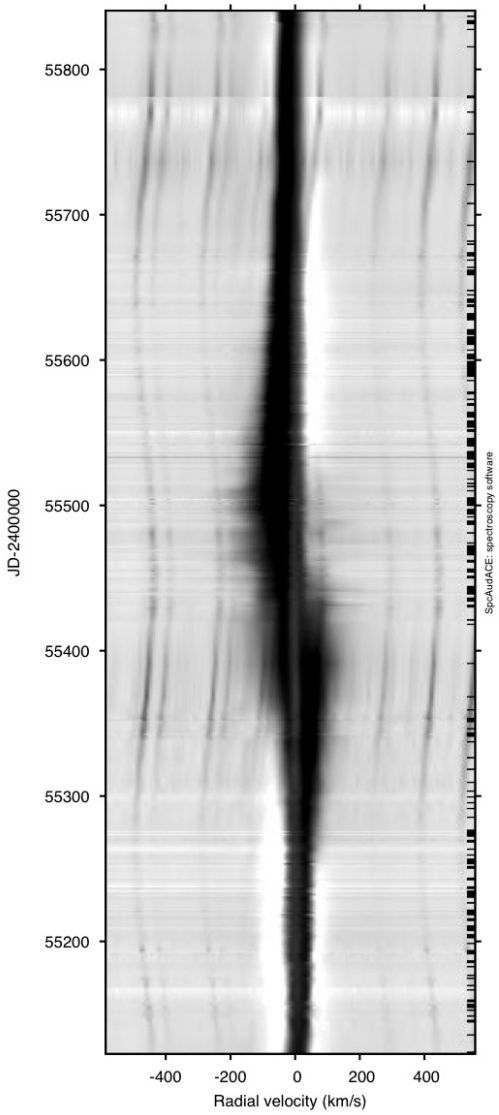

Figure 6. Dynamical spectrum of Hα line from JD 2455120.605 to JD 2455840.48. Interpolation between spectra was used to get a smooth image. Sinusoidal lines at both Hα line edges are telluric lines lying in line profiles that are corrected from heliocentric velocity. The black dashes along the right axis show the actual observation dates.

High Cadence Measurement of Neutral Sodium and Potassium Absorption During the 2009–2011 Eclipse of ε Aurigae

Robin Leadbeater
Three Hills Observatory, The Birches, CA7 1JF, UK; address email correspondence to R. Leadbeater at robin@threehillsobservatory.co.uk

Christian Buil
Castanet Tolosan Observatory, 6 Place Clemence Isaure, 31320 Castanet Tolosan, France

Thierry Garrel
Observatoire de Foncaude, Juvignac, France

Stanley A. Gorodenski
9440 E. Newtown Avenue, Dewey, AZ 86327

Torsten Hansen
Reichau 216, D-87737, Boos, Germany

Lothar Schanne
Observatory for Stellar Spectroscopy Völklingen, Hohlstrasse 19, 66333, Völklingen, Germany

Robert E. Stencel
Department of Physics and Astronomy, University of Denver, 2112 East Wesley Avenue, Denver, CO 80208

Berthold Stober
Nelkenweg 14, 66791 Glan-Münchweiler, Germany

Olivier Thizy
Shelyak Instruments, Les Roussets, 38420 Revel, France

Received May 14, 2012; revised July 10, 2012; accepted July 10, 2012

Abstract The results of a spectroscopic survey of ε Aurigae during eclipse using a network of small telescopes are presented. The spectra have a resolution of 0.35 to 0.65Å and cover the period 2008 to 2012 with a typical interval of four days during eclipse. This paper specifically covers variations in the KI 7699Å, Na D, and Mg II 4481Å lines. Absorption started increasing in the KI 7699Å line three months before the eclipse began in optical photometry and had not returned to pre-eclipse levels by the end of the survey in March 2012, seven months after the broadband brightness had returned to normal outside eclipse levels. The contribution of the eclipsing object to the KI 7699Å line has been isolated and shows the excess absorption increasing and decreasing in a series of steps during eclipse ingress and egress. This is interpreted as an indication

of structure within the eclipsing object. The F star is totally obscured by the eclipsing object at the Na D wavelength during eclipse. The radial velocity of the F star and the mean and maximum radial velocity of the eclipsing material in front of the F star at any given time have been isolated and tracked throughout the eclipse. The quasi-periodic variations seen in the F star radial velocity (RV) outside eclipse continued during the eclipse. It is hoped that these results can be used to constrain proposed models of the system and its components.

1. Background

ε Aurigae is a naked eye eclipsing binary system with a period of 27.1 years and a primary eclipse of about two years. Despite having been studied for almost two centuries, our understanding of the exact nature of the system, the primary star, and its largely unseen companion, is still incomplete.

At each eclipse, a new generation of astronomers equipped with the latest technology tackles the problem. A recent multiwavelength study of the system proposed that the spectral class F primary star is most likely an evolved post-AGB star and that a B5V class star is embedded in the cool (~1000 K) opaque material which causes the eclipse (Hoard *et al.* 2010, hereafter referred to as the HHS model). Interferometric measurements made during the 2009–2011 eclipse have established that the eclipsing object is an elongated opaque cigar shaped object, most likely a disc seen almost edge on, which covers the southern half of the star during eclipse (Kloppenborg *et al.* 2010).

Advances in sensor technology and the availability of affordable high resolution spectrographs allowed a network of advanced amateurs using small aperture telescopes to contribute during the 2009–2011 eclipse. The objective was to study the evolution of the optical spectrum of the system throughout the eclipse with improved time resolution compared with that achieved during previous eclipses. Over 800 spectra were collected and these are available online (http://www.threehillsobservatory.co.uk/epsaur_spectra.htm).

2. Observations

This paper specifically covers:

- 275 observations of the neutral potassium line at 7699 Å (hereafter referred to as K 7699) at a mean interval of 4.3 days throughout the eclipse.

- 199 observations of the neutral sodium D lines at 5890/5896 Å (hereafter referred to as Na D) at a mean interval of 4 days during the eclipse, excluding the periods around solar conjunction.

- 137 observations of the singly ionized magnesium line at 4481 Å (hereafter referred to as Mg 4481).

The observations are summarized in Table 1. The K 7699 line observations were made by Leadbeater and Schanne at a resolution of 0.35 Å using Lhires III Littrow spectrographs, modified to reach this wavelength. Various spectrograph designs with resolutions from 0.35–0.65 Å were used for the Na D line observations. The Mg 4481 line measurements were made with the eShel echelle spectrographs of Buil, Thizy, and Garrel at typically 0.5 Å resolution.

2.1. Choice of lines

Outside eclipse, the ε Aur spectrum shows an interstellar K 7699 line (Welty and Hobbs 2001). There is no detectable contribution from the F star spectrum. This was confirmed by examining spectra outside eclipse (Lambert and Sawyer 1986; Welty and Hobbs 2001) recorded at different phases which showed no variation in RV above the level of the measurement uncertainty. If a stellar component was present it would be detectable due to the change in RV of that component. After removal of the constant interstellar component, the remaining K 7699 line uniquely describes the absorption due to the eclipsing component. Spectra of this line had also been taken during the previous eclipse, though at less frequent intervals (Lambert and Sawyer 1986).

The Na D lines also show strong additional absorption during eclipse (Barsony *et al.* 1986); however, the analysis of these lines is more complex due to the presence of components from both the F star and the interstellar medium.

The Mg 4481 line arises from the F-star photosphere and is absent from the cool eclipsing object spectrum due to the high excitation level of the former (Ferluga and Hack 1985), so acts as a reference for changes in the F star RV.

2.2. Reduction of spectra

The spectra were initially individually reduced by each observer (dark, flat, geometric corrections, cosmetics removal, background subtraction, and binning). Except for Stober, whose spectra were normalised using a fit to the continuum, the spectra were also corrected for instrument response using a standard star. No atmospheric extinction correction was applied. Flux is relative to the continuum. The software used by each observer is listed in Table 1.

The spectra were then further reduced and line parameters measured by RL using VISUAL SPEC software. The pre-reduced spectra for each line of interest were first normalized using a fit to the local continuum. To maximize the global precision of the Na D and K 7699 line wavelength calibration, the original calibrations were checked using telluric lines visible in the spectra and small offsets applied as required. There are no tellurics in the Mg 4481 line region so the observers' original ThAr lamp calibrations were used for this line. The estimated residual uncertainty in wavelength is 0.02 Å. The telluric lines were then removed, by dividing by hot line-free star spectra taken with the same

equipment in the case of the K 7699 line spectra or by scaling a standard telluric line template in the case of the Na D lines. Finally the wavelengths of all spectra were corrected to the heliocentric velocity reference frame.

3. Analysis

For this paper, eclipse start and end dates of JD 2455070 and 2455800 have been adopted based on V-band photometric data submitted to AAVSO (Mauclaire *et al.* 2012). The parameters used for calculating the properties of the system are listed in Table 2.

3.1. KI 7699Å line

Figure 1 shows the evolution of the K 7699 line throughout the eclipse. Each row represents an interval of 2 days. The dates of the spectroscopic measurements are marked on the time axis. Intermediate rows between measured spectra are interpolated. Note that the interstellar component (measured from pre-eclipse spectra) has been removed so the plot shows just the contribution from the eclipsing object. Figures 2 and 3 show typical profiles for the K 7699 line with the interstellar component present and removed, respectively.

Figure 4 shows the variation in the strength (equivalent width, EW) of the K 7699 line including the interstellar component, with measurements from the previous eclipse (Lambert and Sawyer 1986) superimposed for comparison. Figure 5 shows the same EWs for the K 7699 line with the interstellar component removed. The estimated uncertainty in EW is 15 mÅ, based on repeat measurements and comparison with coincident observations made by other observers during eclipse ingress (Ketzeback 2009).

The RV trend for the K 7699 line after removal of the interstellar component is shown in Figure 6. The maximum velocity component in the material in front of the F star at any given time during ingress (line profile red edge) and egress (line profile blue edge) is also plotted.

3.2. Na D lines

Figure 7 shows the evolution of the Na D lines throughout the eclipse. Each row represents an interval of 2 days. To produce a consistent set of spectra, higher resolution spectra were filtered to give a common resolution of 0.65 Å. The dates of the spectroscopic measurements are marked on the time axis. Intermediate rows between measured spectra are interpolated. Figure 8 shows typical Na D2-line profiles throughout the eclipse, while Figure 9 shows a selection of full Na D-line profiles at a higher resolution of 0.35 Å obtained during the second half of the eclipse. The total EW of the Na D line (sum of D1 and D2) as a function of time before and during the eclipse is plotted in Figure 10.

The RVs of the Na D lines (mean of D1 and D2) and of the Mg 4481 line as a function of time before and during the eclipse are plotted in Figure 11.

Also shown is a linear fit to the Mg 4481 line data and, for comparison, the radial component of the orbital velocity of the F star (Stefanik *et al.* 2010).

4. Discussion

4.1. The extent of the eclipsing object

Interferometric imaging has shown the drop in brightness during eclipse to be due to an elongated opaque object (a thin rotating disc seen almost edge on) which covers the southern half of the F star (Kloppenborg *et al.* 2010). The changes we see in the spectrum during eclipse arise from absorption within a gaseous region surrounding this opaque object. Increased absorption was first detected in the K 7699 line 95 days before photometric first contact and was still detectable at the end of the survey, 215 days after fourth contact. Adopting a scale of 3.8 AU for the radius of the disc as per the HHS model, we estimate that this gaseous region extends beyond the outer edges of the opaque region by 1.2 AU on the ingress side and at least 2.6 AU on the egress side.

Outside eclipse the Na D lines, a combination of contributions from the F star and the interstellar medium, are not fully saturated. During eclipse, however, the lines saturate and the residual flux in the core of the lines falls close to zero. This is seen particularly clearly in the higher resolution spectra shown in Figure 9 taken during the second half of the eclipse, in which the eclipsing disc component of the line, blue-shifted during this half of the eclipse, shows a distinctly flattened bottom at just 0.03 of the flux relative to the continuum. Given that the opaque region eclipses only the southern half of the F star (as seen in the interferometric images) this suggests that the Na-absorbing region extends at least the F-star radius (0.6 AU) above the opaque region, completely covering the F star.

A small peak is visible, ~10 km/s bluewards of the rest wavelength, in the high resolution Na D absorption lines during the second half of the eclipse (Figure 9). This was also observed during the previous eclipse (Barsony *et al.* 1986). It is likely that this is due to a partial separation of the eclipsing disc/F-star components (both blue-shifted during this half of the eclipse) and the interstellar component. The same effect is seen in the K 7699 line where the separation of the two components is clear (Figure 2).

The EW of the Na D lines at the end of the campaign period was still significantly higher than pre-eclipse values ($p \ll 0.001$, mean 2.20 Å range 2.18–2.24, 8 values RJD 55954–56005 as opposed to mean 1.79 Å range 1.67–1.86, 6 values RJD 54455–54779); however, this could be due at least in part to the relative separation of the components. (Because the line is saturated, the EW will depend on the overlap between the components which, in turn, depends on the relative RV). Extended post-eclipse monitoring could help clarify this.

The EW of both the K 7699 and Na D lines dropped around mid-eclipse. In the case of the saturated Na D line this could be caused, for example, by a

narrowing of the already saturated line profile rather than a net reduction in the amount of absorbing material. This would not be the case for the unsaturated K 7699 line, however, and suggests that either there is less absorbing material in these inner regions of the disc or that the conditions closer to the central star do not allow the particular transition (due to radiation from the central star, for example). The interval between the leading and trailing EW maxima for the K 7699 line is 265 days, which corresponds to a region 2.1 AU in diameter.

There is significant asymmetry in the K 7699 line excess absorption between the leading and trailing regions of the disc. The trailing maximum is 70% higher than the leading maximum (780 mÅ as opposed to 460 mÅ, see Figure 5). As already mentioned, the tail of the absorption extends significantly further on the egress side. The lateral extent of the main region of absorption, however, is similar for both halves (200 days from 30% to maximum absorption during ingress compared with 220 days during egress).

The minimum flux in the K 7699 line profile remained significantly above zero during the eclipse (the minimum level was 0.18 relative to the continuum) so, provided that the material producing this line extends above the disc to the same extent as that for the Na D line, covering the F star completely, we can conclude that when we look at the K 7699 line we are seeing through the full thickness of the material and, therefore, the line profile includes contributions from all depths within the absorbing region in front of the F star at the time.

4.2. Comparison with the previous eclipse

There is good overall agreement between the total K 7699 line EW trend during this eclipse and measurements made by Lambert and Sawyer on this line during the previous eclipse, offset by 9,896 days. The largest differences occur at RJD 55340 and 55615 but Lambert and Sawyer plotted a smooth curve through their more sparse data and attributed the residual scatter to measurement error, so it is not clear if these differences are significant.

4.3. Structure within the disc

The trend of excess K 7699 absorption during eclipse (Figure 5) did not progress smoothly during ingress and egress but proceeded in a series of steps. The steps during ingress have been interpreted as an indication of structure within the disc material (Leadbeater and Stencel 2010). There is no obvious symmetry in these features between ingress and egress, as might be expected for a simple system of concentric circular rings, though more complex structures such as an elliptical system or spiral density waves produced by the tidal influence of the F star, as seen in other circumstellar discs (for example, Muto *et al.* 2012), are not ruled out. (Note that features are also seen in the Na D line total EW trend but these do not correspond with the steps seen in the K 7699 EW and may be caused by interactions between the various components which make up the line. These interactions are discussed in section 4.5.)

4.4. The disc rotation

The trend of the K 7699 line RV after removal of the interstellar component (Figure 6) is smooth throughout the eclipse with little scatter (except at the start and end of eclipse when the line is weak) and no obvious short timescale features. Given the known quasi-periodic variability seen in the RV of the F-star lines (Stefanik *et al.* 2010), this is additional confirmation that the K 7699 line is not significantly contaminated by any contribution from the F star. Since we are seeing through the full depth of the disc at this wavelength, the RV values plotted here are a measure of the mean velocity along our line of sight of all the vectors of the orbiting components of the absorbing material in front of the F star at a particular phase of the eclipse. While it may prove possible to model such a parameter given a detailed description of the properties and distribution of the material surrounding the disc, a perhaps simpler parameter, the maximum velocity component in the line, has also been plotted in Figure 6. This is somewhat more difficult to measure as it involves estimating the wavelength of the edge of the line where it meets the continuum, and this is reflected in the increased scatter. It has the potential, however, to be used to calculate an orbital velocity curve for the disc since, for material in Keplerian orbits, the maximum radial velocity at a given time will be due to the innermost material in front of the F star at that time viewed tangentially and, hence, gives a direct measurement of the orbital speed of that material. This has already been attempted using the data from the first half of the eclipse (Leadbeater and Stencel 2010) where a figure of 5.3 solar masses was estimated for the disc component. However, this value is sensitive to the RV adopted for the eclipsing component as a whole due to its orbital motion, which is not known currently. We speculate that this orbital motion is, at least in part, responsible for the asymmetry seen in the RV curve from ingress to egress, (higher values of RV seen on egress and a declining RV in the later part of the eclipse compared with the level RV during ingress); however, a full orbital solution for the system will be needed to clarify this.

4.5. The radial velocity of the Na D and Mg 4481 lines

The Na D lines are a combination of components from the eclipsing disc, the interstellar medium, and the F star. The interstellar component will be constant as for the K 7699 line but the F star RV will have an orbital component and quasi-periodic variations (Stefanik *et al.* 2010). The net result (Figure 11), although broadly showing the same swing from red to blue during eclipse, is quite different in detail from that of the disc component extracted from the K 7699 line.

Not enough is known currently about the interstellar or F-star components to allow the net effect of the eclipsing disc to be isolated in the Na D line. This might be possible in the future using more data obtained outside of eclipse. (Throughout the orbit, the Na D line F-star component will move

independently of the interstellar component so it should be possible to isolate the two components.) The Na D line also becomes saturated during the eclipse so the line profile is not a simple linear combination of the three components. Nonetheless, we can make some qualitative observations.

The Mg 4481 line is produced by the F star only (Ferluga and Hack 1985) so the RV of this line can be used as a reference for the F-star Na D component RV during eclipse. The Mg 4481 line data clearly show that the quasi-periodic variations in F star RV seen outside eclipse continued during the eclipse. Note in Figure 11 that the Na D-line RV follows these variations in the interval RJD 55080–55150. The disc component then starts to dominate, rapidly increasing the RV to approximately +16 km/s before reversing through mid eclipse to approximately –23 km/s. There is again some correlation between Na D and Mg 4481 RV in the interval RJD 55570–55700, but the disc absorption strongly saturates the Na D lines during this period so the sensitivity to the F-star variations is expected to be low. By about RJD 55800 the RV had returned close to the F star RV as measured by the Mg 4481 line.

5. Further work

Additional spectra taken outside eclipse are needed to determine the extent of the absorption due to the eclipsing disc on the egress side and to separate the interstellar, F-star, and eclipsing disc components in the Na D lines.

The echelle spectra used here to study the Na D and Mg 4481 lines also cover many other lines known to show changes during eclipse (Ferluga and Hack 1985). A similar analysis of these lines may reveal more information about the structure and conditions within the eclipsing disc.

6. Acknowledgements

We are grateful to Jeff Hopkins for organizing the International Campaign for the observation of ε Aur during this eclipse and to all who submitted observations. We thank the ε Aur spectral monitoring team at Apache Point Observatory (W. Ketzeback, J. Barentine, *et al.*) for allowing us access to their K 7699 line data during ingress. We acknowledge with thanks the variable star observations from the AAVSO International Database contributed by observers worldwide and used in this research. R.E.S. is grateful for the bequest of William Herschel Womble to the University of Denver in support of astronomy, and for support under National Science Foundation grant # AST1016678 to the University of Denver.

References

Barsony, M., Mould, J. R., and Lutz, B. L. 1986, *Publ. Astron. Soc. Pacific*, **98**, 637.
Ferluga, S., and Hack, M. 1985, *Astron. Astrophys.*, **144**, 395.
Hoard, D. W., Howell, S. B., and Stencel, R. E. 2010, *Astrophys. J.*, **714**, 549.
Ketzeback, B. 2009, private communication, Apache Point Observatory.
Kloppenborg, B., *et al.* 2010, *Nature*, **464**, 870.
Lambert, D., and Sawyer, S. 1986, *Publ. Astron. Soc. Pacific*, **98**, 389.
Leadbeater, R., and Stencel, R. 2010, arXiv:1003.3617v2 [astro-ph.SR].
Mauclaire, B., *et al.* 2012, *J. Amer. Assoc. Var. Star Obs.*, **40**, 718.
Muto, T., *et al.* 2012, *Astrophys. J., Lett. Ed.*, **748**, L22.
Parthasarathy, M., and Frueh, M. L. 1986, *Astrophys. Space Sci.*, **123**, 31.
Stefanik, R. P., Torres, G., Lovegrove, J., Pera, V. E., Latham, D. W., Zajac, J., and Mazeh, T. 2010, *Astron. J.*, **139**, 1254.
Welty, D., and Hobbs, L. 2001, *Astrophys. J., Suppl. Ser.*, **133**, 345.

Table 1. Summary of observations.

Observer	*Aperture (mm)*	*Spectrograph*	*Reduction Software**	*Number of Observations*		
				K7699	*NaD*	*Mg4481*
Buil	280	eShel**	4	—	96	94
Garrel	280	Lhires III***	1,2		4	
		eShel	4	—	24	24
Gorodenski	405	Lhires III	1,2		26	—
Hansen	280	Lhires III	1,2	—	4	—
Leadbeater	200/280	Lhires III	1,2	259	12	—
Schanne	355	Lhires III	3	16	6	—
Stober	300	custom echelle	3	—	8	—
Thizy	280	eShel	4	—	19	19
TOTAL				275	199	137

**Reduction Software: (1) IRIS (www.astrosurf.com/buil/us/iris/iris.htm); (2) Visual Spec (www.astrosurf.com/vdesnoux/); (3) ESO-MIDAS (www.eso.org/sci/software/esomidas/); (4) AudeLA-ReShel (http://www.audela.org).*

***eShel (www.shelyak.com/dossier.php?id_dossier=47).*
****Lhires III (www.shelyak.com/dossier.php?id_dossier=46).*

Table 2. Adopted system parameters.

Parameter	*Value*	*Reference*
disc radius	3.8 AU	Hoard *et al.* 2010
F star radius	135 $R_{\odot}$	Hoard *et al.* 2010
mean eclipse duration	710 days	Parthasarathy and Frueh 1986

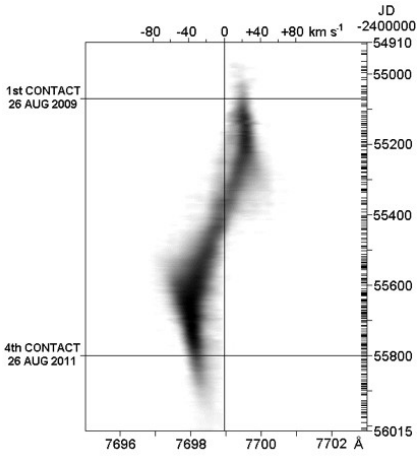

Figure 1. Plot showing the evolution of the K 7699 line after removal of the interstellar component (darker colors signify increased absorption). Tick marks on the right-hand y-axis indicate actual measurements. Intermediate rows are interpolated.

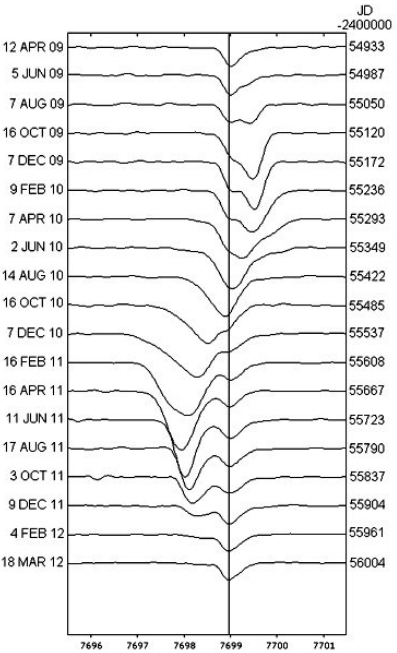

Figure 2. A selection of typical K 7699-line profiles with the interstellar component included.

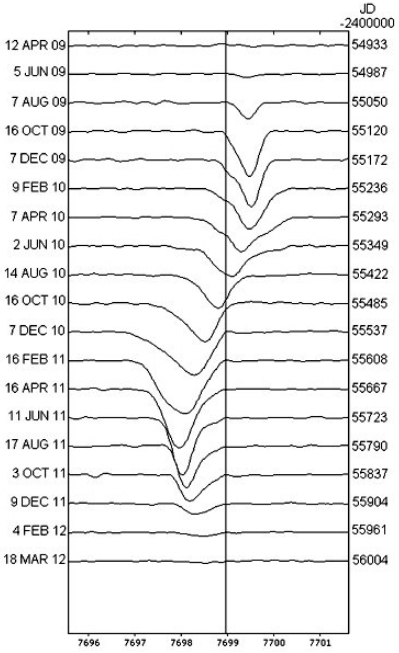

Figure 3. A selection of typical K 7699-line profiles with the interstellar component removed based on pre-eclipse measurements.

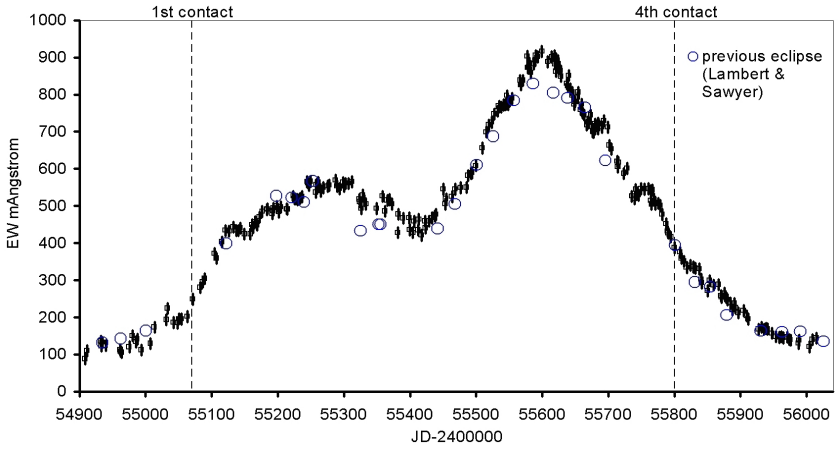

Figure 4. K 7699-line total equivalent width (including the interstellar component) compared with 1983 eclipse data shifted in time by +9,896 days.

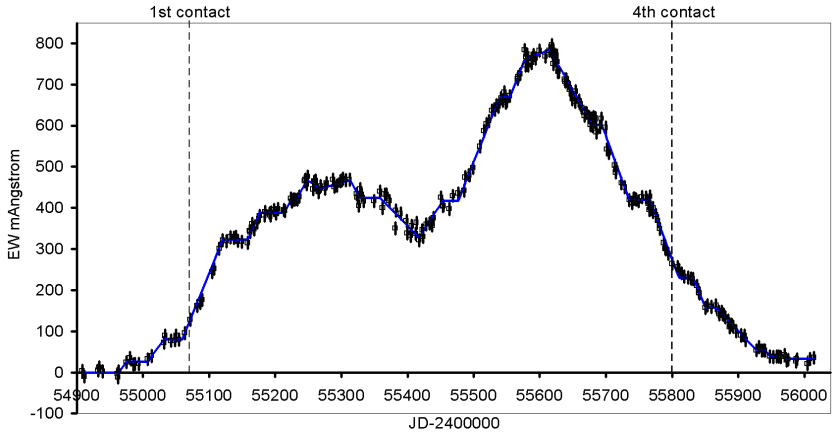

Figure 5. K 7699 excess equivalent width after removal of the interstellar component. The trend line indicates the stepwise progression.

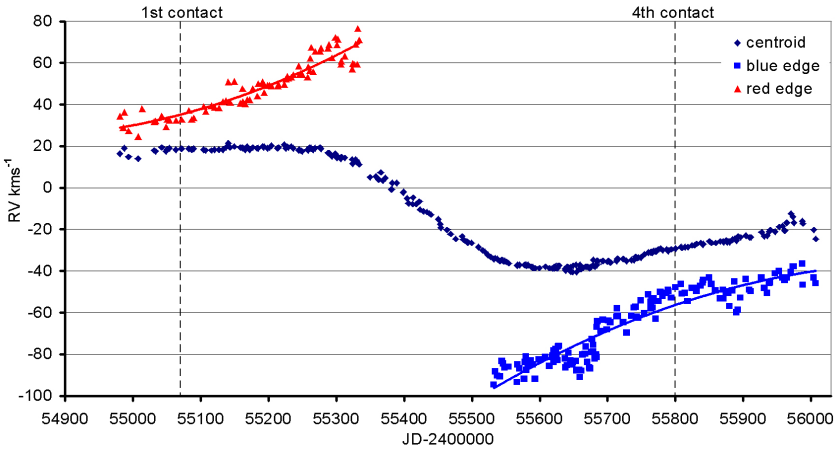

Figure 6. Radial velocity of the K 7699 line (heliocentric). The red (ingress) and blue (egress) edge values are the maximum absolute RV in the line profile.

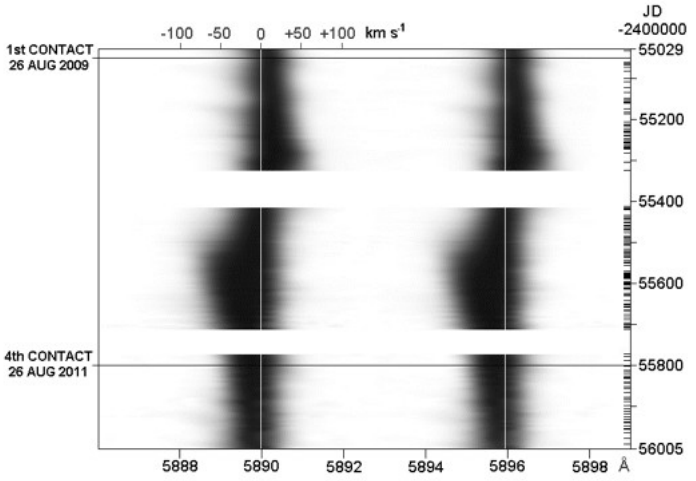

Figure 7. Plot showing the evolution of the Na D lines (darker colors signify increased absorption). Tick marks on the right-hand y-axis indicate actual measurements. Intermediate rows are interpolated. The gaps are the periods around solar conjunction.

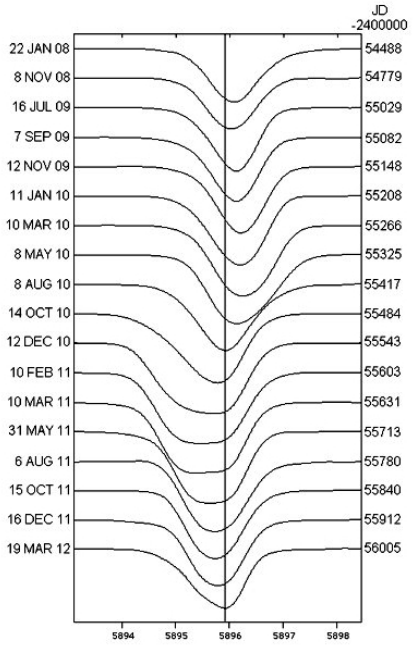

Figure 8. A selection of typical profiles for the Na D2 line at 0.65 Å resolution.

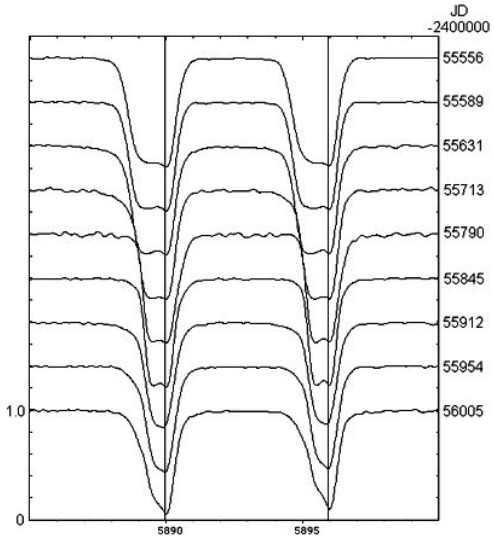

Figure 9. A selection of Na D-line profiles covering the second half of the eclipse at 0.35 Å resolution.

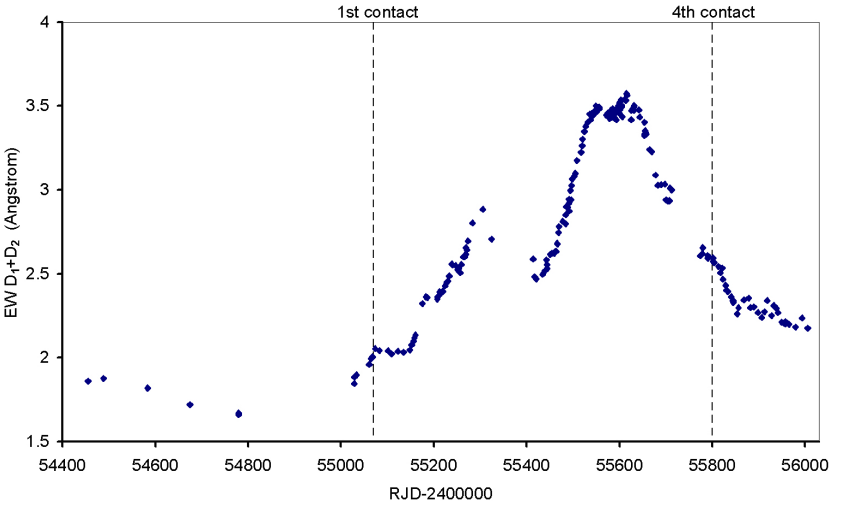

Figure 10. Na D-line equivalent width (sum of both line components) as a function of time before and during eclipse.

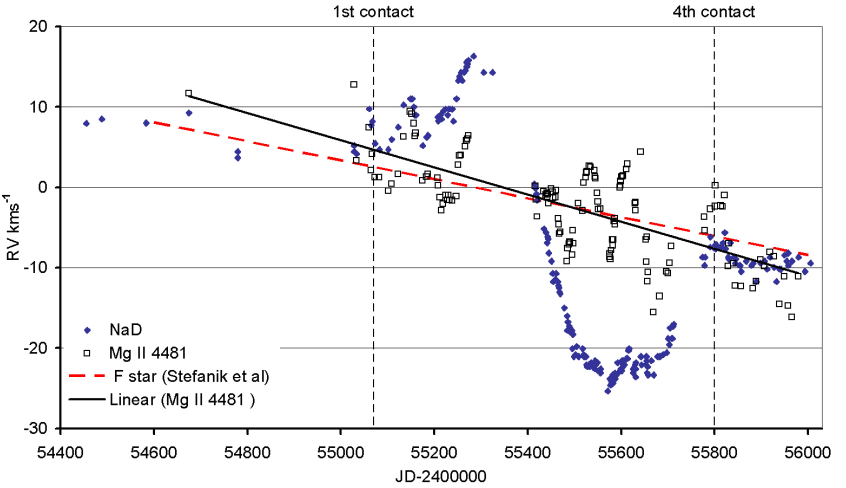

Figure 11. Radial velocity of the Na D lines (mean of both lines) and the Mg 4481 line. A linear fit to the Mg 4481 line data and the F-star RV (based on Stefanik *et al.* 2010) are also shown. All velocities are heliocentric.

Spectroscopic Results From Blue Hills Observatory of the 2009–2011 Eclipse of ε Aurigae

Stanley A. Gorodenski
9440 East Newtown Avenue, Dewey, AZ 86327; stanlep@commspeed.net

Received February 7, 2012; revised February 17, 2012; accepted February 28, 2012

Abstract The purpose of this paper is to report spectroscopic results of ε Aurigae during the 2009–2011 eclipse. Spectra of the sodium D lines and an absorption line occurring at approximately 5853Å were taken from February 13, 2010, to October 10, 2011, with an LHIRES III spectrograph and a 16-inch Meade telescope at Blue Hills Observatory in Dewey, Arizona. Equivalent width and radial velocity data support the presence of a void or ring structure within the eclipsing disk, and they support a central disk clearing around an unseen primary central object. The results also indicate the disk does not end at fourth contact but continues for a significant distance. Analysis of radial velocities demonstrated the profile of the 5853Å line has a disk component in addition to the primary F0 star component. A split line at this location was observed. From the equivalent width profile of the 5853Å line the duration of the split line event was estimated to be 101 days. Other lesser results are presented and discussed.

1. Introduction

ε Aurigae is an eclipsing binary system with a period of 27.1 years and an eclipse that lasts almost two years. The primary star is an F0 star although recent work indicates it may be a highly evolved object (Leadbeater 2011). The eclipse is thought to be caused by a disk of dust rotating around an unseen central object which is in orbit around the primary F0 star. The last eclipse and campaign was 1982–1984. For the 2009–2011 eclipse an international campaign was organized by Dr. Robert E. Stencel and Jeffrey L. Hopkins. There is a major difference between this campaign and the previous one. A lot of the amateur contribution to the previous campaign was in the form of electronic photometry. Since then a range of high performance CCD cameras have become available to the amateur, as well as relatively inexpensive high resolution spectrographs such as SBIG's SGS spectrograph and Shelyak's LHIRES III and eShel spectrographs. The author owns an LHIRES III spectrograph with a resolution greater than 18,000. At the encouragement of Jeff Hopkins, the author worked on the sodium D absorption lines for this campaign.

This paper consists primarily of observations and analyses with some discussion and interpretation. Although the sodium D absorption lines from the disk are confounded with absorption lines from the primary F0 star, no attempt was made to subtract the F0 contribution from the spectra. Doing so requires an

out-of-eclipse estimate of the F0 absorption lines. This can be done, but using it requires one to assume the F0 radial velocities and equivalent widths do not change during the eclipse. The author prefers not to make this assumption and so an out-of-eclipse component was not subtracted. Because such a subtraction would have involved a constant component in any event, it is felt one can still obtain meaningful results and interpretations. In addition to the sodium D lines, this paper also includes a line located at approximately 5853Å. An evaluation of an out-of-eclipse spectrum taken in July 2008 by Olivier Thizy has not been successful in identifying this line. One possibility is Barium II. (The profile is 20080727-031309-epsAur-5x300s_P_1C_FULL.fit and is found at the ε Aur spectral database maintained by Robin Leadbeater at http://www.threehillsobservatory.co.uk/astro/epsaur_campaign/epsaur_campaign_spectra_table.htm.) In lieu of a definite identification, it will be referred to as the 5853Å line in this paper. It exhibits an unexpected line split which will be discussed.

The sodium doublet consists of two lines, D_2 (λ = 5889.95Å) and D_1 (λ = 5895.924Å). Figure 1 is a typical spectrum, normalized, of the sodium D lines region, about 175 Ångstroms wide, taken on February 26, 2010. Figure 2 contains profile examples to illustrate the evolution of the D lines. It also illustrates the resolution capabilities of the LHIRES III spectrograph.

The data contained in Tables 1, 2, 3, and 4, are available for download from the AAVSO ftp site at ftp://ftp.aavso.org/public/datasets/jgoros402a.txt, jgoros402b.txt, jgoros402c.txt, and jgoros402d.txt.

2. Instrumentation and methods

The work was conducted at the author's personal observatory, Blue Hills Observatory (http://users.commspeed.net/stanlep/homepagens.html), located in Dewey, Arizona. The equipment consisted of a Meade 16-inch LX200R telescope (vintage 2006), the LHIRES III spectrograph, an ST8-XME camera for imaging the spectra, and a Meade DSI I camera for guiding. The spectrograph's slit width was set at 22-microns, which enabled the spectrograph to obtain higher resolution spectra than possible with the wider width, usually around 30 to 35 microns, normally used by owners of the LHIRES. Various guiding software was tried and tested. The major ones used were Meade's ENVISAGE and PHD. CCDSOFT captured the images, IRIS (version 5.57) was used to reduce the spectra, and VSPEC and AUDELA were used to calibrate and do additional processing. Great care was taken to obtain very good calibrations using telluric lines. After calibration the telluric lines were removed (using VSPEC) and the spectra were then heliocentric corrected. After all this processing, the reduced spectra were analyzed using SPSS, a statistical software package. The graphs and tables in this paper were produced with SPSS.

Table 1 gives the dates the spectra were taken. Because of the short integration time—only ten minutes—many times more than one spectrum per night were

obtained. The result was a total of seventy spectra over the time period the author participated in the campaign. The data points of these additional spectra per night can be seen in the graphs in this paper.

3. Equivalent width

Equivalent width (EW) was estimated using the method described by Gorodenski (2011). With this method a continuum is estimated with a least squares polynomial regression model. The beginning and end points of a line for the purpose of computing an EW are defined where the line is judged to come in contact with, or cross through, the estimated continuum. At times during the evolution of the Na D lines, the midpoint between the D_2 and D_1 lines drops below the estimated continuum. When this happened the crossover points for estimating the equivalent widths were taken to be midway between the D lines.

Table 1 has the equivalent widths (in Ångstroms) and 95% upper and lower confidence limits for the Na D lines and the 5853Å line. Figures 3 and 4 are plots of the equivalent widths of the Na D_2 and Na D_1 lines, respectively.

The estimated contact dates of the eclipse in B band from Hopkins (2012) are:

1st Contact	August 11, 2009	JD 2455054
2nd Contact	December 19, 2009	JD 2455184
Mid-Eclipse	August 4, 2010	JD 2455412
3rd Contact	March 19, 2011	JD 2455639
4th Contact	May 13, 2011	JD 2455694

The applicable dates (the last three) are shown in all the graphs in this paper.

The disk inclination has been reported to be nearly edge on (Hopkins and Stencel 2008) and at most 90° ± 2° (Kloppenborg 2012). As the disk moves across (eclipses) the star, the amount of disk material contributing to a spectrum should be at a minimum at mid-eclipse, gradually increase to a maximum at third contact, and after third contact it should decline. One would expect equivalent widths to conform to these changing amounts of disk material. The profile of the equivalent widths in Figures 3 and 4 generally agrees with these expectations. The equivalent widths are at a low point (although not the lowest as will be shortly discussed) at mid-eclipse, and they gradually increase after mid-eclipse until they reach a high point at third contact. After third contact they exhibit a decline as expected. However, the decline appears to continue well after fourth contact (150 days beyond fourth contact) when the primary F0 star should be far clear of the disk. The relatively constant slope of the decline for 150 days after the star reached fourth contact indicates the disk material does not abruptly end at this point, but gradually disappears.

There are a few irregularities in the graphs that appear to be real, that is, they are not a sampling error or a problem with the data. One is a dip at

approximately January 16, 2011. The author interprets this as a variation in the amount of disk material, meaning the disk material is not distributed uniformly across the disk and may be patchy or clumpy. This agrees with Leadbeater *et al.* (2011) who interpret structure within the disk as being responsible for the rate of increase of EW during ingress.

The other anomaly, a major one, is at the beginning of the series. The series (profile) of equivalent widths start at a significantly lower level than at mid-eclipse. There is a definite increasing trend that starts from the beginning of the series and peaks on March 28, 2010. (Based on the author's experience with regression analysis, a statistically significant polynomial regression model would fit this part of the series. It should be obvious to the reader that this trend is not random error.) This anomaly over the same time period is also seen in the radial velocity graphs of D_2 and D_1 in Figures 6 and 7, respectively, in the section to follow on radial velocities.

The EW and radial velocity data together are evidence of a ring structure to the disk (Leadbeater and Stencel 2010; Seebode *et al.* 2011), or a large void in the disk (the author's hypothesis). If a ring gap or void exists, there would be less material contributing to a line strength and, hence, the equivalent width would be smaller in value. As the disk moves from first contact to the point where the primary F0 star just clears the inner boundary of the disk, radial velocities should increase, not drop, according to Kepler's Law of Planetary Motion. A large void or ring gap explains the drop in radial velocities for the following reason. Because there would be no disk material in this space there would be no disk material moving in a radial direction away from the observer (the radial velocity values are positive and so the movement would be away from the observer). The contribution to the observed radial velocities then can only come from the parts of the disk on either side of the void. What the observer sees is the radial component (the other component is the proper motion component) of the disk as it rotates. This radial component has a smaller velocity value than material moving directly away from the observer would have at the location of the hypothesized void or ring gap. As the void or gap moves across the primary F0 star, radial velocities start increasing as dust material moves into the line of sight.

Figure 5 is a graph of the 5853Å line equivalent widths. It can be seen that the EW profile is much more variable. However, a second order polynomial regression model, shown in the graph, was statistically significant at the 0.001 level, indicating the 5853Å line profile generally follows the same trend as the Na D lines. (A second order polynomial was statistically significant for both D lines and in the same direction as the 5853Å polynomial but is not displayed in the graphs because of a concern of too much graph clutter.) The large drop that bottoms out between third and fourth contact can be explained by a split line which will be discussed later.

4. Radial velocity and the 5853Å split line

An estimate of radial velocity requires an estimate of the center of a spectral line. Four different kinds of estimates were made with the assistance of VSPEC. They fall into two major categories: EW versus Visual. EW means that the beginning and end points of a line for line center estimation were the same beginning and end points that were used for estimating the line's equivalent width (using the method described in Gorodenski 2011). Because of the frequent occurrence of a long wing on the blue side of the D_2 line, it was felt this method might not give good line center estimates. Therefore, a separate set of estimates was made based on a visual "guess" of the beginning and end points of the lines in VSPEC. An attempt was made to minimize inclusion of asymmetric long wings. Although this Visual estimate is difficult to define, an attempt was made to be as consistent from spectrum to spectrum as much as possible.

Within each of these two categories, that is, EW and Visual, two kinds of line estimates were performed in VSPEC. One was a barycenter line estimate, which will be called "Barycenter," produced by checking a box in VSPEC called "Line Center." The other is a "Gaussian fit" estimate. However, VSPEC uses the line location of the barycenter of the Gaussian fitted line as the line center, that is, the line center estimate is not the estimated parameter of the Gaussian function. However, it will still be called the "Gaussian" estimate.

The line center estimates of each of the sodium D lines consisted of the four types just described. However, the 5853Å line is much weaker than the D lines. Because of this it was felt getting a "Visual" estimate for the 5853Å line would have been very difficult, maybe impossible to consistently estimate. As a result, the beginning and end points for estimating a line were the beginning and end points that were used to estimate the equivalent widths. Consequently, there were only two estimates (in contrast to the four for the D lines), the Barycenter and the Gaussian estimates.

A decision had to be made as to which of the four estimates for sodium and the two for the 5853Å line are the best for computing radial velocities. To do this a standard deviation was computed for each of the line estimation methods for each element line. Table 2 contains these standard deviations. For the 5853Å line the Barycenter estimates have a lower standard deviation than the Gaussian estimates. Hence, the Barycenter estimates were used for computing the 5853Å radial velocities. For both sodium D lines the "Visual" estimates have smaller standard deviations than the "EW" estimates. Within "Visual," the Barycenter estimates have smaller standard deviations. Hence, for the D lines the Visual-Barycenter estimates were used to compute radial velocities. Table 3 contains the line center estimates for all three lines. Table 3 also contains a VSPEC estimate of the line centers of the 5853A split line, the split line mentioned in the introduction of this paper.

Table 4 contains the radial Velocities (km/sec) for Na D_2, Na D_1, 5853Å, and the 5853Å split line. By convention, a positive value indicates a red Doppler shift, that is, the object is moving away from the observer. A negative value means a blue Doppler shift, or an object moving toward the observer.

Figures 6 and 7 are plots of the radial velocities for Na D_2 and Na D_1, respectively, with a statistically significant (0.001) 2nd order polynomial regression line for each. There are a number of things to notice. First, at mid-eclipse it is expected that the radial velocity should be equal to zero. The horizontal solid line is the zero radial velocity line. The estimated points where the interpolated Na D_2 and Na D_1 lines cross the horizontal zero radial velocity line are August 8, 2010, and August 4, 2010, respectively.

However, these are not mid-eclipse estimates because the ε Aur system is moving toward Earth at about 2.5 km/sec, ± 0.9 km/sec. Consequently, what might be a red shift radial velocity of 2.5 km/sec with ε Aur as the frame of reference will appear as a zero km/sec radial velocity from Earth, that is, with Earth as the frame of reference. Therefore, 2.5 km/sec has to be added to the radial velocities in this paper to convert to the ε Aur frame of reference. When this is done, the author's data suggest the mid-eclipse dates for Na D_2 and Na D_1 are August 18, 2010, and August 16, 2010, respectively. Because there is no quantum explanation that could allow the D line to have different mid-eclipse dates, these dates can be taken as independent estimates of the actual mid-eclipse date. Averaging the two gives an estimated mid-eclipse date of August 17, 2010.

The increasing radial velocities from the beginning of the series to March 28, 2010, have already been explained as being due to a possible ring gap, or a possible void in the disk.

The radial velocity curve from about May 6, 2010, to about November 1, 2010, in both Figures 6 and 7 supports the hypothesis that the disk has a central clear area around an unseen central object. In other words, the disk has an outer and inner edge, or boundary. Based on this hypothesis, one would expect a decreasing radial velocity from March 28, 2010 (assuming this part of the curve is at or near the inner boundary on the ingress side of the disk) to mid-eclipse and then an increasing one from mid-eclipse to November 1, 2010 (assuming this part of the curve is at or near the inner boundary on the egress side of the disk) and this is what is observed. The explanation for this expectation is the same as the one given to explain the drop in radial velocities in the above section on equivalent width. Essentially, without central dust, the observer is seeing the disk on both sides of the void. As a result, what is being observed is the radial component (the other component being the proper motion component) to the rotational motion of the disk. As the mid-eclipse is approached this radial component becomes smaller, eventually going to zero. The reverse occurs on the other side of mid-eclipse. This explains the shape and direction of the line between these dates.

As can be seen in Figures 6 and 7, the radial velocities still have not reached the zero radial velocity level after 4th contact. The last data point in the graph is October 10, 2011. This is 150 days past fourth contact. By this time the primary F0 star should be well clear of the disk. Yet, radial velocities on this date are over 8 km/sec (see Table 4). This is additional evidence in support of the EW data that the disk continues well beyond fourth contact.

Figure 8 is the radial velocity plot for the 5853Å line. It is of interest to determine whether this line is undergoing the same radial velocity change as the Na D lines. If it is, then this would be evidence there is a disk component to the 5853Å absorption line. The second order polynomials in Figures 6 and 7 for the D lines are statistically significant (0.001). Although the 5853Å radial velocities exhibit more variability than those of the Na D lines, a statistically significant (0.001) second order polynomial model also fits the data and is in the same direction as the D lines polynomials. This is evidence that there is a disk component to the 5853Å absorption line. However, this is not certain. It could all still be from the primary F0 star.

There is one big difference in the 5853Å line profile compared to the D lines. Starting just after January 27, 2011, the 5853Å radial velocities undergo a large blue shift drop and reach a high of 28.866 km/sec on April 13, 2011 (spectrum number 1 in Table 4). The Na D lines do not exhibit such a drop. The largest blue shift for the D_2 and D_1 lines were 23.842 km/sec and 23.843 km/sec, respectively, on January 17, 2011 (spectrum number 1 in Table 4).

The large drop in the 5853Å radial velocities is caused by the confounding effect of the 5853Å split line. Figure 9 is a graph of the split line radial velocities with a superimposed statistically significant (0.001) first order polynomial regression line. It can be seen the split line radial velocities had already started dropping on January 17, 2011, and reached a high blue shift of 27.954 km/sec on April 26, 2011 (spectrum number 1 in Table 4). These dates do not exactly match those for the 5853Å line but are close. There are two reasons for the inexact match: the split line data is very incomplete, and the line centers could only be roughly estimated in VSPEC. Figure 10 shows the evolution of the split line and illustrates some of the difficulties of getting line center estimates. The profile on December 25, 2010, was included to demonstrate the latter. This profile exhibits what might be called a plateau, not a well defined line such as the one on March 28, 2010.

Such a plateau makes it impossible to estimate a split line center. In addition, there were undoubtedly 5853Å spectra that contained the effects of a split line on EW and radial velocity, but the effect was too small to be noticeable in a line profile.

The start and end dates of the split line phenomenon cannot be determined from the split line data itself, but it appears a reasonable estimate might be obtained from Figure 5, the graph of the 5853Å equivalent widths. A visual inspection of the graph places the start and end of the split line at January 27,

2011, and May 8, 2011, respectively, which gives a duration of 101 days. Kim (2008) reports a 67-day and a 123-day period, although it is not clear what these periods represent, that is, what they are periods of.

5. Conclusion

This paper has demonstrated the high resolution spectroscopic work that can be done with the LHIRES III spectrograph. The paper also demonstrated the following:

1. The profile of the equivalent widths for the Na D lines generally agree with expectations prior to mid-eclipse, at mid-eclipse, and at third contact.

2. The equivalent width data for the D lines support the hypothesis that some of the variation in EW are the result of a non-homogeneous disk, that is, a disk that is patchy or clumpy.

3. The EW data support the hypothesis that the disk does not abruptly end at fourth contact, but gradually trails off.

4. The estimated mid-eclipse date based on the sodium D lines is August 17, 2010. This estimate does not differ substantially from the projected mid-eclipse date (made prior to mid-eclipse) of August 4, 2010.

5. The Na D_2 and D_1 radial velocities reached their highest value, a blue shift, of 23.842 km/sec and 23.843 km/sec, respectively, on January 17, 2011.

6. The EW and radial velocity data support the hypotheses of a ring structure to the disk as others have proposed. The author proposes as an alternative a large void within the disk.

7. The 5853Å line radial velocity profile supports the hypothesis that the 5853Å absorption line has a disk component.

8. The radial velocity data supports the existence of a central clearing around the unseen primary object of the disk, that is, the disk has an inner boundary.

9. The 5853Å absorption profile contains a split line. The estimated duration of the split line event was estimated to be 101 days.

6. Acknowledgements

I would like to thank Jeff Hopkins for encouraging me to join the ε Aur Campaign, and for encouraging me to concentrate my spectroscopy on the sodium D lines region. I would also like to thank Jeff Hopkins for suggesting that I purchase the Meade 16-inch LX200R telescope way back in the year 2005.

It has turned out to be a superb telescope for doing spectroscopy. Without his suggestion I might still be attempting to retrofit my old 12.5-inch Dall-Kirkham, made by a machinist friend, instead of participating in this campaign.

References

Gorodenski, S. 2011, *Soc. Astron. Sci. Newsl.*, **9** (no. 2), 5.

Hopkins, J. L. 2012, ε Aur Campaign website (http://www.hposoft.com/EAur09/Starinfo.html).

Hopkins, J. L., and Stencel, R. E. 2008, *Epsilon Aurigae: a Mysterious Star System*, Hopkins Phoenix Observatory, Phoenix, Arizona.

Kim, H. 2008, *J. Astron. Space Sci.*, **25**, 1.

Kloppenborg, B. 2012, private communication.

Leadbeater, R. 2011, "The International Epsilon Aurigae Campaign 2009–2011. A Description of the Campaign and early Results," arXiv:1101.1435v1 [astro-ph.SR), 67.

Leadbeater, R. 2012, ε Aur spectral database (http://www.threehillsobservatory.co.uk/astro/epsaur_campaign/epsaur_campaign_spectra_table.htm), profile 20080727-031309-epsAur-5x300s_P_1C_FULL.fit.—

Leadbeater, R., and Stencel, R. E. 2010, "Structure of the Disc of Epsilon Aurigae: Spectroscopic Observations of neutral Potassium during Eclipse Ingress," arXiv:1003.3617v2 [astro-ph.SR].

Leadbeater, R., *et al.*, 2011, *Bull. Amer. Astron. Soc.*, **43**, 257.04.

Seebode, S., Howell, S. B., Drumheller, D., Stanford, D., Hoard, D. W., and Stencel, R. E. 2011, *Bull. Amer. Astron. Soc.*, **43**, 257.08.

Table 1. ε Aur, equivalent widths (in Ångstroms) and 95% confidence limits for Na D_2, Na D_1, and the 5853Å line.

Date	*Spectrum Sequence Number*	*Julian Date*	*Na D_2 Lower Conf. Limit (Å)*	*Na D_2 EW (Å)*	*Na D_2 Upper Conf. Limit (Å)*	*Na D_1 Lower Conf. Limit (Å)*	*Na D_1 EW (Å)*	*Na D_1 Upper Conf. Limit(Å)*	*5853Å Lower Conf. Limit (Å)*	*5853Å EW (Å)*	*5853Å Upper. Conf. Limit (Å)*
2010 Feb 13	1	2455240.719352	1.2852	1.3219	1.3587	1.2008	1.2282	1.2555	.0630	.0723	.0815
2010 Feb 13	2	2455240.740081	1.2853	1.3208	1.3564	1.2034	1.2298	1.2562	.0571	.0695	.0820
2010 Feb 13	3	2455240.762222	1.2849	1.3211	1.3573	1.1979	1.2310	1.2641	.0493	.0638	.0782
2010 Feb 14	1	2455241.686528	1.3072	1.3394	1.3717	1.2141	1.2398	1.2656	.0562	.0671	.0780
2010 Feb 14	2	2455241.712986	1.2986	1.3223	1.3459	1.2075	1.2278	1.2481	.0600	.0702	.0804
2010 Feb 14	3	2455241.734444	1.2928	1.3185	1.3442	1.1967	1.2224	1.2481	.0596	.0702	.0808
2010 Feb 19	1	2455246.633507	1.2978	1.3317	1.3656	1.1997	1.2304	1.2612	.0624	.0774	.0924
2010 Feb 19	2	2455246.651863	1.2860	1.3328	1.3795	1.2034	1.2436	1.2839	.0608	.0772	.0937
2010 Feb 19	3	2455246.669815	1.2920	1.3303	1.3685	1.2072	1.2367	1.2662	.0618	.0773	.0928
2010 Feb 19	4	2455246.680093	1.3037	1.3335	1.3632	1.2095	1.2338	1.2582	.0597	.0757	.0916
2010 Feb 26	1	2455253.654190	1.2845	1.3147	1.3449	1.1939	1.2233	1.2526	.0555	.0690	.0826
2010 Mar 04	1	2455259.650289	1.2957	1.3247	1.3536	1.2032	1.2331	1.2631	.0422	.0560	.0698
2010 Mar 04	2	2455259.669225	1.2936	1.3296	1.3655	1.2038	1.2345	1.2651	.0427	.0610	.0792
2010 Mar 04	3	2455259.689699	1.3073	1.3377	1.3681	1.2043	1.2302	1.2561	.0382	.0512	.0642
2010 Mar 13	1	2455268.681319	1.3237	1.3548	1.3858	1.2273	1.2526	1.2780	.0279	.0417	.0555
2010 Mar 13	2	2455268.702488	1.3281	1.3626	1.3971	1.2318	1.2652	1.2986	.0281	.0390	.0498
2010 Mar 13	3	2455268.722338	1.3240	1.3727	1.4215	1.2292	1.2636	1.2979	.0260	.0413	.0566
2010 Mar 28	1	2455283.653206	1.4154	1.4482	1.4810	1.3029	1.3336	1.3642	.0192	.0324	.0456
2010 Mar 28	2	2455283.674873	1.4202	1.4623	1.5043	1.3112	1.3409	1.3706	.0160	.0359	.0558
2010 Mar 28	3	2455283.695197	1.4281	1.4615	1.4948	1.3269	1.3565	1.3860	.0228	.0385	.0543
2010 May 08	1	2455324.636933	1.3779	1.4161	1.4543	1.2704	1.3028	1.3351	.0464	.0622	.0781

Table continued on following pages

Table 1. ε Aur, equivalent widths (in Ångstroms) and 95% confidence limits for Na D_2, Na D_1, and the 5853Å line, cont.

Date	*Spectrum Sequence Number*	*Julian Date*	*Na D_2 Lower Conf. Limit (Å)*	*Na D_2 EW (Å)*	*Na D_2 Upper Conf. Limit (Å)*	*Na D_1 Lower Conf. Limit (Å)*	*Na D_1 EW (Å)*	*Na D_1 Upper Conf. Limit(Å)*	*5853Å Lower Conf. Limit (Å)*	*5853Å EW (Å)*	*5853Å Upper. Conf. Limit (Å)*
2010 May 08	2	2455324.647917	1.3813	1.4145	1.4477	1.2697	1.2976	1.3256	.0496	.0655	.0814
2010 May 08	3	2455324.658241	1.3788	1.4215	1.4642	1.2599	1.2959	1.3319	.0527	.0723	.0920
2010 Aug 05	1	2455413.919329	1.3131	1.4145	1.5159	1.1531	1.2499	1.3467	.0255	.0428	.0600
2010 Aug 05	2	2455413.937581	1.3324	1.4031	1.4739	1.1799	1.2473	1.3147	.0279	.0368	.0457
2010 Aug 05	3	2455413.957431	1.3509	1.4272	1.5036	1.1799	1.2527	1.3255	.0274	.0379	.0484
2010 Sep 24	1	2455463.808264	1.3908	1.4178	1.4447	1.2666	1.2890	1.3114	.0466	.0580	.0694
2010 Sep 24	2	2455463.825220	1.3890	1.4157	1.4424	1.2633	1.2868	1.3103	.0579	.0668	.0756
2010 Oct 08	1	2455477.790775	1.4504	1.4809	1.5115	1.3268	1.3547	1.3825	.0441	.0577	.0712
2010 Oct 08	2	2455477.811817	1.4598	1.4852	1.5106	1.3289	1.3502	1.3714	.0458	.0611	.0764
2010 Nov 04	1	2455504.728750	1.5895	1.6337	1.6778	1.4508	1.4897	1.5286	.0749	.0869	.0990
2010 Nov 04	2	2455504.741042	1.5957	1.6383	1.6809	1.4492	1.4899	1.5305	.0757	.0904	.1052
2010 Nov 04	3	2455504.753403	1.6113	1.6394	1.6675	1.4716	1.4981	1.5246	.0738	.0839	.0940
2010 Dec 07	1	2455537.779896	1.7500	1.7803	1.8105	1.6409	1.6664	1.6920	.0421	.0577	.0732
2010 Dec 07	2	2455537.792292	1.7341	1.7717	1.8092	1.6318	1.6595	1.6871	.0502	.0625	.0748
2010 Dec 07	3	2455537.803646	1.7448	1.7730	1.8011	1.6352	1.6591	1.6831	.0379	.0525	.0672
2010 Dec 25	1	2455555.738889	1.7719	1.8017	1.8316	1.6643	1.6941	1.7239	.0545	.0662	.0780
2010 Dec 25	2	2455555.750000	1.7458	1.8050	1.8641	1.6412	1.6910	1.7409	.0579	.0691	.0804
2011 Jan 17	1	2455578.718461	1.7408	1.7710	1.8012	1.6433	1.6676	1.6920	.1040	.1163	.1286
2011 Jan 17	2	2455578.737396	1.7401	1.7717	1.8033	1.6441	1.6675	1.6909	.1022	.1150	.1278
2011 Jan 27	1	2455588.685625	1.7520	1.7767	1.8014	1.6632	1.6888	1.7144	.1062	.1245	.1428
2011 Jan 27	2	2455588.697546	1.7641	1.8006	1.8371	1.6678	1.6981	1.7285	.0995	.1175	.1354

Table continued on following pages

Table 1. ε Aur, equivalent widths (in Ångstroms) and 95% confidence limits for Na D_2, Na D_1, and the 5853Å line, cont.

Date	*Spectrum Sequence Number*	*Julian Date*	*Na D_2 Lower Conf. Limit (Å)*	*Na D_2 EW (Å)*	*Na D_2 Upper Conf. Limit (Å)*	*Na D_1 Lower Conf. Limit (Å)*	*Na D_1 EW (Å)*	*Na D_1 Upper Conf. Limit(Å)*	*5853Å Lower Conf. Limit (Å)*	*5853Å EW (Å)*	*5853Å Upper. Conf. Limit (Å)*
2011 Feb 12	1	2455604.663553	1.7764	1.8215	1.8665	1.6841	1.7219	1.7597	.0839	.1003	.1166
2011 Feb 12	2	2455604.679606	1.7707	1.8058	1.8408	1.6762	1.7112	1.7462	.0892	.1117	.1341
2011 Mar 05	1	2455625.639016	1.8054	1.8575	1.9095	1.6769	1.7154	1.7538	.0831	.1004	.1177
2011 Mar 05	2	2455625.649919	1.8086	1.8605	1.9124	1.6883	1.7264	1.7645	.0830	.1009	.1188
2011 Mar 05	3	2455625.660567	1.8149	1.8650	1.9150	1.6978	1.7330	1.7681	.0835	.1015	.1195
2011 Mar 05	4	2455625.673125	1.8096	1.8655	1.9215	1.6950	1.7353	1.7756	.0855	.1021	.1187
2011 Mar 10	1	2455630.687222	1.8009	1.8610	1.9211	1.6704	1.7155	1.7606	.0674	.0899	.1125
2011 Mar 10	2	2455630.697222	1.7927	1.8554	1.9181	1.6679	1.7126	1.7573	.0655	.0822	.0989
2011 Mar 10	3	2455630.708461	1.8104	1.8574	1.9043	1.6786	1.7145	1.7504	.0696	.0856	.1015
2011 Mar 23	1	2455643.651956	1.8097	1.8647	1.9196	1.6626	1.7132	1.7638	.0511	.0682	.0852
2011 Mar 23	2	2455643.667616	1.8159	1.8716	1.9272	1.6648	1.7151	1.7654	.0718	.0972	.1225
2011 Mar 23	3	2455643.682164	1.8277	1.8646	1.9015	1.6772	1.7080	1.7388	.0521	.0714	.0908
2011 Apr 02	1	2455653.638958	1.7557	1.8112	1.8668	1.6099	1.6533	1.6966	.0500	.0638	.0776
2011 Apr 02	2	2455653.648762	1.7552	1.8082	1.8611	1.6081	1.6492	1.6904	.0440	.0621	.0802
2011 Apr 13	1	2455664.638056	1.7012	1.7541	1.8070	1.5599	1.5981	1.6362	.0630	.0786	.0941
2011 Apr 13	2	2455664.647801	1.7172	1.7612	1.8052	1.5774	1.6139	1.6503	.0705	.0830	.0954
2011 Apr 13	3	2455664.658252	1.7073	1.7650	1.8228	1.5643	1.6082	1.6522	.0587	.0777	.0967
2011 Apr 26	1	2455677.616528	1.6404	1.6810	1.7215	1.5047	1.5326	1.5605	.0746	.0841	.0936
2011 Apr 26	2	2455677.631076	1.6256	1.6646	1.7035	1.4984	1.5314	1.5643	.0711	.0847	.0983
2011 Apr 26	3	2455677.647581	1.6293	1.6761	1.7228	1.4956	1.5308	1.5660	.0728	.0834	.0940
2011 May 08	1	2455689.627975	1.6196	1.6586	1.6976	1.4791	1.5028	1.5265	.1022	.1113	.1205

Table continued on next page

Table 1. ε Aur, equivalent widths (in Ångstroms) and 95% confidence limits for Na D_2, Na D_1, and the 5853Å line, cont.

Date	*Spectrum Sequence Number*	*Julian Date*	*Na D_2 Lower Conf. Limit (Å)*	*Na D_2 EW (Å)*	*Na D_2 Upper Conf. Limit (Å)*	*Na D_1 Lower Conf. Limit (Å)*	*Na D_1 EW (Å)*	*Na D_1 Upper Conf. Limit(Å)*	*5853Å Lower Conf. Limit (Å)*	*5853Å EW (Å)*	*5853Å Upper. Conf. Limit (Å)*
2011 May 31	1	2455712.626944	1.5604	1.6194	1.6785	1.4383	1.4776	1.5169	.0830	.1014	.1198
2011 Aug 16	1	2455789.862280	1.2727	1.3440	1.4153	1.2160	1.2870	1.3581	.0661	.0850	.1040
2011 Aug 16	2	2455789.876863	1.2920	1.3635	1.4350	1.2244	1.2915	1.3586	.0696	.0787	.0877
2011 Aug 30	1	2455803.851956	1.2969	1.3255	1.3541	1.2218	1.2448	1.2678	.0283	.0402	.0521
2011 Aug 30	2	2455803.865093	1.2985	1.3229	1.3474	1.2259	1.2449	1.2638	.0312	.0429	.0546
2011 Sep 18	1	2455822.813137	1.2674	1.2931	1.3188	1.1765	1.1988	1.2212	.0300	.0402	.0505
2011 Oct 10	1	2455844.770972	1.1888	1.2073	1.2258	1.1119	1.1316	1.1513	.0440	.0519	.0599

Table 2. Standard deviations for line estimation methods.

Line	*Method*	*Mean*	*Std Dev.*
5853Å	EW Barycenter	5853.5185	0.24589
	EW Gaussian	5853.4722	0.31127
Na D_2	EW Barycenter	5889.7920	0.31523
	EW Gaussian	5889.8235	0.30328
	Visual Barycenter	5889.8086	0.30284
	Visual Gaussian	5889.8239	0.30320
Na D_1	EW Barycenter	5895.7780	0.30931
	EW Gaussian	5895.7966	0.30839
	Visual Barycenter	5895.7852	0.30721
	Visual Gaussian	5895.7969	0.30845

Table 3. ε Aur, line center estimates in Ångstroms for Na D_2, Na D_1, the 5853Å line, and the 5853Å split line.

Date	*Spectrum Sequence Number*	*Julian Date*	*Na D_2 (Å)*	*Na D_1 (Å)*	*5853Å Line (Å)*	*5853Å Split Line (Å)*
2010 Feb 13	1	2455240.719352	5890.1240	5896.1199	5853.6636	—
2010 Feb 13	2	2455240.740081	5890.1328	5896.1319	5853.6760	—
2010 Feb 13	3	2455240.762222	5890.1580	5896.1532	5853.6721	—
2010 Feb 14	1	2455241.686528	5890.1130	5896.1122	5853.6458	—
2010 Feb 14	2	2455241.712986	5890.1520	5896.1372	5853.6659	—
2010 Feb 14	3	2455241.734444	5890.1348	5896.1408	5853.6925	—
2010 Feb 19	1	2455246.633507	5890.1841	5896.1650	5853.7409	—
2010 Feb 19	2	2455246.651863	5890.1750	5896.1535	5853.7411	—
2010 Feb 19	3	2455246.669815	5890.1762	5896.1708	5853.7455	—
2010 Feb 19	4	2455246.680093	5890.1769	5896.1693	5853.7587	—
2010 Feb 26	1	2455253.654190	5890.1869	5896.1867	5853.7940	—
2010 Mar 04	1	2455259.650289	5890.2260	5896.2160	5853.9072	—
2010 Mar 04	2	2455259.669225	5890.1948	5896.1877	5853.8784	—
2010 Mar 04	3	2455259.689699	5890.2227	5896.2039	5853.8547	—
2010 Mar 13	1	2455268.681319	5890.2551	5896.2396	5853.8716	—
2010 Mar 13	2	2455268.702488	5890.2340	5896.2190	5853.8145	—
2010 Mar 13	3	2455268.722338	5890.2398	5896.2217	5853.9332	—
2010 Mar 28	1	2455283.653206	5890.2747	5896.2642	5853.6779	5853.7398
2010 Mar 28	2	2455283.674873	5890.2816	5896.2531	5853.7153	5853.7943
2010 Mar 28	3	2455283.695197	5890.2584	5896.2483	5853.7051	—
2010 May 08	1	2455324.636933	5890.2483	5896.2159	5853.7420	—
2010 May 08	2	2455324.647917	5890.2486	5896.2260	5853.8617	—

Table continued on following pages

Table 3. ε Aur, line center estimates in Ångstroms for Na D_2, Na D_1, the 5853Å line, and the 5853Å split line, cont.

Date	*Spectrum Sequence Number*	*Julian Date*	*Na D_2 (Å)*	*Na D_1 (Å)*	*5853Å Line (Å)*	*5853Å Split Line (Å)*
2010 May 08	3	2455324.658241	5890.2334	5896.2057	5853.8222	—
2010 Aug 05	1	2455413.919329	5889.9752	5895.9164	5853.4407	—
2010 Aug 05	2	2455413.937581	5889.9750	5895.9192	5853.4436	—
2010 Aug 05	3	2455413.957431	5889.9444	5895.9222	5853.4442	—
2010 Sep 24	1	2455463.808264	5889.7200	5895.7016	5853.6694	5853.6473
2010 Sep 24	2	2455463.825220	5889.7234	5895.7037	5853.6482	—
2010 Oct 08	1	2455477.790775	5889.6684	5895.6463	5853.4881	—
2010 Oct 08	2	2455477.811817	5889.6509	5895.6249	5853.4813	—
2010 Nov 04	1	2455504.728750	5889.5534	5895.5358	5853.4995	—
2010 Nov 04	2	2455504.741042	5889.5618	5895.5321	5853.5089	—
2010 Nov 04	3	2455504.753403	5889.5641	5895.5408	5853.5117	—
2010 Dec 07	1	2455537.779896	5889.5108	5895.4989	5853.5746	—
2010 Dec 07	2	2455537.792292	5889.5315	5895.5149	5853.5760	5853.6130
2010 Dec 07	3	2455537.803646	5889.5159	5895.4926	5853.5497	—
2010 Dec 25	1	2455555.738889	5889.5171	5895.4846	5853.2774	—
2010 Dec 25	2	2455555.750000	5889.5177	5895.4922	5853.2923	—
2011 Jan 17	1	2455578.718461	5889.4816	5895.4511	5853.3708	5853.5019
2011 Jan 17	2	2455578.737396	5889.4974	5895.4673	5853.3825	—
2011 Jan 27	1	2455588.685625	5889.5192	5895.4856	5853.5203	5853.3694
2011 Jan 27	2	2455588.697546	5889.4865	5895.4618	5853.4414	5853.4001
2011 Feb 12	1	2455604.663553	5889.5145	5895.4847	5853.3657	5853.2924
2011 Feb 12	2	2455604.679606	5889.5255	5895.4939	5853.4441	5853.2943

Table continued on following pages

Table 3. ε Aur, line center estimates in Ångstroms for Na D_2, Na D_1, the 5853Å line, and the 5853Å split line, cont.

Date	*Spectrum Sequence Number*	*Julian Date*	*Na D_2 (Å)*	*Na D_1 (Å)*	*5853Å Line (Å)*	*5853Å Split Line (Å)*
2011 Mar 05	1	2455625.639016	5889.5191	5895.5073	5853.3333	—
2011 Mar 05	2	2455625.649919	5889.5318	5895.5162	5853.3115	5853.2227
2011 Mar 05	3	2455625.660567	5889.5563	5895.5309	5853.3217	5853.2341
2011 Mar 05	4	2455625.673125	5889.5237	5895.4970	5853.3485	5853.1924
2011 Mar 10	1	2455630.687222	5889.5455	5895.5073	5853.2979	5853.2301
2011 Mar 10	2	2455630.697222	5889.5403	5895.5196	5853.3628	5853.2312
2011 Mar 10	3	2455630.708461	5889.5418	5895.5140	5853.3122	5853.2427
2011 Mar 23	1	2455643.651956	5889.5093	5895.4974	5853.1718	—
2011 Mar 23	2	2455643.667616	5889.5394	5895.5094	—	—
2011 Mar 23	3	2455643.682164	5889.5245	5895.5105	5853.2195	5853.3272
2011 Apr 02	1	2455653.638958	5889.5626	5895.5333	5853.0783	—
2011 Apr 02	2	2455653.648762	5889.5392	5895.5210	5853.0749	—
2011 Apr 13	1	2455664.638056	5889.5417	5895.5153	5853.0564	—
2011 Apr 13	2	2455664.647801	5889.5452	5895.5193	5853.0654	—
2011 Apr 13	3	2455664.658252	5889.5331	5895.5135	5853.0611	—
2011 Apr 26	1	2455677.616528	—	—	5853.1024	5853.0742
2011 Apr 26	2	2455677.631076	5889.5672	5895.5349	5853.1409	—
2011 Apr 26	3	2455677.647581	5889.5658	5895.5371	5853.1361	—
2011 May 08	1	2455689.627975	5889.5490	5895.5315	5853.2246	5853.1741
2011 May 31	1	2455712.626944	5889.6136	5895.6052	5853.4914	5853.1330
2011 Aug 16	1	2455789.862280	5889.8000	5895.7474	5853.8034	—
2011 Aug 16	2	2455789.876863	5889.8108	5895.7479	5853.7481	—

Table continued on next page

Table 3. ε Aur, line center estimates in Ångstroms for Na D_2, Na D_1, the 5853Å line, and the 5853Å split line, cont.

Date	*Spectrum Sequence Number*	*Julian Date*	*Na D_2 (Å)*	*Na D_1 (Å)*	*5853Å Line (Å)*	*5853Å Split Line (Å)*
2011 Aug 30	1	2455803.851956	5889.8141	5895.7765	5853.7714	—
2011 Aug 30	2	2455803.865093	5889.8313	5895.7729	5853.7397	—
2011 Sep 18	1	2455822.813137	5889.8196	5895.7627	5853.4599	5853.3919
2011 Oct 10	1	2455844.770972	5889.7865	5895.7378	5853.6354	—

Table 4. ε Aur, radial velocities (km/sec) for Na D_2, Na D_1, the 5853Å line, and the 5853Å split line (negative value = blue Doppler shift; positive value = red Doppler shift).

Date	*Spectrum Sequence Number*	*Julian Date*	*Na D_2 (Å)*	*Na D_1 (Å)*	*5853Å (Å)*	*5853Å Split Line (Å)*
2010 Feb 13	1	2455240.719352	8.856	10.164	2.233	—
2010 Feb 13	2	2455240.740081	9.304	10.774	2.868	—
2010 Feb 13	3	2455240.762222	10.587	11.857	2.668	—
2010 Feb 14	1	2455241.686528	8.296	9.773	1.321	—
2010 Feb 14	2	2455241.712986	10.281	11.044	2.351	—
2010 Feb 14	3	2455241.734444	9.406	11.227	3.713	—
2010 Feb 19	1	2455246.633507	11.915	12.457	6.192	—
2010 Feb 19	2	2455246.651863	11.452	11.873	6.202	—
2010 Feb 19	3	2455246.669815	11.513	12.752	6.427	—

Table continued on following pages

Table 4. ε Aur, radial velocities (km/sec) for Na D_2, Na D_1, the 5853Å line, and the 5853Å split line (negative value = blue Doppler shift; positive value = red Doppler shift), cont.

Date	*Spectrum Sequence Number*	*Julian Date*	*Na D_2 (Å)*	*Na D_1 (Å)*	*5853Å (Å)*	*5853Å Split Line (Å)*
2010 Feb 19	4	2455246.680093	11.549	12.676	7.103	—
2010 Feb 26	1	2455253.654190	12.058	13.561	8.911	—
2010 Mar 04	1	2455259.650289	14.048	15.050	14.709	—
2010 Mar 04	2	2455259.669225	12.460	13.612	13.234	—
2010 Mar 04	3	2455259.689699	13.880	14.435	12.020	—
2010 Mar 13	1	2455268.681319	15.529	16.250	12.885	—
2010 Mar 13	2	2455268.702488	14.455	15.203	9.961	—
2010 Mar 13	3	2455268.722338	14.750	15.340	16.040	—
2010 Mar 28	1	2455283.653206	16.526	17.501	2.965	6.135
2010 Mar 28	2	2455283.674873	16.878	16.937	4.881	8.927
2010 Mar 28	3	2455283.695197	15.697	16.693	4.358	—
2010 May 08	1	2455324.636933	15.183	15.045	6.248	—
2010 May 08	2	2455324.647917	15.198	15.559	12.378	—
2010 May 08	3	2455324.658241	14.424	14.527	10.355	—
2010 Aug 05	1	2455413.919329	1.283	–0.183	–9.183	—
2010 Aug 05	2	2455413.937581	1.272	–0.041	–9.034	—
2010 Aug 05	3	2455413.957431	–0.285	0.112	–9.004	—
2010 Sep 24	1	2455463.808264	–11.707	–11.105	2.530	1.398
2010 Sep 24	2	2455463.825220	–11.534	–10.998	1.444	—
2010 Oct 08	1	2455477.790775	–14.333	–13.917	–6.755	—

Table continued on following pages

Table 4. ε Aur, radial velocities (km/sec) for Na D_2, Na D_1, the 5853Å line, and the 5853Å split line (negative value = blue Doppler shift; positive value = red Doppler shift), cont.

Date	*Spectrum Sequence Number*	*Julian Date*	*Na D_2 (Å)*	*Na D_1 (Å)*	*5853Å (Å)*	*5853Å Split Line (Å)*
2010 Oct 08	2	2455477.811817	–15.224	–15.005	–7.104	—
2010 Nov 04	1	2455504.728750	–20.187	–19.536	–6.171	—
2010 Nov 04	2	2455504.741042	–19.760	–19.724	–5.690	—
2010 Nov 04	3	2455504.753403	–19.643	–19.282	–5.547	—
2010 Dec 07	1	2455537.779896	–22.356	–21.413	–2.325	—
2010 Dec 07	2	2455537.792292	–21.302	–20.599	–2.253	–0.359
2010 Dec 07	3	2455537.803646	–22.096	–21.733	–3.600	—
2010 Dec 25	1	2455555.738889	–22.035	–22.140	–17.547	—
2010 Dec 25	2	2455555.750000	–22.004	–21.753	–16.784	—
2011 Jan 17	1	2455578.718461	–23.842	–23.843	–12.763	–6.049
2011 Jan 17	2	2455578.737396	–23.038	–23.019	–12.164	—
2011 Jan 27	1	2455588.685625	–21.928	–22.089	–5.106	–12.835
2011 Jan 27	2	2455588.697546	–23.593	–23.299	–9.147	–11.262
2011 Feb 12	1	2455604.663553	–22.167	–22.135	–13.024	–16.778
2011 Feb 12	2	2455604.679606	–21.607	–21.667	–9.009	–16.681
2011 Mar 05	1	2455625.639016	–21.933	–20.985	–14.684	—
2011 Mar 05	2	2455625.649919	–21.287	–20.533	–15.800	–20.348
2011 Mar 05	3	2455625.660567	–20.040	–19.785	–15.278	–19.764
2011 Mar 05	4	2455625.673125	–21.699	–21.509	–13.905	–21.900
2011 Mar 10	1	2455630.687222	–20.589	–20.985	–16.497	–19.969

Table continued on next page

Table 4. ε Aur, radial velocities (km/sec) for Na D_2, Na D_1, the 5853Å line, and the 5853Å split line (negative value = blue Doppler shift; positive value = red Doppler shift), cont.

Date	*Spectrum Sequence Number*	*Julian Date*	*Na D_2 (Å)*	*Na D_1 (Å)*	*5853Å (Å)*	*5853Å Split Line (Å)*
2011 Mar 10	2	2455630.697222	–20.854	–20.360	–13.173	–19.913
2011 Mar 10	3	2455630.708461	–20.778	–20.645	–15.764	–19.324
2011 Mar 23	1	2455643.667616	–20.900	–20.879	—	—
2011 Mar 23	2	2455643.651956	–22.432	–21.489	–22.955	—
2011 Mar 23	3	2455643.682164	–21.658	–20.823	–20.512	–14.996
2011 Apr 02	1	2455653.638958	–19.719	–19.663	–27.744	—
2011 Apr 02	2	2455653.648762	–20.910	–20.289	–27.918	—
2011 Apr 13	1	2455664.638056	–20.783	–20.579	–28.866	—
2011 Apr 13	2	2455664.647801	–20.605	–20.375	–28.405	—
2011 Apr 13	3	2455664.658252	–21.220	–20.670	–28.625	—
2011 Apr 26	1	2455677.616528	–24.127	–23.462	—	–27.954
2011 Apr 26	2	2455677.631076	–19.485	–19.582	–24.538	—
2011 Apr 26	3	2455677.647581	–19.556	–19.470	–24.784	—
2011 May 08	1	2455689.627975	–20.411	–19.755	–20.251	–22.838
2011 May 31	1	2455712.626944	–17.123	–16.007	–6.586	–24.943
2011 Aug 16	1	2455789.862280	–7.635	–8.776	9.393	—
2011 Aug 16	2	2455789.876863	–7.085	–8.751	6.561	—
2011 Aug 30	1	2455803.851956	–6.917	–7.297	7.754	—
2011 Aug 30	2	2455803.865093	–6.042	–7.480	6.130	—
2011 Sep 18	1	2455822.813137	–6.637	–7.998	–8.200	–11.682
2011 Oct 10	1	2455844.770972	–8.322	–9.265	0.789	—

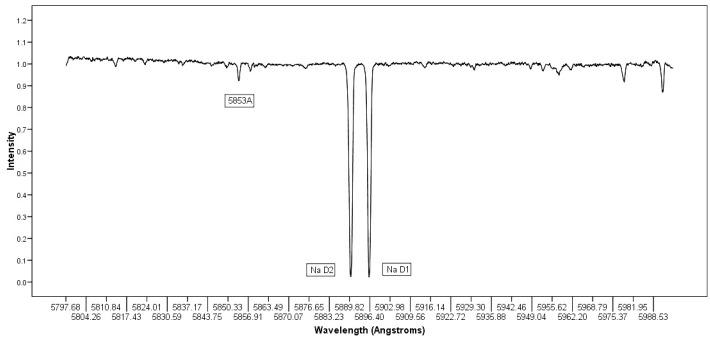

Figure 1. The sodium D lines region encompassing the 5853Å line. This is a normalized spectrum taken on February 26, 2010.

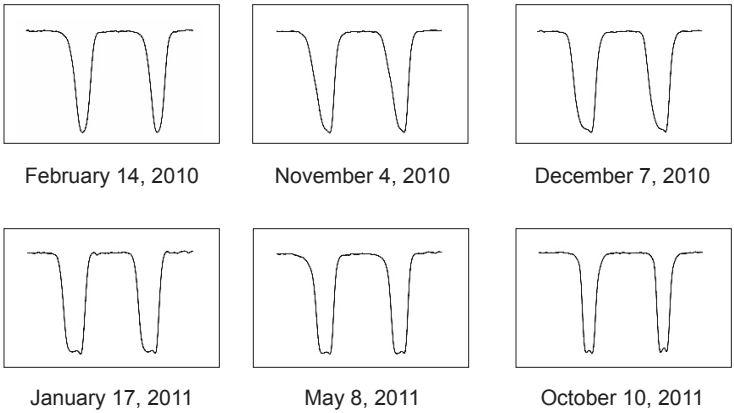

Figure 2. Example spectra to illustrate evolution of the sodium D lines.

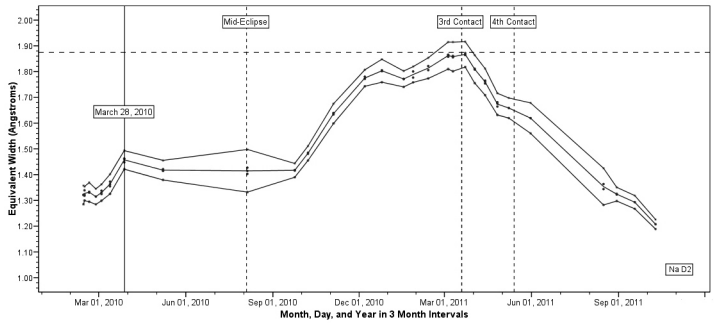

Figure 3. The sodium D_2 line equivalent widths (in Ångstroms) with upper and lower 95% confidence limits.

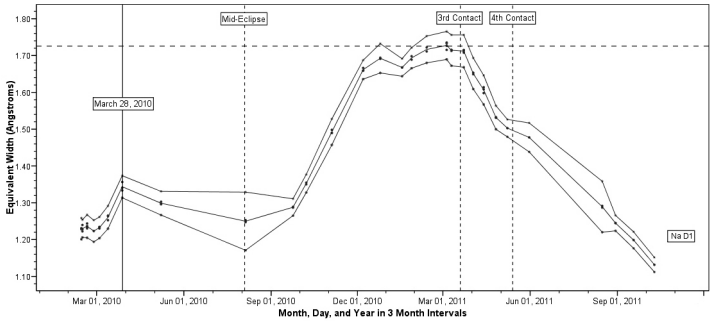

Figure 4. The sodium D_1 line equivalent widths (in Ångstroms) with upper and lower 95% confidence limits.

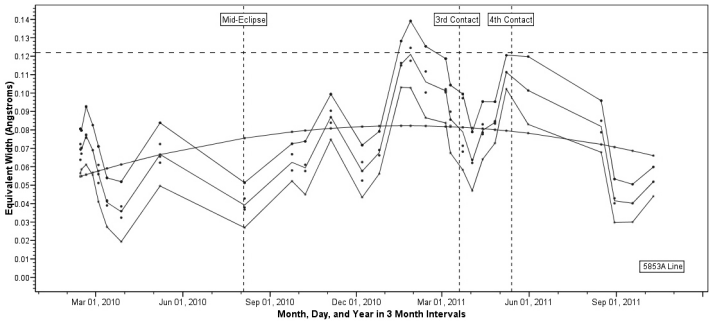

Figure 5. The 5853Å line equivalent widths (in Ångstroms) with upper and lower 95% confidence limits, and a superimposed second order polynomial regression line.

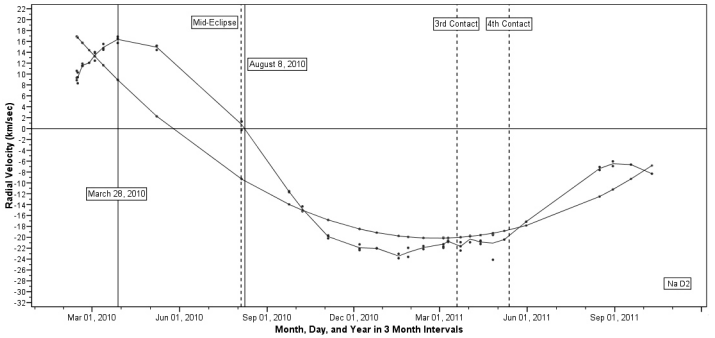

Figure 6. The sodium D_2 radial velocities (km/sec) and a superimposed second order polynomial regression line.

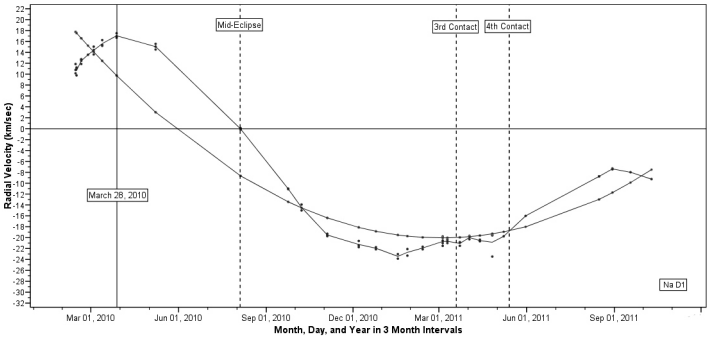

Figure 7. The sodium D_1 radial velocities (km/sec) and a superimposed second order polynomial regression line.

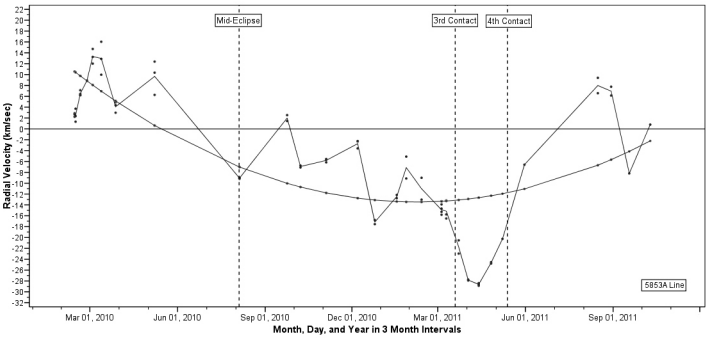

Figure 8. The 5853Å radial velocities (km/sec) and a superimposed second order polynomial regression line.

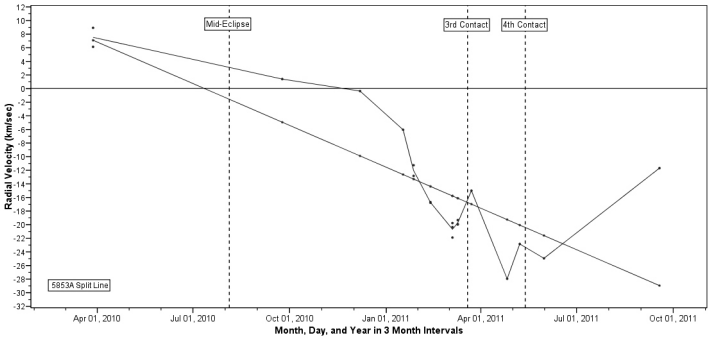

Figure 9. The 5853Å line radial velocities (km/sec) and a superimposed first order polynomial regression line.

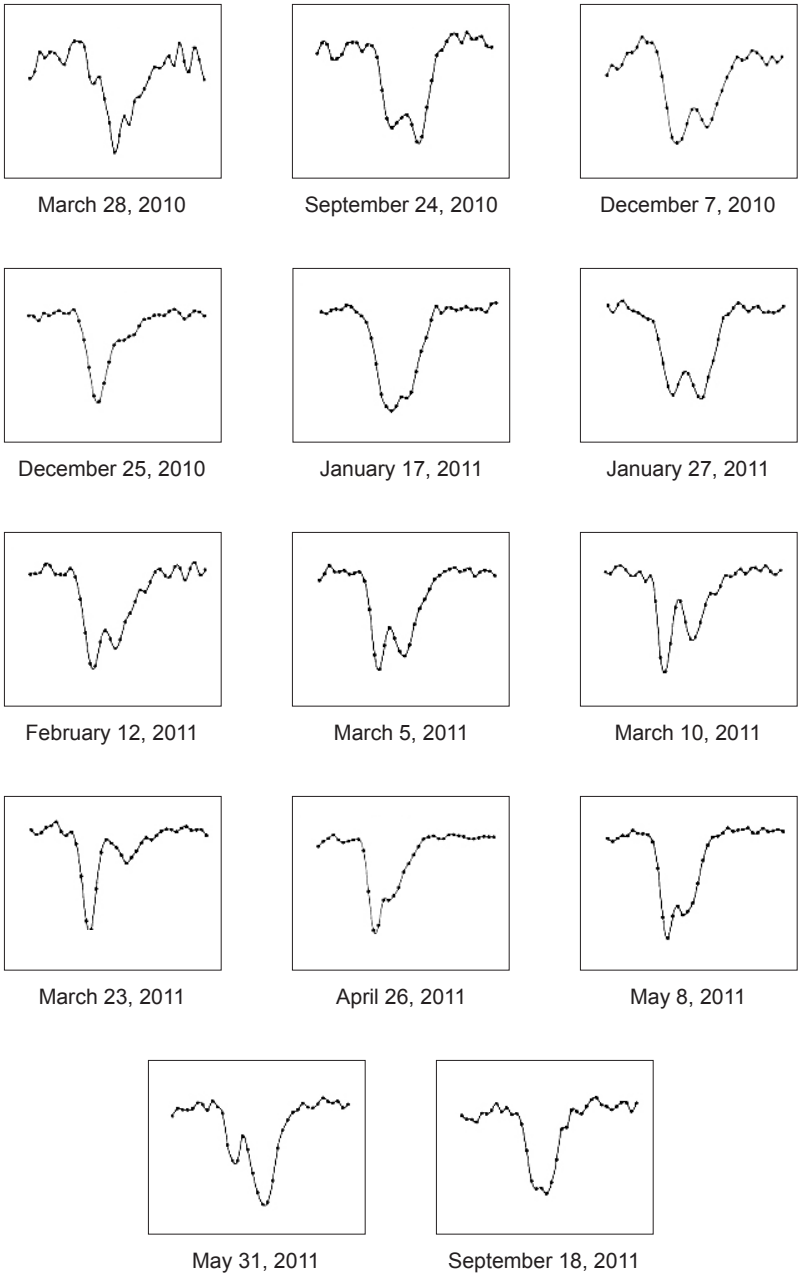

Figure 10. Evolution profiles of the 5853Å split line.

Eclipse Spectropolarimetry of the ε Aurigae System

Kathleen M. Geise
Robert E. Stencel
University of Denver, Department of Physics and Astronomy, 2112 E. *Wesley Avenue, Denver, CO 80208; address email correspondence to kgeise@du.edu*

Nadine Manset
Canada-France-Hawaii Telescope Corporation (CFHT), Waimea Headquarters, 65-1238 Mamalahoa Highway, Kamuela, HI 96743

David Harrington
Jeffrey Kuhn
Institute for Astronomy, University of Hawaii, 2680 Woodlawn Drive, Honolulu, HI 96822

Received April 13, 2012; revised August 27, 2012, October 17, 2012; accepted November 4, 2012

Abstract The recent eclipse of the enigmatic binary star system, ε Aurigae, offered a special opportunity to explore the role of spectropolarimetry in discovery of unknown facets of the objects involved. Here we present spectropolarimetric results for H-alpha, H-beta, Ca I (422.6 nm), and K I (769.9 nm) based on more than 50 epochs of high dispersion spectra obtained with the ESPaDOnS instrument at CFHT during 2006–2012.

1. Introduction

The target, ε Aur, is a single line spectroscopic binary that features an opaque disk, surrounding a hidden companion, that causes a lengthy eclipse every 27 years—for a reading list, see, for example, Stencel *et al.* (2011). Instrumentation advances of the past decade have enabled a remarkable set of new spectropolarimetric data to be obtained during the 2008–2011 eclipse. The ESPaDOnS instrument (Donati 2003) at the Canada-France-Hawaii Telescope obtained more than 50 epochs of full Stokes polarimetry from 3800Å to 10000Å. Prior efforts have revealed broadband polarization changes during eclipses, successfully predicting some disk characteristics, as well as demonstrating post-eclipse variability (Kemp *et al.* 1986; Cole 2012). Spectropolarimetric observations may contribute to our understanding of the system by revealing the nature and distribution of gaseous material in the F-star atmosphere and in the occulting disk. This paper provides a description of data analyzed to date. Our preliminary results indicate that the increased polarization observed in broadband during eclipse is also present in many spectrographic lines.

2. Observations

The data were obtained using the EPSaDOnS instrument at the Canada-France-Hawaii telescope (CFHT). ESPaDOnS is a cross-dispersed échelle spectropolarimeter designed to obtain a complete optical spectrum in a single exposure, with a resolving power of about 70,000. The ε Aur data used in this report were obtained with about 10^6 counts per spectral bin. The normalized intensity (normalized to 1) corresponds to an average uncertainty of about 1×10^{-3}, for a signal-to-noise (S/N) of c. 1000. All four Stokes parameters were taken for each observation (see Table 1 for a log of observations).

We retrieved ESPaDOnS observations of ε Aur from the Canadian Astronomy Data Centre (CADC), CFHT Science Data Archive (http://www1.cadc-ccda.hia-iha.nrc-cnrc.gc.ca/cadc/). Fifty epochs of spectropolarimetric observations of ε Aur span the time from pre-eclipse (beginning February 2006) through the eclipse phases and include post-eclipse observations (for example, January 2012). The data were automatically reduced with Upena, CFHT's reduction pipeline for ESPaDOnS. Upena uses LIBRE_ESPRIT, which is a proprietary data reduction software tool (Donati *et al.* 1997).

2.1. Contributions of polarimetry to the study of ε Aur

Polarization signatures occur when symmetries are broken. Possible sources of polarization are rotation deformities, aspherical winds, tidal distortions in binary systems, the Chandrasekhar effect during eclipse of binary systems, photospheric inhomogeneities including radiation inhomogeneities, and matter streams or accretion. Polarization signatures due to scattering depend upon the nature and distribution of the scatterers: electrons, atomic species, and/or dust grains. Broadband polarization signatures (for example, see Cole 2012; Henson *et al.* 2012; Kemp *et al.* 1986; Coyne 1972) may include contributions from both the continuum and lines that may involve different scattering agents.

The spectropolarimetric observations included in this paper reveal anisotropies in gaseous atomic species intrinsic to the F star, as well as geometric and/or scattering effects of the disk during eclipse. One possible geometric source of polarization in lines during eclipse is the Chandrasekhar effect associated with limb polarization of the F star. One possible source of polarization out-of-eclipse is anisotropy associated with stellar pulsation, for example. Our goal is to identify the source or sources of polarization in the lines both in- an out-of-eclipse revealed by these excellent ESPaDOnS high-resolution observations. ESPaDOnS observations cannot be used to measure continuum polarization (http://www.cfht.hawaii.edu/Instruments/Spectroscopy/Espadons/).

3. Method

Linear polarization, P, was computed using normalized Q and U (that is, Q/I_c and U/I_c) for each wavelength in the observation according to Equation (1) (Bagnulo *et al.* 2009).

$$\frac{P}{I_c} = \sqrt{\left(\frac{Q}{I_c}\right)^2 + \left(\frac{U}{I_c}\right)^2} \tag{1}$$

Percent linear polarization was calculated as follows

$$\%\, p = \frac{P / I_c}{I / I_c} \times 100 \tag{2}$$

Where I/I_c denotes the normalized intensity. Percent q (%q), percent u (%u). and percent v (%v), where q, u, and v are the normalized Stokes parameters, were calculated in a manner similar to Equation (2).

Assessing the true errors in polarimetric measurements is crucial to establishing the physics of the source. We assume that the Stokes parameters Q and U are normally distributed about their true values, but it has been shown that linear polarization follows a Rice distribution (for example, Clarke and Stewart 1986). The Rice probability distribution is given by

$$\mathrm{R}(p \mid p_0, \sigma) = \frac{p}{\sigma^2} \exp\left[\frac{-p^2 + p_0^2}{2\sigma^2}\right] I_0\left(\frac{p p_0}{\sigma^2}\right) \tag{3}$$

Here p_0 is the underlying, true, polarization, I_0 is the zeroth-order modified Bessel function, and the underlying Gaussian noise has variance σ^2. In the limit of high signal-to-noise (S/N), the Rice distribution approaches the normal distribution, with a mean that approaches p_0 and a standard deviation that approaches σ (Vaillancourt 2006). The Rice mean is given by

$$\mu_R = \sqrt{\frac{\pi}{2}}\, \sigma\, L_{1/2}\left(\frac{-\mu^2}{2\sigma^2}\right) \tag{4}$$

Here $L_{1/2}(x)$ is a Laguerre polynomial of order ½, μ is the mean, and σ is the standard deviation. The Rice variance is given by

$$\frac{1}{2}\, \pi\sigma^2\, L_{1/2}^2\left(\frac{-\mu^2}{2\sigma^2}\right) \tag{5}$$

Here $L_{1/2}^2(x)$ is a generalized Laguerre polynomial $L_n^{(\alpha)}(x)$ with n = ½ and $\alpha = 2$. The Rice standard deviation may be found by taking the square root of the variance.

By definition, the parameter p is a positive definite quantity. The individual polarization values calculated from Equation (1) will always be positive and non-zero because the individual values of Q and U will generally be non-zero. At large S/N ($p/\sigma \geq 4$) the maximum likelihood and most probable estimators for the linear polarization (for example, Simmons and Stewart 1985) converge to

$$\hat{p} = \sqrt{(p^2 - \sigma^2)} \tag{6}$$

Equation (6) corrects for the positive bias in the linear polarization calculated using Equation (1) (Clarke 2010). The data presented here are not corrected for interstellar polarization.

The mean value of p may be computed using the mean values of q and u (Clarke and Stewart, 1986) as follows

$$\overline{p} = \sqrt{(\overline{q}^2 + \overline{u}^2)} \tag{7}$$

The barred variables denote the mean.

Linear polarization position angle, Θ, may be computed from Stokes q and u as follows (Bagnulo *et al.* 2009). Position angles will range from 0 to 180 degrees.

$$\Theta = \frac{1}{2}\, tan^{-1}\left(\frac{u}{q}\right) + \Theta_0 \tag{8}$$

$$\Theta_0 = \left\{ \begin{array}{c} 0 \text{ if } q > 0 \text{ and } u \geq 0 \\ 180 \text{ if } q > 0 \text{ and } u < 0 \\ 90 \text{ if } q < 0 \end{array} \right\}$$

$$\Theta = \left\{ \begin{array}{c} 45 \text{ if } q = 0 \text{ and } u > 0 \\ 135 \text{ if } q = 0 \text{ and } u < 0 \end{array} \right\} \tag{9}$$

The ESPaDOnS data are noisier at shorter wavelengths (that is, toward the blue) than longer wavelengths because the detector is less sensitive in the blue. We binned the linear polarization data with a wavelength bin of 0.015 nm using the error-weighted mean (for example, Taylor 1997) to boost signal-to-noise at shorter wavelengths and for deep absorption lines. We determined through trial and error that this was the largest bin size that did not seriously degrade the resolution of the line. In some cases, we combined several epochs (using the error-weighted mean) to further reduce noise prior to wavelength binning, using the criterion that the line profile did not change between binned epochs.

We computed the mean for both q and u using the binned data and then computed the mean linear polarization using Equation (7). The Rice mean and

variance were computed for each p using Equations (4) and (5), adopting the mean polarization for μ in those equations. Finally, we bias-corrected the linear polarization using Equation (6), adopting the Rice standard deviation for σ in that equation. We adopted the error bars given in the pipeline reduction as the uncertainty in both normalized intensity and normalized Stokes parameters and propagated those uncertainties in calculations of percent Stokes (see, for example, error bars in Figure 2). We also propagated the uncertainty (Rice standard deviation) in the calculation of %p (see, for example, error bars in Figure 1).

For polarizations with large S/N, the confidence regions approach those given by a normal Gaussian distribution centered on the bias-corrected value of p, with 2σ corresponding to 95% and 2.6σ corresponding to 99% confidence for $p/\sigma \geq 4$ (Vaillancourt 2006). The maximum likelihood estimator (Equation 6) of the underlying ("true") polarization converges with all other estimators when p/σ is greater than 4. For p/σ greater than 3 and less than 4, the maximum likelihood estimator may not completely correct for bias; the polarization is considered the upper bound. Values of p/σ less than 1.4 correspond to zero polarization (Vaillancourt 2006). We identified spectroscopic regions with significant linear polarization by flagging polarization peaks for $p/\sigma \geq 4$.

We rotated the unbinned data by 27 degrees using a rotation matrix (for example, Code and Whitney 1995; Bagnulo *et al.* 2009) to align instrument north with the rotation axis of the system as described by Kloppenborg *et al.* (2010) before binning by epoch and wavelength. We confirmed that the invariant, $(Q^2 + U^2)$, was conserved under rotation (intensity is unaffected by rotation and %p is unaffected as long as the invariant is conserved).

We verified that the null parameters provided by the ESPaDOnS pipeline contained no signal, indicating that any instrument effects were removed by the data reduction. We were also careful to change the sign of Stokes U as directed by the ESPaDOnS FITS file headers.

4. Analysis

4.1. Linear polarization time series and qu-plots

Initial analysis focused on the stronger lines in order to assess whether the eclipse resulted in changes to the polarization. A sample time-series of H-alpha line profiles and polarizations are shown in Figure 1. A sample plot of %q vs. %u (a qu-plot) is shown in Figure 2. The error bars in the qu-plot are the 1σ-propagated (assumed Gaussian) average uncertainties in both %q and %u. The angle from the +q axis measured counterclockwise to a feature in the qu-plot corresponds to twice the position angle (2Θ) as measured east of north and may be a useful diagnostic of the geometry of the scattering giving rise to the polarization. We were careful to exclude %q and %u contributions from neighboring lines in these plots when possible.

4.2. Hydrogen alpha

We fit the pre-eclipse H-alpha line (rest wavelength 656.280 nm) with a Gaussian function and adopted the HWHM of the Gaussian (c. 25 km s^{-1}) as the line core. We further defined the wings as follows: the blue wing (–125 km s^{-1} to –25 km s^{-1}) and the red wing (25 km s^{-1} to 125 km s^{-1}). Regions outside of these defined areas consistently mapped to (0,0) in the qu-plots. These definitions are maintained throughout the following analysis.

H-alpha exhibited persistent polarization in the line core in all epochs (see Figure 1). During pre-eclipse, the line core accounted for a nearly linear excursion of (–%u, –%q) in the qu-plot (green diamond symbol, Figure 2). The line was largely symmetric, with both red and blue emission wings evident. The line appeared slightly broadened to the red when compared to the Gaussian function. The blue and red emission wings exhibited no polarization features in this binned epoch, or in any pre-eclipse epoch. At no phase did the H-alpha line reach zero intensity.

Harrington and Kuhn (2009) noted the strong presence of spectropolarimetric signatures in and around the absorptive components of the H-alpha emission line in Herbig Ae/Be stars that they called "polarization-in-absorption." They also identified a broad polarization signature across emission features for many classical Be stars in their sample. Herbig Ae/Be stars are embedded in cold gas and dust, which may be equatorially enhanced, whereas classical Be stars are rapid rotators characterized by ionized equatorial material. The equatorial material surrounding these two types of stars contributes to distinctly different polarization signatures. The polarization features we observed in pre-eclipse ε Aur spectra are similar to "polarization-in-absorption"; this suggests that ε Aur does not have an equatorial enhancement of ionized material.

At mid-eclipse, and for many epochs following mid-eclipse, the line exhibited a central emission feature (presumed recombination, see Stencel *et al.* 2011). %p increased, consistent with changes to broadband polarization reported by Cole (2012) and Kemp *et al.* (1986). The core polarization peak appears notched in these epochs, possibly indicating a depolarization associated with the emission core. At mid-eclipse, the blue and red absorption wings exhibited broad %p polarization. There were excursions in the qu-plot for features in the line core (–%q; green diamond symbol), as well as the blue (+%q, +%u; blue square symbol) and red (+%q, –%u; red triangle symbol) absorption wings (Figure 2). These qu-plot excursions were not affected by binning and are evident in several observations around this time.

By late eclipse, the line exhibited a broad, deep, blue-shifted absorption. Normalized intensity dropped to about 10% at the deepest part of the line, but signal-to-noise remained above 700 and the ratio p/σ ranged from 3 to 25 for polarization greater than 0.4%, significant within the Rice statistics. The central core polarization remained strong (>1%) in late eclipse, but the blue wing polarization increased (>0.5% at –100 km s^{-1}), while the red wing polarization

decreased (that is, negligible at 100 km s^{-1}). In the qu-plot, the line core accounted for the –%q features (green diamonds), the blue wing accounted for the +%q features (blue squares), and the red wing polarization (red triangles) was largely concentrated at (0,0) (Figure 2). Thus, the polarization behavior followed the line behavior in this epoch.

The H-alpha line did not return to its pre-eclipse form by the time of our last post-eclipse observation (January 17, 2012). The red emission wing reappeared at about the pre-eclipse level, but the blue emission wing was masked by a broad (> –150 km s^{-1}), shallow (normalized intensity c. 0.9) absorption. Line core polarization remained above 1% and the blue wing polarization feature disappeared. The line core polarization maintained a largely (–%q, +%u; green diamonds) orientation in the qu-plot (see the post-eclipse binned epoch presented in Figure 2).

Clearly, the passage of the rotating, dark disk in front of the F star induces polarization signals away from line center. Continuing observations may be able to demonstrate whether the persistent line core polarization tracks the F star or a disk-tied source velocity around the orbit.

4.3. Hydrogen alpha linear polarization position angle

We calculated the position angle for (%q, %u) pairs for the H-alpha line in mid-eclipse (Figure 3). The data are rotated to the stellar frame and are not binned. Notice that the linear polarization position angle appears randomly scattered outside of the line, which is expected. The position angles that correspond to the line core (± 25 km s^{-1} from rest wavelength) are plotted in green; position angles corresponding to the blue-shifted absorption wing (–125 km s^{-1} to -25 km s^{-1}) are plotted in blue; and position angles corresponding to the red-shifted absorption wing (+25 km s-1 to +125 km s-1) are plotted in red. Position angles only range from 0° to 180° because of the nature of the Stokes parameters; a position angle of 180° is consistent with 0°. Notice the line core polarization is offset by about 90° from the wings. This may be an opacity effect. Compare these data to the mid-eclipse qu-plot (Figure 2).

4.4. Hydrogen beta

Unlike the pre-eclipse H-alpha line, the H-beta line (rest wavelength 486.135 nm) was better fitted by a Lorentzian profile and we adopted the HWHM of this profile (c. 35 km s^{-1}) as the line core. We further defined the wings as follows: the blue wing (–125 km s^{-1} to -35 km s^{-1}) and the red wing (35 km s^{-1} to 125 km s^{-1}) and noted that regions outside of the defined areas consistently mapped to (0,0) in the qu-plots. These definitions are maintained throughout the following analysis.

H-beta also exhibited persistent polarization in the line core in all epochs (see Figure 4). In pre-eclipse, the normalized intensity was at 13%, but the signal-to-noise remained above 1,000. The ratio p/σ was consistently greater

than 4 for %p greater than 0.22%. The –%q excursion in the qu-plot (Figure 5) corresponds to line core polarization and differs in orientation from H-alpha pre-eclipse (see Figure 2). The line itself appeared nearly symmetric and red-shifted by about the velocity of the F star at that phase.

The H-beta line maintained a deep and broad absorption at mid-eclipse that deepened further by late eclipse. %p increased in mid- and late eclipse. At mid-eclipse, the normalized intensity fell to about 5% at the deepest part of the line, but signal-to-noise remained greater than 500. The linear polarization was greatest at the line core, with smaller contributions from the blue and red absorption wings. The ratio p/σ remained consistently greater than 4 for %p $\geq$ 0.2% in this epoch. There were excursions in the qu-plot for features in the line core (–%q; green diamond), as well as the blue (+%q, +%u; blue square) and red (+%q, –%u; red triangle) absorption wings (Figure 5). These qu-plot excursions are similar to those exhibited by H-alpha for this epoch.

By late eclipse, the line exhibited a broad, deep, blue-shifted absorption. The line is clearly saturated in late eclipse, falling to just 1.6% intensity at the deepest point and, although S/N is nearly 200 here, the ratio p/σ is only 1.2; therefore %p = 0. The ratio p/σ ranged from 3 to 11 for %p > 0.4 outside the saturated region. The central core polarization appears to have decreased; the blue wing polarization (outside of the saturated region) increased (>2% at –70 km s^{-1}), while the red wing polarization decreased (c. 0.2% at 70 km s^{-1}) from mid-eclipse levels. In the qu-plot, the line core accounted for the –%q features ($p/\sigma \geq 3$ at –20 km s^{-1}; $p/\sigma \geq 4$ at –10 km s^{-1} and throughout the remainder of the core), the unsaturated blue wing accounted for the +%q features (Figure 5; blue squares) and the red wing polarization was largely concentrated at (0,0). The polarization behavior also followed the line behavior in this epoch and qualitatively resembles the H-alpha polarization.

The H-beta line did not return to its pre-eclipse form by the time of our last post-eclipse observation (January 17, 2012). The line was deeper, broader, and blue-shifted by about –20 km s^{-1} with a strong (c. 1.5%), narrow polarization peak centered on this velocity. The line was deep, but unsaturated, with normalized intensity nearly 8% and signal-to-noise above 500. The ratio p/σ remained above 4 for %p greater than 0.5%. The line core polarization maintained a largely –%q orientation in the qu-plot (see the post-eclipse binned epoch presented in Fig. 5).

4.5. Hydrogen gamma and Hydrogen delta

In pre-eclipse, H-gamma (rest wavelength 434.047 nm) appeared to exhibit low-level polarization features, but there were insufficient data points corresponding to $p/\sigma \geq 4$. H-delta (rest wavelength 410.008 nm) in pre-eclipse showed no polarization features. By mid-eclipse, both lines became saturated, making analysis of line core polarization impossible. However, both lines exhibited absorption wing polarization meeting the $p/\sigma \geq 4$ criteria.

These features exhibited excursions in the qu-plot of +%u for blue-shifted absorption and –%u for red-shifted absorption for both lines, which is consistent with both H-alpha and H-beta polarization during this epoch. The lines remained saturated in late eclipse and there were no significant polarization features post-eclipse for either line.

4.6. Potassium (769.896 nm)

The K I line (rest wavelength 769.896 nm) described here is the weaker line of a doublet that arises from the ground state. The out-of-eclipse line is thought to have an interstellar origin (Welty and Hobbs, 2001). The K I 769.896 nm line exhibited no polarization signatures until after mid-eclipse. We identified no F-star contribution; varying absorption and polarization features described below may be attributed to the disk.

In pre-eclipse, the line profile remained constant; the stellar radial velocity was red-shifted with respect to the line rest wavelength (see Figure 6); and no linear polarization features were observed (see examples, Figures 6 and 7). A Gaussian fit to the line profile returned a HWHM of 0.02 nm.

After first contact, the line exhibited a red-shifted (about 20 km s^{-1}) feature initially about the same depth as the line core (normalized intensity about 0.7) that deepened to a normalized intensity of about 0.3. There were no significant ($p/\sigma \geq 3$) polarization features evident until after second contact. The weak (c. 0.3%), narrow linear polarization feature that appeared after second contact was centered on the red-shifted component of the line.

By mid-eclipse the line appeared deeper and broader than during pre-eclipse epochs. A broad, weak (< 0.2%) linear polarization feature appeared which was centered on the line (see Figure 6). In Figure 6, the ratio p/σ is greater than 3 for polarization above 0.1% and is greater than 4 for polarization above 0.15%; the polarization is significant by Rice statistics. The stellar radial velocity was not shifted with respect to the line rest wavelength at mid-eclipse.

The line developed a broad, blue-shifted component after mid-eclipse. Polarization remained low (below 0.2%) until late eclipse, when the line was very broad. We fit a Gaussian function to the late eclipse line profile; the fit yielded a HWHM of 0.05 nm, more than twice the HWHM measured in pre-eclipse. The Gaussian centroid corresponded to a shift of –20 km s^{-1} from the rest wavelength. A larger (c. 0.5%) polarization feature was centered on the blue-shifted component of the line in this epoch (see Figure 6), which corresponded to a (–%q, +%u; blue squares) loop in the qu-plot (Figure 7). The star's radial velocity became blue-shifted with respect to the line rest wavelength after mid-eclipse.

The line retained a blue-shifted component after 4th contact that decreased in breadth and depth over time. There were no polarization features evident after 4th contact. The line had nearly returned to its pre-eclipse form by our last observation (January 17, 2012).

We examined the stronger line of the K I doublet, (rest wavelength 766.490 nm) and discovered that it exhibited line profile and polarization variations similar to the weaker line. At late eclipse, the line exhibited a broad, blue-shifted absorption component. A linear polarization feature was centered on the blue-shifted component and the qu-plot also exhibited a (–%q, +%u) loop.

4.7. Calcium (422.673 nm)

The Ca I line (rest wavelength 422.673 nm) described here arises from the ground state and shows a persistent core polarization signature in pre-, mid- and late eclipse phases (Figure 8). The late eclipse polarization appeared dramatically greater than the pre-eclipse phase. After first contact, the Ca I line exhibits variations similar to the K I line, with an additional absorption component at about +20 km s^{-1} from the line rest wavelength before mid-eclipse and a blue-shifted additional absorption component developing at about –20 km s^{-1} after mid-eclipse.

We fit the pre-eclipse Ca I line with a Gaussian function and adopted the HWHM of the Gaussian (36 km s^{-1}) as the line core. The Gaussian centroid was displaced from rest by 0.08 nm (24 km s^{-1}), but the calculated radial velocity of the star was only 8 km s^{-1} for this epoch. We confirmed the Gaussian HWHM using data for two later epochs (20081216, 20080213) when the Gaussian centroid and stellar radial velocity were more closely aligned. We defined the wings as follows: the blue wing (–125 km s^{-1} to –36 km s^{-1}) and the red wing (36 km s^{-1} to 125 km s^{-1}). Regions outside of these defined areas consistently mapped to (0,0) in the qu-plots. These definitions are maintained throughout the following analysis.

The line appeared asymmetric in the pre-eclipse epoch (Figure 8) with a red absorption component extending beyond the line core, at about 50 km s^{-1}. A large (c. 1%) polarization peak was nearly centered on the star and a smaller (0.4%) linear polarization peak was associated with the red-shifted component.

The presence of two peaks in %p for this pre-eclipse epoch may be attributed to one of the following: (1) the line is optically thick at the line core (as with H-alpha), (2) more than one asymmetric region contributes to the Ca I 422.6 nm polarization, or (3) the line contains a blend of species with varying degrees of polarization. Two species, Fe I (422.743 nm, 3.3 eV, doublet) and Ti II (422.733 nm, 1.13 eV, multiplet 33), are candidates for possible blended species corresponding to the velocity offset of c. 50 km s^{-1}. The possible blended feature persisted at about the same polarization strength throughout the time series. The corresponding Fe I doublet (422.545 nm) to our candidate line exhibited no polarization in any epoch. The two other members of the Ti II multiplet (421.818 nm and 420.592 nm) did not show polarization features. Hack (1959) identified a Ti II line of comparable energy to our candidate Ti II line (Ti II, 454.5 nm, 1.13 eV, multiplet 30) as a solely F star line. The feature

at c. 50 km s^{-1} may be a Ti II component attributable to the F star.

The qu-plot (Figure 9) describes two dominant position angles for the line in this pre-eclipse epoch; the excursion of (–%q, +%u; green diamonds) corresponds to the line core and the excursion (+%q; red triangles) corresponds to the red wing. The position angles corresponding to the excursions in the qu-plot differ by about 90 degrees.

The Ca I 422.6 nm line increased in %p by mid-eclipse (peak polarization >1% centered at the line rest wavelength. The polarization increased from mid- through the late eclipse and broadened on the blueward side as the blue absorption component appeared in the spectra.

The qu-plot (Figure 9) corresponding to mid-eclipse may be complicated by the presence of a possible blended line. The line core corresponds to (–%q, +%u; green diamonds), the excursion of (+%q, +%u; red triangles) corresponds to the red absorption wing (a possible blend) and the blue-shifted absorption corresponds to (–%q, –%u; blue squares). A similar scenario corresponds to the late eclipse qu-plot, with the notable exception that the degree of polarization has obviously increased for the line center at (–%q, +%u; green diamonds).

The %p decreased after 4th contact and the line returned to its pre-eclipse shape. The linear polarization exhibited two peaks in %p, one centered on the F star and the other offset from the F star velocity by about +50 km s^{-1}, centered on the presumed Ti II feature. The qu-plot (Figure 9) describes two dominant position angles for the line in post eclipse; the excursion of (–%q; green diamonds) corresponds to the line core and the excursion (+%q; red triangles) corresponds to the red wing.

We examined other Ca I lines to discover if the polarization behavior of the ground state transition was consistent with other energy transitions of this atomic species. Another Ca I line (rest wavelength 430.774 nm) arises from a higher energy level (1.9 eV) and exhibited similar line profile changes during eclipse, however, there were insufficient data points corresponding to $p/\sigma \geq 4$ to compare polarization changes of this line with changes observed in the ground state Ca I line. We observed no linear polarization signatures in other Ca I lines of comparable energy transition levels to the Ca I line at 430.774 nm.

The polarization behavior of this line suggests that Ca I (422.6 nm) traces polarization associated with the F star itself, as well as disk effects. Kim (2008) noted a 67-day out-of-eclipse light variation. We speculate that the F star polarization features we observed might be associated with upwelling and large scale bright convective regions.

4.8. Circular polarization and Stokes V

We identified no significant Stokes V (circular) polarization signal in any of the spectral lines we have described. Our preliminary assessment is that there are no significant circular polarization features in the data set. The presence of circular polarization signatures could indicate that magnetic fields are present

and contribute to polarization; the lack of signal suggests that magnetic fields are not a major contributor to the polarization we observed.

5. Results

The presence of persistent polarization in spectral lines such as H-alpha, H-beta, and the Ca I 422.6 nm line out-of-eclipse suggests that asymmetry persists in the F star for extended periods. H-alpha polarization was identified in ESPaDOnS observations of ε Aur dated February 7 and 8, 2006 (Harrington and Kuhn 2009), at phase 0.925, more than three years before the recent eclipse and about two years before periastron. Those observations, as well as the H-alpha observations presented here, indicated that the blue and red emission wings are not polarized, suggesting possible symmetry in the emitting region (at these shifted velocities/temperatures), or insufficient optical depth to generate detectable polarization from scattering in the region. We also observed that the H-alpha line does not saturate, unlike H-beta and others in the Balmer series. This suggests that a broad emission exists, contributing additional H-alpha photons to the line core.

We observed that H-alpha and H-beta exhibited different position angles in pre-eclipse. The H-beta absorption may indicate the presence of equatorially aligned hydrogen gas—the optically thick component scattering at 90 degrees perpendicular to the optically thin component. The H-alpha polarization position angles may include a component from interstellar polarization, or they may indicate a more complex distribution of hydrogen gas at those energies. Chadima *et al.* (2011) demonstrated that the atmosphere of the disk starts to be projected against the F star as early as three years before the beginning of the photometric eclipse; our observations seem to corroborate their findings.

H-alpha and H-beta showed similar mid- and late eclipse behavior in qu-space. The line cores and wings seem to agree about the range of angles involved, suggesting that the dominant features arise from the same orientation in the sky (gaseous material above and below the disk). An offset of 90 degrees between line core and absorption wings is consistent with the effect opacity may have on scattering.

The polarization behavior of the K I 769.9 nm line confirmed that this line has no F-star component; the line may be considered a bellwether for low excitation lines affected by the disk during eclipse. Limb polarization cannot be the sole contributor to polarization signatures during eclipse (for example, Kemp *et al.* 1986) because this line cannot have a limb polarization component. The disk exhibited significantly stronger polarization features in late eclipse than in any other eclipse epoch. Many observers have noted the asymmetry in the line (for example, Leadbeater *et al.* 2012). The increase in polarization may indicate that the density of scattering material increased in late eclipse. Pearson and Stencel (2012) note the "dawn" face of the disk may rotate into the

line-of-sight during late eclipse epochs. The warmed, presumably sublimated, material could contribute to the increased resonant scattering in the line. The position angles of scattering in late eclipse deviate from strict equatorial or polar alignment; modeling is required to replicate the late-eclipse Stokes %q and %u behavior.

The pre-eclipse polarization features of the Ca I 422.6 nm line showed contributions from the F star as well as from the eclipse. The increase in polarization in late eclipse is consistent with the K I line behavior and may also suggest an increase in the density of scattering material.

The spectral and linear polarization features presented here are a sample of the features present in the data set. Only a few epochs have been presented for brevity. We found significant changes to linear polarization in lines such as H-alpha, H-beta, Ca I 422.6 nm, and K I 796.6 nm presented here.

6. Conclusions and next steps

The analysis present here is a work in progress and is not a final word. There are many spectral features whose linear polarization characteristics remain to be described. We are optimistic about the potential in these data to help characterize polarization features that may be attributed to the F star itself, as well as the polarization that arises from the eclipsing disk. Our next steps in a subsequent paper will include identification and classification of spectral features that exhibit polarization, an analysis of the position angle of linear polarization features (to fully describe the linear polarization vector), and an analysis of scattering behavior when the F star is not uniformly eclipsed.

7. Acknowledgements

The authors are grateful for support of this work in part from a bequest in support of astronomy from the estate of William Herschel Womble. Based on observations obtained at the Canada-France-Hawaii Telescope (CFHT), which is operated by the National Research Council of Canada, the Institut National des Sciences de l'Univers of the Centre National de la Recherche Scientique of France, and the University of Hawaii. We would like to thank Roberto Casini, Elizabeth Griffin, Philip Judge, Brian Kloppenborg, Bruce Lites, and Jan Stenflo for helpful discussions.

The authors are very grateful to the referee, John Landstreet, for many helpful suggestions and improvements to the work.

References

Bagnulo, S., Landolfi, M., Landstreet, J.D., Landi Degl'Innocenti, E., Fossati, L., and Sterzik, M. 2009, *Publ. Astron. Soc. Pacific*, **121**, 993.
Chadima, P., *et al.* 2011, *Astron. Astrophys.*, **530**, 146.
Clarke, D. 2010, *Stellar Polarimetry*, Wiley-VCH, Hoboken, NJ.
Clarke, D., and Stewart, B. G. 1986, *Vistas Astron.*, **29**, 27.
Code, A., and Whitney, B. 1995, *Astrophys. J.*, **441**, 400.
Cole, G. 2012, *J. Amer. Assoc. Var. Star Obs.*, **40**, 787.
Coyne, G. 1972, *Ric. Astron.*, **8**, 311.
Donati, J.-F. 2003, in *Solar Polarization*, Eds. J. Trujillo-Bueno and J. Sanchez Almeida, ASP Conf. Proc., 307, Astron. Soc. Pacific, San Francisco, 41.
Donati, J.-F., Semel, M., Carter, B.D., Rees, D. E., and Collier Cameron, A. 1997, *Mon. Not. Roy. Astron. Soc.*, **291**, 658.
Hack, M. 1959, *Astrophys, J.*, **129**, 291.
Harrington, D., and Kuhn, J. 2009, *Astrophys. J., Suppl. Ser.*, **180**, 138.
Henson, G., Burdette, J., and Gray, S. 2012, in *Stellar Polarimetry: From Birth to Death*, AIP Conf. Proc. 1429, Amer. Inst. Physics, Melville, NY, 140.
Kemp, J. C., Henson, G. D., Kraus, D., Beardsley, I., Carroll, L., Ake, T., Simon, T., and Collins, G. 1986, *Astrophys. J., Lett. Ed.*, **300**, 11.
Kim, H. 2008, *J. Astron. Space Sci.*, **25**, 1.
Kloppenborg, B., *et al.* 2010, *Nature*, **464**, 870.
Leadbeater, R., *et al.* 2012, *J. Amer. Assoc. Var. Star Obs.*, **40**, 729.
Pearson, R. L., and Stencel, R. E. 2012, *J. Amer. Assoc. Var. Star Obs.*, **40**, 802.
Simmons, J. F., and Stewart, B. G. 1985, *Astron. Astrophys.*, **142**, 100.
Stefanik, R. P., Torres, G., Lovegrove, J., Pera, V. E., Latham, D. W., Zajac, J., and Mazeh, T. 2010, *Astron. J.*, **139**, 1254.
Stencel, R., *et al.* 2011 *Astron. J.*, **142**, 174.
Taylor, J. 1997, *Introduction to Error Analysis, the Study of Uncertainties in Physical Measurements*, 2nd Edition, University Science Books, New York.
Vaillancourt, J. 2006, *Publ. Astron. Soc. Pacific*, **118**, 1340.
Welty, D., and Hobbs, L. 2001, *Astrophys. J., Suppl. Ser.*, **133**, 345.

Table 1. Log of observations.

Comment[a]	*Gregorian*	*RJD*[b]	*Phase*[c]
	2006-01-07	3774.93	0.926
	2008-08-25	4704.04	0.019
	2008-10-18	4757.92	0.025
	2008-12-07[d]	4807.82	0.030
	2008-12-08[d]	4808.83	0.030
	2008-12-09[d]	4809.83	0.030
	2008-12-10[d]	4810.83	0.030
	2008-12-16	4817.05	0.031
	2009-02-13	4875.71	0.036
	2009-02-14	4876.70	0.037
	2009-02-17	4879.85	0.037
	2009-05-04	4955.72	0.045
1st contact	2009-08-22	5060	
	2009-09-04	5079.05	0.057
	2009-09-05	5080.07	0.057
	2009-09-08	5083.15	0.057
	2009-09-11	5086.11	0.058
	2009-09-25	5100.05	0.059
	2009-09-26	5101.02	0.059
	2009-09-29	5104.03	0.060
	2009-10-02	5107.02	0.060
	2009-10-07	5112.01	0.060
	2009-10-10	5115.16	0.061
	2009-11-29	5165.11	0.066
	2009-12-02	5168.00	0.066
	2009-12-04	5169.80	0.066
	2009-12-07	5173.14	0.067
	2009-12-08	5174.14	0.067
	2010-01-02	5198.77	0.069
2nd contact	2010-01-02	5200	
	2010-01-26	5222.71	0.072
	2010-01-28	5224.70	0.072
	2010-03-08	5263.72	0.076
mid-eclipse	2010-07-06	5390	
	2010-07-23	5401.12	0.090
	2010-08-01[d]	5410.13	0.090
	2010-08-05[d]	5414.11	0.091
	2010-10-16	5485.91	0.098
	2010-10-18	5487.90	0.098
	2010-10-19	5488.99	0.098

Table continued on next page

Table 1. Log of observations, cont.

Comment[a]	*Gregorian*	*RJD*[b]	*Phase*[c]
	2010-10-21	5490.93	0.099
	2010-11-15	5516.02	0.101
	2010-11-16	5517.14	0.101
	2010-11-17	5517.96	0.101
	2010-11-22[d]	5522.89	0.102
	2010-11-24[d]	5524.99	0.102
	2010-12-19	5549.74	0.105
3rd contact	2011-03-18	5620	
4th contact	2011-05-21	5720	
	2011-08-17	5791.13	0.129
	2011-11-01	5867.13	0.137
	2011-11-15d	5880.99	0.138
	2011-11-16d	5882.16	0.138
	2012-01-06	5933.00	0.143
	2012-01-17	5943.78	0.144

Notes: [a]RJD for eclipse taken from Stencel et al. *(2011); [b]Julian date—2450000; [c]Time of periastron and period from Stefanik* et al. *(2010) 2434723+9896.0E; [d]Epoch binning as follows: early—binned 20081207, 20081208, 20081209, 20081210; mid—binned 20100801 and 20100805; late—binned 201122 and 20111124; post—binned 20111115, 2011116.*

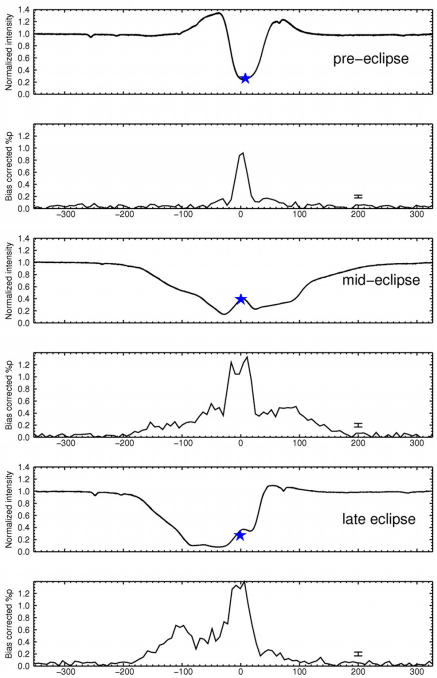

Figure 1. Time series of H-alpha (656.280 nm) line and %p profiles for pre-, mid-, and late-eclipse epochs. Velocity is centered on the line rest wavelength. The F-star radial velocity is indicated by a star symbol. Note the star is slightly red-shifted pre-eclipse and blue-shifted late eclipse. Polarization data are epoch- (see text) and wavelength-binned (bin size 0.015 nm). Average errors in %p are shown.

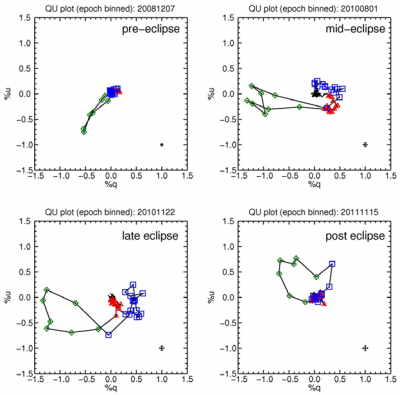

Figure 2. QU-plots of H-alpha (656.280 nm) for pre-, mid-, late, and post-eclipse epoch and wavelength binned data. The first date of each binned epoch is given. Average error bars are shown. Note the QU-plot is nearly linear in pre-eclipse. The prominent excursion (–%q, –%u; green diamonds) corresponds to the line core (± 25 km s^{-1}). Absorption wing contributions appear in mid- and late-eclipse. The blue wing corresponds to (+%q, +%u; blue squares) and the red wing corresponds to (+%q, –%u; red triangles) in mid-eclipse. By late eclipse, the red wing polarization has largely disappeared (near 0,0) and the large +%q excursion is blue wing polarization. The line core polarization is (+%u, –%q; green diamonds) in post eclipse. These data have been rotated into the stellar frame (see text for description).

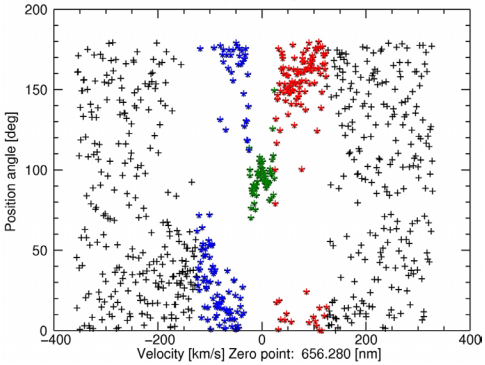

Figure 3. Position angle calculated for (%q, %u) pairs for the H-alpha line in mid-eclipse. The data are rotated to the stellar frame and unbinned. Notice that the linear polarization position angle appears randomly scattered outside of the line, which is expected. The position angles that correspond to the line core (± 25 km s^{-1} from rest wavelength) are plotted in green; position angles corresponding to the blue-shifted absorption wing (–125 km s^{-1} to –25 km s^{-1}) are plotted as blue star-shapes; and position angles corresponding to the red-shifted absorption wing (+25 km s^{-1} to +125 km s^{-1}) are plotted as red star-shapes. Position angles only range from 0° to 180° because of the nature of the Stokes parameters; a position angle of 180° is consistent with 0°. Notice the line core polarization is offset by about 90° from the wings. This may be an opacity effect. Compare these data to the mid-eclipse QU-plot (Figure 2) and mid-eclipse line profile (Figure 1).

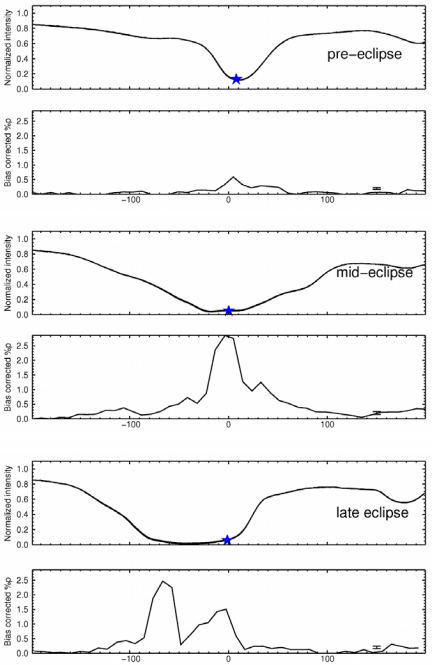

Figure 4. Time series of H-beta (486.135 nm) line and %p profiles for pre-, mid-, and late-eclipse epochs. Velocity is centered on the line rest wavelength. The F-star radial velocity is indicated by a star symbol. Polarization data are epoch- (see text) and wavelength binned (bin size 0.015 nm). Average errors in %p are shown. The line is clearly saturated in late eclipse, falling to just 1.6% intensity at the deepest point and, although S/N is nearly 200 here, the ratio p/σ is only 1.2; therefore %p = 0. The ratio p/σ ranges from 3 to 11 for %p > 0.4 outside the saturated region.

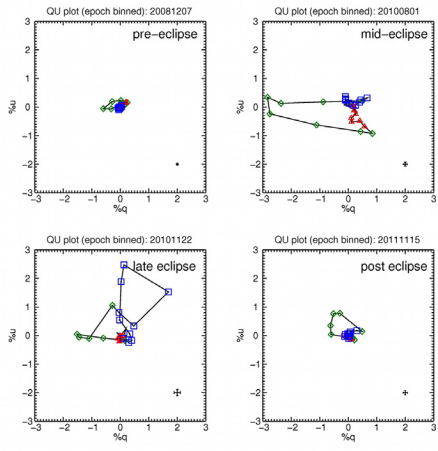

Figure 5. QU-plots of H-beta (486.135 nm) for pre-, mid-, late-, and post-eclipse epoch- and wavelength-binned data. The first date of each binned epoch is given. Average error bars are shown. Absorption wing contributions appear in mid- and late-eclipse. The blue wing corresponds to (+%q, +%u; blue squares) and the red wing corresponds to (+%q, –%u; red triangles) in mid-eclipse. Line core is –%q (green diamonds). By late eclipse, the red wing polarization has disappeared (centered on 0,0) and the large +%q excursion is blue wing polarization (blue squares). The line core polarization is +%u in post eclipse. These data have been rotated into the stellar frame (see text for description).

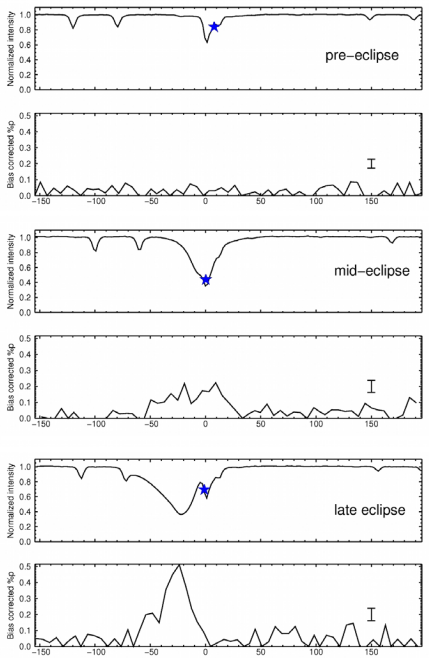

Figure 6. Time series of a K I (769.896 nm) line and %p profiles for pre-, mid-, and late-eclipse epochs. Velocity is centered on rest wavelength. Polarization data are epoch- (see text) and wavelength-binned (bin size 0.015 nm). The out-of-eclipse line is thought to have an interstellar origin. Note the star is red-shifted pre-eclipse, but the line core is not red-shifted and the line exhibits no polarization features. Disk contributions to the line in late eclipse are blue-shifted and exhibit polarization features.

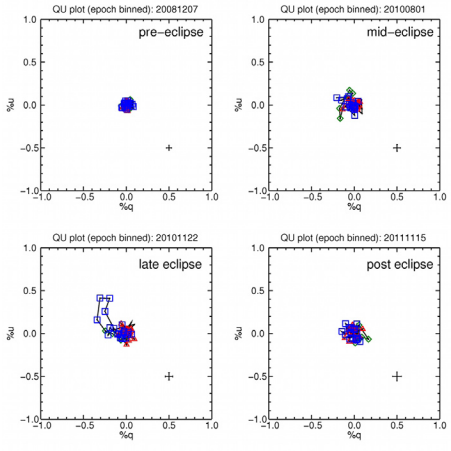

Figure 7. QU-plots of K I (769.896 nm) for pre-, mid-, late-, and post-eclipse epoch- and wavelength-binned data. The first date of each binned epoch is given. Average error bars are given. The out-of-eclipse line is thought to have an interstellar origin (for example, Welty and Hobbs, 2001). Note there are no polarization features pre-eclipse or post eclipse. Disk contributions appear after mid-eclipse. The (–%q, +%u; blue squares) excursion corresponds to the blue-shifted absorption wing. These data have been rotated into the stellar frame (see text for description).

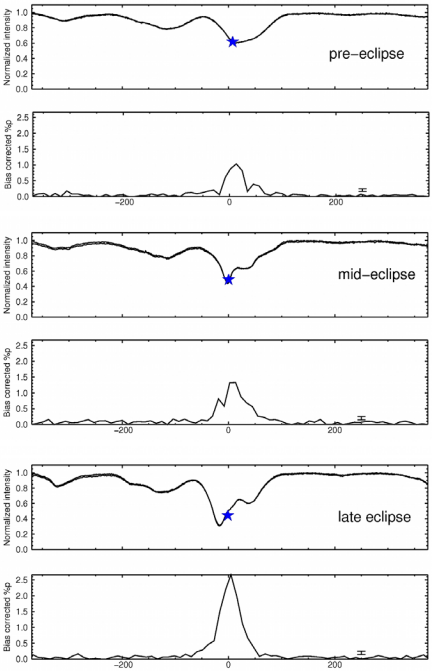

Figure 8. Time series of a Ca I (422.673 nm) line and %p for pre-, mid-, and late-eclipse epochs. Velocity is centered on the line rest wavelength. This line corresponds to a ground state transition. Note the dramatic increase in linear polarization in later epochs. The data are epoch- (see text) and wavelength-binned (bin size 0.015 nm). Average errors in %p are shown.

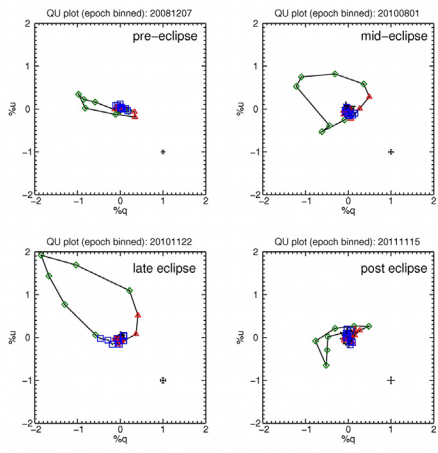

Figure 9. QU-plots of Ca I (422.673 nm) for pre-, mid-, late-, and post-eclipse epoch- and wavelength-binned data. The first date of each binned epoch is given. Average error bars are shown. Absorption wing contributions appear in mid- and late-eclipse. The QU-loop (green diamonds) largely corresponds to line core, with small red wing contributions in +%q in mid-eclipse (red triangles). By late-eclipse, the QU-loop has grown with small –%q contributions from the blue wing (blue squares) and +%q contributions from the red wing. The "flattened" QU-loop corresponds to line core (green diamonds) in post eclipse. These data have been rotated into the stellar frame (see text for description).

Polarimetry of ε Aurigae, From November 2009 to January 2012

Gary M. Cole
Starphysics Observatory, 14280 W. Windriver Lane, Reno, NV 89511; garycole@mac.com; www.starphysics.com

Received March 20, 2012; revised May 17, 2012; accepted June 25, 2012

Abstract During the 2010–2012 eclipse of ε Aurigae, the author obtained linear polarization measurements during 200 nights of observation over three observing seasons. These observations began before second contact and have extended some six months into the post-eclipse period. Measurements were made in V, B, and R photometric bands. The polarization of ε Aurigae was observed to vary by nearly 0.6% peak to valley during this period in cycles of varying duration. These variations resemble, at a qualitative level, those seen by Kemp and Henson during the 1984 eclipse egress. In particular they show evidence of local polarization activity extending well past 4th contact.

1. Introduction

ε Aurigae is an F-type supergiant star approximately 2,000 light years distant. Normally seen at magnitude 3, it undergoes an 18-month-long eclipse every 27 years. The secondary object acts as an opaque disk, partially covering the primary, which dims the system's light by approximately one magnitude. While the disk is assumed to contain a hot embedded star, the spectrum of the secondary has not been observed.

At the suggestion of Dr. Robert Stencel (University of Denver) in May 2009, the author began a series of broadband polarimetric observations of ε Aur during its recent eclipse. The purpose was to extend measurements obtained during the 1984 eclipse by Dr. Jim Kemp and colleagues (Kemp *et al.* 1986) and followed up by his student, Dr. Gary Henson (Henson 1989).

Those observations had revealed significant variations in polarization during and after the eclipse. Dr. Stencel suggested that similar observations during the recent eclipse should be useful for comparison.

Observations reported herein were made over the course of three observing seasons. Season 1 from November 2009 to February 2010, season 2 from September 2010 to May 2011, and season 3 from July 2011 into January 2012. Ongoing instrument development led to significant improvements in the quality of measurements over the course of this work.

2. Instrumentation

There are no commercial sources for small telescope astronomical polarimeters. My instruments have been purpose-built for this project following the general concepts used on the Hawaii 88-inch telescope as described in Masiero *et al.* (2007).

An imaging telescope becomes a dual beam polarimeter with the introduction of a rotating half wave retarder and a calcite beamsplitter. The waveplate material used is an achromatic polymer of the same specification as in the Hawaii instrument. The beamsplitter is a 13-mm calcite Savart plate fabricated by Halbo Optics, which provides a separation of 1 mm at the CCD focal plate. This is approximately 135 arc seconds at the plate scale used on the C8 telescope and 55 arc seconds on the C14. This is more than enough to cleanly separate the slightly defocused and astigmatic star images. The initial waveplate rotator was constructed with a USB-controlled servo motor and plastic gearing.

The Savart plate and a focal reducer were mounted into the nose of an SBIG ST6 camera. The rotator, BVR filter selector, and camera were attached to a C8 optical tube and the entire assembly was mounted onto an existing automated C14 telescope.

This arrangement was used for the first season of observing. For the second season, the camera was replaced with a SBIG ST402 camera. This greatly reduced thermal noise and reduced download time. The rotator, which had frequent breakdowns and poor gearing, remained in use until February of 2010 when it was replaced with a high precision rotator engineered by Optec, Inc.

For the final season of this work, the instrument was reconfigured to work in the C14 optical system. The waveplate rotator was mounted between the focuser and the existing four-way instrument selector. A double fold orthogonal mirror assembly relays the beam into the Savart + camera assembly.

These ongoing changes have yielded significant improvements in data quality over the course of this project. In the first season of measurements, the uncertainty, Δp, in the degree of linear polarization was $\sim \Delta p \pm 0.1\%$; in the second season this was improved to $\sim \Delta p \pm 0.05\%$, and further refined to $\sim \Delta p \pm 0.03\%$ in the third.

Note: The Johnson BVR photometric filters are used in series with a 400-700nm luminance filter so as to match the effective range of the achromatic waveplate. This results in a slightly reddened B and a slightly truncated R bandpass.

3. Calibration

A Polarimeter can exhibit systematic error due to 1) instrumental polarization, 2) co-ordinate frame miss-alignment, and 3) modulation inefficiency.

Instrumental polarization is detected by observing zero polarization standard stars. Several hundred measurements of such stars indicate that such instrumental effects, if present, are less than 0.03% and show no preferred orientation.

The angle of polarization, θ, is defined by IAU conventions as an angle from the North-South line, towards East. The measured angle, therefore, must be adjusted so as to maintain this convention. The first level of adjustment is to set the "zero point" of the waveplate to replicate the convention. This was done using an externally-mounted sheet polarizer oriented along the declination axis. A second step was to refine the fiduciary angle by using measurements of standard stars.

In practice, the author has found it very difficult to maintain the angular precision of the instrument over the course of these observations. Frequent rotator breakdowns, mechanical rotation, and reconfigurations have disturbed the effective alignment and hence the reported angles. Frequent observations of HD 21291, whose stability was affirmed from HPOL measurements (U. Wisconsin 2012), were used for angular correction.

The modulation efficiency was checked by comparing large sets of instrumental results with catalog values for stars of known high polarization. The results obtained match expected values within the experimental uncertainties. No corrections for modulation efficiency have been made.

4. Observing procedure

An automated procedure has been developed for collecting and reducing the data for each measurement and posting the results to a summary file for that object. A detailed calculation report and all data files are retained.

The telescope is slewed to the target. A filter is selected and an initial image frame is taken. The image is dark-subtracted and the target star pair is located.

An appropriate exposure time is calculated based upon the maximum pixel level of the original image. Three dark images are obtained from which a median dark image is assembled. The system then collects from four to eight data sets, each consisting of four data frames taken at different waveplate positions. Each frame is dark-subtracted using the median dark for the series.

The entire sequence is repeated using a shorter exposure time if any pixel in any image exceeds a preset sub-saturation threshold.

The original rotator was stepped through angular positions of 0, 22.5, 45, and 67.5 degrees for each set because moving in a consistent direction minimized gear errors. Once the new rotator was installed the images were taken in 0, 45, 22.5, 67.5 order so that the pairs of images used to determine each of the two Stokes parameters were taken as closely in time as possible. The waveplate was then stepped by 90 degrees for each subsequent data set to minimize the effects of any irregularities in the angular setting of the waveplate.

5. Data reduction

A floating square aperture that is aligned to the centroid of each star is sized to capture 97.5% of the total signal on the first frame. This aperture size is then used for all images in the data set. A larger concentric aperture is used to estimate the background signal. The dual beam method is self-calibrating and does not require flat fielding, but this is subject to the requirement that the star images are recorded onto the same pixel locations within each data pair. To maintain this requirement, any data sets that have excessive motion between frames are excluded from calculations.

Once the intensity values have been extracted from all data sets of the observation, the degree of polarization and angle are computed according to the methods of Tinbergen (1996). The same are calculated for each individual data set for comparison. The error that can be ascribed to photon statistics is calculated according to the method of Serkowski (1974).

The polarization value is adjusted for zero point bias according to the method described by Clarke (2010). The value of this adjustment is typically less than 0.01% for our observations and insignificant in terms of the uncertainty associated with each measurement; the S/N ratio is high and the value of p is large relative to the measurement uncertainties.

6. Target observations

In Table 1 the result for 200 nights of observation are presented. Each measurement consists of multiple sets of four images taken at waveplate positions of 0, 22.5, 45, and 67.5 degrees. On many nights in which several measurements were obtained, these have been averaged. The errors estimated for each polarization measurement are stated in the adjoining columns. The angles are shown in the rightmost three columns. The errors associated with the angles are discussed in the next section.

7. Sources of uncertainty

Observations prior to March of 2011 were subject to imprecise waveplate positioning. The original rotating device used plastic gears to translate servo motion. As each cog of the main gear corresponds to nearly 3 degrees, a small range of random variation is inevitable. There was also an infrequent problem of "hopping." According to the analysis done by Ramaprakash *et al.* (1998), any uncertainty of angular positioning generates a polarization uncertainty of similar magnitude. Hence if a ±1 degree error actually occurred from time to time, it would add 0.05% to the uncertainty of an individual measurement. This source of this problem was reduced by at least a factor of 25 when the Optec Rotator was installed late in season 2.

Observations from this site encounter significant turbulence, bad seeing, wind buffeting, and imperfect guiding. The effects of seeing are to move the center of illumination and to change the distribution of light within each star image. These factors induce small random errors into the results that are difficult to quantify. An examination of the reported variations in closely-spaced time sequential measurements suggest that the data carry error about 50% greater than predicted simply from the photon flux.

For the data presented in this paper, the errors reported in the table and charts for each measurement are double those calculated based upon the photon statistics of the actual images. The author believes this provides a conservative estimate of the true uncertainty in total polarization.

The uncertainty in reported angles of polarization is much worse that that of the magnitude of polarization because 1) it is derived from measurements of standard stars which have at least equivalent uncertainty, and 2) because there were frequent mechanical adjustments made during the course of observations. The author believes that the angles reported contain both random and systematic errors that may reach the level of ± 1 degree.

8. Discussion

The polarization measurements (%) in the *BVR* photometric bands are plotted as a time series in Figure 1. The first season of observations covers the time approaching the second contact during the eclipse. The polarization values (p) are high and are matched again in the early part of the second half of the second season leading up to the end of the eclipse. The third observing season is beyond the eclipse phase and shows strong polarization activity with falls and recoveries covering several tens of days with amplitudes much the same as during the eclipse. Particularly on the protracted fall of some 70 days at the beginning of the second season, soon after mid-eclipse, the color dependence of the polarization clearly shows in Figure 1, with the values of p falling from *B* through *V* to *R*.

Figure 2 displays p and the position angle, θ, for the *V* band over the three seasons. There appears to be a correlation between the three peaks of p and troughs in θ during the second season, but this is not quite as apparent post-eclipse. This behavior indicates that the variable intrinsic polarization is at a significant angle to that of the large interstellar component.

Several researchers, including the team at the Pine Bluff Observatory of the University of Wisconsin, have made synoptic, out-of-eclipse observations of this binary system. During 1990 to 1996, their measurements revealed p(V) values varying from 1.96% to 2.06% with θ(V) ~ 144 degrees. This we assume to be the interstellar component.

Figure 3 displays the normalized Stokes parameters q and u as a function of time. Direct comparison of the polarimetric behavior of this eclipse with

that reported by Kemp *et al.* (1986) of the previous one cannot be made as the earlier authors provide normalized Stokes parameter time-line plots with the q,u values expressed in a co-ordinate frame at 5 degrees relative to the standard equatorial system. However, as the angular difference between frames is very small, strong qualitative comparisons can be made.

In particular, the behavior of both q and u during the egress phase is extremely similar with small oscillations in q and a smooth rise in u in both data sets followed by a rapid decline. The magnitude and frequency of variation in both data sets show considerable similarity but not direct repetition except at egress.

A standard method for investigation of polarimetric data is to plot the normalized Stokes parameters q,u as Cartesian co-ordinates. This has been done in Figure 4 for all the V-band data. Although the scatter of the plotted points is very large, simple inspection shows that there is a trend. This becomes more readily apparent when the data are grouped into smaller temporal segments as has been done in Figure 5. While each segment has a different origin in the q,u-plane, the slopes during these four selected time intervals are close to being parallel. This is shown more clearly in Figure 6 where the four segments are overlaid. Translating these gradients into celestial angles, the polarizational movement appears along position angles between 7 and 22 degrees. Given the level of error in the raw data, these values are close to that (5 degrees) taken by Kemp *et al.* (1986) from the astrometric data of van de Kamp (1978) as being related to the orbital plane direction projected on to the sky. The uncertainty of this angle is not given by Kemp *et al.* (1986) and it is difficult to ascertain the best value from the sketch provided by van de Kamp (1978). As the trend angles are close to the estimate of the orbital projection angle, short-term polarization changes, chiefly affecting the q values, can be surmised as originating from scattering by clumpy material in the orbital plane. The drifts may be affected by introduction of new clumps and their decay, or by changes in their distance from the illuminating star. As to why the origin of the trend lines moves about to produce the more blurred picture that Figure 5 presents, with significant changes in the u parameter, a more sophisticated model is required.

Finally, there appears to be correlation however between several of the *U* band photometric maxima of the recent eclipse (ε Aur campaign 2011) and the polarimetric maxima in these data. In particular, at JD 2455460, at JD 2455545, and at egress the values of *U* and p seem to move together.

9. Future work

In future seasons it is the author's intention to monitor the system in the same frequent manner as during the eclipse to confirm the nature of the variability and search for short-term periodicities. A simultaneous program of *U* and *B* photometry will be added to search for any direct correlation between the optical and polarimetric variability.

10. Acknowledgements

The author extends his thanks to Dr. Robert Stencel of the University of Denver, without whose thoughtful advice and encouragement this project would not have been completed. Also thanks to Dr. Stencel for kindly providing a copy of Henson (1989).

Thanks also to Bolder Vision Optik, of Boulder, Colorado, for the waveplate materials and to Optec, Inc., Lowell, Michigan, for the design and fabrication of the waveplate rotator.

This research has made use of the SIMBAD and VizieR databases operated at CDS, Strasbourg, France and of NASA's Astrophysics Data System.

The author acknowledges the Citizen Sky project of the AAVSO and the National Science Foundation.

References

Clarke, D. 2010, *Stellar Polarimetry*, Wiley-VCH, Hoboken, NJ.

ε Aurigae campaign. 2011, http://www.hposoft.com/Plots09/UBBand.jpg.

Henson, G. D. 1989, Ph.D. dissertation (September), Univ. Oregon.

Kemp, J. C., Henson, G. D., Kraus, D., Beardsley, I., Carroll, L., Ake, T., Simon, T., and Collins, G. 1986, *Astrophys. J., Lett. Ed.*, **300**, L11.

Masiero, J., Hodapp, K., Harrington, D., and Lin, H. 2007, *Publ. Astron. Soc. Pacific*, **119**, 1126.

Ramaprakash, A. N., Gupta, R., Sen, A. K., and Tandon, S. N. 1998, *Astron. Astrophys., Suppl. Ser.*, **128**, 369.

Serkowski, K. 1974, in *Planets, Stars, and Nebulae Studied With Photopolarimetry*, ed. T. Gehrels, Proc. IAU Collq. 23, Univ. Arizona Press, 136.

Tinbergen, J. 1996, *Astronomical Polarimetry*, Cambridge Univ. Press, Cambridge, 100.

Univ. Wisconsin, Space Astronomy Laboratory. 2012, HPOL spectropolarimeter website (http://www.sal.wisc.edu/HPOL/).

Van de Kamp, P. 1978, *Astron. J.*, **83**, 975.

Table 1. Observations of ε Aurigae polarization from JD 2455145 to 2455944 in V, B, and R photometric bands.

JD	*V %Pol*	*%Err*	*B %Pol*	*%Err*	*R %Pol*	*%Err*	*V* θ	*B* θ	*R* θ
2455145	2.474	0.07	—	—	—	—	—	—	—
2455150	2.482	0.05	—	—	2.381	0.1	—	—	—
2455151	2.307	0.09	—	—	—	—	—	—	—
2455154	2.259	0.11	—	—	2.22	0.04	—	—	—
2455155	2.454	0.14	—	—	2.396	0.05	—	—	—

Table continued on following pages

Table 1. Observations of ε Aurigae polarization from JD 2455145 to 2455944 in V, B, and R photometric bands, cont.

JD	*V %Pol*	*%Err*	*B %Pol*	*%Err*	*R %Pol*	*%Err*	*V* θ	*B* θ	*R* θ
2455159	2.357	0.09	—	—	2.334	0.1	—	—	—
2455168	2.145	0.05	—	—	2.147	0.09	—	—	—
2455169	2.249	0.04	—	—	2.206	0.07	—	—	—
2455191	2.218	0.1	—	—	—	—	—	—	—
2455201	2.201	0.14	—	—	—	—	—	—	—
2455202	2.112	0.08	—	—	2.208	0.09	—	—	—
2455210	2.287	0.08	—	—	2.271	0.07	—	—	—
2455211	2.314	0.1	—	—	2.246	0.14	—	—	—
2455212	2.325	0.09	—	—	—	—	—	—	—
2455220	2.271	0.04	2.299	0.06	—	—	—	—	—
2455449	2.168	0.06	2.232	0.06	2.104	0.06	139.8	138.7	140.9
2455450	2.197	0.06	2.192	0.06	2.136	0.06	140.2	139.1	141.2
2455451	2.194	0.07	2.209	0.07	2.239	0.07	139.6	140.1	139.3
2455452	2.212	0.07	2.236	0.06	2.18	0.07	139.1	138.3	140.9
2455453	2.233	0.05	2.223	0.05	2.166	0.06	139	138.3	140.8
2455454	2.238	0.07	2.233	0.06	2.148	0.07	139.5	138.4	141.1
2455455	2.176	0.04	2.215	0.03	2.132	0.04	139.3	138.7	141.3
2455456	2.208	0.04	2.225	0.04	2.193	0.04	138.9	138.9	139.5
2455458	2.222	0.05	2.293	0.05	2.183	0.05	139.2	138.2	141.3
2455462	2.244	0.06	2.27	0.06	2.138	0.06	139.2	138.3	140.6
2455463	2.193	0.05	2.264	0.04	2.136	0.05	139.1	137.7	140.7
2455464	2.246	0.06	2.262	0.05	2.309	0.06	139	138.8	139.1
2455465	2.142	0.06	2.197	0.06	2.189	0.06	138.8	138.2	138.4
2455467	2.218	0.05	2.283	0.05	2.203	0.05	139.4	138.4	140.8
2455468	2.222	0.06	2.243	0.05	2.144	0.08	139.9	139	141.3
2455469	2.188	0.06	2.198	0.06	2.179	0.06	138.9	137.6	140.7
2455470	2.144	0.07	2.191	0.06	2.085	0.07	139.6	138.9	141.2
2455478	2.154	0.05	2.171	0.05	2.117	0.06	141	139.9	143
2455479	2.12	0.06	2.193	0.05	2.127	0.06	141.2	140.3	142.3
2455480	2.118	0.07	2.105	0.07	2.119	0.06	140.5	140.7	140.7
2455481	2.125	0.06	2.135	0.06	2.07	0.06	141.2	139.9	142.7
2455482	2.13	0.07	2.149	0.07	2.117	0.07	141.8	140.5	143.1
2455483	2.142	0.06	2.142	0.06	2.097	0.07	141.8	140.8	143.5
2455484	2.133	0.06	—	—	2.168	0.07	142	—	142.9
2455485	2.148	0.06	2.154	0.06	2.119	0.06	140.9	140.3	142.8
2455489	2.114	0.06	2.101	0.06	2.068	0.07	142	140.8	142.5
2455490	2.103	0.05	2.126	0.06	2.184	0.05	140.6	140.8	140.1
2455501	2.152	0.04	2.1	0.03	2.085	0.03	141.16	140.56	142.36
2455502	2.083	0.04	2.113	0.04	2.015	0.04	141.8	141.4	143.1

Table continued on following pages

Table 1. Observations of ε Aurigae polarization from JD 2455145 to 2455944 in V, B, and R photometric bands, cont.

JD	*V %Pol*	*%Err*	*B %Pol*	*%Err*	*R %Pol*	*%Err*	*V* θ	*B* θ	*R* θ
2455503	2.093	0.05	2.127	0.04	2.05	0.06	142	141.2	143.8
2455504	2.082	0.05	2.057	0.05	2.044	0.07	141.4	141	142.7
2455505	2.083	0.06	—	—	—	—	141.8	—	—
2455507	2.063	0.04	2.065	0.03	2.029	0.04	140.8	140.1	142.9
2455509	2.083	0.05	2.081	0.07	2.076	0.06	142.2	141.8	145
2455512	2.042	0.06	2.029	0.05	1.993	0.05	142.6	142	144.7
2455513	2.036	0.06	2.031	0.06	1.962	0.06	141.9	140.7	143.6
2455514	2.063	0.07	—	—	2.041	0.09	141.2	—	142.9
2455515	2.111	0.08	2.043	0.07	2.004	0.07	141.2	141.6	143.4
2455516	2.1	0.06	2.025	0.05	2.022	0.06	141.2	140.4	142.5
2455517	2.061	0.06	2.045	0.06	2.026	0.06	141	141	142.3
2455518	2.031	0.06	—	—	—	—	141.8	—	—
2455532	2.225	0.06	2.189	0.04	2.186	0.05	140	139.9	141.9
2455537	2.234	0.06	2.266	0.06	2.214	0.06	138.1	137.5	138.7
2455542	2.278	0.07	2.328	0.06	2.158	0.07	145.1	146	146.5
2455543	2.262	0.05	2.285	0.04	2.205	0.04	137.1	136.4	138.4
2455547	—	—	—	—	2.175	0.06	—	—	138.8
2455554	2.246	0.08	2.219	0.05	2.146	0.07	137.4	136.1	140
2455555	2.246	0.06	2.243	0.06	2.174	0.06	137.3	136.3	139.3
2455558	2.154	0.07	2.199	0.06	2.207	0.08	138	136.9	140.7
2455565	2.115	0.05	2.15	0.05	2.091	0.05	139.7	139.5	141.6
2455566	2.122	0.05	2.124	0.05	2.021	0.05	138.7	137.8	140.7
2455567	2.122	0.06	2.104	0.05	2.064	0.06	138.4	137.6	140.2
2455568	2.113	0.05	2.102	0.04	2.015	0.05	139	138.2	140.9
2455569	2.149	0.05	2.112	0.06	2.088	0.05	138.3	138.5	139
2455570	2.16	0.04	2.113	0.04	2.101	0.04	140.2	139.4	142.8
2455576	2.198	0.07	2.223	0.06	2.194	0.07	139.6	139.1	141.3
2455577	2.316	0.06	2.342	0.04	2.297	0.06	140.1	140.7	141.7
2455578	2.355	0.06	2.239	0.05	2.262	0.06	141.3	140.2	141.2
2455579	2.278	0.06	2.221	0.06	2.197	0.06	140.8	140.2	142.3
2455581	2.304	0.07	2.257	0.06	2.281	0.06	141.2	140.7	142.3
2455582	2.316	0.06	2.297	0.05	2.243	0.06	141	140.6	141.5
2455583	2.336	0.06	2.289	0.05	2.307	0.06	140.7	140.9	142.7
2455584	2.293	0.06	2.274	0.06	2.246	0.05	140.5	140.1	142.9
2455587	2.355	0.07	2.269	0.06	—	—	140.6	140.2	—
2455588	2.297	0.06	2.24	0.05	2.232	0.06	139.9	140.1	141.3
2455589	2.281	0.05	2.277	0.06	2.228	0.06	140.2	139.9	142.5
2455593	2.312	0.06	2.332	0.06	2.27	0.06	139.7	139.3	142.1
2455595	2.257	0.07	2.192	0.06	2.394	0.06	138.4	138.2	140.6

Table continued on following pages

Table 1. Observations of ε Aurigae polarization from JD 2455145 to 2455944 in V, B, and R photometric bands, cont.

JD	*V %Pol*	*%Err*	*B %Pol*	*%Err*	*R %Pol*	*%Err*	*V* θ	*B* θ	*R* θ
2455596	2.359	0.07	2.367	0.07	2.229	0.07	137.8	138.8	139.6
2455597	2.362	0.06	2.343	0.05	2.3	0.05	138.4	138.1	139.3
2455599	2.372	0.06	2.385	0.05	2.253	0.06	137.5	137.5	139.6
2455600	2.425	0.05	2.385	0.04	—	—	137.7	137	—
2455602	2.405	0.08	2.463	0.06	2.34	0.06	136.3	134.9	137.7
2455615	2.298	0.08	2.338	0.07	2.278	0.06	136.65	137.35	136.45
2455616	2.312	0.05	2.289	0.03	2.264	0.04	137.15	137.45	137.05
2455620	2.177	0.05	2.192	0.04	2.159	0.04	138.75	138.85	138.55
2455621	2.184	0.07	2.193	0.04	2.221	0.05	138.85	139.15	138.25
2455629	2.008	0.06	1.995	0.05	1.961	0.08	140.65	141.15	139.35
2455630	1.971	0.04	1.971	0.04	1.949	0.05	140.31	141.41	139.81
2455632	2.03	0.06	—	—	—	—	139.21	—	—
2455633	1.946	0.04	1.922	0.03	1.914	0.04	141.03	141.23	140.73
2455638	1.913	0.07	—	—	1.873	0.06	145.13	—	145.13
2455643	1.872	0.07	1.9	0.06	—	—	—	—	—
2455649	1.975	0.08	1.971	0.05	2.002	0.06	141.24	141.14	140.54
2455651	2.019	0.05	1.988	0.05	2.012	0.05	143.04	142.94	142.24
2455652	2.025	0.04	1.983	0.05	2.013	0.05	141.93	142.03	140.83
2455653	1.979	0.07	2.011	0.06	1.991	0.08	139.63	141.73	140.03
2455654	1.99	0.04	1.959	0.04	1.979	0.04	141.93	141.93	140.83
2455655	1.978	0.07	2.003	0.09	2.005	0.08	141.73	143.03	141.13
2455656	2.005	0.07	1.977	0.06	1.953	0.08	142.83	143.53	141.53
2455657	1.994	0.08	2.01	0.07	2.006	0.07	144.13	144.93	144.23
2455659	2.031	0.05	2.014	0.03	2.028	0.05	142.43	141.73	141.93
2455661	1.96	0.07	—	—	—	—	147.93	—	—
2455662	2.011	0.07	1.996	0.08	2.037	0.06	141.98	142.38	140.38
2455663	2.017	0.05	2.03	0.05	2.02	0.05	142.38	141.88	140.68
2455665	2.021	0.03	2.008	0.04	—	—	142.38	141.68	—
2455667	1.997	0.05	2.017	0.08	—	—	141.38	142.08	—
2455670	1.959	0.08	1.924	0.06	—	—	141.58	140.98	—
2455673	1.937	0.08	—	—	—	—	140.68	—	—
2455676	2.024	0.05	2.048	0.06	—	—	139.68	140.38	—
2455678	2.025	0.05	1.925	0.07	—	—	140.98	140.88	—
2455679	2.058	0.07	2.004	0.07	1.988	0.06	140.98	140.58	140.18
2455682	2.034	0.06	2.004	0.06	2.004	0.06	141.58	141.68	141.98
2455683	2.036	0.09	2.035	0.1	2	0.11	140.58	144.28	139.68
2455684	2.005	0.09	2.069	0.07	—	—	142.38	141.08	—
2455685	1.99	0.06	2.034	0.06	2.025	0.07	142.08	141.58	141.48
2455686	2.017	0.07	—	—	—	—	141.18	—	—

Table continued on following pages

Table 1. Observations of ε Aurigae polarization from JD 2455145 to 2455944 in V, B, and R photometric bands, cont.

JD	*V %Pol*	*%Err*	*B %Pol*	*%Err*	*R %Pol*	*%Err*	*V θ*	*B θ*	*R θ*
2455687	2.118	0.06	—	—	—	—	141.28	—	—
2455762	—	—	2.111	0.04	2.026	0.04	—	144.5	146.6
2455765	2.108	0.03	2.133	0.03	—	—	145.5	145.2	—
2455766	2.094	0.03	—	—	2.077	0.03	145.5	—	144
2455767	2.172	0.03	—	—	—	—	143.3	—	—
2455768	2.125	0.02	—	—	—	—	142.8	—	—
2455769	2.187	0.03	2.181	0.03	2.091	0.03	143.7	144	145.6
2455770	2.161	0.03	2.162	0.02	2.099	0.02	143.4	143.2	144.8
2455771	2.175	0.03	2.148	0.03	2.143	0.03	143.9	144	144.8
2455775	2.203	0.03	2.178	0.03	2.106	0.03	143.8	143.6	145
2455776	2.183	0.03	—	—	2.086	0.02	142.7	—	143.4
2455777	2.137	0.02	2.151	0.02	2.148	0.02	142.5	142.3	142.7
2455778	2.114	0.03	2.132	0.02	2.107	0.02	142.4	143	142.6
2455779	2.118	0.03	2.086	0.02	2.052	0.02	142.9	142.4	144.5
2455780	2.085	0.02	2.086	0.02	2.026	0.02	142.7	142.1	143.7
2455781	2.068	0.03	2.087	0.03	2.051	0.02	143	142.8	144.4
2455782	2.069	0.03	2.072	0.02	1.997	0.03	142.4	141.3	143.6
2455783	2.062	0.03	2.015	0.03	2.056	0.03	141.3	141	141.3
2455784	2.047	0.03	2.077	0.03	2.025	0.02	141.5	141.5	141.2
2455785	2.058	0.03	2.053	0.03	2.018	0.02	142.6	141.8	140.7
2455788	2.054	0.02	2.015	0.02	1.988	0.02	141.8	141.1	142.8
2455789	2.026	0.03	2.003	0.02	1.968	0.02	143.1	142.8	142.7
2455790	2.012	0.03	2.011	0.02	1.986	0.03	142.1	141.2	143.1
2455791	2.063	0.03	2.012	0.02	1.998	0.02	141.6	140.6	142.6
2455792	2.047	0.03	1.992	0.02	1.988	0.03	141.3	140.9	141.7
2455793	2.047	0.02	2.025	0.03	2.006	0.02	141.2	140.6	142.3
2455794	2.05	0.03	1.948	0.03	2.012	0.03	141	140	142.2
2455795	2.057	0.03	2.054	0.03	1.948	0.04	140.8	139.8	141.8
2455796	2.033	0.03	1.973	0.03	1.984	0.03	141.3	141.3	142.4
2455798	2.015	0.03	1.962	0.03	1.935	0.03	141.4	140.4	141.8
2455799	2.003	0.04	1.94	0.03	1.935	0.03	142.6	141.9	143.4
2455801	1.999	0.03	1.939	0.03	1.453	0.03	141.7	141.2	—
2455802	1.999	0.02	1.943	0.02	1.951	0.02	142	141.7	—
2455803	1.976	0.03	1.96	0.02	1.944	0.02	143.1	142.9	143.8
2455821	—	—	1.902	0.03	—	—	—	143.9	—
2455822	1.974	0.03	1.862	0.03	1.91	0.03	143.8	144.2	145.3
2455823	1.947	0.03	1.891	0.03	1.924	0.03	145.4	145.5	145.5
2455824	1.946	0.03	1.878	0.03	1.91	0.03	145.3	145	146
2455825	1.927	0.03	1.874	0.03	1.895	0.03	145.5	145.3	146.2

Table continued on next page

Table 1. Observations of ε Aurigae polarization from JD 2455145 to 2455944 in V, B, and R photometric bands, cont.

JD	*V %Pol*	*%Err*	*B %Pol*	*%Err*	*R %Pol*	*%Err*	*V* θ	*B* θ	*R* θ
2455851	2.07	0.04	2.011	0.03	2.049	0.03	—	—	—
2455853	2.043	0.04	2.019	0.03	2.001	0.03	—	—	—
2455854	2.037	0.03	2.056	0.03	2.025	0.03	145.56	144.36	143.66
2455856	2.036	0.04	2.03	0.04	2.037	0.03	142.41	143.21	142.81
2455857	2.02	0.03	2.063	0.03	1.943	0.03	142.72	142.22	152.92
2455858	2.034	0.02	2.056	0.02	2.041	0.02	143.02	142.72	142.42
2455860	2.071	0.04	2.14	0.03	2.073	0.03	141.99	142.09	141.89
2455861	2.157	0.04	2.189	0.04	2.064	0.04	142.05	143.25	142.25
2455862	2.062	0.03	2.068	0.03	2.019	0.03	142.64	142.64	142.44
2455863	2.065	0.03	—	—	—	—	144.32	—	—
2455865	2.008	0.03	1.964	0.02	1.977	0.03	143.31	142.81	142.61
2455866	1.992	0.02	2.018	0.02	2.02	0.02	143.21	143.01	143.01
2455867	2.01	0.03	1.975	0.02	—	—	142.1	141.9	—
2455876	2.057	0.03	2.091	0.03	2.061	0.02	—	—	—
2455878	2.058	0.04	—	—	—	—	—	—	—
2455881	2.029	0.04	1.983	0.03	2.011	0.03	142.8	141.8	144.2
2455882	2.032	0.03	1.988	0.02	2.032	0.02	143.2	142.3	144.5
2455894	2.005	0.03	2.022	0.02	1.999	0.02	138.1	138.3	138.7
2455895	2.057	0.03	2.005	0.02	2.03	0.03	143.5	143.2	144.8
2455897	2.082	0.03	2.067	0.02	1.989	0.02	143.5	142.6	145.6
2455898	2.128	0.03	2.069	0.02	2	0.03	143.7	143.1	145.6
2455899	2.067	0.03	2.078	0.03	2.039	0.03	143.3	142.7	145.3
2455902	2.091	0.03	2.044	0.02	2.049	0.03	143.2	142.6	144.6
2455903	2.073	0.04	2.064	0.03	2.037	0.03	148.2	142.7	144.9
2455904	2.067	0.03	2.057	0.02	2.018	0.03	144.1	142.7	144.7
2455905	2.078	0.03	2.066	0.02	2.065	0.02	142.8	143.3	145.6
2455906	2.123	0.03	2.06	0.03	—	—	143.7	143	—
2455907	2.105	0.03	2.07	0.04	2.048	0.03	143.6	142.3	144.8
2455908	2.098	0.03	—	—	2.08	0.04	144.4	—	146.8
2455909	2.106	0.03	2.104	0.03	2.048	0.03	143.5	143.7	146.1
2455913	2.101	0.03	2.048	0.02	2.03	0.02	144.3	144	145.7
2455917	2.082	0.02	2.068	0.02	2.068	0.02	144.4	144.1	146
2455918	2.08	0.03	2.089	0.02	2.044	0.02	142.8	142.3	144.1
2455936	2.004	0.03	1.944	0.02	1.919	0.02	145.1	144.6	146.8
2455938	2.04	0.06	2	0.03	—	—	143.7	143.4	—
2455939	1.972	0.02	2.014	0.02	—	—	145.4	146.2	—
2455940	1.951	0.05	1.969	0.03	—	—	—	—	—
2455941	2.011	0.02	—	—	—	—	145.1	—	—
2455944	2.028	0.03	—	—	—	—	—	—	—

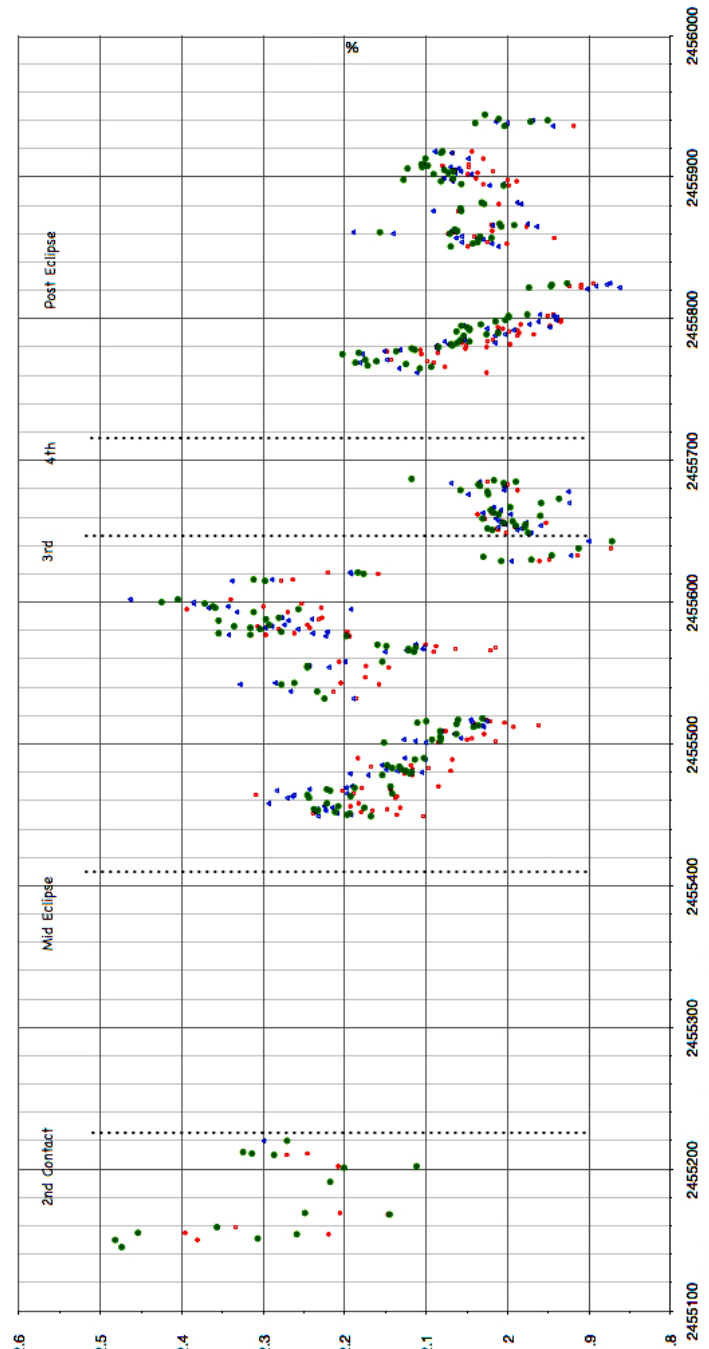

Figure 1. ε Aur eclipse: BVR percentage of polarization. V are circles, B are triangles, R are squares.

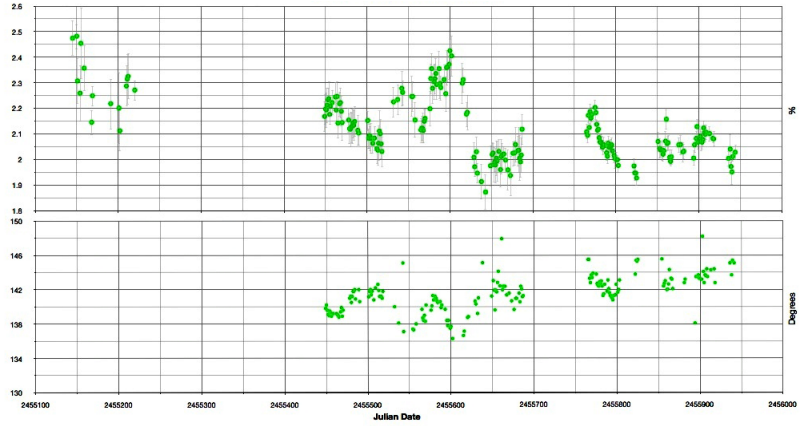

Figure 2. ε Aur eclipse: V percentage of polarization (p) and V position angle (θ).

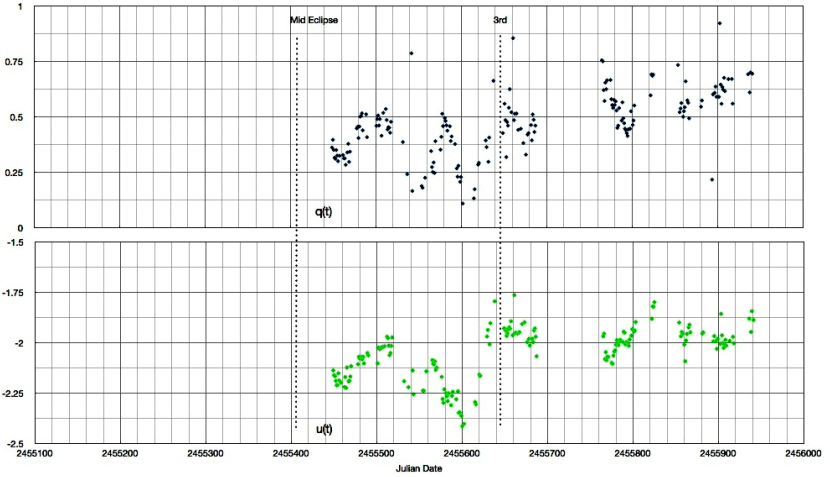

Figure 3. ε Aur eclipse: normalized Stokes parameters as a function of time.

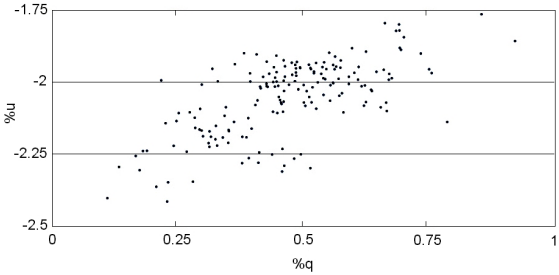

Figure 4. ε Aur eclipse: Stokes u as a function of q for all observations.

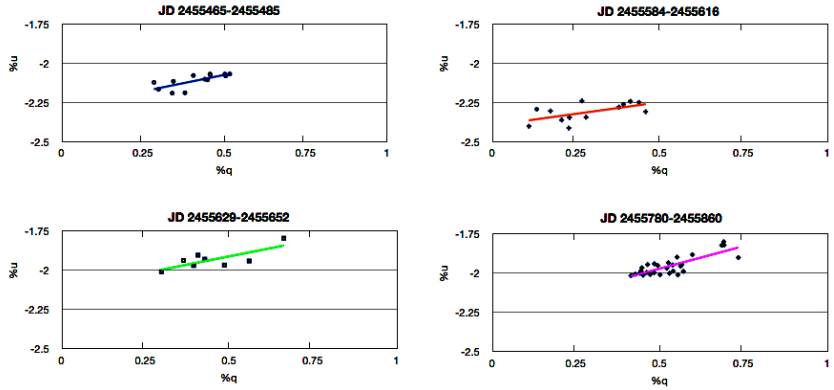

Figure 5. ε Aur eclipse: q,u diagrams for selected epochs.

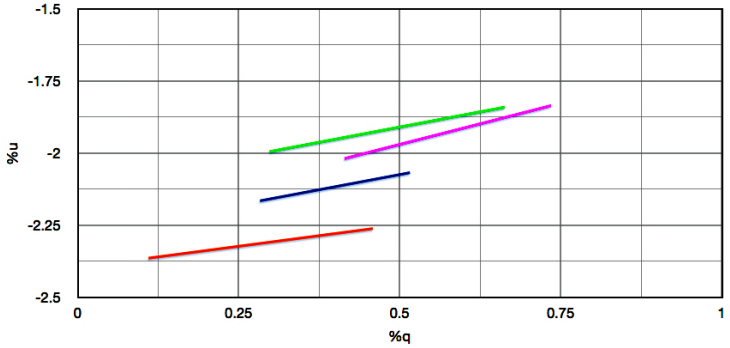

Figure 6. Overlay of 1,u trendlines for selected epochs.

Modeling the Disk in the ε Aurigae System: a Brief Review With Proposed Numerical Solutions

Richard L. Pearson, III
Robert E. Stencel
University of Denver, Department of Physics and Astronomy, 2112 E. Wesley Avenue, Denver, CO 80208; *address email correspondence to richard.pearson@du.edu*

Received April 19, 2012; revised July 19, 2012; accepted August 7, 2012

Abstract Parameters associated with the opaque disk in ε Aurigae are explored in the context of circumstellar and proto-planetary disk theory. The observed blackbody temperatures of the disk, at 550 and 1150 K, are primarily discussed. Brief reviews of previous work are included that describe and attempt to explain this temperature gradient. Heating from only the central B star provides a basal temperature of about 250 K. An accretion rate (from the disk to the B star) of 10^{-7} $M_{\odot}$/yr also provides a similar basal temperature; a rate of 1.5×10^{-5} $M_{\odot}$/yr produces temperatures greater than 3000 K in the disk plane. To include the F star contribution, Monte Carlo radiative transfer tools can be used to examine numerous separation distances between the two stellar components, with the goal of matching the observed and modeled temperatures. An estimation of the distance to ε Aurigae can then be extracted. The proposed method is described here.

1. Introduction

ε Aurigae is a single-line spectroscopic binary that features an opaque disk around a companion that causes lengthy eclipses every 27 years (for a reading list, see Carroll *et al.* 1991; Lissauer *et al.* 1996; Stencel *et al.* 2011). Figure 1 illustrates the configuration. Interferometric imaging proves the existence of a disk and provides some preliminary dimensions for it (Kloppenborg *et al.* 2010), based on a highly uncertain Hipparcos distance of 625 pc (Perryman *et al.* 1997). The eclipse of 2010 provided a wealth of new data, from far-ultraviolet to far-infrared and sub-mm wavelengths (Hoard *et al.* 2010; Stencel *et al.* 2011; Hoard *et al.* 2012). For this work, we are specifically interested in the observed surface temperatures of the disk as stated in Hoard *et al.* (2012) and provided here in Table 1.

There is an unresolved concern in regards to pinpointing the evolutionary state of ε Aur. Two parts of this concern deal with the stellar masses and the distance to the system. First, the masses are unknown, but the bright primary star resembles an F0 supergiant that may contain as much as 15–25 $M_{\odot}$, or as little as 3–4 $M_{\odot}$ (if it is an overluminous post-AGB star, as in Guinan and Dewarf

2002). Little to no optical spectrum exists for the disk-shrouded companion and thus it cannot be classified directly. Spectroscopic information provides a mass function value of 2.53 (Stefanik *et al.* 2010) and admits distance-dependent mass ratios of 0.5–1.1. Eclipse data and ultraviolet fluxes suggest the hidden companion could be a ≈ 6 $M_{\odot}$ B5V star (Hoard *et al.* 2010), with the bright star an approximately 3 $M_{\odot}$ hyper-luminous post-AGB star in a rapid state of evolution (Lambert and Sawyer 1986; Takeuti 1986a; Saito *et al.* 1987; Sheffer and Lambert 1999).

Second, the actual distance to ε Aur is not well defined. The system is at the limit of a valid Hipparcos parallactic distance. There also seems to be intrinsic variability in the F star, which provides a varying star photocenter for the parallactic measurements (Kloppenborg *et al.* 2011). Of course, an accurate distance measurement refines the constraints on the system's physical parameters (for example, stellar masses, star-to-disk separations, and so on). Some of the typical parameters, using the high-error Hipparcos distance, are listed in Table 1.

Previous analytical and numerical modeling techniques have focused on resolving the questionable state of ε Aur, by understanding the disk to constrain certain parameters of the entire system. These include disk thickness limitations (Lissauer *et al.* 1996), disk temperature studies (Takeuti 1986b; Hoard *et al.* 2010; Takeuti 2011), and spectral energy distribution (SED) matching (Muthumariappan and Parthasarathy 2012), for example. Many of these models used the Hipparcos distance to define parameters and/or used only specific parts of the system in the modeling (that is, considering only the disk and B star).

In order to support the plethora of observations, modeling techniques must further explore the complete nature of this disk. The observed minimum and maximum disk temperatures (T_{noon} = 1150 ± 50 K and T_{midnight} = 550 ± 50 K) provide an avenue of investigation (Hoard *et al.* 2012). One can look to reproduce these temperatures in analytical and numerical studies, by examining four ε Aur disk-heating scenarios:

1. radiation from the central star (section 2.1),
2. accretional heating from the disk onto the central star (section 2.2),
3. radiation from the central and companion stars (section 2.3), and
4. radiation from stars plus accretional heating (also section 2.3).

The motivation of this paper is to describe the need to build a complete model of the ε Aur system by using numerical modeling techniques and the observed temperatures. From this, a distance can be determined (as described in section 2.3.2), thereby clarifying the evolutionary state. Sections 2.1 and 2.2 establish possible disk basal temperatures and clarify that the observed temperature gradient must be achieved by an external source. Section 2.3

describes how numerical modeling of all heating components can aid in system constraints. This paper presents a brief review of previous modeling techniques and proposes additional numerical solutions.

2. Disk heating

A very useful tool in constraining certain parameters of the system are the disk temperatures. By matching observationally constructed SEDs with blackbody temperature curves, two temperatures have been established (Hoard *et al.* 2012). Half of the disk facing opposite the F star is the "midnight'' side and found to be 550 ± 50 K. The side facing the F star, "noon," is found to have a temperature of 1150 ± 50 K. Deciphering how and why the disk exhibits the observed temperature gradient is important in understanding the actual state of the system.

We explore heating effects on the disk by three different sources: heating from the central star, accretional heating, and the exterior stellar source are all investigated below. Brief reviews of prior work are included as well.

2.1. Central star input

We first consider a discussion concerning the effect of the central star radiation on the surrounding disk. Takeuti (1986b) analytically solved for the temperature and scale height of the disk at specified radii, based on a central B star of 4 $M_{\odot}$, 3 $R_{\odot}$, and $T_{\rm eff}$ = 15000 K. Blackbody equilibrium temperatures of 355 and 263 K were found at disk radii of 2 and 3 AU, respectively. No numerical radiative transfer analysis was performed. The significance of these values is discussed below.

More recently, Muthumariappan and Parthasarathy (2012, hereafter M&P) investigated the composition, dust particle size, outer radius temperature, and mass of the disk in ε Aur, using a two-dimensional, photon-tracking Monte Carlo code. Their SED results were based on energy input only from an internal B5V star. The system was assumed to be at the Hipparcos distance. They created models with dust compositions of amorphous carbon, ISM distribution (60% silcates and 40% carbonates), and amorphous silicates. Also, particle size distributions corresponding to minima--maxima ranges of 0.05–0.2 μ*m* and 10–100 μ*m* were applied. A Kurucz flux model of a 7700 K, F0Iae post-AGB star was combined with the output SEDs. Then, comparisons were made with the observationally determined SED.

Their SED fitting resulted in a 5×10^{-3} $M_{\odot}$ disk composed of carbonates, with grain sizes 10–100 μ*m*, and an outer disk temperature of 252 K at $R_{\rm out}$ = 3.8 AU. The other models result in outer disk temperatures of 261–293 K. These are, obviously, lower than the either of the observed $T_{\rm midnight}$ or $T_{\rm noon}$. Takeuti (1986b) determined a very comparable temperature, as stated above. Though M&P provide no discussion concerning this, these findings indicate

that models based solely on the interior B5V radiation provide a possible basal heating level which can be compared against observation. Further implications of this basal temperature are discussed in section 2.3.

2.2. Accretion input

We now explore the disk temperature, specifically T_{midnight}, based solely on accretional heating from the disk to the central star. Armitage (2010, specifically section 3.3 therein) describes a set of general disk equations describing accreting, Keplerian disk systems (for additional discussion, see Lin and Papaloizou 1985). Turbulent motion is used as the primary source of angular momentum transport within the disk; it is portrayed as a turbulent viscosity in Equation 1 of Table 2. The Shakura-Sunyaev α parameter (Shakura and Sunyaev 1973) is used to define the disk's viscosity.

The equations displayed in Table 2 have been adopted from Armitage (2010) and applied to the ε Aur disk. A previous iteration of this analytical calculation is found in Takeuti (1986b), who uses a form of Equations 5, 9, and 10 in Table 2 (along with a central B star as described in the first paragraph of section 2.1) to calculate temperatures and scale heights at various disk radii. Updated temperatures and scale heights, as well as additional parameters such as disk mass and density, are presented in Table 3.

If the central star mass (M_{star}), accretion rate ($\dot{M}$), and disk radius (r_{disk}) are known, the equations in Table 2 depend only upon the mass absorption coefficient (κ), the mean molecular weight (μ), and the viscosity parameter (α). Therefore, by defining these six terms, a full set of parameters describing the system can be output. The opacity temperature dependence ($\kappa = \kappa_0 T$) and constant ($\kappa = 5 \times 10^{-3}$ cm^2 g^{-1}) were selected from Lin and Papaloizou (1985) and Pollack *et al.* (1985). A molecular weight of 1.5 was selected, which is low enough to admit that the disk has a high gas-to-dust ratio, but shows it is not completely made of hydrogen gas ($\mu = 1$). Hartmann *et al.* (1998) determined $\alpha = 0.01$ for T Tauri star disks and that has been adopted here. Accretion rates were obtained from Pequette *et al.* (2011a), who concludes that having a $\dot{M} \neq 0$ was a possible way to reproduce comparable model SEDs to the observed. Pequette *et al.* (2011a) state that only a high accretion rate provides an appropriate UV-to-IR ratio. For the analytic calculations here, two typical accretion disk rates of 10^{-6} and 10^{-7} $M_\odot$/yr were used along with 1.5×10^{-5} $M_\odot$/yr from Pequette *et al.* (2011a, 2011b).

Once each of the input variables have been specified, all other parameters become uniquely determined. Selected output variables are displayed in Table 3. Of note, the 10^{-6} and 10^{-7} accretion rates produce disk masses ($2.9–9.25 \times 10^{-3}$ $M_\odot$) comparable to the mass predicted by M&P (5×10^{-3} $M_\odot$); the 1.5×10^{-5} accretion rate produces a disk mass about ten times that of M&P.

For disk thickness-to-radius ratio comparisons, an observed value of 0.08 is given in Table 1. This ratio was calculated from the angular measurements of the

observed thickness of the disk and its radius. Lissauer *et al.* (1996) shows plots of z/R_d, which is equivalent to Nh/R_{out} where N is an integer number of scale heights in a distance z. The analytical calculations in Table 3 show that for the highest accretion rate, none of the Nh/R_{out} values fall near 0.08. However, ratios from the 10^{-6} and 10^{-7} accretion rates are comparable. The 10^{-6} rate allows for $N = 1$ or $N = 2$, depending on the central star mass. The 10^{-7} rate seems to prefer either $N = 2$ or $N = 3$, which also coincides with the Lissauer *et al.* (1996) models.

If we assume a dust sublimation temperature of 1500 K, then the T_c values for the highest accretion rate are too large, especially if particles are supposed to be coalescing into protoplanetary objects. However, as seen in Figure 2, the only $\dot{M}$ to output a $T_{\rm disk}$ near the observed midnight temperature is the 1.5×10^{-5} $M_\odot$/yr rate. If accretional heating was solely responsible for providing the observed 550 K "midnight" temperature, then the predicted disk mass from the high accretion rate must be discussed. The disk mass from Table 3 is 41×10^{-3} $M_\odot$, or 43 Jupiter masses, which is much larger than any previous prediction. Were the disk mass more along the lines of the M&P 5×10^{-3} $M_\odot$, the timescale for the disk would be about 330 years; since eclipse light curves of ε Aur have shown fairly consistant magnitude drops for almost 170 years, a timescale of only 330 years seems very unlikely. The existence of a mass transfer stream (from the F star to the disk), however, could extend the life of the disk. Nevertheless, the predicted mass, high T_c values, and large h/R_{out} ratios dismiss the likelihood of a high accretion rate present in ε Aur. However, it does not dismiss the presence of a lower accretional rate.

Accretional heating alone is not able to support the observed temperature distribution (550–1150 K) on the disk. However, just as in section 2.1, the low $T_{\rm disk}$ output from the lower accretion rates may be able to provide a lower bound temperature for the disk in the ε Aur system. The effect and relationship with the other heating mechanisms are discussed at the end of section 2.3.

2.3. Companion star input

The two previous sections have illustrated the importance of including the F0 star's radiation in the modeling to explain the disk's azimuthal temperature gradient. Though an examination of separate heating components can provide specific constraints (that is, a basal temperature), the next step is to include all of the components of the system. A brief review of previous work relating to the disk temperature is described to further justify the need for new numerical computations. The results of these new calculations will help provide an independent measurement of ε Aur's distance.

2.3.1. Previous analytical studies

As previously mentioned, Takeuti (1986b) calculated disk temperatures and scale heights from two separate radiation sources. Putting them together, Takeuti (1986b) postulates a possible disk configuration: a cool, thin disk

near "midnight" and subject only to the central star's radiation; a crescent-shaped, optically thick region dominated by the F star's radiation; and a small, optically thin region, directly opposite the F star near the disk's edge. Using this configuration, a steady-state disk assumption, and a limiting $T_{\text{midnight}} = 500$ K, an accretion rate of 2×10^{-11} $M_{\odot}$/yr is found. This accretion rate would not produce the observed UV excess (Hoard *et al.* 2010). Takeuti (1986b) outlines that further ultraviolet and infrared observations are needed to resolve the questions concerning the system.

Twenty-five years later, Takeuti (2011) performed some analytical calculations that explored the outer-edge disk temperature variation along the disk plane, as heated by F0 and B5V stars. The Hipparcos distance of 625 pc was used to generate linear separations in the system. It is noted that since the "noon" temperature is the average temperature of the F0-facing side of the disk—similar to the average "midnight" temperature over the half of the disk facing away from the F0 star—the maximum temperature at "noon" will be slightly greater than the average value, T_{noon} (see Figures 1 and 2, as well as Table 2 in Takeuti 2011). Exploratory calculations consisting of physically descriptive heat capacities provided variable temperatures around the disk. However, the implications (composition, particle size, and so on) of the heat capacities chosen were not considered. A maximum temperature of 1200 K provided an upper limit for the calculations. Temperatures at the "midnight" position were found to be 250, 500, and 750 K. Scale heights were also calculated to provide an additional physical correlation with prescribed models. Accretional heating was ignored during this calculation. The work of Takeuti (2011) provides helpful constraints that can be used in numerical model calculations.

2.3.2. Proposed numerical analysis

The processing power and speed of current computers allow numerical simulations to effectively demonstrate physical configurations of astronomical systems quickly. For ε Aur, using a three-dimensional (3D), photon-tracking Monte Carlo code will permit an inspection of disk temperatures according to radiation from both stellar components, as well as accretional heating. However, the unknown (or rather, the known but highly uncertain) distance creates significant problems in analyzing the radiation effects on the disk. Therefore, a distance-—independent of any observations other than temperature—can be determined, based on the reproduction of the known temperatures, T_{noon} and T_{midnight}, on the disk.

Figure 3 displays the process by which a distance can be determined. First, a distance (d^{Model}) is selected. Then, d^{Model} is used to convert all of the well-determined angular separations into linear measurements. These parameters are then input into the Monte Carlo code. Next, the Monte Carlo code outputs a dust temperature file (described as "Disk Temperatures" in the figure). The points along the outer edge of the disk facing the F star, will be averaged—$\langle T_{\text{noon}}^{\text{Model}} \rangle$—

and compared with $\langle T_{\text{noon}}^{\text{Observed}} \rangle$. If the modeled temperatures do not equal the observed, another distance is chosen and the process is continued. However, if the temperatures are equivalent, then the system can be defined by the chosen distance and additional parameters are calculated.

There will be an inherent range of distances that are capable of matching the averaged "noon" temperature, due to the observed temperature having an associated error of ± 50 K. However, the distance ranges should be sufficiently small to provide conclusive results. Once the distance has been established (with a certain amount of uncertainty), further systems parameters can be finalized: the mass function, the mass ratio, the two stellar masses, and the stellar radii. Knowing these, the evolutionary state of the system can be clarified.

Another feature that can be explored is the disk's cooling (and heating) rate. However, the numerical modeling only provides a temperature snapshot of the "stable" system. No rotation of the disk is accounted for, and hence, the dust distributed in the disk has no prior incident heat or radiation. Therefore, the output temperatures only account for the snapshot of heating the dust receives at the specific moment being examined; a temperature distribution will still be present along the outer ridge of the disk (for example, $T_{\text{noon}} > T_{\text{midnight}}$), due to shielding effects of the flared disk and the increased distance from the F star radiation. A temperature profile of the disk can be constructed (see Figure 4 for an example) and examined.

Comparisons of the snapshot temperature profile can be compared against a profile of a rotating disk. If a disk rotation is assumed, the dust particles directly in line with the companion F star, at "noon," will heat up to some temperature, T_{noon}. As the disk's dust rotates, the amount of radiation from the F star decreases; this allows the dust to begin its cooling process. The dust begins to heat up again when it again receives the F star radiation (see Takeuti 2011). The rate at which the heating and cooling occurs is highly dependent on the composition of the dust. Once the maximum and minimum temperatures are acquired in the numerical process outlined above, temperature-time profiles can be created following Takeuti (2011). Various disk compositions will result in various temperature-time profiles. The shape and slope of profile can be compared with the snapshot temperature profiles to assess the compatibility of the two.

There are a few other input parameters that will need to be fully explored. For instance, the accretion rate. Since it is an unknown, numerous iterations with various values of $\dot{M}$ will need to be compared at each chosen distance. Limitations have been placed on $\dot{M}$ previously, but since this is the first complete 3D numerical analysis of the whole system, a full range of accretional rates will be explored. Another required input is the density, composition, and particle size distribution of the disk. These aspects have a large impact on how the disk material interacts with the various heating sources and how it cools. Each will be explored with the technique described above. A complete set of solutions are forthcoming.

Currently, two 3D Monte Carlo codes are available that permit the inclusion of external radiation sources: Dullemond (2012) describes RADMC-3D, which uses a combination of FORTRAN and IDL packages; HYPERION is outlined in Robitaille (2011), using FORTRAN and PYTHON to complete its analysis. Both have the ability to model non-symmetric systems, which illustrates the power of 3D modeling.

2.3.3. A simple example of a 3D numerical calculation

To demonstrate the primary results from this 3D method, a hypothetical example is described here. Following the prescribed outline in Figure 3, an arbitrary distance of 830 pc was chosen. This places a user-defined F0 star (7750 K, $150\,R_{\odot}$, $3\,M_{\odot}$) about 30 AU from a disk-enveloped B5V star (15000 K, $4\,R_{\odot}$, $6\,M_{\odot}$) in RADMC-3D. A silicate disk was modeled with inner and outer radii of 1 and 4 AU. Only 10000 photon packets were launched during the radiative transfer calculation, creating a very statistically poor set of solutions; however, this is sufficient for this conjectured calculation.

The average disk-plane temperature at $R_{\text{out}} = 4$ AU of the F0-facing disk was about 1500 K. This temperature is higher than the values predicted by Takeuti (2011) and $\langle T_{\text{noon}}^{\text{Observed}} \rangle$, but still relatively reasonable. The area of the disk at the "noon" position maxed at about 2500 K, which is significantly higher than the Takeuti (2011) estimation of about 1600 K. An average "midnight" temperature of about 900 K was found, which is also larger than the $\langle T_{\text{midnight}}^{\text{Observed}} \rangle$. A complete analysis, as described previously, is not presently provided. A graphical representation is shown in Figure 4.

It is noted that this brief example uses only a silicate disk and provides no accretional heating. A full analysis will examine the disk composition and will include an accretional rate. Still, the disregard for accretional heating may be a plausible assumption based on the B5V temperature: if the outward radiation pressure from the B5V star is large enough, it would severely limit the mass flow from the disk to the B5V star.

A final note is made here concerning the $\langle T_{\text{midnight}}^{\text{Observed}} \rangle$ and the coldest temperature of the RADMC-3D model. A basal temperature of about 250 K was found in sections 2.1 and 2.2. The work by Takeuti (2011) place this basal temperature near the "dusk" position on the disk (refer to Figure 1). Therefore, one can expect the observed T_{midnight} to be larger than at "dusk." However, in this hypothetical calculation, an average basal temperature was found at about 500 K. Adjustments to the distance, separation, composition, transmissivity, and/or other input parameters of the system can be made to find reasonable and comparable "dusk," "noon," and "midnight" temperatures.

Though just a hypothetical numerical calculation, this example shows that the temperature results will be able to provide distance and disk composition predictions. It outlines the usefulness of incorporating both stars in a numerical simulation and the need to explore the effects of accretional heating.

3. Conclusion

We have demonstrated the need for future analytical and numerical models of ε Aur to include the radiation effects of the companion star. Additionally, we have proposed a way to determine the distance to the system by using the observed temperatures. A brief review of previous disk temperature modeling was provided to give context to the proposed numerical solutions. Further clarification regarding the evolutionary state of the ε Aur system may result from the described analysis.

4. Acknowledgements

We appreciate the expert advice provided by Brian Kloppenborg while constructing this article.This work was supported in part by the bequest of William Herschel Womble in support of astronomy at the University of Denver, for which we are grateful.

References

Armitage, P. J. 2010, *Astrophysics of Planet Formation*, ed. P. J. Armitage, Cambridge Univ. Press, Cambridge.

Carroll, S. M., Guinan, E. F., McCook, G. P., and Donahue, R. A. 1991, *Astrophys. J.*, **367**, 278.

Dullemond, C. P. 2012, RADMC-3D: A new multi-purpose radiative transfer tool (http://www.ita.uni-heidelberg.de/ dullemond/software/radmc-3d/).

Guinan, E. F., and Dewarf, L. E. 2002, in *Exotic Stars as Challenges to Evolution*, ed. C. A. Tout and W. van Hamme, ASP Conf. Ser., 279, Astron. Soc. Pacific, San Francisco, 121.

Hartmann, L., Calvet, N., Gullbring, E., and D'Alessio, P. 1998, *Astrophys. J.*, **495**, 385.

Hinkle, K. H., and Simon, T. 1987, *Astrophys. J.*, **315**, 296.

Hoard, D. W., Howell, S. B., and Stencel, R. E. 2010, *Astrophys. J.*, **714**, 549.

Hoard, D. W., Ladjal, D., Stencel, R. E., and Howell, S. B. 2012, *Astrophys. J., Lett. Ed.*, **748**, L28.

Kloppenborg, B. K., Hemenway, P., Jensen, E., Osborn, W., and Stencel, R. 2011, *Bull. Amer. Astron. Soc.*, **43**, 230.05.

Kloppenborg, B., *et al.* 2010, *Nature*, **464**, 870.

Lambert, D. L., and Sawyer, S. R. 1986, *Publ. Astron. Soc. Pacific*, **98**, 389.

Lin, D. N. C., and Papaloizou, J. 1985, in *Protostars and Planets II*, ed. D. C. Black and M. S. Mattews, Univ. Arizona Press, Tucson, 981.

Lissauer, J. J., Wolk, S. J., Grith, C. A., and Backman, D. E. 1996, *Astrophys. J.*, **465**, 371.

Muthumariappan, C., and Parthasarathy, M. 2012, *Mon. Not. Roy. Astron. Soc.*, **423**, 2075.

Pequette, N., Stencel, R., and Whitney, B. 2011a, *Bull. Amer. Astron. Soc.*, **43**, 225.05.

Pequette, N., Stencel, R., and Whitney, B. 2011b, private communication.
Perryman, M. A. C., *et al.* 1997, *Astron. Astrophys.*, **323**, L49.
Pollack, J. B., McKay, C. P., and Christoerson, B. M. 1985, *Icarus*, **64**, 471.
Robitaille, T. P. 2011, *Astron. Astrophys.*, **536**, A79.
Saito, M., Kawabata, S., Saijo, K., and Sato, H. 1987, *Publ. Astron. Soc. Japan*, **39**, 135.
Shakura, N. I., and Sunyaev, R. A. 1973, *Astron. Astrophys.*, **24**, 337.
Sheffer, Y., and Lambert, D. L. 1999, *Publ. Astron. Soc. Pacific*, **111**, 829.
Stefanik, R. P., Torres, G., Lovegrove, J., Pera, V. E., Latham, D. W., Zajac, J., and Mazeh, T. 2010, *Astron. J.*, **139**, 1254.
Stencel, R. E., Creech-Eakman, M., Hart, A., Hopkins, J. L., Kloppenborg, B. K., and Mais, D. E. 2008, *Astrophys. J., Lett. Ed.*, **689**, L137.
Stencel, R. E., *et al.* 2011, *Astron. J.*, **142**, 174.
Takeuti, M. 1986a, *Astrophys. Space Sci.*, **120**, 1.
Takeuti, M. 1986b, *Astrophys. Space Sci.*, **121**, 127.
Takeuti, M. 2011, *Publ. Astron. Soc. Japan*, **63**, 325.

Table 1. Adopted ε Aur system parameters using d = 625 pc.

Parameter	*Value*	*Comments**
Primary Star		
Temperature, T_F	7750 K	Based on F0 type and SED
Radius, R_F	150 $R_\odot$	interferometric diameter (1)
Mass, M_F	3 $M_\odot$	disk radial velocity (2)
Secondary Star		
Temperature, T_B	15000 K	Determined as B5V, from far-UV and He 10830 (3)
Radius, R_B	4 $R_\odot$	Based on B5V
Mass, M_B	6 $M_\odot$	Based on B5V
Disk		
Inner Radius, R_{in}	1 AU	Assumed
Outer Radius, R_{out}	3.8 AU	(4)
Observed Inclination	89°	(4) and (5)
Disk Temperature	550–1150 K	Midnight to noon, relative to F star phase (6)
Observed Thickness/R_{out}	0.08	(4)
Total number density at R_{out}	1.6×10^{12} cm^{-3}	obtained from CO lines (7)

**References: (1) Stencel et al. (2008); (2) Lambert and Sawyer (1986); (3) Stencel et al. (2011); (4) Kloppenborg et al. (2010); (5) Hoard et al. (2010); (6) Hoard et al. (2012); (7) Hinkle and Simon (1987).*

Table 2. Analytic disk equations, adopted from Armitage (2010).

Variable	*Equation*	*Units*	*Equ. No.*
viscosity	$\nu = \alpha c_s h$	$cm^2\ s^{-1}$	1
sound speed	$c_s^2 = \frac{k_B T_c}{\mu m_p}$	$cm\ s^{-1}$	2
angular velocity	$\Omega^2 = G M_{\rm star} / r^3_{\rm disk}$	s^{-1}	3
density	$\rho = \frac{1}{\sqrt{2\pi}} \frac{\Sigma}{h}$	$g\ cm^{-3}$	4
scale height	$h = \frac{c_s}{\Omega}$	cm	5
mid-plane temperature	$T_c^4 = \frac{3}{4} \tau T^4_{\rm disk}$	K	6
optical depth	$\tau = \frac{1}{2} \Sigma \kappa$		7
opacity	$\kappa = \kappa_0 T_c$	$cm^2\ g^{-1}$	8
mass flow	$\nu\Sigma = \frac{\dot{M}}{3\pi}$	$g\ s^{-1}$	9
effective disk temperature	$T^4_{\rm disk} = \frac{9}{8} \frac{\nu}{\sigma} \Sigma \Omega^2 \left(1 - \sqrt{\frac{R_{\rm star}}{r_{\rm disk}}}\right)$	K	10
surface density	$\Sigma^4 = \frac{64\sigma}{27\kappa_0} \Omega \left(\frac{\mu m_p}{\alpha k_B}\right)^3 \left(\frac{\dot{M}}{3\pi}\right)^2 \left(1 - \sqrt{\frac{R_{\rm star}}{r_{\rm disk}}}\right)$	$g\ cm^{-2}$	11

Table 3. Analytical solutions using silicate dust.

$\kappa = \kappa_0 T_c$, $\kappa_0 = 5 \times 10^{-3}\ cm^2\ g^{-1}\ K^{-1}$, $\alpha = 0.01$, $\mu = 1.5$						
	$M_B = 6\ M_\odot$			$M_B = 8\ M_\odot$		
$\dot{M}$ [$M_\odot$/yr]	1.5×10^{-5}	10^{-6}	10^{-7}	1.5×10^{-5}	10^{-6}	10^{-7}
Σ [$10^2\ g\ cm^{-2}$]	67	17	5.5	70	18	57
$M_{\rm disk}$ [$10^{-3}\ M_\odot$]	34	8.9	3.5	41	9.2	2.9
$T_{\rm disk}$ [K]	520	270	150	560	290	160
T_c [K]	3600	920	290	4000	1000	330
h [$10^{12}\ cm$]	6.7	3.4	1.9	6.2	3.1	1.8
h [AU]	0.45	0.23	0.13	0.41	0.21	0.12
$3\ h/R_{\rm out}$	0.36	0.18	0.10	0.32	0.17	0.093
$2\ h/R_{\rm out}$	0.24	0.12	0.07	0.22	0.11	0.062
$h/R_{\rm out}$	0.12	0.06	0.03	0.11	0.055	0.033
n [$10^{13}\ cm^{-3}$]	16	8.1	4.5	18	9.2	5.2

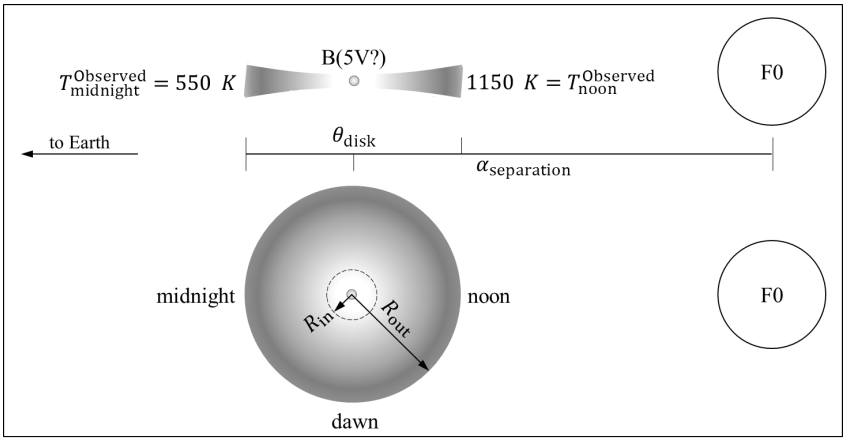

Figure 1. Side and top-view sketches (not-to-scale) of the ε Aur system. Parameters coincide with values given in Table 1.

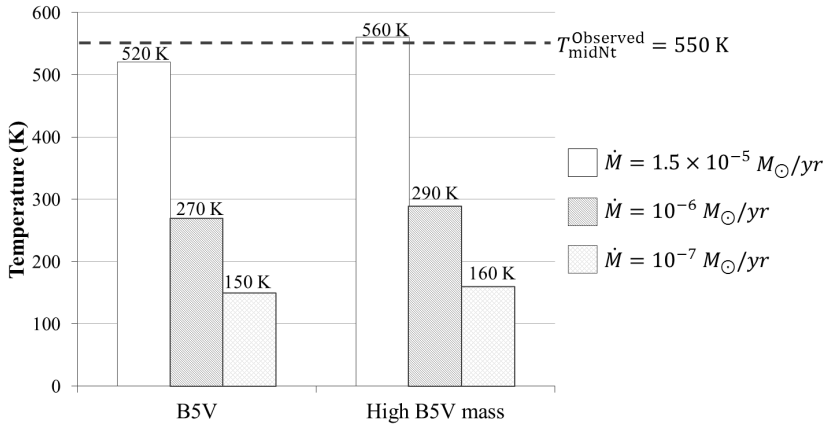

Figure 2. A chart displaying disk temperatures, T_{disk}, at the outer radius of the ε Aur disk. These are results of an analytical study of the system. Two different central star masses were used in the calculations: M_B = 6 $M_{\odot}$ and M_B = 8 $M_{\odot}$. The dotted line represents the known observed temperature, $\langle T^{\text{Observed}}_{\text{midnight}} \rangle$. Note that the only model to reach and exceed this value predicts a very high accreting rate of 1.5 × 10^{-5} $M_{\odot}$/yr, which is not physical for the ε Aur system. Though the other accretion rates do not provide a matching temperature, they do compare to the minimum disk temperatures stated by Muthumariappan and Parthasarathy (2012) and Takeuti (2011).

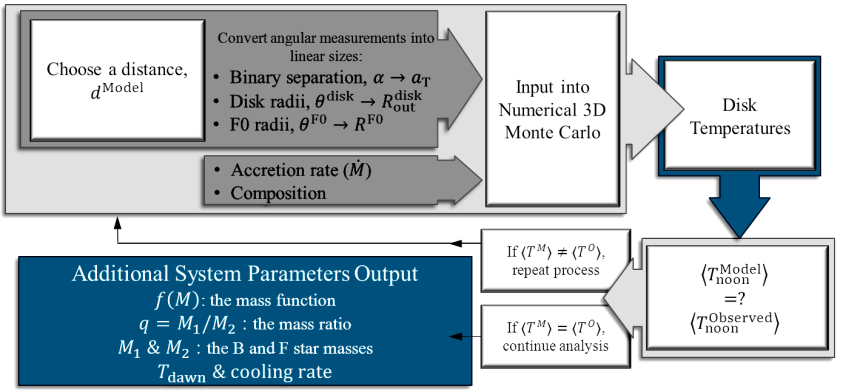

Figure 3. A schematic showing the process of solving for the distance to ε Aur. Note that there are a few other input parameters besides just the binary separation. These include dust composition, dust molecular weight, and dust density distributions. See text for further information regarding analytical studies and numerical modeling, specifically with RADMC-3D.

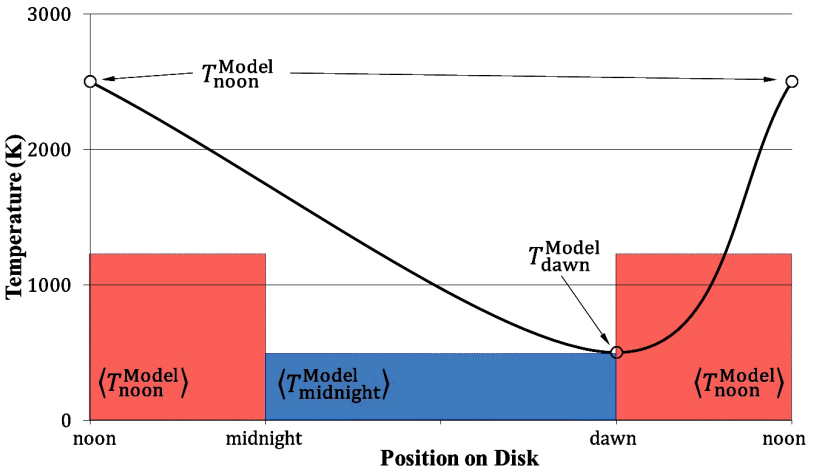

Figure 4. A plot describing the temperature distribution from a hypothetical numerical modeling reconstruction of ε Aur, from RADMC-3D. The average "noon" and "midnight" temperatures were calculated by averaging the temperatures located at the outer edge of the disk, in the associated areas of the disk. The minimum and maximum temperatures associated with the numerical modeling are shown, as well as a hypothetical temperature gradient represented by the solid black line. Again, the line is not a fit to actual data: it is simply a graphical representation of a possible temperature distribution on the disk, outlined by the minimum and maximum temperatures. No accretional heating or disk rotation was used.

A Demonstration of Accurate Wide-field V-band Photometry Using a Consumer-grade DSLR Camera

Brian K. Kloppenborg
Department of Physics and Astronomy, University of Denver, 2112 East Wesley Avenue, Denver, CO 80208; bkloppen@du.edu

Roger Pieri
37 C rue Charles Dumont, 21000, Dijon, France; roger.pieri@wanadoo.fr

Heinz-Bernd Eggenstein
Vogelbeerweg 34, 31515 Wunstorf, Germany; heinz-bernd.eggenstein@vspb.de

Grigoris Maravelias
Physics Department, University of Crete, GR-71003 Heraklion, Crete, Greece; gmaravel@physics.uoc.gr

Tom Pearson
1525 Beachview Drive, Virginia Beach, VA 23464; tandjpearson@verizon.net

Received May 8, 2012; revised July 3, 2012; accepted July 3, 2012

Abstract The authors examined the suitability of using a Digital Single Lens Reflex (DSLR) camera for stellar photometry and, in particular, investigated wide field exposures made with minimal equipment for analysis of bright variable stars. A magnitude-limited sample of stars was evaluated exhibiting a wide range of (*B–V*) colors taken from four fields between Cygnus and Draco. Experiments comparing green channel DSLR photometry with VT photometry of the Tycho 2 catalogue showed very good agreement. Encouraged by the results of these comparisons, a method for performing color-based transformations to the more widely used Johnson V filter band was developed and tested. This method is similar to that recommended for Tycho 2 VT data. The experimental evaluation of the proposed method led to recommendations concerning the feasibility of high precision DSLR photometry for certain types of variable star projects. Most importantly, we have demonstrated that DSLR cameras can be used as accurate, wide field photometers with only a minimal investment of funds and time.

1. Introduction

Digital Single Lens Reflex (DSLR) cameras have been successfully used by astrophotographers since the advent of these imaging devices. Shortly after their introduction, several studies examined the suitability of DSLRs for photometry. Because they are not designed for photometry, these cameras present a unique set of challenges. For instance, DSLR sensors are manufactured with a Bayer array of red, green, and blue filters placed over individual sensor pixels. Unfortunately,

the center wavelengths of these filters do not match the wavelengths of standard Johnson filters. Furthermore, features that improve image quality like built-in software noise reduction also distort the true photometric signature of stars of interest. Fortunately, camera manufacturers have given consumers access to the RAW pixel data, which is often free of any on-camera processing or noise reduction.

Examples of photometry testing of DSLRs include work by Hoot (2007). He tested a Canon EOS 350D as a stellar photometer by imaging a series of Landolt field stars. Using the Landolt V, B, and R filters, he computed offsets and color and extinction transformations. Hoot found significant (~ 0.13 mag.) uncertainties in the color correction coefficients that were far in excess of the instrumental RMS (~ 0.003 mag.) values. From this he concluded there must be some outlying systematic effect causing the low quality of fit. Furthermore he found that "no single exposure set taken with this DSLR family of camera can accurately span more than 2.5 magnitudes." Outside of this narrow window, the errors increase rapidly, therefore decreasing the utility of using DSLR cameras for fields with wide magnitude ranges.

Subsequent to publication of Hoot's article, DSLR cameras were put to the test on various astronomical targets. Littlefield (2010) and Guyon and Martinache (2011) have shown DSLR cameras are capable of 10 milli-magnitude or better photometry that is suitable for tracking transiting exoplanets. Fiacconi and Tinelli (2009) have shown DSLR cameras can track pulsating variable stars, like XX Cyg. All three of these studies made use of differential photometry that does not require a precise transformation to a standard photometric system. A recent study by Pata *et al.* (2010) shows that such transformations are indeed possible, provided that the spectral properties of the observed stars are known.

As part of the American Association of Variable Star Observers' (AAVSO) Citizen Sky Project, several participants elected to use DSLR cameras to track the 2009–2011 eclipse of ε Aurigae (Stencel 2008; Guinan and Dewarf 2002). The success of this method (Kloppenborg and Pearson 2011; Kloppenborg *et al.* 2011) inspired our work which confirms that DSLR cameras can indeed be used as accurate, photometrically calibrated, wide-field photometers over a wide range of colors and nearly five magnitudes of brightness with a very modest investment of time and equipment. What they lack in flexibility, DSLR cameras make up for in price and portability.

2. Procedure

2.1. Instrumentation and experimental setup

For our work we used a standard Canon 450D, without modifications to the filters, and two Nikkor lenses adapted to the Canon body. The 450D has a 22.2 × 14.8 mm, 12-megapixel CMOS sensor and is equipped with a 14-bit analog-to-digital converter. We verified the camera's linear response over most

of its dynamic range by comparing sensor response to a series of illuminated targets. Target brightness levels were measured using a dedicated photometer. At ISO 100, the 450D appears to be linear (within ± 0.5 %) up to 14,300 ADU, where the camera sharply departs from the linear trend (full well saturation). The ADC clipping level occurred at ~15,800 ADU, rather than the expected 16,384 for a 14-bit camera. The calibration factor at ISO 100 has been measured to 2.27 e-/ADU. Therefore the 1 electron to 1 ADU calibration setting resides somewhere between ISO 200 and ISO 400. Above this setting, the dynamic range of the camera is reduced. We used standard Nikkor 200-mm and 85-mm lenses whose fields of view are 6.36 × 4.24 degrees and 15 × 10 degrees, respectively.

We measured the spectral response of our camera's Red (R), Green (G), and Blue (B) Bayer array filters. Figure 1a is a plot of the Canon 450D G filter compared to the Johnson's V filter definition (Maíz Apellániz 2006). We found the G channel is shifted blueward by 12 nm relative to Johnson's V-filter. A transformation equation is, therefore, required to adapt DSLR measurements to this photometric standard. Likewise, we found a 2-nm blue shift between Tycho VT and DSLR G (see Figure 1b), but this shift is nearly negligible. This result is quite interesting as it shows there should be little to no correction between the 450D G channel and Tycho VT. These properties will be verified and discussed in greater detail below.

Of note are some useful features of this camera to a photometrist. The camera has a 10× magnified live-view display that is very useful when defocusing. Unfortunately, we found it is often not possible to frame the field of interest by using the live view at 1× zoom. Instead we used the optical viewfinder with a right angle adapter added. Additionally, we used a red dot finder at times. To best simulate the facilities available to other observers, we mounted our camera on a small, undriven, equatorial mount to accelerate framing of the chosen fields. A simple tripod can also be used.

2.2. Choice of star fields

Our star fields were selected to optimize testing the limits of DSLR photometry and the related post-processing steps. In choosing our test field we intentionally excluded regions in the plane of the Milky Way to avoid blending target stars with potentially unseen, but detectable, background stars. Our four fields are found between the constellations Cygnus and Draco bounded by R.A. $19^h\ 48^m$ to $18^h\ 05^m$ and Dec. +48° 07' to +54° 28'. These fields total 15.85 × 6.36 degrees or 101 square degrees and have ~ 283 stars between V = 3.7 and 8.75 with (*BT–VT*) values of –0.2 to 2 (see Figures 2a and 2b). Of these, Vizier and VOPlot report 76 stars are at risk of blending within the photometric aperture and 27 stars are suspected variables (see Table 1). Most stars in the field are AFG and K spectral types, with a few B- and M-type stars (see Figure 2c). Because of the limited number of M-stars, we were not able to check the known transformation issues involving these objects (Perryman *et al.* 1997). We also

obtained images from a second, larger region using the 85-mm lens. This area extended between R.A. $19^h\,48^m$ to $17^h\,10^m$ and Dec. +44° to +59° in three fields. These data have significant field distortions near the edge of the FOV that must be dealt with delicately. We will discuss these data and our method of reduction in a future publication. For the remainder of our discussion we shall refer to our observed fields as CD3S, CD4S, CD5S, and CD6S as summarized in Table 2.

2.3. Data acquisition

Our observations began on July 14, 2011, and ended on September 28, 2011. All imaging was done from the same location: +47° 19' N, +05° 01' E at 250 *m* altitude. All data were taken in groups of 10 to 15 images (hereafter a "series") with the Canon 450D and Nikkor 200-mm lens at *f*/4, ISO 100 with 12.3-second exposure times, except a few of the CD3S field which uses only 8-second exposures. The number of images per series were chosen to reduce the noise from atmospheric scintillation to a few milli-magnitudes. All images were defocused slightly (see Figure 3) so that the stellar image covers roughly a 10- to 15-pixel diameter (plus trailing during the exposure). Most of the images were acquired within 15 to 30 degrees of the zenith where differential airmass is negligible. Four series for CD5S and CD6S were taken at 40 to 45 degrees of zenith at about 1.5 airmasses. From these images, we found that the brightest stars in our sample ($V \sim 3.7$) have a SNR $\gg$ 1,000 and stars at 7th magnitude have SNR ~200.

Because we used a fixed focal length lens, it was possible to use a flat image recreated every few months. The flat is obtained by imaging a diffusely illuminated, non-glossy, fine-grained white surface (for example, the back of high quality photo paper). A 1% cross-surface uniformity of our flat fielding source has been verified using a dedicated photometer.

3. Data reduction

To reduce our data we employed two main stages. The first stage extracts the instrumental magnitudes and statistical information from the raw camera data, correcting for flat fielding, while the second stage calibrates the data to an absolute photometric system.

3.1. Stage 1

An automated reduction pipeline has been written in APL language running under a Dylog APL environment. This pipeline does the following:

1. Extracts the raw Bayer data in RGGB format from the camera's CR2 files using dcraw (from Dave Coffin, http://www.cybercom.net/~dcoffin/dcraw/).

2. The image is split into three planes formed by the R, (G+G)/2, and B pixels from the Bayer cell. This yields a 2145 × 1428 RGB image.

3. The Canon's systematic offset of 1024 ADU (possibly included in dark) is first subtracted from the raw. The resultant image is then flat fielded. Even though the image looks very uniform, we have noticed a small non-uniformity in the the outer perimeter of our images, and therefore we exclude a 50-pixel-wide border from photometric analysis. We do not apply a dark image as we have found these short exposures at ISO 100 have minimal dark current noise. Any residual cross-image gradients will easily be detected in stage 2, manifesting in the extinction coefficient.

4. Next we create a temporary luminance (R + G + B) image to detect stars. The image is sampled at several points to determine the background and is fit using a polynomial. This function is then subtracted from the image, removing any remaining systematic background. The resulting luminance is again measured and pixels residing above 3-sigma (noise) above the dark level are selected as candidate objects. The area around the brightest pixels are analyzed to determine if they are part of a star. If confirmed, the footprint of the star is measured and its geometric centroid calculated to ensure proper centering during aperture photometry.

5. Because of diurnal motion, our star images are trailed. Therefore we perform aperture photometry using rectangles rather than annuli. Our inner aperture is 21×13 pixels and the outer is 51×51 pixels. The background level for each star, determined from the outer aperture, is subtracted from the foreground aperture and the RGB intensities of the star are extracted.

6. Next, stars are identified using the *Tycho 2* reference catalogue based upon image coordinates and a "tentative" instrumental magnitude relative to the ensemble of stars in the image is computed.

7. Lastly the star ID, RGB intensities (in electrons), R.A., Dec., and image position (X, Y) are written to a file along with aggregate statistics like series mean altitude, means, standard deviations, and signal-to-noise ratio (SNR).

For our analysis we selected only stars whose SNR over a series is greater than 40. Below this limit, a star's SNR is no longer above the 3-sigma criterion for the automated extraction pipeline.

3.1.1. Stellar blending

One downside of wide-field DSLR photometry is that relatively low angular resolution of the camera can blend two nearby stars together. Upon examining our instrumental output table from the steps above, we found a significant number of outliers from the calibration trend we expected. Some of these stars were undoubtedly variables, but in most cases they were affected by blending with faint background stars that fell within the rectangular aperture.

To solve this issue we wrote a small piece of software that uses data from

the *Tycho 2* catalog down to $VT = 13$. All stars that fall within the aperture are selected and their approximate flux is computed. If the background star contribution exceeds 0.012 magnitude, we flag it in our data tables. If the Point Spread Function (PSF) response of the camera were better characterized, we speculate it would be possible to remove the background star contribution, but this was beyond the scope of this paper. Any stars that were affected by blending were not used in our analysis.

3.1.2. Variable stars

In a similar manner to blended stars, we have also flagged variable stars. We have collected aggregate statistics on variability, spectral types, and luminosity from the *Tycho 2* (Høg *et al.* 2000a, 2000b), *Hipparcos Input* (Turon *et al.* 1993), *Hipparcos Main* (Perryman *et al.* 1997), and the *Tycho 2 Spectral Types* (Wright 2003) catalogues. Of our targets, twenty-four were flagged as variable stars from the input catalogs; however, six of these stars showed no sign of variation within our measured accuracy.

3.1.3. Final star selection and output quality

These observations have provided 201 stars from the four fields from VT magnitude 3.8 to 8.8. Of these, 67 have been deselected (18 variables, 52 blended), yielding a total of 134 stars for further processing. Aggregate statistics of these stars are shown in Figures 2a, 2b, and 2c.

3.2. Stage 2

The second stage of data reduction mirrors the techniques employed in the Citizen Sky Intermediate Reduction Spreadsheet. This method transforms the DSLR instrumental G magnitude (denoted using ν hereafter) into the standard photometric system (denoted using capital letters V and B) using the standard transformation coefficient method (compare to Henden and Kaitchuck (1982) and references therein). This method essentially fits the observed instrumental magnitudes to a 3D surface to determine the transformation coefficient (ε), extinction coefficient (k'), and zero-point offset (ζ_ν). The remainder of this section reviews this method by outlining the mathematics required to find these parameters.

3.2.1. Determining ε and ζ_ν

For differential photometry in which airmass may be neglected, the transformation coefficient (ε) and zero point offset (ζ_ν) may be determined using the following equation (Henden and Kaitchuck 1982):

$$(V-\nu)_i = \varepsilon\,(B-V)_i + \zeta_\nu, \qquad (1)$$

where B and V are the catalog B-band and V-band magnitudes, ν is the observed instrumental magnitude, ε is the transformation coefficient, and ζ_ν is the zero-

point offset of the camera. The subscript *i* denotes the i^{th} calibration star in the image. Because of the way in which CMOS sensors are manufactured, we assume, to first order, that the response of each pixel in the camera is nearly identical. Therefore, if proper background and flat subtraction methods have been applied ε and ζ_ν are constant across the field. We may then either solve this equation graphically or use a linear least-squares fit (see Paxson 2010) in order to determine ε and ζ_ν.

After the coefficients are determined, the above equation may be rearranged and the V-band magnitude for the j^{th} target star computed via:

$$V_j = \nu_j + \varepsilon\,(B-V)_j + \zeta_\nu, \tag{2}$$

3.2.2. Airmass corrections

The above method of calibrating is good for images of small angular extent (that is, those with < 3° FOVs) at zenith angles less than 34 degrees. Beyond this point, the differential airmass across the field can contribute significantly to the error. First order airmass corrections may be applied to DSLR images using the following equation (Henden and Kaitchuck 1982):

$$(V-\nu)_i = -k'_\nu X_i + \varepsilon\,(B-V)_i + \zeta_\nu \tag{3}$$

where the newly introduced variable, k'_ν, is the extinction coefficient and X_i is the airmass. This equation has the same functional form as a geometric plane in three dimensions: $z = Ax + By + C$. If we assume that the instrumental magnitude, ν_i, depends only on the terms on the right side of the above equation, then we may solve the above expression for the coefficients ($-k'_\nu$, ε, and ζ_ν) using a minimum of three calibration stars in the field of view. However, if one calibration star is incorrectly identified or the airmass is incorrectly computed, the coefficients will be skewed and the resulting magnitudes for target stars will be invalid. Therefore we alleviate this problem by using multiple calibration stars to compute the coefficients.

A least-squares fit of *n* calibration stars to the plane defined by the equation $z = Ax + By + C$ is found by solving for the coefficient matrix, **X**, in following expressions, using the inverse of **A**:

$$\mathbf{AX} = \mathbf{B} \tag{4}$$

$$\begin{bmatrix} \Sigma_{i=1}^n x_i^2 & \Sigma_{i=1}^n x_i y_i & \Sigma_{i=1}^n x_i \\ \Sigma_{i=1}^n x_i y_i & \Sigma_{i=1}^n y_i^2 & \Sigma_{i=1}^n y_i \\ \Sigma_{i=1}^n x_i & \Sigma_{i=1}^n y_i & \Sigma_{i=1}^n 1 \end{bmatrix} \begin{bmatrix} -k'_\upsilon \\ \varepsilon \\ \zeta_\upsilon \end{bmatrix} = \begin{bmatrix} \Sigma_{i=1}^n x_i z_i \\ \Sigma_{i=1}^n y_i z_i \\ \Sigma_{i=1}^n z_i \end{bmatrix} \tag{5}$$

It is not necessary to write a computer code to solve these equations, as many spreadsheet programs and programming languages already have built-

in routines for such a purpose. For example, EXCEL/OPENOFFICE CALC have the "linest" function which we have employed in the Intermediate Reduction Spreadsheet on the Citizen Sky website. If you wish to write your own reduction code, Python's "scipy.optimize.leastsq" function can be used for this task.

After the coefficients are determined, the magnitude of the j^{th} star in the field of view may be determined by rearranging Equation 6:

$$V_j = \nu_j + -k'_\nu X_j + \varepsilon\,(B-V)_j + \zeta_\nu \quad (6)$$

Note that these equations require that the color of the target stars must be known *a priori*! This places a DSLR camera at a significant disadvantage because even though the Blue and Red channels are measured, they do not correspond to any standard photometric filters. Furthermore, the spectral response of the Red and Blue pixels often are asymmetric with modest red and blue leaks compared to standard filters. This disadvantage can be mitigated by using a catalog that closely responds to DSLR G, thereby resulting in a near-zero value for ε and mitigating the color contribution to final V-band output.

3.3. Verification

In addition to the APL-based pipeline described above, one of us (H.B.E.) created an alternative reduction method that uses AIP4WIN (Berry and Burnell 2005) to stack images, SOURCEEXTRACTOR (Bertin and Arnouts 1996) to automatically find and perform aperture photometry on stars, and SCAMP (Bertin 2006) to perform astrometric star association. The output is then processed in the same manner as step 2 described above using a script we have written in R (Matloff 2011). This second pipeline produced results identical (within uncertainties) to the method described above. Please contact H.B.E. if you are interested in virtual machine image of the freely redistributable components of this pipeline.

4. Results

Our data set consists of nearly 500 images taken in groups of ten, 12-second exposures. These 40 series represent nearly 80 minutes of combined exposure time. From the input catalog of approximately 300 stars brighter than V = 8.8, we detected about 200 stars in our fields that are 3-σ above background noise. From these, we selected 134 stars that were free from blending and not identified as variables (or suspected variables) in catalogues. Overall, stars with $3.5 < V < 7.5$ had a mean uncertainty < 0.01 magnitude or better. Stars in the range $7.5 < V < 8.0$ had an average uncertainty of ~ 0.02 magnitude. Beyond this magnitude, photometric uncertainties rapidly grew $\propto$ 1/SNR. We show typical results for constant and variable stars in Figure 4.

4.1. Choice of calibration catalogue

Following our discussion at the end of section 3.2.2 we have explored the

use of one homogeneous photometric catalog and one inhomogeneous source for stage 2 calibration. In the next few paragraphs we describe the benefits of using a standardized system and caution against using inhomogeneous catalogs for calibration.

4.1.1. Tycho

For our first calibration catalog we used the *Tycho 2 Catalogue* (Høg *et al.* 2000a, 2000b). As discussed above, the difference in transmission between VT and DSLR-G filters is minimal. In Figure 5a and Figure 5b we adjusted DSLR-G to VT using only a zero point offset, ζ_v. The residuals (that is, transformed – catalog) appear normally distributed about zero and show no systematic trends as a function of color, confirming the suspicion that the difference in transmission between the VT and RGB-G filters can be regarded as minimal for the Canon 450D.

4.1.2. ASCC

Unlike Tycho VT, the Johnson V measurements in the ASCC catalog (Kharchenko 2001) should exhibit a modest color transformation coefficient. For almost all of our target stars, ASCC contains VT magnitudes transformed to V_J. In Figure 6a we plot the instrumental magnitude v_{inst} as a function of the ASCC2.5 Johnson V. To demonstrate the color correlation, the difference between instrumental and catalog magnitude is plotted as a function of $(B–V)$ in Figure 4b. Note that unlike our analysis for the VT photometry, and unlike the analysis in Hoot (2007), we find a significant correlation between the residuals and color.

Next we applied the full color calibration to the data to yield Figures 5c and 5d. Aside from a small excursion between $0.4 < (B–V) < 0.5$ (which contains only stars with $V > 8$ with very poor SNR), we find the data are normally distributed. Likewise, residuals as a function of magnitude appear normally distributed within an envelope that is $\propto 1/\mathrm{SNR}$. Combined, these imply that the transformation equations for DSLR G to V_J are valid across our entire range of colors and magnitudes in our sample.

4.1.3. SIMBAD

In Figures 5e, 5f, and 6c we essentially repeat the ASCC experiment using a heterogeneous reference catalog assembled from SIMBAD queries. Both the magnitude and color residual diagrams show a loss of precision of ~ 0.005 mag., with a few stars shifting by as much as 0.02 mag. Although certainly within the statistical uncertainties quoted in the catalog, these deviations are often outside of the internal instrumental uncertainty, implying the deviations are due to errors in the catalog magnitudes. We caution the reader that using aggregate catalogs, like blind queries from SIMBAD, may result in degraded precision. Therefore we suggest that DSLR photometry be performed using a standard reference catalog like ASCC or, preferably, Tycho VT.

5. Conclusion and discussion

We have shown that consumer-grade DSLR cameras can be used as accurate (0.01 mag.) photometers across a wide range of magnitudes and colors. In the next few paragraphs we provide a few comments concerning DSLR photometry and discuss how the reader may alleviate these issues.

5.1. On the number of reference stars

As discussed above, one may calibrate data using the simple method (Equation 2) using only two reference stars and the airmass-corrected version (Equation 6) with only three stars. However, when using these lower limits as a guide, the reader must be aware that an incorrect identification, bad instrumental magnitude, or incorrectly referenced catalog value will significantly degrade (if not invalidate) the results. As a rule of thumb, we recommend six to nine reference stars that bracket the target object(s) in color, airmass, and magnitude so that the values of k', ε, and ζ_v may be interpolated rather than extrapolated.

In many cases, satisfying all of these requirements is not possible. The reader may be tempted to include fainter reference stars, but with that comes larger statistical uncertainty. In our work, we found stars with a SNR > 100 are often acceptable and strongly caution against using any star with a SNR < 100 as a calibrator.

5.2. Airmass corrections

Most of our images were taken fairly close to the zenith (with typical airmasses not exceeding 1.2), therefore the differential extinction across the image was negligible. Two series with the greatest airmass in field CD6S did show a significant correlation of residuals as a function of airmass (compare equation 6). Including airmass correction in the (planar) fit did improve the residuals significantly when compared to the (linear) color-corrected fit. In general, airmass corrections should be applied whenever the differential airmass across the entire FOV multiplied by the extinction coefficient exceed the desired level of accuracy.

5.3. Stellar blending

Of primary concern to a DSLR photometrist is the blending of foreground target/reference stars with fainter background stars. With the technique described above, stars can become blended in three different ways: (1) the formal resolution of the optical setup cannot resolve blended stars, even under ideal atmospheric conditions, (2) defocusing the image causes light from adjacent stars to overlap, or (3) diurnal motion causes an overlap of trails between two nearby stars. In all of these cases, if a comparison star is blended, it will skew the calibration and, potentially, invalidate the results. If the photometric target star(s) are blended, the measured photometry will certainly be invalid.

Before we consider these three cases in further detail, we wish to describe two methods by which blends might be identified. In a large ensemble of stars, blends will only have a limited effect on the resultant photometry. Blended stars can be detected in at least two ways. Given positions from an astrometric catalog and the formal resolution of the imaging setup, stars should be considered blended if the photometric extraction apertures overlap. Software that does this is available from author H.B.E. by request. If the reader wishes to use an empirical method for determining blends, blended stars may be identified by finding stars that skew the photometry error histogram. Typically a visual inspection of the plot that compares measured magnitudes to catalog data will have some obvious outliers. These are most frequently caused by blending, variability, or other sources of error (for example, small clouds).

The three sources of blending deserve further discussion. The method by which the photometrist chooses to decrease blending depends on the science objective they wish to achieve. In our work, a loss of 25% of our sample was inconsequential as we still obtained photometry on 150 stars with only ten 10-second exposures. Of the fifty-two stars that were lost due to blending, almost all of them were due to the limited resolution of the optics. We could have simply increased the angular resolution of our setup by zooming, but then we would require a larger number of exposures.

In the case where stars are blended due to defocusing or trailing, the method of resolving the blend becomes more difficult. In the case of defocus-induced blending, focusing the image is the obvious solution; however, defocusing ensures an accurate measure of the star's light. In the high photon regime, one should decrease the exposure length while proportionally increasing the number of exposures. When analyzing the data, the images should be aligned and stacked. Likewise, for bright stars that become blended due to trailing, the exposure length can be decreased while the number of exposures is proportionally increased.

This advice will likely not extend to the photon-limited, faint star regime. Indeed, the authors are unaware of any study that theoretically discusses the trade-offs between changing the intrinsic resolution, focus, and trail length while providing experimental verification of any published claims. Until such a work is completed, we suggest the reader carefully consider the science they wish to achieve and choose a setup best suited for the job. The procedure we describe herein is ideally suited for wide-field bright-star photometric monitoring, but clearly not for observing faint stars with little photometric variation.

6. Acknowledgements

The authors would like to thank the AAVSO's Citizen Sky project. B.K. acknowledges support from NSF grant DRL-0840188. B.K. thanks Dr. Doug Welch for discussions that piqued his interest in DSLR photometry.

The authors would also like to thank Arne Henden for answering questions concerning photometric calibration databases. We are grateful to the organizers of the Citizen Sky workshops I and II during which we first discussed these efforts. This research has made use of the SIMBAD database, operated at CDS, Strasbourg, France and several online collaborative tools like the AAVSO's IRC channel, Google Docs, and Pastebin.

References

Berry, R., and Burnell, J. 2005, *The Handbook of Astronomical Image Processing*, Willmann-Bell, Richmond, VA.

Bertin, E. 2006, in *Astronomical Data Analysis Software and Systems XV*, eds. C. Gabriel, C. Arviset, D. Ponz, and E. Solano, ASP Conf. Ser., 351, Astron. Soc. Pacific, San Francisco, 112.

Bertin, E., and Arnouts, S. 1996, *Astron. Astrophys., Suppl. Ser.*, **117**, 393.

Fiacconi, D., and Tinelli, L. 2009, *Open Eur. J. Var. Stars*, **114**, 1.

Guinan, E. F., and Dewarf, L. E. 2002, in *Exotic Stars as Challenges to Evolution*, eds. C. A. Tout and W. Van Hamme, ASP Conf. Ser. 279, Astron. Soc. Pacific, San Francisco, 121.

Guyon, O., and Martinache, F. 2011, in *Techniques and Instrumentation for Detection of Exoplanets V*, ed. S. Shaklan, Proc. SPIE, 8151, 815111C, American Inst. Physics, Melville, NY.

Henden, A. A., and Kaitchuck, R. H. 1982, *Astronomical Photometry*, Van Nostrand Reinhold Co., New York.

Høg, E., *et al.* 2000a, *Astron. Astrophys.*, **355**, L27.

Høg, E., *et al.* 2000b, *Astron. Astrophys.*, **363**, 385.

Hoot, J. E. 2007, in *The Society for Astronomical Sciences 26th Annual Symposium on Telescope Science*, Soc. Astron. Sciences, Rancho Cucamonga, CA., 67.

Kharchenko, N. V. 2001, *Kinematika Fiz. Nebesnykh Tel*, **17**, 409.

Kloppenborg, B., and Pearson, T. 2011, *Sky & Telescope*, **121**, No. 4 (April), 64.

Kloppenborg, B., Stencel, R. E., Price, A., Turner, R., and Henden, A. A. 2011, *Bull. Amer. Astron. Soc.*, **43**, 158.12.

Littlefield, C. 2010, *J. Amer. Assoc. Var. Star Obs.*, **38**, 212.

Maíz Apellániz, J. 2006, *Astron. J.*, **131**, 1184.

Matloff, N. 2011, *The Art of R Programming: A Tour of Statistical Software Design* (http://www.amazon.com/Art-Programming-Statistical-Software-Design/dp/1593273843).

Páta, P., Fliegel, K., Klíma, M., Blažek, M., Řeřábek, M. 2010, in *Applications of Digital Image Processing XXXIII*, ed. A. G.Tescher, Proc. SPIE, Amer. Inst. Physics, Melville, NY, 77982H.

Paxson, K. B. 2010, *J. Amer. Assoc. Var. Star Obs.*, **38**, 202.

Perryman, M. A. C., European Space Agency Space Science Department, and the Hipparcos Science Team 1997, T*he Hipparcos and Tycho Catalogues*,

ESA SP-1200 (VizieR On-line Data Catalog: I/239), ESA Publications Division, Noordwiijk, The Netherlands.

Stencel, R. E. 2008, *Bull. Amer. Astron. Soc.*, **40**, 207.

Turon, C., *et al.* 1993, *Bull. Inf. Cent. Donnees Astron. Strasbourg*, **43**, 5.

Wright, C. O., Egan, M. P., Kraemer, K. E., and Price, S. D. 2003, *Astron. J.* **125**, 359.

Table 1. The 27 variable stars detected in our survey.[1]

Tycho Identification	*VT (mag).*	*Series Mean (mag.)*	*Typical SD (mag.)*	*Series Min. (mag.)*	*Series Max. (mag.)*	*No. Sigmas*	*Tycho Classif.*
3528-2121-1	8.077	7.979	0.015	7.954	8.011	2	DA
3529-1447-1	7.648	7.633	0.010	7.600	7.660	3	U
3533-2577-1	5.219	5.195	0.003	5.182	5.209	5	1U
3534-302-1	7.450	7.290	0.010	7.284	7.300	1	1D-
3536-1939-1	7.359	7.379	0.006	7.356	7.420	7	M
3536-2022-1	8.371	8.400	0.023	8.335	8.436	3	C
3538-2150-1	8.436	8.415	0.015	8.351	8.483	5	
3539-137-1	7.759	7.783	0.008	7.757	7.810	3	CU
3539-1700-1	6.831	6.797	0.004	6.702	6.884	24	1U*0.51
3539-2623-1	8.313	8.389	0.015	8.345	8.461	5	3R
3548-2346-1	7.227	7.234	0.005	7.225	7.246	2	U*2.79
3550-579-1	8.339	8.310	0.029	8.276	8.367	2	U*1.25
3551-1744-1	7.459	7.136	0.005	7.103	7.158	7	P
3552-1543-1	8.438	8.464	0.014	8.427	8.513	3	
3552-394-1	8.000	8.078	0.011	7.999	8.223	13	P
3553-999-1	8.260	8.266	0.012	8.249	8.282	1	U
3554-100-1	7.753	7.743	0.007	7.699	7.780	6	1U
3554-1071-1	6.014	6.071	0.003	6.039	6.109	13	5U
3555-686-1	7.559	7.551	0.008	7.525	7.582	4	U
3564-1126-1	8.121	8.129	0.010	8.103	8.173	4	U
3564-3159-1	6.231	6.215	0.003	6.151	6.256	21	5U
3569-331-1	8.117	8.118	0.012	8.061	8.161	5	1U
3908-1123-1	7.652	7.626	0.009	7.620	7.631	1	U
3918-1829-1	5.867	5.932	0.003	5.921	5.943	4	3U
3920-1660-1	8.451	8.401	0.014	8.367	8.431	2	D
3920-1971-1	3.884	3.873	0.002	3.861	3.880	6	C5
3934-27-1	7.405	7.413	0.007	7.374	7.436	6	U

[1] *Most stars have min./max. values that are 2+ times the typical nightly standard deviation. Of particular interest are TYC 3536-2022-1 which was labeled as "stable" in the Tycho 2 input and main catalogs. Stars TYC 3538-2150-1 and TYC 3552-1543-1 have no variability designation. All three stars have no variability designation in SIMBAD. Tycho classifications are: S=Standard, C=Stable in input/main catalog, U, P, M, R = confirmed variables. Numbers in Tycho classifications indicate variation type, see Perryman* et al. *(1997), and Wright* et al. *(2003) for designations.*

Table 2. Summary of the observed fields and exposure information.

*Field**	*Center*		*Near TYC*	*No. Series*	*No. Images*	*No. Days*	*No. Stars*	*Air-mass*
	R.A. *h m*	*Dec.* ° ′					*V < 8.8*	
CD3S "A"	19 35	+51 16	3568-2325-1	21	245	9	56	1.0–1.14
CD4S "B"	19 09	+51 23	3554-275-1	6	76	3	40	1.02–1.2
CD5S "C"	18 43	+51 30	3539-1697-1	6	76	3	48	1.05–1.34
CD6S "D"	18 15	+51 30	3537-1538-1	7	85	4	57	1.13–1.53

**Fields are 15.9 × 6.4 degrees. The instrumental magnitudes for each of the 40 series of observations are available from R.P. by request.*

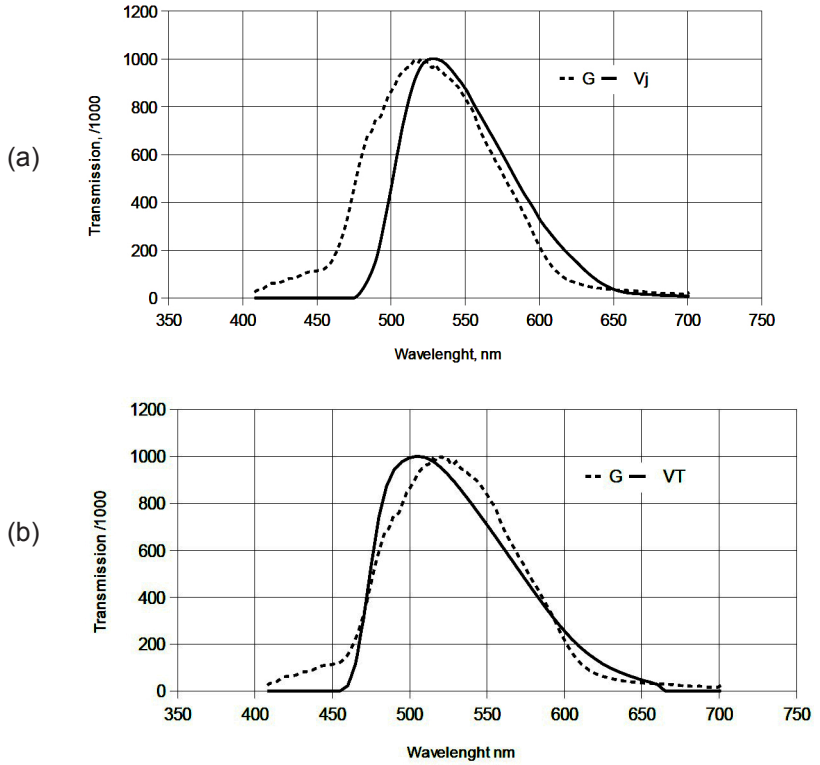

Figure 1. Instrumental response curves of the photometric channels (Photon-count) of the Canon 450D used in this experiment: (a) Johnson V and DSLR G; (b) Tycho VT and DSLR G.

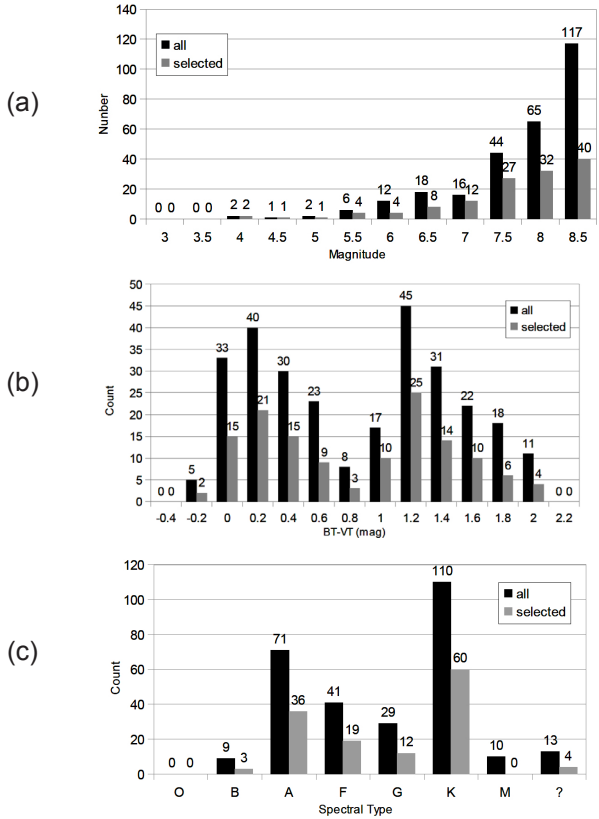

Figure 2. General field properties of the Cygnus-Draco 15.85 × 6.36 deg. fields, used in our experiment, and statistics for selected stars (after rejection of blended and variable stars): (a) magnitude ranges, Tycho 2; (b) (*BT–VT*) color ranges; (c) Approximate spectral types.

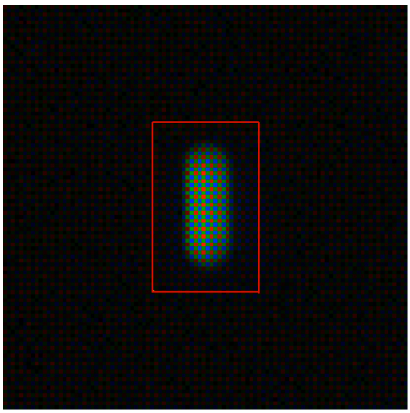

Figure 3. A typical RAW star image from our data set. As mentioned above, we use a non-tracking camera mount, hence the star image shows significant trailing. The Red Green Blue nature of the camera's Bayer array is clarly visible. The 21 × 13 pixel aperture is shown for reference.

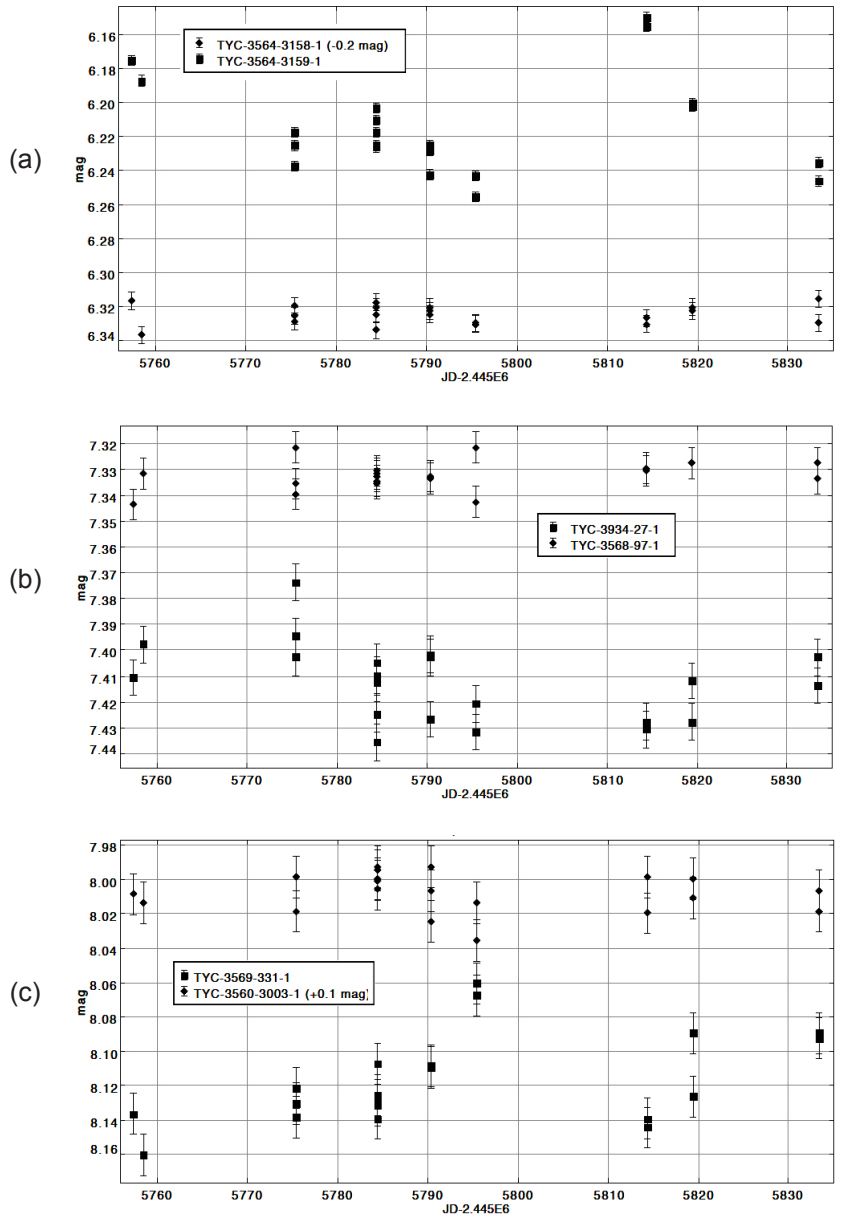

Figure 4. Examples of variable and non-variable stars seen in our data set: (a) nearly constant star TYC 3564-3158-1 and suspected 0.1 mag. variable TYC 3564-3159-1. (b) TYC 3568-97-1 and suspected 0.04 mag. variable TYC 3934-27-1. (c) 0.1 mag. suspected variable TYC 3569-331-1 and nearby stable star TYC 3560-3003-1.

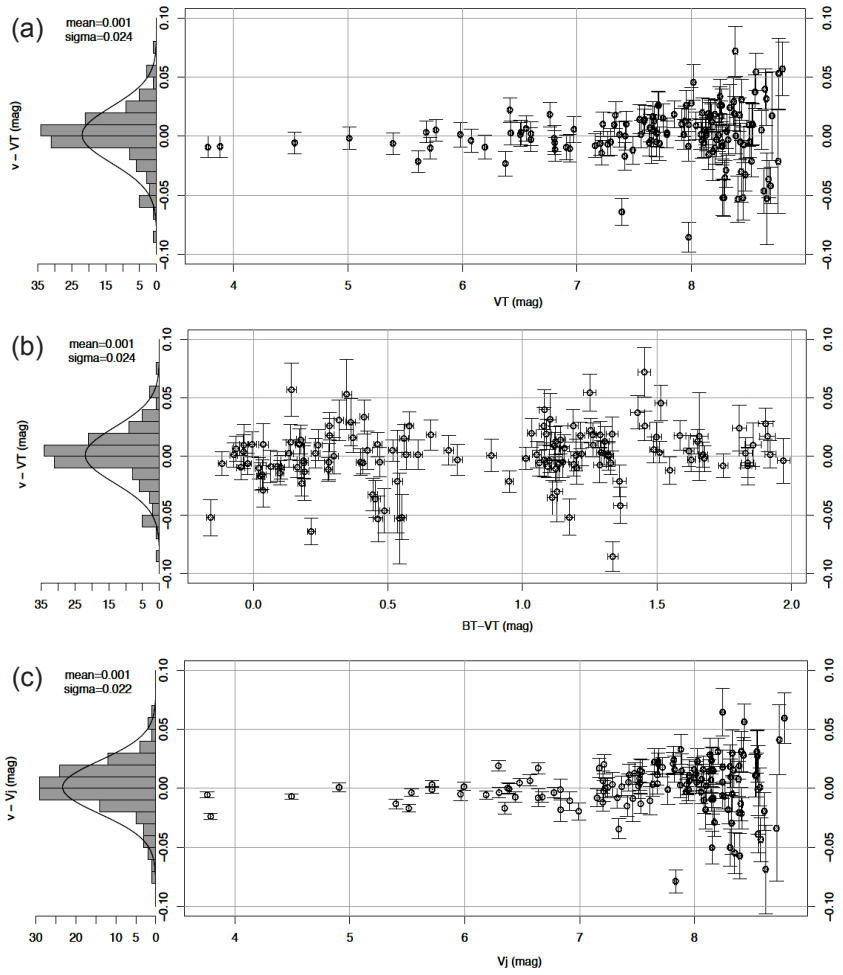

Figure 5 (a, b, c). Residuals of the simple calibration method as a function of color, magnitude, and catalog: (a) Tycho magnitude residuals; (b) Tycho color residuals; (c) ASCC magnitude residuals (figure continued on next page).

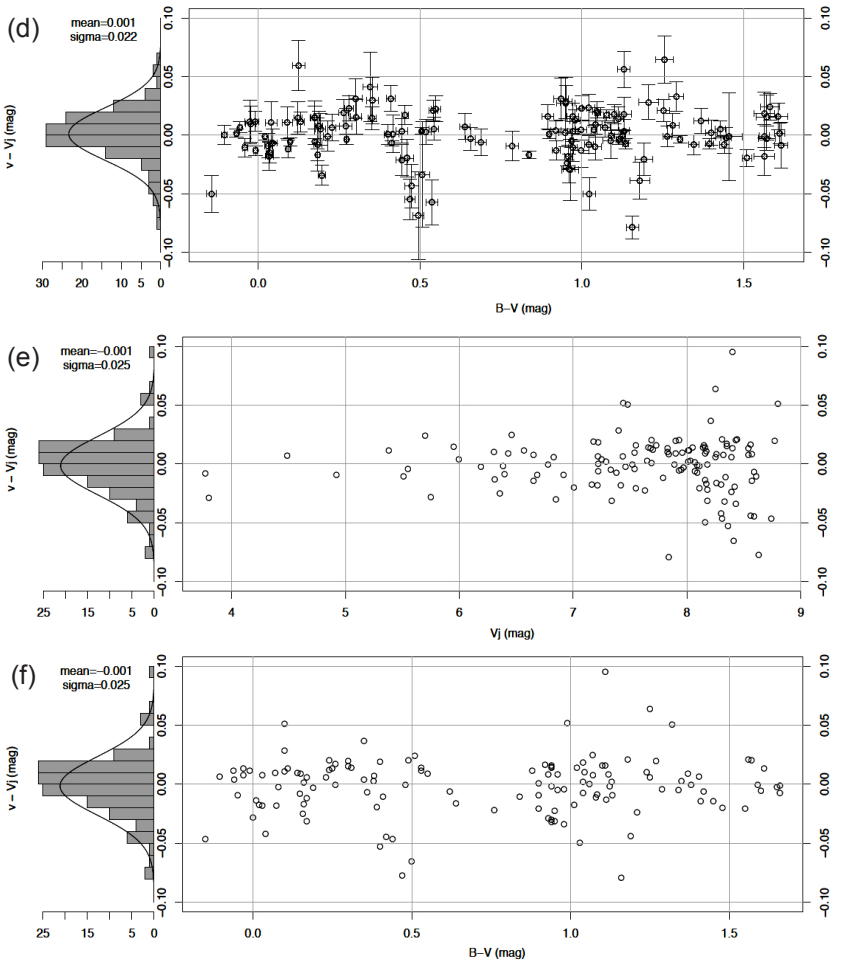

Figure 5 (d, e, f). Residuals of the simple calibration method as a function of color, magnitude, and catalog: (d) ASCC color residuals; (e) SIMBAD magnitude residuals; (f) SIMBAD color residuals. Aside from an increased spread at fainter magnitudes (due to a lower SNR), there appears to be no remaining systematic residuals after application of the calibration procedure discussed above. The statistical distributions of residuals are shown to the left of the *y* axes. All residuals follow a Gaussian distribution with a very small offset (~ 1 mmag). The distribution is typified by a $\sigma = 22$ mmag uncertainty which improves by nearly a factor of two for stars with $V < 8$). This attests to the quality of the catalog and capabilities of the DSLR camera. We believe the SIMBAD results are skewed due to invalid color determinations inherent in a inhomogeneous catalog system.

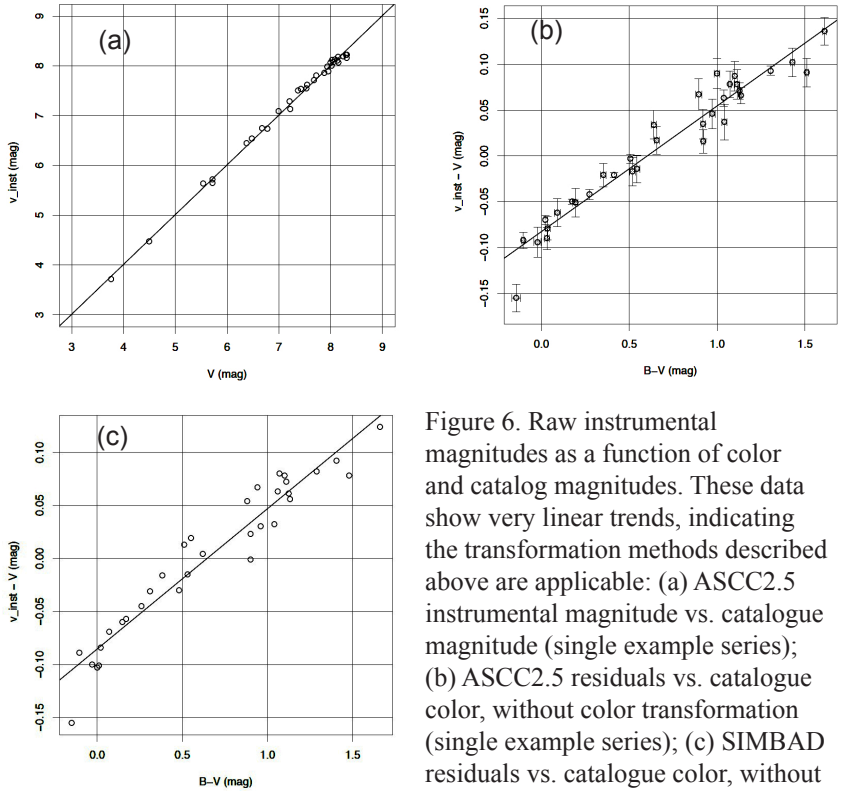

Figure 6. Raw instrumental magnitudes as a function of color and catalog magnitudes. These data show very linear trends, indicating the transformation methods described above are applicable: (a) ASCC2.5 instrumental magnitude vs. catalogue magnitude (single example series); (b) ASCC2.5 residuals vs. catalogue color, without color transformation (single example series); (c) SIMBAD residuals vs. catalogue color, without color transformation (single example series).

Stellar Photometry With DSLR: Benchmark of Two Color Correction Techniques Toward Johnson's VJ and Tycho VT

Roger Pieri
37 C rue Charles Dumont, Dijon, 21000, France; roger.pieri@wanadoo.fr

Received April 24, 2012; revised June 18, 2012; accepted August 17 2012

Abstract DSLRs are now routinely used for measuring the V magnitude of stars through their G channel output. This requires a transformation to Johnson V, using a correction based on the catalogue (B–V) color indices of the stars. This paper reviews the responses of the involved passbands and proposes an alternate solution using a synthetic filter made by combining the three RGB DSLR channels. The assessment of the two techniques through experimentation being uncertain, we have chosen to use a computer simulation instead. This simulation combines the measured spectral responses of the DSLR channels, the atmospheric reddening, and star spectra from the Pickles library.

1. Introduction

The recent ε Aurigae campaign (thanks to AAVSO's Citizen Sky, hereafter "CS") has been a great opportunity to experiment with the DSLR's (Digital Single Lens Reflex) photometry capabilities. We have had to observe under very different conditions, sometimes near zenith, but also at very low elevation and high airmass, during the conjunction period that was an important phase of the eclipse. The typical CS DSLR observer works with a standard DSLR equipped with a regular lens and mounted on a photo tripod. The author's lens is a 200 mm, *f*/4, but most people use shorter focal length, typically 70mm, *f*/2.8. Accurate photometry is achievable down to magnitude 6 with this configuration. Less accurate data can be gathered down to magnitude 8. Ideally, an observation made every few days (when weather permitted) was needed to obtain good coverage of the phenomenon over two years. For an amateur this is possible only near home, most of the time under urban sky conditions, with typically 15 to 20 minutes of observation. This also means under an extinction much worse than any professional observatory would encounter. Not only was neutral extinction a problem, but also reddening at high airmass was making things more complex (unusual for professional observers). A specific observing method and data processing technique has been devised by the Citizen Sky's DSLR team to fit all such conditions. It is known at CS as the "intermediate spreadsheet" method (hereafter "CSIS") and can be found on the CS website (AAVSO Citizen Sky 2009).

A simpler method is also used by CS people when observations are done below airmass 1.5. It is known as the "beginner spreadsheet." It involves only

the color corrections and not the differential extinction across the DSLR field-of-view.

2. Present work

Initially, the author used the tools and publications provided by C. Buil on his website (Buil 2012), his book (Buil 1991), and the tutorials from Citizen Sky (AAVSO Citizen Sky 2009), but soon developed his own software pipeline to make the operations more productive and to experiment with various techniques including a synthetic Johnson V filter.

The goal was to better extract useful data from observations under the poor ε Aur conjunction conditions. Another aim was to push the DSLR to perform at its best in bright star photometry.

The DSLR itself has G- and B-color filters which do not match the standard Cousins-Johnson B and V passbands (hereafter BJ and VJ). The DSLR R channel is too far from the Cousins Rc to be faithfully transformed. A specific transformation and extinction correction technique has been devised to take care of both the G passband and the CS amateur context (Henden and Kaitchuck 1982; Kloppenborg and Pearson 2011). This CSIS technique is based on the catalogue (B–V) and V-magnitude of a star "ensemble" that determines the related correction coefficients.

In the CSIS the differential neutral extinction is determined through a mapping of the magnitude deviations of stars of a large ensemble distributed in the DSLR field-of-view (FOV). To do this, the fully "color corrected" instrumental magnitude of the stars is then compared to the catalogue magnitude of the stars. The resulting magnitude differences that are a function of the differential airmass determine the neutral extinction gradient across the FOV.

Statistics have been extracted from the ε Aur observations and critical cases have been identified in this CSIS technique. The single-equation system (Equation 5) used by the CSIS has some drawbacks depending on the distribution of stars. To overcome that issue the author soon considered a color correction technique independent of the catalogue data using an RGB synthetic filter equivalent to VJ or VT (hereafter "VSF"). It is implemented by combining the three RGB channel signals of the DSLR. The first experiments showed interesting possibilities but it was obvious that an accurate assessment of these techniques was difficult to achieve through observations. Then it was decided to use a computer simulation for that study.

Several options of processing of the neutral part of the extinction in the VSF technique remain under study. The author plans to address it in a future paper based on the best option.

By the way, the present paper addresses only the color aspect of both the CSIS and the author's VSF technique. For such study only the DSLR response and the slope of the atmosphere transmission curve are used in a differential photometry scheme where all stars are at the same airmass.

Carrying out such a simulation needed a library of stellar spectra. The Pickles library (Pickles 1998) has been found to meet the need with its 131 stars from O to M, at all luminosities and several levels of abundance. Other inspiring sources have been the many papers from Bessell: in "UBVRI passbands" (Bessell 1990) he analyzed the issues of various filter implementations used under several photometric systems. The paper includes a synthetic magnitude calculation using the Vilnius spectra library. The approach is very similar to what is reported in this paper. His last paper has an interesting appendix pointing out some issues of such broad passbands (Bessell and Murphy 2011).

The paper from (Tokunaga and Vacca 2005), the photometry introduction of (Romanishin 2006), and a study of the calibration of Tycho-2 and Johnson systems (Apellániz 2006) have also been very informative.

Another important source for the DSLR application is the Hipparcos mission (Perryman *et al.* 1997). Looking at the various system passbands revealed that the Tycho VT passband is comparable to the DSLR green response. In addition the *Tycho-2* catalogue (Høg *et al.* 2000) catalogue is a uniform, very accurate, and reasonably precise reference. This opened a new possibility that will be analyzed hereafter and compared to Johnson VJ using both the CSIS and the VSF techniques.

At this point the author would like to discuss the accuracy of the catalogues compared to what can be obtained through DSLR photometry techniques. Such techniques, based on mapping of magnitude differences, are very sensitive to the catalogue errors. Fortunately, DSLRs have a large FOV that allows one to work with a large ensemble of stars (50 to 100 stars accessible in a 6×4 degree field). This averages both catalogue errors and the imperfect color distribution in the FOV. At a 1000 signal-to-noise ratio the DSLR provides results reproducible within a few millimagnitudes. Most catalogues have larger uncertainties, and from catalogue to catalogue such uncertainties are often much larger; this could affect the determination of both the color transformation coefficient and the differential neutral extinction with the CSIS (as it is based on a mapping of it from an ensemble of stars).

3. Color Passband: DSLR's RGB versus Johnson's VJ and Tycho-2 VT

The DSLR R,G,B channel responses are shown in Figure 1. They have been obtained from a clear day, sunlight observation using a slit and grating mounted in front of the DSLR lens, then corrected from the standard ASTM sun spectrum at 1.5 airmass (ASTM International 2008) and the RGB balance of the grating. It is to be noted that DSLR curves are the responses of the filter stack (R, G, B, IR, and UV cut) plus the sensor and the lens. The linear RAW output of the DSLR has been used; that excludes any processing from the DSLR—in particular, any gamma application or any transformation to sRGB or other color profile. The DSLR was a standard Canon 450D with a CMOS

sensor, 14 bits, equipped with a Nikkor 85 mm lens. Its IR and other filter stack has not been modified.

In the UBVRI (and other) photometric systems (Bessell 1990), magnitudes are calculated from the photon-count from photometric chains of several passbands. Figure 2 shows the Johnson V (hereafter "VJ") passband and its relationship with the DSLR G channel. The version used as reference in this study is the one recommended in the Pickles (Pickles 1998) spectra library. This version is very similar to the one recommended by the CDS. They are used in a number of publications, but other versions also exist (Bessell and Murphy 2011).

Figure 3 shows the relationship between the *Tycho-2* VT passband definition (Apellániz 2006) and the DSLR G channel response curve.

Other DSLR color channels responses could be seen at the website of C. Buil (Buil 2012). They are very similar. Apparently, there are no large differences between recent DSLR or DSC (digital still cameras; large differences may be found in older cameras).

The color filter array of the DSLR is of the Bayer type (Bayer 1975) with a square RG/GB arrangement. That means the G signal is obtained from two sub-pixels instead of only one for R and B. In addition, as shown in Figure 1, the transmission of the red filter is much lower than G and B. As a result the SNR of the G channel is much higher than the B and, in particular, the R channel. The RAW resulting color balance is more or less CIE (Commission Internationale de l'Eclairage) typical (Green *et al.* 2002). In most common usage (sRGB and Jpeg output) the RGB levels are realigned to 1, 1, 1. Then the representation is non-linear (0.45 gamma) coded on 8 bits and to some color profile like sRGB. This study uses only the linear RAW output of R, $G=(G_1+G_2)/2$ and B data (said ADUs, proportional to photon-count, hereafter all photo-count data are denoted as "G", italicized uppercase, and magnitudes as "*Gm*").

The instrumental magnitude, *Gm,* is usually calculated with the equation (Equation 3) from the DSLR G-channel output, *G,* then transformed to VJ *Gtm* using Equation 4. If we compare the G response to the VJ response (Figure 2), there is a large common surface between them both, but also significant differences.

The blue side roll-off is the largest significant difference. The centroid of the G response is at 530 nm and the VJ one at 542 nm. But the blue roll-off of the G response is shifted 26 nm to the blue compared to the steep roll-off of the VJ curve. In addition there is a blue leak at the foot of the curve between 450 and 400 nm.

On the red side the difference is less important and opposite: missing red instead of too much blue. The red side G roll-off is shifted to the blue by about 5 nm. Figure 3 shows the Tycho VT passband which is much more similar to the G channel. The centroids positions are different by only 2 nm. The resulting color correction between both should be minimal. We will also study that case as it offers a real opportunity for DSLR photometry.

4. Atmosphere transmission

The bandwidths of all DSLR-involved passbands are not small. Besides the impact of the mean extinction at the centroid, the passband's internal color balance is affected by the atmosphere transmission variation as a function of the wavelength (essentially the slope of this function). The result is the product of both: the camera response S(λ) and the atmosphere transmission T(λ). This more-or-less moves the resulting centroid to the red. The atmosphere affects all passbands including the references, Johnson's VJ, and Tycho VT. The atmosphere attenuates the short wavelengths more than the long ones. This is shown in Figure 5, extracted from the Moon's solar irradiance table (Desvignes 1991). That effect is weighted by the length of the light path in the atmosphere known as the airmass number (*AM*), after the Beer-Lambert-Bouguer equation:

$$T(\lambda, AM) = e^{-\varepsilon(\lambda)\, AM} \quad (1)$$

Where the airmass *AM* is a function of the star zenithal distance *z* (or elevation $h = 90 - z$), and ε(λ) is the extinction coefficient. In the Desvignes table ε = 0.23 at λ = 550 nm. It could also be extracted from the solar irradiance at AM0 and AM1.5 from the ASTM standard (ASTM International 2008). The solar energy standards better fit our urban amateur sky conditions than the data from professional observatories.

$$M = 1/\cos(z)$$
$$AM = M - 0.0018167 \times (M-1) - 0.002875 \times (M-1)^2 - 0.0008083 \times (M-1)^3 \quad (2)$$

Where *M* is the airmass in a planar homogeneous atmosphere model (valid down to 10 degrees elevation), and *AM* the corrected airmass after the Hardie's approximation (valid down to 5 degrees elevation) (Ilovaisky 2006). These equations are not used in the simulation where the input of the transmission table is directly *AM*.

In the following simulation only the chromatic part of the extinction is used and studied (the transmission slope). The neutral part of it and its differential effect in the DSLR FOV is eliminated by the differential photometry and the fact all stars are set at the same airmass in this simulation.

5. CSIS color transformation from the DSLR *Gm*, instrumental magnitudes, to *Gtm*, VJ, or VT magnitudes

The CSIS color transformation (Henden 2000) is a linear interpolation between the color indices of the stars, the target one and at least two reference stars (an "ensemble" being better). The color index is the magnitude difference between two passbands like $(B_3 - V)$. (Pickles 1998; B3 denotes a specific

Johnson B filter adopted for the Pickles spectra. It is not far from the filter recommended by the CDS.) The magnitude difference from a third passband is linearly interpolated from the known color indices. The interpolation coefficient "k_D" is expected to be specific to a given DSLR. A similar term shall also account for the reddening due to the chromatic part of the atmospheric extinction "k_K". It shall be readjusted for each star field as a function of its distance angle to the zenith. Within 40 degrees of the zenith it accounts for about 2 millimagnitudes only within the usual ±0.7 (B–V) range, then it could be ignored. At airmass 1.5 ~ 4 the impact shall be taken into account (3 ~ 30 millimagnitudes).

$$Gm = m_0 - 2.5 \log (G / G_0) \quad (3)$$

$$Gtm_i = Gm_i + zp + k_D (B_3 - V)_i + k_K (B_3 - V)_i + k_N X_i \quad (4)$$

Gm is the instrumental magnitude from the *G* and G_0 photon-count issued from the green channel of the DSLR respectively for a target star and a comparison star. $(B_3 - V)$ is the catalogue color index of the star (i). *Gtm* is the transformed magnitude of the star. *zp* is the zero-point, the magnitude constant from the instrument. In a given observation k_D and k_K can't be separated when solving the equation system (Equation 5) and shall be replaced by $k_C = k_D + k_K$. In the DSLR FOV, X_i is the differential airmass of the star (i) from the reference star or ensemble.

In the simulation reported in this paper G_0 is the photon-count of an A0V star of magnitude $m_0 = 0$ and $(B_3 - V) \sim 0$ resulting in $zp \sim 0$. Then all stars of the FOV being set at the same airmass, all $X_i = 0$ and k_N are not applicable.

From actual observations, the coefficients for a given DSLR and a given FOV are determined from the catalogue values $(B_3 - V)$ and *Vjm* of several reference stars and their measured *Gm* values (or hereinafter *BT–VT* and *VTm* in the case of Tycho-2).

$$Vjm_i = Gm_i + zp + k_c (B_3 - V)_i + k_N X_i \quad (5)$$

Applying the relation Equation 5 to the observation of more than three stars (i) forms an overdetermined equation system that is solved using the least square error algorithm. This method is used to determine *zp*, k_C, and k_N from this ensemble of stars. Only k_C is used in the reported simulation.

Characterizing the DSLR k_D through observations instead of through simulation is tricky. Such observations should be made under very good sky conditions, near the zenith, using well-documented, stable stars of a matching (B – V) range, at high SNR (>300), and repeated several times. The extinction should be independently checked using the Bouguer's line method (Ilovaisky 2006). If the resulting extinction parameters are far from standard and/or irregular as a function of the star's elevation, the sky conditions should be considered inadequate for a calibration.

6. Definition of a DSLR "VSF" synthetic filter delivering a VJ- or VT-like magnitude

From the analysis of the wavelength response of the DSLR channels we can define another technique to emulate a Johnson VJ chain. The wavelength difference between the blue leak and the B response centroids, and similarly for the red, leads one to think that a compensation would be possible in the form of a synthetic filter combining the RGB channels:

$$Gc = G + a\,R - b\,B \tag{6}$$

$$Gcm = -2.5 \log (Gc / G_0) \tag{7}$$

Where *G,R,B* are the photon-count (or ADUs) from the DSLR raw output, *Gc* and G_0 are the respective photon-counts of a target star and the A0V comparison star ($m = 0$, $B-V \sim 0$), both VSF-filtered, and *Gcm* is the corrected magnitude of the target.

In the following simulation the *a* and *b* coefficients are optimized from the RGB outputs of the DSLR *G,R,B,* and the standard filter output, *Vj,* of the Pickles stars spectra (all photon-count; or *VT* in the case of *Tycho-2*). This optimization of (*a,b*) across the HR diagram is done by solving the overdetermined equation system formed from the relation (Equation 8) using the ensemble of stars (*i*).

$$Vj_i = k\,(G_i + a\,R_i - b\,B_i) \tag{8}$$

It is not recommended to apply Equation 8 to data obtained from observations. The various errors due to the observational conditions and the catalogue uncertainties can have a significant impact on the (*a,b*) coefficients. Such errors can unbalance the corrections from the B and R channels. This could result in a good correction for a given star set but one that is not optimal across the overall (B–V) range. It's better to use the coefficients determined from the RGB pass-bands.

The way (*a,b*) works can be understood as controlling the centroid and the bandwidth of the VSF. When (*a,b*) vary in opposite directions they control the bandwidth, otherwise they shift the centroid of the VSF.

This *G,R,B* combination results in a synthetic filter (VSF) which has a response similar to VJ (or VT) in the visible domain. The VSF passband shape is not exactly the same as VJ but responds similarly to the spectrum continuum (Figure 18). The VSF response to specific features of the spectra, like Balmer's lines of blue stars or molecular bands of the red ones, could differ (Figure 4). A first check has been made using the black body spectrum at various star temperatures with excellent results (within one millimagnitude).

The proposed VSF technique has also been extensively tested on the star field of the ε Aur campaign with excellent results. Under good sky conditions the standard deviation within an ensemble of five stars (*B–V* from –0.18 to 1.22)

and their catalogue values was often as low as a couple of millimagnitudes. But that field had no spectrum-critical star. Next, there are few reference stars of various types having VJ magnitudes known with high accuracy in a single field of 5~15 degrees (DSLR FOV). It has been judged easier, more accurate, and informative to assess this technique through a computer simulation using the coherent Pickles spectra library and the measured RGB responses of the DSLR.

In the CSIS transformation the chromatic part of the extinction is included in k_C, and we see that it shall be set before the determination of the differential neutral extinction in the DSLR FOV.

This can be achieved with the VSF technique by adapting the color balance of the synthetic filter. This is just making the (*a,b*) coefficients adaptive to a measure of the atmospheric reddening (Equation 9). The B_c / G_c ratio of the B,G outputs of the DSLR is an excellent measure of it. It is very stable during an observation and looks much more reliable than any single channel output.

$$a = a_0 + a_1 \, B_c / G_c \qquad b = b_0 + b_1 \, B_c / G_c \tag{9}$$

The B_c / G_c ratio used is that of a reference star in the FOV or of an ensemble centered on the (B–V) range. This atmospheric reddening correction should not be confused with the main filter synthesis operated by Equation 6. It produces only a limited centroid shift of the synthetic filter that compensates for the reddening, and a first order link to (*a,b*) has been found accurate enough for the Canon 450D. A second order could be needed for some older DSLRs having a large blue leak into the G channel.

7. Pickles spectra library

The Pickles library includes 131 spectra of stars with $(B_3 - V)$ from –0.38 to 1.816 and O5 to M10 spectral types. All luminosity classes I to V are represented. The spectra comprise wavelengths 1150 Å to 25000 Å at a resolution of about 500 ($\Delta\lambda / \lambda$). The library has been constructed by combining the data from sixteen other libraries with a dedicated combination and verification methodology. Details may be found in Pickles (1998).

For the purpose of the DSLR simulation the range from 350 nm to 750 nm has been extracted from the original data (Figure 4). The library provides calibrated spectra in energy density per Ångstrom; then the flux has to be converted to photon-count. The original normalization at 5556 Å of the spectra has been readjusted for normalizing the output of the VJ (or VT) passband to zero magnitude at zero airmass for all stars. This makes the assumption the VJ magnitudes are defined on top of the atmosphere after the Johnson definition (Bessell 1990).

Most stars of M spectral type show large color transformation errors. This is due to their spectrum having large absorption molecular bands resulting in their $(B_3 - V)$ colors no longer reflecting the black-body flux and predicting the

correct flux correction to VJ. For M stars, a magnitude correction based on the (V–Rc) color is more appropriate (Rc is not accessible to DSLR except if IR cut and IR dye filters are removed). M stars have been processed separately and 110 O-to-K stars remain in the main analysis.

The ninth star of the library of A0V spectral type has been used as the comparison star (G_0 photon-count) in the magnitude computations. Its VJ (VT) magnitude has been set to zero but the color index determined by its spectrum is 0.015. This induces some few millimagnitudes global shift of the end result.

8. Computer simulation of the DSLR outputs and color processing

The simulation is just the software implementation of Equation 10 to each system passband of that study:

$$G_{ADU} = k\,Np = \frac{k}{hc}\int_{\lambda} \lambda\, F_{\lambda}(\lambda)\, T(\lambda, Am)\, S(\lambda)\, d\lambda \qquad (10)$$

where G is any of RGB channel outputs of the DSLR, k is the sensitivity (or calibration factor) in ADU/photon, and Np is the photon-count. The spectral energy distribution, F(λ), of the Pickles spectra is transformed in the photon-count as $\lambda\, F_{\lambda}(\lambda) / hc$.

$S(\lambda)$ is the overall photonic camera response and $T(\lambda, Am)$ is the atmosphere transmission.

$S(\lambda)$ is successively set to the response of the five passbands VJ, VT, R, G, B, the collecting area being arbitrarily set at 1 cm^2.

In this process the software computes G_{ADU} of all stars at airmass zero and normalizes $F_{\lambda}(\lambda)$ to put all star magnitudes *Vjm* or *VTm* to zero at this level using the reference passbands VJ or VT. Then B_3*jm* or *BTm* and the related color indexes are computed for checking against the original library values.

Next the G_{ADU} of all stars are re-evaluated at each targeted airmass from the normalized $F_{\lambda}(\lambda)$, the atmosphere transmission $T(\lambda, Am)$, and the passband response $S(\lambda)$. The results after integration are the new *Vj* or *VT* and *R, G, B* photon-counts.

The last phase is to compute the end results of both techniques from the photon-counts using Equations 3–4 and 6–7. The results are the final magnitudes *Vjm* (the reference, or *VTm*), *Gtm*, *Gcm* (the corrected results).

Here we should bring to mind that all stars are at the same airmass under evaluation. No differential neutral extinction is involved in the result. These results are the deviations due to the combined camera passbands and the atmospheric reddening, depending on the star's color. They are graphically shown below.

In a first pass the software is also used to compute only *R,G,B* and calibrate the coefficients k_C, a, and b using Equations 5 and 8.

All that computing chain, up to Equation 3 or Equation 7, uses the notion of transmission and photon-count instead of the logarithmic processing usual

in astronomy. This is needed as the VSF technique is additive at the photon-count level and cannot be processed using logs.

This simulation has been implemented in the APL language and performed under a Dyalog APL system.

9. Benchmark results

9.1. Airmass 1 instrumental results under both VJ and VT systems

Johnson System—Figure 6 shows the respective instrumental magnitude deviations at airmass 1 of the Johnson VJ passband, *Vjm*, and the DSLR green channel, *Gm*. *Vjm* was normalized to 0 at airmass 0. The deviations are more or less a linear function of $(B_3 - V)$. The peak-to-peak deviation for *Gm* is about 260 mmg across the color index range of 2.2 magnitudes. The slope is roughly 0.118. This $Gm\,(B_3 - V)$ curve is what we shall use to transform to Johnson VJ.

There is a set of outliers above $(B_3 - V) = 1.1$ magnitude. Those are the M stars, which are bluer than the K stars, although they are cooler, due to large molecular absorption bands in their spectra. Their effective temperature is much lower than expected from their color index defined by the BJ and VJ passbands. In the following they are excluded from the main analysis. This issue has been denoted in the Hipparcos and Tycho report (Perryman *et al.* 1997) and the authors recommend not to transform the M star magnitudes (like Tycho, we can only work with B and V, as the DSLR R is too far from Rc).

The *Vjm* Johnson output itself shows a small deviation at airmass 1 due to the star color—about 10 millimagnitudes across the range. This is small but would need a linear correction when precise photometry is required.

Tycho System—Figure 7 shows the comparative deviations of the Tycho VT passband *VTm* and the DSLR green channel *Gm*, without correction, at airmass 1. *VTm* is normalized to 0 at airmass 0. The *VTm* deviation at airmass 1 is somewhat larger (19 millimagnitudes) than *Vjm*. This is due to the larger and bluer VT passband. The response of the DSLR green channel shows a much smaller deviation than under the Johnson system (23 millimagnitudes peak-to-peak instead of 260). This confirms the analysis (section 3) made from the response curves and their centroids. The outliers are the M stars and a few K stars as seen in the VJ plot (Figure 6), but with a smaller scatter.

This confirmation is important, showing the *Tycho-2* catalogue should be the reference for DSLR photometry. This catalogue is accurate in the magnitude range accessible without a telescope and provides well-quantified uncertainties.

9.2. Airmass 1 to 4 and both VJ and VT passbands

Figures 8 and 9, respectively, show the responses of the Johnson VJ and Tycho VT passbands at airmasses 0, 1, and 4. They show the strong impact of the atmospheric reddening even on such standard filters. At airmass 4, the peak-

to-peak errors are, respectively, 40 and 65 millimagnitudes for *Vjm* and *VTm*. The airmass color shift needs a compensation for the standard passbands.

The following sections compare the CSIS and VSF deviations at airmass 1 and 4 under VJ and VT.

9.3. Johnson's VJ—airmass 1 and 4—CSIS and VSF techniques

Figures 10 to 13 show the deviations of *Gtm* and *Gcm* for the 110 stars of type O-to-K.

CSIS—The CSIS transformation result, *Gtm* (Figures 10 and 12) has been optimized with respectively k_C = 0.135 and 0.098 for airmass 1 and 4. This 0.135 value is in good agreement with the one typically used, at zenith, for our ε Aur observations.

The deviation pattern is similar at both airmasses and forms two lines from a maximum around 5 millimagnitudes at (B_3-V) = 0.33 and a range of 20 millimagnitudes. Using slightly different coefficients for the color index ranges –0.4 ~ 0.33 and 0.33 ~ 1.8 (two different slopes) would improve it. This should reduce the error range to about 8 millimagnitudes except a few outliers. Those outliers are K-type stars that show some problems similar to the M types. On the blue side there are one B3I and one F5I outlier without clear reason to deviate, although the additional violet flux in supergiants is suspected to be the cause.

VSF—The VSF result, *Gcm* (Figures 11 and 13) has been optimized with, respectively, (a = 0.284, b = 0.224) and (a = 0.149, b = 0.244) for airmass 1 and 4. This is just the experimental value for b, and a somewhat higher value for a. But the red correction coefficient has a large variability depending on the experimental conditions due to its weak effect. a equal to or above 0.284 is not uncommon.

The airmass 1 deviation pattern differs from *Gtm* with a well contained section above (B_3-V) = 0.3 within 7 millimagnitudes and no K outlier. At airmass 1 the section below 0.3 shows more dispersed results (within 15 millimagnitudes) of the OBA stars.

The pattern at airmass 4 is reduced to a 12 millimagnitude range but has the same shape as airmass 1. Both are better contained than *Gtm*, the result of the CSIS transformation.

9.4. Tycho VT—airmass 1 and 4—CSIS and VSF techniques

Figures 14 to 17 show the deviations of *Gtm* and *Gcm* for the 110 stars of type O-to-K.

CSIS—The CSIS transformation result, *Gtm* (Figures 14 and 15), has been optimized with, respectively, k_C = 0.009 and –0.019 for airmass 1 and 4. This 0.009 is well in agreement with the value typically used, at zenith, in another massive survey experiment based on *Tycho-2*.

The pattern of the deviations at airmass 1 is more or less similar to that of VJ but with a reduced amplitude of 10 millimagnitudes excluding the

usual outliers. The pivot point has moved about $(B_3 - V) = 0.8$. The outliers also show a reduced deviation.

The overall improvement from the VJ system is more than a factor two. At airmass 4, the pattern amplitude is further reduced, but dominated by the outliers.

VSF—The VSF result, *Gcm* (Figures 16 and 17) has been optimized with, respectively, ($a = –0.085$, $b = 0.073$) and ($a = –0.136$, $b = 0.030$) for airmass 1 and 4.

The deviation patterns at airmass 1 and 4 are nearly identical showing the lowest amplitude of all about 8 millimagnitudes (excluding some outliers). As in the VJ system, using VSF, the late K stars are no problem and the dispersions are not clearly linked to any specific spectral type. At that level of a couple of millimagnitudes it is very possible we are seeing limitations due to the library.

10. Discussion of the simulation results

The accuracy of the simulation results depends upon three items: the spectra library, the passband responses, and the atmosphere extinction model. The last is just a standard model, and the observations clearly show large deviations from such a model. The B_c/G_c ratio dependency to the airmass is usually stable and the neutral extinction much more variable. This is the result of the variability of the high aerosol content of our urban skies. Such a neutral component has no impact and any slope change of $T(\lambda, Am)$ is a color balance difference that would just affect the correction coefficients, not the end error level shown by the simulation (the chromatic and differential neutral corrections are independent in the VSF technique).

The next point is the DSLR response curve accuracy. The passbands have been tested by comparing the simulated RGB outputs with the physical RGB outputs of the DSLR and have been found to be within a couple of percent and corrected. The response curves have been measured using three different reference light sources and found similar. The differences impacted the correction coefficient by less than 2%.

The spectral features: lines, bands, but also some small differences in large bands of the continuum, are expected to be the reason for the star-to-star deviations seen in the simulation results. Then we have a standard deviation from Pickles (hereafter SD) at each wavelength that ranks from 5% to 0.5%. But we don't know the correlation from one wavelength to the next that could form such small "bumps" of the continuum (a few percent) over a bandwidth large enough to interact with the roll-off of the DSLR passbands. In the hypothesis, where we propagate those SDs without any correlation, we will get a worse SD of 3 millimagnitudes at the end which seems somewhat optimistic with regards to the simulation results. Then, if we take the worst case possible correlation, we will get a deviation of 50 millimagnitudes which is obviously

far too large and unlikely. This aspect would need a deeper study of the library construction, which combines a variable number of original spectra depending the wavelength and the star spectral type. There are cases based on a few data only. Anyhow, the Pickles library is an excellent resource and the best of those tested by the author for this work.

The VSF technique has been extensively used during the ε Aur campaign with good results (reports can be found under PROC at Citizen Sky and the AAVSO). It permits us to achieve a fully VJ color response of the DSLR independently from the differential neutral extinction correction (and other error sources). This avoids possible contamination from other factors that exists with the CSIS transformation. This CSIS issue depends on the star color distribution and their position in the field of view. The VSF technique is also independent of the catalogues after its calibration is set.

The VSF technique has been very effective when we had to observe ε Aur at low elevation during the conjunction. It is also very helpful in cases of color change of a variable. This has been recently the case of ζ Aur, for which interesting results have been gathered.

A further improvement of the DSLR photometry will be to use the *Tycho-2* catalogue as a primary reduction reference. The DSLR instrumental color correction is very low under this photometric system; only the high airmass chromatic effect is significant. This shall further improve the accuracy of both color and neutral extinction corrections thanks to the better uniformity and accuracy of this catalogue. If a Johnson's *Vjm* is needed the end result can be converted using the Tycho recommended methods (Perryman *et al.* 1997). A more detailed table of corrections as a function of BT–VT is provided in (Bessell 2000).

11. Conclusion

It is possible to achieve a color correction of the instrumental magnitudes of a DSLR to Vj or VT, within ±5 millimagnitudes, with both the CSIS transformation and the VSF technique. The CSIS transformation would need some refinement (second order coefficient, or two slopes) to achieve it across a wide B–V range under the Johnson system. The color and airmass of the reference stars used in the CSIS should be well-balanced and bracket the target stars in all aspects.

M-star magnitudes are not well-transformable from the DSLR passbands, with possible errors as large as 60 millimagnitudes. Some late K stars could also deviate by 20 millimagnitudes after the CSIS transformation. The luminosity and the abundance of the stars seem not to be significant factors of deviation.

The VSF technique provides the best accuracy, and is independent of the catalogue (B–V), of the differential neutral extinction and other various

error sources. It shows no specific error for the K stars and generally works better with red stars. Using it under the *Tycho-2* system provides a further improvement, reducing the color related errors and also providing a more uniform reference for determining the differential neutral extinction in the field of view of the DSLR.

12. Acknowledgements

The author would like to thank the Citizen Sky staff for their initiative and support during the ε Aur campaign, Brian Kloppenborg for his support and involvement in DSLR photometry, and the referee Mike Bessell for his useful comments on the paper.

This work has made use of the SIMBAD database, operated at CDS, Strasbourg, France.

References

AAVSO Citizen Sky. 2009, "DSLR Photometry Tutorial" (http://www.citizensky.org/content/dslr-documentation-and-reduction).

ASTM International. 2008, "ASTM G173—03(2008) Standard Tables for Reference Solar Spectral Irradiances: Direct Normal and Hemispherical on 37° Tilted Surface" (http://www.astm.org/Standards/G173.htm).

Bayer, B. 1975, Color Imaging Array, U.S. Patent 3,971,065.

Bessell, M. S. 1990, *Publ. Astron. Soc. Pacific*, **102**, 1181.

Bessell, M. S. 2000, *Publ. Astron. Soc. Pacific*, **112**, 961.

Bessell, M. S., and Murphy, S. 2011, *Publ. Astron. Soc. Pacific* (accepted), arXiv:1112.2698v1.

Buil, C. 1991, *CCD Astronomy*, Willmann-Bell, Richmond, VA.

Buil, C. 2012, "Spectroscopy, CCD and Astronomy" (http://www.astrosurf.com/buil).

Desvignes, F. 1991, *Rayonnements Optiques: Radiométrie, Photométrie*, Masson, Paris.

Green, P., and MacDonald, L. (eds.). 2002, *Colour Engineering: Achieving Device Independent Colour*, John Wiley & Sons, Ltd., Chichester, England.

Henden, A. A. 2000, *J. Amer. Assoc. Var. Star Obs.*, **29**, 35.

Henden, A. A., and Kaitchuck, R. H. 1982, *Astronomical Photometry*, Willmann-Bell, Richmond, VA.

Høg, E., *et al.* 2000, *Astron. Astrophys.*, **357**, 367.

Ilovaisky, S. 2006, "Optical Photometry" (www.obs-hp.fr/ecole-ete/Photometry.pdf).

Kloppenborg, B., and Pearson, T. 2011, *Sky & Telescope*, **121**, 64 (April).

Maíz Apellániz, J. 2006, *Astron. J.*, **131**, 1184.

Perryman, M. A. C., European Space Agency Space Science Department, and the Hipparcos Scienc Team. 1997, *The Hipparcos and Tycho Catalogues*, ESA SP-1200 (VizieR On-line Data Catalog: 1/239), ESA Publications Division, Noordwiijk, The Netherlands.

Pickles, A. J. 1998, *Publ. Astron. Soc. Pacific*, **110**, 863.

Romanishin, W. 2006, *An Introduction to Astronomical Photometry Using CCDs*, Univ. Oklahoma, Norman, OK.

Tokunaga, A. T., and Vacca, W. D. 2005, *Publ. Astron. Soc. Pacific*, **117**, 421.

Table 1. CSIS and VSF coefficients to the VJ and VT photometric systems.*

AM	$G_{c\ mean}$	$B_c/G_{c\ mean}$	VJ/k_c	*VJ/a*	*VJ/b*	VT/k_c	*VT/a*	*VT/b*
0	1027	0.805	0.145	0.340	0.217	0.020	–0.064	0.089
1	800	0.750	0.135	0.284	0.224	0.009	–0.085	0.073
2	624	0.701	0.125	0.235	0.231	–0.002	–0.103	0.058
3	488	0.656	0.110	0.190	0.238	–0.012	–0.121	0.045
4	382	0.616	0.098	0.149	0.244	–0.019	–0.136	0.030

**Table 1 shows the various coefficients used in the simulation at various airmasses. "$G_{c\ mean}$" and "$B_c/G_{c\ mean}$" are the mean output intensities of the DSLR channels for the O-to-K spectra "ensemble" (or of a F6V star). The extinction coefficient used is ε = 0.23 at 550 nm. The B_c/G_c ratio is used to measure the atmospheric reddening as a function of the airmass, AM. $G_{c\ mean}$ results from the atmosphere transmission for the G channel after the Moon's model (Desvignes 1991). "k_c", "a", and "b" are the correction coefficients defined in sections 3 and 4, applied to both Johnson and Tycho standards. The values at AM0 are the correction coefficients of the DSLR G channel passband alone, normally invariant.*

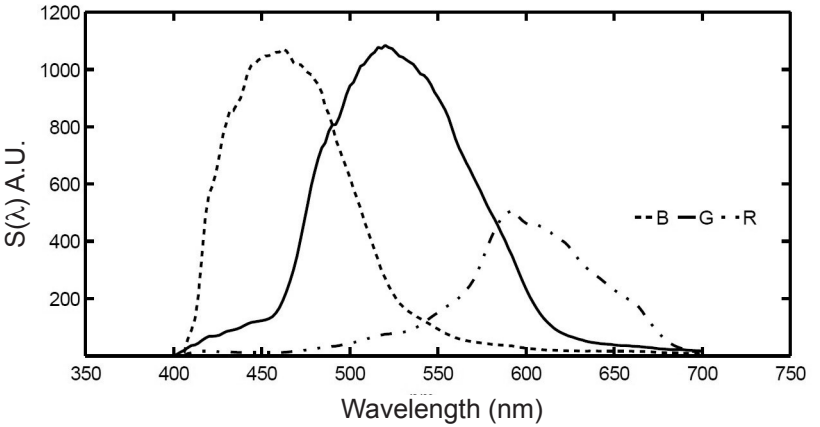

Figure 1. Photonic response of the RGB channels of the Canon 450D DSLR (arbitrary units proportional to S(λ) of equation 10).

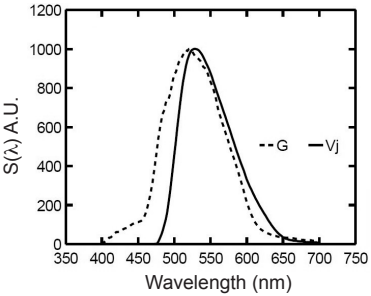

Figure 2. Photonic response of the Johnson VJ passband compared to the DSLR green (G).

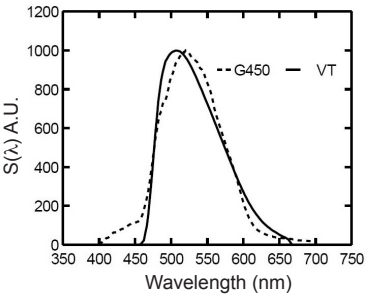

Figure 3. Photonic response of the Tycho VT passband compared to the DSLR green (G).

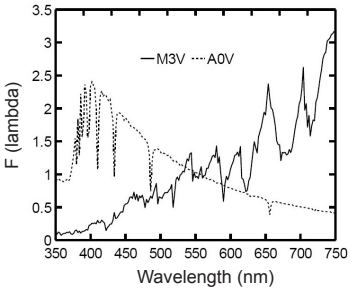

Figure 4. Pickles library (Pickles 1998), samples of M3V and A0V stars of the 131 spectra normalized at 555.6 nm. Spectra are in energy density per wavelength (nm).

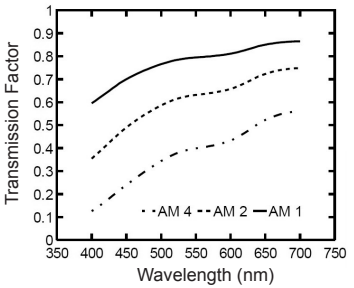

Figure 5. Transmission factor of the atmosphere at airmasses 1, 2, and 4, computed from the solar energy density (Desvignes 1991). The extinction coefficient is 0.23 at 550 nm.

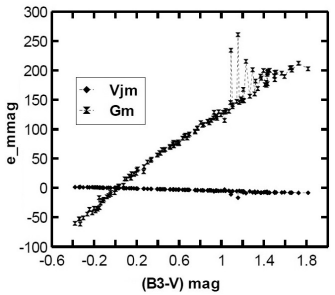

Figure 6. Johnson's Vjm and DSLR Gm magnitude deviation, without correction, at airmass 1 under the Johnson's system. Vjm is normalized at airmass 0.The Gm errors are 11 times those of Figure 7.

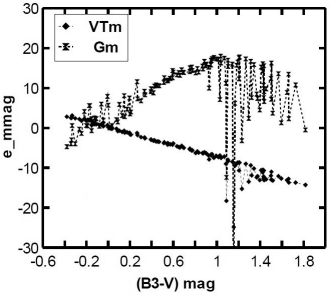

Figure 7. Tycho VTm and DSLR Gm magnitude deviation, without correction, at airmass 1 under the Tycho system. VTm is normalized at airmass 0. The outliers are M stars and a couple of K stars.

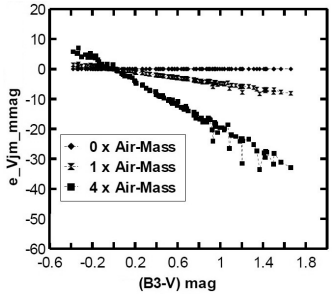

Figure 8. e_Vjm magnitude deviation of the VJ passband at airmass 0, 1, and 4, under the VJ photometric system. The results shown are those of the 110 O-to-K spectra of the library.

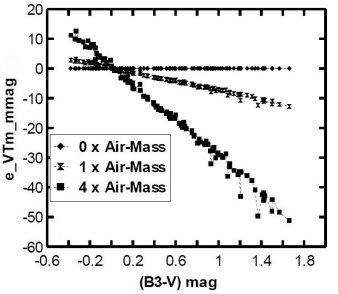

Figure 9. e_VTm magnitude deviation of the VT passband at airmass 0, 1, and 4, under the VT photometric system. The results shown are those of the 110 O-to-K spectra of the library.

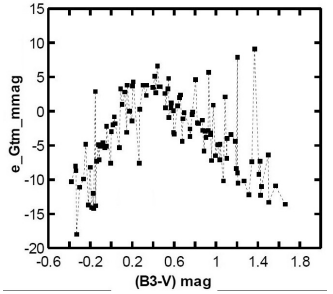

Figure 10. e_Gtm deviation of the CSIS transformation of the Gm DSLR channel to Johnson's Vjm at airmass 1.

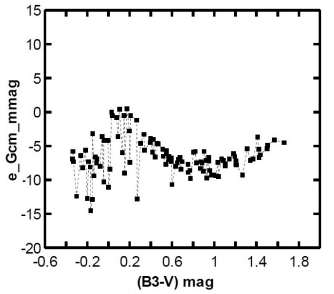

Figure 11. e_Gcm deviation of the VSF filter of the DSLR against Johnson's Vjm at airmass 1.

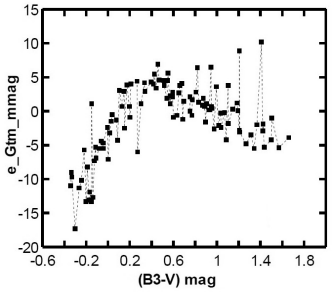

Figure 12. e_Gtm deviation of the CSIS transformation of the Gm DSLR channel to Johnson's Vjm at airmass 4.

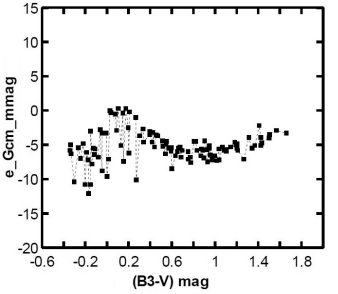

Figure 13. e_Gcm deviation of the VSF filter of the DSLR against Johnson's Vjm at airmass 4.

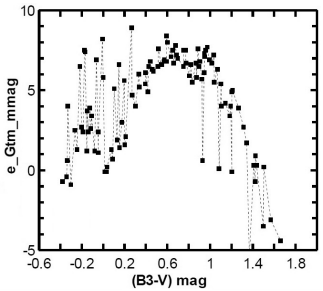

Figure 14. e_Gtm deviation of the CSIS transformation of the Gm DSLR channel to Tycho VTm at airmass 1.

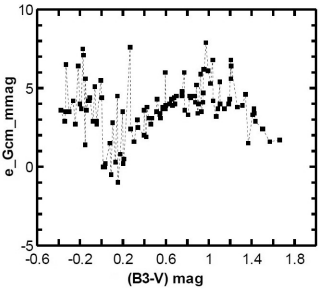

Figure 15. e_Gcm deviation of the VSF filter of the DSLR against Tycho VTm at airmass 1.

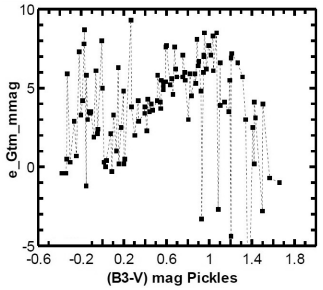

Figure 16. e_Gtm deviation of the CSIS transformation of the Gm DSLR channel to Tycho VTm at airmass 4. Outliers are few K stars.

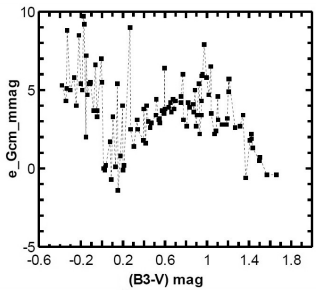

Figure 17. e_Gcm deviation of the VSF filter of the DSLR against Tycho VTm at

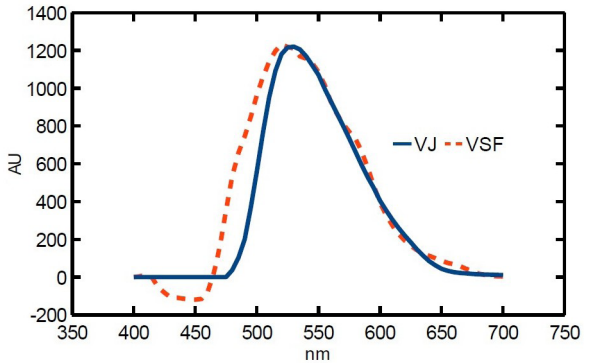

Figure 18. Response of the synthetic filter for a correction to VJ at airmass 0. This correspond to the correction of the DSLR alone. The DSLR R and B outputs are combined to G weighted with the coefficients "a" and "–b" from Table 1 (a = 0.34; b = 0.217). The resulting centroids of the two passbands keep within 1 nm in the –0.4~1.8 (B_3–V) range. The negative section in the blue provides a compensation of the residual excess of the blue roll-off of the VSF. It works like a complementary transformation.

Algorithms + Observations = VStar

David Benn
73 Second Avenue, Klemzig, South Australia; dbenn@computer.org

Received May 15, 2012; accepted June 25, 2012

Abstract VSTAR is a multi-platform, free, open source application for visualizing and analyzing time-series data. It is primarily intended for use with variable star observations, permitting light curves and phase plots to be created, viewed in tabular form, and filtered. Period search and model creation are supported. Wavelet-based time-frequency analysis permits change in period over time to be investigated. Data can be loaded from the AAVSO International Database or files of various formats. VSTAR's feature set can be expanded via plug-ins, for example, to read Kepler mission data. This article explores VSTAR's beginnings from a conversation with Arne Henden in 2008 to its development since 2009 in the context of the AAVSO's Citizen Sky Project. Science examples are provided and anticipated future directions are outlined.

1. Introduction

A conversation with AAVSO Director Arne Hendon at the 23rd National Australian Convention of Amateur Astronomers (NACAA) in 2008 planted the seed for a successor to Grant Foster's DOS-based VSTAR program (Figure 1), initially created for use with the AAVSO's *Hands-on Astrophysics* educational material, later renamed *Variable Star Astronomy*. The motivation for the author was simple: the opportunity to develop an easy to use, powerful data visualization and analysis tool that amateur and professional astronomers would want to use.

Correspondence over the next year culminated in AAVSO staff (including Aaron Price, Arne Henden, and Sara Beck) coming up with an initial specification for a new Java-based multi-platform (WINDOWS, MAC OS X, LINUX, OPENSOLARIS) implementation of VSTAR. Regular communication with Sara Beck commenced in May 2009. Since then, VSTAR development has consumed most of the author's spare time, family and other commitments permitting, and brought a group of passionate people together.

2. Feature overview

Fundamentally, VSTAR's purpose is to permit time series data (ostensibly variable star observations) from a variety of sources to be loaded and analyzed. The initial specification called for data to be loaded from the AAVSO International Database (AID), files conforming to the AAVSO Download

File format, and a simple subset of the latter for personal observations (JD, magnitude, and optionally: error, observer code, and validation flag).

Apart from light curve and phase plot creation, the loaded dataset can be viewed and searched in tabular form. Selection of an observation on a light curve or phase plot is synchronized with observation table row selection, and the reverse is also true. Lists of favorite AID objects can be created. Discrepant observations can be excluded and/or reported to AAVSO Headquarters.

Observation bands can be displayed or hidden through a plot control dialog, which also affects what is seen by default in the observation table. Simple filters can be defined to yield a new series for analysis and the observation table can be searched using regular expressions. See Figures 2 and 3 for examples of different views. Plots can be zoomed and panned. The usual print and save functions are provided.

Binned means can be created for the raw light curve or phased data. Error bars for means and observations can optionally be displayed. An information window shows a breakdown of the loaded dataset by band and a "signal significance" statistic in the form of ANOVA for the band that is the current source for binned means.

The other broad category of functionality is analysis. The first sub-category is period analysis. In VSTAR, this is an implementation of the Date Compensated Discrete Fourier Transform (DCDFT) algorithm (Ferraz-Mello 1981), yielding a power spectrum and table of "top-hits" for a specified series, frequency or period range, and resolution.

From within the DCDFT result window, a phase plot can be created. In addition, one or more periods each with one or more harmonics can be selected to create a model. A model's Fourier coefficients can be viewed along with relative amplitudes and phases. Multiple periods can optionally be refined via the CLEANest (Foster 1995) algorithm. When a model is created, it is also subtracted from the series on which the DCDFT was performed to yield a second, "residuals," series. DCDFT can then be applied to these residuals to look for further signals (periods), a process often called "pre-whitening." See Figure 8 for a sample DCDFT power spectrum and phase plot resulting from a top-hit selection.

The second major analysis capability is time-frequency analysis in the form of the Weighted Wavelet Z-Transform (WWZ; Foster 1996). The user specifies a series, period or frequency range, and resolution, and an analysis of change in period over time is the result. This can be viewed as a 2D graph, a contour plot, a rotatable 3D graph, or in tabular form. Periods can be selected for phase plot creation. Figure 4 shows period change for T UMi between 1913 and 2009. Here the color represents the WWZ statistic, the strength of a periodicity, at a particular time. This example is discussed in Foster (2010).

Another kind of model that can be created is a polynomial fit, along with the corresponding residuals series (for example, for finding the minimum or

maximum magnitude in a cycle of a Mira dataset). Figure 5 shows a polynomial fit of degree 7 for o Cet in the JD range 2451460 to 2451560 along with a 5-day binned means series. The cross-hairs are on the highest point of the curve, at a magnitude of around 3.315 and a JD of around 2451492.8. This example is based upon one found in Foster (2010).

VSTAR's in-built feature set can be enhanced by creating plug-ins (in JAVA). This will be elaborated on in another section. The beginnings of a scripting capability exist, permitting certain operations to be automated.

3. Early development

The original specification led to an initial round of questions. A key decision early on was to move the content from a WORD document to a Wiki (initially hosted by AAVSO). This facilitated a dialogue between the author and the AAVSO through Sara Beck, resulting in the Wiki being annotated with questions and answers. By the end of May 2009, a set of requirements was created that determined what would be developed during phase one.

It was decided that the project would be hosted on SourceForge. AAVSO staff member Richard Kinne helped establish this and argued that VSTAR should be licensed under the Affero GNU Public License, a web-deployment-friendly version of the normal GNU Public License. Feedback on early user interface prototypes was sought from AAVSO staff members.

It was rewarding to reach the point at which VSTAR could be used to load a dataset (for δ Cep) and create a phase plot. Although a simple feature, it was at this point that the author began to glimpse how powerful a tool like this could be.

4. Citizen Sky team

Leading up to the first Citizen Sky workshop in 2009, the VSTAR Software Development team became the first Citizen Sky project, facilitated by Rebecca Turner.

In July 2009, Michael Umbricht, an astronomer at Brown University's Ladd Observatory, contacted the author through Citizen Sky to say that he wanted to help on the project as a tester. After about three months of initial development, Michael's domain knowledge and early feedback on the proto-VSTAR was valuable. Leading up to the first workshop and for quite a few months thereafter, Michael played a key role in testing, promoting VSTAR, and trialling it in a classroom setting.

Soon after the first workshop (around September 2009) Adam Weber joined. He and the author had worthwhile design and implementation discussions. Adam contributed a number of bug fixes and helped to improve the look and feel of VSTAR, especially under MAC OS X.

Nico Camargo, a young artist living in Chicago, attended the first Citizen

Sky workshop and we corresponded afterward. He has played an important role in improving VSTAR's appearance by creating toolbar button and desktop icons. His willingness to help, often at short notice, has been much appreciated.

Over the lifetime of the project numerous people have expressed interest in contributing. Following through was not always possible due to other commitments or because the time and effort required to learn enough about the existing code base to make a contribution was prohibitive. Many who did not directly contribute to development or test often still provided suggestions or encouragement. The Citizen Sky VSTAR development team forum captures the team's interactions. Testing and documentation are not especially popular and it was not generally easy to interest people in these activities. As the team size grew, communication overheads rose, with less time available to the author for software development, compared with the frenetic pace of the first few months. Overheads reduced as the team stabilized.

The most important aspect of the team was the confluence of diverse skills, knowledge, and experience. As lead developer, the author could defer to others with greater domain expertise or artistic skill. Communication media such as Wiki, instant messaging, email, and occasional calls largely compensated for the distance across the Pacific separating the author from most of the team. Questions left with Sara and other team members would often be answered during the author's night. An AAS poster paper covers the team aspect in more detail (Henden *et al.* 2010).

5. Workshops and talks

5.1. Citizen Sky 1

The first Citizen Sky workshop, held at the Adler planetarium in Chicago in August 2009, was an opportunity to receive early feedback from a broader audience about the early implementation of VSTAR. Feedback from Arne Henden and others led to improvements and bug fixes before the first internal deployment to the Citizen Sky VSTAR development team on November 13, 2009.

5.2. NACAA 2010 workshop

The National Australian Convention of Amateur Astronomers (NACAA) is held every two years and has already been mentioned in relation to its role in getting VSTAR started in 2008. Two years later the author ran a full-day workshop at the 24th NACAA. Version 2.0 was released and announced on the AAVSO website in conjunction with that event.

Feedback from Australian and New Zealand amateurs and members of Variable Stars South (VSS) led to several new SourceForge tracker items. It also reinforced to the author certain user interface changes that would improve the end user experience, primarily by increasing the amount of real estate for plots and tables in the main window and moving secondary functions to dialogs (see Figures 6 and 7).

5.3. Citizen Sky 2

At the second Citizen Sky workshop, held at the California Academy of Sciences, San Francisco, in September 2010, the author gave a presentation showing how VSTAR could be used to carry out period analysis, minima identification with a polynomial fit, and an overview of other capabilities added since 2009. Again, the resulting feedback was important for improving the tool.

Leading up to this workshop, Aaron Price created the "5 Star Tutorial" for data analysis, a companion to the Citizen Sky "10 Star Tutorial," for observation of variable stars. The 5 Star Tutorial showed how to use VSTAR to create a binned means series, carry out period search with DCDFT, and create phase plots.

Heinz Bernd-Eggenstein was present at the workshop and showed the author a bug in which VSTAR misbehaved with numeric input in the presence of a German locale being set on the host operating system. Fixing this seemingly simple problem took some weeks after the workshop. Additional locale improvements are on the roadmap, such as providing language specific (for example, German, Spanish, and Portuguese) versions of VSTAR.

5.4. NACAA 2012 update

Four years after the initial conversation with Arne Henden, a talk and demonstration of progress since the 2010 full day workshop was given at the 2nd Variable Stars South Colloquium held in conjunction with the 25th NACAA in Brisbane.

Time spent during breaks with VSS members, in particular Mark Blackford, David Moriarty, Alan Plummer, and Tom Richards, was beneficial as we talked about their use of VSTAR. For example, the need for an ASAS data source plug-in was expressed.

6. From FORTRAN to JAVA

Even before development of VSTAR had begun, Matthew Templeton pointed the author to a paper about the DCDFT algorithm (Ferraz-Mello 1981). Grant Foster had previously written an implementation of DCDFT in BASIC which was subsequently converted to a FORTRAN version by Matthew as part of AAVSO's TS console-based program.

When the time came to implement DCDFT for VSTAR, there were a few choices:

- Implement DCDFT purely based upon the published literature.
- Convert the FORTRAN TS code to JAVA. The author experimented with FORTRAN to JAVA translators, but at the time, none was found to be without important bugs.

- Convert the FORTRAN TS code to C and call from VSTAR as "native methods."
- Convert the FORTRAN TS code to C and then to JAVA.

FORTRAN to C translators exist, in particular F2C. This was made use of in order to be able to source-level debug the TS code in C form when possible bugs in the FORTRAN code were found. The code generated by such translators tends to be cryptic and have dependencies upon special libraries. Calling C code through JAVA's native interface mechanism would have required natively compiled libraries for each operating system, somewhat antithetical to VSTAR's generally platform-independent implementation.

Other than this, there are sufficient incompatibilities between the console and text menu driven nature and data structures of the TS program compared with VSTAR's internals and user interface, that in the end, a mixture of the first and second options was employed.

First, the appropriate literature was read to get an understanding of DCDFT (Ferraz-Mello 1981). Next, a PERL script was written to perform a partial translation of the TS FORTRAN code into JAVA. Next, each line of emitted JAVA code was inspected for logical equivalence with the FORTRAN code. The core algorithms were translated and extracted in this way and exposed to the rest of VSTAR through the appropriate menu items and dialog boxes. For testing purposes, TS was treated as a reference implementation for DCDFT. Unit tests were written for the JAVA implementation of the algorithm and checked (automatically, after some initial manual checking) against the results generated by TS for the same input. The same strategy was used to implement and test WWZ in VSTAR.

There is a difference in emphasis between implementing and testing algorithms from a publication such as Meeus (1991)—which was used for JD calculations in VSTAR—and doing so from the literature. The purpose of a book such as Meeus is to unambiguously describe an algorithm and provide at least minimal test cases. A paper that describes an algorithm does not have quite the same obligation. Hence the approach of using "battled-tested" FORTRAN as a reference implementation and semi-automated translation as opposed to writing from scratch from the literature, while making use of it to bolster understanding of the algorithm. In the end, the key benefit is that the powerful functionality of the FORTRAN TS and WWZ code has been made available in VSTAR, and along the way, some bugs were uncovered in the original FORTRAN code.

7. Plug-ins

VSTAR plug-ins can be created using the JAVA programming language (or in fact, any language that can be compiled to JAVA VIRTUAL MACHINE class files) in order to:

- Load observations from an arbitrary source.
- Perform a custom dataset filtering operation.
- Implement a new period analysis algorithm.
- Carry out an arbitrary operation on the loaded dataset.
- Create a general purpose tool.
- Implement a model creation tool.

Perhaps not too surprising is that observation source plug-ins have so far been the most commonly written or requested, since this makes it possible to load datasets from more diverse sources than those defined by the AAVSO.

To date, observation source plug-ins have been written for Kepler mission public data release FITS files and SuperWASP survey FITS files. Both of these were written in collaboration with Doug Welch. Other users such as Ken Mogul and Alan Plummer prompted the development of an AAVSO simple and extended upload file format observation source plug-in. This format can be hand-crafted or generated by an application such as VPHOT for use in uploading multiple observations to the AAVSO International Database. Some plug-ins, if commonly used like this one, may eventually be added into the core of VSTAR's code base.

An example of the second category was a plug-in written by Sara Beck to show which observations in a loaded dataset were made by observers in, for example, Ireland.

As far as the author is aware, no period analysis plug-ins have been written yet, but two candidates are AoV (Schwarzenberg-Czerny 1989) and Fast Chi-squared (Palmer 2009). Internally, DCDFT and WWZ are treated as plug-ins, implementing the required interfaces, the only difference being that they are not dynamically loaded when VSTAR starts.

An example of the "arbitrary operation" plug-in type was created by the author when AAVSO member Mike Simonsen expressed a need to select datapoints on a light curve plot to determine mean time between selected observations (along with mean magnitude). An example of the last plug-in category is a JD to calendar date calculator. The VSTAR plug-in library (http://www.aavso.org/vstar-plugin-library) and the VSTAR webpage (http://www.aavso.org/v-star-overview) can be consulted for more information.

8. Deployment

JAVA WEBSTART™ is the deployment mechanism used when launching VSTAR from the AAVSO web page and remains the easiest way to begin using VSTAR. WEBSTART™ imposes "security constraints" similar to that imposed by a JAVA applet. It took some time to make VSTAR work properly within these constraints, especially in the presence of dynamically loaded plug-ins.

For each formal release, there were one or more testing releases made available to the Citizen Sky team through WEBSTART™. Each formal release has been accompanied by a downloadable archive (from SourceForge) that can be unzipped and run as a normal local application. More recently, operating-system specific launcher programs/scripts were added to improve the local run-time experience, in particular by making start-up memory allocation equivalent to the WEBSTART™ deployment and by adding a desktop icon for DOS/WINDOWS and MAC OS X.

9. Science examples

This section gives brief examples of how VSTAR has been used for Citizen Science. These examples are not exhaustive, but they are representative.

9.1. Cepheid identification

In an example of professional-amateur collaboration, amateur astronomer Ken Mogul has partnered with Doug Welch, a professional astronomer at McMaster University, on a long-term project using the robotic telescope network AAVSOnet to obtain high-quality photometric time series of Type 2 Cepheids in Sloan griz filters. Ambiguously classified variables (CEP, CEP:) were also included to ensure that their classifications could be improved (Welch 2012). VPHOT is used to process images and VSTAR is used to help eliminate targets that don't meet the project criteria. In Ken's words: "I have also been able to data mine the data for new variables outside the goal of the project. VSTAR has enabled me to make intelligent suggestions to the professional on what to look at and what to dismiss thereby saving the professional time to focus on the big picture" (Mogul 2012).

By using VPHOT and VSTAR together, Ken was easily and quickly able to first reduce the data for every other star, apart from the original target, in the field-of-view being studied, to look for possible variability. Then VSTAR's DCDFT and phase plot features (see Figure 8) enabled him to immediately phase the data into a classification-revealing light curve, such as in the example in Figure 8 of star 2MASS J03145502+5618172 (Mogul 2012). Ken was also able to reclassify GV Aur as a Classical Cepheid as shown in Figure 9.

Again, in Ken's words: "Eventually with enough data, VSTAR will enable me to be at the center of the action conceptually, without my having to spend a great effort to learn and understand things like IRAF. These tools are a shining example of how to make citizen science a viable force going forward. AAVSOnet, VSTAR and VPHOT have enabled me, with no equipment…to go from observing to organizing to analyzing and drawing useful conclusions…with only a computer and Internet connection…a possibility which was almost unimaginable even a decade ago, except to the very far sighted" (Mogul 2012).

9.2. Kepler data mining

Using VSTAR's Kepler data source plug-in and DCDFT and phase plots, Kevin Alton has explored eclipsing variable star systems observed by the Kepler spacecraft, looking for changes in minima/maxima across cycles. According to Kevin, this is a prelude to potentially mapping magnetic activity cycles and/or starspot migration in selected contact binaries (Alton 2012).

9.3. Long term ε Aurigae light curve

Brian Kloppenborg has used VSTAR's WWZ feature to look for changing or multiple periods in ε Aur's long-term photometric archive light curve. Brian commented that nothing has been found so far, as others before him have discovered (Kloppenborg 2012). Brian's use of WWZ exposed a bug in the FORTRAN and JAVA implementation (in the presence of significant gaps in the data). This is now on the inevitable list of things to fix.

9.4. Light curves for illustration in articles

Articles containing light curves saved from VSTAR have appeared in *Australian Sky & Telescope* by VSS member Alan Plummer and by others in VSS newsletters and elsewhere.

9.5. Mira Fourier coefficient team (Citizen Sky)

Apart from acting as a testing ground for DCDFT, Fourier series modelling, and WWZ in VSTAR, the Citizen Sky Mira Fourier coefficient team needed to bulk-download around 400 Mira datasets of fixed duration from the AID. VSTAR can be scripted (only through JAVASCRIPT currently) to automate some operations, such as data file or AID dataset loading. This feature was used to bulk download these Mira observation datasets.

9.6. Period search and phase plots

As part of learning about variable star photometry and analysis in his work on the SPADES project (Richards 2012), VSS member David Moriarty has carried out period search with VSTAR on photometric data obtained for the contact eclipsing binary system TW Cru and compared it to period and epoch values found in GCVS, Dvorak, and Krakow repositories.

10. Future directions

Although still under active development, VSTAR is already proving to be a useful tool for activities ranging from simply exploring light curves in AID to analyzing photometric data so as to determine a star's period. The initial goal for VSTAR was to create a free, easy-to-use tool for basic variable star observation visualization and analysis. User anecdotes suggest that this has been achieved.

Much has been done, but there is still plenty to do. What follows gives some indication of VSTAR's future:

• Parallelization of DCDFT and WWZ to make use of multi-core machines with concurrent JAVA threads mapping to cores.

• Memory footprint reduction. For example, each observation data-point is represented by an object that consumes more memory than it should. Addressing this will permit larger data sets to be loaded.

• Better documentation, in the form of a user manual as opposed to the current minimal Help menu item and occasional articles.

• More analysis features, for example: time of minimum/maximum, for example, for eclipsing binary epoch determination; alternatives to DCDFT, such as AoV and Fast Chi-Squared. These can also be developed by others as plug-ins; O–C analysis; Lowess fit, for example, for minima determination (Foster 2010).

• AAVSO download files can be generated as lines of comma-, tab-, or space-separated values. Unless values are quoted, ambiguity is possible (for example, commas in comments fields). This has been flagged as an issue and will be pursued since some files contain lines that cannot be unambiguously parsed by VSTAR (or any tool), so must be omitted at load time and reported as erroneous to the user.

• Permit toggling between magnitude and flux values for particular kinds of analysis.

• Make plug-in installation and management a less manual process.

• Improve the quality of plots for publication.

• Localization (for example, Spanish, German, Portuguese, or Persian).

• Increasing the power of models, for example: addition of arbitrary terms, such as for observer bias (as permitted by TS); making it easier to accumulate periods throughout the process of pre-whitening for subsequent model creation; merging two or more existing models; model creation from WWZ.

• Although plug-ins can be created to perform arbitrary filtering operations, the current in-built filtering capability is limited to the equivalent of an expression language over a subset of an observation's fields, supporting conjunction (logical AND), relational operations (>, <, =, <=, >=), and negation. This could be made more powerful by permitting expressions containing disjunctions (logical OR) and allowing all observation fields to be used.

• The scripting API should grow to permit more operations to be automated.

- Replacement of direct AID database access with a web service. This would also open up programmatic access to AID to a broader range of applications and devices, but this is something that cannot be done in isolation and is a decision for AAVSO since it has infrastructure implications.
- Other data source plug-ins, such as for ASAS.
- Bug fixes! See the SourceForge tracker for these, the issues above, and others besides (https://sourceforge.net/projects/vstar).
- In general, the SourceForge tracker and change log (updated each release) will continue to document the process of change.

11. Acknowledgements

The author would like to thank Arne Henden and Aaron Price for getting it all started and for ongoing encouragement; and Sara Beck for mentoring, being an AAVSO liason, and providing regular support and enthusiasm. Rebecca Turner has been supportive as Citizen Sky project manager. Doc Kinne provided system administration support, helped establish the SourceForge project site, and sort out license issues. Matthew Templeton patiently answered questions about algorithms. All provided encouragement.

Michael Umbricht, Adam Weber, Nico Camargo, Heinz Bernd-Eggenstein, Jaime Garcia, Doug Welch, Ken Mogul, and Mike Simonsen—VSTAR team members and users—provided feedback, assistance, testing, and encouragement. Thanks also to Grant Foster for writing his light curve analysis book (Foster 2010), introducing me to the R statistical analysis language, and for helpful technical discussions. These people have given generously of their time and talents in response to my questions.

Members of VSS have also provided encouragement, advice for future directions, and better still, have made use of it in their research (for example, Mark Blackford and David Moriarty).

A little more than two years after the VSTAR project started, I received email from Arne Henden to say that I was the recipient of the 2011 AAVSO Director's Award. Considering the previous recipients of this award, I am honored and humbled to have received this. Members of the VSTAR team, and others, helped to make this possible.

My supportive wife Karen and children Nicholas and Heather have become very tolerant of their husband's/father's nocturnal nature, especially over the last few years. Nicholas also helped with the DOS/WINDOWS launcher.

The author greatly appreciates the opportunity to develop VSTAR, to participate in the Citizen Sky and AAVSO communities, and to attend both Citizen Sky workshops.

The title for this paper was inspired by a 1976 book by computer scientist Niklaus Wirth—*Algorithms + Data Structures = Programs.*

On behalf of the AAVSO and the Citizen Sky Project, the author also gratefully acknowledges grant 000379097 from the National Science Foundation.

References

Alton, K. 2012, private communication.
Ferraz-Mello, S. 1981, *Astron. J.*, **86**, 619.
Foster, G. 1995, *Astron. J.*, **109**, no 4, 1889.
Foster, G. 1996, *Astron. J.*, **111**, 1, 555.
Foster, G. 2010, *Analyzing Light Curves, a Practical Guide* (http://www.lulu.com/shop/grant-foster/analyzing-light-curves-a-practical-guide/paperback/product-11037112.html).
Henden, A., Benn, D., Beck, S., Price, A., and Turner, R. 2010, *Bull. Amer. Astron. Soc.*, **42**, 510.
Kloppenborg, B. 2012, private communication.
Meeus, J. 1991, *Astronomical Algorithms*, Willmann-Bell, Richmond, VA.
Mogul, K. 2012, private communication.
Palmer, D. M. 2009, *Astrophys. J.*, **695**, 496.
Richards, T. 2012, "Search for Planets Around Detached Eclipsing Systems," (SPADES; http://www.variablestarssouth.org/index.php?option=com_content&view=article&id=59&Itemid=49).
Schwarzenberg-Czerny, A. 1989, *Mon. Not. Roy. Astron. Soc.*, **241**, 153.
Welch, D. 2012, private communication.

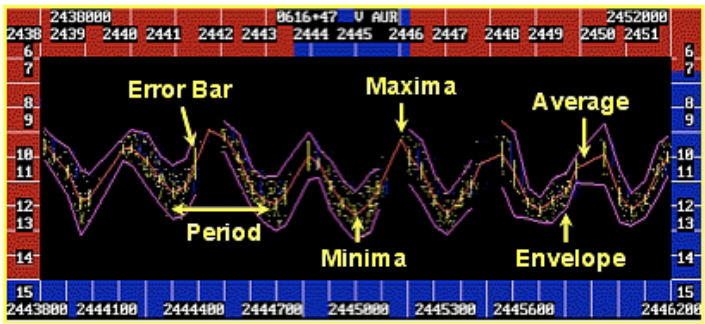

Figure 1. Grant Foster's original DOS-based VSTAR (provided by AAVSO).

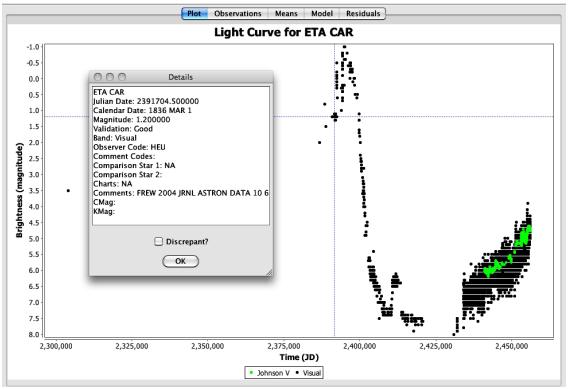

Figure 2. A plot of η Car, an observation selected in the cross-hairs, and a detail dialog.

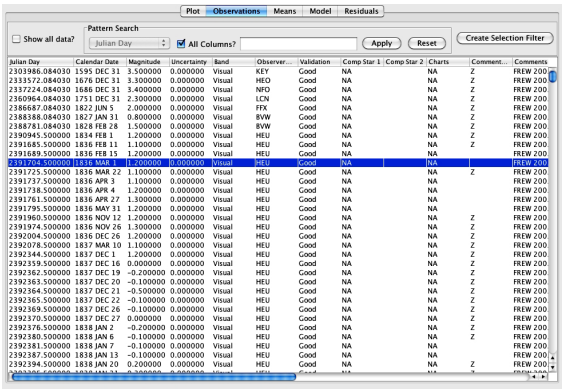

Figure 3. The tabular view of the η Car dataset shown in Figure 2 with the same observation row selected.

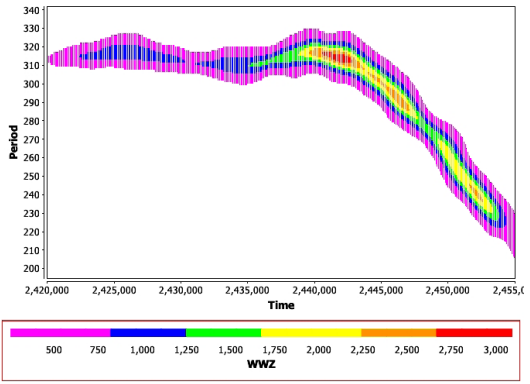

Figure 4. WWZ plot for T UMi showing period change over almost a century.

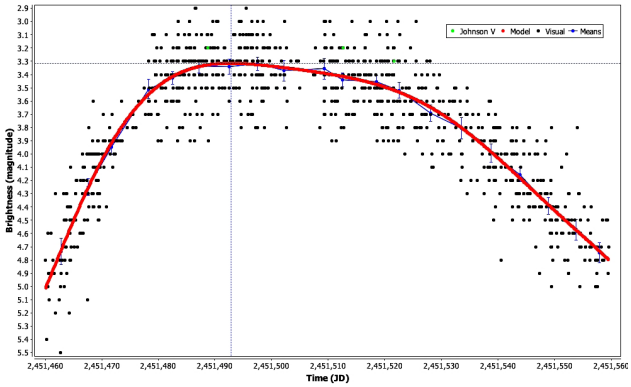

Figure 5. A polynomial fit of degree 7 for o Cet with 5-day binned means.

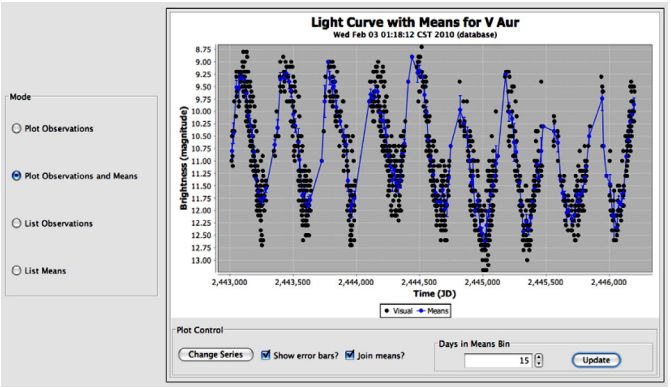

Figure 6. A screen-shot of VSTAR at the time of NACAA 2010.

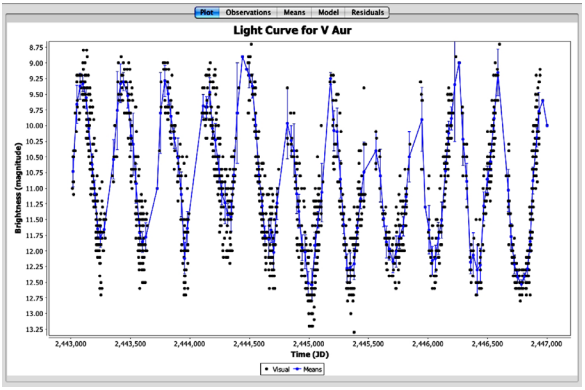

Figure 7. VSTAR's modified interface as it has become since NACAA 2010.

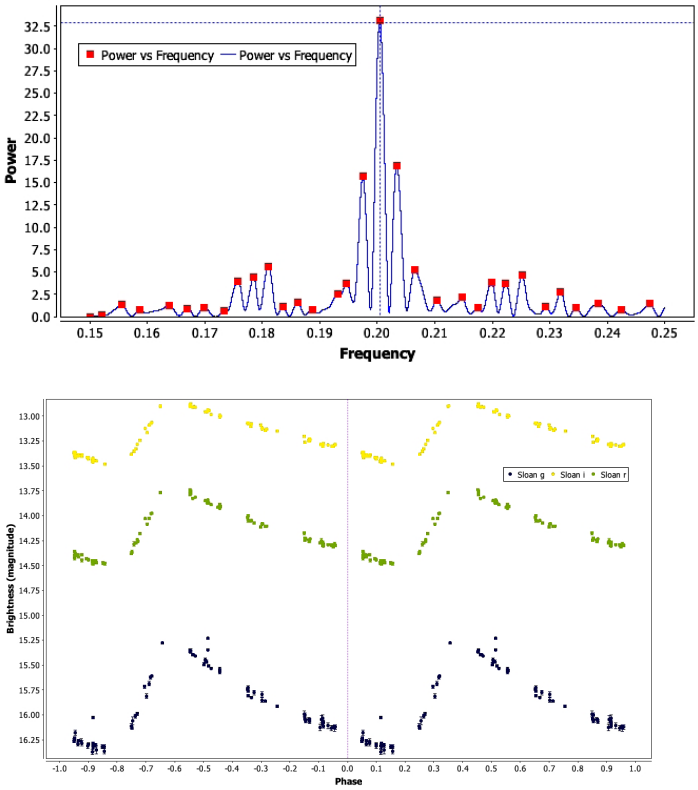

Figure 8. A VSTAR DCDFT power spectrum (upper panel) and phase plot (lower panel) resulting from top-hit period, for 2MAS J03145502+5618172.

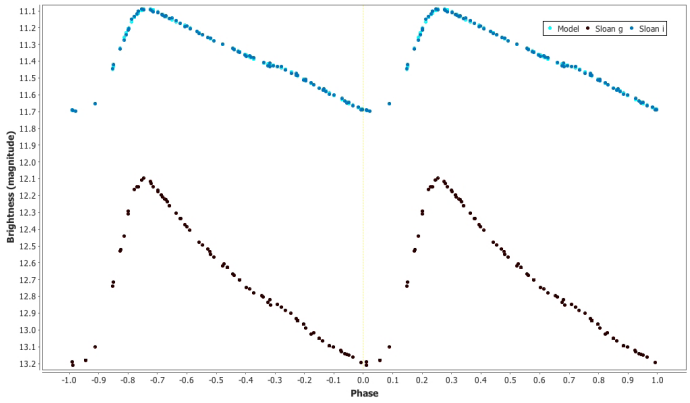

Figure 9. Phase plot for GV Aur resulting from DCDFT period analysis.

An Artist's Note on Art in Science

Nico Camargo
4233 N. Hermitage Avenue, #3A, Chicago, IL 60613; nicocamarg@yahoo.com

Received May 14, 2012; revised October 22, 2012

Abstract I decided to write about art in science by telling personal anecdotes surrounding my involvement in astronomy. These portray what drove me (with a career in the Fine Arts) to try scientific illustration through involvement in the American Association of Variable Star Observers' Citizen Sky project to observe the eclipse of ε Aurigae. These accounts define what I believe to be at the core of being a scientific illustrator: the importance of maintaining accuracy and factual detail without compromising the compelling visuals that evoke curiosity. This, as most people realize, is an important factor in being able to successfully engage the public in science—particularly in astronomy. However, my intention in telling these anecdotes goes deeper than stating the importance of disseminating scientific knowledge through imagery—for which ample examples and literature already exist. Instead, I'm really after contrasting the role of a science illustrator versus that of an artist. In doing so, I will underscore what I believe illustrating phenomena in science really is all about. This note is not intended as a scholarly treatise but rather personal reflections relative to my involvement in Citizen Sky.

1. My introduction to astronomy

On one summer morning in 2009, while I was preparing to begin a painting, I played a daily podcast I sometimes listened to, called 365 Days of Astronomy. That day, a welcoming voice was saying something about an organization called Citizen Sky. She proceeded to describe what was known, at that time, about a peculiar star system in the constellation of Auriga, which had been shrouded in mystery for hundreds of years. Then, she went on to explain that this celestial speck, dubbed ε Aurigae, would be visible by the unaided eye (even under city lights), and most interestingly would be undergoing an eclipse lasting about two years. Because this event only happens every twenty-seven years, she urged the public to assist her organization by collaborating in any relevant way to achieve its mission—to find out more about this star's strange disc-like companion as it transits across said star. As I became intrigued with this weird eclipsing binary system, the narrator mentioned that Citizen Sky would be having a workshop at the Adler Planetarium in Chicago (just a couple of miles from where I lived), and called on those who wished to learn more about ε Aur to help the astronomy community understand this rare phenomenon. I marked my calendar, and when the date came, I eagerly jumped on the train each morning for what would be a

fun weekend of lectures and conversations with passionate, bright individuals trying to set up an unprecedented campaign of observations during the next 640–730 days of eclipse.

My enthusiasm for astronomy was entrenched in curiosity about how the universe works. Very early recollections of Carl Sagan's *Cosmos* and the STS *Challenger* disaster on television are embedded in my memory to this day and had impacted the way I view science. Particularly space exploration intrigued me—from the standpoint of human achievement and engineering advancement—because it was a common topic at the dinner table growing up. That famous image of an astronaut wearing a jet-pack, floating alone in space above Earth, was in my grandfather's home office, and a late 1980s television mini-series about the Apollo missions cemented my utmost admiration, wonder, and thirst for learning about space and the universe. What all of these memories have in common is awe-inspiring imagery. Whether on television or in still pictures, these images, as well as many others (certainly some from science fiction movies as well) would stir my curiosity to learn about what is beyond our home.

Back in Chicago at the Adler Planetarium, I was soaking in all the information available about ε Aur: light curves from past observation campaigns, crude illustrations, data analyses; that, and much more information, provided several possibilities to illustrate what was presumed to be an eclipsing binary system that was just too far to be captured in photographic format—not even with our most powerful observatories. What ε Aur was remained a mystery awaiting resolution, and to me, this meant an opportunity to inspire others with my own space images—ones that would tell what would otherwise be a difficult-to-comprehend celestial conundrum. I met the podcast's voice, Rebecca Turner, and the rest of Citizen Sky crew that weekend and from that point on, I was committed to providing them with illustrations that would help to support their mission.

2. Nature has better imagination

In 2010 Citizen Sky met again, that time in San Francisco, to discuss progress on ε Aur's eclipse and analyses of new data. After lectures, once again, I engaged in conversations with head astronomers and experts on ε Aur to find out what the new leading hypotheses worth illustrating were. I wanted to depict exactly what they envisioned, or more appropriately, what the new information was telling them. About 2,000 light-years away, the only way to bring this eclipsing binary system to life is by imagining and illustrating it, and every new piece of the puzzle meant that we could have a more concrete idea of the system's objects. Evidence of the system's objects' approximate size, positioning, molecular composition, and shape already created an exact model of how ε Aur could look, however, there were new details that dismissed earlier hypotheses.

When I began illustrating ε Aur, I looked at earlier illustrations of the system, as well as ones of other similar systems. One had a black hole with spewing jets of energy coming from the middle of this companion disk—a compelling image that was negated by data confirming that there were no black holes in ε Aur. (That's not to say that impressive jets of energy spewing from black holes don't exist, or haven't been seen—they have.) Another ε Aur illustration had its visible star (what came to be recognized as a large F-type star) pulling mass from the obscure companion through the inner Lagrangian point and creating a disk of material if its own—that idea was also rejected after more solid data came to light. Again, trafficking material between two celestial objects that trespass their Roche Lobe does exist. My point is that at the time, it was anybody's guess what was going on in ε Aur, but as more knowledge was acquired, these guesses were appropriately marginalized. I was supposed to illustrate the new "guesses," and it was my duty to make an attractive image while keeping in mind that any extrapolation of my own would wrongly make the illustration become something other than ε Aurigae—just like the ones prior to mine, just like my first ones.

Today, my favorite eclipsing binary system remains much of a mystery despite hard-earned new data. Its dark, humongous disc-like component could be a planetary system in its infancy, or one in limbo that will never form planets due to gravitational pulls from its inside (where a small B star was found) and the F-star companion. ε Aur could end up being several surprising things (but not too many). However, these plausible surprises, I'm sure, will be fascinating. Nature has a way of revealing herself, in the most "out-there" of ways—she outdoes even science fiction flicks. From planets with four stars, to planetary formation itself, we should just illustrate natural phenomena as honestly as possible, since those images are certainly as (if not more) creative and imaginative than any artist could imagine.

3. Artwork created in support of Citizen Sky and the AAVSO

The work I did related to Citizen Sky and ε Aur was my first in scientific illustration and my first related to astronomy. Artwork I created on behalf of Citizen Sky and the AAVSO included:

- potential designs for the Citizen Sky logo
- seven depictions of the ε Aur system
- icons for the data plotting and analysis software VSTAR, a crucial element of Citizen Sky that is being used by variable star observers and analysts far beyond the original Citizen Sky audience
- illustration for a Citizen Sky participation certificate
- characters for a Citizen Sky comic strip

- illustration commemorating the receipt of the AAVSO's 20 millionth variable star observation
- October page in the American Astronomical Society's 2011 calendar, commemorating the AAVSO's centennial
- potential designs for the AAVSO logo

4. Not apples and oranges, more like apples and onions

As an emerging visual artist, I underwent an intentional shift from nebulous abstract conceptualism to the constrictions of imperative predestinarianism in picture-making. That shift effectively converted me into an illustrator for the time being. This duality must be addressed because, while the juxtaposition of these two different fields has provided an abundance of intellect and creativity in my art, one must understand the extents and limitations that these two fields impose on each other. To say that a scientific illustrator took some artistic liberties when rendering a natural phenomenon implies misdirection—such as fabrication of facts, exaggeration, and image entitlement, to name a few. Conversely, when an artist renders ideas as visual explanations of themselves, without context ambiguity, or abstraction of any kind, this artist becomes an illustrator.

There are certain things in the universe that can't be directly translated into visual form, so we use symbols, approximations, and the imagination. But, scientific illustrators fill in this gap, and they must derive their work from research and scientific hypotheses. A scientific illustrator has the obligation to explain a scientific subject concisely, thoroughly, and accurately, whether the medium is animation or illustration, and in doing so, he or she must excite the imagination without misleading the viewer.

Beauty and aesthetics are very important aspects of scientific imagery. Undoubtedly, science illustrators must make their subject matters visually attractive and unforgettable. That being said, scientific imagery should also be reserved, humble, and have an anonymous quality. It should be economic and focused solely on its depictions, without compromising on its scientific accuracy. Scientific illustrators are not making art; they are not making a personal statement; they are not trying to convey an idea indirectly or per ambiguities and insinuations, nor are they speaking about themselves, abstract concepts (like love or life), or society. Instead, they are providing a precise, hyper-realistic representation (as best as they can) of the physical world and its natural occurrences. Scientific illustrators have formal and conceptual constrictions and are obliged to capture the subject matter explicitly. The artistry in scientific imagery lies in how effective and well-executed the subject matter is, in order to make learning faster, easier, and more enjoyable.

My hope is for other creative individuals to follow the points I lay out in this note, and to remember that the essence of scientific illustration lies in the comprehension of knowledge.

JAAVSO Volume 40, Number 2— other papers received

BVRI Photometry of SN 2011fe in M101

Michael W. Richmond
Physics Department, Rochester Institute of Technology, 84 Lomb Memorial Drive, Rochester, NY, 14623; mwrsps@rit.edu

Horace A. Smith
Department of Physics and Astronomy, Michigan State University, East Lansing, MI 48824; smith@pa.msu.edu

Received March 19, 2012; revised April 4, 2012; accepted April 11, 2012

Abstract We present BVRI photometry of Supernova 2011fe in M101, starting 2.9 days after the explosion and ending 179 days later. The light curves and color evolution show that SN 2011fe belongs to the "normal" subset of type Ia supernovae, with a decline parameter $\Delta m_{15}(B) = 1.21 \pm 0.03$ mag. After correcting for the small amount of extinction in the line of sight, and adopting a distance modulus of $(m - M) = 29.10$ mag to M101, we derive absolute magnitudes $M_B = -19.21$, $M_V = -19.19$, $M_R = -19.18$, and $M_I = -18.94$. We compare the voluminous record of visual measurements of this event to our CCD photometry and find evidence for a systematic difference which depends on color.

1. Introduction

Supernova (SN) 2011fe in the galaxy M101 (NGC 5457) was discovered by the Palomar Transient Factory (Law *et al.* 2009; Rau *et al.* 2009) in images taken on UT 2012 Aug 24 and announced later that day (Nugent *et al.* 2011a). As the closest and brightest type Ia SN since SN 1972E (Kirshner *et al.* 1973), and moreover as one which appears to suffer relatively little interstellar extinction, this event should provide a wealth of information on the nature of thermonuclear supernovae.

We present here photometry of SN 2011fe in the BVRI passbands obtained at two sites, starting one day after the discovery and continuing for a span of 179 days. Section 2 describes our observational procedures, our reduction of the raw images, and the methods we used to extract instrumental magnitudes. In section 3, we explain how the instrumental quantities were transformed to the standard Johnson-Cousins magnitude scale. We illustrate the light curves and color curves of SN 2011fe in section 4, comment briefly on their properties, and discuss extinction along the line of sight. In section 5, we examine the rich history of distance measurements to M101 in order to choose a representative value with which we then compute absolute magnitudes. Using a very large set of visual measurements from the AAVSO, we compare the visual and CCD V-band observations in section 6. We present our conclusions in section 7.

2. Observations

This paper contains measurements made at the RIT Observatory, near Rochester, New York, and the Michigan State University (MSU) Campus Observatory, near East Lansing, Michigan. We will describe below the acquisition and reduction of the images into instrumental magnitudes from each site in turn.

The RIT Observatory is located on the campus of the Rochester Institute of Technology, at longitude 77:39:53 West, latitude +43:04:33 North, and an elevation of 168 meters above sea level. The city lights of Rochester make the northeastern sky especially bright, which at times affected our measurements of SN 2011fe. We used a Meade LX200 *f*/10 30-cm telescope and SBIG ST-8E camera, which features a Kodak KAF1600 CCD chip and astronomical filters made to the Bessell prescription; with 3 × 3 binning, the plate scale is 1.85 seconds per pixel. To measure SN 2011fe, we took a series of 60-second unguided exposures through each filter; the number of images per filter ranged from 10, at early times, to 15 or 20 at late times. We typically discarded a few images in each series due to trailing. We acquired dark and flatfield images each night, switching from twilight sky flats to dome flats in late October. The filter wheel often failed to return to its proper location in the R-band, so, when necessary, we shifted the R-band flats by a small amount in one dimension in order to match the R-band target images. We combined 10 dark images each night to create a master dark frame, and 10 flatfield images in each filter to create a master flatfield frame. After applying the master dark and flatfield images in the usual manner, we examined each cleaned target image by eye. We discarded trailed and blurry images and measured the FWHM of those remaining.

The XVista (Treffers and Richmond 1989) routines STARS and PHOT were used to find stars and to extract their instrumental magnitudes, respectively, using a synthetic aperture with radius slightly larger than the FWHM (which was typically 4" to 5"). As Figure 1 shows, SN 2011fe lies in a region relatively free of light from M101 (see also Supplementary Figure 1 of Li *et al.* 2011). As a check that simple aperture photometry would yield accurate results, we examined high-resolution HST images of the area, using ACS WFC data in the F814W filter originally taken as part of proposal GO-9490 (PI: Kuntz). The brightest two sources within a 5" radius of the position of the SN, R.A. = 14^h 03^m 05.733^s, Dec, = +54° 16' 25.18" (J2000) (Li *et al.* 2011), have apparent magnitudes of $m_I \simeq 21.8$ and $m_I \simeq 22.2$. Thus, even when the SN is at its faintest, in our final *I*-band measurements, it is more than one hundred times brighter than nearby stars which might contaminate our measurements.

Between August and November 2011, we measured instrumental magnitudes from each exposure and applied inhomogeneous ensemble photometry (Honeycutt 1992) to determine a mean value in each passband. Starting in December 2011, the SN grew so faint in the I-band that we combined

the good images for each passband using a pixel-by-pixel median procedure, yielding a single image with lower noise levels. We then extracted instrumental magnitudes from this image in the manner described above. In order to verify that this change in procedure did not cause any systematic shift in the results, we also measured magnitudes from the individual exposures, reduced them using ensemble photometry, and compared the results to those measured from the median-combined images. As Figure 2 shows, there were no significant systematic differences.

The Michigan State University Campus Observatory lies on the MSU campus, at longitude 05:37:56 West, latitude +42:42:23 North, and an elevation of 273 meters above sea level. The *f*/8 60-cm Boller and Chivens reflector focuses light on an Apogee Alta U47 camera and its e2V CCD47-10 back-illuminated CCD, yielding a plate scale of 0.56 arcsecond per pixel. Filters closely approximate the Bessell prescription. Exposure times ranged between 30 and 180 seconds. We acquired dark, bias, and twilight sky flatfield frames on most nights. On a few nights, high clouds prevented the taking of twilight sky flatfield exposures, so we used flatfields from the preceding or following nights. The I-band images show considerable fringing which cannot always be removed perfectly. We extracted instrumental magnitudes for all stars using a synthetic aperture of radius 5.4 seconds.

3. Photometric calibration

In order to transform our instrumental measurements into magnitudes in the standard Johnson-Cousins BVRI system, we used a set of local comparison stars. The AAVSO kindly supplied measurements for stars in the field of M101 (Henden 2012) based on data from the K35 telescope at Sonoita Research Observatory (Simonsen 2011). We list these magnitudes in Table 1; note that they are slightly different from the values in the AAVSO's on-line sequences which appeared in late 2011. Figure 1 shows the location of the three comparison stars.

The AAVSO calibration data included many other stars in the region near M101. In order to check for systematic errors, we compared the AAVSO data to photoelectric BV measurements in Sandage and Tammann (1974). For the five stars listed as A, B, C, D, and G in Sandage and Tammann (1974), which range $12.01 < V < 16.22$, we find mean differences of -0.013 ± 0.038 mag in B-band, and -0.009 ± 0.022 mag in V-band. We conclude that the AAVSO calibration set suffers from no systematic error in B or V at the level of two percent. Unfortunately, we could not find any independent measurements to check the R and I passbands in a similar manner.

In order to convert the RIT measurements to the Johnson-Cousins system, we analyzed images of the standard field PG1633+009 (Landolt 1992) to determine the coefficients in the transformation equations

$$B = b + 0.238\ (043) * (b - v) + Z_B \quad (1)$$

$$V = v - 0.077\ (010) * (v - r) + Z_V \quad (2)$$

$$R = r - 0.082\ (038) * (r - i) + Z_R \quad (3)$$

$$I = i + 0.014\ (013) * (r - i) + Z_I \quad (4)$$

In the equations above, lower-case symbols represent instrumental magnitudes, upper-case symbols Johnson-Cousins magnitudes, terms in parentheses the uncertainties in each coefficient, and *Z* the zeropoint in each band. We used stars A, B, and G to determine the zeropoint for each image (except in a few cases for which G fell outside the image). Table 2 lists our calibrated measurements of SN 2011fe made at RIT. The first column shows the mean Julian Date of all the exposures taken during each night. In most cases, the span between the first and last exposures was less than 0.04 day, but on a few nights, clouds interrupted the sequence of observations. Contact the first author for a dataset providing the Julian Date of each measurement individually.

The uncertainties listed in Table 2 incorporate the uncertainties in instrumental magnitudes and in the offset to shift the instrumental values to the standard scale, added in quadrature. As a check on their size, we chose a region of the light curve, $875 < JD - 2455000 < 930$, in which the magnitude appeared to be a linear function of time. We fit a straight line to the measurements in each passband, weighting each point based on its uncertainty; the results are shown in Table 3. The reduced χ^2 values, between 0.9 and 1.6, indicate that our uncertainties accurately reflect the scatter from one night to the next. The decline rate is smallest in the blue, but it is still, at roughly 130 days after explosion, significantly faster than the 0.0098 mag/day produced by the decay of ^{56}Co.

The MSU data were transformed in a similar way, using only stars A and B. The transformation equations for MSU were

$$B = b + 0.25\ (0.03) * (b - v) + Z_B \quad (5)$$

$$V = v - 0.08\ (0.02) * (b - v) + Z_V \quad (6)$$

$$I = i + 0.03\ (0.02) * (v - i) + Z_I \quad (7)$$

In the equations above, lower-case symbols represent instrumental magnitudes, upper-case symbols Johnson-Cousins magnitudes, terms in parentheses the uncertainties in each coefficient, and *Z* the zeropoint in each band.

Table 4 lists our calibrated measurements of SN 2011fe made at MSU. Due to the larger aperture of the MSU telescope, exposure times were short enough

that the range between the first and last exposures on each night was less than 0.01 day.

4. Light curves

We adopt the explosion date of JD 2455796.687 ± 0.014 deduced by Nugent *et al.* (2011b) in the following discussion. Figure 3 shows our light curves of SN 2011fe, which start 2.9 days after the explosion and 1.1 days after Nugent *et al.* (2011a) announced their discovery.

In order to determine the time and magnitude at peak brightness, we fit polynomials of order 2 and 3 to the light curves near maximum in each passband, weighting the fits by the uncertainties in each measurement. We list the results in Table 5, including the values for the secondary maximum in *I*-band. We again use low-order polynomial fits to measure the decline in the *B*-band 15 days after the peak, finding $\Delta_{15}(B) = 1.21 \pm 0.03$. This value is similar to that of the "normal" SNe Ia 1980N (Hamuy *et al.* 1991), 1989B (Wells *et al.* 1994), 1994D (Richmond *et al.* (1995), and 2003du (Stanishev *et al.* 2007). The location of the secondary peak in *I*-band, 26.6 ± 0.5 days after and 0.45 ± 0.03 mag below the primary peak, also lies close to the values for those other SNe.

Although there is as yet little published analysis of the spectra of SN 2011fe, (Nugent *et al.* 2011b) state that the optical spectrum on UT 2011 Aug 25 resembles that of the SN 1994D; on the other hand, (Marion 2011) reports that a near-infrared spectrum on UT 2011 Aug 26 resembles that of SNe Ia with fast decline rates and Δm_{15} (B) > 1.3. We must wait for detailed analysis of spectra of this event as it evolves to and past maximum light for a secure spectral classification, but this very preliminary information may support the photometric evidence that SN 2011fe falls into the normal subset of type Ia SNe.

We turn now to the evolution of SN 2011fe in color. In order to compare its colors easily to those of other supernovae, we must remove the effects of extinction due to gas and dust within the Milky Way and within M101. Fortunately, there appears to be little intervening material. Schlegel *et al.* (1998) use infrared maps of dust in the Milky Way to estimate $E(B–V) = 0.009$ in the direction of M101. Patat *et al.* (2011) acquired high-resolution spectroscopy of SN 2011fe and identified a number of narrow Na I D_2 absorption features; they use radial velocities to assign some to the Milky Way and some to M101. They convert the total equivalent width of all components, 85mÅ, to a reddening of $E(B–V) = 0.025 \pm 0.003$ using the relationship given in Munari and Zwitter (1997). Note, however, that this total equivalent width is considerably smaller than that of all but a single star in the sample used by Munari and Zwitter (1997), so we have decided to double the quoted uncertainty. Adopting the conversions from reddening to extinction given in Schlegel *et al.* (1998), we compute the extinction toward SN 2011fe to be $A_B = 0.11 \pm 0.03$, $A_V = 0.08 \pm 0.02$, $A_R = 0.07 \pm 0.02$, and $A_I = 0.05 \pm 0.01$.

After removing this extinction from our measurements, we show the color evolution of SN 2011fe in Figures 4 through 6. The shape and extreme values of these colors are similar to those of the normal Type Ia SNe 1994D and 2003du. In Figure 4, we have drawn a line to represent the relationship (Lira (1995); Phillips *et al.* (1999)) for a set of four type Ia SNe which suffered little or no extinction. The $(B-V)$ locus of SN 2011fe lies slightly (0.05 to 0.10 mag) to the red side of this line, especially near the time of maximum $(B-V)$ color. Given our estimates of the extinction to SN 2011fe, this small difference is unlikely to be due to our underestimation of the reddening.

5. Absolute magnitudes

In order to compute the peak absolute magnitudes of SN 2011fe, we must remove the effects of extinction and apply the appropriate correction for its distance. The previous section discusses the extinction to this event, and we now examine the distance to M101. Since the first identification of Cepheids in this galaxy 26 years ago (Cook *et al.* 1986), astronomers have acquired ever deeper and larger collections of measurements. Shappee and Stanek (2011) provide a list of recent efforts, which suggests that Cepheid-based measurements are converging on a relative distance modulus $(m - M) = 10.63$ mag between the LMC and M101. If we adopt a distance modulus of $(m - M)_{\rm LMC} = 18.50$ mag to the LMC, this implies a distance modulus $(m - M)_{\rm M101} = 29.13$ to M101. This is similar to one of the two results based on the luminosity of the tip of the red giant branch, $(m - M)_{\rm M101} = 29.05 \pm 0.06\,({\rm rand}) \pm 0.12\,({\rm sys})$ mag (Shappee and Stanek 2011), though considerably less than the other, $(m - M)_{\rm M101} = 29.42 \pm 0.11$ mag (Sakai *et al.* 2004). We therefore adopt a value of $(m - M)_{\rm M101} = 29.10 \pm 0.15$ mag to convert our apparent to absolute magnitudes. Note that the uncertainty in this distance modulus is our rough average, based on a combination of the random and systematic errors quoted by other authors and the scatter between their values. This uncertainty in the distance to M101 will dominate the uncertainties in all absolute magnitudes computed below.

Using this distance modulus, and the extinction derived earlier for each band, we can convert the apparent magnitudes at maximum light into absolute magnitudes. We list these values in Table 6.

Phillips (1993) found a connection between the absolute magnitude of a type Ia SN and the rate at which it declines after maximum: quickly-declining events are intrinsically less luminous. Further investigation (Hamuy *et al.* 1996; Riess *et al.* 1996; Perlmutter *et al.* 1997) confirmed this relationship and spawned several different methods to quantify it. We adopt the $\Delta m_{15}(B)$ method, which characterizes an event by the change in its B-band luminosity in the 15 days after maximum light. The light curve of SN 2011fe yields $\Delta m_{15}(B) = 1.21 \pm 0.03$ mag, placing it in the middle of the range of values for SNe Ia. Prieto *et al.* (2006) compute linear relationships between the $\Delta m_{15}(B)$ and

peak absolute magnitudes for a large sample of SNe. If we insert our value of $\Delta m_{15}(B)$ into the equations from their Table 3 for host galaxies with small reddening, we derive the absolute magnitudes shown in the rightmost column of Table 6. The excellent agreement with the observed values suggests that our choice of distance modulus to M101 may be a good one.

6. Comparison with visual measurements

Perhaps because it was the brightest SN Ia to appear in the sky since 1972, SN 2011fe was observed intensively by many astronomers. The AAVSO received over 900 visual measurements of the event within six months of the explosion. Since it was observed so well with both human eyes and CCDs, this star provides an ideal opportunity to compare the two detectors quantitatively.

We acquired visual measurements made by a large set of observers from the AAVSO; note that these have not yet been validated. We removed a small number of obvious outliers, leaving 880 measurements over the range $799 < \mathrm{JD} - 2455000 < 984$. For each of our CCD V-band measurements, we estimated a simultaneous visual magnitude by fitting an unweighted low-order polynomial to the visual measurements within N days; due to the decreasing frequency of visual measurements and the less sharply changing light curve at late times, we increased N from 5 days to 8 days at JD 2455840 and again to 30 days at JD 2455865. We then computed the difference between the polynomial and the V-band measurement. Figure 7 shows our results: there is a clear trend for the visual measurements to be relatively fainter when the object is red. If we make an unweighted linear fit to all the differences, we find

$$(\mathrm{visual} - \mathrm{V})_{2011\mathrm{fe}} = -0.09 + 0.19\ (04) * (B - V) \qquad (8)$$

where the number in parentheses represents the uncertainty in the coefficient.

We know of two other cases in which visual and other measurements of type Ia SNe are compared. Pierce and Jacoby (1995) retrieved photographic films of SN 1937C, which were originally described in Baade and Zwicky (1938), re-measured them with a photodensitometer, and calibrated the results to the Johnson V-band using a set of local standards. They compared their results to the visual measurements of SN 1937C made by Beyer (1939) and found

$$(\mathrm{visual} - \mathrm{V})_{1937\mathrm{C}} = -0.63 + 0.53 * (B - V) \qquad (9)$$

We plot this relationship in Figure 7 using a dotted line. Jacoby and Pierce (1996) discussed the differences between visual measurements of SN 1991T from the AAVSO to CCD V-band measurements made by Phillips *et al.* (1992). We have extracted the measurements of Phillips *et al.* (1992) from their Figure 2 and compared them to the visual measurements, using the median of all visual

measurements within a range of 0.5 day to define a value corresponding to each CCD measurement. We show these differences as circular symbols in Figure 7; an unweighted linear fit yields

$$(\text{visual} - \text{V})_{1991\text{T}} = -0.28 + 0.68(10) * (B-V) \quad (10)$$

We find the slope to be the more interesting quantity in these relationships, since the constant offset term may depend on the choice of comparison stars for visual observers. Although at first blush the slopes appear to be quite different, if one examines Figure 7 carefully, one will see that the trend is quite similar for all three SNe if one restricts the color range to $(B-V) > 0.5$. The main difference between these three events, then, lies in the measurements made when the SNe were relatively blue. Could that difference be real? We note that SNe 1991T (definitely) and 1937C (probably) were events with slowly declining light curves and higher than average luminosities, while SN 2011fe declined at an average rate and, for our assumed distance to M101, was of average luminosity. As Phillips *et al.* (1992) describes, the spectrum of SN 1991T was most different from that of ordinary SNe Ia at early times, before and during its maximum luminosity; it is also at these early times that SNe shine with blue light. Could the combination of photometry by the human eye and photometry by CCD really distinguish ordinary and superluminous SNe Ia at early times? The evidence is far too weak at this time to support such a conclusion, but we look forward to testing the idea with future events.

Stanton (1999) undertook a more general study, comparing the measurements of a set of roughly twenty stars near SS Cyg made by many visual observers to the Johnson V as a function of $(B-V)$. He found a relationship

$$(\text{visual} - \text{V}) = 0.21 * (B-V) \quad (11)$$

which we plot with a dash-dotted line in Figure 7. The slope of this relationship is consistent with that derived from the entire SN 2011fe dataset.

7. Conclusion

Our multicolor photometry suggests that SN 2011fe was a "normal" type Ia SN, with a decline parameter $\Delta m_{15}(B) = 1.21 \pm 0.03$ mag. After correcting for extinction and adopting a distance modulus to M101 of $(m - M) = 29.10$ mag, we find absolute magnitudes of $M_B = -19.21$, $M_V = -19.19$, $M_R = -19.18$, and $M_I = -18.94$, which provide further evidence that this event was "normal" in its optical properties. As such, it should serve as an exemplar of the SNe which can act as standardizable candles for cosmological studies. A comparison of the visual and CCD V-band measurements of SN 2011fe reveals systematic differences as a function of color which are similar to those found for other type Ia SNe and for stars in general.

8. Acknowledgements

We acknowledge with thanks the variable star observations from the AAVSO International Database contributed by observers worldwide and used in this research. We thank Arne Henden and the staff at AAVSO for making special efforts to provide a sequence of comparison stars near M101, and for helping to coordinate efforts to study this particular variable star. MWR is grateful for the continued support of the RIT Observatory by RIT and its College of Science. Without the Palomar Transient Factory, the astronomical community would not have received such early notice of this explosion. We thank the anonymous referee for his comments.

References

Baade, W., and Zwicky, F. 1938, *Astrophys. J.*, **88**, 411.
Beyer, M. 1939, *Astron. Nachr.*, **268**, 341.
Cook, K. H., Aaronson, M., and Illingworth, G. 1986, *Astrophys. J., Lett. Ed.*, **301**, L45.
Hamuy, M., Phillips, M. M., Maza, J., Wischnjewsky, M., Uomoto, A., Landolt, A. U., and Khatwani, R. 1991, *Astron. J.*, **102**, 208.
Hamuy, M., Phillips, M. M., Suntzeff, N. B., Schommer, R. A., Maza, J., and Aviles, R. 1996, *Astron. J.*, **112**, 2391.
Henden, A. A. 2012, Observations from the AAVSO International Database, private communication.
Honeycutt, R. K. 1992, *Publ. Astron. Soc. Pacific*, **104**, 435.
Jacoby, G. H., and Pierce, M. J. 1996, *Astron. J.*, **112**, 723.
Kirshner, R. P., Willner, S. P., Becklin, E. E., Neugebauer, G., and Oke, J. B. 1973, *Astrophys. J., Lett. Ed.*, **180**, L97.
Landolt, A. U. 1992, *Astron. J.*, **104**, 340.
Law, N. M., *et al.* 2009, *Publ. Astron. Soc. Pacific*, **121**, 1395.
Li, W., *et al.* 2011, *Nature*, **480**, 348.
Lira, P. 1995, Master's thesis, Univ. Chile.
Marion, H. 2011, *Astron. Telegram*, No. 3599, 1.
Munari, U., and Zwitter, T. 1997, *Astron. Astrophys.*, **318**, 269.
Nugent, P., Sullivan, M., Bersier, D., Howell, D. A., Thomas, R., and James, P. 2011a, *Astron. Telegram*, No. 3581, 1.
Nugent, P. E., *et al.* 2011b, *Nature*, **480**, 344.
Patat, F., *et al.* 2011, arXiv, 1112.0247.
Perlmutter, S., *et al.* 1997, *Astrophys. J.*, **483**, 565.
Pierce, M. J., and Jacoby, G. H. 1995, *Astron. J.*, **110**, 2885.
Phillips, M. M. 1993, *Astrophys. J., Lett. Ed.*, **413**, L105.
Phillips, M. M., Wells, L. A., Suntzeff, N. B., Hamuy, M., Leibundgut, B., Kirshner, R. P., and Foltz, C. B. 1992, *Astron. J.*, **103**, 1632.

Phillips, M. M., *et al.* 1999, *Astron. J.*, **118**, 1776.
Prieto, J. L., Rest, A., and Suntzeff, N. B. 2006, *Astrophys. J.*, **647**, 501.
Rau, A., *et al.* 2009, *Publ. Astron. Soc. Pacific*, **121**, 1334.
Richmond, M. W., *et al.* 1995, *Astron. J.*, **109**, 2121.
Riess, A. G., Press, W. H., and Kirshner, R. P. 1996, *Astrophys. J.*, **473**, 88.
Sakai, S., Ferrarese, L., Kennicutt, R. C., Saha, A. 2004, *Astrophys. J.*, **608**, 42.
Sandage, A., and Tammann, G. A. 1974, *Astrophys. J.*, **194**, 223.
Schlegel, D. J., Finkbeiner, D. P., and Davis, M. 1998, *Astrophys. J., Suppl Ser.*, **500**, 525.
Shappee, B. J., and Stanek, K. Z. 2011, *Astrophys. J.*, **733**, 124.
Simonsen, M. 2011, *Bull. Amer. Astron. Soc.*, **43**, 218.
Stanishev, V., *et al.* 2007, *Astron. Astrophys.*, **469**, 645.
Stanton, R. H. 1999, *J. Amer. Assoc. Var. Star Obs.*, **27**, 97.
Treffers, R. R., and Richmond, M. W. 1989, *Publ. Astron. Soc. Pacific*, **101**, 725.
Wells, L. A., *et al.* 1994, *Astron. J.*, **108**, 2233.

Table 1: Photometry of comparison stars.

Star	*R.A. (J2000)* *h m s*	*Dec. (J2000)* ° ′ ″	*B* *R*	*V* *I*
A	14 03 13.67	+54 15 43.4	14.767±0.065	13.832±0.027
			13.290±0.030	12.725±0.037
B	14 02 54.17	+54 16 29.5	14.616±0.080	13.986±0.037
			13.627±0.039	13.262±0.044
G	14 02 31.15	+54 14 03.9	15.330±0.084	14.642±0.042
			14.283±0.042	13.931±0.073

Table 2. RIT photometry of SN 2011fe.

JD–2455000	B	V	R	I	note
799.56	14.072±0.038	13.776±0.016	13.728±0.011	13.696±0.022	*
800.58	13.321±0.046	13.025±0.013	12.955±0.024	12.942±0.026	
802.56	12.148±0.028	12.049±0.011	11.941±0.020	11.882±0.022	
803.55	11.690±0.023	11.643±0.016	11.512±0.015	11.471±0.024	
804.56	11.310±0.025	11.300±0.009	11.170±0.012	11.147±0.017	
806.54	—	10.659±0.020	10.572±0.028	10.569±0.052	*
808.54	10.346±0.045	10.466±0.029	10.336±0.011	10.402±0.025	
814.53	10.034±0.039	10.014±0.003	10.042±0.084	10.260±0.030	*
815.53	9.981±0.015	10.012±0.012	10.011±0.025	10.320±0.027	
816.53	10.072±0.052	9.998±0.008	10.006±0.035	10.362±0.036	
817.58	10.060±0.072	9.903±0.059	10.031±0.031	10.307±0.019	*
820.53	10.171±0.010	10.082±0.013	10.080±0.014	10.505±0.018	*
822.52	10.326±0.017	10.134±0.006	10.181±0.002	10.630±0.026	
823.53	10.405±0.015	10.185±0.014	10.283±0.015	10.691±0.013	
825.52	10.623±0.030	10.311±0.009	10.428±0.027	10.840±0.018	
827.51	10.829±0.028	10.459±0.016	10.580±0.024	10.918±0.025	
829.51	11.043±0.057	10.574±0.019	10.655±0.017	10.898±0.020	
830.52	11.167±0.014	10.629±0.011	10.672±0.021	10.894±0.015	
832.51	11.423±0.058	10.739±0.011	10.731±0.012	10.855±0.018	*
839.53	12.228±0.016	11.116±0.016	10.850±0.008	10.699±0.033	*
840.50	12.312±0.039	11.180±0.013	10.865±0.024	10.661±0.026	
841.50	12.407±0.049	11.237±0.011	10.925±0.016	10.672±0.031	
842.50	12.503±0.038	11.294±0.006	10.958±0.015	10.680±0.026	
844.50	12.688±0.035	11.430±0.016	11.054±0.016	10.738±0.045	*
852.90	13.098±0.021	11.921±0.014	11.615±0.033	11.255±0.022	
858.48	13.314±0.034	12.144±0.020	11.862±0.013	11.564±0.024	*
859.49	13.290±0.016	12.157±0.010	11.879±0.012	11.634±0.047	*
864.90	13.340±0.037	12.332±0.012	12.085±0.013	11.884±0.010	
868.49	13.364±0.017	12.441±0.014	12.190±0.016	12.038±0.040	
870.90	13.375±0.011	12.478±0.016	12.256±0.008	12.141±0.005	
872.88	13.371±0.041	12.509±0.016	12.343±0.021	12.179±0.008	*
883.92	13.584±0.006	12.826±0.010	12.688±0.011	12.676±0.014	
887.92	13.598±0.012	12.927±0.006	12.796±0.005	12.832±0.013	
889.92	13.699±0.037	12.968±0.019	12.904±0.026	12.909±0.012	
890.93	13.658±0.021	12.988±0.019	12.902±0.011	12.957±0.018	
898.91	13.761±0.037	13.217±0.014	13.155±0.019	13.245±0.027	
905.94	13.831±0.033	13.398±0.013	13.353±0.017	13.470±0.036	
907.92	13.877±0.026	13.442±0.018	13.445±0.027	13.580±0.039	
913.89	13.919±0.035	13.559±0.019	13.624±0.027	13.732±0.025	*
924.92	14.078±0.036	13.811±0.016	13.945±0.025	14.066±0.032	*

table continued on next page

Table 2. RIT photometry of SN 2011fe, cont.

JD–2455000	*B*	*V*	*R*	*I*	*note*
932.94	14.191±0.032	14.006±0.022	14.145±0.020	14.256±0.045	*
935.98	14.219±0.041	14.054±0.017	14.280±0.027	14.384±0.039	*
937.92	14.253±0.026	14.124±0.015	14.325±0.026	14.423±0.036	
942.72	14.298±0.038	14.204±0.025	14.402±0.058	14.506±0.043	*
945.89	14.377±0.033	14.272±0.033	14.523±0.036	14.627±0.045	*
948.86	14.420±0.036	14.336±0.023	14.639±0.031	14.702±0.050	
954.82	14.524±0.044	14.465±0.021	14.757±0.028	14.803±0.040	
966.90	14.716±0.033	14.623±0.024	14.951±0.032	15.034±0.053	
973.67	14.792±0.044	14.754±0.039	15.165±0.060	15.174±0.056	
978.67	14.884±0.046	14.894±0.026	15.340±0.048	15.242±0.054	

* *clouds*

Table 3. Linear fit to light curves 2455875 < JD < 2455930.

Passband	*Slope (mag/day)*	*reduced* χ^2
B	0.0117±0.0006	1.2
V	0.0247±0.0004	1.6
R	0.0312±0.0004	0.9
I	0.0346±0.0006	1.0

Table 4. MSU photometry of SN 2011fe.

JD–2455000	*B*	*V*	*I*	*note*
801.58	12.66±0.02	12.42±0.02	12.36±0.03	
803.56	11.69±0.01	11.60±0.01	11.48±0.02	
806.58	10.80±0.01	10.74±0.01	10.66±0.02	
809.56	10.36±0.02	10.30±0.01	10.28±0.02	
811.56	10.17±0.03	10.08±0.03	10.22±0.02	*
820.54	10.13±0.02	10.06±0.01	10.44±0.02	
822.53	10.27±0.02	10.10±0.01	10.55±0.01	
825.54	10.55±0.03	10.27±0.02	10.87±0.02	*
837.52	11.93±0.02	10.97±0.02	10.66±0.03	
851.50	13.04±0.03	11.83±0.02	11.16±0.03	
857.90	13.18±0.05	12.09±0.04	11.42±0.04	*
867.48	13.27±0.04	12.37±0.03	11.96±0.03	
889.46	13.61±0.03	12.92±0.03	12.89±0.03	
898.47	13.67±0.10	13.14±0.06	13.22±0.08	

* *clouds*

Table 5. Apparent magnitudes at maximum light.

Passband	*JD–2455000*	*Magnitude*
B	816.0±0.3	10.00±0.02
V	817.0±0.3	9.99±0.01
R	816.6±0.4	9.99±0.02
I	813.1±0.4	10.21±0.03
I (sec)	839.7±0.5	10.66±0.01

Table 6. Absolute magnitudes at maximum light, corrected for extinction.

Passband	*Observed*	*Based on* Δm_{15}[b] *magnitude*[a]
B	–19.21±0.15	–19.25±0.03
V	–19.19±0.15	–19.18±0.03
R	–19.18±0.15	–19.19±0.04
I	–18.94±0.15	–18.92±0.03
I (sec)	–18.49±0.15	—

[a] *Based on* $(m - M)_{M101} = 29.10 \pm 0.15$ *mag.*
[b] *Using the relationship from Prieto* et al. *(2006).*

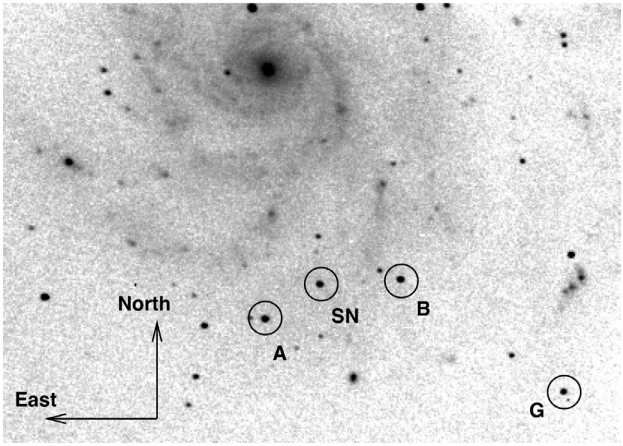

Figure 1. A V-band image of M101 from RIT, showing stars used to calibrate measurements of SN 2011fe. North is up, East to the left. The field of view is roughly 13 by 9 arcminutes.

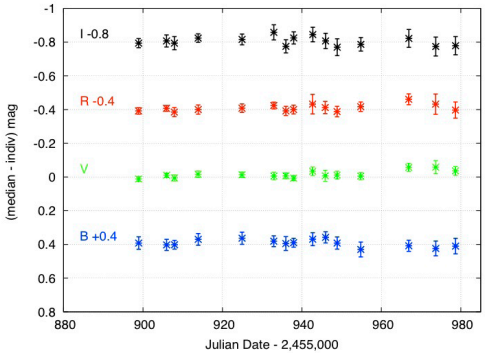

Figure 2. Difference between instrumental magnitudes extracted from median-combined images and from individual images at RIT. The values have been shifted for clarity by 0.4, 0.0, –0.4, –0.8 magnitude in B, V, R, I, respectively.

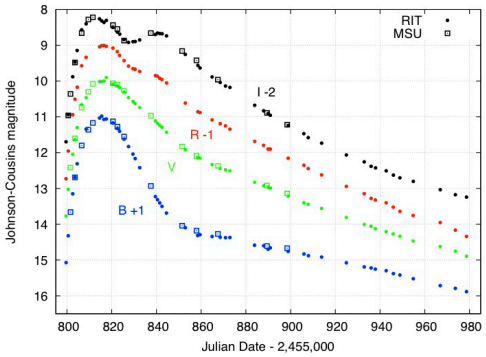

Figure 3. Light curves of SN 2011fe in BVRI. The data for each passband have been offset vertically for clarity.

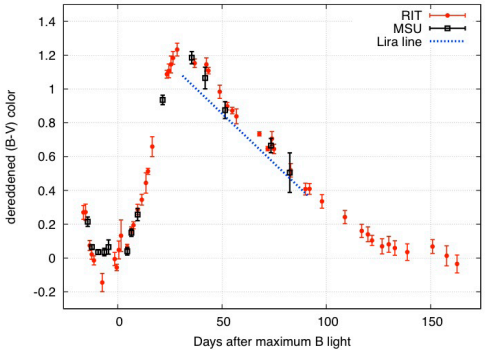

Figure 4. (B–V) color evolution of SN 2011fe, after correcting for extinction.

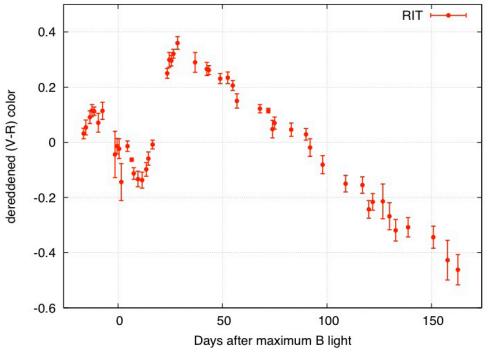

Figure 5. (V–R) color evolution of SN 2011fe, after correcting for extinction.

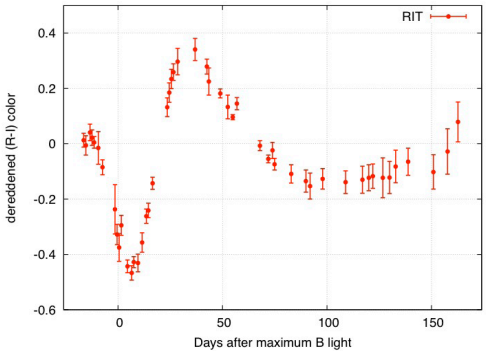

Figure 6. (R–I) color evolution of SN 2011fe, after correcting for extinction.

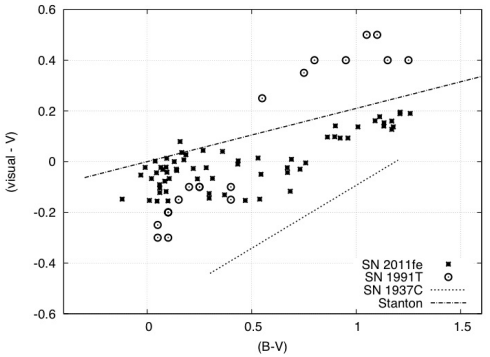

Figure 7. The difference between visual and CCD or photographic measurements, as a function of (B–V) color, for SNe Ia and for variable stars in general.

New Light Curve for the 1909 Outburst of RT Serpentis

Grant Luberda
Wayne Osborn
Yerkes Observatory, 373 W. Geneva St., Williams Bay, WI 53191; email correspondence should be sent to Wayne.Osborn@cmich.edu

Received October 6, 2011; revised October 24, 2011; accepted October 24, 2011

Abstract A new light curve for the 1909 outburst of the unusual nova RT Serpentis has been derived. Published observations have been compiled and new brightness measures determined from archival photographic plates. Modern photometry has been used to place the observations approximately on the *UBV* system. The outburst had an overall increase of at least 5 magnitudes and reached maximum in 1917 May with $B = 11.0$ and $V = 10.1$

1. Introduction

The unusual variable RT Serpentis (= AN 7.1917 = Nova Ser 1909; J2000 coordinates = R.A. $17^h\ 39^m\ 51.98^s$, Dec. –11° 56' 39.0") was discovered by Wolf in 1917 (Wolf 1917) and independently discovered by Barnard two years later (Barnard 1919a). A search of archival photographs showed the object was not visible on any plates prior to 1909 but after outburst remained near maximum brightness for several years (Bailey 1919, Wolf 1919, Shapley 1919) after which it began a slow decline (Shapley 1927). RT Ser is now classified as one of the rare symbiotic novae objects (Nussbaumer 1992).

Our interest in this object began when we came across a plate in the Yerkes collection with the envelope notation "Remarkable variable." Some sleuthing revealed the photograph was one of Barnard's observations of RT Ser during outburst. Our search for a light curve of the event revealed only the old one published by Payne-Gaposchkin and Gaposchkin (1938). It seemed obvious that deriving a new light curve more closely tied to the traditional *UBV* system would be worthwhile.

2. Observational Data

We have collected available observations of the magnitude of RT Serpentis within twenty-five years of its outburst in 1909, i.e., data prior to 1935. The observations are of two types: magnitudes determined from images on photographic plates and visual estimates.

2.1 Photographic Observations

Magnitudes from photographic plates have been published by Wolf (1919),

Barnard (1919a, 1919b), Bailey (1919, 1921), and Shapley (1919, 1923, 1927). The published data have been supplemented in three ways. First, we have made eye estimates of the brightness of RT Ser on forty-two plates found in the Yerkes Observatory collection. Second, we have used the digital copies of the plates of the University of Heidelberg's Bruce Telescope that are available online (http://www.lsw.uni-heidelberg.de/projects/scanproject/) both to make eye estimates and to determine magnitudes through aperture photometry. Third, we have determined rough magnitudes and epochs for the "unpublished Harvard observations" plotted on the Payne-Gaposchkin and Gaposchkin (1938) light curve.

2.2 Visual Observations

Visual observations of RT Ser around the time of its outburst have been published by Mundler (1919), Barnard (1919b), Graff (1919, 1921, 1922, 1927), and Lacchini (1921, 1929, 1933). We also downloaded the 121 data points for RT Ser in the AAVSO International Database (AAVSO 2011) that are within our time window. A review of the AAVSO observations showed that all but three are visual estimates by Lacchini. They include his thirteen published magnitude estimates but with more accurate epochs. For some reason, however, his first eight observations have AAVSO magnitudes between 0.2 and 0.3 magnitude systematically fainter than his published values for those epochs, with the published data being more consistent with his subsequent brightness estimates. There is also one case of an epoch with a ten-day difference. We have adopted the published data in the discrepant cases.

3. Reductions

We endeavored to place the diverse observations approximately on the UBV system. Specifically, pseudo-B and pseudo-V magnitudes were derived for the photographic observations and the visual measures, respectively. We began by determining B and V magnitudes for a comparison star sequence that included the stars that had been used by the earlier investigators. The adopted B and V data are given in Table 1 along with the identification of the stars and the source of the BV photometry. Tycho catalogue data were transformed to the UBV system using the relations of Bessell (2000); AAVSO data are from CCD photometry on the UBVRcIc system. Given the uncertainties in the RT Ser magnitudes, the comparison sequence values are usually given only to a tenth of a magnitude.

3.1 Photographic data

The photographic data sets are from the Yerkes, Heidelberg, and Harvard plate collections. Eye estimates of the brightness of RT Ser using our comparison sequence have been made for the Yerkes plates. These data are given in Table 2

which lists the plate number, the Julian date of mid-exposure, and the pseudo-B magnitude. The first digits of the plate number indicate the aperture of the camera employed, with two or more exposures often being taken simultaneously with different lenses.

Wolf (1919) published magnitudes from Heidelberg plates taken with telescopes of three different apertures. Some plates—those taken with the 41-cm (16-inch) Bruce Telescope—have been digitized and are available online. We downloaded the digitized images of plates showing RT Ser and both performed aperture photometry and made eye-estimates using our comparison sequence; our results are given in Table 3. These data showed that a correction of +2.0 mag is needed to convert Wolf's published magnitudes to approximate B ones, and this factor was used to transform the published data for the undigitized plates.

The observations from the Harvard plates were more difficult to adjust. Magnitudes are given in six different references (Bailey 1919, 1921; Shapley 1919, 1923, 1927; Payne-Gaposchkin and Gaposchkin 1938). Several give the magnitude from the critical 1909 July 9 plate, and we compared the different values to each other and to an eye-estimate we were able to make for this plate using our comparison sequence. Our analysis indicates that all Harvard observations other than those of Shapley (1919) are on the same system (referred to as the "Harvard System"). An empirically derived adjustment of +0.6 magnitude was used to transform the Harvard system to our pseudo-B system; the correction used for the 1919 Shapley data was +0.1 magnitude.

3.2 Visual Observations

In general, the visual observers listed the comparison stars used and their adopted magnitudes. We compared the listed comparison star magnitudes with the stars' V ones to obtain corrections for transforming the visual observations approximately to the V system. The adopted corrections were +1.0 mag for Barnard's observations, +0.9 mag for Graff's, and +1.1 mag for Lacchini's and for the AAVSO data. Mundler's observations were made with a photometer; the correction averaged 0.0 mag but depended slightly on which comparison stars he used for a given observation. We estimate our zero point shifts may be uncertain by up to three tenths of a magnitude.

4. Results

Our derived B and V light curves are shown in Figure 1. The B light curve includes data from plates of the field taken before the outburst. No evidence of the precursor was seen on plates extending back to 1891 (Bailey 1919), with the deepest ones reaching past 16th magnitude. The rise to maximum took place between 1908 June, when the B magnitude was less than 16.4, and 1910 March, when the B magnitude was approximately 12. Unfortunately, few plates are

available that were exposed during the time of rise. There is a Harvard plate of 1909 July 9 that definitely shows RT Ser. One of us (WO) had the opportunity to briefly examine this plate and the brightness was estimated at about 14.9 using our comparison sequence; the value from the corrected Harvard observers' estimates put it at 14.5. We also found two possible images of RT Ser at the plate limit on the digitized Heidelberg plates of 1909 June 9; these indicate a magnitude of roughly 14.5.

From 1910 to 1917, the nova's magnitude gradually increased about one magnitude, reaching a maximum of about B = 11.0 around 1917 May (JD 2421350). This was when the object was discovered by Wolf and began to be followed by the visual observers. The maximum in V was 10.1, indicating a B-V of approximately 0.9.

After maximum, the brightness began a decline, with a rate of about 0.4 magnitude/year for four years after which the rate decreased to less than 0.1 magnitude/year. By 1928 both the B and the V magnitudes had decreased to about 13.0. Thus, the B–V in the 1930s was approximately zero, indicating the nova's color shifted toward the blue as its brightness decreased. This likely reflects the gradual spectral development of strong emission lines, which by 1928 dominate the spectrum (Adams and Joy 1928); these lines would enhance the photographic brightness relative to the visual. Other novae, such T Pyx, have also shown similar color evolution (Schaefer 2010). We caution, however, that both the visual and photographic estimates for the later years are uncertain. In particular, the photographic data after JD 2425100 are from the unpublished observations plotted on Payne-Gaposchkin's graph while the visual observers no doubt relied on comparison stars for which only photographic magnitudes were available for these fainter estimates. Lastly, we note we do not find strong evidence of the brightness fluctuations previously reported.

5. Acknowledgements

We would like to thank Lee Robbins, University of Toronto; Alison Doane, curator of the Harvard plate stacks; Holger Mandel and Markus Demleitner, Zentrum für Astronomie Heidelberg; and Elizabeth Waagen, AAVSO, for their help in gathering data needed for this study. This research made use of NASA's Astrophysics Data System; the SIMBAD database, operated at CDS, Strasbourg, France; and the Digitized Sky Surveys (DSS) produced at the Space Telescope Science Institute under U.S. Government grant NAG W-2166. The DSS images are from photographic data obtained using the Oschin Schmidt Telescope on Palomar Mountain and the UK Schmidt Telescope through funding provided by The National Geographic Society, the National Science Foundation, the Sloan Foundation, the Samuel Oschin Foundation, the Eastman Kodak Corporation, and the UK Science and Engineering Research Council. Finally, we thank the referee for some excellent comments and questions that helped improve the paper.

References

AAVSO 2011, observations from the AAVSO International Database (http://www.aavso.org).
Adams, W. S., and Joy, A. H. 1928, *Publ. Astron. Soc. Pacific*, **40**, 252.
Bailey, S. I. 1919, *Bull. Harvard Coll. Obs.*, No. 680, 1.
Bailey, S. I . 1921, *Bull. Harvard Coll. Obs.*, No. 753, 2.
Barnard, E. E. 1919a, *Astron. J.*, **32**, 37.
Barnard, E. E. 1919b, *Astron. J.*, **32**, 48.
Bessell, M. S. 2000, *Publ. Astron. Soc. Pacific*, **112**, 961.
Graff, K. 1919, *Astron. Nach.*, **210**, 61.
Graff, K. 1921, *Beob.-Zirk. Astron. Nach.*, No. 32, 55.
Graff, K. 1922, *Beob.-Zirk. Astron. Nach.*, No. 25, 45.
Graff, K. 1927, *Beob.-Zirk. Astron. Nach.*, No. 12, 23.
Lacchini, G. 1921, *Beob.-Zirk. Astron. Nach.*, No. 35, 59.
Lacchini, G. 1929, *Beob.-Zirk. Astron. Nach.*, No. 5, 12.
Lacchini, G. 1933, *Astron. Nach.*, **248**, 366.
Mundler, M. 1919, *Astron. Nach.*, **210**, 157.
Nussbaumer, H. 1992, in *Evolutionary Processes in Interacting Binary Stars*, Proc. IAU Symp. 151, eds. Y. Kondo, R. F. Sistero, R. S. Polidan, Kluwer, Dordrecht, and Boston, 429.
Payne-Gaposchkin, C., and Gaposchkin, S. 1938, *Variable Stars*, Harvard Monogr., No. 5, 263.
Schaefer, B. E. 2010, *Astrophys. J., Suppl. Ser.*, **187**, 275.
Shapley, H. 1919, *Publ. Astron. Soc. Pacific*, **31**, 226.
Shapley, H. 1923, *Bull. Harvard Coll. Obs.*, No. 789, 3.
Shapley, H. 1927, *Bull. Harvard Coll. Obs.*, No. 851, 3.
Wolf, M. 1917, *Astron. Nach.*, **204**, 293.
Wolf, M. 1919, *Astron. Nach.*, **208**, 363.

Table 1. Comparison star sequence for RT Ser.

Other ID	R.A. (2000) h m s	Dec. (2000) ° ′ ″	B	V	Photometry Source
BD–11 4436	17:40:31.79	–12:04:51.2	11.3	9.95	Tycho, Heidelberg
BD–11 4426	17:38:40.93	–11:49:36.5	11.65	10.1	Tycho, Heidelberg
BD–11 4433	17:39:48.19	–11:50:22.1	10.75	10.15	Tycho, Heidelberg
BD–12 4801	17:40:07.36	–12:05:05.5	11.2	10.65	Tycho, Heidelberg
BD–11 4434	17:39:56.77	–11:46:26.3	12.5	10.95	Tycho, Heidelberg
AAVSO 110	17:40:48.90	–11:58:33.0	11.5	11.0	Tycho, Heidelberg
TYC 5668-51-1	17:39:55.85	–12:08:20.9	11.55	11.25	Tycho, Heidelberg
AAVSO 114	17:40:48.67	–12:05:54.0	12.0	11.4	Tycho, Heidelberg
AAVSO 120	17:40:03.12	–11:55:55.6	12.9	11.95	AAVSO
AAVSO 123	17:39:36.41	–11:52:26.6	13.2	12.3	AAVSO
AAVSO 130	17:39:32.60	–12:01:26.4	14.5	13.0	AAVSO
AAVSO 132	17:40:13.09	–11:57:23.9	14.7	13.2	AAVSO
AAVSO 136	17:39:43.93	–11:52:16.2	14.4	13.6	AAVSO
AAVSO 139	17:39:32.47	–11:53:51.3	15.0	13.9	AAVSO
AAVSO 145	17:39:38.53	–11:56:44.1	15.6	14.5	AAVSO
AAVSO 150	17:39:54.62	–11:57:24.2	16.2	15.0	AAVSO
AAVSO 153	17:39:45.19	–11:58:01.7	16.4	15.3	AAVSO
AAVSO 160	17:39:52.31	–11:53:56.3	17.3	16.0	AAVSO
AAVSO 164	17:39:52.27	–11:57:16.0	17.9	16.4	AAVSO
AAVSO 174	17:39:49.93	–11:57:10.5	18.5	17.4	AAVSO

Photometry references: AAVSO = sequence star magnitudes listed by AAVSO from CCD photometry, Heidelberg = values from our aperture photometry of Heidelberg plates, Tycho = data in Tycho–2 catalog transformed as per Bessell (2000).

Table 2. Magnitudes of RT Ser from eye-estimates of Yerkes plates.

Plate	Julian Date	B	Plate	Julian Date	B
6B-12	2414813.708	<14.4	10B-979	2420684.697	11.2
10B-89	2416664.717	<12.0	6B-979	2420684.697	11.0
6B-89	2416664.717	<12.9	10B-1268	2421780.695	11.2
10B-90	2416674.733	<15.6	6B-1268	2421780.695	11.2
6B-90	2416674.733	<15.6	10B-1331.5	2421998.938	11.1
10B-99	2416693.635	<15.0	6B-1331.5	2421998.938	11.1
6B-99	2416693.635	<15.6	10B-1340	2422020.930	11.1
10B-100	2416695.6	<14.7	6B-1340	2422020.930	11.0
6B-100	2416695.6	<14.7	10B-1345	2422045.887	11.1
10B-224	2417017.717	<17.3	6B-1345	2422045.887	11.0
6B-224	2417017.717	<14.7	10B-1355	2422088.852	11.0
3B-224	2417017.717	<14.7	6B-1355	2422088.852	11.0

table continued on next page

Table 2. Magnitudes of RT Ser from eye-estimates of Yerkes plates, cont.

Plate	*Julian Date*	*B*	*Plate*	*Julian Date*	*B*
10B-457	2418122.720	<16.4	10B-1366	2422249.551	11.1
6B-457	2418122.720	<16.2	6B-1366	2422249.551	11.1
10B-689	2419158.816	11.8	10B-1423	2422470.866	11.2
6B-689	2419158.816	11.8	6B-1423	2422470.866	11.3
10B-702	2419209.736	11.8			
6B-702	2419209.736	11.7	10R-44	2424319.667	12.4
10B-977	2420681.682	11.2	10R-346	2425449.822	12.9
6B-977	2420681.682	11.2			
10B-978	2420683.702	11.2	24R-5434	2429455.673	14.8
6B-978	2420683.702	11.2	24R-5435	2429455.709	14.8

Table 3. Magnitudes of RT Ser from aperture photometry of digital copies of Heidelberg plates.

Plate	*Julian Date*	*B*	*Plate*	*Julian Date*	*B*
B479a	2415910.459	<14.7	B1784a	2417742.506	<14.7
B480b	2415910.460	<14.7	B1785b	2417742.506	<15.5
B483a	2415912.522	<15.3	B2338a	2418467.467	14.5
B484b	2415912.522	<15.3	B2339b	2418467.467	14.5
B996a	2416636.461	<15.0	B3945a	2421375.485	11.0
B997b	2416636.461	<15.0	B3946b	2421375.485	11.0
B1002a	2416645.479	<15.0	B3949a	2421394.468	11.0
B1003b	2416645.479	<14.7	B3950b	2421394.468	11.0
B1225a	2416994.544	<13.2	B4765a	2423608.478	11.3
B1226b	2416994.544	<13.2	B4766b	2423608.478	11.3
B1249a	2417025.479	<16.4	B4878a	2423936.477	11.5
B1250b	2417025.479	<16.4	B4879b	2423936.477	11.4

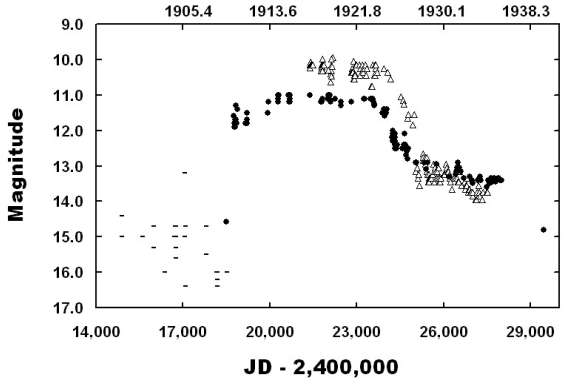

Figure 1. The new light curve of the 1909 outburst of RT Ser. Open triangles are V magnitudes, filled circles are B magnitudes, and the dashes show the B magnitude plate limit when the star was too faint to be detected.

International Observing Campaign: Photometry and Spectroscopy of P Cygni

Ernst Pollmann
Emil-Nolde-Str. 12, 51375 Leverkusen, Germany; ernst-pollmann@t-online.de

Thilo Bauer
Heimerzheimer Str. 2, 53332 Bornheim, Germany

Received February 3, 2012; revised March 19, 2012; accepted March 19, 2012

Abstract In this combined campaign on the Luminous Blue Variable star P Cygni we are trying for the first time by way of contemporaneous measurements of photometric V brightness and Hα equivalent width (EW) to realize a longterm monitoring of the intrinsic Hα-line flux. The photometric observers of AAVSO and BAV (Germany) and a spectroscopic observer group (Japan, France, Spain, Germany) started observing for this campaign in November 2008 at the request of Bernd Hanisch and one of us (EP) in order to continue former investigations whose results were based on multi-daily averaging of V and EW. Additional data from literature enable us to represent the quantitative behavior of the Hα-line flux for the timespan August 2005 to December 2011, which behavior reflects variabilities in mass-loss rate, stellar wind density, and ionization structure.

1. Introduction

The international observing campaign, Photometry and Spectroscopy of P Cygni, begun in 2008 by Bernd Hanisch and one of us (EP) (Templeton 2008a, 2008b), is a cooperative project of the American Association of Variable Star Observers (AAVSO), Active-Spectroscopy-in-Astronomy (ASPA), and Bundesdeutsche Arbeitsgemeinschaft für Veränderliche Sterne (BAV). One goal of the campaign is the monitoring of the behavior of the Hα-line equivalent width (EW) and the contemporaneous changes of the V-band magnitude of P Cyg. Another goal is to gather further information about the intrinsic flux of this spectral line.

As background it should be mentioned that a lot of different investigations during the last decades have been carried out to clarify the causes of brightness and emission strength variation and possible links between them, the extensions of the Hα-emitting wind, and line structures in different spectral areas. One of the earliest interesting investigations of the Hα emission was performed by Scuderi *et al.* (1992) in order to determine properties of the mass-loss.

Five years later, Najarro *et al.* (1997) carried out a detailed parameter study of the line strength, line shape, and energy distribution for the H and HeI spectrum,

in order to understand the nature of P Cygni and its wind. de Jager (2001) described photospheric models to explain outward motions in the atmosphere in context of luminosity and brightness variations. The investigation of the long-term spectral and quasi-simultaneous photometric behavior of P Cygni of Markova *et al.* (2001a, 2001b) was the main impetus to start our campaign.

The (for us) important question of the quantitative evaluation of the Hα emission and its reference to the radial distribution of the emitting regions around P Cyg was investigated in a comprehensive interferometric study by Balan *et al.* (2010). Relative to our investigation, it seems to give certain parallels in the current study of Richardson *et al.* (2011). They are showing in long-term studies the correlation behavior of the continuum flux and (not contemporaneous) photometric V-data, and they conclude that they vary in different manner in context of long-term and short-term timescales (the non-contemporaneous nature of their data is one of the substantial differences from campaign).

In our campaign it is assumed that the variability of the EW is caused by variations of the continuum flux and not by variations of the line flux, which would indicate variations in the stellar wind density. Therefore, the variability of the continuum flux shall be our primary concern when the properties of the stellar winds and rate of mass loss are studied.

Photometric and spectroscopic changes in P Cygni are shown to be anti-correlated on short- and long-term scales. We observed a total change of 35 Å in the equivalent width (EW) of the Hα line and of ~ 0.25 magnitude in the V-band brightness. Our observations extend from JD 2454671 (23 July 2008) through JD 2455880 (14 November 2011).

2. Results

Figures 1 and 2 illustrate our observations. Figure 1 compares of the behavior of the V magnitude (top) and the Hα-EW (below) during our campaign. Figure 2 is a plot of the Hα-EW (black points) as a function of photometric V magnitude (open circles) of P Cyg from Markova *et al.* (2001b).

As can be seen in Figure 1, when the EW decreases, the contemporaneous stellar brightness increases and vice versa. So far, our own results in Figure 1 agree well with the results of Markova *et al.* (2001b), which are shown in Figure 2 for comparison. Strict anti-correlation is expected if the variation of the continuum flux is independent from variations of the EW. If the Hα line flux is constant over time, an increase of the continuum brightness will yield a smaller line flux from the measured EW and vice versa.

To find out if and how the flux obtained from the spectral line profiles varies, the EW measurements are corrected for the effect mentioned in the previous section. From the definitions of

$$EW = \int \frac{l_o - l_\lambda}{l_o} d\lambda \quad (1)$$

and the relation between stellar magnitudes and continuum flux variations $F2 / F1 = 10^{-0.4\,(m2-m1)}$, it follows that the line flux is $F = C\ EW / 10^{\,(0.4\ Vphot)}$.

Here C is a constant factor. In practice, we correct EW with a simple division by $10^{(0.4*Vphot)}$. The derived quantity is then not the line flux in physical units, but a quantity proportional to the physical line flux, corrected for continuum variations. It is important to consider the absolute flux of the line because its variations are caused by the effects of mass loss, stellar wind density, and changes of the ionization state of chemical elements in it.

In the current campaign we have already obtained 122 nearly simultaneous measurements of the EW and the flux in the V-band (Figure 3). Strictly applied, the continuum flux at 6563 Å should be used. But here ΔV is a good approximation since the color indices of P Cygni do not vary greatly (Markova *et al.* 2001b, p. 903).

Figure 3 attempts to display if and to what extent the intrinsic line flux (a continuum-corrected EW) depends on V-magnitude. From a statistical point of view one can say that the low 0.25 correlation coefficient (which should be zero after the continuum correction), with consideration of the measurement uncertainties, suggests the conclusion that the Hα line flux is independent of V-magnitude. With consideration of standard deviation and possibly other kinds of errors, the temporal variation of the line flux of Hα in the plot in Figure 4 will represent the result of variations in the mass loss rate, stellar wind density, and changes of the ionization.The 122 EW and contemporaneous V-measurements of the current campaign are, of course, from a statistical point of view, still not sufficient to make firm statements regarding the simultaneous temporal behavior of V and the intrinsic line flux. In order to achieve this aim, further multiyear, simultaneous spectroscopic and photometric measurements will be continued in this campaign. Maybe then we will have a opportunity to report here again about the state of the results.

3. Acknowledgements

We are grateful to Dr. Dietrich Baade (ESO-München), Dr. Otmar Stahl (Landes, Sternwarte Heidelberg), and Prof. Dr. Edward Geyer (formerly Director Observatorium Hoher List, University Bonn) for their critical comments which led to essential improvements of this work. We also offer many thanks to all the participants of the campaign for their worthwhile contributions and measurements.

The following observers took part at the project: AAVSO (V-magnitude)—Adrian Ormsby, Robert E. Crumrine, Jim Fox, Kate Hutton, Nick Stoikidis, David B. Williams, E. G. Williams, Charles L. Calia, Thomas L. Peairs, Jeffery

G. Horne, Mike Durkin, Desmond Loughney, Wolfgang Vollmann; Spectroscopy (Hα-EW)—Mitsugu Fuji, Benjamin Mauclaire, Joan Guarro, Bernd Hanisch, Ernst Pollmann, Thierry Garrel, Valerie Desnaux, Olivier Thizy, Jean Noel Terry, Christian Buil, Stephane Charbonnel, Pierre Dubreul, Alain Lopez (from Balan *et al.* (2010)).

The EW, V(phot), and line flux data are available at the following website: http://astrospectroscopy.de/Data_PCyg_Campaign/Data%20table%20of%20the%20campaign.txt

References

Balan, A., Tycner, C., Zavala, R. T., Benson, J. A., Hutter, D. J., and Templeton, M. 2010, *Astrophys. J.*, **139**, 2269.

de Jager, C. 2001, in *P Cygni 2000: 400 Years of Progress*, ed. M. de Groot, C. Sterken, ASP Conf. Ser. 233, Astron. Soc. Pacific, 215.

Markova, N., Morrison, N., Kolka, I., and Markov, H. 2001a, *Astron. Astrophys.*, **376**, 898.

Markova, N., Scuderi, S., de Groot, M., Markov, H., and Panagia, N. 2001b, *Astron. Astrophys.*, **366**, 935.

Najarro, F., Hillier, D. J., and Stahl, O. 1997, *Astron. Astrophys.*, **326**, 1117.

Richardson, N. D., Morrison, N. D., Gies, D. R., Markova, N., Hesselbach, E. N., and Percy, J. R. 2011, *Astron. J.*, **141**, 120.

Scuderi, S., Bonanno, G., di Benedetto, R., Spadaro, D., and Panagia, N. 1992, *Astrophys. J.*, **392**, 201.

Templeton, M. R. 2008a, *AAVSO Special Notice*, No. 131 (http://www.aavso.org/node/1555/2811).

Templeton, M. R. 2008b, Campaign page (http://www.aavso.org/lont-term-photometric-campaign-luminous-blue-variable-p-cygni).

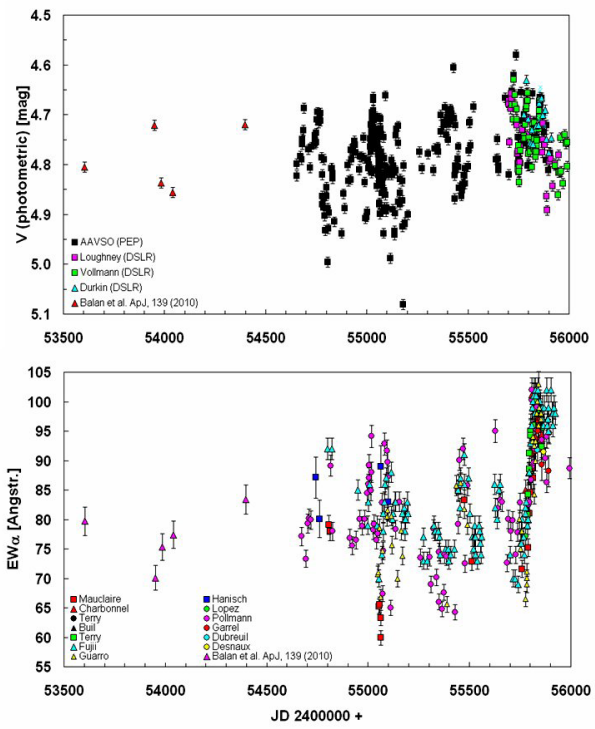

Figure 1. Photometric and spectroscopic observations: V-magnitude (top) and the Hα-EW (bottom) of P Cyg during the campaign (including data of Balan *et al.* 2010).

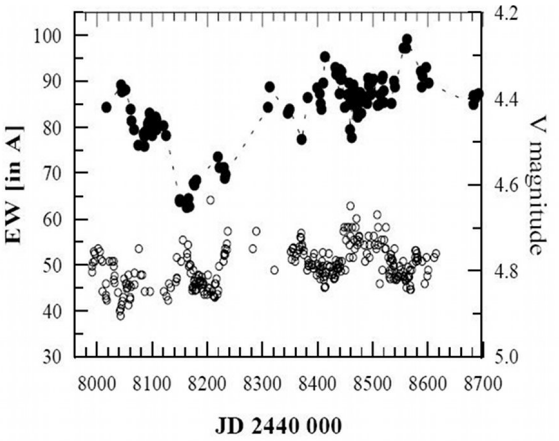

Figure 2. Plot of the Hα-EW (black points) as a function of photometric V-magnitude (open circles) of P Cyg (from Markova *et al.*2001b).

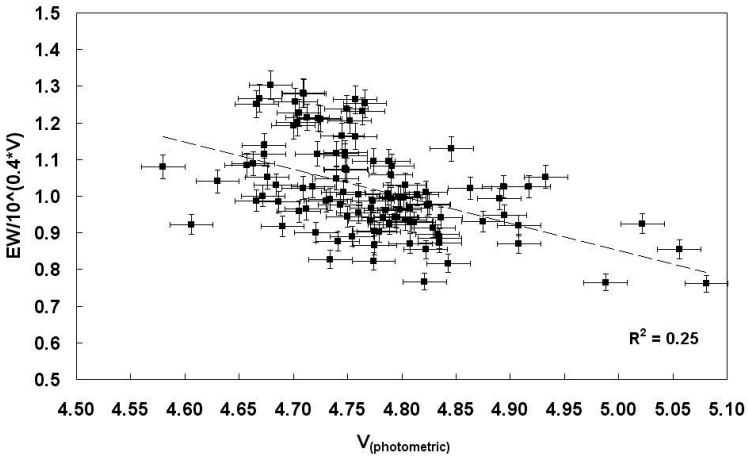

Figure 3. The relationship between line flux and V-magnitude of P Cyg.

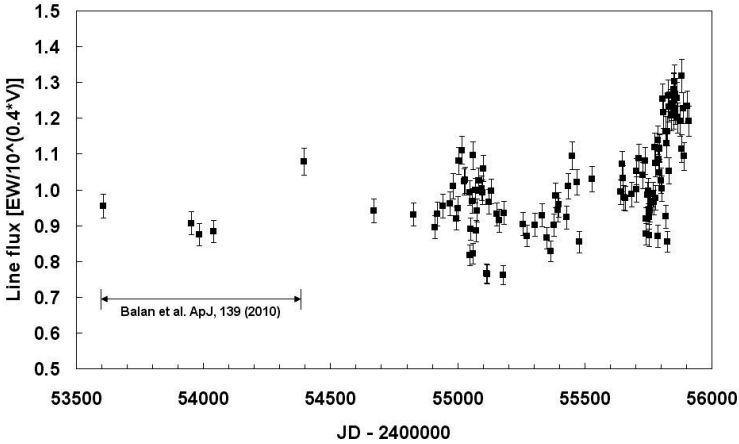

Figure 4. Intrinsic flux of the Hα line of P Cyg, 22 August (JD 2453605) to 15 December 2011 (JD 2455911).

The Pulsation Period of the Hot Hydrogen-Deficient Star MV Sagittarii

John R. Percy
Rong Fu
Department of Astronomy and Astrophysics, University of Toronto, Toronto. ON, M5S 3H4, Canada; john.percy@utoronto.ca

Received January 20, 2012; revised April 30, 2012; accepted April 30, 2012

Abstract MV Sgr is a hot, hydrogen-deficient star which has undergone R CrB fadings. We have used self-correlation analysis and Fourier analysis of CCD V-band photometry in the AAVSO International Database to identify a period of 8.0 days in this star; the amplitude is about 0.03 magnitude. The variability is most likely due to pulsation.

1. Introduction

Hydrogen-deficient stars (Clayton 1996; Werner and Rauch 2008) are a rare but very diverse (Jeffery 2008a) group of objects, in advanced and unusual stages of evolution. In this paper, we are concerned with hydrogen-deficient stars which can undergo the R CrB phenomenon—unpredictable fadings, followed by slow return to maximum brightness. Most of the approximately fifty such stars in our galaxy are cool—"classical" R CrB stars—but a few hot members of the group have been discovered.

There are two proposed mechanisms for producing "classical" R CrB stars: the merger of a helium white dwarf and a carbon-oxygen white dwarf, and a final helium shell flash (Iben *et al.* 1996; Saio and Jeffery 2002). Observational evidence seems to favor the former mechanism, though a few R CrB stars may be produced by the latter mechanism (Clayton 2011). The hot hydrogen-deficient stars do not necessarily arise from the same mechanism(s) as the cool ones, and may in fact have diverse evolutionary histories (De Marco *et al.* 2002).

Many R CrB stars are also pulsating variables, and the pulsation may be partly responsible for the mass loss that leads to the fadings. Pulsating hot hydrogen-deficient variable stars have been classified as PV Tel stars, but Jeffery (2008b) argues that this classification should be replaced by three new classes, based on the pulsation period and mode in the star.

MV Sgr (AAVSO 1838–21, HV 4168, V ~ 13.35) was discovered to be an R CrB star in 1928 by Miss Ida Woods (Hoffleit 1959), and has been studied by various techniques since then (De Marco *et al.* 2002). Its atmospheric properties are T_{eff} = 16,000 ± 500 K and log g = 2.48 ± 0.30, and pulsations had not been found in MV Sgr as of 2008 (Jeffery 2008b).

Since observations of this star have been made by AAVSO observers, one of

the purposes of this paper is to provide feedback to the observers, showing the kind of science that can be done with their observations. An additional purpose is to demonstrate how undergraduate students (such as co-author Fu) can carry out useful research with archival variable star data.

2. Data, analysis, and results

Visual and CCD V-band data were taken from the American Association of Variable Star Observers International Database (AID; Henden 2012). There were a total of 2,315 visual observations, and 138 CCD V-band observations. The former were made by 33 different observers; the latter were made by G. Di Scala, M. Simonsen, J. Temprano, and D. Wells.

The most numerous V-band observations were in the season JD 2455644–2455852. Self-correlation analysis (Percy and Mohammed 2004) of these showed a clear period of about 8.0 days, with a full amplitude of about 0.03 magnitude, and at least eight repeating minima, indicating coherent variability (Figure 1). Self-correlation anaysis of the whole V-band dataset showed a period of 8.0 ± 0.1 days, with a similar amplitude. The mean error of the observations, as determined from the intercept on the vertical axis, is 0.03 magnitude. Self-correlation analysis of the visual data did not show a detectable signal, which is probably due to the small amplitude and the much higher noise level.

The analysis was repeated with Fourier analysis, using the PERIOD04 software (Lenz and Breger 2005). For the V-band data, in the season JD 2455644–2455852, and in the whole dataset, the highest peaks were at frequencies of 0.128 cycle/day (period 7.8 days) and and 0.122 cycle/day (period 8.2 days), respectively; the latter spectrum is shown in Figure 2. In each case, the highest peak was only slightly higher than the next-highest peak. It did, however, agree with the period found from self-correlation analysis. For the visual data, the highest peak was at a frequency of 0.204 cycle/day (period 4.9 days), but this was only slightly higher than the noise level, and may not be significant, especially considering the small amplitude and the much higher noise level in the visual data.

3. Discussion and conclusions

MV Sgr displays a period of 8.0 days, which we assume to be due to pulsation. The signal is not strong, but it is quite clear in the self-correlation diagram, and is consistent with the results of the Fourier analysis. This enables us to place the star in Jeffery's (2008b) PV Tel I sub-class.

MV Sgr was not known to be pulsating (Saio and Jeffery 1988; Jeffery 2008b). We now have one more piece of useful information about this star. Also, the discovery of pulsation provides further support for the possible connection between pulsation and the R CrB phenomenon in hydrogen-deficient stars.

4. Acknowledgements

We thank the AAVSO observers and staff for making and archiving the visual and CCD observations used in this study, and the referee Geoff Clayton for his useful suggestions. This study was supported by the Ontario Work-Study Program.

References

Clayton, G. C. 1996, *Publ. Astron. Soc. Pacific*, **108**, 225.

Clayton, G. C. 2011, in *Asymmetric Planetary Nebulae V*, eds. A. A. Zijlstra, F. Lykou, I. McDonald, and E. Lagadec, Jodrell Bank Centre for Astrophysics, Manchester, UK, 157.

De Marco, O., Clayton, G. C., Herwig, F., Pollacco, D. L., Clark, J. S., and Kilkenny, D. 2002, *Astron. J.*, **123**, 3387.

Henden, A.A., 2012, Observations from the AAVSO International Database, private communication.

Hoffleit, D. 1959, *Astron. J.*, **64**, 241.

Iben, I., Jr., Tutukov, A. V., and Yungelson, L. R. 1996, *Astrophys. J.*, **456**, 750.

Jeffery, C. S. 2008a, in *Hydrogen-Deficient Stars*, eds. K. Werner, and T. Rauch, ASP Conf. Ser. 391, Astron. Soc. Pacific, San Francisco, 3.

Jeffery, C. S. 2008b, *Inf. Bull. Var. Stars*, No. 5817, 1.

Lenz, P., and Breger, M. 2005, *Commun. Astroseismology*, **146**, 53.

Percy, J. R., and Mohammed, F. 2004, *J. Amer. Assoc. Var. Star Obs.*, **32**, 9.

Saio, H., and Jeffery, C. S. 1988, *Astrophys. J.*, **328**, 714.

Saio, H., and Jeffery, C. S. 2002, *Mon. Not. Roy. Astron. Soc.*, **333**, 121.

Werner, K., and Rauch, T., eds. 2008, *Hydrogen-Deficient Stars*, ASP Conf. Ser. 391, Astron. Soc. Pacific, San Francisco.

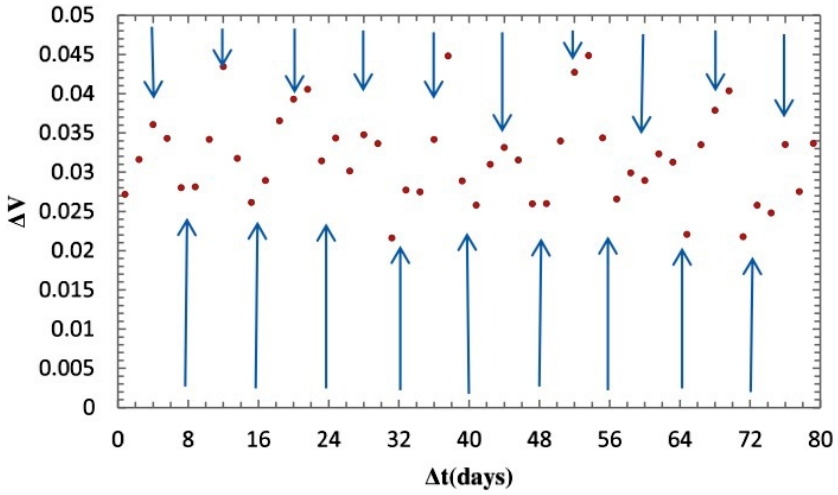

Figure 1. Self-correlation diagram for CCD V-band observations of MV Sgr during the season JD 2455644–2455852 when the observations are most numerous. There are repeating minima at multiples of 8.0 days: 8, 16, 24 (weak), 32, 40, 48, 56, 64... days, and maxima at 4, 12, 20, 28 (weak), 36, 44, 52... indicating coherent variability. These minima and maxima are marked. The minima (including at $\Delta t = 0$), do not extend below 0.025 because this is the average error of the observations. The minima and maxima die out at large Δt because of the scarcity of Δ magnitudes with these Δt values.

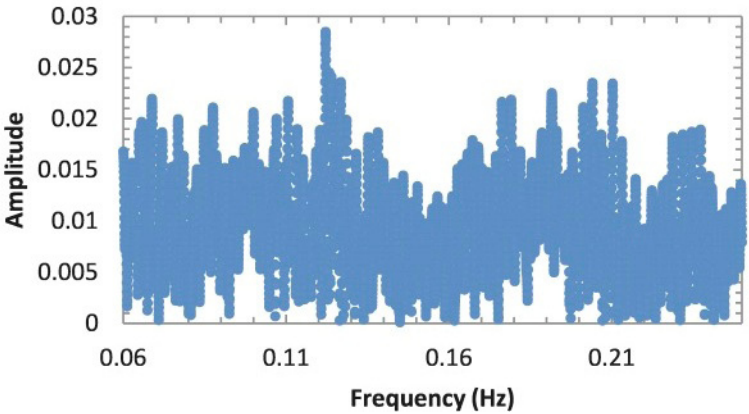

Figure 2. Fourier spectrum for CCD V-band observations of MV Sgr. The highest peak is at a frequency corresponding to a period of 8.0 days.

GEOS RR Lyrae Survey: Blazhko Period Measurement of Three RRab Stars—CX Lyrae, NU Aurigae, and VY Coronae Borealis

Pierre de Ponthière
15 Rue Pré Mathy, Lesve, Profondeville 5170, Belgium

Jean–François Le Borgne
14, Avenue Edouard Belin, F–31400 Toulouse, France

F. Fumagalli
Calina Observatory, Carona, Switzerland

Franz–Josef Hambsch
12 Oude Bleken, Mol, 2400, Belgium

Tom Krajci
P. O. Box 1351, Cloudcroft, NM 88317

J.-M. Llapasset
66 Cours de Lassus, F–66000 Perpignan, France

Kenneth Menzies
318A Potter Road, Framingham, MA 01701

Marco Nobile
via Cantonale 53, 6942 Savosa, Switzerland

Richard Sabo
2336 Trailcrest Drive, Bozeman, MT 59718

Received December 14, 2011; revised December 28, 2011; accepted January 9, 2012

Abstract We present the results of collaborative observations of three RR Lyrae stars (CX Lyr, NU Aur, and VY CrB) which have a strong Blazhko effect. This work has been initiated and performed in the framework of the GEOS RR Lyr Survey (Groupe Européen d'Observations Stellaires). From the measured light curves, we have determined the times and the magnitudes at maximum. The times of maxima have been compared to ephemerides to obtain the (O–C) values and from a period analysis of these (O–C) values, the Blazhko period is derived. The Blazhko periods of NU Aur (114.8 days) and VY CrB (32.3 days) are reported here for the first time and a more accurate period for CX Lyr (68.3 days) has been obtained. The three stars are subject to strong Blazhko effect, but this effect has different characteristics for each of them. When we compare the variations of magnitude at maximum and variations of (O–C) values with

respect to the Blazhko phase, these variations are in phase, in opposition, or even in quadrature.

1. Introduction

The main objective of the GEOS RR Lyr Survey is to follow the variations of period and Blazhko effect of bright and well-studied RR Lyrae stars. These variations are followed in the long term with TAROT robotic telescopes (Le Borgne *et al.* 2007 and Poretti *et al.* 2008). The second objective of the survey is the observation of Blazhko effect of under-studied RR Lyrae stars. The results presented here are in keeping with this objective.

The RR Lyrae stars of Bailey type ab (RRab) are pulsating stars with a period between 0.4 and 0.7 day. Some RRab stars exhibit a phase and amplitude modulation. This phenomenon, known for a century, is called the Blazhko effect. It is recognized that this effect is still not well understood. RRab stars exhibiting the Blazhko effect appear to show a variety of characteristics. Recent continuous, high precision photometry from the Kepler satellite documents a period doubling for some RR Lyrae stars (Szabó *et al.* 2010). With our ground–based small aperture telescopes and their limited photometric accuracy, we attempt to determine the Blazhko period of neglected RRab stars. Monitoring during several years is needed to determine the Blazhko period and to characterize the Blazhko behavior. We have analyzed the variations of the magnitude at maximum and (O–C) value with respect to the Blazhko phase for three different stars (CX Lyr, NU Aur, and VY CrB).

After dark and flat field corrections with the MAXIM DL software (Diffraction Limited 2004), aperture photometry was performed using either AIP4WIN (Berry and Burnell 2001) or LESVEPHOTOMETRY (de Ponthière 2010), a custom software which also evaluates the SNR and estimates magnitude errors. No color corrections have been applied to the measured magnitudes. The times of maxima of the light curves have been evaluated with the same custom software fitting the light curve with a smoothing spline function (Reinsch 1967). We have used the ANOVA algorithm of PERANSO (Vanmunster 2007) to derive the Blazhko period from the times of maxima.

2. CX Lyr

The star CX Lyr is classified in the *General Catalogue of Variable Stars* (GCVS; Samus *et al.* 2011) as an RRab variable star with a period of 0.61664495 day. CX Lyr observations during the second half of 2008 (JD 2454637 to 2454783) have been previously reported by de Ponthière *et al.* (2009). During a new observation campaign from 2009 to 2011 (JD 2455041 to 2455807), we obtained forty–one new maxima.

The comparison stars used by the authors are given in Table 1. The star

coordinates and magnitudes in *B* and *V* bands were obtained from the NOMAD catalogue (Zacharias *et al.* 2011). C1 was used as magnitude reference and the others as check stars. The choice of different comparison stars creates a magnitude offset due to their color differences. This offset has been evaluated by comparing the magnitudes of a common check star and taken into account. Table 2 provides the list of these new observations and Figure 1 shows the (O–C) values. For the sake of completeness, observations obtained by G. Maintz (Huebscher *et al.* 2008, 2010) and older GEOS observations are included in the table as they are used in the present analysis.

A linear regression of all available (O–C) values has provided a new pulsation period of 0.616758 day. The (O–C) values have been re–evaluated with this new pulsation period. The new elements are:

$$HJD = 2454677.5692 \pm 0.0031 + (0.6167582 \pm 0.0000031)\ E \qquad (1)$$

These values are very close to the values reported previously (de Ponthiere *et al.* 2009).

$$HJD = 2454677.5688 \pm 0.0037 + (0.61675 \pm 0.000024\ )\ E \qquad (2)$$

The Blazhko period was determined by a period analysis of the (O–C) values with the ANOVA algorithm. The most significant period is 68.3 ± 0.4 days (5.34 c/y). The periodogram presented in Figure 2 indicates other peaks at 56.6 days (6.45 c/y), 84.1 days (4.34 c/y), and 113.3 days (3.22 c/y) which are one-year sampling aliases.

There is also another peak at 136 days, that is, twice the most significant period. Data from the year 2010 (JD 2455300 to 2455500) indicate that the successive Blazhko cycles are not identical (Figure 1). The variations of successive cycles create spectral response at a multiple of the fundamental period. An (O–C) folded light curve at 136 days, would show two maxima. A similar period analysis of the magnitude at maximum with the ANOVA algorithm has provided similar conclusions.

The folded (O–C) and magnitude at maximum curves versus the Blazhko phase are given in Figure 3a and 3b. It can be seen that these two curves are nearly in phase, with the minima reached at the same Blazhko phase.

3. NU Aur

The star NU Aur is classified in the GCVS (Samus *et al.* 2011) as an RRab variable star with a period of 0.53941672 day and a Blazhko period of 179 days. During a first observation campaign, between December 2006 and February 2007 (JD 2454081 to 2454135), the eighteen obtained maxima clearly showed a strong Blazhko effect but did not allow a determination of the Blazhko period. The observation of seventy–five maxima resulted from a second series of observations between December 2008 and March 2011

(JD 2454752 to 2454640). The comparison stars are documented in Table 3. Star coordinates and *B* and *V* magnitudes are those found in the AAVSO's Comparison Star Database (VSD). The times of maximum and (O–C) values are given in Table 4 and Figure 4. The observations of G.Maintz have already been published by Huebscher *et al.* (2009) and those of K. Menzies published by Samolyk (2011).

A linear regression on the (O–C) values has provided the following elements:

$$HJD = 2454752.4603 \pm 0.0014 + (0.5394148 \pm 0.0000015)\ E \qquad (3)$$

To determine the Blazhko period we have performed a period analysis of the (O–C) values with the ANOVA algorithm. The corresponding periodogram presented in Fig. 5a indicates that the values of the four prominent peaks include:

Period (days)	Cycles / year	Peak value
114.4	3.192	49.6
170.1	2.148	56.7
227.1	1.600	47.3
339.6	1.074	53.4

The first two peaks (114.4 ± 1.7 and 170.1 ± 2.6 days) are an alias pair. One frequency is the alias at one cycle per year of the other. The third period (227.1) days is approximately double the first one (114.4). The period of 170.1 days is close to the value reported in the GCVS (175 days). These aliases are artifacts arising from gaps between normal 6–month observing seasons. With the Spectral Window tool in PERANSO, we have tried to determine which peaks are artifacts of the seasonal sampling. This algorithm calculates the pattern caused by the structure of gaps in the observations. The output of the Spectral Window is given in Figure 5b, where it can be seen that the artifact peaks are broad. The list of prominent peaks is:

Period (days)	Cycles / year	Peak value
91.1	4.007	0.08
103.4	3.536	0.06
128.8	2.834	0.07
145.2	2.517	0.16
181.4	2.013	0.12
244.2	1.494	0.28
362.2	1.008	0.60

This Spectral Window analysis indicates that the first peak (114.4 days) of the ANOVA analysis is not an artifact due to seasonal sampling. The second peak (170.1 days) is close to the 181.4 peak of the Spectral Window analysis and could be an artifact. The Blazhko period is probably 114.4 ± 1.7 days, but

we can not eliminate the second possible period of 170.1 ± 2.6 days. More observations are needed to remove this ambiguity.

Using the adopted period of 114.4 days, the folded (O–C) and magnitude at maximum curves versus the Blazhko phase are given in Figure 6a and 6b. It can be seen that these two curves are not in phase as was the case for CX Lyr. For NU Aur star the two curves are in quadrature.

4. VY CrB

The star VY CrB is classified in the GCVS (Samus *et al.* 2011) as an RRab variable star. VY CrB is also designated as GSC 2576–0980 (Space Telescope Science Institute 2001). It was identified as an RRab star on photographic plates by Antipin (1996). VY CrB is herein identified as Antipin's Var 23 with a period of 0.462957 day.

We observed two maxima of VY CrB in April 2007 (JD 2454215 and 2454216) and forty–nine maxima between April 2010 and August 2011 (JD 2455302 to 2455784). The selected comparison stars are given in Table 5. Star coordinates and *B* and *V* magnitude are obtained from the NOMAD catalogue. The times of maximum and (O–C) values are given in Table 6 and Figure 7. This table also includes a previous observation obtained by A. Paschke (Agerer and Huebscher 2002).

A linear regression of the (O–C) values has provided the following elements:

$$HJD = 2455302.5032 \pm 0.0013 + (0.4629461 \pm 0.0000010)\ E \qquad (4)$$

As for the other stars, the Blazhko period has been derived with the ANOVA algorithm applied to the (O–C) values. The corresponding periodogram is given in Figure 8. The periods for the two prominent peaks are: 32.3 ± 0.1 and 64.6 ± 0.2 days, which differ by a factor of two. As for CX Lyr, the non–repetitive behavior of the Blazhko effect generates spectral response at multiples of the fundamental period. With a Blazhko period of 64.4 days we would have two (O–C) maxima per cycle, so we retained the Blazhko period value of 32.3 ± 0.1 days.

The folded (O–C) and magnitude at maximum versus the Blazhko period of 32.3 days are given in Figure 9a and 9b. It can be seen that these two curves are in phase opposition: the maximum value of (O–C) occurs when the magnitude at maximum is at its minimum value.

5. Blazhko behavior comparison

It is interesting to plot the magnitude at maximum versus the (O–C) values. If these quantities were varying in time as sinusoids and were in phase, the resulting graph would be a straight line in the first and third quadrants. If they were in phase opposition, the graph would be a straight line in the second

and fourth quadrants and if they were in quadrature the graph would exhibit a circle. The periodical variations of magnitude at maximum and the (O–C) values are not sinusoidal, but the corresponding parametric representation will nevertheless provide useful information.

These graphs for the three stars are given in Figure 10. For the CX Lyr, the points are scattered along two segments forming a right angle but the general trend is a slope at 45 degrees indicating that (O–C) and magnitude at maximum are in phase as shown in Figures 3a and 3b. The points along the vertical segment correspond to the Blazhko phases between 0.0 and 0.5 and the other points along the horizontal segment correspond to the second part of the Blazhko period.

In the diagram of NU Aur, the points with a magnitude fainter than 12.9 are grouped on a circle, the magnitude at maximum and (O–C) values are in phase quadrature as shown in Figures 6a and 6b. The group of points with a magnitude fainter than 12.9 are created by the non–repetitive behavior from Blazhko cycles. The full data set for NU Aur covers more than ten Blazhko cycles.

In the VY CrB graph, the points are scattered along a curve with a slope of about 135 degrees. The magnitude at maximum and (O–C) curves are in phase opposition.

For CX Lyr and VY CrB, the (O–C) errors are larger when the magnitudes at maximum are at their greatest value. This is partially due to a lower SNR but mainly because the light curve at maximum is flatter, which leads to a less precise maximum measurement.

6. Conclusions

This study indicates that regular observations over several seasons or years by amateurs can lead to the characterization of the Blazhko effect of RR Lyr stars: this is one of the main objectives of the professional–amateur program "GEOS RR Lyr Survey." These results should encourage amateurs to join in measurement campaigns.

The measurement of RR Lyrae stars having a strong Blazhko effect highlights the fact that this effect is not standard from one star to another, as satellite-based observations (CoRot and Kepler) have shown. Each star has a particular behavior and it may not repeat exactly from one cycle to another. A complete astrophysical model of Blazhko effect for RRab stars should be able to explain these behavior differences.

7. Acknowledgements

This research made use of the GEOS RR Lyr database http://rr–ly.ast.obs–mip.fr, hosted by Institut de Recherche en Astrophysique et Planétologie, Toulouse, France, and of the SIMBAD database, operated at CDS, Strasbourg,

France. The authors acknowledge AAVSO Director Arne Henden and the AAVSO for the use of the AAVSONet telescopes at Sonoita (Arizona) and Cloudcroft (New Mexico). They would also like to thank G. Maintz and A. Paschke for their contributions to the GEOS database.

The authors wish to recognize their affiliation with the following organizations or institutions: Pierre de Ponthière—AAVSO, Groupe Européen d'Observations Stellaires, France (GEOS); Jean–François Le Borgne—GEOS, Université de Toulouse, France; F. Fumagalli—GEOS; Franz–Josef Hambsch—AAVSO, Bundesdeutsche Arbeitsgemeinschaft für Veränderliche Sterne e.V., Germany (BAV), GEOS, Vereniging Voor Sterrenkunde, Belgium (VVS); Tom Krajci—AAVSO; Kenneth Menzies—AAVSO, GEOS; Marco Nobile—GEOS; Richard Sabo—AAVSO, GEOS.

References

Agerer, F., and Huebscher, J. 2002, *Inf. Bull. Var. Stars*, No. 5296, 1 (*BAV Mitteilungen* No. 152).

Antipin, S. V. 1996, *Inf. Bull. Var. Stars*, No. 4343, 1.

Berry, R., and Burnell, J. 2001, *The Handbook of Astronomical Image Processing*, Willmann–Bell, Richmond, VA.

de Ponthière, P. 2010, LESVEPHOTOMETRY automatic photometry software, http://www.dppobservatory.net

de Ponthière, P., Le Borgne, J. –F., and Hambsch, F. –J. 2009, *J. Amer. Assoc. Var. Star Obs.*, **37**, 117.

Diffraction Limited 2004, MAXIM DL image processing software, http://www.cyanogen.com

Groupe Européen d'Observation Stellaire (GEOS) 2011, GEOS RR Lyr Database, http://rr–lyr.ast.obs–mip.fr/

Huebscher, J., Lehmann, P. B., Monninger, G., Steinbach, H. –M., and Walter, F. 2010, *Inf. Bull. Var. Stars*, No. 5941, 1 (*BAV Mitteilungen* No. 212).

Huebscher, J., Steinbach, H. –M., and Walter, F. 2008, *Inf. Bull. Var. Stars*, No. 5830, 1 (*BAV Mitteilungen* No. 193).

Huebscher, J., Steinbach, H. –M., and Walter, F. 2009, *Inf. Bull. Var. Stars*, No. 5874, 1 (*BAV Mitteilungen* No. 201).

Le Borgne, J. F., *et al.* 2007, *Astron. Astrophys.*, **476**, 307.

Poretti, E., *et al.* 2008, *Mem. Soc. Astron. Ital.*, **79**, 471.

Reinsch, C. H. 1967, *Numer. Math.*, **10**, 177.

Samolyk, G. 2011, *J. Amer. Assoc. Var. Star Obs.*, **39**, 23.

Samus, N. N., *et al.* 2011, *General Catalogue of Variable Stars* (GCVS database, Version 2011Jan), http://www.sai.msu.su/gcvs/gcvs/index.htm

Space Telescope Science Institute 2001, *The Guide Star Catalog*, Version 2.2 (VizieR On–line Data Catalog: I/271), STScI, Baltimore.

Szabó, R., *et al.* 2010, *Mon. Not. Roy. Astron. Soc.*, **409**, 1244 (http://arxiv.org/abs/1007.3404).

Vanmunster, T. 2007, PERANSO period analysis software, http://www.cbabelgium.com and http://www.peranso.com

Zacharias, N., Monet, D., Levine, S., Urban, S., Gaume, R., and Wycoff, G. 2011, The Naval Observatory Merged Astrometric Dataset (NOMAD), http://www.usno.navy.mil/USNO/astrometry/optical–IR–prod/nomad/

Table 1. Comparison stars for CX Lyr.

Identification	*R.A. (2000)* h m s	*Dec. (2000)* ° ′ ″	*B*	*V*	*B–V*	*DPP*	*Hambsch*	*Sabo*
GSC 2121–2818	18 51 51.48	+28 49 08.15	11.129	10.548	0.581	C1		
GSC 2121–2053	18 51 37.00	+28 51 16.32	11.054	10.565	0.489	C2		C2
GSC 2121–1980	18 51 14.25	+28 43 37.01	13.29	12.74	0.55	C3	C1	C1
GSC 2121–2842	18 51 07.01	+28 45 12.52	13.8	13.1	0.7		C2	

Table 2. List of measured maxima of CX Lyr.

Maximum HJD	*Error*	*O–C (day)*	*E*	*Magnitude*	*Error*	*Filter*	*Observer*
2454238.4240	0.0050	–0.0139	–712	—	—	—	F. Fumagalli
2454278.5276	0.0014	0.0004	–647	—	—	—	F. Fumagalli
2454280.3802	0.0015	0.0027	–644	—	—	—	F. Fumagalli
2454362.4056	0.0014	–0.0007	–511	—	—	—	G. Maintz
2454637.4929	0.0026	0.0125	–65	12.329	0.050	V	F.-J. Hambsch
2454661.5051	0.0020	–0.0289	–26	12.308	0.050	V	F.-J. Hambsch
2454677.5688	0.0018	–0.0009	0	12.152	0.006	V	P. de Ponthière
2454685.5930	0.0020	0.0055	13	12.062	0.026	V	P. de Ponthière
2454692.3815	0.0013	0.0096	24	12.051	0.005	V	P. de Ponthière
2454708.4197	0.0019	0.0121	50	12.235	0.006	V	P. de Ponthière
2454711.5050	0.0040	0.0136	55	12.237	0.040	V	P. de Ponthière
2454719.5020	0.0050	–0.0072	68	12.297	0.026	V	P. de Ponthière
2454724.4300	0.0040	–0.0133	76	12.331	0.007	V	P. de Ponthière
2454729.3630	0.0030	–0.0144	84	12.324	0.006	V	P. de Ponthière
2454750.3518	0.0016	0.0047	118	12.134	0.012	V	P. de Ponthière
2454758.3736	0.0012	0.0086	131	12.156	0.020	V	P. de Ponthière
2454774.4100	0.0030	0.0093	157	12.293	0.020	V	P. de Ponthière
2454782.3940	0.0030	–0.0246	170	12.363	0.022	V	P. de Ponthière
2454983.4954	0.0024	0.0137	496	12.333	0.008	V	P. de Ponthière
2455041.4761	0.0032	0.0191	590	12.158	0.008	V	P. de Ponthière

Table continued on next page

Table 2. List of measured maxima of CX Lyr, cont.

Maximum HJD	*Error*	*O–C (day)*	*E*	*Magnitude*	*Error*	*Filter*	*Observer*
2455046.4025	0.0025	0.0115	598	12.296	0.013	V	F.-J. Hambsch
2455049.4886	0.0035	0.0138	603	12.294	0.010	V	P. de Ponthière
2455052.5695	0.0085	0.0109	608	12.295	0.015	V	P. de Ponthière
2455057.4596	0.0060	–0.0331	616	—	—	V	G. Maintz
2455060.5485	0.0084	–0.0279	621	12.371	0.010	V	P. de Ponthière
2455062.3950	0.0010	–0.0317	624	—	—	V	G. Maintz
2455062.3977	0.0032	–0.0290	624	12.432	0.009	V	F.-J. Hambsch
2455094.5062	0.0025	0.0081	676	12.065	0.015	V	P. de Ponthière
2455096.3587	0.0015	0.0103	679	12.042	0.008	V	P. de Ponthière
2455295.5698	0.0015	0.0085	1002	12.087	0.011	V	P. de Ponthière
2455303.5902	0.0012	0.0111	1015	12.021	0.010	V	P. de Ponthière
2455308.5270	0.0020	0.0138	1023	12.024	0.011	V	P. de Ponthière
2455311.6080	0.0025	0.0110	1028	12.073	0.020	V	P. de Ponthière
2455312.8464	0.0018	0.0159	1030	12.162	0.012	V	F.-J. Hambsch
2455320.8601	0.0019	0.0117	1043	12.307	0.011	V	F.-J. Hambsch
2455333.7745	0.0040	–0.0258	1064	12.397	0.012	V	F.-J. Hambsch
2455353.5350	0.0025	–0.0015	1096	12.303	0.012	V	P. de Ponthière
2455363.4131	0.0025	0.0084	1112	12.122	0.030	V	P. de Ponthière
2455369.5828	0.0020	0.0106	1122	12.050	0.010	V	P. de Ponthière
2455374.5167	0.0020	0.0104	1130	12.030	0.010	V	P. de Ponthière
2455379.4518	0.0020	0.0114	1138	12.056	0.009	V	P. de Ponthière
2455382.5342	0.0015	0.0100	1143	12.121	0.009	V	P. de Ponthière
2455387.4662	0.0023	0.0080	1151	12.188	0.010	V	P. de Ponthière
2455392.3970	0.0030	0.0047	1159	12.286	0.010	V	P. de Ponthière
2455395.4753	0.0040	–0.0008	1164	12.337	0.009	V	P. de Ponthière
2455398.5497	0.0074	–0.0102	1169	12.364	0.009	V	P. de Ponthière
2455408.3959	0.0035	–0.0321	1185	12.325	0.010	V	P. de Ponthière
2455429.4044	0.0025	0.0066	1219	12.189	0.011	V	P. de Ponthière
2455440.5115	0.0017	0.0121	1237	11.988	0.009	V	P. de Ponthière
2455442.3601	0.0020	0.0104	1240	11.980	0.012	V	P. de Ponthière
2455445.4485	0.0015	0.0150	1245	12.009	0.008	V	P. de Ponthière
2455461.4862	0.0040	0.0170	1271	12.284	0.011	V	P. de Ponthière
2455470.7015	0.0065	–0.0191	1286	12.427	0.011	V	F.-J. Hambsch
2455479.3298	0.0047	–0.0254	1300	12.371	0.010	V	P. de Ponthière
2455492.3090	0.0075	0.0019	1321	12.347	0.018	V	P. de Ponthière
2455649.5879	0.0020	0.0075	1576	12.053	0.009	V	P. de Ponthière
2455670.5422	0.0044	–0.0080	1610	12.343	0.010	V	P. de Ponthière
2455713.7302	0.0013	0.0069	1680	12.025	0.006	V	K .Menzies
2455745.7679	0.0020	–0.0268	1732	12.464	0.004	V	R. Sabo
2455746.3925	0.0026	–0.0189	1733	12.401	0.013	V	P. de Ponthière
2455807.4625	0.0034	–0.0080	1832	12.366	0.010	V	P. de Ponthière

Table 3. Comparison stars for NU Aur.

Identification *R.A. (2000)* *h m s*	*Dec. (2000)* ° ′ ″	*B*	*V*	*B–V*	*DPP*	*Hambsch*	*Menzies*	*Sabo*
GSC 1857–1453								
05 08 58.82	+28 42 08	13.32	12.53	0.795	C1	C1	C1	C1
GSC 1857–1288								
05 08 59.15	+28 43 20.2		13.67			C2		
GSC 1857–1288								
05 08 59.17	+28 43 20.3	14.46	13.77	0.69	C2		C2	C2
GSC 1857–938								
05 08 34.00	+28 45 07.6	13.322	12.326	0.996	C3	C3	C3	C3

Table 4. List of measured maxima of NU Aur.

Maximum HJD	*Error*	*O–C (day)*	*E*	*Magnitude*	*Error*	*Filter*	*Observer*
2454081.4445	0.0100	0.0204	–1244	—	—	—	J.-M. Llapasset
2454083.5942	0.0005	0.0125	–1240	—	—	—	J.-M. Llapasset
2454088.4454	0.0010	0.0089	–1231	—	—	—	J.-M. Llapasset
2454089.5225	0.0005	0.0072	–1229	—	—	—	J.-M. Llapasset
2454090.6033	0.0005	0.0092	–1227	—	—	—	J.-M. Llapasset
2454091.6733	0.0010	0.0003	–1225	—	—	—	J.-M. Llapasset
2454096.5397	0.0005	0.0120	–1216	—	—	—	J.-M. Llapasset
2454100.3214	0.0005	0.0178	–1209	—	—	—	J.-M. Llapasset
2454107.3333	0.0010	0.0173	–1196	—	—	—	J.-M. Llapasset
2454114.3359	0.0005	0.0075	–1183	—	—	—	J.-M. Llapasset
2454121.3493	0.0005	0.0085	–1170	—	—	—	J.-M. Llapasset
2454128.3628	0.0010	0.0096	–1157	—	—	—	J.-M. Llapasset
2454135.3748	0.0005	0.0092	–1144	—	—	—	J.-M. Llapasset
2454456.3178	0.0004	–0.0001	–549	—	—	—	G. Maintz
2454752.4570	0.0040	0.0000	0	13.042	0.011	C	P. de Ponthière
2454759.4820	0.0030	0.0126	13	13.028	0.008	C	P. de Ponthière
2454774.5770	0.0020	0.0040	41	12.899	0.012	C	P. de Ponthière
2454787.5310	0.0040	0.0120	65	12.860	0.007	C	P. de Ponthière
2454801.0080	0.0030	0.0036	90	12.737	0.005	V	P. de Ponthière
2454804.7820	0.0040	0.0017	97	12.875	0.005	V	P. de Ponthière
2454808.0200	0.0030	0.0032	103	12.845	0.005	V	P. de Ponthière
2454827.4315	0.0018	–0.0043	139	12.854	0.007	C	P. de Ponthière
2454828.5107	0.0017	–0.0039	141	12.838	0.007	C	P. de Ponthière
2454829.5870	0.0030	–0.0064	143	12.846	0.009	C	P. de Ponthière
2454829.5900	0.0020	–0.0034	143	12.852	0.009	V	P. de Ponthière
2454830.6570	0.0030	–0.0153	145	12.878	0.009	V	P. de Ponthière

Table continued on following pages

Table 4. List of measured maxima of NU Aur, cont.

Maximum HJD	*Error*	*O–C (day)*	*E*	*Magnitude*	*Error*	*Filter*	*Observer*
2454830.6610	0.0030	–0.0113	145	12.902	0.014	V	P. de Ponthière
2454831.7451	0.0017	–0.0060	147	12.849	0.008	V	P. de Ponthière
2454832.8202	0.0016	–0.0097	149	12.875	0.008	V	P. de Ponthière
2454833.9020	0.0030	–0.0067	151	12.891	0.009	V	P. de Ponthière
2454838.7576	0.0014	–0.0059	160	12.931	0.011	V	P. de Ponthière
2454841.4540	0.0050	–0.0066	165	12.927	0.023	V	P. de Ponthière
2454843.6114	0.0018	–0.0068	169	12.936	0.013	V	P. de Ponthière
2454844.6863	0.0012	–0.0108	171	12.902	0.012	V	P. de Ponthière
2454845.7661	0.0015	–0.0098	173	12.900	0.011	V	P. de Ponthière
2454846.3070	0.0020	–0.0083	174	—	—	—	J.-M. Llapasset
2454846.8450	0.0020	–0.0097	175	12.898	0.010	V	P. de Ponthière
2454850.6150	0.0020	–0.0156	182	12.904	0.010	V	P. de Ponthière
2454851.6940	0.0040	–0.0155	184	12.946	0.009	V	P. de Ponthière
2454852.7740	0.0020	–0.0143	186	12.932	0.006	V	P. de Ponthière
2454857.6330	0.0040	–0.0100	195	13.018	0.008	V	P. de Ponthière
2454860.3380	0.0050	–0.0021	200	13.021	0.016	V	P. de Ponthière
2454861.4150	0.0040	–0.0039	202	13.040	0.018	V	P. de Ponthière
2454862.4960	0.0040	–0.0018	204	13.034	0.017	V	P. de Ponthière
2454884.6190	0.0018	0.0051	245	13.007	0.008	V	P. de Ponthière
2454887.3170	0.0020	0.0061	250	—	—	—	J.-M. Llapasset
2454888.3980	0.0020	0.0083	252	—	—	—	J.-M. Llapasset
2454891.6396	0.0030	0.0133	258	13.017	0.011	V	P. de Ponthière
2455100.9247	0.0031	0.0053	646	—	—	V	R. Sabo
2455106.8653	0.0036	0.0123	657	12.995	0.019	V	F.-J. Hambsch
2455113.8751	0.0028	0.0097	670	12.937	0.017	V	F.-J. Hambsch
2455114.9502	0.0040	0.0060	672	12.961	0.036	V	F.-J. Hambsch
2455119.8273	0.0035	0.0283	681	12.971	0.019	V	F.-J. Hambsch
2455120.8963	0.0029	0.0185	683	12.923	0.011	V	F.-J. Hambsch
2455121.9780	0.0023	0.0214	685	12.889	0.009	V	F.-J. Hambsch
2455122.5074	0.0030	0.0113	686	12.878	0.010	V	F.-J. Hambsch
2455127.9098	0.0034	0.0196	696	12.797	0.019	V	F.-J. Hambsch
2455128.9865	0.0039	0.0175	698	12.783	0.003	V	F.-J. Hambsch
2455135.9890	0.0120	0.0076	711	12.674	0.008	V	F.-J. Hambsch
2455155.4042	0.0019	0.0038	747	12.703	0.009	V	F.-J. Hambsch
2455175.3210	0.0020	–0.0378	784	—	—	—	M. Nobile
2455182.9060	0.0032	–0.0046	798	12.890	0.013	V	F.-J. Hambsch
2455189.3650	0.0040	–0.0186	810	12.867	0.015	V	F.-J. Hambsch
2455208.8035	0.0030	0.0010	846	13.014	0.008	V	F.-J. Hambsch
2455241.7199	0.0025	0.0130	907	12.963	0.010	V	F.-J. Hambsch

Table continued on next page

Table 4. List of measured maxima of NU Aur, cont.

Maximum HJD	*Error*	*O–C (day)*	*E*	*Magnitude*	*Error*	*Filter*	*Observer*
2455247.6585	0.0030	0.0180	918	12.862	0.009	V	F.-J. Hambsch
2455261.6812	0.0048	0.0159	944	12.898	0.009	V	F.-J. Hambsch
2455479.6006	0.0025	0.0115	1348	12.713	0.013	V	P. de Ponthière
2455481.7610	0.0026	0.0142	1352	12.741	0.010	V	F.-J. Hambsch
2455492.5516	0.0034	0.0165	1372	12.717	0.026	V	P. de Ponthière
2455511.9491	0.0020	–0.0050	1408	12.686	0.010	V	F.-J. Hambsch
2455528.6650	0.0024	–0.0110	1439	12.781	0.012	V	F.-J. Hambsch
2455531.8989	0.0031	–0.0135	1445	12.847	0.010	V	F.-J. Hambsch
2455538.9143	0.0040	–0.0105	1458	13.014	0.010	V	F.-J. Hambsch
2455540.5315	0.0075	–0.0116	1461	13.044	0.013	V	K. Menzies
2455542.6905	0.0041	–0.0103	1465	13.026	0.013	V	F.-J. Hambsch
2455543.7760	0.0048	–0.0036	1467	13.062	0.011	V	F.-J. Hambsch
2455545.9362	0.0042	–0.0010	1471	13.016	0.011	V	F.-J. Hambsch
2455548.6347	0.0036	0.0004	1476	13.066	0.008	V	R. Sabo
2455554.5716	0.0050	0.0037	1487	13.115	0.013	V	K. Menzies
2455555.6427	0.0035	–0.0040	1489	13.031	0.011	V	K. Menzies
2455571.3082	0.0060	0.0184	1518	13.057	0.016	V	P. de Ponthière
2455572.3921	0.0038	0.0235	1520	13.063	0.010	V	F.-J. Hambsch
2455575.6360	0.0060	0.0309	1526	13.045	0.001	V	F.-J. Hambsch
2455583.7160	0.0031	0.0197	1541	12.941	0.012	V	F.-J. Hambsch
2455589.6450	0.0047	0.0151	1552	12.919	0.012	V	K. Menzies
2455627.3941	0.0030	0.0051	1622	12.767	0.015	V	P. de Ponthière
2455627.3945	0.0016	0.0055	1622	12.775	0.006	V	F.-J. Hambsch
2455640.3375	0.0040	0.0025	1646	12.787	0.015	V	P. de Ponthière

Table 5. Comparison stars for VY CrB.

Identification *R.A. (2000)* *h m s*	*Dec. (2000)* ° ′ ″	*B*	*V*	*B–V*	*DPP*	*Hambsch*	*Menzies*	*Sabo*
GSC 2576–1883								
16 06 45.0	+33 19 35.756	12.265	11.638	0.627	C1		C1	C1
GSC 2576–1372								
16 05 53.7	+33 20 17.166	14.97	13.71	1.26	C2	C1	C2	
GSC 2576–740								
16 06 13.7	+33 19 05.222	14.36	13.58	0.78	C3	C2	C3	C2
GSC 2576–1021								
16 06 05.5	+33 25 00.460	16.77	14.65	2.12	C4	C3	C4	

Table 6. List of measured maxima of VY CrB.

Maximum HJD	*Error*	*O–C (day)*	*E*	*Magnitude*	*Error*	*Filter*	*Observer*
2451615.5930	0.005	–0.0153	–7964	—	—	—	A. Paschke
2454215.5169	0.002	0.0089	–2348	—	—	—	J.-M. Llapasset
2454216.4421	0.002	0.0082	–2346	—	—	—	J.-M. Llapasset
2455302.4926	0.0013	–0.0105	0	13.480	0.009	C	P. de Ponthière
2455303.4196	0.0018	–0.0094	2	13.510	0.012	C	P. de Ponthière
2455309.4562	0.0031	0.0088	15	13.662	0.009	C	P. de Ponthière
2455310.3791	0.0023	0.0059	17	13.702	0.011	C	P. de Ponthière
2455321.4822	0.0021	–0.0017	41	13.548	0.008	C	P. de Ponthière
2455352.5027	0.0024	0.0015	108	13.602	0.008	C	P. de Ponthière
2455364.5240	0.0014	–0.0138	134	13.376	0.009	C	P. de Ponthière
2455370.5535	0.003	–0.0026	147	13.557	0.013	C	P. de Ponthière
2455371.4812	0.0024	–0.0008	149	13.570	0.009	C	P. de Ponthière
2455377.5180	0.008	0.0177	162	13.733	0.030	C	P. de Ponthière
2455378.4431	0.0053	0.0170	164	13.719	0.014	C	P. de Ponthière
2455384.4469	0.0033	0.0025	177	13.614	0.009	C	P. de Ponthière
2455390.4495	0.0016	–0.0132	190	13.352	0.009	C	P. de Ponthière
2455391.3773	0.0015	–0.0113	192	13.343	0.009	C	P. de Ponthière
2455396.4673	0.0016	–0.0137	203	13.343	0.007	C	P. de Ponthière
2455397.3939	0.0017	–0.0130	205	13.372	0.007	C	P. de Ponthière
2455410.3855	0.0048	0.0161	233	13.737	0.009	C	P. de Ponthière
2455441.3929	0.0029	0.0062	300	13.743	0.014	C	P. de Ponthière
2455461.2817	0.0015	–0.0116	343	13.347	0.008	C	P. de Ponthière
2455480.2825	0.0036	0.0084	384	13.676	0.009	C	P. de Ponthière
2455627.4899	0.003	–0.0007	702	13.555	0.010	C	P. de Ponthière
2455640.4717	0.007	0.0186	730	13.754	0.011	C	P. de Ponthière
2455622.8556	0.0054	–0.0056	692	13.316	0.058	V	K. Menzies
2455644.6183	0.0026	–0.0013	739	13.581	0.009	C	P. de Ponthière
2455645.5423	0.003	–0.0032	741	13.559	0.009	C	P. de Ponthière
2455646.4724	0.0041	0.0010	743	13.613	0.022	C	P. de Ponthière
2455602.9682	0.005	0.0137	649	13.717	0.015	V	F.-J. Hambsch
2455608.9772	0.005	0.0044	662	13.680	0.018	V	F.-J. Hambsch
2455609.9030	0.005	0.0043	664	13.661	0.025	V	F.-J. Hambsch
2455614.9834	0.0028	–0.0077	675	13.413	0.015	V	F.-J. Hambsch
2455615.9087	0.003	–0.0083	677	13.370	0.019	V	F.-J. Hambsch
2455622.8554	0.002	–0.0058	692	13.294	0.012	V	F.-J. Hambsch
2455629.8069	0.004	0.0016	707	13.582	0.018	V	F.-J. Hambsch
2455640.9245	0.007	0.0085	731	13.690	0.024	V	F.-J. Hambsch
2455646.9268	0.003	–0.0075	744	13.432	0.014	V	F.-J. Hambsch
2455647.8531	0.003	–0.0071	746	13.382	0.013	V	F.-J. Hambsch

Table continued on next page

Table 6. List of measured maxima of VY CrB, cont.

Maximum HJD	*Error*	*O–C (day)*	*E*	*Magnitude*	*Error*	*Filter*	*Observer*
2455653.8707	0.0022	–0.0078	759	13.276	0.013	V	F.-J. Hambsch
2455654.7969	0.0019	–0.0075	761	13.276	0.013	V	F.-J. Hambsch
2455660.8238	0.003	0.0011	774	13.545	0.014	V	F.-J. Hambsch
2455665.9194	0.0053	0.0043	785	13.695	0.018	V	F.-J. Hambsch
2455666.8510	0.0044	0.0101	787	13.715	0.020	V	F.-J. Hambsch
2455671.4845	0.0039	0.0141	797	13.748	0.011	C	P. de Ponthière
2455672.4003	0.0047	0.0040	799	13.769	0.012	C	P. de Ponthière
2455714.5166	0.0013	–0.0077	890	13.337	0.007	C	P. de Ponthière
2455715.4414	0.0014	–0.0088	892	13.325	0.007	C	P. de Ponthière
2455760.8215	0.003	0.0027	990	13.690	0.011	V	R. Sabo
2455739.5326	0.0041	0.0093	944	13.608	0.009	C	P. de Ponthière
2455775.6294	0.0025	–0.0036	1022	13.494	0.013	V	K. Menzies
2455784.4199	0.003	–0.0091	1041	13.367	0.010	C	P. de Ponthière

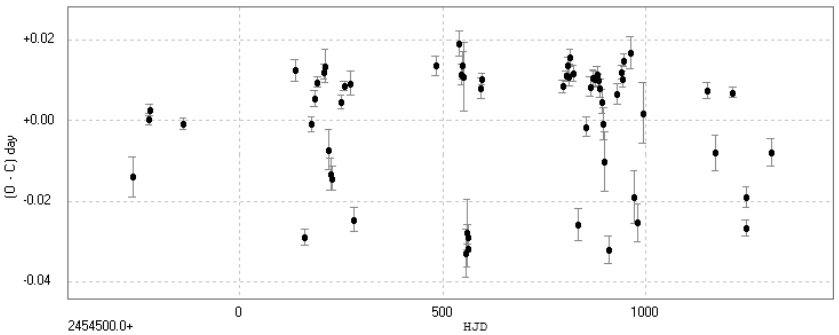

Figure 1. CX Lyr (O–C).

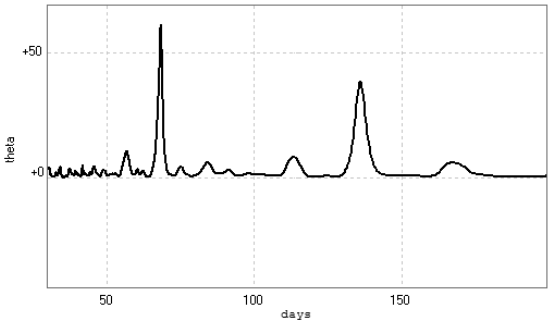

Figure 2. CX Lyr (O–C) periodogram.

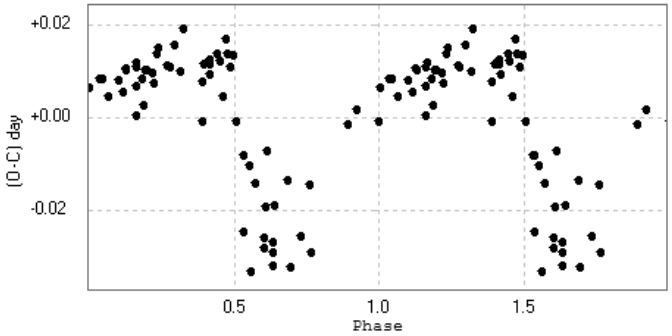

Figure 3a. CX Lyr (O–C) at maximum versus Blazhko phase.

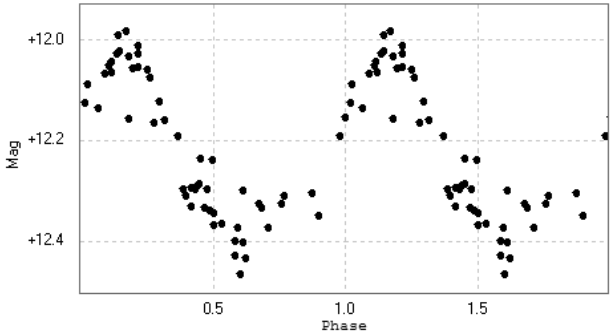

Figure 3b. CX Lyr magnitude at maximum versus Blazhko phase.

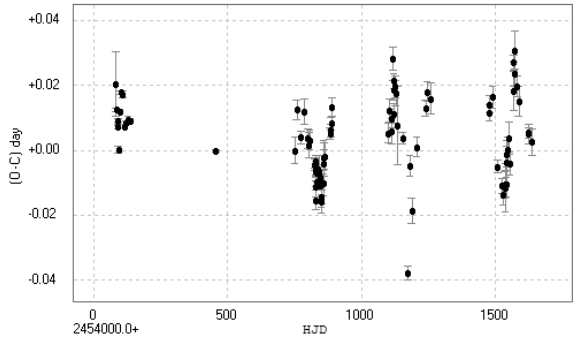

Figure 4. NU Aur (O–C).

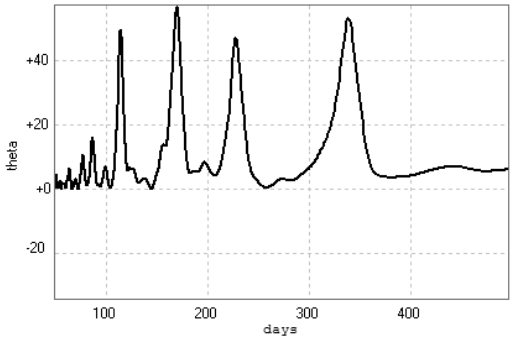

Figure 5a. NU Aur (O–C) periodogram.

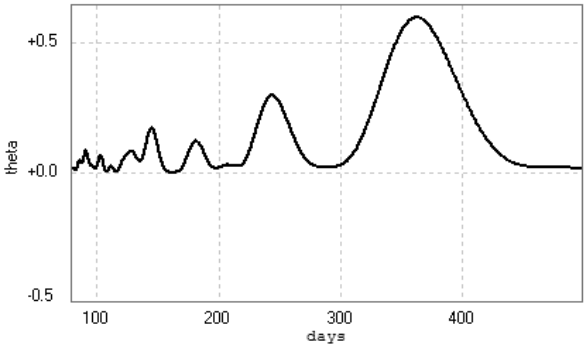

Figure 5b. NU Aur spectral window.

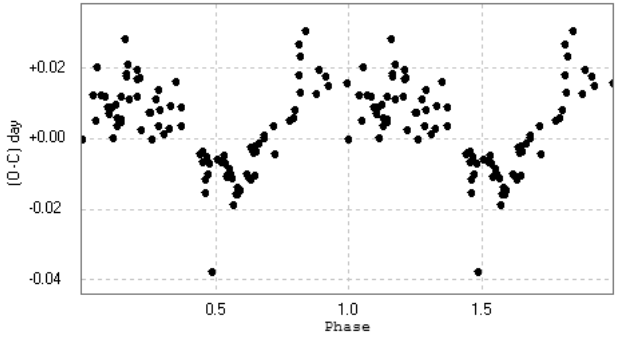

Figure 6a. NU Aur (O–C) at maximum versus Blazhko phase.

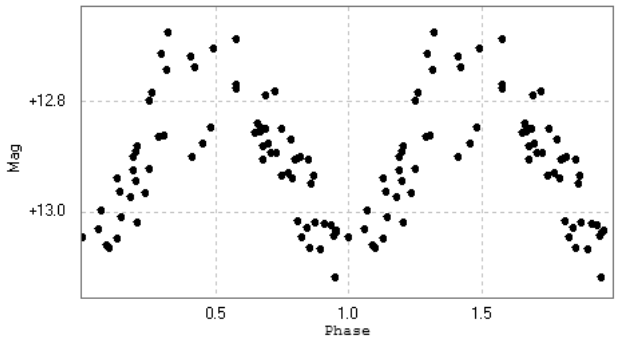

Figure 6b. NU Aur magnitude at maximum versus Blazhko phase.

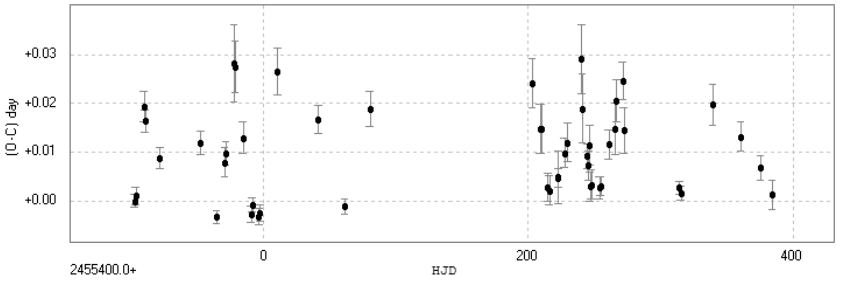

Figure 7. VY CrB (O–C).

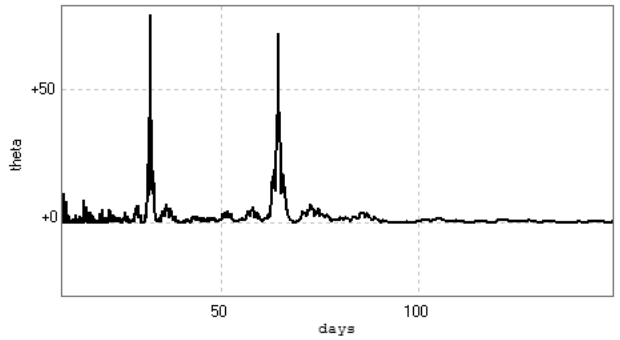

Figure 8. VY CrB (O–C) periodogram.

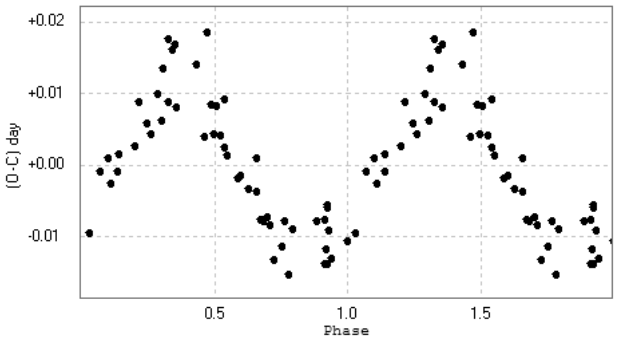

Figure 9a. VY CrB (O–C) at maximum versus Blazhko phase.

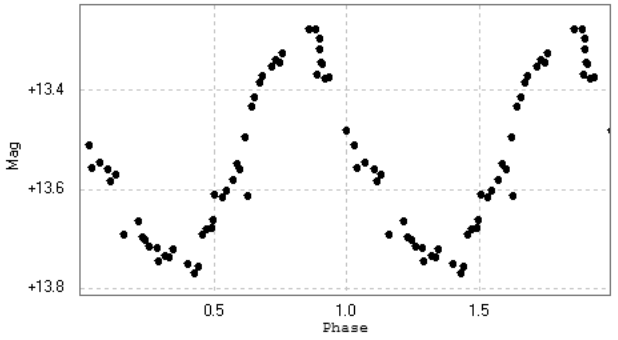

Figure 9b. VY CrB magnitude at maximum versus Blazhko phase.

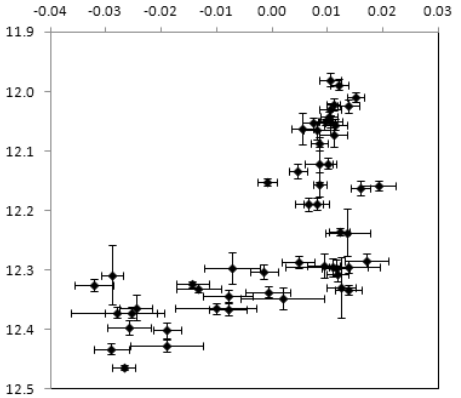

Figure 10a. CX Lyr magnitude at maximum versus (O–C) values.

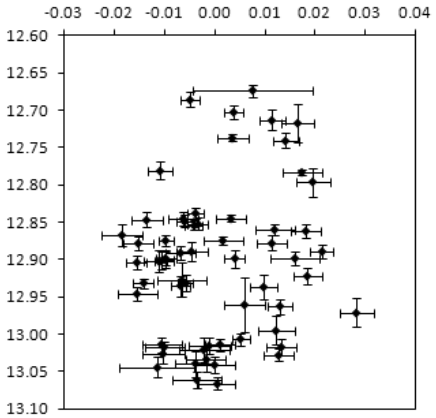

Figure 10b. NU Aur magnitude at maximum versus (O–C) values.

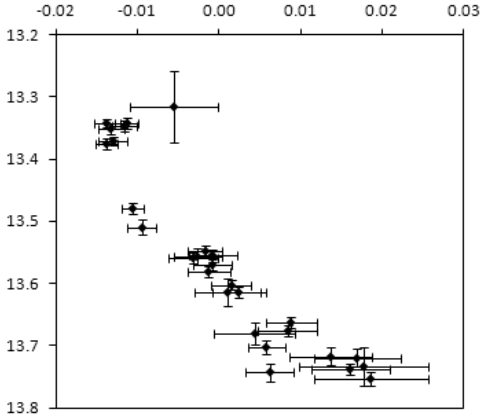

Figure 10c. VY CrB magnitude at maximum versus (O–C) values.

Recent Maxima of 55 Short Period Pulsating Stars

Gerard Samolyk
P.O. Box 20677, Greenfield, WI 53220; gsamolyk@wi.rr.com

Received January 6, 2012; accepted January 6, 2012

Abstract This paper contains times of maxima for 55 short period pulsating stars (primarily RR Lyrae and δ Scuti stars). This represents the CCD observations received by the AAVSO Short Period Pulsator (SPP) section in 2011 along with some earlier data.

1. Recent observations

The accompanying list contains times of maxima calculated from CCD observations made by participants in the AAVSO's Short Period Pulsator (SPP) Section. This list will be web-archived and made available through the AAVSO ftp site at ftp:ftp.aavso.org/public/datasets/jsamog402.txt. These observations were reduced by the writer using the PERANSO program (Vanmunster 2007). Column F indicates the filter used. The error estimate is included.

RR Lyr stars in this list, along with data from earlier AAVSO publications, are included in the GEOS database at: http://rr-lyr.ast.obs-mip.fr/dbrr/dbrr-V1.0_0.php. This database does not include δ Scuti stars.

The linear elements in the *General Catalogue of Variable Stars* (Kholopov *et al.* 1985) were used to compute the O–C values for most stars. For a few exceptions where the GCVS elements are missing or are in significant error, light elements from another source are used: VY CrB (Antipin 1996), AH Leo (Schmidt *et al.* 1995), VY LMi (Henden and Vidal-Sainz 1997), and GW UMa (Hintz *et al.* 2001).

References

Antipin, S. V. 1996, *Inf. Bull Var. Stars*, No. 4343, 1.
Henden, A. A., and Vidal-Sainz, J. 1997, *Inf. Bull Var. Stars*, No. 4535, 1.
Hintz, E. G., Bush, T. C., and Rose, M. B. 2005, *Astron. J.*, **130**, 2876.
Kholopov, P. N., *et al.* 1985, *General Catalogue of Variable Stars*, 4th ed., Moscow.
Schmidt, E. G., Chab, J. R., and Reiswig, D. E. 1995, *Astron. J.*, **109**, 1239.
Vanmunster, T. 2007, PERANSO period analysis software, http://www.peranso.com

Table 1. Recent times of maxima of stars in the AAVSO RR Lyrae program.

Star	JD(max) Hel. 2400000 +	Cycle	O–C	F	Observer	Error
SW And	55786.7504	85137	–0.3869	V	R. Sabo	0.0009
SW And	55793.8288	85153	–0.3850	V	R. Sabo	0.0014
SW And	55815.9392	85203	–0.3886	V	R. Sabo	0.0014
SW And	55827.8846	85230	–0.3847	V	R. Sabo	0.0023
SW And	55844.6873	85268	–0.3887	V	K. Menzies	0.0006
SW And	55852.6494	85286	–0.3876	V	R. Sabo	0.0015
SW And	55874.7608	85336	–0.3902	V	R. Sabo	0.0012
XX And	55796.8764	23120	–0.4746	V	R. Sabo	0.0020
XX And	55833.7370	23171	–0.4741	V	R. Sabo	0.0015
ZZ And	55891.6583	56017	0.0266	V	K. Menzies	0.0009
AT And	55808.8146	21827	–0.0041	V	R. Sabo	0.0025
AT And	55832.8716	21866	–0.0068	V	R. Sabo	0.0020
AT And	55847.6745	21890	–0.0099	V	R. Sabo	0.0026
AT And	55868.6556	21924	–0.0039	V	R. Sabo	0.0026
AT And	55889.6287	21958	–0.0059	V	N. Simmons	0.0020
DM And	55857.7959	31949	0.0667	V	K. Menzies	0.0018
SW Aqr	55777.9087	66798	–0.0022	V	R. Sabo	0.0007
SW Aqr	55790.7716	66826	0.0002	V	R. Sabo	0.0009
SW Aqr	55806.8453	66861	–0.0017	V	R. Sabo	0.0010
SW Aqr	55836.7000	66926	–0.0017	V	R. Sabo	0.0010
AA Aqr	55824.7823	57607	–0.1347	V	R. Sabo	0.0015
TZ Aur	55844.8578	91766	0.0127	V	K. Menzies	0.0006
TZ Aur	55844.8597	91766	0.0146	V	G. Samolyk	0.0011
TZ Aur	55869.9259	91830	0.0136	V	R. Sabo	0.0009
BH Aur	55596.4980	28163	–0.0010	V	K. Menzies	0.0012
BH Aur	55835.9501	28688	0.0039	V	R. Sabo	0.0014
BH Aur	55872.8920	28769	0.0025	V	K. Menzies	0.0009
BH Aur	55919.8685	28872	0.0018	V	R. Sabo	0.0012
NU Aur	55575.6370	30616	0.2937	V	K. Menzies	0.0020
NU Aur	55576.7099	30618	0.2878	V	K. Menzies	0.0023
NU Aur	55589.6434	30642	0.2753	V	K. Menzies	0.0031
NU Aur	55857.7213	31139	0.2631	V	K. Menzies	0.0013
RS Boo	55683.7390	36872	0.0069	V	K. Menzies	0.0015
RS Boo	55762.6015	37081	0.0055	V	K. Menzies	0.0006
ST Boo	54957.6753	57491	0.0754	V	R. Poklar	0.0018
ST Boo	55748.6354	58762	0.1041	V	K. Menzies	0.0015
ST Boo	55759.8333	58780	0.1007	V	R. Sabo	0.0013
ST Boo	55791.5561	58831	0.0867	V	K. Menzies	0.0010

Table continued on following pages

Table 1. Recent times of maxima of stars in the AAVSO RR Lyrae program, cont.

Star	*JD(max) Hel. 2400000 +*	*Cycle*	*O–C*	*F*	*Observer*	*Error*
SZ Boo	55624.6954	53526	0.0118	V	K. Menzies	0.0020
TV Boo	55666.7388	99364	0.0756	V	R. Poklar	0.0014
TV Boo	55743.6272	99610	0.0744	V	K. Menzies	0.0021
TW Boo	55746.7935	54212	–0.0665	V	R. Sabo	0.0008
UU Boo	55647.6959	42815	0.2347	V	K. Menzies	0.0014
UY Cam	55905.759	76170	–0.095	V	G. Samolyk	0.004
RW Cnc	55596.5712	29314	–0.3343	V	K. Menzies	0.0024
RW Cnc	55906.8342	29881	–0.3331	V	G. Samolyk	0.0015
TT Cnc	55615.7041	27813	0.1189	V	R. Poklar	0.0012
TT Cnc	55914.8750	28344	0.0982	V	K. Menzies	0.0012
RR Cet	55826.8102	40948	0.0099	V	R. Sabo	0.0020
RR Cet	55852.8042	40995	0.0116	V	R. Sabo	0.0013
RR Cet	55913.6401	41105	0.0144	V	R. Sabo	0.0020
RU Cet	55897.6386	27412	0.1202	V	R. Sabo	0.0037
RZ Cet	55875.7351	43025	–0.1840	V	R. Sabo	0.0025
RZ Cet	55896.6656	43066	–0.1885	V	R. Poklar	0.0021
TU Com	55628.6952	57760	0.1216	V	K. Menzies	0.0023
TU Com	55648.5661	57803	0.1347	V	K. Menzies	0.0018
TU Com	55719.6807	57957	0.1307	V	K. Menzies	0.0019
VY CrB	55760.8200	30207	–0.1321	V	R. Sabo	0.0019
XX Cyg	55798.6319	84108	0.0025	V	K. Menzies	0.0004
XZ Cyg	55740.7980	24895	–2.1385	V	N. Simmons	0.0011
DM Cyg	55772.7961	31416	0.0683	V	R. Sabo	0.0010
DM Cyg	55785.8154	31447	0.0720	V	R. Sabo	0.0015
DM Cyg	55797.5700	31475	0.0705	V	K. Menzies	0.0008
DM Cyg	55803.8663	31490	0.0689	V	R. Sabo	0.0011
DM Cyg	55809.7499	31504	0.0745	V	R. Sabo	0.0012
DM Cyg	55825.6998	31542	0.0697	V	R. Sabo	0.0012
DM Cyg	55835.7749	31566	0.0681	V	R. Sabo	0.0011
DM Cyg	55852.5725	31606	0.0713	V	K. Menzies	0.0009
DM Cyg	55862.6500	31630	0.0722	V	R. Sabo	0.0013
DM Cyg	55875.6641	31661	0.0706	V	R. Sabo	0.0009
RW Dra	55754.8872	36976	0.1972	V	R. Sabo	0.0008
RW Dra	55767.7599	37005	0.2253	V	R. Sabo	0.0006
RW Dra	55814.7015	37111	0.2177	V	R. Sabo	0.0006
RW Dra	55825.7456	37136	0.1889	V	R. Sabo	0.0009
RW Dra	55829.7266	37145	0.1836	V	R. Sabo	0.0013
RW Dra	55833.7180	37154	0.1888	V	R. Sabo	0.0013

Table continued on following pages

Table 1. Recent times of maxima of stars in the AAVSO RR Lyrae program, cont.

Star	JD(max) Hel. 2400000 +	Cycle	O–C	F	Observer	Error
RW Dra	55865.6079	37226	0.1887	V	R. Sabo	0.0013
RW Dra	55873.5769	37244	0.1852	V	R. Sabo	0.0009
XZ Dra	55733.7791	28973	–0.1425	V	K. Menzies	0.0013
XZ Dra	55794.7806	29101	–0.1326	V	K. Menzies	0.0007
XZ Dra	55847.6739	29212	–0.1305	V	R. Sabo	0.0017
XZ Dra	55874.8360	29269	–0.1287	V	R. Sabo	0.0024
RR Gem	55563.3943	35757	–0.4458	V	M. Martinengo	0.0009
RR Gem	55575.7103	35788	–0.4465	V	R. Poklar	0.0008
RR Gem	55584.4513	35810	–0.4463	V	M. Martinengo	0.0008
RR Gem	55586.4336	35815	–0.4505	V	A. Marchini	0.0005
RR Gem	55596.7671	35841	–0.4471	V	G. Samolyk	0.0008
RR Gem	55603.5197	35858	–0.4488	V	K. Menzies	0.0009
RR Gem	55603.5198	35858	–0.4487	V	N. Simmons	0.0009
RR Gem	55833.9453	36438	–0.4633	V	R. Sabo	0.0010
RR Gem	55862.9464	36511	–0.4659	V	R. Sabo	0.0010
RR Gem	55868.9045	36526	–0.4675	V	R. Sabo	0.0009
RR Gem	55901.8832	36609	–0.4656	V	R. Sabo	0.0010
RR Gem	55915.7883	36644	–0.4663	V	R. Sabo	0.0012
GQ Gem	55578.7200	44258	–0.1941	V	K. Menzies	0.0019
GQ Gem	55605.5376	44305	–0.1932	V	K. Menzies	0.0023
TW Her	55741.7979	85577	–0.0142	V	R. Sabo	0.0007
TW Her	55761.7789	85627	–0.0132	V	R. Sabo	0.0006
TW Her	55775.7646	85662	–0.0135	V	R. Sabo	0.0006
TW Her	55797.7417	85717	–0.0144	V	R. Sabo	0.0010
TW Her	55823.7159	85782	–0.0142	V	R. Sabo	0.0006
TW Her	55872.4671	85904	–0.0142	V	K. Menzies	0.0005
VX Her	55767.7440	74702	0.0009	V	R. Sabo	0.0010
VX Her	55798.7055	74770	–0.0030	V	R. Sabo	0.0009
VZ Her	55751.6914	43065	0.0728	V	N. Simmons	0.0010
AR Her	55757.8655	30434	–1.3137	V	R. Sabo	0.0023
AR Her	55798.7326	30521	–1.3390	V	R. Sabo	0.0010
AR Her	55806.7177	30538	–1.3444	V	R. Sabo	0.0012
DL Her	55785.7309	29710	0.0390	V	R. Sabo	0.0016
DY Her	55745.7557	150078	–0.0270	V	R. Sabo	0.0007
DY Her	55761.8064	150186	–0.0285	V	R. Sabo	0.0011
DY Her	55777.7105	150293	–0.0279	V	R. Sabo	0.0006
LS Her	55786.6014	120367	0.0228	V	K. Menzies	0.0020
SZ Hya	55611.7238	27795	–0.2801	V	G. Samolyk	0.0021

Table continued on following pages

Table 1. Recent times of maxima of stars in the AAVSO RR Lyrae program, cont.

Star	*JD(max) Hel. 2400000 +*	*Cycle*	*O–C*	*F*	*Observer*	*Error*
SZ Hya	55624.6736	27819	–0.2241	V	R. Poklar	0.0010
SZ Hya	55639.6686	27847	–0.2718	V	G. Samolyk	0.0026
SZ Hya	55653.6876	27873	–0.2211	V	R. Poklar	0.0012
UU Hya	55649.7164	30868	0.0036	V	R. Poklar	0.0011
DH Hya	55648.7256	50046	0.0777	V	R. Poklar	0.0009
RR Leo	55604.6817	27209	0.1104	V	R. Poklar	0.0009
RR Leo	55666.6594	27346	0.1102	V	K. Menzies	0.0013
RR Leo	55905.9802	27875	0.1150	V	G. Samolyk	0.0014
TV Leo	55635.7908	27635	0.1192	V	G. Samolyk	0.0014
TV Leo	55664.7188	27678	0.1145	V	R. Poklar	0.0018
WW Leo	55567.8683	34313	0.0446	V	K. Menzies	0.0027
WW Leo	55648.6415	34447	0.0365	V	G. Samolyk	0.0018
WW Leo	55648.6480	34447	0.0430	V	K. Menzies	0.0039
AA Leo	54196.5951	24388	–0.0751	V	G. Lubcke	0.0013
AH Leo	55576.8477	14856	0.0293	V	K. Menzies	0.0018
VY LMi	55565.8731	9652	0.0049	V	K. Menzies	0.0011
VY LMi	55603.7593	9724	0.0086	V	K. Menzies	0.0024
SZ Lyn	55838.8355	146965	0.0227	V	G. Samolyk	0.0014
SZ Lyn	55875.8397	147272	0.0227	V	R. Sabo	0.0008
SZ Lyn	55890.9069	147397	0.0231	V	G. Samolyk	0.0007
SZ Lyn	55921.7637	147653	0.0229	V	N. Simmons	0.0008
SZ Lyn	55921.8832	147654	0.0219	V	N. Simmons	0.0010
RZ Lyr	55747.6734	28488	–0.0232	V	G. Samolyk	0.0013
RZ Lyr	55756.8719	28506	–0.0271	V	R. Sabo	0.0012
RZ Lyr	55770.6657	28533	–0.0368	V	K. Menzies	0.0019
RZ Lyr	55771.6878	28535	–0.0372	V	R. Sabo	0.0007
RZ Lyr	55777.8244	28547	–0.0355	V	R. Sabo	0.0009
RZ Lyr	55793.6703	28578	–0.0381	V	R. Sabo	0.0012
RZ Lyr	55816.6874	28623	–0.0270	V	R. Sabo	0.0017
RZ Lyr	55837.6507	28664	–0.0246	V	R. Sabo	0.0008
RZ Lyr	55862.7012	28713	–0.0250	V	R. Sabo	0.0017
CX Lyr	55745.7667	36772	1.1336	V	R. Sabo	0.0025
AV Peg	55744.8970	30623	0.1366	V	R. Sabo	0.0015
AV Peg	55760.9014	30664	0.1356	V	R. Sabo	0.0011
AV Peg	55771.8337	30692	0.1374	V	R. Sabo	0.0011
AV Peg	55792.9147	30746	0.1382	V	R. Sabo	0.0010
AV Peg	55798.7691	30761	0.1370	V	K. Menzies	0.0009
AV Peg	55807.7492	30784	0.1384	V	R. Sabo	0.0010

Table continued on next page

Table 1. Recent times of maxima of stars in the AAVSO RR Lyrae program, cont.

Star	JD(max) Hel. 2400000 +	Cycle	O–C	F	Observer	Error
AV Peg	55823.7558	30825	0.1397	V	R. Sabo	0.0013
AV Peg	55832.7326	30848	0.1379	V	R. Sabo	0.0010
AV Peg	55864.7437	30930	0.1382	V	R. Sabo	0.0008
AV Peg	55868.6454	30940	0.1362	V	K. Menzies	0.0012
AV Peg	55872.5512	30950	0.1382	V	K. Menzies	0.0006
BH Peg	53952.8716	22758	–0.1271	V	G. Samolyk	0.0027
BH Peg	54372.7303	23413	–0.1188	V	G. Samolyk	0.0023
BH Peg	55759.8356	25577	–0.1224	V	R. Sabo	0.0017
BH Peg	55825.8398	25680	–0.1404	V	R. Sabo	0.0017
BH Peg	55834.8125	25694	–0.1416	V	R. Sabo	0.0024
RV UMa	54219.6391	19536	0.1079	V	G. Lubcke	0.0013
RV UMa	55607.9182	22502	0.1211	V	G. Samolyk	0.0017
RV UMa	55634.6024	22559	0.1259	V	N. Simmons	0.0011
RV UMa	55634.6039	22559	0.1274	V	G. Samolyk	0.0015
RV UMa	55763.7830	22835	0.1219	V	R. Sabo	0.0013
RV UMa	55807.7821	22929	0.1234	V	R. Sabo	0.0024
AE UMa	55584.5518	232282	0.0002	V	G. Samolyk	0.0006
AE UMa	55584.6348	232283	–0.0028	V	G. Samolyk	0.0007
AE UMa	55584.7285	232284	0.0049	V	G. Samolyk	0.0011
AE UMa	55584.8102	232285	0.0006	V	G. Samolyk	0.0006
AE UMa	55584.8936	232286	–0.0020	V	G. Samolyk	0.0005
AE UMa	55584.9814	232287	–0.0003	V	G. Samolyk	0.0008
AE UMa	55890.7752	235842	0.0029	V	G. Samolyk	0.0004
AE UMa	55890.8557	235843	–0.0026	V	G. Samolyk	0.0007
AE UMa	55890.9446	235844	0.0003	V	G. Samolyk	0.0007
AE UMa	55907.7213	236039	0.0037	V	G. Samolyk	0.0009
AE UMa	55907.8063	236040	0.0026	V	G. Samolyk	0.0006
AE UMa	55907.8872	236041	–0.0025	V	G. Samolyk	0.0007
GW UMa	55921.7701	19301	0.0021	V	G. Samolyk	0.0013
GW UMa	55921.9671	19302	–0.0041	V	G. Samolyk	0.0011

The Ross Variable Stars Revisited. II

Wayne Osborn
O. Frank Mills
Yerkes Observatory, 373 W. Geneva Street, Williams Bay, WI 53191; email correspondence should be sent to Wayne.Osborn@cmich.edu

Received May 23, 2012; accepted June 15, 2012

Abstract Better magnitudes and epochs have been determined for 190 of the 379 confirmed and suspected variable stars discovered by Ross from 1925 to 1931. Accurate positions have been determined for those objects for which unambiguous identifications had been lacking. These include a number of cases for which Ross's published coordinates have large errors.

1. Introduction

This is the second of two papers giving identifications and improved magnitudes and epochs for the suspected variable stars discovered by F. Ross of Yerkes Observatory in the period 1925 and 1931. Paper I (Osborn and Mills 2011) discussed those stars in Ross's first, second, seventh, eighth, ninth, and tenth lists of variables (Ross 1925, 1926a, 1928b, 1929, 1930, 1931). This paper gives our results for the remaining stars—those in Ross's third, fourth, fifth, and sixth lists (Ross 1926b, 1927a, 1927b, 1928a).

The rationale for this work along with our methods were described in Paper I and will not be repeated here. We will merely say that we have re-examined the original photographic plates used by Ross for his discoveries to unambiguously identify the objects and determine better magnitudes and epochs of observation than those published by Ross. The only change in our procedure was to include data from the *Third U.S. Naval Observatory CCD Astrograph Catalog* (UCAC3; Zacharias *et al.* 2010) in determining our approximate B magnitudes.

2. Results

Our results are presented in Table 1. The columns give, respectively, the Ross star number, the corresponding variable star name (and, when needed, another identification below), the Julian Dates (actually JD – 2400000.0) and B magnitudes for the two compared plates. The epochs are geocentric, that is, they have not been converted to heliocentric ones. Following each table are notes for many of the stars; these give such information as errors detected in Ross's papers and comments on the identification.

Of the 190 stars considered in this paper, 159 are named variables, twenty-two are suspected variables listed in the NSV catalogue (Samus *et al.* 2009),

seven were observations of minor planets, one is a missing BD star, and one a variable BL Lac object (Baument and Cudworth 1981). Of the NSV objects, we do not see the variation seen by Ross for R118 using the same plate material, and the supposed variations of R119 and R164 may be due to plate flaws.

The case of R148 is interesting, this being a listing in the *Bonner Durchmusterung* catalogue (Argelander 1903), BD+34°531, for which Ross found there is no corresponding star (irrespective of the fact that Ross's 1875 coordinates were incorrectly precessed from the BD's 1855 position). His note card for this star has the comment "Kustner writes this was in the sky certainly on Oct 21, 1856." To us it seems possible that BD+34°531 resulted from some error by the compilers of the BD. The star with the same number in the +33° zone, BD+33°531, lies at the same right ascension and just slightly south. The following compares the BD catalogue entries for the two stars:

BD+34°531 (mag. = 9.3):	R.A. $02^h43^m39.5^s$, Dec. +34° 01.6' (revised coordinates)
	R.A. $02^h43^m40.5^s$, Dec. +34° 00.6' (originally published coordinates)
BD+33°531 (mag. = 9.3):	R.A. $02^h43^m40.7^s$, Dec. +33° 57.5'

That both stars lie so close to the zone boundary, the revision in the position for the missing star, and the similarity in number, magnitude, and coordinates for the two stars suggest confusion with the data may have led to two catalogue entries from the observations of just one object.

With this paper, all the Ross variables have been reviewed and we can now expand upon Marsden's (2007) comments concerning the Ross observations that were of minor planets. For the fifteen such cases, the average difference between the actual time of exposure of the plate and Marsden's computed time was 0.0d with an RMS dispersion of 0.15d, strong confirmation that our Julian Dates have been calculated correctly. The average difference between our pseudo-B magnitudes and the expected V magnitudes for the minor planets is 0.9 mag, or 0.75 if one discrepant value is omitted. Not only is this in good agreement with the average (B–V) of around 0.8 for minor planets (Zellner *et al.* 1975), it supports both that Ross's estimates were visual magnitudes and that our estimates are approximately on the B system.

As mentioned in Paper I, Ross's note cards contain comments for a number of the stars, including some visual observations by him or his colleagues with the Yerkes 40-inch refractor. This information is presented in an appendix, Table A, so it will not be lost.

3. Corrections to paper I

Soon after the publication of Paper I, a reader brought to our attention

several errors. Most involve the ten stars we had noted as "not listed in NSV catalog." We had used SIMBAD to check for cross identifications between the Ross variables and NSV objects, but it was pointed out that a number of NSV objects had yet to be incorporated into the SIMBAD database. Using the on-line version of the *General Catalogue of Variable Stars* (http://www.sai.msu.su/gcvs/cgi-bin/search.htm) all ten objects turned out to indeed have NSV numbers. These identifications and a few other corrections to Paper I are given Table 2.

4. Acknowledgements

This research made use of the SIMBAD database, operated at CDS, Strasbourg, France, and the Digitized Sky Surveys (DSS) produced at the Space Telescope Science Institute under U.S. Government grant NAG W-2166. The DSS images are from photographic data obtained using the Oschin Schmidt Telescope on Palomar Mountain and the UK Schmidt Telescope through funding provided by The National Geographic Society, the National Science Foundation, the Sloan Foundation, the Samuel Oschin Foundation, the Eastman Kodak Corporation, and the UK Science and Engineering Research Council.

References

Argelander, F. W. A. 1903, *Bonner Durchmusterung des Nordlichen Himmels*, 2nd corrected ed. (*BD Catalogue*), A. Marcus and E. Weber's Verlag, Bonn.

Baumert, J. H., and Cudworth, K. 1981, *Inf. Bull. Var. Stars*, No. 2039, 1.

Bedient, J. R. 2003, *Inf. Bull. Var. Stars*, No. 5478, 1.

Bidelman, W. P., and Cudworth, K. 1981, *Inf. Bull. Var. Stars*, No. 2055, 1.

Bidelman, W. P., and van Altena, W. F. 1972, *Inf. Bull. Var. Stars*, No. 744, 2.

Harwood, M. 1960, *Ann. Sterrewacht Leiden*, **21**, 387.

Marsden, B. G. 2007, *Perem. Zvezdy*, **27**, 3.

Osborn, W., and Mills, O. F. 2011, *J. Amer. Assoc. Var. Star Obs.*, **39**, 186.

Ross, F. E. 1925, *Astron. J.*, **36**, 99 (first list of variables).

Ross, F. E. 1926a, *Astron. J.*, **36**, 122 (second list of variables).

Ross, F. E. 1926b, *Astron. J.*, **36**, 167 (third list of variables).

Ross, F. E. 1926c, *Astron. J.*, **36**, 172 (third list of proper motion stars).

Ross, F. E. 1927a, *Astron. J.*, **37**, 91 (fourth list of variables).

Ross, F. E. 1927b, *Astron. J.*, **37**, 155 (fifth list of variables).

Ross, F. E. 1928a, *Astron. J.*, **38**, 99 (sixth list of variables).

Ross, F. E. 1928b, *Astron. J.*, **38**, 144 (seventh list of variables).

Ross, F. E. 1929, *Astron. J.*, **39**, 140 (eighth list of variables).

Ross, F. E. 1930, *Astron. J.*, **40**, 34 (ninth list of variables).

Ross, F. E. 1931, *Astron. J.*, **41**, 88 (tenth list of variables).

Samus, N. N., *et al.* 2012, *General Catalogue of Variable Stars*, published online at http://www.sai.msu.su/gcvs/cgi-bin/search.htm.

Zacharias, N., *et al.* 2010, *Astron. J.*, **139**, 2184.

Zellner, B., Wisniewski, W. Z., Andersson, L., and Bowell, E. 1975, *Astron. J.*, **80**, 986.

Table 1. Identifications and improved data for Ross Variables 105–294.

Ross	*Variable / Other identification*	*First JD 2400000+*	*B*	*Second JD 2400000+*	*B*
105	RV Del	17062.949	14.2	24384.707	13.1
106	RX Del	17062.949	13.1	24384.707	15.2:
107	RZ Del	17062.949	14.4	24384.707	13.1
108	SS Del	17062.949	13.6	24384.707	<16.6
109	ST Del	17062.949	13.3	24384.707	12.5
110	V830 Cyg	18447.816	13.5	24460.540	14.8
111	SW Del	17062.949	15.7	24384.707	13.8
112	V833 Cyg	18447.816	14.6	24460.540	13.9
113	GR Cyg	18447.816	13.0	24460.540	15.7:
114*	NSV 13523	18447.816	<15.6	24460.540	14.1
	2MASS 21051394+3837134				
115*	NSV 13558	18447.816	<15.3	24460.540	14.4
	2MASS 21080005+3734183				
116	DU Cyg	18447.816	13.8	24460.540	12.1
117	NSV 13612	18447.816	14.4	24460.540	15.4
	2MASS 21133238+4258055				
118*	NSV 13622	18447.816	15.4	24460.540	15.5
	2MASS 21151328+3828514				
119*	NSV 13624	18447.816	15.5:	24460.540	15.3
	2MASS 21153512+3639576				
120	V837 Cyg	18447.816	15.1	24460.540	14.4
121	V1812 Cyg	18447.816	13.7	24460.540	16.7
122	V1338 Cyg	18447.816	<15.2	24460.540	14.7
123	EL Peg	17791.674	13.5	24475.517	<16.0
124	CX Peg	17791.674	14.1	24475.517	<16.0
125	AX Peg	17791.674	12.7	24475.517	11.8
126	GW Cyg	19275.660	15.7	24413.628	13.9
127*	AQ Lac	18542.776	13.1	24413.628	<14.9
128	EL Lac	18542.776	13.5	24413.628	<14.9
129	AS Lac	19275.660	12.8	24413.628	<16.8
130*	AV Lac	19275.660	13.6	24413.628	<15.6

Table continued on following pages

Table 1. Identifications and improved data for Ross Variables 105–294, cont.

Ross	*Variable / Other identification*	*First JD 2400000+*	*B*	*Second JD 2400000+*	*B*
131	UY Lac	18542.776	11.6	24413.628	14.0
132	V458 Lac	18542.776	12.5	24413.628	13.3
133	DG Cas	17793.658	14.2	24473.565	15.5
134	FK Cas	17793.658	14.2	24473.565	13.0
135	FN Cas	17793.658	13.5	24473.565	15.3:
136*	NSV 308			24468.681	13.5
	Minor planet (137) *Meliboca*				
137	AH Per	17832.732	13.9	24497.569	<16.4
138	AI Per	17832.732	13.5	24497.569	15.3
139	AK Per	17832.732	12.8	24497.569	<16.8
140	AL Per	17068.872	14.5	24494.628	13.7
141	GH Per	17911.641	12.4	24557.563	13.6
142	EV Tau	17910.642	12.8	24497.668	<14.5
143	DQ Tau	17562.706	12.3	24768.666	15.7
144*	V1800 Ori	17562.706	15.8	24768.666	<16.8
145	HW Mon	16795.951	12.4	24557.645	<14.4
146	UW Pup	16795.951	13.6	24557.645	<15.2
147	AO Gem	17698.616	12.5	24557.740	16.5
148*	BD+34°531	–755.5		24497.569	<15.4
149	NSV 1351	19665.796	11.2	24577.543	14.7
	2MASS 03490755+1430533				
150	EP Ori	16737.913	14.6	24577.587	13.1
151	FG Ori	16737.913	11.5	18955.805	16.4
152	V1802 Ori	16737.913	13.8	24577.587	<16.9
153	DG Ori	16737.913	13.3	24577.587	<15.4
154	AQ Aur	16736.844	<15.9	24578.573	14.6
155	DU Aur	16736.844	12.8	24578.573	<16.1
156	V1794 Ori	17679.590	15.1	24577.643	12.5
157	EQ Aur	19503.592	13.7	24578.649	13.0
158	AZ Mon	16937.685	12.6	24584.670	<14.5
159	AH Mon	16937.685	15.0	24584.670	12.9
160*	NSV 3506	16937.685	14.5	24584.670	<15.9
	2MASS 07172610+0137388				
161	HU Mon	16937.685	15.7	24584.670	12.7
162	YZ Pup	16885.761	13.1	24588.603	11.6
163	FF Pup	16885.761	<14.4	24588.603	13.0

Table continued on following pages

Table 1. Identifications and improved data for Ross Variables 105–294, cont.

Ross	*Variable / Other identification*	*First JD 2400000+*	*B*	*Second JD 2400000+*	*B*
164*	NSV 3982	20566.684	14.2	24591.691	15.2
	2MASS 08173168+0602094				
165	V425 Hya	20566.684	13.9	24591.691	14.7
166*	NSV 4168	19151.703	<15.7	24579.689	13.3
	Near 08:41:37, +72:27.6				
167	VX Vir	17623.693	13.8	24624.706	15.5
168*	NSV 6188	16889.8	14.1		
	Minor planet (106) *Dione*				
169	TW UMa	17324.7	12.0	24641.699	13.7:
170	AA Vir	16889.8	13.8	24648.667	15.6
171	TW Lib	16971.751	<16.0	24639.756	12.7
172	WX Ser	18064.655	12.5	24624.765	<15.0
173	UU Lib	16994.791	17.1:	24646.787	12.6
174	V872 Sco	16994.791	<16.6	24646.787	13.5
175	AY Her	16586.707	14.6	24651.718	12.4
176	KT Oph	17686.845	<15.9	24671.814	13.3
177	KU Oph	17686.845	<16.0	24671.814	13.4
178	VZ Ser	17686.845	14.6	24671.814	<15.5
179	YZ And	19630.720	12.2	24886.560	14.6
180	GV Cas	18154.727	13.2	24855.547	14.0
181	TZ Psc	18995.519	<14.2	24904.572	11.6
182	BB Ari	18619.618	<16.8	24846.601	13.2
183	V413 Per	19743.601	<17.2:	24914.572	14.3
184*	NSV 1224	17859.672	16.6	24855.708	14.7
185	KL Eri	19027.584	14.0	24879.635	15.2
186	XY Tau	19004.600	16.4:	24874.613	13.0
187	NV Per	20457.619	14.5	24904.654	<16.2
188	CO Ori	18622.795	11.2	24878.708	13.1
189	YY Tau	18622.795	15.7:	24878.708	13.6
190*	NSV 2777	18622.795	13.4		
	Minor planet (714) *Ulula*				
191	EO Ori	16938.688	14.8	24943.1	13.1
192	DD Ori	16938.688	11.8	24943.1	12.8
193	FT Mon	17616.693	12.8	24879.732	14.5
194*	NSV 2975	16938.688	14.4	24943.1	13.7
	2MASS 06285910+0819492				

Table continued on following pages

Table 1. Identifications and improved data for Ross Variables 105–294, cont.

Ross	*Variable / Other identification*	*First JD 2400000+*	*B*	*Second JD 2400000+*	*B*
195	VX Mon	16938.688	14.6	24943.1	12.9
196	EE Gem	16938.688	<16.4	24943.1	13.9
197	AY Mon	16938.688	15.7	24943.1	12.8
198	UZ Mon	18216.922	11.8	24907.722	<14.9
199	VZ CMi	18216.922	<14.4	24907.722	12.0
200*	OI 090.4	20569.668	14.1	24886.845	15.4
201	ST Cnc	20569.668	15.9	24886.845	14.0
202	SU Cnc	20569.668	12.5	24886.845	<14.3
203	VW Cnc	20569.668	16.4	24886.845	13.3
204*	NSV 4018			24948.607	13.2
	Minor planet (554) *Peraga*				
205*	TU Hya	20567.684	11.5	24913.729	<15.9
206*	NSV 5338	18406.601	12.1		
	Minor planet (26) *Proserpina*				
207*	AS Her	18447.681	10.1	24684.703	14.7
208	V2582 Oph	18447.681	<15.6	24684.703	13.3
209	V440 Oph	18447.681	12.6	24684.703	<15.6
210	V2588 Oph	18447.681	14.0	24684.703	15.1
211	BI Her	17656.887	13.9	24668.765	<16.0
212	MW Her	17656.887	<16.6	24668.765	12.4
213	V374 Oph	17656.887	13.7	24668.765	<16.0
214	CY Aql	16653.832	13.9	24830.516	15.1:
215	EM Aql	16653.832	16.4	24830.516	12.8
216	DM Aql	16653.832	11.7	24830.516	14.8
217	ES Aql	16653.832	13.0	24830.516	<15.5
218*	V986 Aql	16653.832	14.6	24830.516	<14.7
219	V607 Aql	16653.832	13.6	24830.516	<15.5
220	GT Aql	16653.832	14.6	24830.516	<14.9
221	EG Peg	19237.686	13.2	24849.540	<15.7
222	VX Cep	18179.694	12.0	24851.551	<14.8
223	EY Peg	17471.621	14.6	24841.515	13.3
224	NSV 14639	20072.558	14.0	24879.531	16.2
	2MASS J23364663+1643317				
225*	NSV 14640	20072.558	14.5	24879.531	<16.8
	2MASS J23364891+1643341				
226	V419 Peg	20072.558	15.2	24879.531	14.2

Table continued on following pages

Table 1. Identifications and improved data for Ross Variables 105–294, cont.

Ross	*Variable / Other identification*	*First JD 2400000+*	*B*	*Second JD 2400000+*	*B*
227	EO Cas	18179.694	15.6	24851.551	13.5
228*	DU Peg	19630.720	12.5	24886.560	15.4
229	TY Cnc	20576.610	13.7	24918.639	12.6
230*	NSV 4333	20576.610	12.4		
	Minor planet (389) *Industria*				
231*	NSV 4352	20576.610	13.9		
	Minor planet (242) *Kriemhild*				
232	SW Cnc	20576.610	12.9	24918.639	11.7
233	AL Hya	20576.610	14.6	24918.639	12.4
234	VX Crv	16963.717	13.4	24994.676	<15.9
235	U Crv	16963.717	11.4	24994.676	15.9
236	V Crv	16963.717	12.8	24994.676	<15.8
237	V429 Sct	18525.643	14.2	25142.589	16.5
238	CI Sct	18525.643	14.4	25142.589	15.4
239*	NSV 11532	18525.643	14.6	25142.589	14.8
	UCAC3 162–217813				
240	V358 Sgr	18525.643	14.3	25142.589	15.2
241	NSV 11649	18525.643	13.5	25142.589	15.4
	2MASS 19011546–1148397				
242	V920 Sgr	19980.642	<13.8	25127.587	12.7
243*	CN Aql	18525.643	12.1	25142.589	<14.0
244*	V1940 Sgr	19980.642	12.2	25127.587	14.5
245	EK Sgr	18525.643	13.4	25142.589	14.6
246	V923 Sgr	19980.642	<13.2	25127.587	12.9
247	V918 Aql	18525.643	13.6	25142.589	<14.6
248	CU Aql	18525.643	12.2	25142.589	<13.7
249*	NSV 11953	16676.835	13.2	25125.646	<15.7
	2MASS 19221196+2234390				
250	DI Aql	19980.642	<13.9	25127.587	12.3
251	XY Vul	16676.835	12.9	25125.646	<14.5
252*	V976 Aql	17038.936	14.2	25174.566	<16.2
253	KU Aql	17038.936	<15.5	25174.566	13.8
254	V1137 Aql	17038.936	14.6	25174.566	15.4
255	CE Vul	16676.835	13.5	25125.646	14.5:
256	V452 Aql	17038.936	14.7	25174.566	<15.5
257	V453 Aql	17038.936	<15.5	25174.566	15.1

Table continued on following pages

Table 1. Identifications and improved data for Ross Variables 105–294, cont.

Ross	*Variable / Other identification*	*First JD 2400000+*	*B*	*Second JD 2400000+*	*B*
258	LR Aql	17038.936	14.5	25174.566	<15.9
259	V536 Aql	17038.936	14.1	25174.566	15.5
260	V827 Aql	17038.936	14.8	25174.566	<15.9
261	MU Aql	17038.936	12.7	25174.566	14.4
262*	DY Aql	20427.606	11.8	25138.573	11.0
263	QX Aql	19658.588	13.3	25127.663	<14.7
264	SZ Cap	20427.606	<15.2	25138.573	12.4
265	NSV 12804	20427.606	14.0	25138.573	13.0
	2MASS 20071642–1315180				
266	SS Cap	20427.606	<16.0	25138.573	12.5
267	V581 Aql	19658.588	13.2	25127.663	15.2
268	QY Aql	17888.664	13.0	25142.704	11.2
269	ST Cap	20427.606	12.3	25138.573	<15.1
270	V586 Aql	17888.664	13.0	25142.704	15.1
271*	NSV 12941	17888.664	14.2	25142.704	<15.6
	2MASS 20144760+1454058				
272	V499 Aql	20427.606	11.3	25138.573	12.1
273	RU Del	17888.664	15.2	25142.704	12.4
274	QZ Aql	17888.664	<14.8	25142.704	13.6
275*	NSV 13012	17888.664	13.1	25142.704	14.4
	2MASS 20200672+0805420				
276	V335 Aql	19658.588	12.1	25127.663	14.7
277	EP Aql	18887.667	11.9	25175.551	<14.8
278	RW Del	17888.664	13.2	25142.704	14.5
279*	NSV 13086	17888.664	<14.7	25142.704	13.6
	2MASS 20263913+0852343				
280	NSV 13100	18887.667	16.4	25175.551	14.4
	2MASS 20284168–0531369				
281	CQ Del	17888.664	<16.1	25142.704	13.1
282	RY Del	17888.664	<15.5	25142.704	12.5
283	ET Aql	18887.667	14.2	25175.551	12.2
284*	V384 Cyg	20387.639	14.9	25176.561	12.3:
285	BT Aqr	18887.667	12.5	25175.551	11.7
286*	LN Cyg	20387.639	13.6	25176.561	13.7:
287*	NSV 13469	20387.639	13.7	25176.561	12.7:
	2MASS 21015589+3159129				

Table continued on following pages

Table 1. Identifications and improved data for Ross Variables 105–294, cont.

Ross	*Variable / Other identification*	*First JD 2400000+*	*B*	*Second JD 2400000+*	*B*
288*	DI Cyg	20387.639	12.6	25176.561	<13.7:
289	SX Del	18886.630	14.4	25128.597	13.1
290*	GQ Cyg	20387.639	<15.1	25176.561	11.8:
291*	V471 Cyg	20387.639	12.9	25176.561	12.2:
292	AS Peg	18886.630	11.8	25128.597	15.5
293	AP Peg	18886.630	12.3	25128.597	14.9
294	AY Peg	19713.684	14.9	25128.677	13.6

**Notes:*

R114: Marsden (2007) showed this suspected variable was not a minor planet observation.

R115: Marsden (2007) showed this suspected variable was not a minor planet observation.

R118: Probably not variable. Ross indicated a variation of two magnitudes between his two epochs, but we do not see a brightness change for the star he marked as the variable on his finding chart, nor for any nearby star, on these same plates.

R119: Probably not variable. The brightening detected by Ross on the 1909 plate taken with the 10-inch camera seems to result from a plate flaw—a dark smudge that does not look like a star image. No brightening was seen on the 6-inch plate. Ross (1926c) discussed plate flaws found on his plates in his paper that gave the proper motion stars detected in the R119 field.

R127: Ross published his fainter magnitude as 15 but his note card has 15(?). We do not believe the variable was seen but that Ross detected the close companions to the variable.

R130: Ross' published declination has a 28' error but his finding chart and our re-examination of the plates confirm this identification.

R136: Bidelman and Cudworth (1981), Bedient (2003), and Marsden (2007) showed object seen in 1925 was a minor planet.

R144: Marsden (2007) showed this suspected variable was not a minor planet observation.

R148: This special case is discussed in the paper.

R160: Marsden (2007) showed this suspected variable was not a minor planet observation.

R164: The apparent variability is probably due to a plate flaw. The star image is brighter on the 1915 10-inch plate, but not on the 6-inch plate taken simultaneously.

R166: Marsden (2007) showed this suspected variable was not a minor planet observation.

R168: Marsden (2007) showed object seen in 1905 was a minor planet.

R184: Ross' published magnitudes for the two epochs are reversed.

R190: Marsden (2007) showed object seen in 1909 was a minor planet.

R194: Only Ross' 10-inch plate could be located so we could not confirm the variability on the second plate set.

R200: Baumert and Cudworth (1981) identified this as the BL Lac object Ohio I 090.4.

R204: Marsden (2007) showed object seen in 1927 was a minor planet.

R205: Date of second observation was 1927 Feb 1, not Feb 2 as published by Ross.

Table continued on next page

Table 1. Identifications and improved data for Ross Variables 105–294, cont.

Notes (continued):

R206: Bedient (2003) and Marsden (2007) showed object seen in 1909 was a minor planet.

R207: Ross inverted the identifications of variable and comparison star on his finding chart.

R218: Marsden (2007) showed this object was not a minor planet observation. We found Ross' published coordinates are in error. His finding chart and our re-examination of the plates confirm this identification.

R225: Marsden (2007) showed this suspected variable was not a minor planet observation.

R228: Ross' published magnitudes for the two epochs are reversed.

R230: Marsden (2007) showed object seen in 1915 was a minor planet.

R231: Marsden (2007) showed object seen in 1915 was a minor planet.

R239: This star is very close to QT Sct, but a careful comparison of the finding chart for that object (Harwood 1960) with the field suggests R239 is not the same object as QT Sct.

R243: Ross' published declination has an 11' error but re-examination of the plates by both Bidelman and van Altena (1972) and ourselves as well as the Ross finding chart confirm this identification.

R244: Ross' published declination has a 2.3° error but his finding chart and our re-examination of the plates confirm this identification.

R249: Marsden (2007) showed this suspected variable was not a minor planet observation.

R252: Ross' published declination has a 30' error but his finding chart and our re-examination of the plates confirm this identification.

R262: Ross' published position has a 21' error but his finding chart and our re-examination of the plates confirm this identification.

R271: Marsden (2007) showed this suspected variable was not a minor planet observation.

R275: The variable may be the star slightly north of our adopted identification.

R279: Marsden (2007) showed this suspected variable was not a minor planet observation.

R284: Ross' published right ascension has a 21' error but his finding chart confirms this identification. The 1927 Oct 22 plates could not be located and the listed magnitude for this date is based on Ross' estimate.

R286: The 1927 Oct 22 plates could not be located but Ross' finding chart confirms this identification. The listed magnitude for this date is based on Ross' estimate.

R287: The 1927 Oct 22 plates could not be located but Ross' finding chart confirms this identification. The listed magnitude for this date is based on Ross' estimate. The variability was confirmed on a 1922 Nov. 26 plate (JD 2,423,385.535) which gave a magnitude of 12.6.

R288: The 1927 Oct 22 plates could not be located but Ross' finding chart confirms this identification. The listed magnitude for this date is based on Ross' estimate.

R290: The 1927 Oct 22 plates could not be located but Ross' finding chart confirms this identification. The listed magnitude for this date is based on Ross' estimate.

R291: The 1927 Oct 22 plates could not be located but Ross' finding chart confirms this identification. The listed magnitude for this date is based on Ross' estimate.

Table 2. Corrections to published data in paper I, Osborn and Mills (2011).

Ross	*Corrected data*
29	JD of 15.0 mag. observation is 2418122.720; Ross's published date was incorrect
66	Star is NSV 11974
67	Star is NSV 12000
72	Star is NSV 12194
76	Star is NSV 12573
103	Star is NSV 14720
295	Star is NSV 00670
300	Star is NSV 10725; optical transient (not X-ray) source ROTSE1 J182240.62+293115.0
303	Star is NSV 11012
317	Star is NSV 12257
368	Star is NSV 06117

Appendix

Ross's note cards for his earlier discoveries contain entries showing that observations of some of the suspected variables were made with the 40-inch refractor by him or collaborators. The following table reproduces these notes verbatim, omitting the common note that the object might be an asteroid. A "v" refers to the variable while letters (a, b, m, n) refer to comparison stars that are indicated on the finding charts. For those cases where a visual magnitude estimate was made, we follow the reproduced comments with the approximate Julian Date of the observation and approximate V magnitude, derived by using modern magnitude values for the comparison stars.

Table A. Ross's notes and derived V magnitude estimates.

Ross	*Comments on Ross's note cards reproduced verbatim*	*JD*	*m(V)*
114	1925 Dec 7: 40''v = a = b (found by Sullivan on pl 73)	24492.6	12.9
137	1926 Nov 10: Nothing brighter than 16^m in this place	24830.6	<16
144	1926 Nov 10: b 1^m v 1^m m	24830.6	16:
152	1926 Nov 10: invis. <16^m	24830.6	<16
153	1926 Nov 10: v 0.5^m b	24830.6	12.1
158	1926 Nov 10: v quite red! b 3 v 2 a	24830.6	12.0
160	1926 Nov 10: m 3 v 1 n	24830.6	12.8

GSC 4552-1643: a W UMa System With Complete Eclipses

Dirk Terrell
Department of Space Studies, Southwest Research Institute, 1050 Walnut Street, Suite 300, Boulder, CO 80302; terrell@boulder.swri.edu

John Gross
Sonoita Research Observatory, 1442 E. Roger Road, Tucson, AZ 85719; johngross3@msn.com

Received October 6, 2011; revised October 17, 2011; accepted November 17, 2011

Abstract Observations and analysis of GSC 4552-1642 are presented and the system is shown to be a W UMa system with complete eclipses. The total/annular nature of the eclipses results in a photometric mass ratio that should be reliable but the light curves do have appreciable amounts of third light.

1. Background

GSC 4552-1643 is listed as star 828321 in the Gettel, *et al.* (2006; hereafter GGM) catalogue of overcontact binary stars with an orbital period of about 0.27 day. Visual inspection of the light curve given by GGM showed that it might have complete eclipses. Given the greatly strengthened analysis that complete eclipses can provide, we began observing the system with Johnson B and V and Cousins I filters at the Sonoita Research Observatory in Sonoita, Arizona. We used the 20-inch telescope equipped with a Santa Barbara Instrument Group Research STL 6303 CCD camera. Calibration (bias, dark, flat) and aperture photometry were done with IRAF. Observations were made on six nights in March and April 2011 with a total of 283 observations in the B filter, 459 in V, and 436 in I. GSC 4552-0002 was used as the comparison star and GSC 1399-0059 was the check star. The images were reduced using IRAF to bias and dark subtract the frames before flatfielding, and the calibration frames were created by median-combining at least twenty raw images. Aperture photometry was performed on the images using the IRAF PHOT package. Data from the AAVSO Photometric All-Sky Survey (APASS) (Henden *et al.* 2010) for the stars are shown in Table 1. The comparison minus check star values showed no variability greater than 0.01 magnitude over the course of the observing run.

2. Analysis

We analyzed our observations with the most recent version of the PHOEBE program (Prša and Zwitter 2005) which is based on the Wilson-Devinney program (WD; Wilson and Devinney 1971; Wilson 1979). The J–H value from

2MASS (Skrutskie *et al.* 2006) is 0.40 ± 0.03, which corresponds to an effective temperature of about 5600 K (Kenyon and Hartmann 1995). The B–V value from APASS is 0.78 ± 0.08, corresponding to a temperature of around 5400 K. Since the J–H and B–V values are in good agreement, we set the mean effective temperature of star 1 (the star eclipsed at primary minimum) equal to 5500 K for the light curve solution. The adjusted parameters were the orbital inclination (i), the mean effective temperature of the secondary (T2), the mass ratio (q), the modified surface potential of the common envelope (–1), the heliocentric Julian date of the primary minimum (HJD_0), the orbital period (P), the bandpass luminosity of the primary (L1), and third light (l_3). Unadjusted parameters such as the gravity darkening exponents (g_1, g_2) and bolometric albedos (A_1,A_2) were set to their theoretically expected values for convective envelopes (0.32 and 0.5, respectively). The square root limb darkening law, using the Van Hamme (1993) coefficients (x_1,x_2,y_1,y_2), gave the best fits to the light curves. We used WD mode 3, appropriate for overcontact binaries of this type. The derived parameter values are shown in Table 2. The third light values are the ratio of the third light value to the total system light at quadrature. The fit shows that the slightly deeper eclipse (by 0.01 magnitude in V) is the partial one, technically making this an A-type system, but the light curve clearly shows asymmetries and large scatter, so we cannot make that classification with high confidence. Figure 1 shows the fits to the observations.

In W UMa systems like this, there is an astrophysical interest in the temperature difference of the two components. The primary star's temperature is estimated from the observed B–V and J–H colors with an approximate error of 200 K from the observational errors of the colors. The light curve solution gives the error in T_2, given the assumed T_1 from the observed colors. Thus the true uncertainty in T_2 is similar to the uncertainty in T_1. However, the uncertainty in the temperature difference, T_2–T_1, is similar to the formal solution error in T_2 since T_1 is assumed to be fixed. To illustrate this, we re-did the light curve analysis with T_1 = 5700 K and found T_2 = 5858 K, for a temperature difference of 158 K, compared to a value of 152 K for the solution in Table 1. So, while the individual temperatures are uncertain at the level of 200 K, the uncertainty in their difference is much smaller, of order 10–20 K.

3. Conclusions

Because of its total/annular eclipses and overcontact configuration, we might expect the photometric mass ratio to be well-determined (Terrell and Wilson 2005). However, Terrell and Wilson (2005) did not consider the effect of third light on the mass ratio determination. This system shows appreciable third light, with the flux from the third body comparable to that of the secondary star at quadrature. Simulations like those of Terrell and Wilson (2005) are underway to determine how third light might affect their findings, although we do not

expect it to have a large effect on the mass ratio determination. As discussed by Terrell and Wilson (2005), the photometric mass ratio for a totally eclipsing overcontact system is accurate because of the high accuracy to which the ratio of the stellar radii can be determined. Since third light affects the depths of both eclipses, rather than one or the other strongly, we do not expect the ratio of the radii to be strongly affected, and the photometric mass ratio should be reasonably accurate. The luminosity ratio in this system is, however, not so extreme as to preclude the ability to measure a spectroscopic mass ratio, so this system could have its absolute dimensions determined accurately because of the complete eclipses, even if the photometric mass ratio should prove to be inaccurate due to third light issues. A spectroscopic study of this system is sorely needed.

References

Gettel, S. J., Geske, M. T., and Mc Kay, T. A. 2006, *Astron. J.*, **131**, 621.
Henden, A. A., Terrell, D., Welch, D., and Smith, T. C. 2010, *Bull. American Astron. Soc.*, **42**, 515.
Kenyon, S. J., and Hartmann, L. 1995, *Astrophys. J., Suppl. Ser.*, **101**, 117.
Prša, A., and Zwitter, T. 2005, *Astrophys. J.*, **628**, 426.
Skrutskie, M. F., *et al.* 2006, *Astron. J.,* **131**, 1163.
Terrell, D., and Wilson, R. E. 2005, *Astrophys. Space Sci.,* **296**, 221.
Van Hamme, W. 1993, *Astron. J.,* **106**, 2096.
Wilson, R. E. 1979, Astrophys. J., **234**, 1054.
Wilson, R. E., and Devinney, E. J. 1971, *Astrophys. J.,* **166**, 605.

Table 1. Colors of the variable, comparison, and check stars.

	Star	*B–V*
Variable	GSC 4552-1643	0.78 ± 0.08
Comparison	GSC 4552-0002	0.92 ± 0.08
Check	GSC 4552-0059	0.50 ± 0.06

Table 2. Parameters for the light curve solution.*

Parameter	*Value*
i	88.9 ± 0.6°
T_2	5652 ± 10 K
q	0.327 ± 0.004
Ω_1	2.435 ± 0.008
HJD_0	2452500.187 ± 0.002
P	0.2698999 ± 0.0000001 day
$L_1/(L_1+L_2)_B$	0.687 ± 0.010
$L_1/(L_1+L_2)_V$	0.697 ± 0.009
$L_1/(L_1+L_2)_I$	0.705 ± 0.009
$l_{3\ B}$	0.163 ± 0.008
$l_{3\ V}$	0.185 ± 0.007
$l_{3\ I}$	0.212 ± 0.008
A_1, A_2	0.5 (fixed)
g_1, g_2	0.32 (fixed)
x_1, y_1 (B filter)	0.77, 0.09 (fixed)
x_1, y_1 (V filter)	0.46, 0.35 (fixed)
x_1, y_1 (I filter)	0.19, 0.48 (fixed)
x_2, y_2 (B filter)	0.72, 0.14 (fixed)
x_2, y_2 (V filter)	0.43, 0.37 (fixed)
x_2, y_2 (I filter)	0.18, 0.48 (fixed)

** The quoted errors are the formal errors from the differential corrections solution. Since the primary star's temperature is estimated from the observed B–V and J–H colors with an approximate error of 200 K; the secondary star's uncertainty in temperature is similar. The formal error is more indicative of the precision to which the solution can fit the ratio of the stellar temperatures, rather than the absolute temperatures.*

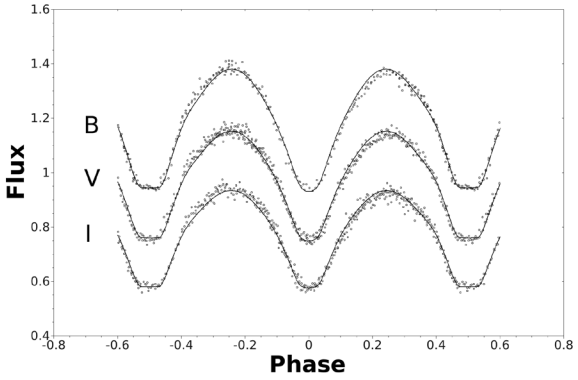

Figure 1. BVI light curves of GSC 4552-1643 and the fits from the Wilson-Devinney solution given in Table 2.

VSX J071108.7+695227: a Newly Discovered Short-period Eclipsing Binary

Mario Damasso
Astronomical Observatory of the Autonomous Region of the Aosta Valley, fraz. Lignan 39, 11020 Nus (Aosta), Italy; INAF associated; mario.damasso@studenti.unipd.it and m.damasso@gmail.com

and

Dept. of Physics and Astronomy, University of Padova, vicolo dell'Osservatorio 3, I-35122 Padova, Italy

Davide Cenadelli
Paolo Calcidese
Astronomical Observatory of the Autonomous Region of the Aosta Valley, fraz. Lignan 39, 11020 Nus (Aosta), Italy; INAF associated

Luca Borsato
Dept. of Physics and Astronomy, University of Padova, vicolo dell'Osservatorio 3, I-35122 Padova, Italy; INAF-OAPd associated

Valentina Granata
Dept. of Physics and Astronomy, University of Padova, vicolo dell'Osservatorio 3, I-35122 Padova, Italy

Valerio Nascimbeni
Dept. of Physics and Astronomy, University of Padova, vicolo dell'Osservatorio 3, I-35122 Padova, Italy; INAF-OAPd associated

Received March 28, 2012; revised April 13, 2012; accepted April 16, 2012

Abstract We report the discovery of an EW variable, VSX J071108.7+695227, with a short orbital period of ~0.238 day. This period is very close to the lower limit of ~0.22 day that has been found for EW systems. Here we present and discuss photometric and spectroscopic data of the variable, collected at the Astronomical Observatory of the Autonomous Region of the Aosta Valley and at the Asiago Astrophysical Observatory. The light curves show some asymmetries and the spectra suggest a dK4 classification for the two components. It could be interesting to carry out further observations of this system at different epochs because such systems frequently show variations in period and in the features of the light curve.

1. Introduction

We report the discovery of VSX J071108.7+695227 (= 2MASS J0711 0876+6952276), a short-period eclipsing binary system. We classify it as an EW type variable. This variable, located in the constellation Camelopardalis (R.A. 07^h 11^m 08.76^s; Dec. +69° 52' 27.6"; epoch J2000.0), was discovered thanks to photometric observations performed at the Astronomical Observatory of the Autonomous Region of the Aosta Valley (OAVdA), and at the Asiago Observatory. The system has an estimated orbital period of ~0.238 day.

The variable deserves further investigation mostly because the assessed period is very short and pretty close to the sharp cut-off at the lower limit of ~0.22 day found by Norton *et al.* (2011) for these binaries. Only a minor percentage of EW variables have periods shorter than ours. For example, Rucinski (2006) found that only a few tens out of the 4,638 EW systems of the ASAS sample have a period shorter than or similar to ours, Weldrake *et al.* (2007) found only two out of fifty-eight short period eclipsing binaries to have $P < 0.238$ day, and Miller *et al.* (2010) about ten out of 533. To date, the largest sample of EW systems with a period shorter than ours is made up of the fifty-three EW binaries with $P < 0.2314$ day listed by Norton *et al.* (2011). Moreover, such close systems show several features that change over time, as the orbital period and the shape of the light curves, as we discuss below.

All this considered, we pursued a photometric and spectroscopic analysis of our variable aimed at better characterizing its physical properties. We determined B, V, and R light curves, we assigned the two components to a spectral type, we looked for possible activity indicators in the spectra like emission lines, and we sought asymmetries in the light curves.

2. Instrumentation and methodology

Since the end of 2008, at the OAVdA is underway the implementation of an extensive observational campaign aimed at finding small-sized extrasolar planets around M dwarfs using the photometric transit method (Damasso *et al.* 2010; Giacobbe *et al.* 2012). The first observations of VSX J071108.7+695227 were perfomed at the end of December 2011, during the commissioning tests of the new telescope array which will be used for a five-year survey of hundreds of M dwarfs in the solar neighborhood. The array is composed of four identical 40-cm *f*/8.4 Ritchey-Chrétien telescopes, each on a 10 MICRON QCI2000 mount and equipped with a FLI ProLine 1001E CCD camera.

After the discovery, we photometrically followed up on the binary system with the main telescope present in OAVdA, an 81-cm f/7.9 Ritchey-Chrétien coupled to a back-illuminated CCD camera FLI ProLine PL 3041-BB and standard BVRI filters. The sensor is 2048 px × 2048 px, with a pixel area of 15 × 15 μm^2. The system has a FoV of 16.5 × 16.5 $arcmin^2$ with a

plate scale of 0.48"/pixel (binning 1 × 1). We present and discuss here the data collected with this telescope. In Figure 1 we present one of our frames and indicate our system.

2.1. Photometric data

The scientific frames taken during the discovery night and the follow-up observations were reduced and analyzed with the software package TEEPEE (Transiting ExoplanEts PipElinE) developed by some of the authors. A detailed description of the basic functions of the TEEPEE pipeline is provided in Damasso *et al.* (2010). In short, the final result of the data processing is the generation of the differential light curves of all the stars in the CCD field which were automatically recognized in every frame of the series. The ensemble photometry is obtained testing up to twelve apertures. The best set of comparison stars is automatically determined for a pre-selected target from a list of the 100 brightest objects found in the field, excluding the ones too close to the CCD borders. The aperture and set of reference stars selected at the end of the data processing are the ones which give the smallest RMS for the entire light curve of the object of interest.

Figure 2 (a, b, c) shows the normalized differential light curves of VSX J071108.7+695227 obtained in B, V, and R filters on January 16, 2012, during the follow-up observations with the 81-cm telescope. The differential magnitudes are calculated as the difference between the average instrumental magnitudes of the comparison stars and the instrumental magnitudes of the variable star. The comparison stars automatically selected by the TEEPEE pipeline for each filter are listed in Table 2. The light curves clearly unveil the EW variability type for the object and the observations cover almost 1.75 times the orbital period of the two components of the system, which we estimated to be ~0.238 day using the Fast Chi-Squared algorithm described in Palmer (2009) and freely available at http://public.lanl.gov/palmer/fastchi.html. Figure 3 shows the normalized V-band light curve folded according to the orbital period. The zero epoch is HJD(0) = 2455943.438.

We estimate a mean V magnitude for the object through the relations described in Pavlov (2009), which use the *J–K* color index from the *2MASS* catalogue (Skrutskie *et al.* 2006) and the U_f and U_a magnitudes from the *UCAC-3* catalogue (USNO 2012):

$$V_f = 0.531 \cdot (J–K) + 0.906 \cdot U_f + 0.95 \pm 0.08 \quad (1)$$

$$V_a = 0.529 \cdot (J–K) + 0.9166 \cdot U_a + 0.83 \pm 0.08 \quad (2)$$

Averaging the two values found from (1) and (2) results in $V = 14.37$, where $J = 12.631$, $K = 11.923$, $U_f = 14.366$, and $U_a = 14.396$.

Using the following conversion relations between the *USNO A2.0* (Monet *et al.* 1998) and Landolt BR magnitudes (Kidger 2003):

$$B = 1.097 \cdot \mathrm{USNO}(B) - 1.216 \quad (3)$$

$$R = 1.031 \cdot \mathrm{USNO}(R) - 0.417 \quad (4)$$

where USNO(B) = 14.8 and USNO(R) = 13.9, we obtained B = 15.0 and R = 13.9.

Moreover, the star also appears in the APASS catalogue (AAVSO 2012), which provides other estimates for B and V magnitudes: $B = 15.485 \pm 0.368$; $V = 14.468 \pm 0.289$.

2.2. Spectroscopic data

To better characterize the variable and look for possible activity indicators like emission lines, on January 26, 2012, we took nine consecutive spectra with the 182-cm Copernico telescope at the Asiago Observatory (http://www.pd.astro.it/asiago/), using the AFOSC CCD camera. Two different optical configurations were used (grism3 and grism8) with different dispersion and spectral coverage. The main features of these configurations are summarized in Table 1. We took five spectra using the grism3 and four with the grism8.

In Figure 3 we overplotted (solid and dashed) vertical lines corresponding to the orbital phases at which the nine spectra of the system were collected. It can be seen that the first ones (with both configurations) were taken at maximum brightness. They are shown in Figure 4. The other spectra do not show sizeable differences as compared to these, at least at the low dispersion accessible to us. It can be noticed, however, that they were taken at a not very different phase.

3. Discussion

At the epoch of our observations the light curves of the variable showed some clear asymmetries, as expected from such short-period systems. The most significant is an evident O'Connell Effect as the magnitude of the two maxima is different (Davidge and Milone 1984). The conventional way to assess the size of this effect is to measure the peak magnitude after the primary (deepest) minimum subtracted from the peak magnitude after the secondary minimum. From Figure 2 we derive that $\Delta B \sim \Delta V \sim \Delta R \sim + 0.05$. Furthermore, a closer inspection of the B curve reveals a small "shoulder" along the rise towards both the secondary maxima. This is possibly due to the ocurrence of starspots.

In fact, it is well-known that that EW variables are usually heavily spotted systems, as theoretically predicted by Binnendijk (1970). He was the first to propose that dark spots exist on the surfaces of the components to explain the asymmetry and variability of the light curves at different epochs. This hypothesis was later demonstrated by Doppler imaging (see for instance Hendry and Mochnacki 2000). One of the authors of the present paper already dealt with this issue and detected the presence of starspots in light curves taken at different epochs of one EW variable with an orbital period of ~0.355 day (Damasso *et al.* 2011).

Starspots are a possible explanation of the O'Connell Effect as well, but there is much uncertainty in this respect (Wilsey and Beaky 2009).

It would be interesting to collect new data of this system at different epochs to put in evidence possible evolutions that our data, taken during a single night, cannot reveal. In particular, short-period systems like ours can show variations in period or in the shape of the light curves, like an inversion of the primary and secondary maxima leading to an O'Connell Effect with opposite sign (see for example the case of V523 Cas treated in Zhang and Zhang 2004).

Let us now turn to the discussion of the spectroscopic data. The spectra in Figure 4 display the typical shape of K stars, without any evident superposition of different spectral types. This suggests that both components have similar spectra and surface temperatures. This is in accordance with the fact that the minima in the light curves are almost equal in deepness.

W UMa binaries are expected to be located within or in proximity of the main sequence stars (Bilir *et al.* 2005). This can be confirmed by our spectra: the prominence of the MgH band around 5200 Å and the tooth-shaped MgH feature around 4770 Å strongly suggest that the stars are dwarfs (Gray and Corbally 2009, p. 262).

To obtain a more precise classification, we resorted to the lines highlighted in Figure 4(c): the CaI line at 6162 Å, the BaII-FeI-CaI blend at 6497 Å, and the Hα line at 6563 Å. The latter directly correlates with temperature, while the first two inversely correlate with temperature, so that the CaI or BaII-FeI-CaI blend to Hα ratio is a useful temperature indicator.

Although in late-type stars it is often difficult to spot out an actual continuum to refer to, we calculated the equivalent widths of these three lines which are only indicative. They are:

$W\lambda$ (CaI) = 1.7 Å
$W\lambda$ (blend) = 0.8 Å
$W\lambda$ (Hα) = 0.4 Å

We decided to compare our spectra to the ones tabulated by Allen and Strom (1995) because they possess a spectral coverage and resolution quite similar to ours. The CaI to Hα ratio suggest a dK4 classification.

A further clue as to how to classify the two stars can be given by the slight difference in depth of the two minima. Such difference is nearly equal to 0.05 magnitude, that is, ~4.7% in flux. Calling $T_{1,2}$ the surface temperatures of the two components we can roughly infer that $(T_1 / T_2)^4 \sim 1.047 \rightarrow T_1 / T_2 \sim 1.012$, that is, the component 1 is hotter than the component 2 by 1.2 %. At temperatures between 4000 and 5000 K this means a difference of ~50 K. Unfortunately, the surface temperature of lower main sequence stars is not easy to calculate and within a same spectral type there can be a variance of more than 100 K (see for example Casagrande *et al.* 2006). Hence, the calculated temperature

difference cannot be safely assumed as to testify a difference of spectral type between the two components. In the end, we rest upon a dK4 classification for both components. In addition, this conclusion is consistent with a classification based on the color indices: according to Cox (2000) a dK4 star is expected to have $J–H = 0.58$ and $H–K = 0.11$, and our variable has $J–H = 0.583$ and $H–K = 0.125$.

Furthermore, we can try to deduce the masses of the two stars. If we call *a* the overall semi-major axis of the system (that is, the sum of the two semi-major axes with respect to the center of mass) expressed in AUs, T the period expressed in years, and $M_{1,2}$ the masses of the two components expressed in solar units, we have:

$$a^3 = T^2(M_1 + M_2) \quad (5)$$

From our photometric data we deduce $T = 0.238$ day $= 6.516 \times 10^{-4}$ yr. A mid-K dwarf typically has a mass $M \sim 0.7 – 0.75$; assuming $M_1 + M_2 = 1.45$, it results that $a \sim 1.27 \times 10^6$ km.

Assuming both components to have a radius R 0.75 – 0.8 with respect to the Sun, that is, about 5×10^5 km, we have a ~2.5R. This is fine because W UMa variables are supposed to be almost touching each other.

Moreover, one could ask how large a Doppler broadening such an orbital pattern would entail in spectra. Let us assume a circular orbit. At the time of maximum in the light curve we should have an overall Doppler broadening of the order of:

$$\Delta\lambda / \lambda = v / c = 2\pi a / (T_c) = 1.29 \times 10^{-3} \quad (6)$$

If we consider the Hα line at 6563Å we have that $\Delta\lambda \sim 8$ Å, that is, the width of the line should extend about from 6554.5 to 6571.5Å. If we consider the CaI line at 6162 we have $\Delta\lambda$ 8Å, that is, the width of the line should extend about from 6154 to 6170Å. These values are consistent with our spectra, but because of the low dispersion we can attain we believe we cannot draw any sure conclusion in this respect.

We finally looked for possible activity indicators in the spectra like emission lines, but we found none at the level of resolution accessible to us.

4. Acknowledgements

Authors Damasso, Cenadelli, and Calcidese are supported by grants provided by the European Union, the Autonomous Region of the Aosta Valley and the Italian Department for Work, Health and Pensions. The OAVdA is supported by the Regional Government of the Aosta Valley, the Town Municipality of Nus and the Mont Emilius Community. The telescope which led to the discovery of the variable star has been funded by the Fondazione Cassa di Risparmio di Torino (CRT). This

research has made use of the SIMBAD database, operated at CDS, Strasbourg, France, and of the NASA Astrophysics Data System Bibliographic Services.

References

AAVSO. 2012, APASS: The AAVSO Photometric All-Sky Survey (http://www.aavso.org/apass), AAVSO, Cambridge, MA.

Allen, L. E., and Strom, K. 1995, *Astron. J.*, **109**, 1379.

Bilir, S., Karataş, Y., Demircan, O., Eker, Z. 2005, *Mon. Not. Roy. Astron. Soc.*, **357**, 497.

Binnendijk, L. 1970, *Vistas Astron.*, **12**, 217.

Casagrande, L., Portinari, L., and Flynn, C. 2006, *Mon. Not. Roy. Astron. Soc.*, **373**, 13.

Cox, A. N. 2000, *Allen's Astrophysical Quantities*, 4th ed., Springer, New York.

Damasso, M., *et al.* 2010, *Publ. Astron. Soc. Pacific*, **122**, 1077.

Damasso, M., *et al.* 2011, *Open Eur. J. Var. Stars*, No. 138, 1.

Davidge, T. J., and Milone, E. F. 1984, *Astrophys. J., Suppl. Ser.*, **55**, 571.

Giacobbe, P., *et al.* 2012, *Mon. Not. Roy. Astron. Soc.*, **424**, 3101.

Gray, R. O., and Corbally, C. J. 2009, *Stellar Spectral Classification*, Princeton Univ. Press, Princeton, NJ.

Hendry, P. D., and Mochnacki, S. W. 2000, *Astrophys. J.*, **531**, 467.

Kidger, M. R. 2003, "The USNO A2.0 photometric scale compared to the standard Landolt BVR magnitudes" (http://quasars.org/docs/USNO_Landolt.htm, accessed April 2012).

Miller, V. R., Albrow, M. D., Afonso, C., and Henning, T. 2010, *Astron. Astrophys.*, **519A**, 12.

Monet, D. *et al.* 1998, *USNO-A V2.0 Catalog of Astrometric Standards,* U.S. Naval Observatory, Flagstaff, AZ.

Norton, A. J., *et al.* 2011, *Astron. Astrophys.*, **528A**, 90.

Palmer, D. M. 2009, *Astrophys. J.*, **695**, 496.

Pavlov, H. 2009, "Deriving a V magnitude From UCAC3" (http://www.hristopavlov.net/Articles/index.html).

Rucinski, S. M. 2006, *Mon. Not. Roy. Astron. Soc.*, **368**, 1319.

Skrutskie, M. F., *et al.* 2006, *The Two Micron All Sky Survey, Astron. J.,* **131**, 1163.

U.S. Naval Observatory. 2012, *UCAC-3* (http://www.usno.navy.mil/USNO/astrometry/optical-IR-prod/ucac).

Weldrake, D. T. F., Sackett, P. D., and Bridges, T. J. 2007, *Astron. J.*, **133**, 1447.

Wilsey, N. J., and Beaky, M. M. 2009, in *The Society for Astronomical Sciences 28th Annual Symposium on Telescope Science* (May 19–21, 2009), Soc. Astron. Sci., Rancho Cucamonga, CA, 107.

Zhang, X.B., and Zhang, R.X. 2004, *Mon. Not. Roy. Astron. Soc.*, **347**, 307.

Table 1. Optical configurations used to acquire the spectra of the variable.

Configuration	*Spectral coverage*	*Mean dispersion*	*Resolution*
grism3	~3700 – ~5850Å	~2.1Å/px	~650
grism8	~5950 – ~8000Å	~2.0Å/px	~1900

Table 2. Comparison stars used for differential photometry in B, V, and R bands.

Star	*R.A.* *h m s*	*Dec.* ° ′ ″	*Band*
UCAC-3 320-037770	07 09 19.041	+69 55 06.66	B V
UCAC-3 320-037772	07 09 21.093	+69 56 00.27	B
UCAC-3 320-037776	07 09 24.095	+69 56 59.02	B V R
UCAC-3 320-037779	07 09 28.970	+69 51 43.34	B R
UCAC-3 320-037783	07 09 32.398	+69 50 57.44	B
UCAC-3 320-037784	07 09 32.649	+69 58 42.06	B
UCAC-3 320-037787	07 09 34.315	+69 49 49.11	B V R
UCAC-3 320-037794	07 09 42.534	+69 50 59.13	B
UCAC-3 320-037795	07 09 43.173	+69 54 42.21	B
UCAC-3 320-037798	07 09 45.939	+69 55 15.41	B
UCAC-3 320-037799	07 09 47.551	+69 52 26.48	B
UCAC-3 320-037820	07 10 09.948	+69 55 17.80	B
UCAC-3 320-037821	07 10 11.189	+69 50 45.90	B
UCAC-3 320-037823	07 10 14.455	+69 50 34.28	R
UCAC-3 320-037827	07 10 20.912	+69 49 40.04	B V R
UCAC-3 320-037828	07 10 21.806	+69 52 30.72	B
UCAC-3 320-037831	07 10 23.959	+69 51 24.78	B R
UCAC-3 320-037835	07 10 31.401	+69 53 52.17	B
UCAC-3 320-037849	07 10 38.339	+69 57 18.61	B
UCAC-3 320-037857	07 10 42.666	+69 49 14.61	B
UCAC-3 320-037860	07 10 44.576	+69 51 52.55	B
UCAC-3 320-037862	07 10 47.011	+69 51 35.23	B
UCAC-3 320-037867	07 10 54.909	+69 52 17.17	B V R
UCAC-3 320-037871	07 11 03.636	+69 52 31.88	B
UCAC-3 320-037876	07 11 07.800	+69 51 27.49	B V
UCAC-3 320-037881	07 11 10.879	+69 51 29.52	B V
UCAC-3 320-037885	07 11 14.572	+69 56 07.65	B V R
UCAC-3 320-037896	07 11 27.544	+69 48 08.74	B
UCAC-3 320-037901	07 11 32.558	+69 52 03.82	B V R
2MASS 07110649+6947296	07 11 06.492	+69 47 29.61	B
2MASS 07094405+6952413	07 09 44.051	+69 52 41.40	B

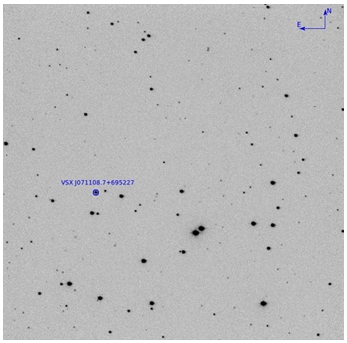

Figure 1. The star field of VSX J071108.7+695227, with the variable star target highlighted. The scale of the image is 16.5 × 16.5 arcmin^2. North is up and east is to the left.

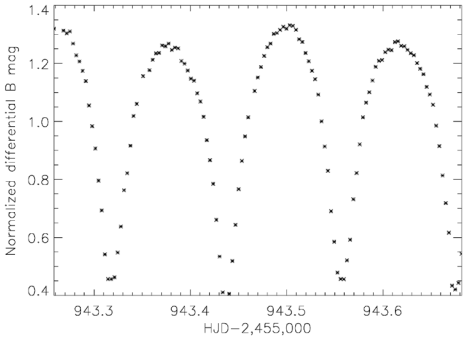

Figure 2a. Differential light curve of the variable star VSX J071108.7+695227 in B filter. The data were collected on January 16, 2012.

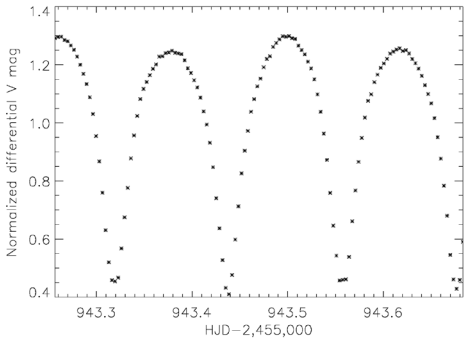

Figure 2b. Differential light curve of the variable star VSX J071108.7+695227 in V filter. The data were collected on January 16, 2012.

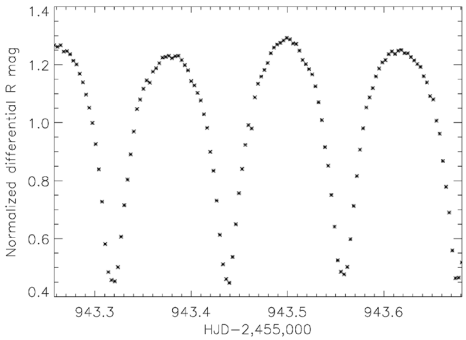

Figure 2c. Differential light curve of the variable star VSX J071108.7+695227 in R filter. The data were collected on January 16, 2012.

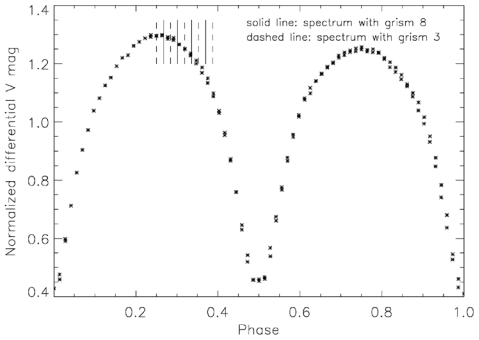

Figure 3. Differential light curve of VSX J071108.7+695227 in V band folded according to the orbital period ~0.238 days.

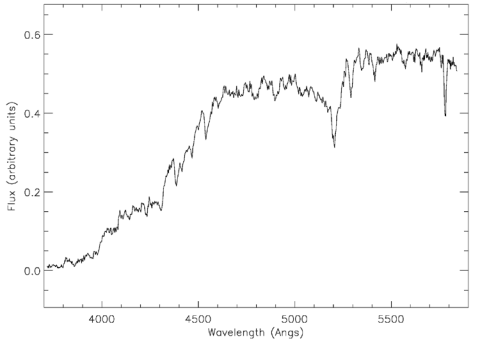

Figure 4a. Spectra of the variable star VSX J071108.7+695227 at maximum brightness, taken with grism3. The mid epoch of the exposure is HJD 2455953.493615.

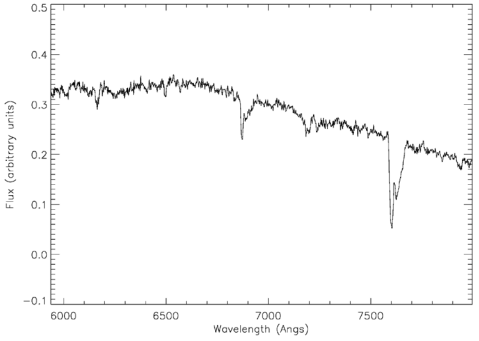

Figure 4b. Spectra of the variable star VSX J071108.7+695227 at maximum brightness, taken with grism8. A magnified region is displayed in Figure 4c. The mid epoch of the exposure is HJD 2455953.497677.

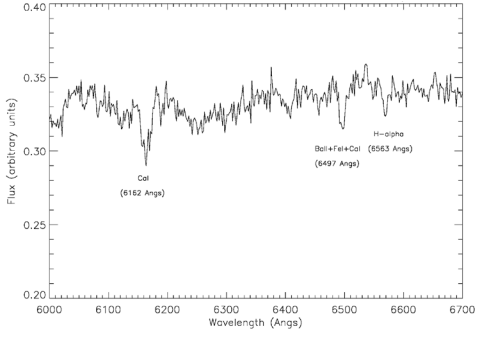

Figure 4c. A magnified region of the spectra of the variable star VSX J071108.7+695227 at maximum brightness, taken with grism8. The mid epoch of the exposure is HJD 2455953.497677.

Variability Type Determination and High Precision Ephemeris for NSVS 7606408

Riccardo Furgoni
Keyhole Observatory, Via Fossamana 86, S. Giorgio di Mantova (MN), Italy; riccardo.furgoni@alice.it

and

Associazione Astrofili Mantovani—Gorgo Astronomical Observatory MPC 434, S. Benedetto Po (MN), Italy

Received May 11, 2012; revised June 4, 2012; accepted June 14, 2012

Abstract A photometric campaign analysis of the star NSVS 7606408 has been conducted in order to determine the type of variability and high accuracy ephemeris. By combining the obtained data with other datasets available, it was tried to improve the determination of the period, highlighting, however, a possible minimal change of the period over the years. At May 2, 2012, the ephemeris calculated for this variable star is HJDmin = $(2456015.44998 \pm 1.1 \times 10^{-4}) + E \times (0.35482573 \pm 3 \times 10^{-8}) + E^2 \times (2.4 \times 10^{-10} \pm 1 \times 10^{-11})$

1. Introduction

In recent years many wide field photometric surveys have led to the discovery of a large number of variable stars of different types. These include: NSVS (Northern Sky Variability Survey—an extensive variability survey of the sky north of Dec. −38° with daily time-sampling and a one-year baseline, by the Los Alamos National Laboratory; SuperWASP (Wide Angle Search for Planets)—UK's leading extra-solar planet detection program comprising a consortium of eight academic institutions, including Cambridge University, the Instituto de Astrofisica de Canarias, the Isaac Newton Group of telescopes, Keele University, Leicester University, the Open University, Queen's University Belfast, and St. Andrew's University; ASAS (All Sky Automated Survey)—a low-cost project dedicated to constant photometric monitoring of the whole available sky, which is approximately 10^7 stars brighter than 14th magnitude—the project's ultimate goal is detection and investigation of any kind of photometric variability. Despite this, there has never been made a precise study of many of them with the aim of determining the class of variability and obtaining phase plots with a reasonably low scattering. Most of the instruments dedicated to large-scale research use short focal length telescopes which give extremely crowded images of star fields, making the photometric measurements difficult and sometimes inaccurate. The databases generated by these surveys, however, are a particularly valuable source of data in obtaining confirmations

of newly discovered variable stars and in allowing a precise determination of the periods of regular variables. Having data concerning a large period of time makes period determination much more effective.

2. Instrumentation used

The data were obtained with a Celestron C8 Starbright, a Schmidt-Cassegrain optical configuration with aperture of 203 mm and central obstruction of 34%.

The telescope was positioned at coordinates: 45° 12' 32" N 10° 50' 20" E (WGS84), in a rural area with low to medium light pollution. The telescope was equipped with a focal reducer Baader Planetarium Alan Gee II able to bring the focal length from 2030 mm to 1396 mm. The focal ratio was reduced to *f*/6.38 from the original *f*/10.

The pointing was maintained with a Syntha NEQ6 mount with software SYNSCAN 3.27 guided through a Baader Vario Finder telescope equipped with a Barlow lens capable of bringing the focal length of the system to 636 mm and focal ratio of *f*/10.5.

The guide camera has been a Magzero MZ-5 with Micron MT9M001 monochrome sensor equipped with an array of 1280 × 1024 pixels. The size of the pixels is 5.2 µm × 5.2 µm for a resulting sampling of 1.68 arcsec/pixel.

The CCD camera has been a SBIG ST8300m with monochrome sensor Kodak KAF8300 equipped with an array of 3352 × 2532 pixels. The pixels are provided with microlenses for improving the quantum efficiency, and the size of the pixels is 5.4 µm × 5.4 µm for a resulting sampling of 0.80 arcsec/pixel. The camera has a resolution of 16 bits with a gain of 0.37e-/ADU and a full-well capacity of 25,500 electrons. The dark current is 0.02e-/pixel/sec at a temperature of –15° C. The typical read noise is 9.3e-RMS.

The camera is equipped with 1,000× antiblooming: after exhaustive testing it has been verified that the zone of linear response is between 1,000 and 20,000 ADU, although at up to 60,000 ADU the loss of linearity is less than 5%. The CCD is equipped with a single-stage Peltier cell $\Delta T = 35 \pm 0.1$° C which allows cooling at a stationary temperature.

3. Data collection

The observations were performed with the CCD at a temperature of –5° C in binning 1 × 1. The exposure time was 55 seconds with a delay of 1 second between the images and an average download time of 11 seconds per frame. The star has been observed with a maximum pixel intensity of about 3,400 ADU and SNR 80. The comparison star had pixels with maximum intensity of about 4,000 ADU and SNR 100. The check star had pixels with maximum intensity of about 4,200 ADU and SNR 110. All stars have ADU intensity within the region of linear response of the CCD.

The observations were carried out without the use of photometric filters to maximize the signal-to-noise ratio. The spectral sensitivity of the CCD, as shown in Figure 1, is maximum at a wavelength of 540 nm, making the data more compatible with a magnitude CV (Clear Filter—Zero Point V).

The observations were conducted over eight nights as presented in Table 1.

The CCD control program was Software Bisque's CCD SOFT V5. Once the images were obtained, calibration frames were taken for a total of 30 dark of 55 sec at –5° C, 80 darkflat of 2 sec at –5° C, and 100 flat of 2 sec at –5° C. The darkflats and darks were taken only the first observation session and used for all other sessions. The flats were performed for each session as the position of the CCD camera could be varied slightly, as well as the focus point.

The calibration frames were combined with the method of the median and the masterframes obtained were then used for the correction of the images taken. All images were then aligned and an astrometric reduction was made to implement the astrometrical coordinate system WCS in the FITS header. These operations were conducted entirely through the use of software MAXIMDL V5.18 made by Diffraction Limited.

4. The measurement of NSVS 7606408

The star to be measured was observed within the Northern Sky Variability Survey (NSVS; Wozniak *et al.* 2004), which is a photometric survey for stars with an optical magnitude between 8 and 15.5. The research was conducted during the first generation of the Robotic Optical Transient Search Experiment (ROTSE-I) using a robotic system composed by four photographic lenses without photometric filters connected to CCDs. The research was conducted by Los Alamos National Laboratory (New Mexico) in order to cover the entire northern hemisphere of the sky. In a year of work between 1999 and 2000 an average of 150 photometric measurements for 14 million stars was made.

At the end of this research an automatically extended data analysis was made that led to the discovery of variable stellar sources. NSVS 7606408 has been recognized as a source with confirmed variability (Shaw *et al.* 2009). Identification data for this star are as follows:

Name:	NSVS 7606408
Position (UCAC3):	R.A. (2000), $11^h\ 48^m\ 56.586^s$, Dec. (2000) +26° 02' 30.07"
Cross Identifications:	GSC2.2 N201201146 CMC14 114856.5+260230 USNO-B1.0 1160-0187403 NOMAD1 1160-0192011 PPMX 114856.5+260230

UCAC3 233-104554
2MASS J11485658+2602301
SDSS J114856.58+260229.9

Proper motion (PPMX): pm R.A. = –0.08 mas/yr; pm Dec. = 2.39 mas/yr

AAVSO VSX period: 0.17740547 day (from Shaw *et al.* 2009)

The star field containing the variable star is shown in Figure 2.

The star's brightness was measured with MAXIMDL V5.18 software, using the aperture ring method. With a FWHM of the observing sessions at times arrived at values of 5" it was decided to choose values providing an adequate signal-to-noise ratio and the certainty of being able to properly contain the whole flux sent from the star. I have used the following apertures:

Aperture radius, 12 pixels; Gap width, 2 pixels; Annulus thickness, 8 pixels

The choice of making observations without the use of photometric filters required a proper study of the field in order to identify comparison stars with color similar to the variable under study, and with adequate signal-to-noise ratio, to obtain as accurate differential photometry as possible.

The choice was made by analyzing the measures relating to photometric 2MASS (Skrutskie *et al.* 2006) bands J, H, and K as mentioned in the *Carlsberg Meridian Catalog 14* (CMC14; Copenhagen Univ. Obs. *et al.* 2006). In the absence of precise measures of the magnitude in the standard V Johnson-Cousins, for stars used in the analysis it was decided to derive their V magnitude from the catalog CMC14 r' magnitude as described in Dymock and Miles (2009). This way ensures a good reliability and a final error theoretically not more than 0.05 magnitude in V. The conversion formula is as follows:

$$V_{\text{Johnson-Cousins}} = 0.6278 \times (J_{\text{2MASS}} - K_{\text{2MASS}}) + 0.9947 \times r'_{\text{CMC14}} \; (9 < r' < 16) \qquad (1)$$

The possible spectral type has been derived from the 2MASS J–H value instead, as shown in CMC14. The method is described in Stead and Hoare (2002) with the results as shown in Table 2.

Within the star field analyzed, only two stars have an adequate signal-to-noise ratio and color similar to the variable under study. Their position with respect to the variable is shown in Table 3 and Figure 3.

Through differential photometry the average magnitude of NSVS 7606408 is 13.572 ± 0.006 CV determined by placing the comparison star's magnitude at 13.325 CV. Whereas the variability of the star is by far superior to the gap that this value has with the V magnitude derived from CMC14 (= 13.641), it can be considered an acceptable result. The mean magnitude error for all the sessions is 0.006 CV. For the longest observing session the light curves of the

variable star and the check star in relation to the comparison star are shown in Figure 4.

The check star shows an almost complete absence of significant trends: this fact shows that the color index of stars used is good enough for differential photometry carried out in unfiltered conditions.

5. Data analysis

Before proceeding further in the analysis, the time of the light curves obtained was heliocentrically corrected (HJD) in order to ensure a perfect compatibility of the data with observations carried out even at a considerable distance in time.

From here on, the obtained dataset will be referred to as FRIC in this work, (FRIC being the author's AAVSO observer code).

The determination of the period was calculated using the software PERIOD04 (Lenz and Breger 2005), using a Discrete Fourier Transform (DFT). The average zero-point (average magnitude of the object) was subtracted from the dataset to prevent the appearance of artifacts centered at a frequency 0.0 of the periodogram. All the data points were weighted in relation to the amount of the magnitude error. The periodogram was calculated with a frequency range from 0 to 25 cd^{-1} (cycles per day) and step 0.00118537583 cd^{-1}. The result is shown in Figure 5.

The calculated frequency is 5.636659(89) cd^{-1} (SNR 12.9) with an amplitude of 0.164 ± 0.001 CV. The period thus appears to be 0.1774100(28) day with a time of minimum 2456008.35376(17) HJD. The calculation of the uncertainties was carried out with PERIOD04 using the method described in Breger *et al.* (1999). The resulting phase diagram is shown in Figure 6.

In the VSX catalogue (Watson *et al.* 2012) maintained by the American Association of Variable Stars Observers (AAVSO), the star is listed as a possible eclipsing variable W UMa-type or as a pulsating variable δ Sct. By observing this phase diagram one can see that the curve shape much more resembles the rotation of an eclipsing variable rather than a pulsating one. In general, it is not easy to distinguish between EW eclipsing binaries and pulsating stars such as δ Sct or RRC since many of them have symmetric light curves, and sometimes comparable periods. In any case it is possible to distinguish them using the following criteria:

- The minima of the EW variables are generally sharper than maxima.
- The minima of the EW variables may have slight differences in depth.
- The EW variables can have maxima with slight differences in intensity before and after the primary minimum (O'Connell Effect) (Liu and Yang 2003).

- The RRC variables may have light curves slightly asymmetrical with the growth phase slightly steeper than the descending phase.

Based on these considerations and the more plausible classification of this variable as a W UMa system, I propose a new period for NSVS 7606408 equal to P = 0.3548200(28) day and HJD_{min} = 2456015.45016(17). The new phase diagram is shown in Figure 7. The low dispersion phase diagram allows us to recognize the following parameters:

- The minima centered at phase 0 and 0.5 are sharper than maxima present at phases 0.25 and 0.75.

- Primary minimum placed at phase 0 is deeper than the minimum placed at phase 0.5. The difference in intensity is estimated on the order of 0.028 ± 0.005 magnitude (the result is obtained by calculating the difference between the average value of the data places between phase 0.95 and phase 0.05 and those located between phase 0.45 and phase 0.55).

- The maximum placed at phase 0.25 is slightly less bright than the maximum placed at phase 0.75. The difference in intensity is estimated on the order of 0.013 ± 0.005 magnitude (the result is obtained by calculating the difference between the average value of the data places between phase 0.2 and phase 0.3 and those located between phase 0.7 and the phase 0.8).

The observations suggest that this system should be classified as a eclipsing variable W UMa (EW-type star) with a perceptible difference between primary and secondary minimum and the existence of a probable O'Connell effect.

6. Other photometric data for NSVS 7606408

As a series of photometric measurements are accurate and provided with low scatter, the temporal extension of them is a key requirement to allow an accurate determination of the period. The longer their extension, in fact, the more noticeable will be the effect that a minimum error in the determination of the period will lend to the phase diagram obtained. Even the phenomenon of aliasing tend to decrease if in the presence of temporal coverage sufficiently long and provided with adequate resolution. My observations give a phase plot with reduced dispersion; until now, no phase diagram has been published for NSVS 7606408, except that associated with NSVS data, which however, is plagued by a very noticeable scattering.

It was therefore decided to evaluate all the existing photometric observations for this star able to provide a reasonable amount of data to improve the period specified above.

The following surveys were taken into consideration:

• NSVS The star is listed as NSVS 7606408. There are 233 observations made from April 5, 1999, to March 30, 2000, with a mean magnitude of 13.72 ± 0.07 (the original data are 275 points but are reduced to 233 after the rejection on the flag N Good Points). The data were obtained through the SkyDot service operated by Los Alamos National Laboratory (Sky Database for Objects in Time-Domain. Data at http://skydot.lanl.gov/nsvs/star.php?num=7606408&mask=32004). I have made a heliocentric correction of the data.

• SuperWASP The star is listed as 1SWASP J114856.59+260230.1. There are 5,916 observations made from May 2, 2004, to May 17, 2008 with a mean magnitude of 13.73 ± 0.04 (Tamflux2). The data, provided by the Public SWASP Archive in the form of Data Fits, were extracted using fv software, only for the values Tmid, Tamflux2, and Tamflux2_Err. (Tmid = HJD Mean Time of Exposure from JD Reference which is 2453005.5; Tamflux2 = Original flux (Tamuz) corrected on the basis of a decorrelation technique highlighted by Collier Cameron et al. (2006). This flux is provided in microvegas and its conversion to magnitudes is given by the formula mag. = 15 – 2.5 log(Flux); Tamflux2_err = error calculated on flux Tamflux2.) The SuperWASP data are already heliocentrically corrected and even for the average time of exposure. The wide availability of data related to this dataset led me to make a selection on those that showed the Tamflux2_Err less than 0.05 magnitude. The number of observations used is thus down to 3,158 with a time span fom May 4, 2004, to May 16, 2007, and a mean magnitude of 13.706.

• ASAS The star is listed as ASAS 114858+2602.5. Only data relating to ASAS- 3 (V-Magnitude) are present, not to ASAS-2 (I-Magnitude). There are 139 observations made from January 2, 2003, to March 2, 2009, with a mean magnitude of 13.67 ± 0.03. (The original data are 279 points but are reduced to 139 after discarding all those with flag D (worst data, probably useless) and all those having at least one measure invalid (Mag0; Mag1; Mag2; Mag3; Mag4 = 29.999. The average magnitude was calculated by performing for each given data the average of the values Mag1, Mag2; Mag3; Mag4 corresponding to different apertures used for the calculation of the stellar flux.) The data were provided by the Astronomical Observatory, University of Warsaw, and are already heliocentrically corrected.

Table 4 shows the period determinations for each dataset using the software PERIOD04. (When the same criteria used for determining the period and uncertainties of FRIC dataset data were also used here, they have been omitted.) The respective phase diagrams and Fourier spectra are shown in Figures 8 through 13.

7. Combining the available data

Due to the different spectral sensitivity of the CCDs used in these surveys (as well as the lack or the use of different filters), the combination of the datasets can not be trusted as regards the determination of the amplitude variation. Using the DFT, only the SWASP dataset shows an amplitude of variation at all similar to the FRIC dataset (0.164 ± 0.001) while all the other datasets show slightly different values. Moreover, the NSVS and ASAS datasets have a strong scattering which could make inaccurate the combined Fourier analysis. Since it is unclear how these differences affect the DFT of the combined data, only the FRIC and SWASP datasets will be used in combination for this calculation. In this case, the DFT may be used only to obtain a possible period to be used as a good starting point for a more detailed O–C analysis.

In order to combine the datasets it was first necessary to normalize the mean magnitude of the SWASP, NSVS, and ASAS datasets to the average value of the FRIC dataset. (For the NSVS and ASAS datasets the offset has been applied only for the realization of the combined phase diagram shown in Figure 15.) The applied offsets are given in Table 5.

The periodogram obtained, calculated on the frequency between 0 and 15 (cd^{-1}) with steps of 0.00001712275 (cd^{-1}) is shown in Figure 14.

The choice of combining the two datasets has led to a significant reduction in errors relating to the period, the amplitude variation and the determination of the time of primary minimum.

The calculated period is 5.63656978 (8) cd^{-1} (SNR = 13.068), which corresponds to $2P = 0.35482573\,(3)$ day, the amplitude is 0.1645 ± 0.0007 mag. with $HJD_{min} = 2456015.44998\,(11)$. The resulting phase diagram for all the datasets based on these new parameters is given in Figure 15.

Visually we can see that the NSVS dataset, which is the earliest in time, is clearly not in phase with the FRIC and SWASP. Trying to slightly vary the period to improve the phase of NSVS we immediately lose the coincidence of other datasets. Now it would be necessary to use an O–C analysis even if the NSVS, ASAS, and SWASP datasets did not have a sampling rate that allows to verify precisely the times of minimum. Due to the fact that there are no observations in the literature regarding the time of minimum for this variable star we will proceed as follows: for each dataset will be taken as times of minimum the times in which the light intensity is less than magnitude 13.75. (The low numbers of ASAS data and their high dispersion renders them useless for this type of analysis. This dataset was not used for the creation of the O–C diagram.) Obviously, because of scattering, even this calculation will be noisy, but if a period change is present, the O–C diagram should show the typical shape (Figure 16).

Compared to the primary minimum observed on 2456015.44998 (11) HJD, the earlier NSVS primary minimum that best represents the time shift with

respect to the calculated ephemeris is out of phase by 0.042 (1) day. Here it is important to remember that the vertical shape of the different minima in the graph is due solely to the uncertainty of the derived time of timimum related to the dataset's scattering. I have used for fitting a second order polynomial and the good result obtained suggests that we are faced with a progressive slowing of the period. Now, if we assume that the period is slowing down for a probable mass transfer between the two stars, is necessary to calculate how much each cycle must slow down to accumulate in 13,326 cycles a time shift of 0.042 (1) day. (These are the complete cycles that the star has made since the earlier NSVS primary minimum until HJD_{min} = 2456015.44998 ± 0.00011 HJD.)

It is necessary that the period increases $4.8 \times 10^{-10} \pm 1 \times 10^{-11}$ days at each cycle to be able to accumulate a time shift of 0.042 (1) day in 13,326 cycles. As the calculation is based on very small quantities it is necessary to provide a double check: it is possible to evaluate the reliability of this prediction by looking at the data provided by PERIOD04 concerning the calculation of the period of each dataset.

If the period really increases by this small amount in each cycle it is necessary that in the 13,326 cycles which separate the two minima it is increased by 6.396×10^{-6} days. The period calculated by PERIOD04 for the earlier NSVS dataset is 0.3548184 (14) day and if we add to this the value 6.396×10^{-6} days we obtain 0.3548248 (14), which is very close to the period obtained by PERIOD04 for the FRIC and SWASP data combined as shown in Table 5.

In other words, the different length of the period found by the DFT in the measurements carried out in 1999 and 2000 by NSVS in comparison with those carried out more recently is very similar to the variation of the period calculated with the O–C diagram.

8. Conclusions

By combining the available data I have tried to classify the star NSVS 7606408, originally considered in the literature a possible W UMa- or δ Sct-type variable star with a period of 0.17740547 day. Analyzing the obtained data it is believed possible to identify the type of variability and a precise calculation of the ephemeris. The final resulting data are as follows:

Star name	NSVS 7606408
Equatorial coordinates (UCAC3)	R. A. (2000) $11^h\ 48^m\ 56.586^s$ Dec. (2000) +26° 02' 30.07"
Variability type	Eclipsing binary W UMa
Actual Period	$0.354825732 \pm 3 \times 10^{-8}$ day
Amplitude variation (primary min – primary max)	

$$13.743 \pm 0.005\,\mathrm{CV} - 13.403 \pm 0.005\,\mathrm{CV} = (0.340 \pm 0.005\,\mathrm{CV})$$

Difference between primary and secondary minimum

$$13.743 \pm 0.005\,\mathrm{CV} - 13.715 \pm 0.005\,\mathrm{CV} = (0.028 \pm 0.005\,\mathrm{CV})$$

Difference between primary and secondary maximum

$$13.403 \pm 0.005\,\mathrm{CV} - 13.416 \pm 0.005\,\mathrm{CV} = (0.013 \pm 0.005\,\mathrm{CV})$$

Effects present O'Connell Effect

Ephemeris $HJD_{min} = (2456015.44998 \pm 1.1 \times 10^{-4}) + E \times (0.35482573 \pm 3 \times 10^{-8}) + E^2 \times (2.4 \times 10^{-10} \pm 1 \times 10^{-11})$

9. Aknowledgements

I wish to thank Mrs. Antonella Finotti for her support in revising the text, and Stefano Brangani, Ph.D., for his valuable comments on the mathematical aspects of this work.

References

Breger, M., *et al.* 1999, *Astron. Astrophys.*, **349**, 225.

Collier Cameron, A., *et al.* 2006, *Mon. Not. Roy. Astron. Soc.*, **373**, 799.

Copenhagen Univ. Obs., *et al.* 2006, *Carlsberg Meridian Catalog 14* (CMC14), VizieR On-line Data Catalog: I/304.

Dymock, R., and Miles, R. 2009, *J. British Astron. Assoc.*, **119**, 149.

Lenz, P., and Breger, M. 2005, *Commun. Asteroseismology*, **146**, 53.

Liu, Q. -Y., and Yang, Y. -L. 2003., *Chin. J. Astron. Astrophys.*, **3**, 142.

Shaw, J. S., *et al.* 2009, "Finding periodic variables in the NSVS" (https://www.physast.uga.edu/~jss/nsvs/).

Skrutskie, M. F., *et al.* 2006, *Astron. J.*, **131**, 1163.

Stead, J. J., and Hoare, M. G. 2002, "New Empirical Intrinsic Colours for the 2MASS and UKIDSS Photometric Systems" (http://www.ast.leeds.ac.uk/~phy2j2s/Intrinsic_Stead10.pdf).

Watson, C., Henden, A. A., and Price, A. 2012, AAVSO International Variable Star Index VSX (Watson+, 2006-2011), VizieR On-line Data Catalog: B/vsx.

Wozniak, P. R., *et al.* 2004, *Astron. J.*, **127**, 2436.

Table 1. Activity log for the data collection concerning the FRIC dataset. The NExT value indicates the Net Exposure Time which is the session duration spent in pure photons collection.

Date (dd-mm-yyyy)	*UTC Start (hh:mm:ss)*	*UTC End (hh-mm-ss)*	*NExT[1] (hh-mm-ss)*	*Useful Exposures*	*Airmass Min*	*Airmass Max*
21-03-2012	18:41:11	22:34:41	02:55:07	202	1.065	1.767
22-03-2012	18:35:15	21:07:47	01:54:24	135	1.153	1.783
25-03-2012	20:57:53	22:44:12	01:19:44	94	1.058	1.149
26-03-2012	19:11:22	00:49:43[2]	04:13:38	294	1.058	1.459
28-03-2012	20:08:08	00:45:15[3]	03:27:50	240	1.058	1.230
22-04-2012	19:24:59	21:29:28	01:39:55	109	1.058	1.122
27-04-2012	20:38:54	23:29:46	02:17:30	150	1.058	1.282
02-05-2012	19:38:20	23:04:29	02:42:15	177	1.058	1.266

[1] Net Exposure Time: session duration spent in photon collection. [2] 00:49:43 of 27-03-2012. [3] 00:45:15 of 29-03-2012.

Table 2. 2MASS Colors and Spectral Type relation as described in Stead and Hoare (2002).

Spectral Type	*No. stars per subtype*	*H–K (UKIDSS)*	*J–H (UKIDSS)*	*H–K (2MASS)*	*J–H (2MASS)*	*e(H–K)*	*e(J–H)*
Main sequence intrinsic colors O8V to M0V							
O8V	6	–0.10	–0.19	–0.10	–0.21	0.017	0.019
O9V	23	–0.10	–0.15	–0.09	–0.17	0.009	0.011
B0V	24	–0.10	–0.17	–0.09	–0.19	0.008	0.010
B1V	54	–0.09	–0.16	–0.08	–0.17	0.006	0.008
B2V	105	–0.06	–0.14	–0.06	–0.15	0.004	0.005
B3V	101	–0.05	–0.12	–0.05	–0.13	0.004	0.005
B4V	35	–0.04	–0.10	–0.04	–0.11	0.007	0.008
B5V	125	–0.03	–0.10	–0.03	–0.11	0.004	0.004
B6V	70	–0.02	–0.09	–0.02	–0.10	0.006	0.006
B7V	85	–0.02	–0.08	–0.02	–0.09	0.005	0.006
B8V	240	–0.02	–0.08	–0.01	–0.09	0.003	0.003
B9V	351	0.00	–0.06	0.00	–0.06	0.002	0.003
A0V	195	0.00	–0.04	0.00	–0.04	0.003	0.004
A2V	353	0.02	–0.02	0.02	–0.02	0.002	0.003
A5V	215	0.03	0.02	0.03	0.03	0.003	0.004
F0V	232	0.04	0.09	0.04	0.10	0.003	0.004
F2V	245	0.03	0.13	0.04	0.14	0.003	0.004
F5V	231	0.05	0.16	0.05	0.18	0.003	0.004

table continued on next page

Table 2. 2MASS Colors and Spectral Type relation as described in Stead and Hoare (2002), cont.

Spectral Type	*No. stars per subtype*	*H–K (UKIDSS)*	*J–H (UKIDSS)*	*H–K (2MASS)*	*J–H (2MASS)*	*e(H–K)*	*e(J–H)*
F8V	146	0.05	0.19	0.06	0.21	0.004	0.005
G0V	115	0.06	0.22	0.07	0.25	0.005	0.006
G2V	95	0.06	0.24	0.07	0.27	0.005	0.006
G5V	141	0.06	0.28	0.07	0.31	0.005	0.006
G8V	171	0.06	0.35	0.07	0.38	0.004	0.005
K0V	136	0.07	0.37	0.08	0.40	0.005	0.006
K2V	47	0.08	0.40	0.09	0.44	0.008	0.010
K5V	20	0.12	0.50	0.13	0.55	0.014	0.019
M0V	12	0.19	0.60	0.21	0.67	0.015	0.019
Giant intrinsic colors: G4III to M5III.							
G5III	156	0.127	0.436	0.188	0.465	0.008	0.008
G8III	585	0.128	0.458	0.119	0.487	0.004	0.005
K0III	514	0.132	0.493	0.123	0.522	0.004	0.005
K2III	578	0.174	0.581	0.166	0.613	0.006	0.006
K5III	426	0.223	0.778	0.215	0.814	0.014	0.014
M0III	179	0.237	0.808	0.230	0.845	0.023	0.022
M2III	353	0.243	0.903	0.235	0.941	0.017	0.017
M5III	73	0.327	0.912	0.320	0.956	0.041	0.041

Table 3. Comparison star positions and information with respect to NSVS 7606408.

Object	*R.A. (2000) UCAC3* *h m s*	*Dec. (2000) UCAC3* *° ′ ″*	*2MASS J–H*	*CMC14 r'mag*	*CMC14 derived V mag.*	*Probable spectral type*
NSVS7606408	11 48 56.586	+26 02 30.07	0.226	13.532	13.641	F8V-G0V
Comp. Star[1]	11 49 09.986	+25 55 32.92	0.229	13.192	13.325	F8V-G0V
Check Star[2]	11 49 37.454	+26 14 48.23	0.208	13.145	13.275	F5V-F8V

[1] Cross references for comparison star: GSC2.2 N201201182; CMC14 114909.9+255532; USNO-B1.0 1159-0186938; NOMAD1 1159-0191730; PPMX 114909.9+255532; UCAC3 232-105102; 2MASS J11490997+2555328; SDSS J114909.99+255532.8

[2] Cross references for check star: GSC2.2 N20120112; CMC14 114937.4+261448; USNO-B1.0 1162-0194828; NOMAD1 1162-0199537; PPMX 114937.4+261448; UCAC3 233-104578; 2MASS J11493745+2614483; SDSS J114937.45+261448.2

Table 4. Period determination results for each dataset, using PERIOD04 software.

Dataset	*Checked Range*	*Step*	*SNR*	*Period (days)*	*Amplitude*
NSVS	0–25 (cd^{-1})	0.00013895 (cd^{-1})	7.4	0.3548184 (14)	0.170 ± 0.005
SWASP	0–25 (cd^{-1})	0.0000452 (cd^{-1})	11.9	0.35482227 (13)	0.164 ± 0.001
ASAS	5–6 (cd^{-1})	0.0000222 (cd^{-1})*	4.0	0.3548227 (14)	0.157 ± 0.027

** Several problems afflicting this dataset: high scattering, a few observations available. Despite this, forcing the search for a frequency only between 5 (cd^{-1}) and 6 (cd^{-1}) we obtain a result consistent with other datasets.*

Table 5. Offsets applied to the mean magnitude of each dataset used.

Dataset	*Original mean mag.*	*Applied offset*	*New mean mag.*
FRIC (Furgoni, R.)	13.572	—	—
SWASP	13.73	–0.158	13.572
NSVS	13.72	–0.148	13.572
ASAS	13.67	–0.098	13.572

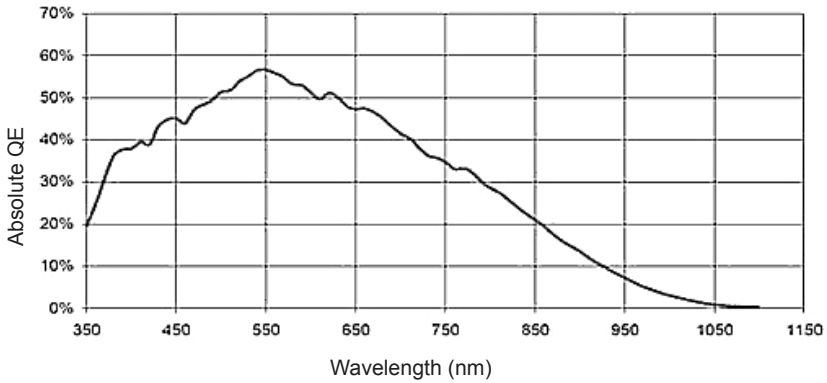

Figure 1. Quantum Efficiency of the Kodak KAF8300 monochrome sensor with microlens, equipping the CCD SBIG ST8300m used for the data collection of this study.

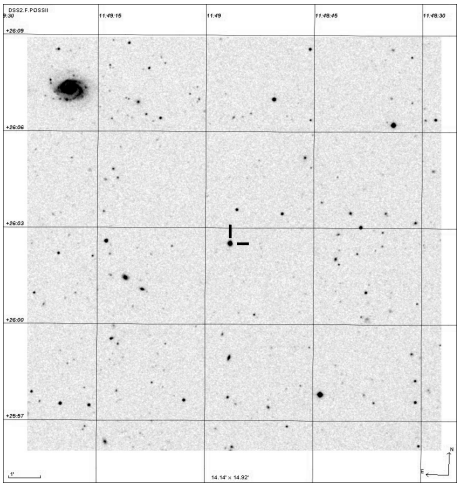

Figure 2. DSS image centered on NSVS 7606408. In the top-left side of the field the galaxy NGC 3902 is clearly visible. North is up, East to the left.

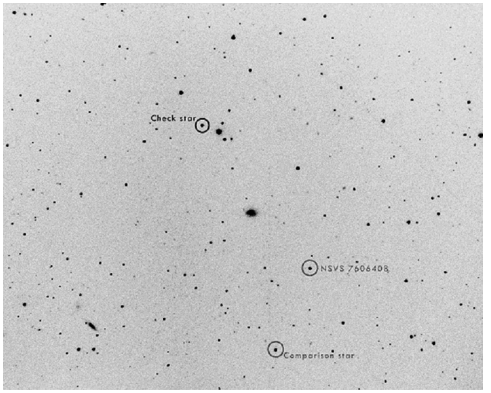

Figure 3. Star field containing NSVS 7606408, the comparison star UCAC3 232-105102 and the check star UCAC3 233-104578. North is up, East to the left.

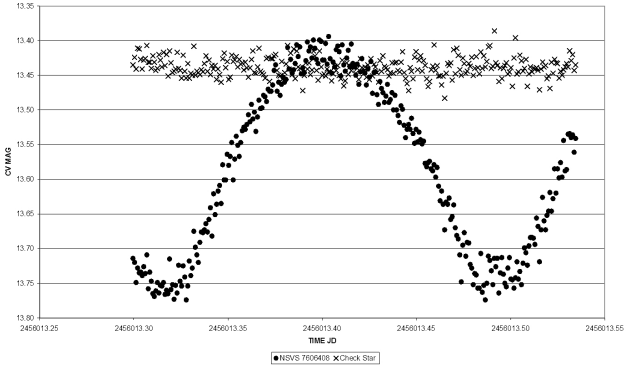

Figure 4. Differential photometry of NSVS 7606408 and the check star UCAC3 233-104578 in relation to the comparison star UCAC3 232-105102. The 26/03/2012 session is shown, which is the longest one. The check star shows an almost complete absence of significant trends: this fact shows that the color index of stars used is good enough for differential photometry carried out in unfiltered conditions.

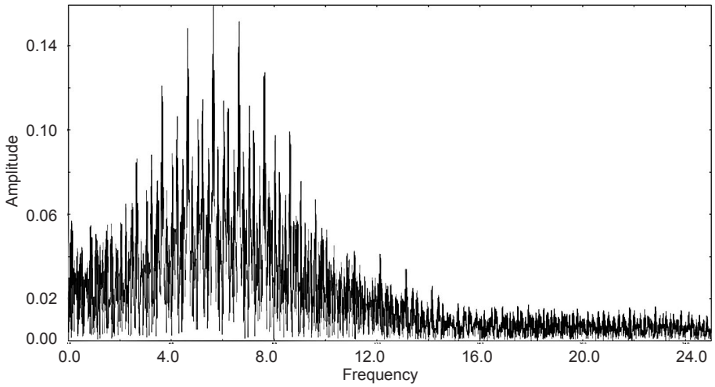

Figure 5. Fourier spectrum of the FRIC dataset weighted in relation to the magnitude error. The periodogram was calculated with a frequency range from 0 to 25 cd^{-1} (cycles per day) and step 0.00118537583 cd^{-1}.

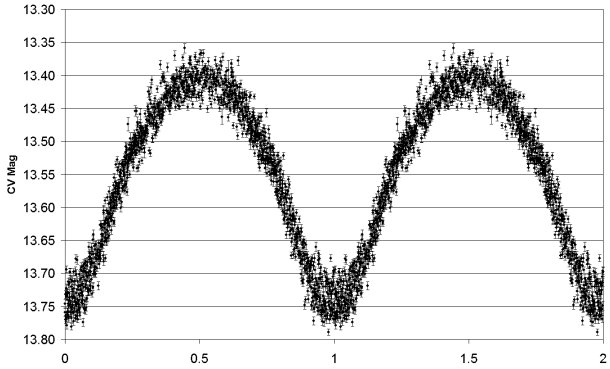

Figure 6. Phase plot of the FRIC dataset with period 0.1774100 day.

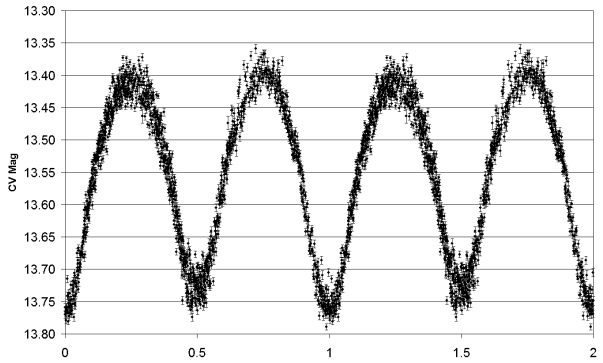

Figure 7. Phase plot of the FRIC dataset with period 0.3548200 day. The shape of a W Uma type variable star is evident.

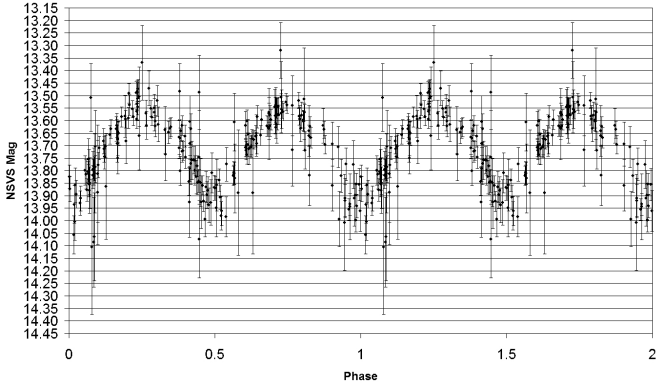

Figure 8. Phase plot of the NSVS dataset with period 0.3548184 day.

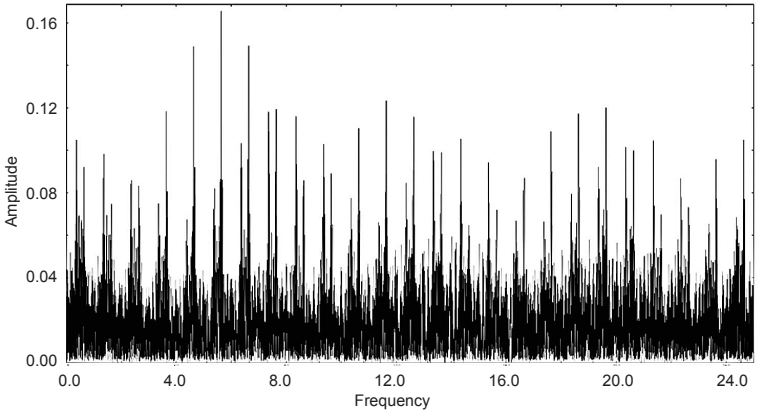

Figure 9. Fourier spectrum of the NSVS dataset weighted in relation to the magnitude error. The periodogram was calculated with a frequency range from 0 to 25 cd^{-1} (cycles per day) and step 0.00013895 (cd^{-1}).

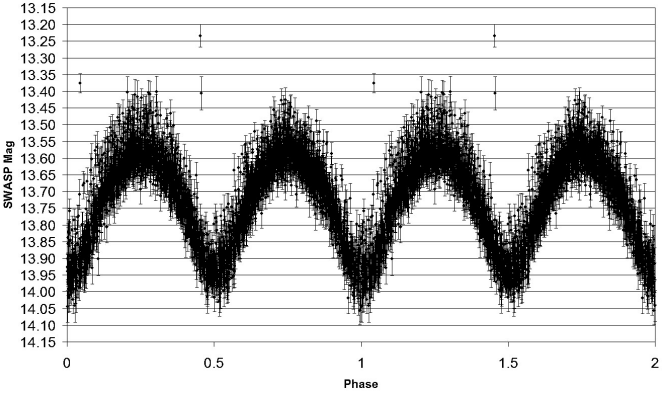

Figure 10. Phase plot of the SWASP dataset with period 0.35482227 day.

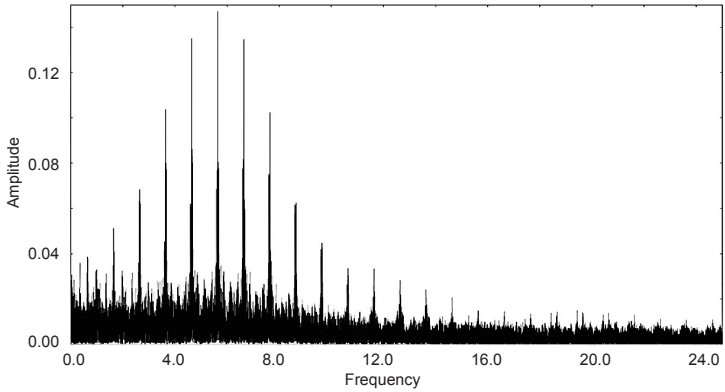

Figure 11. Fourier spectrum of the SWASP dataset weighted in relation to the magnitude error. The periodogram was calculated with a frequency range from 0 to 25 cd^{-1} (cycles per day) and step 0.0000452 (cd^{-1}).

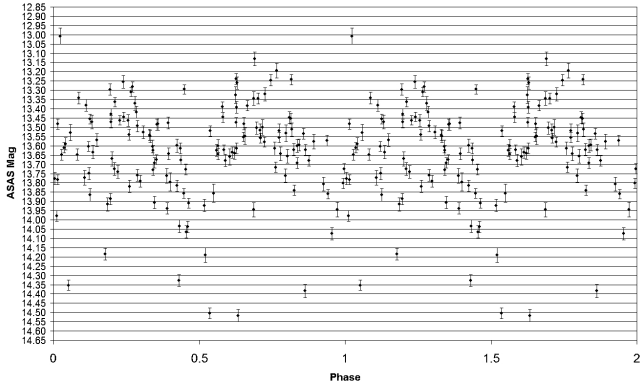

Figure 12. Phase plot of the ASAS dataset with period 0.3548227 day.

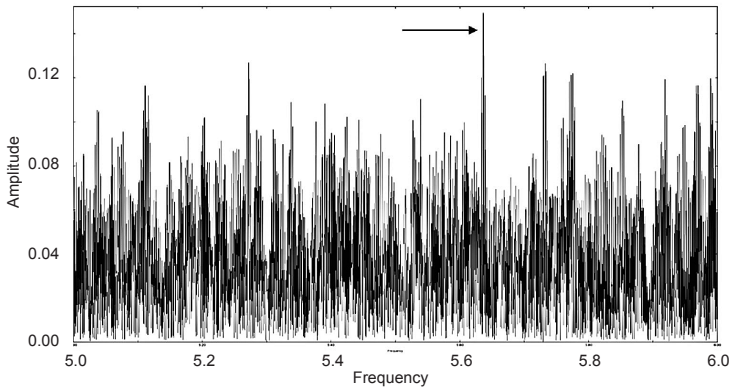

Figure 13. Fourier spectrum of the ASAS dataset weighted in relation to the magnitude error. The periodogram was calculated with a frequency range from 0 to 25 cd^{-1} (cycles per day) and step 0.0000222 (cd^{-1}). The arrow marks the significant peak.

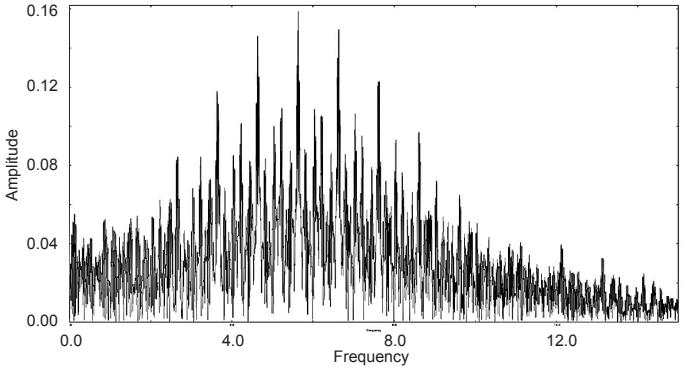

Figure 14. Fourier spectrum of the FRIC + SWASP datasets. An offset of –0.158 mag has been applied to SWASP to normalize the mean magnitude to that of FRIC. The periodogram was calculated with a frequency range from 5 to 6 cd^{-1} (cycles per day) and step 0.00001712275 (cd^{-1}).

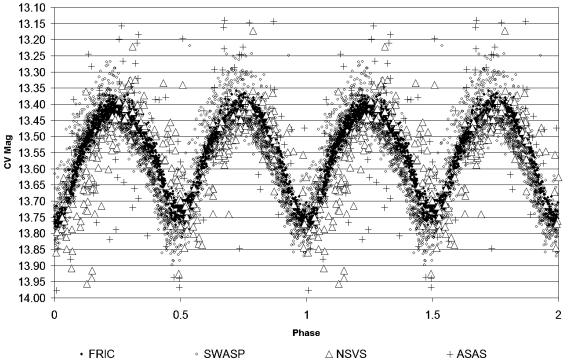

Figure 15. Phase plot of FRIC, SWASP, NSVS, and ASAS dataset with period of 0.35482573 day. We can see that the NSVS dataset, which is the earliest in time, is clearly not in phase with the FRIC and SWASP.

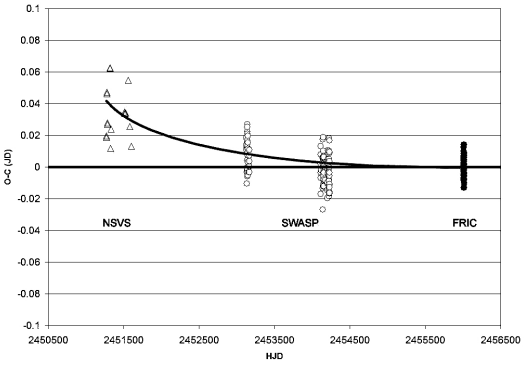

Figure 16. O–C analysis for the time of primary minimum of NSVS 7606408.

Is MP Geminorum an Eclipsing Binary With a Very Long Period?

Dietmar Böhme
Dorfstrasse 11, D-06682 Nessa, Germany; dietmar-nessa@t-online.de

Received September 7, 2011; revised January 26, 2012; accepted January 27, 2012

Abstract Perhaps MP Gem is a very long-period eclipsing binary star. Only nine observations of a minimum exist to this day. The author observed the star on plates of the Sonneberg Observatory and did not find any further minima. Continued monitoring by CCD observers is recommended.

1. Introduction

Hoffmeister (1963) discovered the variable star MP Gem in the field ν Gem of the "Sonneberger Felderplan" (Figure 1). He wrote: "the star is invisible 1944 February 24/25 (2 plates), February 25/26 (7 plates), on all other plates bright, perhaps with very low changes. On neighboring days no plates exist. Perhaps an Algol-like star with a long period." I have checked these plates again and can confirm that the star was invisible on those dates.

Gessner (1973, where MP Gem is listed as S 7958 Gem on p. 589) observed MP Gem on all plates available at Sonneberg in 1973. She could not find any further minima and noted: "the variable consists of components, the southern component is blue (Palomar atlas, page 417)." The variable is the south component.

No further observations of the star are known. I therefore have observed the star on all 119 later plates of the Sonneberg sky patrol from the years 1981 to 1994. I could not find any further minima. A light curve for MP Gem is shown in Figure 2, based on magnitudes estimated from the Sonneberg plates. The comparison star was USNO 1050-04327215 (mpg 15.6).

2. Discussion and conclusion

Brightness measurements in BVRIJHK of the star exist in different catalogs. These measurements show that it probably is a star of spectral type A.

The star is about 16th magnitude in V and so could be monitored easily with amateur telescopes. The VSP chart is very good for finding, but most planetarium programs (Guide 8.0) show the star at a faulty position. The correct position is R.A. $06^h\,48^m\,33.3^s$, Dec. $+19^\circ\,37'\,15''$ (J2000). I would like to call for the observation of the star, so that it is possible to confirm the period, which is presumably very long.

References

Hoffmeister, C. 1963, *Astron. Nachr.*, **287**, 169.
Gessner, H. 1973, *Veröff. Sternw. Sonneberg.*, **7**, 589.

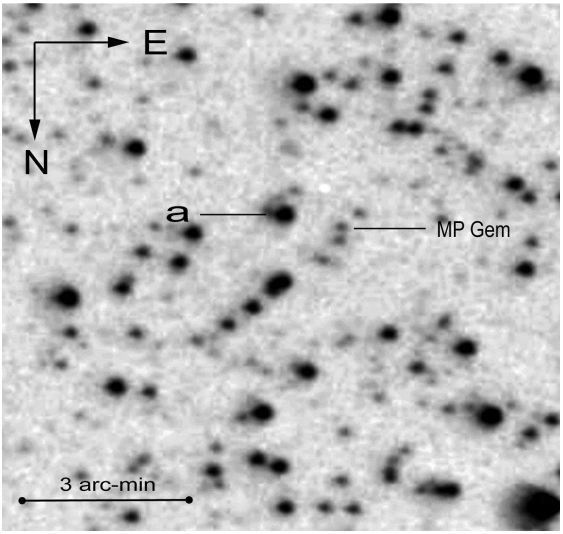

Figure 1. Field of view of MP Gem (Sonneberg Sky Patrol). Star "a" is USNO 1050-04324543.

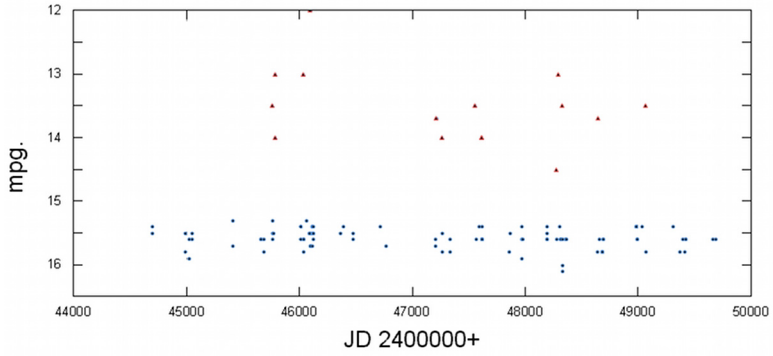

Figure 2. Light curve of MP Gem (uper data) from magnitudes estimated from the Sonneberg plates. The comparison star was USNO 1050-04327215 (mpg 15.6, lower data). Triangles indicate star not visible/fainter-than.

Recent Minima of 150 Eclipsing Binary Stars

Gerard Samolyk
P.O. Box 20677; Greenfield, WI 53220; gsamolyk@wi.rr.com

Received January 23, 2012; accepted January 23, 2012

Abstract This paper continues the publication of times of minima for eclipsing binary stars from observations reported to the AAVSO EB section. Times of minima from observations made from April 2011 through December 2011 along with some unpublished times of minima from older data are presented.

1. Recent Observations

The accompanying list contains times of minima calculated from recent PEP and CCD observations made by participants in the AAVSO's eclipsing binary program. This list will be web-archived and made available through the AAVSO ftp site at ftp://ftp.aavso.org/public/datasets/gsam2j402.txt. This list, along with the eclipsing binary data from earlier AAVSO publications, is also included in the Lichtenknecker database administrated by the Bundesdeutsche Arbeitsgemeinschaft für Veränderliche Sterne e. V. (BAV) at: http://www.bav-astro.de/LkDB/index.php?lang=en. These observations were reduced by the observers or the writer using the method of Kwee and Van Worden (1956). The standard error is included when available. Column F in Table 1 indicates the filter used. A "C" indicates a clear filter.

The linear elements in the *General Catalogue of Variable Stars* (GCVS; Kholopov *et al.* 1985) were used to compute the O–C values for most stars. For a few exceptions where the GCVS elements are missing or are in significant error, light elements from another source are used: CD Cam (Baldwin and Samolyk 2007), CW Cas (Samolyk 1992a), V1115 Cas (Kholopov et al. 2011), Z Dra (Danielkiewicz-Krośniak and Kurpińska-Winiarska 1996), DF Hya (Samolyk 1992b), EF Ori (Baldwin and Samolyk 2005), GU Ori (Samolyk 1985). Light elements for V471 Cas, BC Eri, V728 Her, CD Lyn, V1128 Tau, KM UMa, and MS Vir are from up-to-date linear elements of eclipsing binaries (Kreiner 2012). O–C values listed in this paper can be directly compared with values published in the *AAVSO Observed Minima Timings of Eclipsing Binaries* series.

References

Baldwin, M. E., and Samolyk, G. 2005, *Observed Minima Timings of Eclipsing Binaries No. 10*, AAVSO, Cambridge, MA.

Baldwin, M. E., and Samolyk, G. 2007, *Observed Minima Timings of Eclipsing Binaries No. 12*, AAVSO, Cambridge, MA.

Danielkiewicz-Krośniak, and E. Kurpińska-Winiarska, M., eds. 1996, *Rocznik Astron.* (SAC 68), **68**, 1.

Kholopov, P. N., *et al.* 1985, *General Catalogue of Variable Stars*, 4th ed., Moscow.

Kholopov, P. N., *et al.* 2011, *General Catalogue of Variable Stars*, Online Edition (http://www.sai.msu.su/gcvs/gcvs/index.htm).

Kreiner, J. M. 2012, Up-to-date linear elements of eclipsing binaries (http://www.as.up.krakow.pl/ephem/).

Kwee, K. K., and Van Worden, H. 1956, *Bull. Astron. Inst. Netherlands*, **12**, 327.

Samolyk, G. 1985, *J. Amer. Assoc. Var. Star Obs.,* **14**, 12.

Samolyk, G. 1992a, *J. Amer. Assoc. Var. Star Obs.,* **21**, 34.

Samolyk, G. 1992b, *J. Amer. Assoc. Var. Star Obs.,* **21**, 111.

Table 1. Recent times of minima of stars in the AAVSO eclipsing binary program.

Star	*JD (min) HJD 2400000+*	*Cycle*	*O–C (day)*	*F*	*Observer*	*Standard Error (day)*
RT And	55850.6541	23387	–0.0094	V	K. Menzies	0.0001
WZ And	55836.6375	21511	0.0569	V	G. Samolyk	0.0002
XZ And	55836.7518	23473	0.1738	V	G. Samolyk	0.0001
AB And	55748.7710	59173.5	–0.0284	V	K. Menzies	0.0002
AB And	55793.5776	59308.5	–0.0273	R	L. Corp	0.0004
AB And	55838.3811	59443.5	–0.0292	R	L. Corp	0.0001
AB And	55838.5476	59444	–0.0286	R	L. Corp	0.0002
AB And	55890.3218	59600	–0.0296	R	L. Corp	0.0001
AB And	55906.5850	59649	–0.0291	V	G. Samolyk	0.0002
BD And	55824.9533	45069	0.0095	V	R. Sabo	0.0003
BX And	55873.6462	31707	–0.0586	V	K. Menzies	0.0001
BX And	55906.5895	31761	–0.0615	V	G. Samolyk	0.0002
DS And	55864.7039	19517	0.0036	V	N. Simmons	0.0002
CX Aqr	55907.5249	34990	0.0128	V	G. Samolyk	0.0001
OO Aql	55773.6378	33861	0.0509	V	K. Menzies	0.0003
OO Aql	55773.6378	33861	0.0509	V	N. Simmons	0.0002
OO Aql	55790.3637	33894	0.0528	R	L. Corp	0.0001
OO Aql	55793.4035	33900	0.0518	R	L. Corp	0.0002
OO Aql	55825.3320	33963	0.0527	R	L. Corp	0.0006

Table continued on following pages

Table 1. Recent times of minima of stars in the AAVSO eclipsing binary program, cont.

Star	*JD (min) HJD 2400000+*	*Cycle*	*O–C (day)*	*F*	*Observer*	*Standard Error (day)*
SS Ari	55866.6860	41475	–0.2936	V	R. Poklar	0.0002
SX Aur	55923.6455	13025	0.0154	V	R. Poklar	0.0002
TT Aur	55890.6875	25998	–0.0134	V	G. Samolyk	0.0001
TT Aur	55902.6839	26007	–0.0116	V	R. Poklar	0.0003
TT Aur	55914.6787	26016	–0.0115	V	N. Simmons	0.0001
AP Aur	55874.7679	23589.5	1.3617	V	K. Menzies	0.0001
AP Aur	55890.7106	23617.5	1.3636	V	G. Samolyk	0.0003
CL Aur	55838.8305	18380	0.1490	V	G. Samolyk	0.0002
CL Aur	55924.6936	18449	0.1509	V	R. Poklar	0.0002
EP Aur	55872.8002	50022	0.0160	V	K. Menzies	0.0001
HP Aur	55797.9141	9166	0.0608	V	R. Sabo	0.0002
HP Aur	55889.6847	9230.5	0.0600	V	G. Samolyk	0.0003
IM Aur	55844.7034	12290	–0.1109	V	G. Samolyk	0.0002
TU Boo	55654.6273	69655.5	–0.1359	V	K. Menzies	0.0002
TU Boo	55718.6727	69853	–0.1371	V	N. Simmons	0.0001
TY Boo	55718.2987	66965	0.0780	C	Y. Ogmen	0.0001
TZ Boo	55666.7288	53956.5	0.0655	V	K. Menzies	0.0004
TZ Boo	55699.7121	54067.5	0.0639	V	G. Samolyk	0.0004
TZ Boo	55704.3151	54083	0.0609	C	Y. Ogmen	0.0001
TZ Boo	55716.6510	54124.5	0.0645	V	K. Menzies	0.0003
VW Boo	55745.6648	71781	–0.1936	V	G. Samolyk	0.0002
Y Cam	55923.6781	3921	0.3973	V	G. Samolyk	0.0002
SV Cam	55893.6696	22424	0.0539	V	R. Poklar	0.0001
CD Cam	55905.7874	4113	–0.0009	V	G. Samolyk	0.0004
AM CMi	55897.8921	30076	0.2010	V	K. Menzies	0.0003
TY Cap	55836.6486	7758	0.0731	V	G. Samolyk	0.0002
TV Cas	55838.7074	6199	–0.0261	V	G. Samolyk	0.0003
TW Cas	55844.5549	9687	–0.0070	V	G. Samolyk	0.0003
TW Cas	55864.5530	9701	–0.0054	V	N. Simmons	0.0002
CW Cas	55914.5221	44791.5	–0.0642	V	G. Samolyk	0.0002
IR Cas	55875.6672	19850	0.0080	V	R. Poklar	0.0001
IS Cas	55857.6111	14706	0.0667	V	K. Menzies	0.0001
OR Cas	55872.7162	9362	–0.0248	V	K. Menzies	0.0001
V380 Cas	55798.6136	22216	–0.0684	V	N. Simmons	0.0003
V380 Cas	55836.6183	22244	–0.0673	V	N. Simmons	0.0002
V380 Cas	55844.7634	22250	–0.0658	V	K. Menzies	0.0002
V380 Cas	55889.5527	22283	–0.0666	V	G. Samolyk	0.0005
V471 Cas	55923.6121	8538.5	0.0016	V	G. Lubcke	0.0002

Table continued on following pages

Table 1. Recent times of minima of stars in the AAVSO eclipsing binary program, cont.

Star	JD (min) HJD 2400000+	Cycle	O–C (day)	F	Observer	Standard Error (day)
V471 Cas	55923.6122	8538.5	0.0017	I	G. Lubcke	0.0001
V1115 Cas	55923.5541	7842	–0.0551	I	G. Lubcke	0.0001
V1115 Cas	55923.5542	7842	–0.0550	V	G. Lubcke	0.0007
SU Cep	55806.6959	32706	0.0065	V	G. Samolyk	0.0001
WW Cep	55836.7798	20088	0.3280	V	G. Samolyk	0.0001
WZ Cep	55747.6643	66373	–0.1081	V	N. Simmons	0.0001
XY Cep	50702.637	2491	–0.0258	C	S. Cook	
XY Cep	51465.637	2766	–0.0207	C	S. Cook	
DK Cep	55836.5917	22564	0.0367	V	G. Samolyk	0.0001
DL Cep	55747.8256	13371	0.0561	V	G. Samolyk	0.0003
EG Cep	55689.8277	24045	0.0133	V	G. Samolyk	0.0001
EK Cep	55810.6345	3796	0.0098	V	G. Samolyk	0.0001
GK Cep	49311.725	11341	0.0622	C(PEP)	R. Benge	0.0004
GK Cep	50675.721	12798	0.0774	C	S. Cook	0.0003
GK Cep	51057.682 :	13206	0.0864	C	S. Cook	0.0005
SS Cet	55905.6333	4524	0.0369	V	G. Samolyk	0.0001
SS Cet	55911.5810	4526	0.0366	V	R. Poklar	0.0008
TT Cet	55811.9036	47877	–0.0658	V	R. Sabo	0.0002
TT Cet	55888.6840	48035	–0.0665	V	R. Poklar	0.0001
TW Cet	55891.6792	42664.5	–0.0267	V	R. Poklar	0.0001
TX Cet	55903.6244	17306	0.0087	V	R. Poklar	0.0002
RW Com	55921.9726	66989	–0.0082	V	G. Samolyk	0.0002
RW Com	55924.9399	67001.5	–0.0077	V	K. Menzies	0.0001
RZ Com	55666.5871	61532.5	0.0444	V	K. Menzies	0.0002
CC Com	55664.6330	73095	–0.0136	V	N. Simmons	0.0003
TW CrB	52428.8443	24675	0.0283	V	S. Dvorak	0.0002
TW CrB	53091.9185	25801	0.0312	V	S. Dvorak	0.0003
TW CrB	55748.3357	30312	0.0410	R	Y. Ogmen	0.0001
ZZ Cyg	55810.6136	17197	–0.0603	V	G. Samolyk	0.0001
AE Cyg	55867.5625	11640	–0.0053	V	N. Simmons	0.0003
CG Cyg	55759.7491	25881	0.0668	V	K. Menzies	0.0002
CG Cyg	55785.6255	25922	0.0664	V	N. Simmons	0.0001
DK Cyg	55479.7104	37137	0.0916	V	G. Samolyk	0.0003
DK Cyg	55810.6074	37840	0.0932	V	N. Simmons	0.0002
KR Cyg	55838.5786	31630	0.0173	V	G. Samolyk	0.0005
V388 Cyg	55790.6151	16108	–0.0934	V	N. Simmons	0.0001
V401 Cyg	55812.6005	20554	0.0735	V	N. Simmons	0.0001
V456 Cyg	55769.6862	12184	0.0474	V	K. Menzies	0.0003

Table continued on following pages

Table 1. Recent times of minima of stars in the AAVSO eclipsing binary program, cont.

Star	*JD (min) HJD 2400000+*	*Cycle*	*O–C (day)*	*F*	*Observer*	*Standard Error (day)*
V466 Cyg	55770.7815	19400	0.0065	V	K. Menzies	0.0004
V836 Cyg	55744.5868	16668	0.0220	R	L. Corp	0.0005
V1073 Cyg	50657.644 :	15251	–0.0839	C	S. Cook	
V1073 Cyg	54085.5347	19613	–0.1132	V	V. Petriew	0.0004
TT Del	55806.6615	3683	–0.0888	V	G. Samolyk	0.0002
TY Del	55778.4084	10762	0.0558	R	L. Corp	0.0011
TY Del	55792.7025	10774	0.0564	V	R. Sabo	0.0003
DM Del	50309.745	6876.5	–0.0594	C	S. Cook	
DM Del	55773.4976	13345	–0.0923	R	L. Corp	0.0006
FZ Del	55792.6349	31241	–0.0389	V	N. Simmons	0.0001
Z Dra	55921.6210	4477	–0.0196	V	G. Samolyk	0.0001
TZ Dra	52494.5844	11002	–0.0114	V	S. Dvorak	0.0003
TZ Dra	53309.5192	11943	–0.0152	V	S. Dvorak	0.0003
AX Dra	52435.5845	45177	–0.0536	V	S. Dvorak	0.0001
AX Dra	52975.9090	46128	–0.0534	V	S. Dvorak	0.0001
BV Dra	50590.685	17472	–0.0144	C	S. Cook	
BV Dra	51056.629	18803	–0.0097	C	S. Cook	
S Equ	55777.6736	3836	0.0624	V	N. Simmons	0.0001
SV Equ	50309.550	12403	0.0800	C	S. Cook	
SV Equ	50310.004	12403.5	0.0935	C	S. Cook	
YY Eri	55836.8182	44340	0.1436	V	G. Samolyk	0.0001
YY Eri	55906.7428	44557.5	0.1432	V	G. Samolyk	0.0001
YY Eri	55926.6762	44619.5	0.1440	V	R. Poklar	0.0001
BC Eri	53304.8230	1526	0.0011	V	S. Dvorak	0.0020
BC Eri	53369.6753	1649	0.0014	V	S. Dvorak	0.0004
SX Gem	55854.8866	26940	–0.0498	V	R. Sabo	0.0004
WW Gem	55858.8461	24135	0.0206	V	K. Menzies	0.0003
HR Gem	52549.8571	20796	0.0146	V	S. Dvorak	0.0001
HR Gem	52578.7190	20823	0.0145	V	S. Dvorak	0.0002
RX Her	55336.7469	12463	0.0011	V	G. Samolyk	0.0004
RX Her	55795.6170	12721	–0.0005	V	N. Simmons	0.0002
SZ Her	55673.7814	16880	–0.0227	V	K. Menzies	0.0001
SZ Her	55836.5822	17079	–0.0235	V	G. Samolyk	0.0001
TT Her	55745.6655	17268	0.0385	V	G. Samolyk	0.0001
TU Her	55747.6338	5155	–0.2158	V	G. Samolyk	0.0003
LT Her	55752.3184	13834	–0.1306	C	Y. Ogmen	0.0001
LT Her	55778.3450	13858	–0.1211	C	Y. Ogmen	0.0001
V728 Her	51704.6717	–1688	0.0075	V	J. Howell	0.0004

Table continued on following pages

Table 1. Recent times of minima of stars in the AAVSO eclipsing binary program, cont.

Star	JD (min) HJD 2400000+	Cycle	O–C (day)	F	Observer	Standard Error (day)
V728 Her	52752.8244	536	0.0030	V	S. Dvorak	0.0004
VZ Hya	55923.5621	5395	0.0040	R	L. Corp	0.0003
DF Hya	55654.5906	38919	–0.0106	V	N. Simmons	0.0001
DF Hya	55878.9067	39597.5	–0.0101	V	K. Menzies	0.0001
FG Hya	52347.5530	22509.5	–0.0578	V	S. Dvorak	0.0010
FG Hya	52629.8087	23370.5	–0.0655	V	S. Dvorak	0.0006
FG Hya	53025.8222	24578.5	–0.0730	V	S. Dvorak	0.0006
FG Hya	53088.6048	24770	–0.0702	V	S. Dvorak	0.0003
SW Lac	55856.4707	32992	–0.1009	R	L. Corp	0.0002
VX Lac	55889.5903	9894	0.0787	V	G. Samolyk	0.0001
CM Lac	55907.5513	17998	–0.0041	V	G. Samolyk	0.0002
CO Lac	55751.8415	18297	–0.0019	V	N. Simmons	0.0003
CO Lac	55775.7447	18312.5	–0.0029	V	K. Menzies	0.0002
UV Leo	55664.3946	28702	0.0349	R	L. Corp	0.0001
UZ Leo	55661.4231	25663.5	–0.0913	R	L. Corp	0.0005
XY Leo	55653.4706	37237	0.0637	R	L. Corp	0.0004
AM Leo	55659.3644	35992.5	0.0125	R	L. Corp	0.0004
AP Leo	55653.4048	37450	–0.0293	R	L. Corp	0.0003
AP Leo	55659.4298	37464	–0.0293	R	L. Corp	0.0004
SW Lyn	52629.7070	13437	0.0371	V	S. Dvorak	0.0001
SW Lyn	53012.9317	14032	0.0441	V	S. Dvorak	0.0001
CD Lyn	51956.8230	–120	0.0026	V	S. Dvorak	0.0010
CD Lyn	51979.5681	–115	0.0003	V	S. Dvorak	0.0003
FL Lyr	55718.6648	8033	–0.0020	V	G. Samolyk	0.0001
β Lyr	55836.21	529	1.55	R	G. Samolyk	0.01
β Lyr	55836.22	529	1.56	V	G. Samolyk	0.02
β Lyr	55836.30	529	1.64	B	G. Samolyk	0.02
β Lyr	55842.51	529.5	1.38	V	G. Samolyk	0.02
β Lyr	55842.60	529.5	1.47	B	G. Samolyk	0.02
β Lyr	55842.61	529.5	1.48	R	G. Samolyk	0.03
RW Mon	55874.9343	11644	–0.0737	I	R. Sabo	0.0001
EP Mon	55914.8879	20056	0.0323	V	G. Samolyk	0.0002
V451 Oph	55751.4441	4970	–0.0038	R	L. Corp	0.0004
V501 Oph	52475.3887	22278	–0.0053	V	L. Baldinelli	0.0005
V501 Oph	52506.3610	22310	–0.0074	V	L. Baldinelli	0.0004
EF Ori	55911.7618	2199	0.0050	V	G. Samolyk	0.0003
ER Ori	55890.8172	33690	0.1000	V	G. Samolyk	0.0001
ER Ori	55915.7982	33749	0.1005	V	R. Sabo	0.0001

Table continued on following pages

Table 1. Recent times of minima of stars in the AAVSO eclipsing binary program, cont.

Star	*JD (min) HJD 2400000+*	*Cycle*	*O–C (day)*	*F*	*Observer*	*Standard Error (day)*
FR Ori	52265.7152	27632	0.0191	V	S. Dvorak	0.0002
FR Ori	52342.5496	27719	0.0184	V	S. Dvorak	0.0001
FR Ori	54102.6977	29712	0.0243	V	R. Poklar	0.0001
FR Ori	54139.7893	29754	0.0231	V	J. Bialozynski	0.0006
FT Ori	55925.6701	4627	0.0167	V	R. Poklar	0.0001
GU Ori	55921.7978	27305	–0.0499	V	G. Samolyk	0.0003
U Peg	55844.6258	51585	–0.1430	V	G. Samolyk	0.0001
AT Peg	52270.5261	6152	0.0079	V	S. Dvorak	0.0002
AT Peg	52976.5136	6768	0.0123	V	S. Dvorak	0.0005
BB Peg	55790.5999	33267.5	–0.0046	V	K. Menzies	0.0001
BB Peg	55837.5955	33397.5	–0.0043	V	G. Samolyk	0.0001
BB Peg	55845.5487	33419.5	–0.0041	V	K. Menzies	0.0001
BX Peg	55838.6233	41521	–0.1058	V	G. Samolyk	0.0001
BX Peg	55845.6342	41546	–0.1055	V	K. Menzies	0.0001
GP Peg	55786.6940	14912	–0.0481	V	K. Menzies	0.0001
RT Per	55882.6933	26497	0.0747	V	R. Poklar	0.0001
RV Per	55914.6450	7027	–0.0015	V	G. Samolyk	0.0001
XZ Per	55837.9646	10707	–0.0593	V	R. Sabo	0.0001
IT Per	53339.7475	15620	0.0054	V	S. Dvorak	0.0003
IT Per	54095.8632	16113	–0.0058	V	J. Bialozynski	0.0006
IT Per	54115.8064	16126	–0.0011	V	J. Bialozynski	0.0006
V432 Per	52503.8691	51722	–0.0092	V	S. Dvorak	0.0002
V432 Per	52629.5940	52113	0.0026	V	S. Dvorak	0.0001
V432 Per	52973.8089	53183.5	0.0335	V	S. Dvorak	0.0002
β Per	55837.7575	3556	0.1100	V	G. Samolyk	0.0002
Y Psc	55836.6946	2709	–0.0092	V	G. Samolyk	0.0001
RV Psc	55868.6393	56837	–0.0527	V	R. Poklar	0.0001
CC Ser	55701.6856	35308	0.9687	V	G. Samolyk	0.0002
Y Sex	50519.621	20850	0.0276	C	S. Cook	
Y Sex	51608.635	23444	0.0213	C	S. Cook	
RW Tau	55806.8207	3656	–0.2463	V	G. Samolyk	0.0001
CT Tau	55874.8717	15702	–0.0567	V	K. Menzies	0.0001
EQ Tau	55826.9198	45741	–0.0260	V	R. Sabo	0.0001
EQ Tau	55844.8411	45793.5	–0.0255	V	G. Samolyk	0.0002
EQ Tau	55865.6639	45854.5	–0.0250	V	K. Menzies	0.0001
EQ Tau	55921.6445	46018.5	–0.0255	V	G. Samolyk	0.0001
V1128 Tau	55923.3619	11210	0.0009	R	L. Corp	0.0002
V1128 Tau	55923.5154	11210.5	0.0017	R	L. Corp	0.0006

Table continued on next page

Table 1. Recent times of minima of stars in the AAVSO eclipsing binary program, cont.

Star	*JD (min) HJD 2400000+*	*Cycle*	*O–C (day)*	*F*	*Observer*	*Standard Error (day)*
V Tri	55837.8148	53594	–0.0045	V	G. Samolyk	0.0001
X Tri	55806.8448	13694	–0.0792	V	G. Samolyk	0.0001
X Tri	55881.6520	13771	–0.0802	V	R. Poklar	0.0001
X Tri	55920.5129	13811	–0.0807	V	N. Simmons	0.0001
RS Tri	55790.7941	9351	–0.0386	V	K. Menzies	0.0003
RV Tri	55905.5500	13099	–0.0352	V	G. Samolyk	0.0001
W UMa	55906.9130	30396	–0.0706	V	G. Samolyk	0.0001
TX UMa	55921.8507	3566	0.1958	V	G. Samolyk	0.0001
TY UMa	55717.6631	45650.5	0.3022	V	K. Menzies	0.0002
UX UMa	55757.2760	93173	0.0024	C	Y. Ogmen	0.0001
VV UMa	55914.9607	14693	–0.0501	V	G. Samolyk	0.0001
XZ UMa	55648.6327	7756	–0.1072	V	N. Simmons	0.0001
XZ UMa	55907.7609	7968	–0.1109	V	G. Samolyk	0.0001
KM UMa	55692.2752	9072	–0.0017	C	Y. Ogmen	0.0001
AH Vir	55698.6342	24254	0.2349	V	N. Simmons	0.0003
AX Vir	50567.641	32735	0.0018	C	S. Cook	
AX Vir	52402.6425	35347	0.0049	V	S. Dvorak	0.0001
BF Vir	52406.6237	9891	0.0618	V	S. Dvorak	0.0005
BF Vir	53097.8067	10970	0.0698	V	S. Dvorak	0.0001
MS Vir	52371.7634	–410.5	0.0033	V	S. Dvorak	0.0003
MS Vir	52407.6931	–295.5	0.0026	V	S. Dvorak	0.0003
MS Vir	53150.6746	2082.5	0.0060	V	S. Dvorak	0.0003
AW Vul	55784.6403	11779	–0.0159	V	N. Simmons	0.0001
BE Vul	55718.8180	10056	0.0825	V	G. Samolyk	0.0001
BE Vul	55763.8270	10085	0.0823	V	R. Sabo	0.0001
BE Vul	55788.6603	10101	0.0829	V	N. Simmons	0.0001
BS Vul	55779.6050	26279	–0.0273	V	K. Menzies	0.0001
BT Vul	55773.7433	17851	0.0021	V	K. Menzies	0.0004
BU Vul	55837.6585	39199	0.0189	V	G. Samolyk	0.0001
CD Vul	55747.8599	13820	–0.0010	V	G. Samolyk	0.0002
ER Vul	54008.7294	19806	0.0158	V	V. Petriew	0.0023
ER Vul	54078.5378	19906	0.0147	V	V. Petriew	0.0006

The Variable Stars South Eclipsing Binary Database

Tom Richards
Director, Variable Stars South, Pretty Hill Observatory, P.O. Box 323, Kangaroo Ground, Vic 3097, Australia; tom.richards@variablestarssouth.org

Received October 1, 2012; revised October 18, 2012; accepted October 18, 2012

Abstract Variable Stars South (VSS) has three active projects using electronic detectors to study eclipsing binaries, especially EAs. In addition to supplying JD observational data to the AAVSO International Database, VSS maintains a database of observed times of minima (ToM) and linear light elements derived from the ToMs. This database, located on the VSS website www.variablestarssouth.org, is updated monthly. In addition, the same page links to the areas for the three projects which maintain extensive observational and analytic data.

1. Introduction

Variable Stars South (VSS) is an online organization of astronomers interested in studying southern variable stars. It is a research section of the Royal Astronomical Society of New Zealand. All information about VSS including its collected data can be found on its website, www.variablestarssouth.org. VSS primarily acts as a host to projects organized by individuals or teams, and three such are:

- Equatorial Eclipsing Binaries (EEB), joint with the British Astronomical Association Variable Star Section; leader Tom Richards.
- Search for Planets around Detached Eclipsing Binaries (SPADES); leaders Simon O'Toole (Australian Astronomical Observatory) and Tom Richards.
- Southern Binaries DSLR (SBD), leader Mark Blackford.

Although these projects have very different goals, they all collect and analyze electronic (DSLR and CCD) time series data on eclipses of binary star systems. Information about each project, including science cases, observational requirements, and guides for observers and analysts, as well as observational data and analyses, can be found under the Research Projects menu on the VSS website. Collaboration in these projects is open to any astronomer with appropriate equipment. The eclipse data from the three projects are collected into a single downloadable file, the VSS Eclipsing Binary Database. JD data from these observations are also supplied by individual observers to the AAVSO International Database—a requirement on all VSS observational projects. There is no fixed northerly limit to the targets in any of the projects—the main requirement is to be well observable from temperate southern latitudes. At present the most northerly target is LT Her in SPADES, at +09° 57' 52".

2. The VSS EB database

Typically, when an observer in one of the projects obtains a measureable time series on an eclipse, an analysis is carried out to determine time of minimum (ToM) and other results of interest, which are then stored in the project's area on the VSS website. For example, in the SPADES observation area, one may find under the sub-area for each target system:

- Excel Observation Files of every observation set obtained—all to a fixed format, as submitted by the observer.
- An Excel Results File maintained by the analyst responsible for that target system, containing: all ToMs measured from the Observation File data; sets of linear light elements (LEs) published by others (such as GCVS); calculations of O–C of the ToMs against a published LE set (such as GCVS); and where sufficient measured ToMs exist, a linear estimate of the LEs from the ToMs.
- A PERANSO (www.peranso.com) file of all the observational data in the project for the target, and associated information and plots.
- A text file of all the HJD data for the target obtained in the project.

The VSS EB database consolidates ToM and LE data obtained and recorded in the three projects in their own different ways, so that researchers have a "one-stop shop" for such commonly required data. At present, it contains data on 91 systems. The file itself is in CSV plain text format. It is updated monthly (that's an intention, not a promise!) to contain new data and also to refine or correct old data as improved analyses are carried out. Some old data, such as "eyeball" estimates of poorly recorded minima intended as rough guides to observers, may even be removed when better data become available.

The format of the file is given below. It may change in future when it becomes apparent that a change would be for the better; but it is always accompanied by a Readme file specifying the current format.

System—Name of the binary system. Format is constellation abbreviation, then GCVS identification where available, with 3-digit V... identifications expanded with a leading "0" (for example, Ara V0536). Where the GCVS identification is not available the constellation abbreviation is retained then another catalogue identifier is used, whose provenance should be obvious. The table is sorted lexically on this column, so, for example, "Sco" entries precede "Sgr", and "Gru RU" precedes "Gru W".

Next come five columns recording ToM measurements:

Type—p = primary min, s = secondary min.

HJD_min—Measured HJD of minimum, to the same number of significant decimal places as the error (next column). The rows for a given system are sorted on HJD_min, earliest first.

Error—Measured uncertainty in HJD_min, to one or two significant figures.

Min V mag—Measured magnitude of minimum in Johnson V band.

Min B mag—Measured magnitude of minimum in Johnson B band.

Min R Mag—Measured magnitude of minimum in Cousins R band.

Notes—Any useful information on the preceding data.

Next come four columns recording measured linear light elements. In rows where these occur, they are derived from linear regressions on the minima measurements recorded in that row and the preceding rows for that system. Thus it is possible to count the number of data points in the regression; and for a given system later rows will have regressions based on more data points.

E0—The HJD zero epoch for the elements, to the same number of significant decimal places as the error (next column). This will be close to one of the measured minima in this or preceding rows.

E0 error—The measured uncertainty in E0, to one or two significant figures.

P—The measured orbital period of the system in days, to the same number of significant decimal places as the error (next column).

P error—The measured uncertainty in P, to one or two significant figures.

Other data follow:

Spectrum—Spectral type and/or class, derived from a spectrum taken for the project. This is entered into the last row for the system that exists at the time the spectral analysis was carried out.

Project—Abbreviation of the project name.

3. Conclusion

The VSS EB database is a downloadable file in CSV text-only format containing data on southern eclipsing binaries obtained in three VSS projects. The data, updated monthly, consist of measured times of minima, light elements, and spectra. At present it contains data on 91 systems.

A Note on the Variability of V538 Cassiopeiae

Gustav Holmberg
Karl XI-gatan 8A, SE-222 20 Lund, Sweden; 5063.gustav.holmberg@gmail.com

Received December 28, 2011; revised February 9, 2012; accepted February 13, 2012

Abstract CCD observations of V538 Cas have been made on nine nights during three weeks using the AAVSO Bright Star Monitor. No significant variations were found.

1. Discovery

Weber (1958a) discovered variations in the star BD +60° 201 (HD 7681, HIP 6084, R.A. $01^h\ 18^m\ 07.2^s$ Dec. +61° 43' 04" (J2000)) by analyzing plates taken between 1942 and 1958. The star was found to vary between 9.0 and 9.6 photographic magnitude and Weber, who did not publish a light curve, suspected it could be an eclipsing variable of the Algol type. A further study of the star was made by Häussler (1974) who used 135 patrol camera plates to find the star varying irregularly between 9.44 and 10.01 photographic magnitude. He classified it as an irregular variable star, type Isb.

On the basis of these studies, the star was designated V538 Cas. The entry in the *General Catalogue of Variable Stars* (GCVS; Samus *et al.* 2011) of the star has type Isb and gives the magnitude range as 9.4–10.6 photographic magnitude, and spectral type K5III. Later observations have re-classified the spectrum as M0 III (Henry *et al.* 2000).

2. New observations

V538 Cas is, at 7.7V, a bright star. It is thus a suitable object for the AAVSO Bright Star Monitor (BSM; AAVSO 2009). This instrument aims at filling a niche in current photometric telescope ecology where not many CCD-equipped telescopes are operating: there are interesting stars that are difficult to observe using most modern telescopes because the stars are too bright and risk saturating the CCD detector. Finding suitable comparison stars for bright stars in telescopes with small fields of view can also be a challenge. Several of the current photometric surveys, such as NSVS and ASAS, only measure stars fainter than about eighth magnitude, giving much room for work for an instrument such as the Bright Star Monitor. The BSM is a 6-cm *f*/6.2 refractor with a SBIG ST-8XME CCD with a field of view of 84' × 127', operated for AAVSO by Tom Krajci at the Astrokolkhoz facility in New Mexico.

30-second (V) and 60-second (B) exposures of V538 Cas were obtained

with the BSM on nine nights during three weeks in November and December 2011. The images were analyzed using VPHOT (AAVSO 2011) and the brightness of the star measured relative to an ensemble of five stars. The results (Table 1) show very small or no significant variations during this time interval.

These observations are in line with other measurements from the post-photographic era. A photometric study by Henry *et al.* found slight short-time scale variations on the order of a hundredth of magnitude (Henry *et al.* 2000). Hipparcos (Perryman *et al.* 1997) consistently measured V538 Cas around 7.75 with variations on the order of hundredths of a magnitude. TASS, The Amateur Sky Survey (2012), observed the star on four occasions during three weeks, finding a constant brightness, also in the vicinity of 7.75. Together with the new observations reported here, this leads the present author to conclude that V538 Cas, at least today, does not show the type of variations once attributed to it.

3. Discussion

Although not the primary purpose of this short communication, an attempt will also be made to try to resolve the discrepancy between data showing rapid variations on the order of 0.6 magnitude or more, and data showing no or very small variations in the star known as V538 Cas.

One possibility is of course that this star has changed its behavior since the mid-20th century. Another is that Weber's initial guess, that this is an EA star, is correct and that further eclipses have not been covered in the observations made with the BSM, Hipparcos, TASS, and by Henry *et al.* But can there be another explanation?

A similar discrepancy found in the literature may provide a clue. Weber, also in 1958, published his discovery of a Cepheid in the open cluster NGC 7789, varying between photographic magnitude 11.2 and 12.2. The discovery was confirmed by another observer, Romano (Weber 1958b). Cepheids in open clusters have great astrophysical importance, and Weber's finding was therefore followed up. Burbidge and Sandage found no variations at all in the star in their photographic photometry of the cluster using the 100-inch Hooker telescope (Burbidge and Sandage 1958). Furthermore, Starrfield's photoelectric monitoring of the star with a 24-inch reflector at Lick during three hours per night during three nights found no variations in the star. Photographic photometry on a series of plates taken with the 20-inch Carnegie astrograph at Lick gave a similar result: constant brightness (Starrfield 1965). Measurements on plates from the Harvard College Observatory plate archives gave a similar result (Janes 1977).

Thus, we have two cases in which Weber found variations of quite large amplitude, both of which were first confirmed by another observer using similar type of cameras (Weber used small-scale photographic cameras) that was not confirmed by later observers. Starrfield, in trying to resolve this discrepancy,

pointed out that a possible solution could be the small plate scale of Weber's camera; the suspected variable star was therefore imperfectly separated from another star, and seeing variations could produce a spurious impression of variability (Starrfield 1965). Perhaps this or some other photographic effect can account for the variations found in V538 Cas by Weber and Häussler.

4. Acknowledgements

The author wishes to thank AAVSO Director Arne A. Henden for his generous support. This research has made use of the SIMBAD database (CDS 2007), operated at CDS, Strasbourg, France.

References

AAVSO 2009, The Bright Star Monitor (www.aavso.org/bsm).

AAVSO 2011, VPHOT online photometric analysis tool (www.aavso.org/vphot).

Burbidge, E. M., and Sandage, A. 1958, *Astrophys. J.*, **128**, 174.

Centre de Donnees astronomiques de Strasbourg 2007, SIMBAD Astronomical Database, http://simbad.u-strasbg.fr/simbad/

Häussler, K. 1974, *Inf. Bull. Var. Stars*, No 887, 1.

Henry, G., Fekel, F., Henry, S., and Hall, D. 2000, *Astrophys. J., Suppl. Ser.*, **130**, 201.

Janes, K. A. 1977, *Astron. J.*, **82**, 35.

Perryman, M. A. C., European Space Agency Space Science Department, and the Hipparcos Science Team 1997, *The Hipparcos and Tycho Catalogues*, ESA SP-1200, ESA Publications division, Noordwiijk, The Netherlands (Hipparcos data on V538 Cas accessed using http://www.rssd.esa.int/hipparcos_scripts/HIPcatalogueSearch.pl?hipepId=6084).

Samus, N. N., *et al.* 2011, *General Catalogue of Variable Stars*, online version (http://www.sai.msu.su/gcvs/gcvs/index.htm), Sternberg Astron. Inst., Moscow.

Starrfield, S. 1965, *Publ. Astron. Soc. Pacific*, **77**, 206.

The Amateur Sky Survey (TASS) 2012, http://sallman.tass-survey.org/servlet/markiv/template/TassPlot.vm?object_id=6293418

Weber, R. 1958a, *J. Obs.*, **41**, 74.

Weber, R. 1958b, *Astronomie*, **72**, 80.

Table 1. Bright Star Monitor measurements of V538 Cas in November–December 2011.

JD	*Magnitude*	*filter*
2455881.85384	9.422	B
2455881.85444	7.696	V
2455882.80720	9.433	B
2455882.80782	7.715	V
2455888.78655	9.422	B
2455888.78714	7.713	V
2455889.68596	9.455	B
2455889.68656	7.699	V
2455892.65948	9.429	B
2455892.66008	7.715	V
2455893.65671	9.425	B
2455893.65730	7.718	V
2455894.67079	9.435	B
2455894.67139	7.702	V
2455895.65212	9.404	B
2455895.65272	7.697	V
2455896.64828	9.399	B
2455896.64888	7.706	V

A Practical Approach to Transforming Magnitudes onto a Standard Photometric System

David Boyd
5 Silver Lane, West Challow, Wantage, OX12 9TX, UK; davidboyd@orion.me.uk

Received December 30, 2011; revised March 15, 2012; accepted April 5, 2012

Abstract We describe a practical implementation, convenient for amateur use, of a method of transforming instrumental magnitudes onto a standard photometric system in differential CCD photometry.

1. Introduction

Most amateur astronomers using a CCD camera to measure the brightness of an object of interest, be it a variable star, an asteroid, or some other distant light source, employ a procedure called differential photometry. In this the magnitude of the target object is found by comparing its brightness to other stars in the same field of view whose magnitudes are known. The measure of an object's brightness found by integrating the image of the object recorded by the CCD is called its instrumental magnitude. Increasingly amateurs are being encouraged to observe using photometric filters and to transform their measured instrumental magnitudes onto one of the standard photometric magnitude systems.

Transforming instrumental magnitudes in this way greatly increases their usefulness for scientific analysis. They can be combined with similarly-transformed measurements from other observers into a single internally-consistent dataset. The most common standard photometric system in use by amateurs today is the Johnson-Cousins UBVRI system and it is this which we shall use here, in particular its BVRI subset. However, the approach described is applicable to any standard system.

There are two main reasons why instrumental magnitudes differ from standard magnitudes: atmospheric extinction and a mismatch between the response of the equipment in use and the standard system. By observing stars whose magnitudes are very accurately known ("standard" stars), corrections can be found which enable instrumental magnitudes to be transformed onto the standard system. Over the years several formulations of these transformations have been devised and published, usually with the expectation that photometric skies will be readily available for their use. We describe here a variation on previously published methods which amateurs may find better suited to conditions they are likely to experience.

First we explain how atmospheric extinction and instrumental characteristics affect observations and briefly discuss the scope of applicability of the proposed

approach. Next we describe the transformation equations and discuss choosing standard stars. We then explain how to find the transformation parameters and use them to transform instrumental magnitudes and color indices. Finally we use measurements of Landolt standard fields to illustrate the benefits of transforming instrumental magnitudes.

2. Atmospheric extinction and instrumental transformation

Atmospheric extinction has two principal causes: scattering of incident light by aerosols including dust and water vapor, and molecular Rayleigh scattering. Aerosol scattering is relatively uniform across the spectrum, rising slowly at shorter wavelengths, and is the dominant cause of extinction at wavelengths longer than about 500 nm. Rayleigh scattering increases very rapidly at shorter wavelengths and dominates at the blue end of the spectrum. The amount of aerosol scattering can vary widely depending on the aerosol content of the atmosphere, whereas Rayleigh scattering remains relatively constant. Further information about atmospheric extinction can be found in (Green 1992) and (Stubbs *et al.* 2007).

Wavelength-independent scattering is represented by a first order extinction coefficient multiplied by the air mass in the direction of the star, and wavelength-dependent scattering by the product of a second order extinction coefficient, the air mass, and the color index of the star. Since first order extinction is primarily caused by aerosol scattering it can potentially change rapidly during a single night or from night to night as the dust or moisture content of the atmosphere changes. Second order extinction is mainly due to Rayleigh scattering and is generally considered to be stable over time at a given location. Because of the rapid rise in Rayleigh scattering at the blue end of the spectrum, second order extinction should primarily affect measurements made through a B filter while measurements through V, R, and I filters will be much less affected.

The presence of a thin layer of cloud or haze reduces the incoming light equally at all wavelengths, as verified experimentally (Honeycutt 1971). In practice this adds a constant "gray" term to atmospheric extinction, which has the effect of changing the image zero point. Thin cloud is often difficult to detect visually but its presence need not prevent good quality photometry provided it is uniform and stable (Hardie 1959). Nevertheless, the most reliable results will always be obtained under clear skies.

In practice all BVRI filter and CCD detector combinations differ in their spectral response from the standard Johnson-Cousins system. This means that they will produce results which differ from the standard system and this difference will vary with the color of the star. Since the mismatch is usually small, it is normally assumed that it can be corrected by a linear term comprising the product of an instrumental transformation coefficient and the color index of the star. Provided the instrumental components do not change, any change in

the transformation coefficient, for instance due to long term changes in the transmission properties of the optical components and filters, is likely to be small and slow.

So, while first order extinction may change from night to night, and even during a single night as atmospheric conditions change, any changes in second order extinction at the same location and instrumental transformation with the same equipment are likely to happen only slowly over time as noted in Welch (1979) and Harris *et al.* (1981). It would nevertheless be prudent to remeasure them at regular intervals to monitor for any such change.

3. Applicability

The approach to obtaining transformation parameters described here is aimed at those using CCD cameras to image the sky through sufficiently long focal length optical equipment that the field of view is small, typically less than one degree across. In photometry it is normally good practice to work above an altitude of about 30 degrees, corresponding to an air mass of 2, to avoid the worst effects of atmospheric extinction. Under these circumstances we can assume that all stars being measured in the same image are at the same zenith distance and hence are measured through the same air mass. The error introduced by this assumption is, in the worst case, only a few thousandths of a magnitude. It should be noted however that under some circumstances, for example when imaging large fields using DSLR cameras or imaging close to the horizon where air mass increases rapidly with reducing altitude, it may not be valid to assume that all stars in the image have the same air mass and a more rigorous analysis must be carried out.

4. The transformation equations

We take as our starting point the following equations which are conventionally used to transform instrumental magnitudes (in lower case) into magnitudes in a standard photometric system (in upper case), see for example Da Costa (1992) and Warner (2009).

$$B = b - k'_b X - k''_{bbv} X(B-V) + T_{bbv}(B-V) + Z_b \quad (1)$$

$$V = v - k'_v X - k''_{vbv} X(B-V) + T_{vbv}(B-V) + Z_v \quad (2)$$

where B and V are the standard B- and V-band magnitudes of the star, b and v are the instrumental magnitudes of the star measured in B and V filters, k'_b and k'_v are the B- and V-band first order extinction coefficients, k''_{bbv} and k''_{vbv} are the B- and V-band second order extinction coefficients for the (B–V) color index, X is the air mass of the star, T_{bbv} and T_{vbv} are the B- and V-band instrumental transformation coefficients for the (B–V) color index, and Z_b and Z_v are the

B- and V-band image zero points which are of course the same for all stars in an image.

We adopt the convention that the first, or only, letter in a subscript indicates the filter passband, while the second and third letters indicate the relevant color index.

As we noted earlier, rapid atmospheric changes may cause first order extinction coefficients and image zero points to vary from image to image, whereas second order extinction and instrumental transformation coefficients should remain constant or change only slowly over time.

The first order extinction, second order extinction, and instrumental transformation coefficients have usually been determined by separate processes. The two common methods of finding the extinction coefficients are the Bouguer and Hardie methods. The Bouguer method involves following a close group of standard stars as they move through a wide range of air mass over the course of a night. The Hardie method requires closely timed observations of pairs of red and blue standard stars at widely separated air masses. Both methods depend on atmospheric extinction remaining constant over the wide ranges of time and/or the sky involved in making these measurements. Instrumental transformation coefficients are found by observing a closely spaced group of stars with a wide range of colors at low air mass. Descriptions of these methods can be found in, for example Welch (1979) and Romanishin (2002).

However, as pointed out in (Harris *et al.* 1981), determining these parameters separately in this way is sub-optimal and usually requires iteration to obtain the best solution. They argue that it is better to make use of all observations together to determine the required parameters. Our approach is a simplified version of that described by Harris *et al.* which meets the needs of differential CCD photometry and may be easier for amateurs to implement in practice. It has the merit of reaching a solution in stages with graphical verification at each stage rather than a "black-box" multilinear least squares approach. This makes it easier to spot problems with individual stars, internal inconsistencies within the data, or human error.

We can rearrange equations (1) and (2) as follows:

$$(B–b) = T_{bbv}(B–V) – k''_{bbv}X(B–V) + Z_b – k'_bX \quad (3)$$

$$(V–v) = T_{vbv}(B–V) – k''_{vbv}X(B–V) + Z_v – k'_vX \quad (4)$$

and then rewrite them as:

$$(B–b) = C_{bbv}(B–V) + Z'_b \quad (5)$$

$$(V–v) = C_{vbv}(B–V) + Z'_v \quad (6)$$

where $C_{bbv} = T_{bbv} – k''_{bbv}X$ incorporates the B-band instrumental transformation and second order extinction correction for the (B–V) color index, $C_{vbv} = T_{vbv} – k''_{vbv}X$ is a similar term for the V-band, $Z'_b = Z_b – k'_bX$ incorporates the B-band

image zero point and first order extinction correction, and $Z'_v = Z_v - k'_v X$ is a similar term for the V-band.

Since we are working with small fields and can assume all stars in the image being measured have the same value of air mass X, the terms C_{bbv}, C_{vbv}, Z'_b, and Z'_v are the same for all stars in the image. If we plot (B–b) against (B–V) for all stars in an image, the gradient will give us C_{bbv} at the value of X for that image, and similarly plotting (V–v) against (B–V) gives C_{vbv}.

Similar equations to (5) and (6) relate magnitudes measured using other filters and color indices. For example:

$$(R-r) = C_{rvr}(V-R) + Z'_r \quad (7)$$

$$(I-i) = C_{ivi}(V-I) + Z'_i \quad (8)$$

where definitions of the terms C_{rvr}, C_{ivi}, Z'_r, and Z'_i follow by analogy with those above.

Hence, if we can measure values of C_{bbv}, C_{vbv}, C_{rvr}, and C_{ivi} (henceforth described collectively as the C parameters where, generically, $C = T - k''X$), each with the corresponding value of X, then we can determine the instrumental transformations T and second order extinction coefficients k". As we shall see, these are the parameters required to transform differential CCD photometry.

5. Sources of standard stellar magnitudes

In order to measure these parameters, we need to identify groups of stars which (a) will fit within a small CCD field of view, (b) contain as many stars as possible with accurately known magnitudes in each of the filter passbands, and (c) span as large a range of color index as possible.

Traditionally, the gold standard for calibration is the set of equatorial standard stars measured over many years by Arlo Landolt, see Landolt (1992, 2009, 2011). These have a root mean square (rms) V magnitude uncertainty of about 0.004 mag. While Landolt standard stars have the advantage of being visible from all latitudes, for observers far from the terrestrial equator they do not rise very high in the sky and so traverse a relatively small range of air mass. Using only those standard stars would necessitate extrapolating to air mass values outside this range, a procedure which would inevitably reduce accuracy. Using only Landolt stars therefore limits the accuracy attainable when trying to account for air mass dependent effects. Another slight drawback of Landolt stars is that it is sometimes difficult to include many of them with a wide range of color index within a typical CCD field.

For this reason we investigated using groups of secondary standard stars which have themselves been calibrated using Landolt stars, in particular ones which culminate near the zenith at higher latitudes and can therefore be observed at or near an air mass of 1. Suitable fields of stars have been measured in the B,

V, R, and I passbands by Arne Henden as an aid to selecting comparison stars for variables and are available from Henden (2012). When selecting stars from these fields to use as secondary standards, we excluded those which had fewer than ten observations, large measurement uncertainties, or close companions which might compromise their measurement. Also, stars significantly out of line in magnitude-color plots with the majority of stars in the same field were excluded on the grounds that their magnitudes may be incorrect or they might be variable. The ten brightest stars in each field satisfying these selection criteria have been used. The magnitude uncertainties of these stars are larger than for Landolt standard stars, but this is in part compensated by having more stars per field with a wider range of color. The stars used in the example given here were from fields around the variables EE Cep, TT Cas, V504 Per, and Var Cas 06 (also known as VSX J000921.8+543943—the bright gravitational microlens variable).

Figure 1 shows stars in the field of Var Cas 06. The circled stars were used as secondary standards and have V magnitudes in the range 11.373–13.889 with rms uncertainty 0.024 and B–V color indices in the range 0.125–1.716.

The availability of accurately measured stellar magnitudes across much of the sky from photometric surveys such as the AAVSO APASS survey (AAVSO 2012) should greatly increase the availability of high quality secondary standard stars suitable for this purpose.

6. Finding the instrumental transformation and second order extinction coefficients

First we select a suitable field containing stars with known, accurately-measured B, V, R, and I magnitudes covering as wide a range of colors as possible, such as the one shown in Figure 1. We identify the stars in the field we intend to use as our secondary standards. We then wait for a clear night with stable sky conditions when the field is well placed and take between five and ten images of the field through each filter. We take care to record the brightest stars with as high signal to noise as possible in each filter while avoiding non-linearity or saturation of the CCD. This typically takes only a few minutes for each filter during which we require the sky conditions to remain clear. We calibrate the images using dark and flat fields and using aperture photometry measure the instrumental magnitudes b, v, r, and i for each of our standard stars in each image taken with the corresponding filter. We then calculate mean values and standard deviations of b, v, r, and i for each star over all the images taken with each filter. We also calculate a mean value of X of all the stars in all the images taken with each filter.

To check that sky conditions have indeed remained stable throughout each set of images, we can compare standard deviations of the instrumental magnitudes of each star in each filter with the estimated measurement uncertainties output by the photometry software. If the former are substantially larger than the latter,

it is an indication that sky conditions were probably unstable and the results should not be used for calibration purposes.

We know values of (B–V), (V–R), and (V–I) and can calculate values of (B–b), (V–v), (R–r), and (I–i) for each standard star. We can also calculate the uncertainties on (B–b), and so on, for each star by adding the quoted uncertainty on its standard magnitude B and the standard deviation of its instrumental magnitude b in quadrature.

We plot (B–b) vs (B–V), (V–v) vs (B–V), (R–r) vs (V–R), and (I–i) vs (V– I). Assuming the transformations we are seeking are linear, we expect the data points to lie approximately on a straight line. If the line is horizontal, it indicates that our measured instrumental magnitude has no color dependency. If, as is more likely, the line is at an angle to the horizontal it means that there is a color dependency in our observations which we need to correct.

Figure 2 shows magnitude-color plots of (B–b) vs (B–V), (V-v) vs (B–V), (R–r) vs (V–R), and (I–i) vs (V–I) for stars in the field of the variable EE Cep. The equipment used was a 0-35m SCT, SXVR-H9 CCD camera, and Astrodon dichroic B, V, R, and I filters.

From equations (5) to (8) the gradients of straight lines fitted to the data points in these plots give values of the C parameters at the mean air mass X calculated for each filter, and we can calculate their uncertainties from the scatter in the data points about the fitted lines.

We repeat this process for several more fields of secondary standard stars satisfying our selection criteria and covering as wide a range of air mass as possible. Each field provides values of the C parameters and a corresponding value of X for each filter. The data do not all have to be collected on the same night since, as noted earlier, these parameters should be stable over time so data from several nights can be combined.

Since for each of the C parameters, $C = T - k''X$, if we now plot the value of the C parameter for each filter against the corresponding value of X and make weighted linear fits, we can obtain values for the instrumental transformation (T) and second order extinction (k") coefficients for each filter with estimates of their uncertainties. In these fits we weight each value of C with the inverse square of its uncertainty.

Figure 3 shows plots of the C parameters vs X obtained from twelve sets of observations of four fields imaged over two nights. Also shown in these plots are the straight lines representing the fits for T and k".

Table 1 lists the values of the instrumental transformation and second order extinction coefficients found from these analyses. Remember our convention is that the first letter in a subscript indicates the filter passband, while the second and third letters indicate the relevant color index.

The second order extinction coefficients for the V, R, and I filter passbands are small and consistent with zero within experimental uncertainty. This is as expected given that extinction in these filters is primarily due to aerosol

scattering which has minimal wavelength dependency. Therefore, consistent with conventional wisdom, we will assume these have a value of zero. The second order extinction coefficient for the B filter is significantly non-zero as expected from the rapid rise in Rayleigh scattering at shorter wavelengths.

By observing several fields of secondary standard stars covering a wide range of color and air mass, slight differences between the assumed "standard" magnitudes for individual stars and their "true" values are averaged out. In this way we can offset the lower accuracy in the magnitudes of our secondary standard stars compared to primary standards.

7. First order extinction coefficients

Values of the first order extinction coefficients k' are not calculated directly and are not needed for differential CCD photometry with small fields where we assume X is constant over the field. They are contained in the image zero points Z' = Z – k'X in eqns (5) to (8). Values of Z' can be found from intercepts of the linear fits in Figure 2 at color index 0 but in general these will not yield consistent values of Z and k' since these parameters vary with changes in atmospheric transparency. Nevertheless, if conditions are sufficiently stable during one night, we might expect Z and k' to remain approximately constant. In that case, if we plot the values of Z' for each filter against the corresponding values of X for data obtained on that night, we should get a straight line whose gradient gives the mean value of k' for the appropriate filter on that night (see Figure 4). The corresponding values of k' are listed in Table 2. As expected, k' gradually diminishes as the wavelength increases, reflecting the reduction in aerosol scattering at longer wavelengths.

8. Transforming instrumental magnitudes to standard magnitudes

Now we have all the parameters needed to transform instrumental magnitudes measured in differential CCD photometry onto the BVRI standard magnitude system. In doing this it is easier to work with equations which contain only instrumental rather than standard magnitudes on the right hand side. By simple manipulation of eqns (5) to (8) we derive the equations we require.

$$B = b + C'_{bbv}\,(b–v) + z_b \tag{9}$$

$$V = v + C'_{vbv}\,(b–v) + z_v \tag{10}$$

$$R = r + C'_{rvr}\,(v–r) + z_r \tag{11}$$

$$I = i + C'_{ivi}\,(v–i) + z_i \tag{12}$$

where the C' parameters are related to the original C parameters as follows:

$$C'_{bbv} = C_{bbv} / (1 - C_{bbv} + C_{vbv}), \quad (13)$$

$$C'_{vbv} = C_{vbv} / (1 - C_{bbv} + C_{vbv}), \quad (14)$$

$$C'_{rvr} = C_{rvr} / (1 - C_{vvr} + C_{rvr}), \quad (15)$$

$$C'_{ivi} = C_{ivi} / (1 - C_{vvi} + C_{ivi}), \quad (16)$$

and the various "z" terms on the right hand side are image zero points which are the same for all stars in an image.

Since, generically, $C = T - k''X$ and the values of T and k" are known (see Table 1), if we know the air mass X of an image we can calculate the values of the appropriate C parameters and hence the C' parameters.

Suppose we want to find the standard V magnitude of a variable star in a field containing several comparison stars with known magnitudes. We take several images of the field through B and V filters and measure the instrumental magnitudes b and v of the variable and comparison stars in each image. Knowing the mean air mass X of the stars in each image we calculate $C_{bbv} = T_{bbv} - k''_{bbv}X$ and $C_{vbv} = T_{vbv} - k''_{vbv}X$ and hence C'_{vbv} from equation (14) for each image. Using equation (10) and knowing the standard and instrumental magnitudes for the comparison stars, we can determine the zero point z_v for each image. Since we know the instrumental b and v magnitudes of the variable, we can again use equation (10) to calculate its standard V magnitude in each image. Finally, using these individual measurements of the V magnitude of the variable, we can compute its mean and standard deviation.

A similar procedure will yield values for B, R, and I calculated from the measured instrumental magnitudes b, v, r, and i using eqns (9), (11), and (12).

9. Transforming color indices

The transformation equations for color indices can be found from equations (9) to (12).

$$(B–V) = C'_{bv} (b–v) + z_{bv} \quad (17)$$

$$(V–R) = C'_{vr} (v–r) + z_{vr} \quad (18)$$

$$(V–I) = C'_{vi} (v–i) + z_{vi} \quad (19)$$

where

$$C'_{bv} = 1 / (1 - C_{bbv} + C_{vbv}), \quad (20)$$

$$C'_{vr} = 1 / (1 - C_{vvr} + C_{rvr}), \quad (21)$$

$$C'_{vi} = 1 / (1 - C_{vvi} + C_{ivi}), \quad (22)$$

$$z_{bv} = (z_b - z_v) \quad (23)$$

$$z_{vr} = (z_v - z_r) \quad (24)$$

and

$$z_{vi} = (z_v - z_i). \quad (25)$$

Here the two subscript letters indicate the relevant color index.

10. Implementation

In practice, the two procedures described above—finding the transformation parameters and using them to transform instrumental magnitudes to standard magnitudes—are quite straightforward to implement in a spreadsheet.

11. Transforming magnitudes measured for Landolt standard fields

As an application of this approach, BVR-filtered instrumental magnitudes were measured for stars in three Landolt standard fields and transformed as described above. The rms residuals between the standard and derived magnitudes before and after transformation are shown in Table 3. These results clearly show the improvement achieved by transforming magnitudes onto the standard system.

12. Conclusion

We have described and demonstrated a practical approach to finding and applying the transformations required to bring instrumental magnitudes onto a standard photometric system in differential CCD photometry. This includes correcting for second order atmospheric extinction where appropriate. It is possible to use well-measured secondary standard stars in fields spanning a wide range of declinations to enable full coverage of the air mass range from observing sites far from the terrestrial equator. Sky conditions must remain clear and stable for long enough to obtain short series of filtered images of the fields required to cover the required range of air mass. These images can be obtained on several nights and the results combined. This approach may be easier for some observers, particularly those operating at high terrestrial latitudes, to use than other approaches.

13. Acknowledgements

I am grateful to Dr. Chris Lloyd and Dr. Richard Miles for helpful suggestions in preparing this paper and to Brian Warner for stimulating my thoughts on this subject. Constructive comments from an anonymous referee have helped to clarify and improve the paper.

References

AAVSO. 2012, APASS: The AAVSO Photometric All-Sky Survey (http://www.aavso.org/apass), AAVSO, Cambridge, MA.

Da Costa, G. S. 1992, in *Astronomical CCD Observing and Reduction Techniques*, ed. S. B. Howell, Astron. Soc. Pacific, San Francisco, 90.

Green, D. W. E. 1992, *Int. Comet Q.*, **14**, 55.

Hardie, R. 1959, *Astrophys. J.*, **130**, 663.

Harris, W. E., Fitzgerald, M. P., and Reed, B. C. 1981, *Publ. Astron. Soc. Pacific*, **93**, 507.

Henden, A. H. 2012, "Calibration fields" (ftp://ftp.aavso.org/public/calib/).

Honeycutt, R. K. 1971, *Publ. Astron. Soc. Pacific*, **83**, 502.

Landolt, A. 1992, *Astron. J.*, **104**, 340.

Landolt, A. 2009, *Astron. J.*, **137**, 4186.

Landolt, A. 2011, "Equatorial standards" (http://www.cfht.hawaii.edu/ObsInfo/Standards/Landolt/).

Romanishin, W. 2002, "An Introduction to Astronomical Photometry Using CCDs" (http://homepage.usask.ca/~ges125/Astronomy/wrccd4a.pdf).

Stubbs, C. W., *et al.* 2007, *Publ. Astron. Soc. Pacific*, **119**, 1163.

Warner, B. 2009, Photometry Workshop, Soc. Astron. Sciences, 28th Annual Symposium on Telescope Science, held May 19–21, 2009, Big Bear Lake, CA.

Welch, D. 1979, *J. Roy. Astron. Soc. Canada*, **73**, 370.

Table 1. Instrumental transformation and second order extinction coefficients.

Transformation Coefficients		*Second Order Extinction Coefficients*	
T_{bbv}	0.0295 ± 0.0104	k''_{bbv}	–0.0199 ± 0.0067
T_{vbv}	–0.0335 ± 0.0091	k''_{vbv}	0.0016 ± 0.0055
T_{rvr}	–0.1262 ± 0.0164	k''_{rvr}	–0.0077 ± 0.0102
T_{ivi}	–0.0642 ± 0.0165	k''_{ivi}	0.0019 ± 0.0095

Table 2. First order extinction coefficients for data obtained on one night under stable conditions.

First Order Extinction Coefficients	
k'_b	0.376 ± 0.015
k'_v	0.245 ± 0.016
k'_r	0.224 ± 0.025
k'_i	0.166 ± 0.029

Table 3. rms residuals between standard and derived B, V, and R magnitudes before and after transformation for stars in three Landolt standard fields.

Field	*Air mass*	*rms residuals between standard and derived magnitudes*					
		untransformed			*transformed*		
		B	*V*	*R*	*B*	*V*	*R*
98-185	1.63	0.064	0.028	0.033	0.021	0.008	0.008
98-618	1.64	0.035	0.026	0.055	0.015	0.007	0.008
114-750	1.57	0.031	0.018	0.031	0.009	0.007	0.009
Mean	—	0.043	0.024	0.040	0.015	0.007	0.008

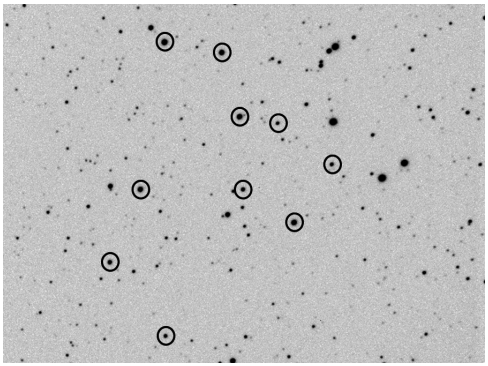

Figure 1. Stars in the field of Var Cas 06 used as secondary standards.

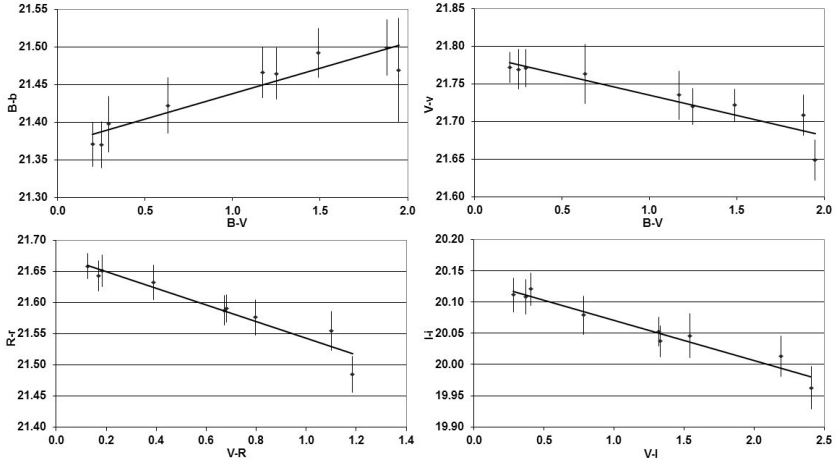

Figure 2. (B–b) vs (B–V), (V–v) vs (B–V), (R–r) vs (V–R) and (I–i) vs (V–I) for stars measured in the field of the variable EE Cep.

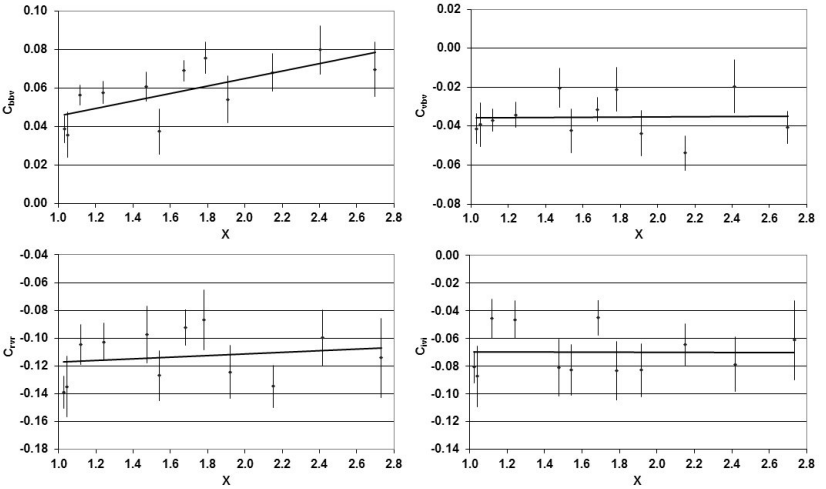

Figure 3. C_{bbv}, C_{vbv}, C_{rvr}, and C_{ivi} vs X for 12 sets of observations of four fields imaged over two nights.

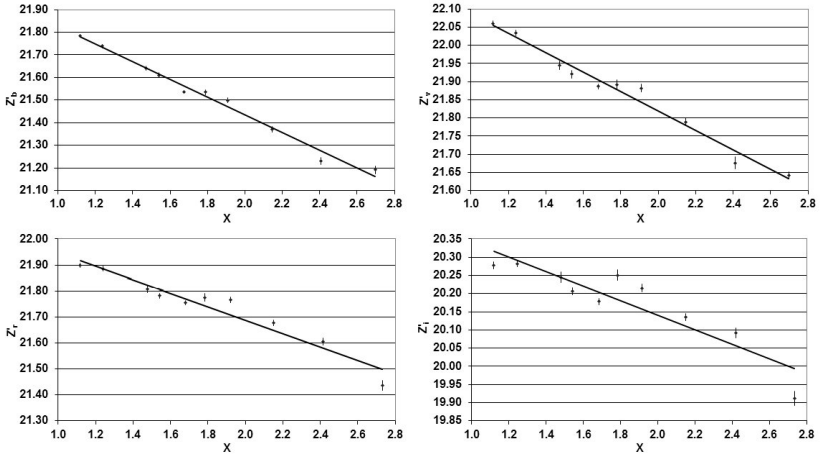

Figure 4. Z'_b, Z'_v, Z'_r, and Z'_i vs X for the data from one night under stable conditions.

ROAD (Remote Observatory Atacama Desert): Intensive Observations of Variable Stars

Franz-Josef Hambsch
Oude Bleken 12, B-2400 Mol, Belgium; M31@telenet.be

Presented at the 101st Spring Meeting of the AAVSO, Big Bear Lake, CA, May 22–24, 2012

Received August 23, 2012; revised October 1, 2012; accepted October 2, 2012

Abstract

The author discusses his new remote observatory under pristine skies and the intensive observations of variable stars he is accomplishing. The stars under investigation are mainly cataclysmic variables, observed in response to AAVSO, CBA, and VSNET alerts; other types, such as RR Lyrae stars, were also observed. Examples are presented of dense observations of different cataclysmic variables as well as an RR Lyrae star. Featured is the first bright outburst of SV Ari (Nova Ari 1905) since its discovery, as well as the first outburst of UGWZ candidate BW Scl. Results for VW Hyi, another cataclysmic variable, will also be shown. Furthermore, an intensively observed RR Lyrae star will be highlighted.

1. Introduction

It is an amateur astronomer's dream to observe under pristine dark and clear skies nearly every night like at the sites where the professional astronomical observatories are located. Such a dream normally never comes true. However, modern techniques and infrastructures in most countries make it possible nowadays to observe from remote sites using off-the-shelf technology. The author installed a remote observatory under the dark skies of the Atacama Desert close to the town of San Pedro de Atacama, Chile. The telescope is housed at SPACE (San Pedro de Atacama Celestial Exploration (http://www.spaceobs.com/index.html)). The owner, also an amateur astronomer, formerly worked at the European Southern Observatory (ESO) at the big telescope sites in Chile. In 2003 he started SPACE, which has been extended to telescope hosting for the last couple of years. I contacted him in 2009 and decided to establish my observatory at his place.

Unfortunately, delivery of the telescope took much longer than anticipated, and only in July 2011 was I able to install the dome, mount, and telescope. Since August 1, 2011, the remote observatory has been producing data every clear night. So far, in less than 8.5 months of operation, this amounted to about 220 data-taking nights. Not bad, is it not?

I am collaborating on the observation of cataclysmic variable stars with J. Patterson of the Center for Backyard Astrophysics (CBA) and T. Kato of the VSNET email alerts. Since I am also interested in observing RR Lyrae stars, I collaborate with the Groupe Européen d'Observations Stellaires (GEOS). In Belgium, I am a member of the Werkgroep Veranderlijke Sterren (WVS) on High Amplitude Delta Scuti (HADS) stars. I am also member of the AAVSO and the German Bundesdeutsche Arbeitsgemeinschaft für Veränderliche Sterne (BAV).

During the many clear nights I gather a lot of data on many stars. Since space here is limited, I restrict myself to some highlights: the outbursts of SV Ari, BW Scl, and VW Hyi; and I also look at an RR Lyrae-type star with a strong Blazhko effect.

2. Observatory

The remote observatory in Chile houses a 40-cm *f*/6.8 Optimized Dall-Kirkham (ODK) from Orion Optics, England. The CCD camera is from Finger Lakes Instruments (FLI) and contains a Kodak 16803 CCD chip with 4k × 4k pixels of 9 μm size. The filter wheel is also from FLI and contains photometric BVI filters from Astrodon.

Figure 1 shows an image of the remote telescope in Chile. It is housed in a clamshell dome, making easy movement of the telescope possible without the need to follow with a shutter of a normal dome. Images of a night's session are either acquired with ACP or CCDCOMMANDER automation software. Further analysis in terms of determination of the brightness of the stars is done using a program developed by P. de Ponthierre (2010). The data are then finally submitted to the AAVSO.

3. SV Arietis (Nova Arietis 1905)

As a first example, I show the results of the campaign on SV Arietis (Nova Ari 1905). SV Ari was discovered on November 6, 1905, by M. and G. Wolf (1905) in Heidelberg, Germany, at a photographic magnitude of 12.0. It was reported that it had brightened from magnitude 22.1. Himpel and Jantsch (1943) reported a possible sighting in September 1943, at a magnitude of 15.7, but this was not confirmed. No brightness increase has been observed for this star ever since.

Then, on 2011 August 2.788 UT, R. Stubbings observed the field of SV Ari and saw an object at magnitude 15.0. He sent an alert via the mailing list cvnet-outburst to ask for confirmation. The outburst information was also given via the VSNET mailing list. This lead to the confirmation by G. Masi (2011) and R. Fidrich (2011). I saw those alerts via VSNET, and since G. Masi immediately took a time series and observed superhumps, I also decided to go after this star

and started a time series at August 2.844 UT, just 1.34 hours after the initial discovery. A first analysis of the data of G. Masi by the Kyoto team (Ohshima *et al.* 2011) showed that the star is probably an SU UMa type dwarf nova with a superhump period of about 1.54 hours. The present outburst seems also not as bright as the one during the discovery of magnitude 12. However, another mail from T. Kato (2011a) on VSNET reported that probably the original brightness estimate was too optimistic as it seems that many brightness determinations of M. Wolf were about 2 magnitudes too bright.

Figure 2 shows the observations I made of this star over a period of more than two weeks. During this period the star dropped more than one magnitude in brightness. Figure 2 also clearly shows individual nightly brightness variations of about 0.3 magnitude.

Figure 3 shows the time series observation made during the first night. Clearly a superhump of 0.3 magnitude is visible. The magnitude of the superhumps reduced to about 0.15 magnitude after a couple of days.

Based on the analysis by the Kyoto team, there have been distinct stages in the evolution of superhumps in SV Ari. The mean period before August 4 was 0.05574(18) day which since then shortened to 0.05519(5) day. Also, later data showed that SV Ari was gradually declining (~ 0.05 mag./day). This seemed very slow for an ordinary SU UMa type dwarf nova. Thus, this object might be a WZ Sge-type dwarf nova. This information is based on e-mail exchanges via VSNET. Towards the end of August 2011, SV Ari had dimmed towards magnitude 18.

4. BW Sculptoris

Another example of an intensively followed star is BW Sculptoris, which went into its first-ever observed outburst on 2011 October 21. BW Scl is also a cataclysmic variable star. On the same day the *AAVSO Special Notice #261* (AAVSO 2011a) was published mentioning the outburst of BW Scl. It was visually observed by M. Linnolt on October 21.3146 at a magnitude of 9.6 (visual). The outburst was confirmed by A. Plummer at magnitude 9.4 (visual). The star has conflicting classifications in the literature and is probably a WZ Sge-type dwarf nova. On October 25, the *AAVSO Alert Notice 449* (AAVSO 2011b) was issued concerning this outburst.

I had already been follwing this star in its pre-outburst phase. However, I missed the outburst, as I thought the star was not doing much, and ceased observing it on October 14—just a week before the outburst took place. Of course, I restarted observations immediately after the news was spread and followed the star over a period of 2.5 months. Figure 4 shows the development of the brightness over the full observing period.

After a few days nice superhumps of about 0.25 magnitude developed, as can be seen in Figure 5. After a week into the outburst the early superhump

period was determined to be 0.054308(3) day by Kato (2011b). After a rapid declining phase from magnitude 11.7 to about magnitude 14, nice superhumps of 0.3 magnitude developed, beginning at about JD 2455877.

5. VW Hydri

At the request of professional astronomers from South Africa (P. Woudt (2011)), I began observations of VW Hyi just as the star went into superoutburst, although that was a surprise to the pros, as the superoutburst was not expected yet. My observations triggered satellite observations of the star.

VW Hyi is a popular cataclysmic variable in the Southern sky. Many studies have been performed on this star; see, for example, AAVSO (2010). During quiescence the star is at magnitude 14.4, Normal outbursts happen on average every 27.3 days and last about 1.4 days. The superoutburst happens on average every 179 days and lasts for about 12.6 days. Figure 6 shows impressively this behavior of VW Hyi with one superoutburst and two normal outbursts.

The star develops strong superhumps during its outburst as can be seen in Figure 7. The variation of those humps reaches 0.5 magnitude.

6. Example of an RR Lyr star, V1820 Ori

This type of variable is named after the prototype, the variable star RR Lyrae in the constellation Lyra. RR Lyr stars are pulsating horizontal branch stars with a mass of about one-half of our Sun's. Their period is short, typically less than one day.

My interest in observing RR Lyr stars is, on the one hand, due to the short period of those stars—within one night you can see quite a change in brightness. On the other hand, the stars also show some brightness modulations, known as the Blazhko effect. Back in 1907 S. Blazhko observed this effect for the first time in the star RW Dra (see Smith 2004). The Blazhko effect is not well-understood and needs further observational campaigns. Recently due to the Kepler and CoRoT satellite missions, more insight into this phenomenon has been gained as the satellites can, of course, observe the stars continuously, which is impossible for Earth-bound observations. Nevertheless, observations from Earth are also very valuable, as can be seen in many publications on this subject in the astronomical literature. Figure 8 shows the phase diagram of the RR Lyr star V1820 Ori, which has been observed from Chile over a full season (more than 3 months). It is obvious from the figure that the light curve is not regular, the maximum brightness is changing over more than 0.5 magnitude, and the moment of maximum time is changing. So a rather complex light curve is the result. Presently the data are under analysis, and I intend to publish the results.

7. Conclusion

The remote observatory under pristine skies in the Atacama Desert of Chile opens up great possibilities to observe variable stars. Intensive follow-up observations over many days, weeks, or even months are possible due to the stable weather conditions. The given examples show impressively what is possible. I welcome collaborations in order to contribute to scientific research of common interest.

References

AAVSO. 2010, Variable Star of the Month (http://www.aavso.org/vsots_vwhyi).

AAVSO. 2011a, *AAVSO Special Notice #261*, AAVSO, Cambridge, MA.

AAVSO. 2011b, *AAVSO Alert Notice 449*, AAVSO, Cambridge, MA.

de Ponthierre, P. 2010, LesvePhotometry software (http://www.dppobservatory.net/AstroPrograms/Software4VSObservers.php).

Fidrich, R. 2011, e-mail to cvnet-outburst.

Himpel, K., and Jantsch, E. 1943, *Beob.-Zirk. Astron. Nachr.*, **25**, 105.

Kato, T. 2011a, vsnet-alert e-mail message 13544 (http://ooruri.kusastro.kyoto-u.ac.jp/mailarchive/vsnet-alert/13544).

Kato, T. 2011b, vsnet-alert e-mail message 13799 (http://ooruri.kusastro.kyoto-u.ac.jp/mailarchive/vsnet-alert/13799).

Masi, G. 2011, vsnet-alert e-mail message 13538 (http://ooruri.kusastro.kyoto-u.ac.jp/mailarchive/vsnet-alert/13538).

Ohshima, T., *et al.* 2011, vsnet-alert e-mail message 13543 (http://ooruri.kusastro.kyoto-u.ac.jp/mailarchive/vsnet-alert/13543).

Smith, H. A. 2004, *RR Lyrae Stars*, Cambridge Univ. Press, Cambridge, 103.

Wolf, M., and Wolf, G. 1905, *Astron. Nachr.*, **169**, 415.

Woudt, P. 2011, private communication.

Figure 1. Photo of the remote telescope installation in Chile.

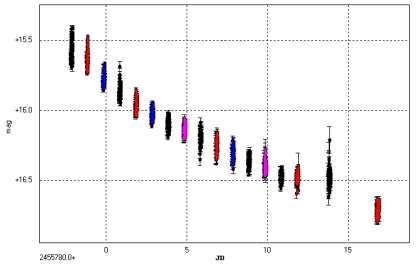

Figure 2. Light curve of the observations of SV Ari over a period of more than two weeks. Different colors represent observations during different nights.

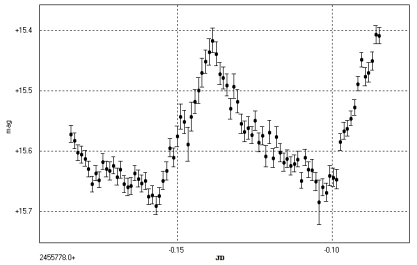

Figure 3. Light curve of the observations of SV Ari showing a superhump during one night of observation.

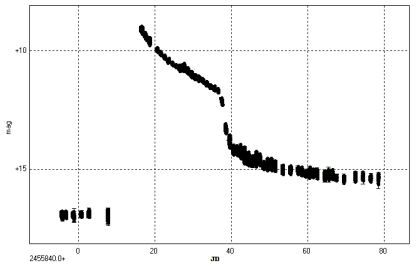

Figure 4. Light curve of the observations of BW Scl over a period of nearly three month.

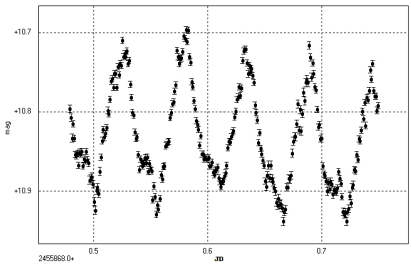

Figure 5. Light curve of the observations of BW Scl showing several superhumps during one night of observation.

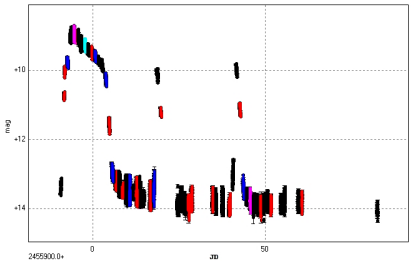

Figure 6. Observations of VW Hyi during superoutburst and normal outburst. Different colors represent observations during different nights.

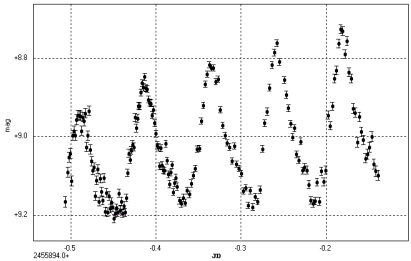

Figure 7. Observations of VW Hyi during one night at the top of the superoutburst clearly showing strong superhumps.

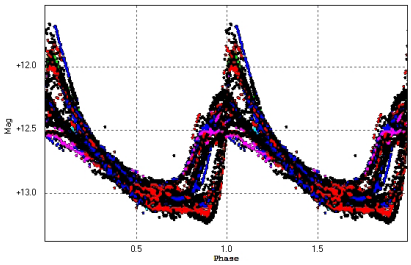

Figure 8. Phase diagram of the observations of V1820 Ori over a period of nearly three months. Different colors represent observations during different nights.

The AAVSO 2011 Demographic and Background Survey

Aaron Price
AAVSO Headquarters, 49 Bay State Road, Cambridge, MA 02138;aaronp@aavso.org

Kevin B. Paxson
20219 Eden Pines, Spring, TX 77379; kbpaxson@aol.com

Received February 16, 2012; revised March 13, 2012; accepted March 13, 2012

Abstract In 2011, the AAVSO conducted a survey of 615 people who are or were recently active in the organization. The survey included questions about their demographic background and variable star interests. Data are descriptively analyzed and compared with prior surveys. Results show an organization of very highly educated, largely male amateur and professional astronomers distributed across 108 countries. Participants tend to be loyal, with the average time of involvement in the AAVSO reported as 14 years. Most major demographic factors have not changed much over time. However, the average age of new members is increasing. Also, a significant portion of the respondents report being strictly active in a non-observing capacity, reflecting the growing mission of the organization. Motivations of participants are more aligned with scientific contribution than with that reported by other citizen science projects. This may help explain why a third of all respondents are an author or co-author of a paper in an astronomical journal. Finally, there is some evidence that participation in the AAVSO has a greater impact on the respondents' view of their role in astronomy compared to that expected through increasing amateur astronomy experience alone.

1. Introduction

The AAVSO is a large, multinational citizen science organization dating back to 1911. The organization has experienced significant change in the past two decades (Williams and Saladyga 2011), yet our last survey of membership was conducted in 1994. As the organization begins planning for the future, it was time to use data to characterize those who are active and contributing to the AAVSO, in all its forms. These data can be compared with current assumptions and beliefs of the organization and also used as a tool for planning new initiatives and direction.

2. Prior surveys

The AAVSO has conducted a number of membership surveys in the past 35 years. These surveys included a mix of demographic (such as "age"),

programmatic (such as "observing trends") and operational (such as "evaluation of staff") items.

In 1976, AAVSO Director Janet Mattei, with staff members Linda M. Blizzard and Josefa M. Manella, mailed a survey to members. The survey included sections on headquarters operations, communications, observations, meetings, and publications. Approximately 200–300 responses were received and are stored in the AAVSO archives (AAVSO 1976). However, no known tabulation or report of the responses is known to exist.

In January of 1980, the AAVSO mailed a second survey to members. It was a smaller survey, with ten questions focused on demographics and observing activities. A summary of results were reported in Waagen (1980). 267 surveys were returned as of the writing of that report. None of the questions on the 1980 survey were also on the 1976 survey, so the two surveys could be seen as complementary.

In 1994, Wayne M. Lowder designed a survey of members and observers in response to a request by a recently convened Futures Studies Group. The survey had 79 items divided into sections focused on demographics, publications, other resources of information, astronomical activities, observing, headquarters operations, meetings, and use of personal computers. 420 surveys were returned and tabulated by AAVSO staff (Tanja Foulds, Shawna Helleur, Dennis Milon, and Barbara Silva). Results were presented to the Futures Studies Group in the form of an executive summary written by Lowder in September 1994, which exists in the AAVSO archives (Lowder 1994). The Futures Study Group presented results to the AAVSO Council at the AAVSO Annual Meeting in October 1994 (Hazen 1995).

The AAVSO has also run a few surveys over the past few years focused on more specific topics. In 2010, the AAVSO conducted a survey with eight questions about AAVSO meeting experiences. This survey was distributed exclusively online through the AAVSO website and received 88 responses. Since 2009, the AAVSO's Citizen Sky project has asked participants a few optional demographic questions when they first registered for the Citizen Sky website. 1,385 of these responses were analyzed in a paper by Price and Lee (in press) and some of those data are included here.

3. Survey design and methodology

The goal of the 2011 survey was to better characterize the AAVSO membership so that staff and the Council can make better decisions regarding membership activities and future directions of the organization, such as testing current assumptions about members and also looking for unexpected results in the data. As such, the survey items were designed to report on the respondents' educational and professional backgrounds and their experience in the AAVSO and astronomy in general.

The survey was designed prior to the known existence of the previous surveys. Yet the items on the surveys are often quite similar, which we feel is a testament to the validity of the chosen items. Twenty of those who were privately invited to take the survey tested the first draft. Only technical changes came out of that pilot test. The survey has a maximum of 27 items (see Appendix A). However, some items are conditioned only to appear based on certain responses to earlier items and all items were optional. So the response rate varies item-to-item.

The survey was placed on the Survey Monkey website so that results could be automatically tabulated. We posted the survey's URL to the AAVSO Discussion Group (~490 subscribers) and on the AAVSO web site (417 reads). We sent an e-mail to those who were current AAVSO members or who had made an observation within the last five years (~2,400 e-mails). We identified eight people who met that criteria but who did not have e-mail addresses on record. For them, we printed a copy of the survey and sent it using postal mail. A total of 691 valid responses were received to the online survey and four of the printed surveys were returned.

We tabulated the results into an Excel spreadsheet. For the open-ended items, we coded them into a set of categories that included 99% or more of the responses. When a particular item response could fit into more than one category, the first category mentioned in the response was used. This was based on the assumption that the first item mentioned by the respondent was the most important to them. The ranking items were scored on an ordinal scale (the highest ranking item is assigned a "1" and the rest are ranked accordingly). We treated items that were not answered as missing data. We made our final analysis with the PASW Statistics 18 software (formerly SPSS Statistics, now IBM SPSS Statistics).

3.1. Definitions

For the purposes of this survey, we refer to *respondents* as anyone who answered at least one item of the survey. Also, we combined Charge-Coupled Device (CCD), Photoelectric Photometry (PEP), and Digital Single-Lens Reflex (DSLR) technologies beneath the umbrella term of *digital technologies*. *Visual observations* include any observation made with the eye, which includes naked eye, binoculars, and telescopic observations made with an eyepiece. *Membership status* was assigned based on AAVSO headquarters records as of January 2012.

The profession categories included items were taken from the U.S. Department of Labor categories used in the 2011 U.S. Census (U.S. Dept. of Labor 2011). The categories of objects were taken from the highest level categories used by the Variable Star Index (VSX) (AAVSO 2011), which are based on categories originally developed by the *General Catalogue of Variable Stars* (GCVS; Kholopov *et al.* 1985).

4. Results

4.1. Age

The mean age of survey respondents is 53 (N=671; Figure 1). There is no significant difference between the mean ages of men and women, nor of the mean ages between digital and visual observers. The 1994 survey reports frequencies instead of means. The mean frequency category was "41–50" (N=420). Citizen Sky members report a mean age of 41 (N=1,385). *Sky & Telescope* magazine reports a mean subscriber age of 51 (New Track Media 2010).

The AAVSO maintains an archive of membership applications dating back to 1911. Almost all applications include either the applicant's age or birthdate. We randomly selected 615 applications and plotted their age as of the moment they joined the organization (Figure 2). There are some gaps in the data from incomplete records (namely 1911–1918, 1922–1928, and 2004–2008). Over the entire 100-year period, the average age of an AAVSO membership applicant was 37 years old. During 1911–1921, the average new member age was 40 years. New member age dropped to 28 years during the years 1967–1977 and was 51 years for the years 2001–2011.

The average age of observers does not vary much among the various observing techniques included in the survey (Figure 3). The age of PEP observers is the only category that stands out. We found slightly more variation between the average ages of those engaged in non-observing activities (Figure 4). In particular, the more "high-tech" activities of programming and data mining tend to have slightly younger participants.

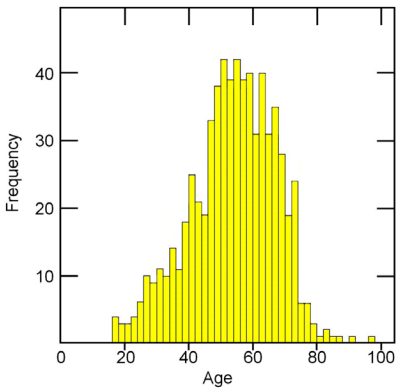

Figure 1. Histogram of age of survey respondents. The mean age is 53.31; Standard Deviation = 13.384; N = 671.

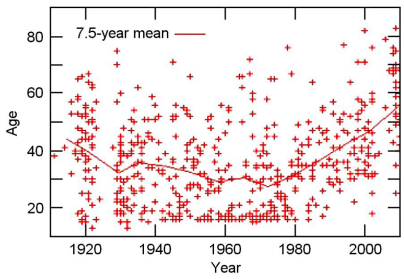

Figure 2. Age of new member applicants.

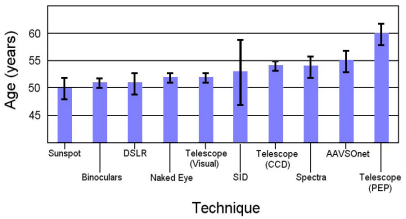

Figure 3. Average age of survey participants as a function of observing technique.

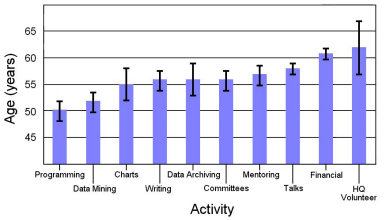

Figure 4. Average age of survey participants as a function of non-observing activity.

4.2 Years active

"Years active" is a variable computed from subtracting the first year a respondent reported to be active in the AAVSO from 2011. It represents an approximation of how long survey respondents have been active in the organization. The mean is 14.3 years (SD=15, N=598). There seems to be a drop off at years 2 and 5, after which drop out rates flatten (Figure 5). Members of the AAVSO tend to be involved in the organization for six years longer than non-members, a difference which is statistically significant, $F(1,503)=22.0$, $p<.001$.

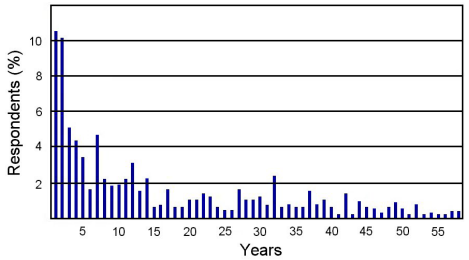

Figure 5. Number of years active of all 2011 survey respondents.

The 1994 survey included frequencies of the number of years respondents have observed variable stars (note a slight difference between their question about "observing" and our question about "being active") separated into 5-year bins (Figure 6), so we were unable to compute a mean. The only major difference between the 1994 and 2011 distributions is a drop off after 30 years that appears in the 1994 survey, but not in the 2011 survey.

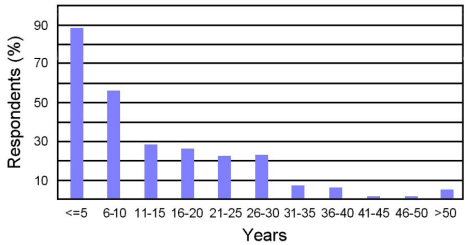

Figure 6. Number of years active of observers only, from 1994 survey.

In order to get more detail from the period around the 1980 survey, we randomly selected 26 observers from the AAVSO International Database (AID) who had submitted observations in 1977 (chosen to match the same interval between 1994 and 2011) and pulled their original membership application to set a date for their joining of the organization. We computed the difference between that date and 1977 as their AAVSO Age (Figure 7). The mean age was 10.8 years. The mean AAVSO Age of members in the 2011 survey was 16.8 years. The distributions are similar, but not the same. The drop-offs seen in the 2011 survey at years 2 and 5 occur in the 1977 data, but a year or two later. Overall, the trends are very similar.

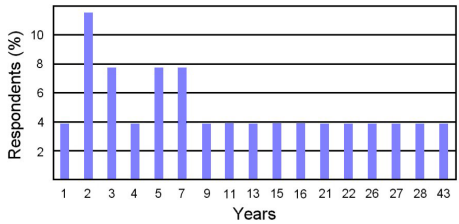

Figure 7. Years of activity of members and observers active in 1977 (N = 26).

4.3 Membership status

Membership status was determined by looking up an observer code or e-mail address (when provided) in the AAVSO membership database on January 18, 2012. At that time, 54% of respondents were official members of the AAVSO. In the 1994 survey, 85% of the respondents were members of the organization (N=417), according to self-reported data. In the 1994 survey, we received observations from 660 observers. In 2011, we received observations from 1,050 observers. The observer/membership ratio difference may reflect more the growth of observers rather than the loss of members. The AAVSO does not keep a record of membership totals per year.

We also looked for a relationship between membership status and whether the respondent reports to be an active observer or not. We found no significant relationship. However, for those who were active, there was a significant relationship between the techniques they used and their membership status, $F(390,8)=2.21$, $p=.03$ (Figure 8). The most interesting result is that 60% of telescopic CCD observers (N=143) are members and 43% of telescopic visual observers (N=138) are members. This difference is statistically significant, $F(315, 1)=7.36$, $p<.01$.

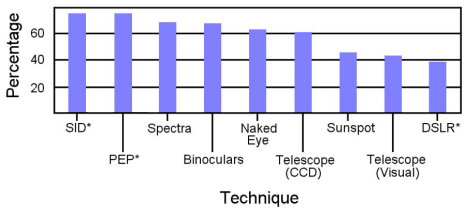

Figure 8. Membership rates for particpants as a function of various observing techniques (* = categories with fewer than 15 member respondents).

4.4. Gender

92% of respondents identified as male (N=634) and 8% identified as female (N=44). The mean age for women is 49, while the mean age for men is 53, however the difference is not statistically significant (p=.06). The low sample of females makes it difficult to look for relationships between gender and other variables in the survey. In the 1994 survey, the distribution was 94% male and 6% female, very close to the current ratio. *Sky & Telescope* reports a gender ratio of 95% male and 5% female in their 2010 advertising rate card (New Track Media 2010). The Citizen Sky gender distribution is 78% male, 19% female, and 3% unreported (N=1,385).

4.5 Country

108 different countries were represented in our survey results. About 49% of respondents were from the United States. The rest were widely distributed among the other 107 countries (Figure 9). 28 countries were represented by members and 46 countries were represented by active observers.

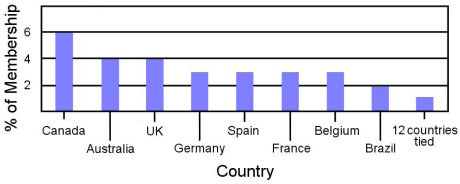

Figure 9. Top countries represented by membership, excluding the United States.

4.6 Formal education

Almost a quarter of the respondents claimed to have a terminal degree (Ph.D., M.D., J.D., and so on) in their field (Figure 10). About 76% report a Bachelor's degree or higher, which is close to *Sky & Telescope's* rate of 77% (New Track Media 2010).

There is a significant relationship between profession and observation type, $F(9,438)=3.44$, $p<.01$. Most of that significance is due to the increased education levels of the spectroscopic observers (N=32) and decreased education levels reported by the sunspot observers (N=22) (Figure 11).

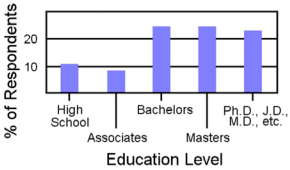

Figure 10. Reported formal education of respondents (N = 656).

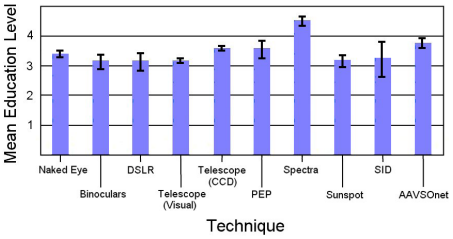

Figure 11. Average formal education of the users of various observation techniques. Education level reflects the categories in Figure 10 in ascending order.

There are also some correlations between education and the type of objects the respondents favored to observe (Table 1). Specifically, those with less of a formal education tend to be more interested in novae (N=421, q=.139, p < .001) and the Sun (N=404, q=.121, p < .05). Also, those with more of a formal education tend to be more interested in rotating variables (N=354, q=–.107, p < .05). All of these relationships are considered small by traditional social science standards (Cohen's Guidelines).

Table 1. Intercorrelations between formal education and interest in objects.

CV	*EB*	*Extra-galactic*	*Novae*	*Non-Stellar*	*Pulsating*	*Rotating*	*Sun*	*YSO*
Formal Education								
–.044	–.055	.074	.139*	.022	–.055	–.107**	.121**	–.049

*$p < .01$, **$p < .05$.

4.7. Profession

The reported distribution of professions (N=615) can be broken down into two categories of high and low (Figure 12). The most common professions were in science, computer science, engineering, and education. Those four categories account for about 57% of the respondents. The rest of the other categories were roughly even, with management and health care leading the group. Building and Grounds Cleaning had the fewest responses.

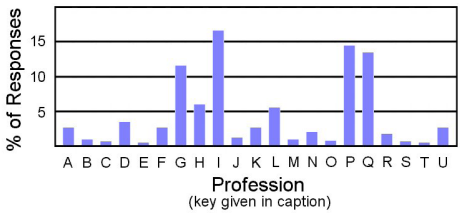

Figure 12. Distribution of professions according to U.S. Department of Labor categories: a. Transportation and material; b. Sales and related; c. Protective service; d. Production; e. Personal care and service; f. Office and administrative support; g. Mathematical and computer; h. Management; i. Life, physical, and social science; j. Legal; k. Installation, maintenance and repair; l. Healthcare practitioners and technical; m. Food preparation and serving; n. Financial; o. Farming, fishing, and forestry; p. Engineering, architecture and surveyors; q. Education, training, and library; r. Construction and extraction; s. Community and social services; t. Building and grounds cleaning; u. Arts, design, entertainment.

The 1994 survey had a similar question, but with fewer profession categories to choose from. Table 2 is a comparison of results from the two surveys in categories that are similar. In general, there is not much difference that cannot be explained by differences in the definition/labeling of categories between the surveys.

Table 2. Comparison of 1994 and 2011 reported professions (selected).

1994 Category	*2011 Category*	*1994 Response (%)*	*2011 Response (%)*
Scientific/Technical	Life, Physical, and Social Science	41	17 (31*)
Professional Astronomer	(none)	12	13**
Educator	Education, Training, and Library	18	14
Computer Specialist	Mathematical and Computer Scientists	9	11
Business Management	Management	5	6
Sales/Marketing	Sales, and Related	1	1

*When combining this category with "Engineering, Architecture, and Surveyors."

**Taken from astronomy experience responses (see text).

4.8. Astronomy experience

Almost half (49%) of the respondents classified themselves as having an advanced level of experience in astronomy (Figure 13). There is a significant but low positive correlation between astronomy experience and the variable we call "Years Active" ($r = .208$, $p < .001$). There is also a significant correlation between age and astronomy experience, $r = .087$, $p < .05$, but it is weaker than the relationship with Years Active. In fact, when controlling for Years Active through an ANCOVA, age is no longer a significant predictor of experience, $F(67, 587) = 1.11$, $p = .125$.

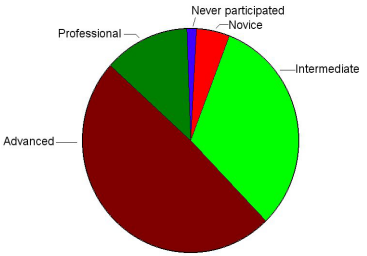

Figure 13. Astronomy experience levels of of respondents (N = 658).

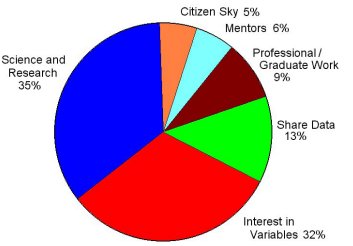

Figure 14. Sources of motivation to participate in the AAVSO (N = 351).

4.9. Motivation

Supporting science and research ("citizen science") is the most popular reason respondents gave for being active in the AAVSO. A close second is an interest in variable stars (Figure 14). Around 9% of respondents are active in the AAVSO due to professional or graduate student research.

4.10. Barriers to activity

To investigate barriers to activity we asked an open-ended question worded as: "If you are not currently active in the AAVSO, what is the main reason?" Almost all respondents who previously reported to be inactive (N=192) provided an answer to this item. Note the vague definition of "active" in the question. We purposely allowed the respondent to define activity in their own way so as to include those who would otherwise be active in non-observing contexts. Time (43%) was by far the main reported reason respondents were inactive (Figure 15). Other astronomy interests was second (14%), followed by a lack of equipment/poor location (12%). Much of poor location comments were reported as problems with light pollution.

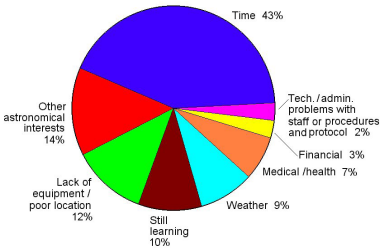

Figure 15. Major reasons to be inactive / barriers to activity (N = 192).

4.11. Referral sources

People learn about the AAVSO from a variety of sources (Figure 16). Word of mouth (25%) is most common, followed closely by other astronomy club or conferences (19%), *Sky & Telescope* magazine (19%), and the Internet (18%). The 1994 survey also included a question about referral sources. It was stated as: "How did you first hear about the AAVSO?" and had 427 responses (Figure 17).

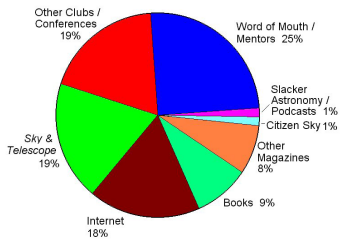

Figure 16. Referral sources in the 2011 survey.

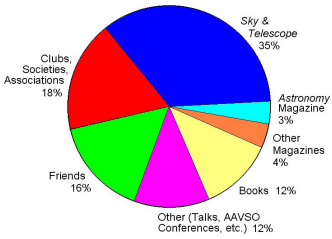

Figure 17. Referral sources in the 1994 survey.

The biggest difference between the 1994 and 2011 surveys is the 35% to 19% drop in referral share attributed to *Sky & Telescope* magazine. *Sky & Telescope* has long been an important source of branding for the organization, but it has dropped in significance. This is likely due to the ability of the AAVSO to reach amateur astronomers directly through the Internet. If you add up the

referral share of the "Internet" and "*Sky & Telescope*" in this survey it reaches 37%, which is very close to the 35% share in the 1994 survey (and in line with general societal trends). Club and books continue to have similar shares between the 1994 and 2011 surveys, at 18%–19% and 12%–9% respectively. Interestingly, non-*Sky & Telescope* magazines also have a similar share between surveys, at 7%–8%.

In the 2011 survey, we coded talks into the "Word of mouth" category. If you combine the "Other (talks…)" and "Friends" categories in the 1994 survey, then they too have a similar share with the 2011 "Word of mouth" category at 28%–25%.

The 1980 survey included a referral question as well. It was stated as: "Source of information about the AAVSO?". Waagen (1980) divided the responses into 5 categories (Figure 18). In general, they are consistent with the other surveys. The major difference being the large share books held in 1980 (21%) as opposed to 1994 (12%) and 2011 (9%). Club referrals also dropped between 1980 (23%) and 1994 (18%) while remaining consistent from 1994 to 2011 (19%).

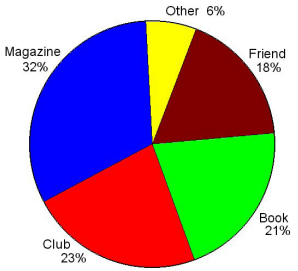

Figure 18. Referral sources in the 1980 survey.

4.12. Observation activity

We asked respondents to declare whether they consider themselves active observers or not. We did not define the term "active." Almost two-thirds (63%) of the respondents report to be active (Figure 19). Similarly, the 1994 survey asked observers to classify themselves into various categories of activity. 78% chose a category denoting activity and 22% chose a category denoting inactivity. Thus, the percentage of inactive observers has increased since the last survey. In the 1980 survey, 93% reported to be "an observer."

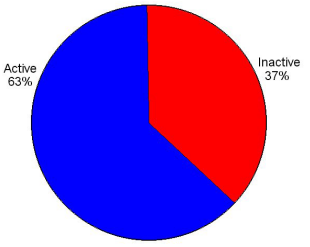

Figure 19. Active and inactive observer rates (N = 691).

We were interested to see whether the increase in inactive observers was related to any of the non-observing activities in the AAVSO. An ANOVA (ANalysis Of Variance) found a significant difference between the active and inactive groups based on whether they are also active in a non-observing activity, $F(10,644) = 1.9$, $p < 0.05$. Figure 20 is a plot of the mean observation activity value (lower number means more active) grouped by non-observing activities listed in this survey. It is of no surprise that the many active observers are those involved in the chart process, since charts have a direct impact on observing. It is also interesting that the least active are those involved in financial aspects of the organization. Programmers tend to be active observers as well. Beyond that, the rest of the categories are roughly even.

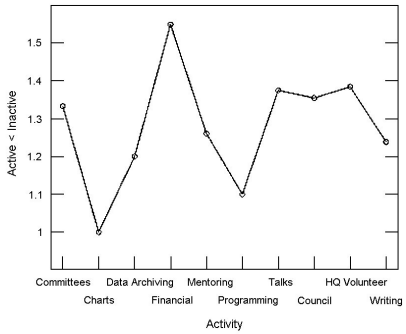

Figure 20. Activity rates of respondents who participate in non-observing activities.

4.13. Faintest observation

We asked observers to report the magnitude of the faintest observation they "typically" observe (Figure 21). We then asked whether that observation was made visually or with "CCD/DSLR/PEP/Other Digital system." This was more useful than asking if a person was a "visual or CCD" observer since many use both techniques. Instead, this question tells us which technique they used to get their faintest observation, which will almost always be "CCD"

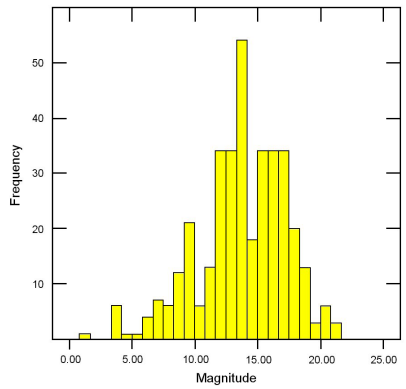

Figure 21. Faintest observations (magnitude) "typically" recorded by respondents. Mean = 13.75; Standard Deviation = 3.45; N = 365.

for CCD/combined observers and "visual" for visual-only observers (for a more detailed discussion of observation type see the observation technology section). The goal of these questions was to establish magnitude ranges for visual or CCD campaigns. Observers were divided roughly in half between the two (Figure 22). The mean faintest visual observation was 12.02 and the mean faintest CCD observation was 13.75. The visual distribution drops off sharply around magnitude 15–16 while the CCD distribution fades more gradually until around magnitude 20 (Figure 23).

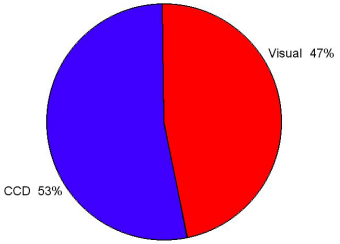

Figure 22. How the faintest observation in Figure 21 is measured.

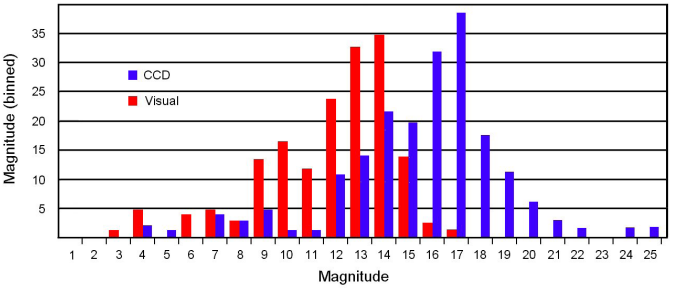

Figure 23. Distribution of the faintest "typical" observation made through CCD or visual measurements.

4.14. CCD origins

We were interested in how often visual observing is used as a stepping stone to digital observing. We asked digital observers: "If you are a CCD/DSLR/PEP observer, did you begin as a visual observer who migrated to CCD/DSLR/PEP or did you begin as a CCD/DSLR/PEP observer?" About half of the respondents report beginning as a visual observer (Figure 24).

This result is somewhat biased because it includes the generation of AAVSO observers who began when visual was the only option. When we looked at the answers of only those who became active within the last 10 years (using the "Years Active" variable, N = 119) we found 67% began with CCD and only 33% began as visual observers. If we tighten the window further and only look at the last 5 years (N = 79), we don't find much additional difference as about 28% of CCD observers began as visual observers (Figure 25). Currently, visual observing is an effective entry point for roughly a quarter of new AAVSO CCD observers.

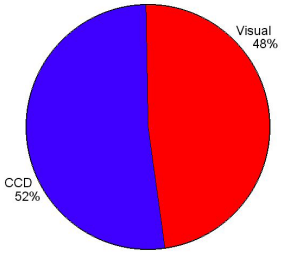

Figure 24. Background (origins) of active CCD observers.

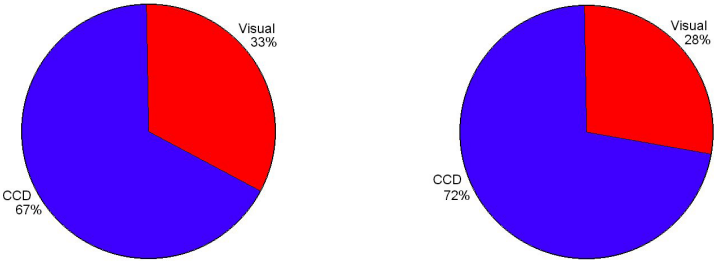

Figure 25. Backround (origins) of active CCD observers for the last 10 years (left), and last 5 years (right).

4.15. Observation technology

We provided respondents with a list of observation technologies and asked them to select which types they "actively use" (N = 460, Figure 26). Interestingly, 40% of those who reported to be telescopic CCD observers are also active as visual telescopic (N = 54) or naked eye (N = 34) observers. Also, the number of those who reported to be observers utilizing spectra (N = 32) was surprising, since the organization has no formal group or section to standardize this activity. Lastly, more than half of all observers use multiple observing techniques (Figure 27).

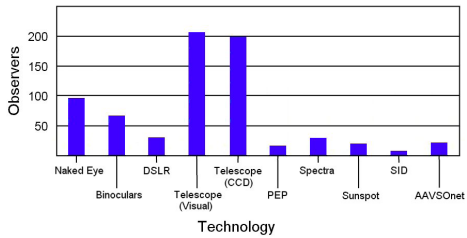

Figure 26. Number of active observers using various observation technologies.

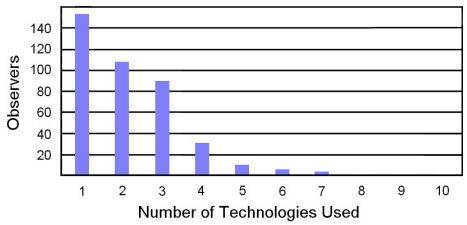

Figure 27. Number of different observing technologies used by active observers.

4.16. Non-observing activities

By far, the most popular non-observing activities involved public outreach (Figure 28). Specifically, giving talks and writing about the AAVSO. Prior surveys did not include items to address participation in these areas. We found no significant relationships between non-observing activity and observation technology or with membership status.

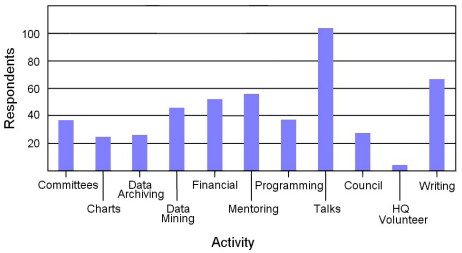

Figure 28. Number of respondents participating in various non-observation activities.

4.17. Object interest

When asked to rank objects by interest, we find a clustering of objects into two categories: highly ranked (Pulsating, CV, EB, Novae, Extragalactic) and lesser ranked (YSO, Sun, Rotating, Non Stellar) (Figure 29). Respondents were only allowed to provide one object for each ranking. However, they were not required to rank every object. Some respondents only ranked the objects they were most interested in (example: they only ranked the top 5). In a separate tabulation, we assigned a ranking of 9 (the lowest rank possible) to those objects that had missing data, with the justification that the respondent had no interest in that object. The only major difference is that the drop off between the highly ranked group and the lesser ranked group increases. 33 types of objects were included in the "Other" category (Table 3). Many of these types of objects could be included in existing survey categories.

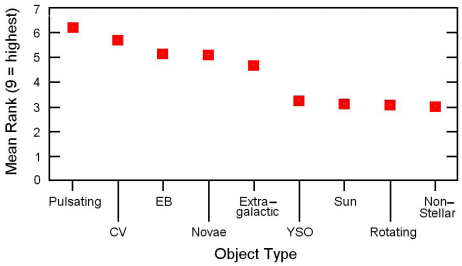

Figure 29. Popularity of various variable star object types.

4.18. Meeting attendance

The mean number of meetings attended by a respondent was 1.5 (N = 584; Figure 30). However, that number is significantly skewed because of four respondents of reported between 20–60 meetings. The overall survey median value is 0, meaning that the vast majority of respondents had not attended an AAVSO meeting before. By excluding those who have not attended any

Table 3. Objects included in the "Other" field.

"Other" Objects	*Number*	*"Other" Objects*	*Number*
Exoplanets	17	HAD's	1
Asteroids	9	Supernovae	1
RCB's	6	Cool Supergiants	1
Be, Shell or GCAS stars	4	Central-planetary nebulae	1
Symbiotic variables	3	Thermal pulse candidates	1
Carbon	3	AGB's	1
Spotted or RS CVn	2	Emission line stars	1
GRB's	2	Mira's	1
HMXB's	2	NSV's	1
Globular variables	2	ISM	1
Non-specific (general)	2	RR Lyr	1
Bright variables	2	Del Sct	1
Recurrent novae	2	SX Phe	1
SR's	2	Neutron stars	1
Irregulars	1	White dwarfs	1
Double or multiple	1	Interesting stellar spectra	1
Infra-red stars	1		

meetings, and the two persons who reported 40 and 60 meetings, then the average meeting attendance is 4.2. This number reflects the number of meetings someone would typically attend if they have attended at least one.

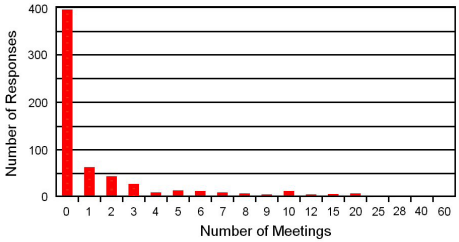

Figure 30. Number of AAVSO meetings attended by respondents.

We looked for relationships between meeting attendance and the type of observations people make and the types of non-observing activities they participate in (Figure 31). For types of observations, we found no significant relationships. For non-observing activities, we did find a significant relationship, $F(573, 10) = 15.4$, $p < .001$. However, most of that statistical relationship is due to those who selected "HQ Volunteer." We believe this to be a perplexing variable because those who volunteer at Headquarters tend to live near Headquarters, thus attend the annual meeting quite often. In Figure 31, we zoomed in on the other categories. The main difference between the activities that involve more investment of initiative (writing, programming, mentoring, and so on) than in activities that are more procedural-based. Finally, members are more likely to

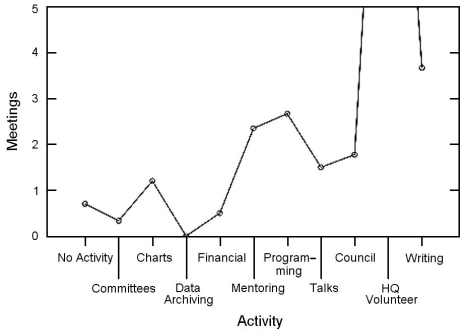

Figure 31. Number of meetings attended by participants of various non-observing activities.

attend meetings (mean = 2.5 meetings) than nonmembers (mean = 0.3 meetings). This difference is statistically significant, $F(1, 483) = 31.1$, $p < .001$.

4.19. Paper authorship

A little over a third of the respondents reported to be either an author or coauthor of a paper in an astronomical journal (36%). None of the prior surveys included paper authorship.

5. Discussion

Overall, the 2011 survey depicts those participating in AAVSO activities as similar to those described in the 1980 and 1994 surveys. They are largely male, older, highly educated, and tend to work in scientific or technical fields. Most are active observers and have been affiliated with the AAVSO for decades.

The survey also suggests areas of significant change over time. First, the average age of new members has been increasing. This began in the 1980s and has continued. Originally, the increase in age was mostly attributed to the loss of younger members. More recently it can also be attributed to an increase in older members. The overall size of the organization's membership has not diminished over this same time period. This "greying of astronomy" is an issue that affects amateur astronomy as a whole. The average age of a *Sky & Telescope* subscriber was 39 in 1979, 48 in 1998, and 51 in 2010 (Beatty 2000; New Track Media 2010). An analysis of the average age of professional American astronomers found an increase of around half a year per year in the mid 1980s (Thronson and Lindstedt 1986). However, the AAVSO Citizen Sky project has been more successful in recruiting younger observers. It reports a mean age of 41 (N = 1,385). For comparison, the median age in the United States as of the 2010 census was 37. The cause behind this trend is complicated and multifaceted. One issue could be the impact of the cold war space race on interest in science in the 1950s and 1960s. Another could be the increasing entertainment options for a decreasing amount of personal time. Amateur astronomy has also become a largely high-tech endeavor requiring significant initial financial investment.

A more detailed investigation of the age question is planned for a future study. Another major difference between surveys is where and how respondents heard about the AAVSO. The Internet is replacing many of the referrals which previously may have come through *Sky & Telescope* magazine. It is interesting that referrals from books and non-*Sky & Telescope* magazines have not changed much between the 1994 and 2011 surveys. This suggests the issue may be specific to *Sky & Telescope*, perhaps due to its previously dominant position as a major referring source and/or because *Sky & Telescope* is more closely associated with advanced amateur astronomers than casual readers. It is possible that the Internet is impacting newsstand sales (casual readers) less than circulation sales (more advanced readers).

In terms of observing methodology, active observers are pretty evenly divided between digital and visual observing. Since the 1990s, there has been discussion about competition between the two types of observing. However, we found that 40% of telescopic CCD observers are also visual observers. Also, about half of all CCD observers and a quarter of new CCD observers began as visual observers. This suggests the line distinguishing these two groups is much fuzzier than has been advertised.

There are some surprising results as well. First, AAVSO activity is related to a greater increase in self-efficacy in astronomy than one would find through increased astronomy experience alone (as measured through age). That is, it is possible that the demands of variable star research have a greater impact on how one views their knowledge of astronomy than the activity of the typical amateur astronomer. This could hint at greater learning taking place in active citizen science projects when compared to typical amateur astronomy projects. A future study is planned to investigate this result. A second surprise was the number of respondents who report to be active in the AAVSO, but also report to be inactive observers. This reflects the increased scope of the AAVSO over the past two decades. When the past two surveys were conducted, non-observing activities were not even considered unless they were in support of observing. Now, many participants of the AAVSO are dedicated to important projects such as programming, analysis of data, public outreach, and so on. Observing is still the heart of the AAVSO, with 60% of those who report participation in at least one non-observing activity also report to be active observers. Another surprise was the high level of education reported. Over half of participants report a graduate degree, with 24% reporting a terminal degree in their field (Ph.D., M.D., J.D., and so on). Also, 13% identify as professional astronomers (N = 86). One of the most interesting surprises is the number of countries represented by AAVSO membership (108). This may reflect the significant work that volunteers have put into translating our training materials into other languages, but it is likely a bigger reflection of the universal appeal of variable stars. There are simply so many types of stars and so many open questions, that almost anyone can find a project or object of interest. Finally, the number of respondents who have

authored or coauthored a paper in a scientific journal was quite high (36%). This is one of the major distinguishing characteristics between the AAVSO and other citizen science organizations, who tend to focus on using participants to contribute data for professionals to analyze and publish.

Raddick, *et al.* (2010) identified 12 categories of motivation from Galaxy Zoo participants through analysis of interviews and online forum posts. As with our survey, their categories were reduced from open-ended discussion (in their case, interviews were also included). In areas where our categories overlap with theirs, we find similarities and some significant differences in motivation rates. They report only 1% of their responses are motivated by "science" while "science and research" was the motivation of 35% of our respondents, which was our highest category of motivation. The Galaxy Zoo primary motivation category was "astronomy" at 39%. If that refers to interest in astronomy, then it is analogous to our "interest in variable stars" category that was cited by 32% of our respondents. Our two groups report the same level of motivation in terms of contributing data to a greater cause. 13% of the Galaxy Zoo participants cite a desire to "contribute" as a motivation of their participation while an identical 13% of our respondents cite a desire to "share data."

This study has a number of limitations. First, it is a study of active or recently active participants of the AAVSO. Some data, such as the ranked interest in types of objects, will be skewed towards current operations (people interested in exoplanets, for example, may have dropped out of the organization). So this data should not be used as a guide for the future, but only as a snapshot of the present. Second, the coding of the open-ended items was limited to one code per item. So it may oversimplify the results of those items. There is a striking similarity between our results and past surveys on these items, which suggests strong validity. Finally, this is self reported data. Thus it includes biases caused by human nature and different definitions of terminology. For example, some respondents report to be professional astronomers yet also report to not have a Ph.D. We are not stating they are not professionals, just that respondents will have difference definitions of the term "professional." To some, it requires a "Ph.D." while for others it denotes publishing in journals while still others apply the term to anyone contributing scientifically to astronomical research at any level.

6. Conclusion

This is a summary report of the AAVSO 2011 Demographic Survey, which included current and recent AAVSO participants. Compared with past surveys of this type, it shows an organization that is largely similar in demographics. Respondents were active in a wide variety of observing and non-observing activities and are interested in a wide variety of objects. The AAVSO reflects a "big tent" mentality, with room for everyone interested in variable stars.

There are signs in the data of some challenges, such as a population that is growing older and the presence of a very significant gender gap. However, these are not limited to the AAVSO alone. As a descriptive analysis, we make no predictions for the future. However, the results can be used, along with other surveys and analysis, to identify future paths and opportunities for the organization.

References

AAVSO 1976, AAVSO Archives, JAM Adm., Box 3 and 4, Survey of Membership, AAVSO, Cambridge, MA.

AAVSO 2011, Variable Star Index (http://vsx.aavso.org).

Beatty, K. 2000, *Sky & Telescope*, **100**, 3.

Hazen, M. L. 1995, *J. Amer. Assoc. Var. Star Obs.*, **23**, 143.

Kholopov, P. N., *et al.* 1985, *General Catalogue of Variable Stars*, 4th ed., Moscow.

Lowder, W. M. 1994, AAVSO Archives, JAM Org., Box 3B, Futures Study (2), AAVSO, Cambridge, MA.

New Track Media 2010, *Reader Demographics Rate Card*, **51**, 1.

Price, C. A., and Lee, H. -S. *J. Assoc. Res. Sci. Teach.*, in press.

Raddick, M. J., Bracey, G., Gay, P. L., Lintott, C. J., Murray, P., Schawinski, K., Szalay, A. S., and Vandenberg, J. 2010, *Astron. Education Rev.*, **9**, 1.

Thronson, H. A., and Lindstedt, S. L. 1986, *Publ. Astron. Soc. Pacific*, **98**, 941.

U.S. Department of Labor, Bureau of Labor Statistics. 2011 (November 1), List of SOC Occupations (retreived from http://www.bls.gov/oes/current/oes-stru.htm).

Waagen, E. O. 1980, *J. Amer. Assoc. Var. Star Obs.*, **9**, 92.

Williams, T. R., and Saladyga, M. 2011, *Advancing Variable Star Astronomy: The Centennial History of the American Association of Variable Star Observers*, Cambridge Univ. Press, Cambridge.

Appendix A

This is the printed version of the AAVSO 2011 Demographic survey. All items are worded exactly as they appeared online, except for the state and country items, which included drop down lists. In a few areas, screen shots of the online form were used in the printed survey as well.

AAVSO 2011 Demographic survey

1. What is your name? _____
2. If you have an observer code, what is it? _____
3. Do you want a copy of the summarized results of this survey?
   If so, enter your email address here: _____
4. What is your gender? _____
5. What is your age? _____
6. Zip code or postal code: _____
7. In what country do you live? _____
8. In which state or territory is your primary residence? _____
9. What is your highest level of completed formal education? (circle one)

- High School or equivalent
- Associates degree (2-year) or equivalent
- Bachelors degree (4-year) or equivalent
- Masters degree or equivalent
- M.D./J.D/Ph.D or equivalent

10. What is your primary field of profession? (circle one)
    (the following list is from the U.S. Department of Labor)

- Arts, Design, Entertainment, Sports and Media
- Building and Grounds Cleaning and Maintenance
- Community and Social Services
- Construction and Extraction
- Education, Training and Library
- Engineering, Architecture and Surveyors
- Farming, Fishing and Forestry
- Financial
- Food Preparation and Serving Related
- Health Care Practitioners and Technical
- Installation, Maintenance and Repair
- Legal
- Life, Physical and Social Science
- Management
- Mathematical and Computer Scientists
- Office and Administrative Support
- Personal Care and Service
- Production
- Protective Service
- Sales and Related
- Transportation and Mateiral-Moving
- Other (please specify) _____

11. What is your level of astronomy experience? (circle one)

- Novice with very basic astronomy experience
- Intermediate level
- Advanced level but not in a professional capacity
- Professional astronomer, astrophysicist, etc.

12. What do you consider was the *first* year you were active in the AAVSO? (ex: 1975, 1990, etc.)
_____
13. What was the main reason you became active in the AAVSO at that time?
_____
14. How did you hear/learn about the AAVSO? _____
15. If you are active in the AAVSO right now, what is your current main interest? _____
16. If you are not currently active in the AAVSO, what is the main reason? _____
17. Are you an active variable star observer? (circle one) Yes No
18. Of all the observing techniques you may use, what is the magnitude of the faintest positive variable star observation that you routinely make (do not count fainterthans)? _____
19. How do you make those faint observations? (check one)
    _____ Visual _____ CCD/DSLR/PEP/Other Digital system

20. If you are a CCD/DSLR/PEP observer, did you begin as a visual observer who migrated to CCD/DSLR/PEP or did you begin as a CCD/DSLR/PEP observer? (check one)
__I began making variable star observations as a visual observer who migrated to CCD/DSLR/PEP/etc.
__I began making variable star observations as a CCD/DSLR/PEP/etc. observer.

21. Select the following observing techniques that you actively use (circle as many that apply):

- Naked eye
- Binoculars
- DSLR
- Telescope visual
- Telescope CCD
- Telescope PEP
- Spectroscopy
- Sunspot counting
- SID monitoring
- AAVSONet or other robotic systems
- Other (please specify):

22. Select the following nonobserving activities in which you are currently active (circle as many that apply):

- AAVSOnet hardware or software support
- Actively contributing to a committee, division or section
- Chart/Sequence Development
- Data archiving
- Data mining
- Financial support (beyond membership fees)
- Mentoring
- Programming
- Public Speaking and Teaching
- Have served on Council at any point in time
- Volunteering at HQ
- Writing
- Other (please specify):

23. Please rank the types of objects you are most interested in (fill in the circle).
Please choose only one item for each rank. For example, only one object should be assigned a "1", only one object should be assigned a "2", etc.

1 = Most Interested 5 = Neutral 9 = Least Interested

	1	2	3	4	5	6	7	8	9
Rotational Variables	○	○	○	○	○	○	○	○	○
Cataclysmic Variables (Dwarf Novae, Novalike, etc.)	○	○	○	○	○	○	○	○	○
Non-stellar Objects	○	○	○	○	○	○	○	○	○
Young Stellar Objects	○	○	○	○	○	○	○	○	○
Eclipsing Binaries	○	○	○	○	○	○	○	○	○
Novae	○	○	○	○	○	○	○	○	○
Pulsating Variables (Cepheids, Miras, RR Lyr, etc.)	○	○	○	○	○	○	○	○	○
Extragalactic Objects (supernovae, blazars, etc.)	○	○	○	○	○	○	○	○	○
The Sun	○	○	○	○	○	○	○	○	○
Other (please specify)	_____								

24. How many AAVSO meetings have you attended? _____
25. If 1 or more, in what year did you last attend an AAVSO meeting? _____
26. Have you been an author or coauthor of a paper submitted to an astronomical journal (JAAVSO included—check one)? _____ Yes _____ No
27. Do you have any general comments you'd like to share?

The Citation of Manuscripts Which Have Appeared in *JAAVSO*

Arlo U. Landolt
Department of Physics and Astronomy, Louisiana State University, Baton Rouge, LA 70803; landolt@phys.lsu.edu

Received May 3, 2012; revised May 14, 2012; accepted May 15, 2012

Abstract A study is presented of the use by the astronomical community of the manuscripts published in *The Journal of the American Association of Variable Star Observers* (*JAAVSO*).

1. Introduction

The Journal of the American Association of Variable Star Observers (*JAAVSO*) was established in 1972 as "a place where professional and non-professional astronomers can publish papers on research of interest to the observer" (Mayall 1972). Mayall went on to write that "the new journal would include Abstracts of papers presented at AAVSO meetings, various Committee reports, Minutes of the Meetings of the AAVSO's Council, Observer's Totals, and Book Reviews." Additional insights concerning the formation and development of *JAAVSO* are discussed in the AAVSO's centennial history (Williams and Saladyga 2011). The content of *JAAVSO* has evolved over recent years, now containing less of the business and more of the scholarship of the organization.

The current authors and readers of *JAAVSO* are a mixture of amateur and professional astronomers. These individuals have an abiding interest in celestial phenomena which vary in brightness and color. The kinds of data presented in *JAAVSO* manuscripts have changed over time. Historically, the data primarily were visual or photographic. At present, data may be visual, photoelectric, or CCD-based. Both the precision and accuracy of the published data have improved with time. Suffice it to say that the authors of *JAAVSO* papers are a varied and talented population.

On the whole, and certainly historically, *JAAVSO* papers dwelled more on data acquisition and data presentation. Data interpretation is not pursued to the extent one finds in the professional journals. It is important that there be a journal such as *JAAVSO* for it provides an opportunity to a broader community to write and to publish useful and quality research.

2. Method

The Astrophysics Data System (ADS) is headquartered at the Smithsonian Astrophysical Observatory at Harvard. It is funded by NASA and contains

bibliographic databases, is a digital library, thereby providing access to astronomical information to the world via the World Wide Web. Once in the ADS, and in the Journal/Volume/Page section, a particular journal's code can be entered; for *JAAVSO*, that code is "JAVSO." Next, the desired journal volume number can be entered. This step leads to Query Results which list the papers in their order of appearance in the specified volume. The existence of the letter C indicates that the article was cited. Clicking on the C brings up the citing articles, whose numbers then may be counted.

It transpires that the ADS does not index all articles in a given volume in its article, or paper, count. Two volumes, numbers one and nineteen (which appeared in 1972 and 1990, respectively), were carefully searched in an effort to ascertain which titles were not included by the ADS. In volume one, the Treasurer's Report, Observer Totals, and Committee Reports were not indexed as articles. Similarly, in volume nineteen, the Introduction to the volume, the listing of the papers at First European Meeting of the AAVSO, the Minutes of the Annual Meeting, the Director's annual report, the Committee Reports, and the Treasurer's report were not identified by the ADS. All these written items have the characteristic that they are not astronomical research articles, hence a likely reason for omission from the ADS index count. Another reason for inclusion or omission is that the decision to include or not include depended on the decision maker, different from time to time. This study was limited to papers containing astronomical data.

This exercise reviewed the thirty-nine volumes of *JAAVSO* which were published in the interval 1972 through 2010. The review, the counting of the citations, of the authored articles identified by the ADS, was completed on October, 28, 2011.

A file was created whose function was to contain a count of the number of times each paper in a given volume was cited. This file contained a matrix constructed with the volumes listed in the row, and the possible number of citations, from zero to n, listed in the column. The matrix was filled in by tabulating the citations present, or not, if there were none. As an example, volume one contained thirty-one articles, as defined by the ADS, of which twenty papers never were cited, five papers were cited once, four papers were cited twice, one paper was cited three times, and one paper was cited four times, for a total of twenty citations for the volume.

3. Results

Some aspects of this investigation have been tabulated in Table 1. The Table contains the following information: the volume number in the first column, the year of publication in the second column, the number of papers which appeared in the volume in column three, and the total number of citations received by the papers in that volume in column four. Column five contains the number

of citations due to *JAAVSO* authors for a given volume, or, another way of describing it, column five gives the number of citations in column four which are by *JAAVSO* authors. The last column provides the percentage of the citations which were due to *JAAVSO* authors. This column is of interest because it indicates whether only individuals who publish in *JAAVSO* are citing *JAAVSO* papers. The goal of this table is to compare the number of citations by the astronomical community as a function of volume, with the number of citations by *JAAVSO* authors.

The information tabulated in Table 1 indicates that 1,545 papers were published in *JAAVSO* over its first thirty-nine years, a rate of 39.6 papers per volume. Those 1,545 papers have been cited 1,296 times, or, 0.84 citations per paper.

Of the total 1,296 citations, 464, or 35.8%, were citations by other *JAAVSO* authors. And, 64.2%, about two-thirds, of all citations to *JAAVSO* papers came from the greater astronomical community. A total of 1,296 citations in thirty-nine volumes leads to 33.2 citations per volume.

The last column in Table 1 provides the percentage of *JAAVSO* author citations for each volume. On the average, 37% of the citations to papers in a given volume are by *JAAVSO* authors.

Eighteen papers in these thirty-nine volumes were cited ten or more times. The paper with the most citations, nineteen, was by Percy, *et al.*, 1985, *JAAVSO*, vol. 14, p. 1. Appendix 1 lists the eighteen papers in chronological order, and which were cited at least ten times, through October 28, 2011. The number in brackets for each listed paper provides the citation count for that paper. The purpose in listing the most cited papers is to show the breadth of the projects found useful by the user community. It should be emphasized that a small number of citations does not mean that a paper has no value. Indeed, such a paper's content may be crucial to a citer's own research.

In summary, one can say that the articles, the papers, which appear in the issues of *JAAVSO*, are read by, and are cited by, researchers across the amateur and professional community.

References

Mayall, M. M. 1972, *J. Amer. Assoc. Var. Star Obs.*, **1**, 1.

Williams, T. R., and Saladyga, M. 2011, *Advancing Variable Star Astronomy: The Centennial History of the American Association of Variable Star Observers*, Cambridge Univ. Press, Cambridge.

Table 1. Citation counts of papers published in *JAAVSO*, volumes 1 through 39.

Vol.	*Year*	*Number of Papers*	*Total Number of Cites*	*Number of JAAVSO Cites*	*Percent JAAVSO Cites*
1	1972	31	20	13	65.0
2	1973	25	41	23	56.0
3	1974	20	40	11	27.5
4	1975	12	13	4	30.8
5	1976	33	30	6	20.0
6	1977	36	19	7	36.8
7	1978	45	44	12	27.3
8	1979	42	20	12	60.0
9	1980	39	24	12	50.0
10	1981	52	40	20	50.0
11	1982	35	22	5	22.7
12	1983	29	11	6	54.5
13	1984	30	5	2	40.0
14	1985	31	49	22	44.9
15	1986	62	68	45	66.2
16	1987	35	31	18	58.1
17	1988	39	40	18	45.0
18	1989	45	54	19	35.2
19	1990	47	42	9	21.4
20	1991	76	47	18	38.3
21	1992	60	83	31	37.3
22	1993	32	48	8	16.7
23	1994	15	12	6	50.0
24	1995	13	17	4	23.5
25	1996	45	41	16	39.0
26	1997	30	45	10	22.2
27	1998	14	33	7	21.2
28	1999	44	61	15	24.6
29	2000	56	48	8	16.7
30	2001	37	29	6	20.7
31	2002	45	36	7	19.4
32	2003	25	23	3	13.0
33	2004	58	48	18	37.5
34	2005	43	16	11	68.8
35	2006	100	23	9	39.1
36	2007	23	11	7	63.6
37	2008	43	25	5	20.0
38	2009	36	19	6	31.6
39	2010	62	18	5	27.8

Appendix 1

Papers published in JAAVSO having the most citations. The papers are listed in chronological order. The number in brackets for each listed paper provides the citation count for that paper.

JAAVSO, **2**, 52, 1973 [11]
Dinerstein, H., "VX Sagittarii: A Variable at Many Wavelengths."

JAAVSO, **10**, 1, 1981 [16]
Stanton, R. H., "Photoelectric Measures of AAVSO Comparison Star Sequences—Part Two."

JAAVSO, **14**, 1, 1985 [19]
Percy, J. R., Fabro, V. A., and Keith, D. W., "The Application of Visual Observations to the Study of a Small Amplitude Variable Star: Rho Cassiopeiae."

JAAVSO, **15**, 243, 1986 [15]
Belserene, E. P., "O–C by Computer."

JAAVSO, **17**, 34, 1988 [10]
Kiplinger, A. L., Mattei, J. A., Danskin, K. H., and Morgan, J. E., "Low-amplitude long-term modulations resembling solar cycles in SS Cygni."

JAAVSO, **21**, 42, 1992 [10]
Wing, R. F., "Three-Color Narrow-Band Photoelectric Photometry of Red Variables."

JAAVSO, **21**, 111, 1992 [11]
Samolyk, G., "A Period Update for the Five Eclipsing Biinary Stars: SS Ari, TY Boo, DF Hya, Z Lep, and TY UMa."

JAAVSO, **22**, 105, 1993 [18]
Oppenheimer, B. D., and Mattei, J. A., "Analysis of Long-Term AAVSO Observations of RS Ophiuchi."

JAAVSO, **24**, 106, 1995 [10]
Mattei, J. A., and Foster, G., "Dramatic Period Decrease in T Ursae Minoris."

JAAVSO, **26**, 115, 1997 [11]
Hoffleit, D., "History of the Discovery of Mira Stars."

JAAVSO, **26**, 57, 1997 [11]
Mattei, J. A., "Introducing Mira Variables."

JAAVSO, **27**, 101, 1998 [14]
Turner, D. G., "Monitoring the Evolution of Cepheid Variables."

JAAVSO, **27**, 97, 1998 [14]
Karovska, M., Carilli, C. L., and Mattei, J. A., "Possible Jet Formation in the Symbiotic System CH Cyg."

JAAVSO, **28**, 5, 1999 [14]
Turner, D. G., Horsford, A. J., and MacMillan, J. D., "Monitoring Cepheid Period Changes from Saint Mary's University."

JAAVSO, **31**, 27, 2002 [14]
Zijlstra, A. A., and Bedding, T. R., "Period Evolution in Mira Variables."

JAAVSO, **32**, 89, 2003 [11]
Sokoloski, J. L., "Symbotic Stars as Laboratories for the Study of Accretion and Jets: A Call for Optical Monitoring."

JAAVSO, **33**, 9, 2004 [17]
Percy, J. R., and Mohammed, F., "Self-Correlation Studies of RV Tauri Variables and Related Objects."

JAAVSO, **37**, 90, 2008 [11]
Majaess, D. J., Turner, D. G., Lande, D. J., and Moncrieff, K. E, "The Exciting Star of the Berkeley 59/Cepheus OB4 Complex and Other Chance Variable Star Discoveries."

Abstracts of Papers and Posters Presented at the Joint Meeting of the Society for Astronomical Sciences and the American Association of Variable Star Observers (AAVSO 101st Spring Meeting), Held in Big Bear Lake, California, May 22–24, 2012

Fast Spectrometer Construction and Testing *(Abstract)*

John Menke
22500 Old Hundred Rd, Barnesville, MD 20838; john@menkescientific.com

Abstract This paper describes the construction and operation of a medium resolution spectrometer used in the visual wavelength range. It is homebuilt, but has built in guiding and calibration, is fully remote-operable, and operates at a resolution R = 3000. It features a fast *f*/3.5 system, which allows it to be used with a fast telescope (18-inch *f*/3.5) with no Barlow or other optical matching devices.

Observations Using a Bespoke Medium Resolution Fast Spectrograph *(Abstract)*

John Menke
22500 Old Hundred Rd, Barnesville, MD 20838; john@menkescieentific.com

Abstract Designing and building a medium resolution (R = 3000) spectrograph was the relatively easy part. The really challenging part is learning how to use it: learning the characteristics of the spectrograph, choosing the right kind of astronomical problems, learning the best methods of taking data, and figuring out how to analyze the results. I have used several observing projects to "commission" this system, including measuring the Doppler shifts in several WUMa type stars. I will briefly describe the spectrograph but discuss in more detail the early experiences of using it.

Enhancing the Educational Astronomical Experience of Non-Science Majors With the Use of an iPad and Telescope *(Abstract)*

Robert M. Gill
Michael J. Burin
California State University, San Marcos, Physics Department, 333 S.Twin Oaks Valley Rd., San Marcos, CA 92096; rgill@csusm.edu, mburin@csusm.edu

Abstract General Education (GE) classes are designed to broaden the understanding of all college and university students in areas outside their major interest. However, most GE classes are lecture type and do not facilitate hands-on experimental or observational activities related to the specific subject matter. Utilizing several astronomy application programs (apps), currently available for the iPad and iPhone, in conjunction with a small inexpensive telescope allows students unique hands-on experiences to explore and observe astronomical objects and concepts independently outside of class. These activities enhance the student's overall GE experience in a unique way not possible prior to the development of this technology.

The Rotational Period of the Sun Using the Doppler Shift of the Hα Spectral Line *(Abstract)*

Robert M. Gill
California State University, San Marcos, Physics Department, 333 S.Twin Oaks Valley Rd., San Marcos, CA 92096; rgill@csusm.edu

Abstract The fact that the sun rotates is obvious by observing the daily motion of sunspots. The overall sunspot movement to the west is a result of this solar rotation. However, solar rotation can also be determined by observing the solar spectrum at the solar limbs. The absorption lines in the spectrum will display a Doppler shift since the east limb is coming toward the observer and the west limb is moving away. The velocity of the limb, relative to the observer, can be determined from these spectral line shifts. Knowing the solar radius, the rotational period can be calculated.

A Single Beam Polarimeter *(Poster abstract)*

Jerry D. Horne
3055 Lynview Drive, San Jose, CA 95148; jdhorne@hotmail.com

Abstract As astronomical polarimetry is an emerging field of study for amateur astronomy, the background, theory, and instrumentation of astronomical polarimetry is reviewed. Additionaly, the design and construction of a simple single beam polarimeter is presented, together with the results of its initial calibration.

Index to Volume 40

Author

Subject

AAVSO INTERNATIONAL DATABASE

PHOTOMETRY, VISUAL

VARIABLE STAR OBSERVING ORGANIZATIONS

VARIABLE STARS (GENERAL)

VARIABLE STARS (INDIVIDUAL); OBSERVING TARGETS